Cranfield University

RMCS, Shrivenham
Department of Aerospace, Power and Sensors

Mutual Interference Between Jets and Intakes in STOVL Aircraft

A thesis submitted for the degree of
EngD

by
A J Saddington

Supervised by
Dr K Knowles and Dr R G Matthews

September 1997

This thesis is submitted in partial fulfilment of
the requirements for the degree of EngD

ALL MISSING PAGES ARE BLANK

IN

ORIGINAL

Abstract

During wind tunnel testing of jet-lift, short take-off and vertical landing (STOVL) aircraft it is usual to simulate the jet efflux but not the intake flows. The intakes, which are commonly faired over or are unpowered, are generally tested in separate wind tunnel experiments. The forces acting on the wind tunnel model are determined by the linear addition of the forces obtained from the two separate tests. There is some doubt as to whether this is a valid approach.

A systematic experimental investigation was, therefore, conducted to determine the magnitude of any jet/intake interference effects on a generic jet-lift STOVL aircraft in transitional flight, out of ground effect. Comparisons made between separate and simultaneous jet and intake testing concluded that a mutual jet/intake interference effect does exist. The existence of this interference means that the aerodynamic wing lift loss in transitional flight deduced from isolated jet and intake testing is less than the lift loss obtained from simultaneous jet and intake testing.

The experimental research was supplemented by some simplified computational fluid dynamics (CFD) studies of elements of the flow-field about the aircraft using the k-ε turbulence model. The numerical modelling enabled aspects of the flow-field around the aircraft to be visualised which could not easily be done using the experimental apparatus.

It is a requirement of the EngD programme that part of this thesis must address a management topic linked to the research. In this case the management aspects of wind tunnel project work were examined. A scenario was developed which established a requirement for a large-scale, low-speed wind tunnel with a Reynolds number capability of 20 million. A study was performed on the decision-making process and investment appraisal methods used in the procurement of such a wind tunnel.

Acknowledgements

The author wishes to express his gratitude to Dr Kevin Knowles for initially setting up the research work and for his expert guidance and supervision throughout the four years of the project. Thanks are also due to Dr Ron Matthews for his assistance with and supervision of the management work contained in this thesis and to Dr Robin Bruce of DERA Farnborough for establishing the research parameters.

The general assistance of the laboratory managers, Alan Norris and Mark Eyles is gratefully acknowledged. Thanks also go to Dr Mark Finnis for his expert programming skills, to Dr Alastair Senior for his assistance with the CFD software and to Dr Marek Myszko for his help with the experimental facilities.

Declaration

No portion of the work presented in this thesis has been submitted in support of an application for another degree or qualification at this or any other University or Institution of Learning.

Contents

1. Introduction **1**

1.1 Background....3

1.1.1 Entwicklungsring Sud (EWR) VJ101C....3

1.1.2 Dassault Mirage III-V....3

1.1.3 Vereinigte Flugtechnische Werke (VFW) - Fokker VAK191B....4

1.1.4 Yakovlev Yak-38 'Forger'....4

1.1.5 Yakovlev Yak-141 'Freestyle'....5

1.1.6 The 'Harrier' family of STOVL aircraft....5

1.2 The future - JSF....6

1.3 Research field....7

1.4 Research objectives....8

2. STOVL Interference Effects **15**

2.1 Hovering out of ground effect....17

2.1.1 The free jet....17

2.1.2 Jet-induced interference effects....18

2.1.2.1 The effect of jet decay rate....19

2.1.2.2 The effect of nozzle pressure ratio (NPR)....21

2.1.2.3 The effect of nozzle length and projection....22

2.1.2.4 The effect of planform shape and position....23

2.1.2.5 The effect of off-axis nozzle positions....23

2.2 Transition out of ground effect....24

2.2.1 The free jet in a cross-flow....24

2.2.1.1 Correlation parameters....25

2.2.1.2 Jet trajectory....26

2.2.2 Jet-induced interference effects....27

2.2.2.1 The effect of velocity ratio, V_e....28

2.2.2.2 The effect of area ratio, A_n/S....29

2.2.2.3 The effect of nozzle geometry....29

2.2.2.4 The relative location of wing and jet....30

2.2.2.5 The effect of nozzle vector angle, δ_j....31

2.2.2.6 Lift improvement devices (LIDs)....31

2.2.3 Interference effects between jet(s) and intake(s)....32

2.3 STOVL aircraft in ground effect....35

2.3.1 Jet impingement 35
2.3.2 Wall jet flows 36
2.3.3 Fountain flows between multiple jets 36
2.3.4 The ground vortex 36
2.3.5 Hot gas ingestion 37
2.4 Summary 37

3. Experimentation **49**

3.1 Design and construction of the wind tunnel model 51
3.1.1 Jet simulation 52
3.1.2 Jet nozzles 53
3.1.3 Intakes 54
3.1.4 Wing 55
3.1.5 Fuselage 56
3.2 Experimental facilities 57
3.2.1 Wind tunnel 57
3.2.1.1 Description 57
3.2.1.2 Speed control hardware 58
3.2.1.3 Calibration 59
3.2.1.4 Speed control software 60
3.2.1.5 Wind tunnel interference 60
3.2.2 Compressed air supply 61
3.2.2.1 Description 61
3.2.2.2 Pressure control hardware 62
3.2.3 Additional instrumentation 62
3.2.4 Pressure control and data acquisition software 63
3.2.5 Pressure loss through the intake and ducting 64
3.2.5.1 Wind tunnel model 64
3.2.5.2 90 degree bend, diameter 65 mm 64
3.2.5.3 Straight duct, diameter 65 mm 65
3.2.5.4 Conical diffuser, 65 mm to 225 mm diameter 65
3.2.5.5 90 degree bend, 225 mm diameter 65
3.2.5.6 Straight duct, 225 mm diameter 65
3.2.5.7 Total pressure loss 65
3.2.6 Estimation of the intake mass flow rate 66
3.3 Experimental programme 66
3.4 Error analysis 68
3.5 Summary 69

4. Experimental Results **91**

4.1 Experimental procedure....93
4.1.1 Changes introduced following the Phase 1 experiments....94
4.2 Schlieren photography....94
4.3 Repeatability....95
4.4 Data reduction....95
4.5 Presentation of results....95
4.6 The effect of the jet on the wing....96
4.6.1 The influence of effective velocity ratio, V_e....97
4.6.1.1 Wing upper surface....98
4.6.1.2 Wing lower surface....99
4.6.1.3 The net effect....99
4.6.2 The influence of NPR (constant nominal mass flow rate)....100
4.6.2.1 Wing upper surface....100
4.6.2.2 Wing lower surface....101
4.6.2.3 The net effect....101
4.6.3 The influence of NPR (constant nozzle area)....102
4.6.3.1 Wing upper surface....102
4.6.3.2 Wing lower surface....103
4.6.3.3 The net effect....103
4.6.4 The influence of nozzle position....103
4.6.4.1 Wing upper surface....103
4.6.4.2 Wing lower surface....104
4.6.4.3 The net effect....104
4.7 The effect of the intakes on the wing....105
4.7.1 Wing upper surface....105
4.7.2 Wing lower surface....106
4.7.3 The net effect of the intake on the wing....106
4.8 The effect of the jet on the intake flow....107
4.8.1 Lower outer surface....107
4.8.2 Lower inner and upper inner surfaces....109
4.8.3 Upper outer surface....109
4.8.4 The net effect of the jet on the intake flow....110
4.9 Comparison of separate and simultaneous jet and intake testing....110

4.9.1 The influence of effective velocity ratio, V_e 111
4.9.2 The influence of NPR (constant nominal mass flow rate) 112
4.9.3 The influence of NPR (constant nozzle area)..... 112
4.9.4 The influence of nozzle position..... 112
4.10 Summary..... 113
4.10.1 The effect of the jet on the wing..... 113
4.10.2 The effect of the intakes on the wing 113
4.10.3 The effect of the jet on the intakes..... 114
4.10.4 The effect of the jet and intakes on the wing..... 114
4.10.5 Comparison between separate and simultaneous jet and intake testing 114

5. Numerical Modelling 163

5.1 Introduction..... 165
5.2 Turbulence..... 165
5.3 The governing equations..... 166
5.4 The closure problem..... 168
5.5 Reynolds averaging..... 168
5.5.1 Time-averaging the incompressible equations 168
5.6 Turbulence modelling 170
5.6.1 The Boussinesq eddy-viscosity 170
5.6.2 Prandtl's mixing-length model 170
5.6.3 One-equation models..... 171
5.6.4 Two-equation models 171
5.7 Compressibility effects..... 172
5.7.1 Compressible-flow closure approximations..... 174
5.8 The PHOENICS program 174
5.8.1 Flow types 174
5.8.2 Grid types and arrangement..... 175
5.8.3 Solution algorithm..... 175
5.8.4 Operating system and versions..... 176
5.9 Previous PHOENICS modelling work..... 176
5.10 Summary..... 177

6. Numerical Modelling Results 179

6.1 Aim of the numerical modelling..... 181
6.2 Convergence 181
6.3 NACA 1408 aerofoil..... 182

6.3.1 Computational grid 182
6.3.2 Flow conditions 182
6.3.3 Boundary conditions 183
6.3.4 Results 183
6.4 Round free jet 184
6.4.1 Computational grid 185
6.4.2 Flow conditions 185
6.4.3 Boundary conditions 186
6.4.4 Results 187
6.4.4.1 Velocity profiles in a subcritical jet 187
6.4.4.2 Velocity profiles in an underexpanded jet 189
6.4.4.3 Centre-line velocity decay 189
6.4.4.4 Free jet spreading rate 190
6.4.4.5 Comments on the k-ε turbulence model 191
6.5 Round jet in crossflow 192
6.5.1 Computational grid 192
6.5.2 Flow conditions 193
6.5.3 Boundary conditions 193
6.5.4 Results 193
6.5.4.1 Jet trajectories (δ_j = 90 degrees) 193
6.5.4.2 Jet trajectories (δ_j = 60 degrees) 195
6.6 Summary 195

7. Management Aspects of Wind Tunnel Project Work 211

7.1 Commercial justification for the research 213
7.2 Project management 213
7.2.1 Project time schedule 213
7.2.2 Project costs 214
7.3 Analysis of the likely impact on DERA Farnborough 215
7.4 Procurement of a new low-speed wind tunnel 215
7.4.1 Market impact from a new low-speed wind tunnel 216
7.4.2 A review of low-speed wind tunnels in Europe 217
7.4.3 The US National Wind Tunnel Complex 218
7.4.4 A proposed new low-speed wind tunnel 219
7.4.4.1 Construction costs 220
7.4.4.2 Operating costs 221
7.5 Capital investment decisions 223
7.6 The decision-making process 224

7.7 Opportunity cost of investment 225
7.8 Financial evaluation - appraisal methods 226
7.8.1 Traditional methods 226
7.8.1.1 Payback 226
7.8.1.2 Average accounting rate of return 227
7.8.2 Discounted cash flow methods 228
7.8.2.1 Net present value 228
7.8.2.2 Internal rate of return 231
7.8.2.3 Discounted payback 232
7.8.3 Problems associated with financial appraisal methods 233
7.9 Broader frameworks for investment appraisal 234
7.9.1 Strategic methods 234
7.9.2 The Information Economics Model 235
7.9.3 Combined operational effectiveness and investment appraisal (COEIA) 237
7.10 Suitability of investment appraisal methods to wind tunnel construction projects 240
7.11 Summary 242

8. Conclusions and Recommendations 249

8.1 Conclusions 251
8.1.1 Experimental work 251
8.1.2 Numerical modelling 252
8.1.3 Management work 253
8.2 Recommendations for future work 254

References 257

A. Determination of the Theoretical Effective Velocity Ratio 269

B. Phase 1 Experimental Data 273

C. Phase 2a Experimental Data (Constant Nozzle Mass Flow Rate) 311

D. Phase 2b Experimental Data (Constant Nozzle Area) 351

E. PHOENICS q1 Input Files 391

Nomenclature

Abbreviations

AEW	airborne early warning
APRA	Advanced Projects Research Agency
ARR	accounting rate of return
ASTOVL	advanced short take-off and vertical landing
BAe	British Aerospace
BFC	body-fitted co-ordinates
CALF	Common Affordable Lightweight Fighter
CFD	computational fluid dynamics
CIL	Computer Instrumentation Limited
COEIA	combined operational effectiveness and investment appraisal
CofG	centre of gravity
DERA	Defence Evaluation and Research Agency
ETW	European Transonic Wind Tunnel
EWR	Entwicklungsring Sud
HP	high pressure
IRR	internal rate of return
JAST	joint advanced strike technology
JSF	joint strike fighter
LES	large-eddy simulation
LID	lift improvement device
LP	low pressure
MDAL	master data and assumptions list
MoD	Ministry of Defence
MRF	Multi-role Fighter
NACA	National Advisory Committee for Aeronautics
NASA	National Aeronautics and Space Administration
NPR	nozzle pressure ratio $\left\{\frac{P_c}{p_a}\right\}$
NPV	net present value
P&W	Pratt and Witney
RMCS	Royal Military College of Science
RS	Radio Spares
SAM	surface-to-air missile

STOL	short take-off and landing
STOVL	short take-off and vertical landing
TPS	turbine-powered simulator
UK	United Kingdom
US	United States (of America)
USA	United States of America
USAF	United States Air Force
USMC	United States Marine Corps
USN	United States Navy
VAAC	Vectored-thrust Aircraft Advanced Control
VFW	Vereinigte Flugtechnische Werke
V/STOL	vertical/short take-off and landing
VTOL	vertical take-off and landing

Symbols

a_{2d}	two dimensional lift curve slope
A	area (m^2)
$b_{x,y,z}$	power law exponent to determine grid spacing in the x, y and z directions (see Equation 6.1)
c	wing chord (m)
C_l	sectional lift coefficient per unit span $\left\{\frac{l}{q_\infty c}\right\}$
C_L	lift coefficient $\left\{\frac{L}{q_\infty S}\right\}$
C_{ni}	intake normal force coefficient $\left\{\sum \frac{p_i - p_\infty}{q_\infty}\right\}$
c_p	specific heat at constant pressure [1005] ($Jkg^{-1}K^{-1}$)
C_p	pressure coefficient $\left\{\frac{p - p_\infty}{q_\infty}\right\}$
C_y	net cash flow arising at the end of year y (£)
$C_{\varepsilon 1}$	k-ε model coefficient [1.44]
$C_{\varepsilon 2}$	k-ε model coefficient [1.92]
C_μ	k-ε model coefficient [0.09]
d	diameter (m)

$\overline{D}$	angular mean planform diameter $\left\{\frac{1}{\pi}\int_0^{2\pi}\left(r(\theta)-\frac{d_{ne}}{2}\right)\mathrm{d}\theta\right\}$ (m)
f	surface friction coefficient
F	thrust (N)
g	acceleration due to gravity [9.81] (ms^{-2})
h	height (m) or specific enthalpy (Jkg^{-1})
i	index
i, j, k	unit vectors (in Cartesian co-ordinates)
k	turbulent kinetic energy (J) or cost of capital (£)
k_1, k_2	constants in Equations 2.1, 2.3 and 2.6
k_{t1}, k_{t2}	constants in Equation 3.3
k_p	static pressure offset
l	length (m) or sectional lift (N)
L	lift (N)
l_m	mixing length (m)
m	constant used in Equation 2.9
M	Mach number or moment (Nm)
$\dot{m}$	mass flow rate (kgs^{-1})
n	constant used in Equation 2.9
N	number of samples in a population
nx, ny, nz	number of grid cells in the x, y and z directions
p	static pressure (Pa)
P	total pressure (Pa)
Per	perimeter (m)
Pr_t	turbulent shear layer Prandtl number [0.5]
p_{tn}	wind tunnel nozzle static pressure
p_{ts}	wind tunnel settling chamber static pressure
q	dynamic pressure (Pa)
r	radius (m)
R	specific gas constant [287.1] ($Jkg^{-1}K^{-1}$)
Re	Reynolds number $\left\{\frac{\rho\bar{V}l}{\mu}\right\}$
S	planform area (m^2)
S_i	body force tensor (N)
t	time (s)
T	temperature (K)
T_0	total temperature (K)

Tu	turbulence intensity
u_i	velocity tensor (ms^{-1})
u, v, w	instantaneous velocity components (ms^{-1})
$\mathbf{V}$	velocity vector (ms^{-1})
V	general velocity (ms^{-1})
V_e	effective velocity ratio $\left\{\frac{V_\infty}{V_j}\sqrt{\frac{\rho_\infty}{\rho_j}}=\frac{M_\infty}{M_j}\sqrt{\frac{p_\infty}{p_j}}\right\}$
x_i	Cartesian co-ordinate tensor (m)
x, y, z	Cartesian co-ordinates (m)
$y_{½}$	local jet half width (m)
$z_{\alpha/2}$	number of standard deviations for a given probability
α	wing incidence (degrees) or constant in Equation 2.9
β	constant in Equation 2.9
γ	ratio of specific heats [1.4]
δ	local shear layer width (m)
δ_{ij}	Kronecker delta { = 1 if $i=j$, otherwise = 0}
δ_j	jet vector angle (see Figure 4.12b)
Δ	incremental
ε	rate of dissipation of turbulent kinetic energy (Js^{-1})
ζ	enstrophy (a measure of vorticity and used in the k-ζ turbulence model)
η	efficiency
η_t	tunnel power factor
θ	angular distance (degrees)
κ	thermal conductivity ($Wm^{-1}K^{-1}$)
μ	molecular viscosity $\left\{1.458\times10^{-6}\frac{T^{1.5}}{T+110.4}\right\}(kgm^{-1}s^{-1})$
ν	kinematic viscosity $\left\{\frac{\mu}{\rho}\right\}$ (m^2s^{-1})
ν_t	turbulent (eddy) viscosity (m^2s^{-1})
ρ	density (kgm^{-3})
σ_k	k-ε model closure coefficient [1.0]
σ_ε	k-ε model closure coefficient [1.3]
σ_ϕ	standard deviation of $\phi(t)$
$\sigma[\,]$	standard deviation of [ ]
τ_{ij}	stress tensor

$\phi(t)$	time-dependent variable
Φ	dissipation function

Subscripts and superscripts

a	atmospheric
c	settling chamber
f	flap
i	intake
i	point at which maximum value occurs (see Equation 2.2)
ie	intake equivalent
j	jet
max	maximum
n	nozzle exit condition
ne	nozzle equivalent
(root)	wing root
t	wind tunnel working section
w	water
x	(e.g. q_x) position along the x-axis to which the variable refers
∞	freestream
[^]	estimate of [ ]
$^-$	(e.g. $\overline{\phi}$) denotes time-mean variable
$^\sim$	(e.g. $\widetilde{\phi}$) denotes Favre-averaged variable
$'$	(e.g. ϕ') denotes fluctuating variable in Reynolds averaging
$''$	(e.g. ϕ'') denotes fluctuating variable in Favre averaging

Variables used in PHOENICS q1 files

CFLOW	–	freestream velocity
CGAS	–	specific heat at constant pressure
DAMB	–	ambient density
DIAM	–	nozzle diameter
DJETS	–	nozzle exit static density
DJETT	–	nozzle exit total density
ENUL	–	laminar kinematic viscosity
EPINJET	–	dissipation of turbulent kinetic energy in the jet
EPINCF	–	dissipation of turbulent kinetic energy in the freestream
GAMMA	–	ratio of specific heats

MACH – nozzle exit Mach number

MAXV – maximum velocity (used to determine Courant number)

MINL – minimum cell width (used to determine Courant number)

NPR – nozzle pressure ratio

P1 – first phase static pressure

PAMB – ambient pressure

PRESS0 – reference total pressure (PAMB)

RELXEP – false time step relaxation value for the dissipation rate of turbulent kinetic energy.

RELXKE – false time step relaxation value for the turbulent kinetic energy

RELXU – false time step relaxation value for the u velocity component

RELXV – false time step relaxation value for the v velocity component

RELXW – false time step relaxation value for the w velocity component

RGAS – specific gas constant

RHO1 – first phase static density

RHO1B – parameter associated with the command RHO1=GRND5

TAMB – ambient temperature

TINT – turbulence intensity

TKEIN – turbulent kinetic energy

TJETS – jet exit static temperature

TJETT – jet exit total temperature

TMP1 – first phase static temperature

TMP1A – parameter associated with the command TMP1=GRND5

TMP1B – parameter associated with the command TMP1=GRND5

WJET – jet exit velocity

XPWR – power law expansion in the x-direction

YPWR – power law expansion in the y-direction

ZPWR – power law expansion in the z-direction

1 Introduction

Chapter One opens by introducing and discussing the background to short take-off and vertical landing (STOVL) jet-lift aircraft. This is followed by a brief discussion of some of the better-known aircraft designs, culminating in the present day situation where only one STOVL aircraft (the Harrier) is in service.

Next, the future for STOVL aircraft is discussed with reference to the JSF project. The three original competing designs are described, with particular emphasis on the methods used for the vertical flight mode.

The research is primarily concerned with some of the aerodynamic problems associated with the design, wind tunnel testing and operation of jet-lift STOVL aircraft. In the final section, the aims and objectives of the research project are described.

1.1 Background

The idea of short take-off and vertical landing (STOVL) aircraft is not a new one. Serious research and configuration development has been going on since the mid 1950s producing over 50 vertical/short take-off and landing (V/STOL) and short take-off and landing (STOL) aircraft that have reached the flight stage. But in 1997, there is still only one operational STOVL aircraft in the world, the British Aerospace/McDonnell Douglas Harrier/AV-8B. Vertical flight has been achieved through the use of rotors, propellers, jets or some combination of these. The aircraft of interest here, however, are jet-supported vehicles of which there have been many research and development types built over the years. They make use of either lightweight lift-engines in addition to one or more cruise engines, cruise engines with a swivelling nozzle system, or a combination of both types, installed in either the airframe or in wing pods. Some of the better known jet-lift STOVL aircraft are now described. More details of these and other STOVL aircraft can be found in HIRSCHBERG, 1997.

1.1.1 Entwicklungsring Sud (EWR) VJ101C

First flown in 1963, the EWR VJ101C (see Figure 1.1) was a single seat vertical take-off and landing (VTOL) experimental aircraft which was built and tested to provide data for a definitive Mach 2 VTOL interceptor. The aircraft had a high wing and was powered by six Rolls-Royce RB145 engines each producing 12.2 kN (2750 lb) of thrust. Its chief design feature was the use of wingtip engine pods, each containing two RB145 engines, which swivelled through a total angle of 94 degrees. The wingtip engines had supersonic intakes which could translate forward exposing slots to let extra air into the engines for take-off and landing. The remaining two engines were mounted in a fixed vertical attitude in tandem in the fuselage centre section behind the cockpit. In their vertical thrust position, the two wing-tip pods combined with the fuselage lift engines to form a triangular jet lifting system which enabled hovering, roll and pitch control to be achieved by differential thrust modulation. Yaw control in the hover was accomplished by differential pod swivelling. Mach 1 was exceeded several times in flight trials.

1.1.2 Dassault Mirage III-V

An attempt at a supersonic STOVL aircraft was made by converting an existing design, the Dassault Mirage III, to STOVL capability. This was achieved by the installation of eight 24.0 kN (5400 lb) thrust Rolls-Royce RB162 lift engines, four on either side of the propulsion engine air intake duct. The aircraft first flew in February 1965 and was capable of Mach 2 in level flight. Designated Mirage III-V, it is shown hovering in Figure 1.2. The aircraft only ever took off from a special porous

pad to reduce 'suckdown' interference effects. Control jets in the nose, tail and wingtips provided attitude control in the hover. The lift engine air intake covers were rear-hinged to admit ram air for engine starting. Although the aircraft had VTOL capability and Mach 2 performance, the eight lift engines added 1360 kg (3000 lb) of extra weight, severely reducing its payload/range capability and the project was cancelled.

1.1.3 Vereinigte Flugtechnische Werke (VFW) - Fokker VAK191B

The VAK191B (Figure 1.3) was designed as a subsonic VTOL tactical reconnaissance strike fighter and had a similar layout to the Hawker P.1127, which in turn evolved into the familiar Harrier. It was powered by one 44.5 kN (10000 lb) thrust Rolls-Royce RB193, four-nozzle, vectored thrust turbofan and two Rolls-Royce RB162-81 lift jets. The lift engines were installed fore and aft of the centrally-mounted RB193 engine and inclined to exhaust 14 degrees aft of vertical. The air intakes for the lift engines were covered by semi-circular doors hinged at the sides. There was no need to use ram air to spin the lift engines up to speed, since on-board starting was provided. Lift engine exhausts were covered by pairs of transverse-hinged rectangular doors. The air intakes for the vectored thrust engine were at the sides of the fuselage just behind the cockpit. The intakes were much smaller than those for the Harrier and were optimised for fast forward flight. The front 0.91 metre-long (3 feet) section of each intake was separate from the fuselage, and could slide forward about 0.25 m (10 inches), creating an additional slot through which the engine could 'suck' more air during transition and hover. Control was by means of reaction nozzles at nose, tail and wingtips using air bled from the compressors of all three engines. The first flight was made in October 1964 but the research contract for the project ended in December 1972 after which the three aircraft were retained as flight systems test beds in the Panavia Tornado programme.

1.1.4 Yakovlev Yak-38 'Forger'

The Soviet-developed Yak-38 'Forger' (Figure 1.4) used a lift plus lift/cruise layout to achieve STOVL capability. Two in-line Rybinsk lift engines (29.8 kN (6700 lb) thrust each) were mounted immediately behind the cockpit inclined with the engine exhaust 13 degrees to the rear. One 57.8 kN (13000 lb) thrust Tumansky turbojet engine was mounted in the centre fuselage and exhausted through two hydraulically actuated vectoring nozzles, one on each side just aft of the trailing edge of the wing. The first prototype flew in 1971 and was in service by 1976. The primary role was fleet defence, reconnaissance and anti-ship strike, but the aircraft was never used in combat. The Forger was removed from service in 1992-1993.

1.1.5 Yakovlev Yak-141 'Freestyle'

The Yak-141 programme was initiated in 1975, about the same time as the Yak-38 was first being introduced into service. The supersonic 'Freestyle' (Figure 1.5) was optimised for air defence. The first conventional flight was made in 1987 and the first hover in 1989. In flight testing, the Freestyle achieved a maximum speed of Mach 1.7 and manoeuvrability was claimed to be very good. It was powered by one lift engine mounted behind the cockpit and one lift/cruise engine, the latter having a rotating nozzle to vector exhaust gases downwards. Severe ground erosion problems were encountered with the lift/cruise engine particularly in reheat mode. Development work was stopped in 1991 due to shrinking Soviet defence budgets.

1.1.6 The 'Harrier' family of STOVL aircraft

The Hawker-Siddeley P.1127 design was first conceived in 1957 powered by an 48.9 kN (11000 lb) Bristol-Siddeley Pegasus 1 vectored thrust engine. The P.1127 made its first double transition in 1961. In 1962, the UK, US and Germany initiated a tripartite programme, funding nine improved P.1127 'Kestrels' for use with the UK-led tri-national squadron which conducted operational trials. These used Pegasus 5 engines with thrust increased to 69.0 kN (15500 lb) Following the Kestrel operational trials the first of six production-designed 'Harrier' developmental aircraft flew in 1966. The production Harrier, powered by an 84.5 kN (19000 lb) Pegasus Mk. 101, entered service in 1969 with the Royal Air Force as the GR1 and with the US Marine Corps as the AV-8A. A navalised version, the Sea Harrier FRS1, entered service with the Royal Navy in 1980. McDonnell Douglas, together with British Aerospace, began developing the AV-8B/GR5 Harrier II in 1974, with flight testing commencing in 1981. With a more powerful engine, a larger, composite, supercritical wing, optimised lift improvement devices (LIDs) and other improvements, the Harrier II was able to double the payload and range when making short take-offs compared with the GR1/AV-8A.

The current aircraft, designated GR5/AV-8B (Figure 1.6), is powered by a Rolls-Royce Pegasus Mark 105 vectored thrust turbofan engine developing 105.9 kN (23800 lb) of thrust (more than double that of the Pegasus which powered the P.1127) mounted in the fuselage such that the resultant thrust vector passes very close to the aircraft centre of gravity at any nozzle vector angle. Air exhausting from the forward 'cold' nozzles at approximately 150°C and 350 ms^{-1} is supplied from the low pressure (LP) compressor. The rear 'hot' nozzles are supplied from the LP turbine at 670°C and 550 ms^{-1}. A reaction control system, drawing air from the high pressure (HP) compressor provides pitch, roll and yaw control in the hover. The use of aerodynamic control surfaces and the reaction control system, gives the Harrier superior control response at low forward speeds (up to about 60 ms^{-1}) compared with a conventional aircraft. To date it is still the most successful STOVL de-

sign in the world, and with the withdrawal from service of the Yak 38 'Forger', is currently the only STOVL aircraft in regular service.

1.2 The future - JSF

The development of an improved (particularly supersonic) STOVL military aircraft has been an attractive goal for many aircraft companies all over the world especially in Europe and the USA. Research is currently underway in the UK and the USA to develop the next generation of STOVL aircraft. The aim is to design an aircraft with all the advantages of STOVL but without compromising too greatly the performance of a conventional aircraft. Significant design features will include stealth and supercruise capability. The reduced radar cross section provided by a stealthy design is important because it greatly reduces enemy detection capability [PENNEY, 1996]. Supercruise, the ability to accelerate to and exceed Mach 1 without the need for afterburning, is important for a number of reasons. It increases the lethal envelope of any weapon fired due to the increased kinetic energy at launch. Supercruise also provides optimum fuel flow at combat airspeeds thus allowing a larger radius of action. Finally, supercruise minimises the exposure of an aircraft to surface-to-air missile (SAM) threats as it greatly reduces a SAM's available firing envelope [PENNEY, 1996]. Currently there is no STOVL aircraft in regular service with a stealthy design or a supersonic capability. The Harrier GR5/AV-8B has a maximum level flight Mach number of 0.90.

The current Joint Strike Fighter (JSF) programme is the result of merging a number of US programmes which were aimed at supplementing the F-22 and F/A-18E/F in USAF, USN and USMC service. Initially the USAF's Multi-role Fighter (MRF) and US Navy's advanced fighter programmes were rolled into a common programme specification which became Joint Advanced Strike Technology (JAST) which was to include the study of a STOVL derivative. The Advanced Projects Research Agency (APRA) was also funding Advanced STOVL (ASTOVL) studies under the joint service Common Affordable Lightweight Fighter (CALF) programme. Finally CALF was merged with JAST and united with some other work done by various companies under both government and private funding to form JSF. As well as merging these various programmes, JSF is designed to produce service aircraft from around 2008 rather than being a technology demonstration programme.

The UK has agreed to fund 35% of the STOVL portion of the programme. Initially 20% of this contribution was direct funding of about £8 million, the rest coming via the results of UK research such as the Vectored-thrust Aircraft Advanced Control (VAAC) Harrier programme and a BAe/Rolls-Royce integrated flight and propulsion controls programme.

There were initially three design teams in the JSF programme: McDonnell Douglas/Northrop-Grumman/British Aerospace; Boeing and Lockheed Martin. Of the

three proposals for the JSF competition Boeing's propulsion system is most like the Harrier's vectored thrust, direct lift configuration. The aircraft is a tail-less delta with a chin-mounted intake and twin fins (Figure 1.7). The engine is a modified Pratt and Witney (P&W) F119 with a 20% bigger fan to increase thrust. A two-dimensional cruise nozzle will close in STOVL mode allowing mixed core and fan air to be ducted to two retractable nozzles aligned with the centre of gravity (CofG). A series of attitude control nozzles which take air from the fan provide hover pitch, yaw and roll control. A translating intake lip opens in the STOVL mode to improve low-speed intake performance.

The Lockheed Martin-led JSF (Figure 1.8) also borrows from previous STOVL aircraft, in this case the Yak-141. The engine is again a P&W F119, this time modified to power a shaft-driven lift-fan mounted in the fuselage behind the cockpit. The main engine has a Rolls-Royce vectoring nozzle (non-afterburning) which can be rotated through 110 degrees downwards or 10 degrees upwards. It can also be vectored left and right for yaw control. To cope with the additional mass flow demands of the main engine during STOVL operations, an additional intake is provided on the top of the rear fuselage. There are also two ducts under the wings, taking air from the bypass duct for STOVL roll control. The lift-fan will be a two-stage, contra-rotating unit with an Allison-designed nozzle which will allow the air stream to be vectored forward 20 degrees, backward 60 degrees and 8 degrees to port or starboard. The lift-fan is driven from a gearbox linked to the main engine LP compressor stage through a dry clutch.

The McDonnell Douglas JSF design (Figure 1.9) features a lift plus lift/cruise engine arrangement. The main engine uses an axisymmetric pitch-yaw thrust vectoring nozzle which, in STOVL mode, operates in conjunction with a General Electric GEA-FXL lift engine. The lift engine is located behind the cockpit and is enclosed by doors when not in use. Its exhaust can be vectored through 50 degrees through the use of vanes at the nozzle exit. The main engine's contribution to STOVL flight is via two nozzles behind the main undercarriage legs which are fed from diverted exhaust flow. These can also be vectored for control to 5 degrees forward, 45 degrees rearward and via lateral flaps to 30 degrees outboard and 7 degrees inboard.

In November 1996 the Pentagon eliminated the McDonnell Douglas design from the programme, reducing the teams to two. Contracts to build a flying prototype were awarded to Boeing and Lockheed Martin. It has subsequently been announced that British Aerospace has joined with the Lockheed Martin team, maintaining a UK presence in the JSF programme.

1.3 Research field

STOVL aircraft introduce many aerodynamic characteristics unique to their operation. The flow-fields surrounding the aircraft, during hover near the ground and

during transition from hover to wing-borne flight, are of particular importance. The problems of interest include (but are not limited to) the airframe forces and moments due to the motion of the aircraft, due to the jets and their entrainment flowfield and due to the intake flows. These are generally complex effects which have to be checked by wind tunnel tests of the chosen configuration. One area that has not been systematically investigated is the possible mutual interference between the jets and intakes on the aircraft.

It is essential to test new STOVL designs for jet interference during the transition phase. This is done by feeding high pressure air to accurately-scaled vectoring nozzles incorporated into a wind tunnel model. These nozzles may be live (fixed to the model) or earthed (isolated from the model). The intakes, which are commonly faired over or are unpowered, are generally tested in separate wind tunnel experiments. The model is tested over the appropriate Mach number range, and the forces and moments are measured with the jets on and off, to assess the jet interference effects. The overall forces and moments on the aircraft are then deduced by linear addition of the separate jet interference results and the intake test results. This procedure, however, will ignore any mutual interferences between jets, intakes and airframes which may produce 'non-linearly additive' airloads.

There is considerable doubt over whether the current test procedure is sufficient for some of the modern STOVL configurations discussed above [BRUCE, 1997]. These tend to have large intake mass flows, large auxiliary intakes, forward mounted jets and large wings. The intake flows are likely to be affected by jet interference (and the jet paths may be affected by intake interference), and this may cause additional lift losses and pitching moments which would not be identified by conventional intake tests or jet interference tests. These could have a critical effect on the aircraft stability and the rate at which the nozzles can be vectored to accelerate/decelerate the aircraft through the transition phase.

Unfortunately, it is particularly difficult to design a force/moment wind tunnel model with simultaneous jet and intake flows. If intake flows were to be simulated on a model, a large duct would usually be required, which must be shielded from the model to cause minimal flow interference. Turbine powered simulator (TPS) units are very difficult to install within STOVL models, with their relatively close intake-to-nozzle spacing and their remote forward jets.

1.4 Research objectives

The primary objective of the current research project was to determine the significance (if any) of the jet/intake interference effects described above.

In co-operation with DERA Farnborough, an investigation has, therefore, been conducted at RMCS to quantify the magnitude of these interference effects on a generic STOVL jet-lift aircraft. Both jet and intake flows were simulated at realistic condi-

tions. Measurements were taken of wing and intake pressure distributions and from these wing and intake loads were inferred. An extensive parametric study has been conducted looking at variations in flight speed, nozzle position, nozzle area, nozzle pressure ratio and aircraft configuration.

The experimental research has been supplemented by some simplified computational fluid dynamics (CFD) studies of elements of the flow-field about the aircraft.

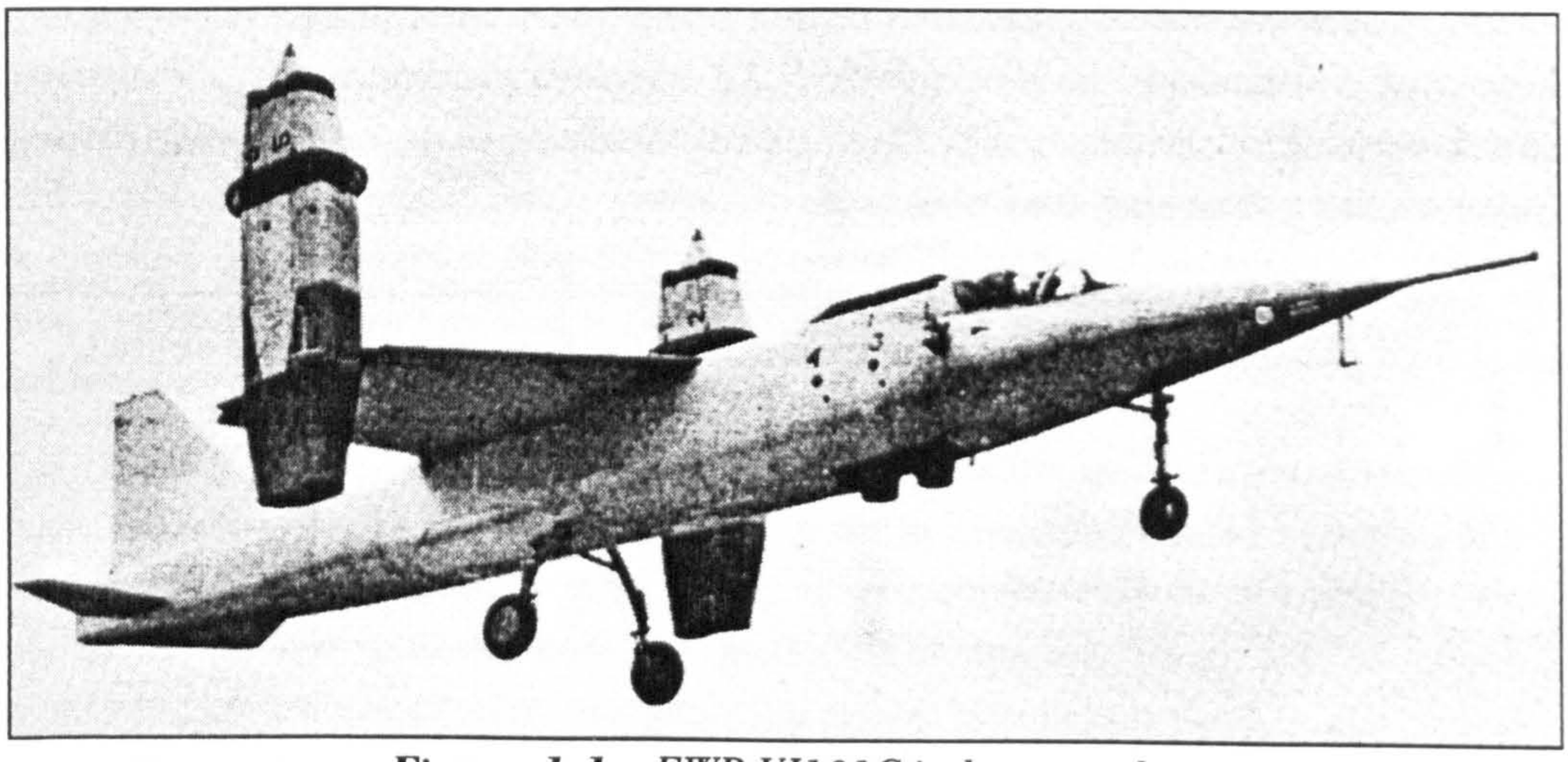

***Figure 1.1** - EWR VJ101C in hover mode.*

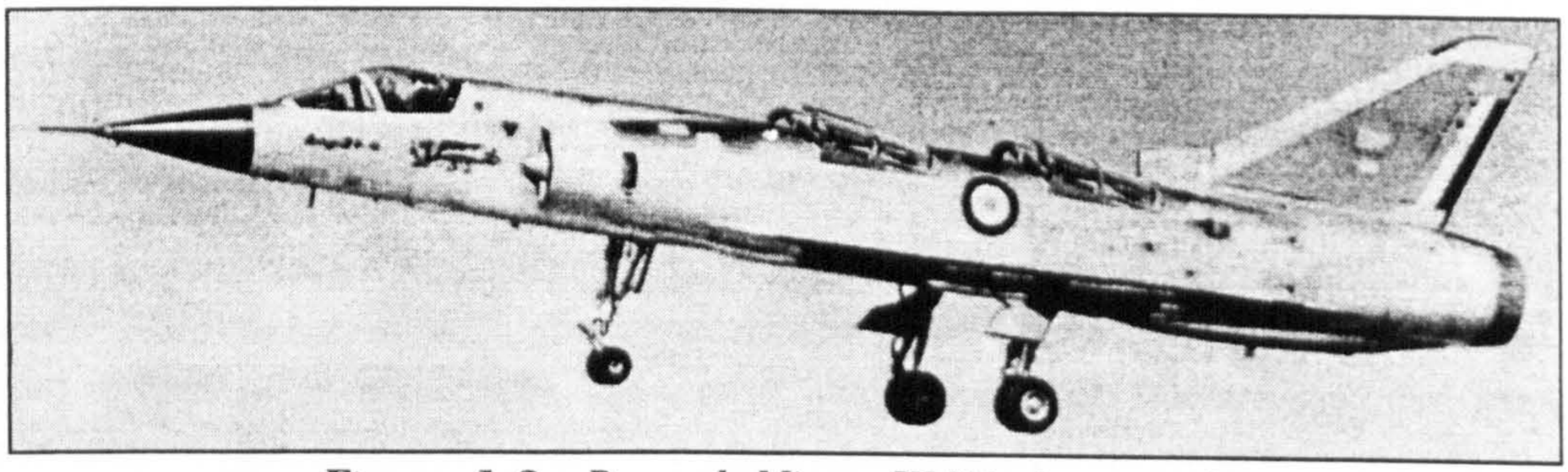

***Figure 1.2** - Dassault Mirage III-V in hover mode.*

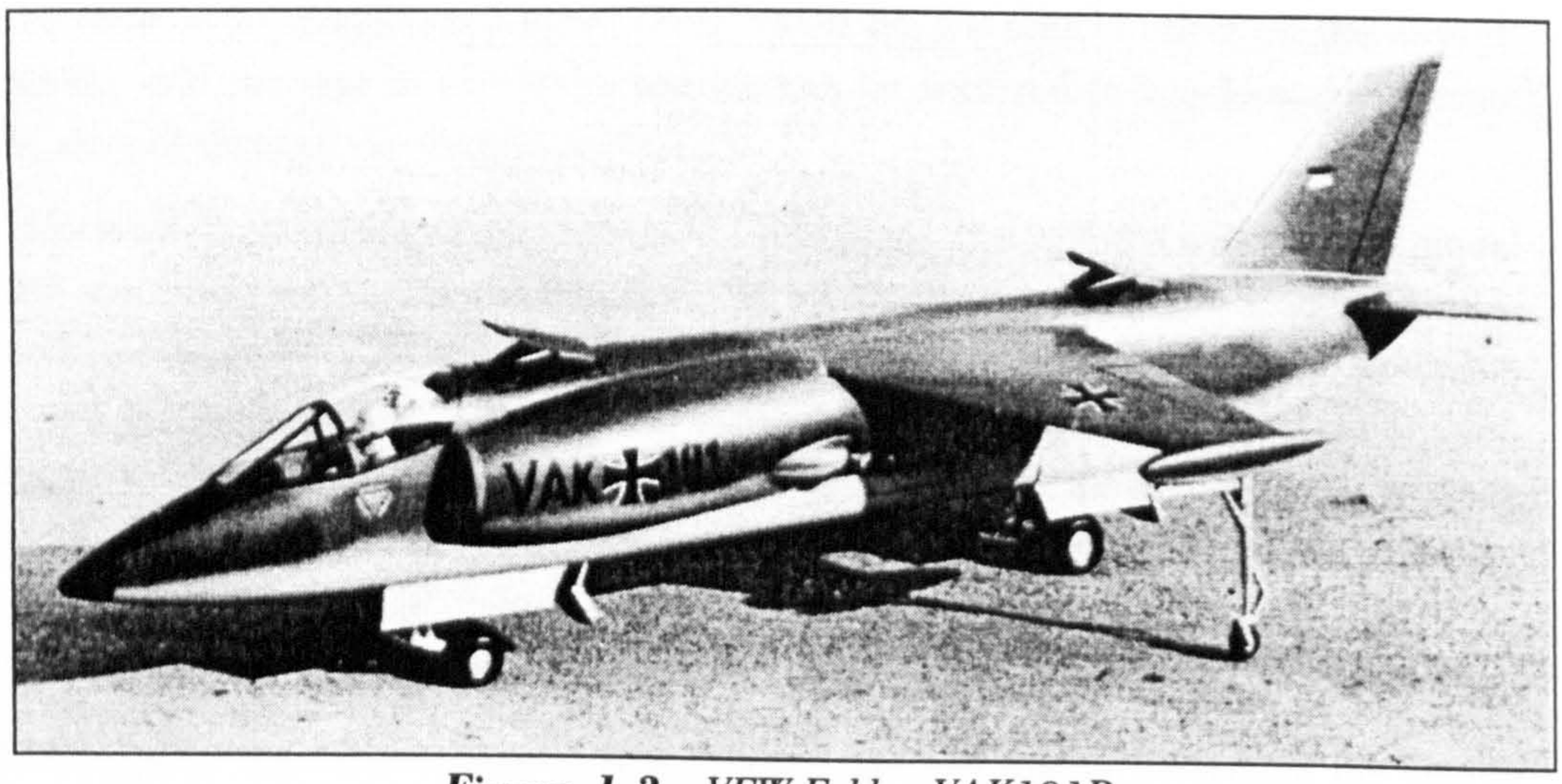

***Figure 1.3** - VFW Fokker VAK191B.*

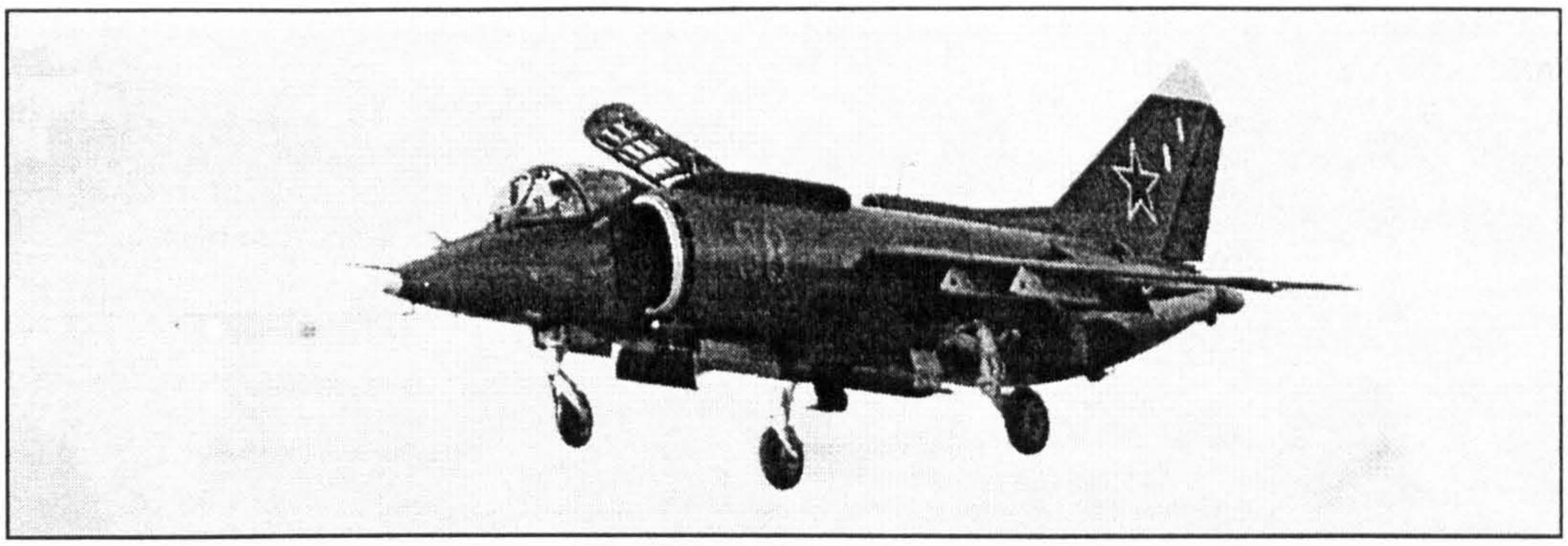

Figure 1.4 *- Yakovlev Yak-38 'Forger' in hover mode.*

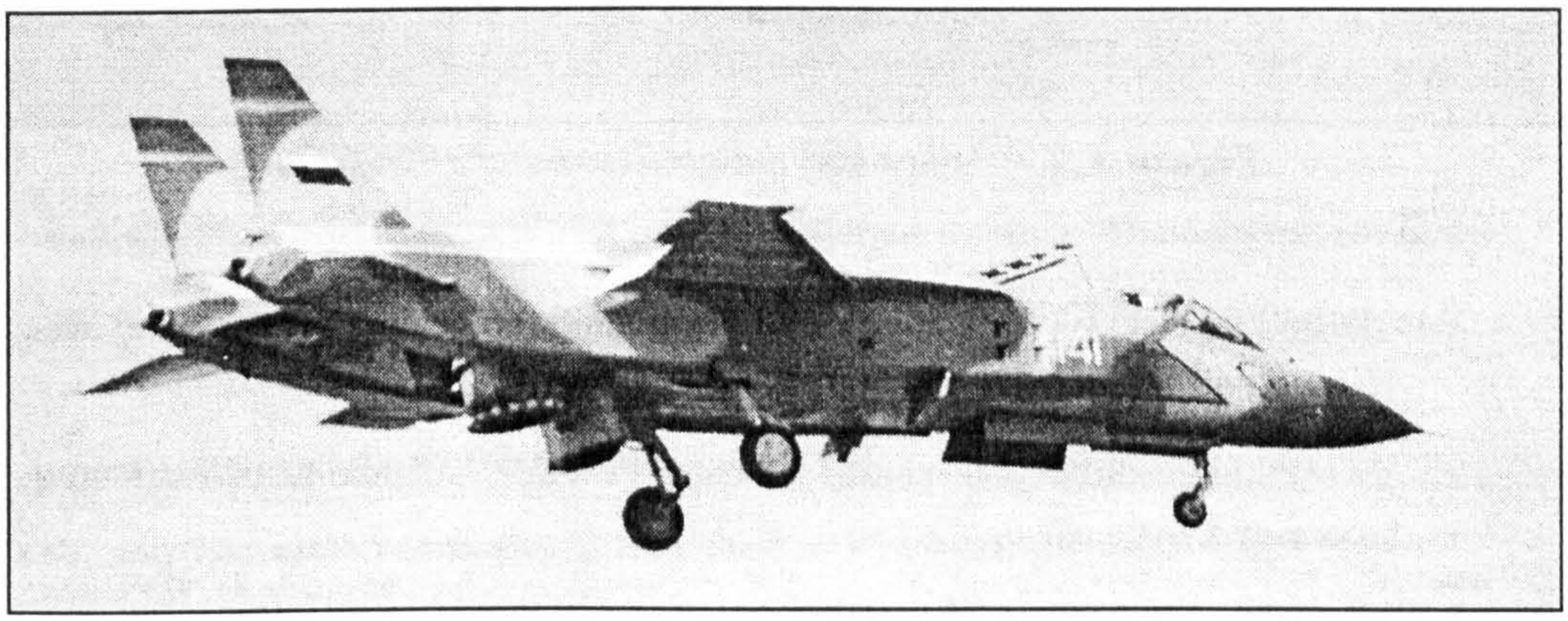

Figure 1.5 *- Yakovlev Yak-141 'Freestyle' in hover mode.*

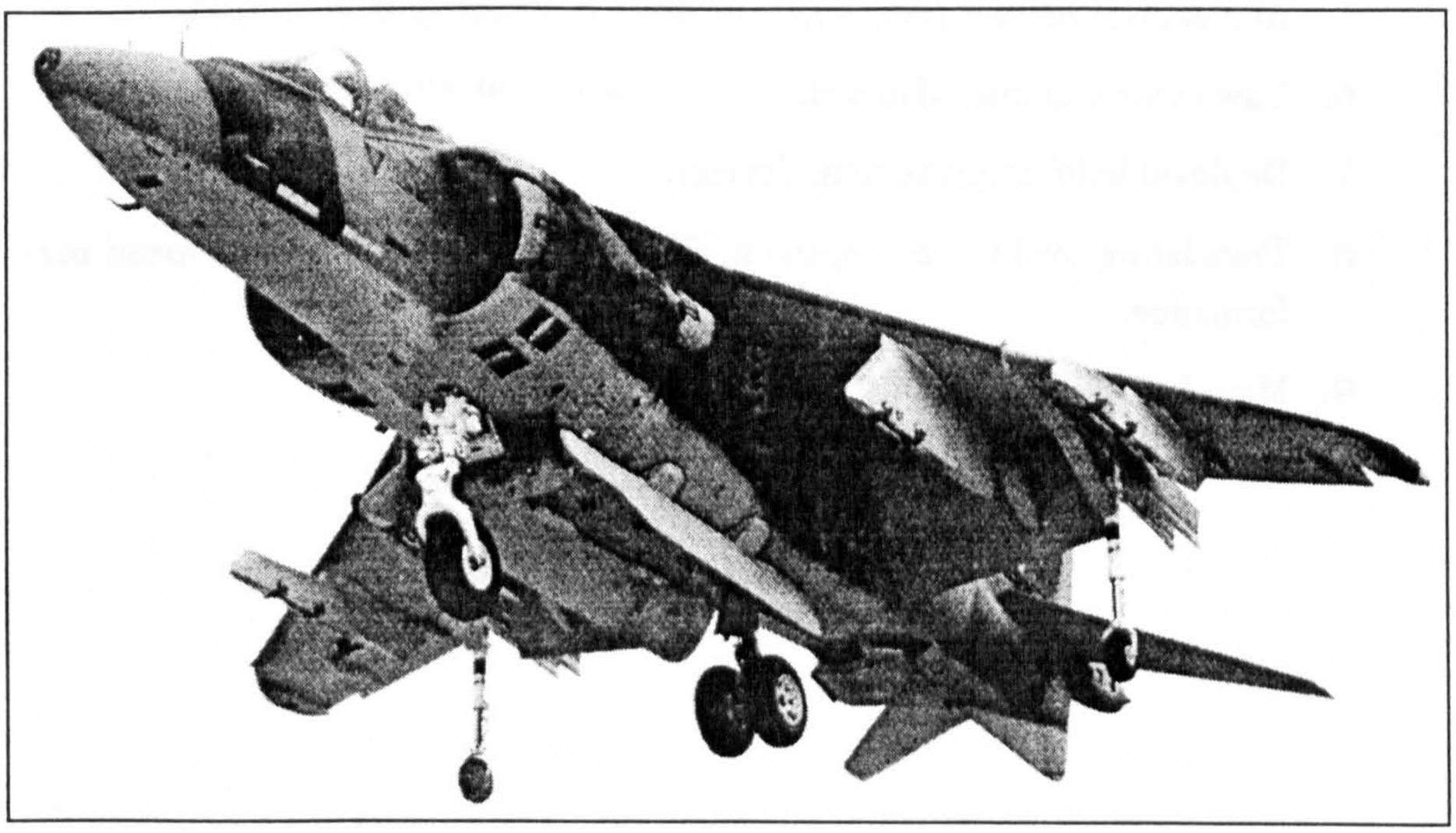

Figure 1.6 *- Harrier GR5/AV-8B in hover mode.*

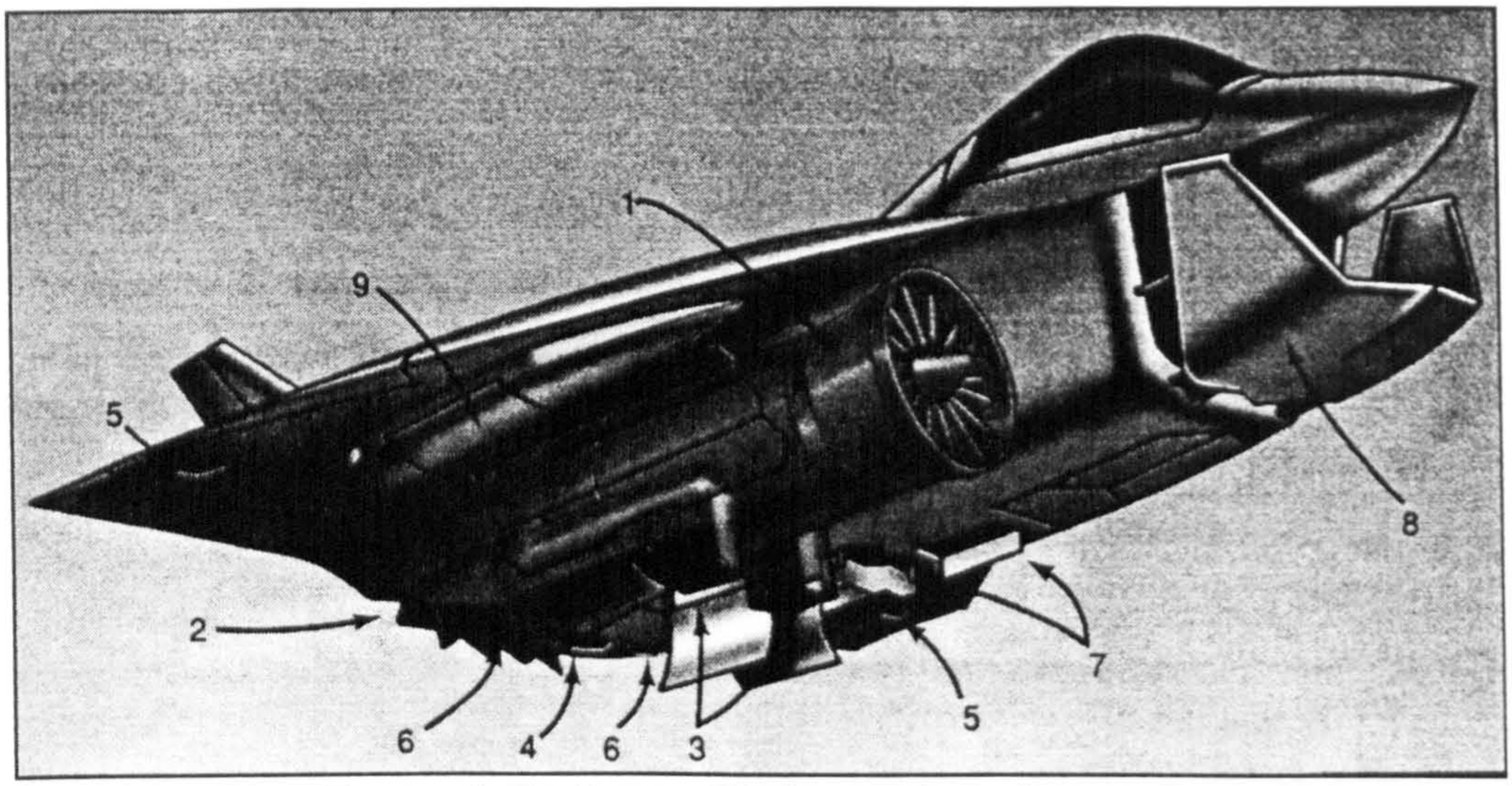

***Figure 1.7** - Boeing JSF design (December 1996).*

1. Modified P&W F119 engine - 20% bigger fan to increase thrust. Rolls-Royce direct lift system.
2. Two dimensional cruise nozzle - closed in STOVL mode to divert mixed core and bypass air to:
3. Vectoring, retractable lift nozzles.
4. Pitch control nozzles (fan air).
5. Roll control nozzles (fan air).
6. Yaw control nozzles (fan air).
7. Deployable lift improvement devices.
8. Translating cowl intake - opens in STOVL mode to improve low-speed performance.
9. Main landing gear pods.

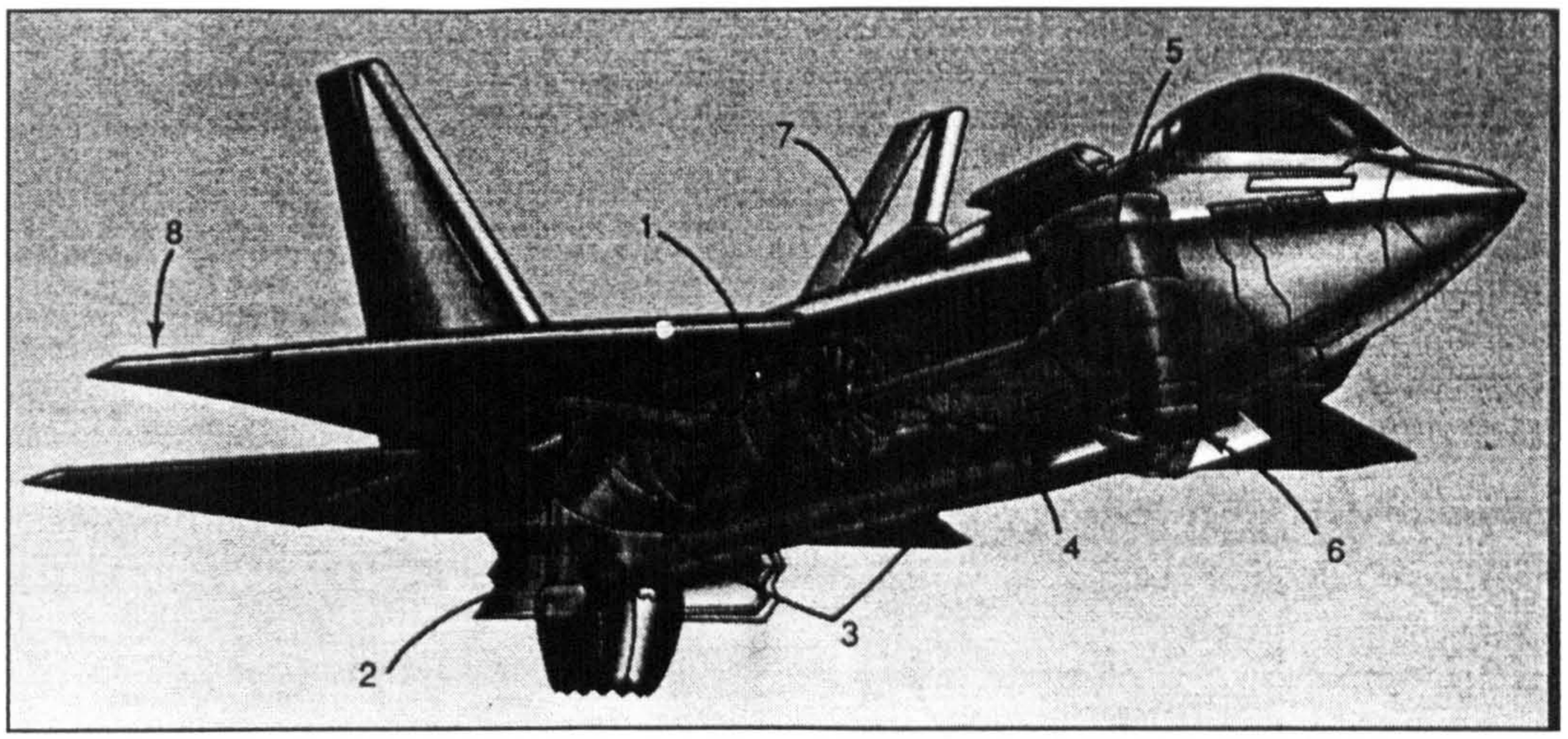

Figure 1.8 *- Lockheed Martin JSF design (December 1996).*

1. Pratt and Witney F119 engine modified to power shaft-driven lift-fan.
2. Rolls-Royce nozzle vectors core thrust up to 110 degrees forward, and left/right for yaw control, on STOVL mode.
3. Roll offtake ducts all bypass air to roll-control nozzles in the wing.
4. Dry clutch connects lift-fan shaft to F119 low-pressure spool.
5. Allison/Rolls-Royce two-stage counter-rotating shaft-driven lift-fan.
6. Retractable D-section nozzle vectors lift-fan thrust from 20 degrees forward to 60 degrees aft of vertical.
7. Main engine auxiliary intake.
8. Folding wingtips.

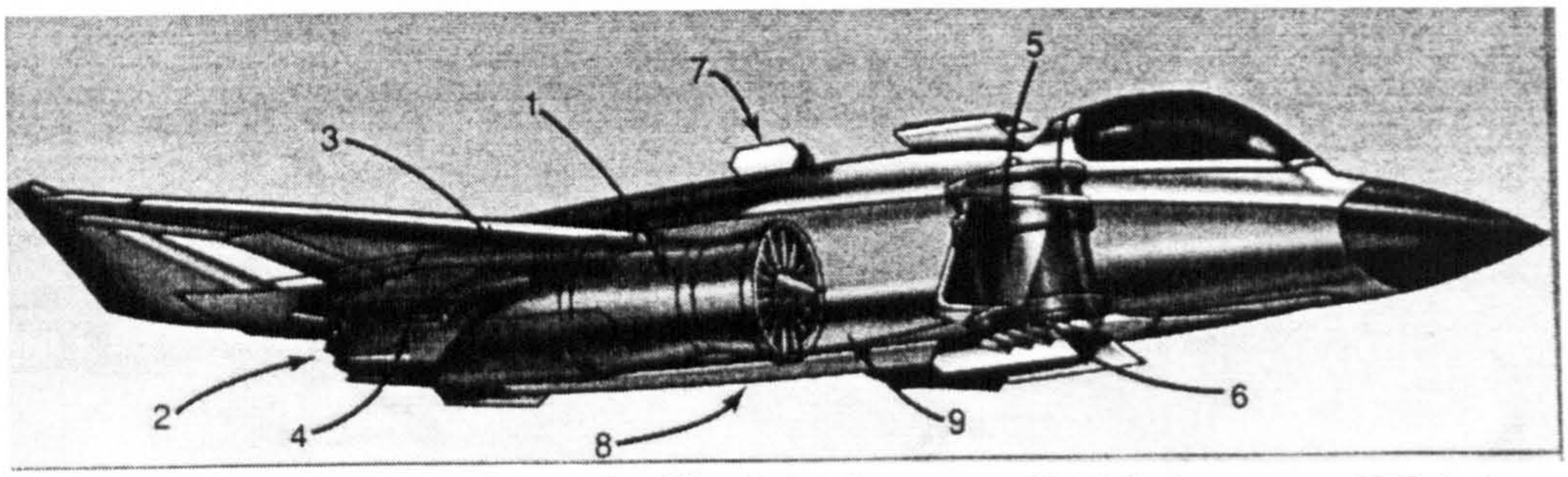

***Figure 1.9** - McDonnell Douglas/Northrop Grumman/British Aerospace JSF design (December 1996).*

1. Pratt and Witney F119 engine.
2. Low-observable axisymmetric, multi-axis thrust-vectoring cruise nozzle.
3. General Electric lift module - blocker/diverter valve diverts mixed core and bypass exhaust to:
4. Lift nozzles - vanes deflect thrust for roll and yaw control.
5. General Electric/Allison/Rolls-Royce GEA-FXL lift engine.
6. Lift-engine exhaust - vanes deflect thrust fore and aft.
7. Main engine auxiliary intakes.
8. Expandable weapons bay.
9. Side weapons bays.

2 STOVL Interference Effects

This chapter reviews previous work carried out on STOVL interference effects which were thought to be beneficial to the general understanding of the current research topic. This mainly concentrates on out of ground effect studies of free jets and jets in crossflow. Particular attention has been paid to experiments involving jets and intakes simulated together.

2.1 Hovering out of ground effect

The basic flow-field associated with hovering out of ground effect is illustrated in Figure 2.1. In all cases, the lifting jets issuing from the aircraft mix with ambient air to generate extremely complicated three-dimensional flow phenomena. In general, when one or more jet-lift engines are installed in an aircraft fuselage or wing, and exhaust vertically downwards, a small lift loss is induced by the entrainment action of the jet(s). Before looking at the aerodynamic interaction between the jet(s) and aircraft configurations hovering out of ground effect it is important to understand the characteristics of an isolated free jet emerging from a convergent nozzle.

2.1.1 The free jet

The general structure of a turbulent free jet is well understood. If one considers the flow issuing from a circular convergent nozzle, three variations of the flow pattern are possible, depending on the nozzle pressure ratio (NPR, the ratio of settling chamber total pressure, P_c, to ambient static pressure, p_a). The three variations are the subsonic jet, the underexpanded jet and the highly underexpanded jet. The idealised structural features of each of these variations are shown in Figure 2.2 [DONALDSON & SNEDEKER, 1971].

Note that with a convergent-divergent nozzle an additional flow pattern exists, that of the overexpanded jet. This occurs when the nozzle is operating off-design at too high a NPR. The divergent section of the nozzle accelerates the flow to supersonic speeds but in doing so the static pressure of the jet at the nozzle exit is below that of the surrounding ambient air. On exiting the nozzle, the jet flow re-compresses through a series of oblique shocks [ANDERSON, 1990]. Since only convergent nozzle flows are considered here, the overexpanded case will not be discussed further.

The subsonic jet is characterised by a potential core, an area of constant velocity in which no viscous mixing occurs, surrounded by a region in which mixing between jet and ambient fluid takes place. Several nozzle diameters downstream, the mixing region has spread inward enough to reach the centreline, and the core region no longer exists. Beyond this point, the mixing region continues to spread as the velocity decays at a rate required to conserve axial momentum. In this portion of the jet, the mean velocity profiles approach the self-similar shape of the fully expanded jet. Such a jet exists in air for isentropic nozzle pressure ratios from 1 to 1.893.

When the sonic, or critical, pressure ratio is reached, a very weak normal shock forms at the nozzle exit. This shock changes rapidly with increasing pressure ratio, however, and at a NPR of approximately 2.0, the familiar pattern of 'shock diamonds' or 'cells' composed of intersecting oblique shocks is established in the core. This structure exists, for a sonic exit, until the NPR is about 4.0. The term

'moderately underexpanded' is used to denote jets within this pressure ratio interval. Due to the additional expansion required in the unconfined jet flow beyond the nozzle, the boundaries of what was the potential core in the subsonic case are now determined by the requirement of pressure equilibrium between the outermost portion of the flow within the shock structure and the surrounding ambient air. The inward diffusion of the mixing region, however, continues, and ultimately results in the dissipation of the potential core. Downstream of the core, after the jet has become subsonic, the spreading and decay rates would be expected to be those of a totally subsonic jet.

At NPRs greater than 4.0, the form of the shock structure in the initial cell begins to change. Along the centreline, where the expansion is a maximum, the pressure becomes so low relative to ambient pressure that the recompression in the remainder of the cell reaches the limiting value for conical shocks, and the required compression takes place through an observable normal shock disc. Once this disc forms, the jet is said to be 'highly underexpanded'. As the NPR is further increased, the shock disc increases both in strength and diameter. Immediately downstream of the disc, the flow is subsonic. Since the surrounding flow in the oblique shock region remains supersonic, a slip line exists at the boundary between the two concentric regions. For a fairly high degree of underexpansion, (NPR = 7.0), this subsonic core region is quickly accelerated and becomes supersonic once again near the beginning of the second cell. In this case the second cell may resemble the first and even possess a normal shock similar to that in the first cell. For very high pressure ratios, the structure downstream of the first cell is dominated for a great distance by the very strong normal shock in the first cell, and no other normal shocks are present. The flow then decays through a structure of oblique shocks. The mixing region surrounds the core as usual, but its radial diffusion is small, with the result that the core of the highly underexpanded jet can be extremely long. Far downstream, the usual subsonic decay takes place.

2.1.2 Jet-induced interference effects

For a simple circular planform with a single central round jet having a uniform exit velocity distribution (Figure 2.3), the reduction in lift is about 2 percent of the installed thrust F, for a nozzle area to planform area ratio $A_N/S = 0.01$ [WILLIAMS & WOOD, 1966]. This lift loss reduces steadily, but non-linearly, as the ratio A_N/S increases, becoming only about 0.5% for $A_N/S = 0.11$ and negligible if A_N/S is greater than 0.25. The lift losses on the plate arise from the entrainment action of the jet which mixes with the surrounding air and sets up a cross-flow over the bottom of the plate, thereby inducing a suction pressure.

2.1.2.1 The effect of jet decay rate

The lift loss created by various arrangements of nozzles was the subject of an investigation by GENTRY & MARGASON, 1966. Some tests were to be carried out using a circular plenum chamber whereas others were to use a rectangular plenum chamber. The latter was designed to fit inside the fuselage of a wind tunnel model and was smaller than ideally desired. Results using the different plenum chambers could only be compared if the same basic lift loss was obtained using both plenum chambers. The first part of the investigation, therefore, was to obtain a comparison of the loads induced on a circular plate by a single nozzle from the rectangular plenum chamber for comparison with an identical plate-nozzle configuration on the more ideal circular plenum chamber. As shown in Figure 2.4, the loads induced on the circular plate mounted on the original rectangular plenum were three to four times as large as those induced on the same plate-nozzle arrangement with the circular plenum chamber.

Measurements of the velocity profile obtained from the rectangular plenum indicated a distorted velocity distribution with a deficit at the centre, whereas the flow from the circular plenum had a uniform 'top hat' velocity profile. The flow through the rectangular plenum was found to be very turbulent and it was suspected that the high turbulence levels were causing the higher induced loads. To confirm the hypothesis, fairings and baffles were added to the rectangular plenum chamber to improve the flow quality and a strut was inserted in the circular plenum to degrade the flow quality. This also produced a much greater distortion of the exit velocity profile than was present on the original rectangular plenum chamber. Figure 2.4 shows that these changes increased the lift loss for the circular plenum chamber and greatly reduced the losses for the rectangular plenum chamber. A summary of the lift losses at NPRs of 1.5 and 2.0 is shown in Table 2.1.

***Table 2.1** - Induced loads on a circular plate, $A_n/S = 0.0144$ (GENTRY & MARGASON, 1966).*

Plenum Chamber Type	$\frac{\Delta L}{F}$***(NPR = 1.5)***	$\frac{\Delta L}{F}$***(NPR = 2.0)***
Original cylindrical	-0.0085	-0.0087
Modified cylindrical	-0.0130	-0.0130
Original rectangular	-0.0342	-0.0263
Modified rectangular	-0.0149	-0.0141

The lift losses did not correlate with the exit velocity distribution. They were found, however, to correlate with the rate of decay of the jet with distance downstream from the nozzle exit as shown by the curves at the bottom of Figure 2.4. These curves show the peak non-dimensional dynamic pressure in the jet at a non-dimensional

distance downstream of the nozzle. The circular plenum chamber gave the smallest lift loss and had the lowest decay rate. The original rectangular plenum produced the greatest lift loss and had the highest decay rate. The modifications made to the circular and rectangular plenum chambers produced jets with similar decay rates, giving similar lift losses. The correlation was also found to hold true for multiple-jet configurations. Figure 2.5 compares the lift loss and decay rates for three different jet arrangements (all using the modified rectangular plenum chamber). An empirical equation was developed [GENTRY & MARGASON, 1966] to predict the lift loss per unit thrust based on the jet decay rate and model geometry:

$$\frac{\Delta L}{F} = \sqrt{\frac{S}{A_n}} k_1 k_2 \tag{2.1}$$

where k_1 = -0.009 and

$$k_2 = \sqrt{\frac{-\left\{\partial\left(q_x/q_n\right) \Big/ \partial\left(x/d_{ne}\right)\right\}_{max}}{\left(x/d_{ne}\right)_i}} \tag{2.2}$$

where x is the distance along the nozzle axis, the origin of which is at the exit plane. The lift loss is therefore proportional to the square-root of the maximum rate of decay of the jet divided by the distance to the point at which this occurs. The correlation showed good agreement with the test data.

It is clear that the use of rapid mixing nozzles, if installed on a STOVL aircraft, will have a detrimental effect on the aircraft's hover performance. These nozzles, which are currently being developed for reduced radar and infra-red signatures and for minimising ground erosion problems, are designed to promote high decay rates of the jet potential core. The use of these nozzles will inevitably incur an installation penalty possibly doubling the lift loss [WILLIAMS & WOOD, 1966].

When multiple jets are dispersed over the planform, the percentage lift loss is greater than for the corresponding single jet of the same equivalent diameter ratio, d_{ne} [WILLIAMS & WOOD, 1966]. This is partly due to the increased mixing rate, but also to the additional pressure drop produced on the lower surface between the jets because of the constricting effect of the jets themselves on the entrained flow. This does not appear, however, to be a strong effect and the lift loss seems unlikely to exceed 5 percent unless the jets are arranged in rows or elongated narrow slots, thus tending to enclose a significant amount of the planform area.

The lift loss data of GENTRY & MARGASON, 1966 mentioned above were obtained using small cold jets with an equivalent diameter of 57 mm (2.25 inches). In order to establish whether these findings were representative of full size configurations a

second investigation was undertaken [MCLEMORE, 1966] using a Pratt and Witney J85 engine. The engine was equipped with two alternative jet pipes; one for a single jet investigation, and one with a special exhaust ducting to produce a four-jet configuration. The tests were run with three different sizes of rectangular plates to produce three different ratios of planform area to jet area. The comparison of these real engine data with the model results (Figure 2.6) shows good agreement.

With regard to rapid mixing nozzles, mentioned above, there have been numerous studies carried out over the years. As an example of the findings, BRADBURY, 1981 reports on some tests which were carried out on a large 203 mm (8 inch) diameter nozzle with various arrangements of circumferentially placed tabs. The square tabs, with sides equal to one sixteenth of the diameter of the nozzle, were equally spaced around the nozzle circumference and protruded into the jet path. Measurements were made of the jet decay rate for two, four and eight tabs. Interestingly, the fewer the tabs, the greater the jet decay rate, but no explanation was given for this. It was found that the effect of the tabs was to produce a circumferential variation in the flow direction and these flow angle variations caused large distortions in the jet cross-section increasing the mixing rate within the jet.

Comparisons of experiments conducted using jets of different temperature [KUHN & MCKINNEY, 1965], [HAMMOND, 1966] suggest that temperature does not appear to have an appreciable effect on the jet decay rate except for the circular nozzle. Figure 2.7 shows the effect of nozzle configuration and temperature on jet decay.

These studies have demonstrated the need for information on the jet decay rate for actual engines to be used in STOVL aircraft. If accurate lift loss data are to be obtained from wind tunnel models then the decay rate of the simulated jets should accurately match those of the full size installation.

2.1.2.2 The effect of nozzle pressure ratio (NPR)

GENTRY & MARGASON, 1966 observed that the measured lift losses showed a reduction with increasing NPR for a constant nozzle to planform area ratio. At the time a theoretical model was not available to explain this. NPR effects were looked at, however, in an extensive study of jet-induced lift effects undertaken by SHUMPERT & TIBBETTS, 1969. Tests were conducted on a 14 percent scale model of a jet VTOL aircraft with a fuselage-mounted lift system at pressure ratios of 1.4, 1.7, 2.0 and 2.3. It was discovered that the lift loss did not follow the correlation proposed by GENTRY & MARGASON, 1966 (Equation 2.1). The results showed that there was a measurable discrepancy between the lift losses at different NPRs for a constant nozzle area and a modification to Equation 2.1 was proposed:

$$\frac{\Delta L}{F} = \sqrt{\frac{S}{A_n}}(\mathrm{NPR})^{-0.64} k_1 k_2 \qquad (2.3)$$

The constant k_1 was found to be aircraft configuration dependent and for the tests conducted, varied between -0.01 and -0.016. k_2 was unchanged (see Equation 2.2). As this correlation suggests, an increase in NPR is seen to result in a decrease in percentage lift loss. This effect was found to be similar for all configurations. The NPR effect described above is explained by the jet entrainment rate of different NPR jets. At an axial distance, x, downstream of the nozzle exit plane, the ratio of extra entrained mass flow rate to the total mass flow rate at the nozzle exit is given by [RANSOM & SMY, 1984]:

$$\frac{\Delta \dot{m}_x}{\dot{m}_n} = 0.32 \frac{x}{d_n} \sqrt{\left(\frac{\rho_a}{\rho_j} \right)} \tag{2.4}$$

As NPR is increased (and hence the jet density), the ratio of mass flow rate entrained into the jet is reduced. Hence the decay rate of a high NPR jet will be less than that of a lower NPR jet. SHUMPERT & TIBBETTS, 1969 also conducted experiments at constant thrust, i.e. the nozzle area was reduced as the NPR was increased. Varying NPR at constant thrust had no measurable effect on lift loss.

A more direct, easier to use method for estimating these hover lift losses was developed by KOTANSKY, 1984. Correlation of data from various single and multiple jet configurations resulted in the following equation:

$$\frac{\Delta L}{F} = -0.0002528 \sqrt{\frac{S}{A_n}} \left[(\mathrm{NPR})^{-0.64} \left(\frac{\mathrm{Per}_{\mathrm{total}}}{d_{ne}} \right) \right]^{1.581} \tag{2.5}$$

This equation implicitly accounts for the higher decay rate of multiple jet configurations in terms of equivalent nozzle diameter but does not account for higher decay rates caused by jet exit conditions involving high entrainment rates i.e. rapid mixing nozzles. If higher than normal turbulence and decay rates are involved, KOTANSKY suggests that Equation 2.3 should be used.

2.1.2.3 The effect of nozzle length and projection

GENTRY & MARGASON, 1966 investigated the effect of nozzle length and projection on induced loads for a single round jet with the modified rectangular plenum chamber (see Section 2.1.2.1) and with rectangular-planform plates. In these experiments, nozzle length was defined as the distance from the bottom of the settling chamber (the start of the nozzle profile) to the nozzle exit plane. Nozzle projection, by contrast, was the distance the nozzle exit plane extended below the planform surface. The findings are summarised in Table 2.2 for NPRs of 1.5 and 2.0.

Extending the nozzle length caused a slight reduction in the lift loss for the case of zero projection. Measurements of the jet decay rate for the different nozzle lengths showed that the shortest nozzle had the highest decay rate. A further reduction in lift loss was obtained by projecting the nozzle through the circular plate distances of

$0.5d_n$ and $1.0d_n$. This reduction is due to the increased distance between the plate and the free surface of the jet which is entraining air.

***Table 2.2** - Lift loss for various nozzle lengths and projections, A_n/S = 0.0105 (GENTRY & MARGASON, 1966).*

Nozzle length (d_n)	*Nozzle projection (d_n)*	$\frac{\Delta L}{F}$ *(NPR=1.5)*	$\frac{\Delta L}{F}$ *(NPR=2.0)*
0.248	0.0	-0.0187	-0.0175
0.910	0.0	-0.0163	-0.0155
1.410	0.0	-0.0163	-0.0148
0.910	0.5	-0.0130	-0.0129
1.410	0.5	-0.0133	-0.0126
1.410	1.0	-0.0116	-0.0107

2.1.2.4 The effect of planform shape and position

In order to determine the effect of planform shape on the induced lift loss, GENTRY & MARGASON, 1966 tested four plate shapes on their circular plenum chamber (see Section 2.1.2.1). The four shapes were circular, square, rectangular (aspect ratio 1.52) and triangular (equilateral). In all cases the ratio of nozzle exit area to plate area, A_n/S was 0.0144 and the centre of the nozzle was located at the centroid of the plate. There was no measurable effect of planform shape on the lift loss. The effect of wing height was also investigated. As would be expected, a low wing configuration had more lift loss than a mid-mounted wing which in turn performed worse than a high wing. This is due to the relative proximity of the wing to the mixing region of the jet.

The effect of planform lip shape was investigated by ING & ZHANG, 1994. An experiment was carried out to study the parameters affecting single-jet ground-effect hover lift loss and to identify the cause behind the large discrepancies in lift loss between the experiments of WYATT, 1964 and CORSIGLIA *et al.*, 1990, commonly known as the 'Wyatt anomaly'. The cause of the discrepancies was traced to a single geometrical parameter, planform plate edge geometry which significantly affected the flow separation underneath the plate. The out of ground effect lift loss was found to be insensitive to the edge geometry.

2.1.2.5 The effect of off-axis nozzle positions

The effect of positioning a nozzle away from the fuselage centre-line was part of a study carried out by WELTE, 1974. Tests on a model of the VTOL transporter, Dornier Do-31, indicated that a centrally located jet will produce more lift loss than a peripherally located jet. The podded lift engines installed at the wing tips induced

a lift loss of 2.2 percent compared with 3.6 percent for the lift/cruise engine installed below the inner wing section. WELTE postulated that the constant k_1 in Equation 2.2 above is universal and an additional term could be introduced into the equation to take into account configuration effects. The following equation was developed:

$$\frac{\Delta L}{F} = \frac{\overline{D}}{d_{ne}}\left(\frac{P_n}{p_a}\right)^{-0.64} k_1 k_2 \qquad (2.6)$$

where $\overline{D}$ is the angular mean planform diameter and is given by:

$$\overline{D} = \frac{1}{\pi}\int_0^{2\pi}\left\{r(\theta) - \frac{d_{ne}}{2}\right\}\mathrm{d}\theta \qquad (2.7)$$

k_1 = -0.009 and k_2 is unchanged from Equation 2.2.

It was found that for the lift/cruise engines, both Equations 2.3 and 2.6 predicted the lift loss quite well, 4.0 percent and 3.4 percent respectively. With the peripherally located lift engines at the wing tip, Equation 2.3 failed to produce a satisfactory result, again predicting 4.0 percent (as would be expected) compared with 2.4 percent for Equation 2.6. These tests demonstrate the validity of using Equation 2.6 for predicting percentage lift losses for all nozzle locations.

This section has described the characteristics of free jets and their influence on a hovering STOVL aircraft. Hover lift losses have been shown to be dependent on a number of configuration-specific factors. Additional information on free jets and hovering out of ground effect can be found in; WOOD, 1967; BARCHE, 1974; KNOTT & HARGREAVES, 1974; LEYLAND, 1984; KUHN, 1986 and MARGASON, 1987.

2.2 Transition out of ground effect

The transition from hover to wing-borne flight is a very important design consideration for STOVL aircraft. This is the flight regime relevant to the current research project. Figure 2.8 shows the aerodynamic phenomena around a STOVL aircraft in transition out of ground effect. In the transition from hovering to conventional flight, the streams from the lifting jet(s) are swept back by the freestream and are rolled up into pairs of vortices. These vortices, along with the entrainment action and blockage effect of the jet(s), induce suction pressures on the bottom of the configuration beside and behind the jet(s) and a smaller region of positive pressure ahead of the jet(s). In most cases, these induced pressures result in a nose-up pitching moment and a loss of lift on the aircraft.

2.2.1 The free jet in a cross-flow

The jet in cross-flow has received considerable research attention because it is a fundamental fluid dynamic phenomenon with many applications such as smoke

plumes from chimneys, the dispersal of liquids in streams, jet engine combustors and reaction control jets on rockets and missiles. The most widely-studied application, however, is related to STOVL aircraft.

A jet exhausting into a cross-flow generates a complex flow-field with several distinguishable features. When the jet efflux exits the nozzle it is deflected by the freestream to follow a curved path downstream while its cross-section changes. For the case of a circular jet, near the nozzle exit, consider the pressure distribution due to potential flow around a rigid circular cylinder where $C_p = 1 - 4\sin^2\theta$. There are stagnation points (C_p = 1) upstream (θ = 0°) and downstream (θ = 180°) and minimum pressures (C_p = -3) at the lateral edges (θ = 90° and 270°). As a consequence, the jet flow spreads laterally into an oval shape. At the same time the cross-flow shears the jet fluid along the lateral edges downstream to form a kidney-shaped cross-section. At increasing distances along the jet path this shearing folds the downstream face over itself to form a vortex pair which dominates the flow. Associated with the vortex pair is the flow induced into the wake region of the jet from the freestream. Figure 2.9 [MARGASON, 1993] shows the topology of a jet in cross-flow.

When the locus of maximum vorticity is projected to the symmetry plane the resultant line is called the vortex path. There is also a locus of maximum velocities in the symmetry plane which is called the jet centreline path. Also shown in Figure 2.9 are the secondary vortices, the horseshoe vortex and the wake vortex street.

2.2.1.1 Correlation parameters

Early jet in cross-flow investigations usually characterised the test condition by the ratio of freestream velocity to jet exit velocity, V_∞/V_j. It was soon recognised that this ratio was not appropriate for hot jets. WILLIAMS & WOOD, 1966 observed that non-dimensional increments in lift, drag and pitching moment were primarily, but not solely, a function of jet to freestream velocity ratio. The influence of jet Reynolds number (based on nozzle diameter) and model Reynolds number (based on wing chord) on jet interference effects were secondary. They showed that the influence of temperature and compressibility effects could better be accounted for by the use of an effective velocity ratio (Equation 2.8) and this is still widely used by most researchers.

$$V_e = \frac{V_\infty}{V_j}\sqrt{\frac{\rho_\infty}{\rho_j}} = \frac{M_\infty}{M_j}\sqrt{\frac{p_\infty}{p_j}} \tag{2.8}$$

For STOVL applications the magnitude of V_e for transition to wing-borne flight depends on the pressure ratio of the lifting propulsion device. For high pressure ratio jet engines, transition will occur with $V_e < 0.2$; for the Harrier, transition will occur with $V_e < 0.3$; and for lift fans with low pressure ratios, transition will occur with $V_e < 0.5$ [MARGASON, 1993].

2.2.1.2 Jet trajectory

One property of jets in cross-flow which has received a lot of research attention is the jet trajectory [e.g. KEFFER & BAINES, 1962; SHAW & MARGASON, 1973; STOY & BEN-HAIM, 1973; RANSOM & WOOD, 1974; TAYLOR & WATKINS, 1981]. The most common parameter for defining the trajectory is the locus of maximum velocity; however, other definitions are sometimes used depending on the preference of the researcher. These trajectory definitions include: the locus of maximum stagnation pressure; the locus of maximum dynamic pressure; the locus of maximum stagnation temperature and the line of maximum vorticity. Since none of these definitions will give the same trajectory, it is necessary to exercise great care when comparing data from different sources.

Nearly all the work done to establish a jet trajectory has used a subsonic jet in a subsonic cross-flow. MARGASON, 1993, gives the empirical equation for the jet centreline trajectory to be:

$$\frac{x}{d_n} = \alpha V_e^n \left(\frac{z}{d_n}\right)^m + \frac{z}{d_n}\beta \cot(\delta_j) \tag{2.9}$$

where x is the distance in the freestream direction and z is the distance perpendicular to the cross-flow (in the free jet direction). The z and x origins are taken as the centre of the nozzle exit. When the nozzle vector angle is 90 degrees (i.e. perpendicular to the cross-flow), the second term in Equation 2.9 becomes zero. The empirical approaches correlate the experimental data using similarity laws to obtain the jet trajectory. Empirical equations for jets with a 90 degree vector angle have been developed by KAMOTANI & GREBER, 1972, CHAISSAING *et al.*, 1974, FEARN & WESTON, 1978, BRADBURY, 1981 and AHMED, 1996. For jets with varying vector angles, empirical equations have been developed by IVANOV, 1963, SHANDOROV, 1966 and MARGASON, 1968. Table 2.3 summarises the coefficients and exponents used by these researchers as well as the range of applicability for their equations.

Equation 2.9 has been plotted using an effective velocity ratio, V_e, of 0.25 which covers the range of applicability for most of the researchers. Figure 2.10 shows the jet trajectories for a nozzle vector angle of 90 degrees while Figure 2.11 shows the trajectories for a vector angle of 60 degrees. The equations derived by the researchers show good agreement with each other. There are slight variations in the initial depth of penetration and the rate of jet deflection. These can probably be accounted for by variations in the initial jet and cross-flow conditions in the experiments from which the empirical equations are derived. In particular the turbulence intensities of the jet and cross-flow, which will affect the mixing rate between the two, will have a strong influence on the jet penetration and curvature. ZHANG & HURST, 1990 have observed that with supersonic jets, where the turbulence intensity in the jet may be high (due to the breakdown of the shock structure), the jet centreline trajectory will ultimately lead to less penetration than for a subsonic jet. The equation derived by

AHMED, 1996 confirms this, predicting a much greater initial penetration and subsequently a more rapid bending of the jet than predicted by most subsonic jet equations. This brings into question the applicability of using subsonic jet trajectory empirical equations with supersonic jets.

***Table 2.3** - Jet trajectory equation terms and applicability*

Author(s)	α	n	m	β	V_e	δ_j
KAMOTANI & GREBER, 1972	1.38	2.61	2.78	n/a	0.13-0.26	90°
CHAISSAING *et al.*, 1974	$(0.59+V_e)^{-2.6}$	2.60	2.60	n/a	0.16-0.42	90°
FEARN & WESTON, 1978	1.08	2.68	2.95	n/a	0.10-0.33	90°
BRADBURY, 1981	1.08	2.70	3.00	n/a	0.08-0.43	90°
AHMED*,1996	0.51	3.33	3.70	n/a	0.06-0.08	90°
IVANOV, 1963	1.00	2.60	3.00	1.00	0.03-0.71	60°-120°
SHANDOROV, 1966	1.00	2.00	2.55	$(1+V_e)^2$	0.21-0.71	45°-90°
MARGASON, 1968	$\frac{1}{4\sin^2\delta_j}$	2.00	3.00	1.00	0.10-0.85	30°-180°

There have also been some integral methods developed which consider the deflecting mechanisms of a jet by taking into account either a pressure force or cross-flow momentum entrainment or both [WOOLER, 1969; SNEL, 1974; SICLARI *et al.*, 1975; SUCEC & BOWLEY, 1976; ADLER & BARON, 1978; FEARN, 1986]. More recently the use of computational fluid dynamics (CFD) has given researchers an addition numerical tool to enable the jet trajectory to be determined [ROTH, 1987; BAKER *et al.*, 1993].

2.2.2 Jet-induced interference effects

In general the jet-induced interference effects in transition are characterised by a loss in lift and a nose-up pitching moment. Figure 2.12 illustrates typical trends for a tail-off configuration [MARGASON, 1966]. The left hand graph shows the lift divided by the thrust as a function of the angle of attack with the pitching moment as a function of the angle of attack on the right. In hover, the jets produce a lift which is equal to the net thrust. At forward velocity the wing develops additional lift. In the absence of interference effects, lift from these two sources could be added together

* *Ahmed used a supersonic jet from a convergent-divergent nozzle.*

to produce the solid curve. The jet-induced effects, however, cause a loss in lift, and the actual lift measured in a wind tunnel is shown by the symbols. The difference between the calculated and measured curves is the interference lift loss, which is generally independent of angle of attack. The rolling up of the jet wakes into contra-rotating vortices is the primary cause of the interference effects in transitional flight [MARGASON, 1966]. The vortices change the flow-field in the near-field and induce additional suction pressures on the lower surface of the fuselage and wing of the aircraft.

The interaction between the jet and the cross-flow means that positive pressures are generated on surfaces ahead of the jet and negative pressures behind. SPREEMAN, 1960, measured negative pressures as high as 3 to 4 times the freestream dynamic pressure. The pressures diminished with distance from the jet but extended 10 to 15 jet diameters downstream and 5 to 10 diameters to each side of the jet. The combination of positive pressures ahead of the jet and negative pressures behind gives a nose-up pitching moment.

There have been many studies made of jet-induced interference effects over the past 30 years or so. Most have tended to concentrate on the effect of the jet on the airframe and little attention has been paid to modelling intake flows. Tests have been carried out on a variety of models ranging from simple flat plates or delta wings to complex scaled representations of full-size aircraft. This section aims to describe parameters which have been observed to influence the jet-induced interference effects. Due to the very complex nature of the flow-fields surrounding STOVL aircraft in transition, it is very difficult to isolate the effects which different parameters may have on any particular configuration. As such only general trends can be identified. More detailed information can be obtained from the individual reports.

2.2.2.1 The effect of velocity ratio, V_e

The lift loss on a typical STOVL aircraft in hover has already been discussed and is of the order of 2 to 3 percent of the installed thrust. Early experiments conducted by WILLIAMS & WOOD, 1966, on a simple rectangular-wing model with a centrally-located jet established that the lift increment $\Delta L/F$ falls steadily below its static value as the effective velocity ratio V_e is raised from zero. The lift loss was accompanied by the expected nose-up pitching moments again increasing as V_e was raised. The observed interference effects are due partly to the steady growth of the downward load from jet interference on the lower surface behind the jet and partly from the rearward movement of the centre of this jet interference load. Also, the normal component of thrust will be reduced because of the jet deflection.

As the velocity ratio is increased further, the lift loss reduces but the nose-up pitching moment continues to increase. This may be due to two main factors. Firstly the configuration being tested may be generating aerodynamic lift which will offset the

lift loss. Secondly the very high jet deflection angles involved may put the jet interference close to the trailing edge of the wing. The jets may then act as a crude jet-flap on the wing lower surface and thereby generate extra lift by super-circulation.

For practical VTOL aircraft, velocity ratios below about 0.3 are of primary concern during transition with jet-lift schemes although values as high as 0.5 could be of importance with high by-pass ratio engines or lift fan arrangements.

2.2.2.2 The effect of area ratio, A_n/S

The interference lift loss is strongly sensitive to the ratio of nozzle area to planform area, A_n/S. With the configuration mentioned above (Section 2.2.2.1), WILLIAMS & WOOD, 1966, observed that the lift loss increases as the area ratio is decreased and the relationship is approximately linear for a simple wing/jet geometry. A larger planform provides more area over which the interference pressures can act thereby increasing the lift loss. At very low area ratios, $A_n/S < 0.0016$, L/F actually fell to zero! For more practical area ratios (between 0.01 and 0.04 for a typical STOVL aircraft) the lift loss and accompanying nose-up moments are less severe, a maximum lift loss of 25 percent was recorded with an area ratio of 0.01.

2.2.2.3 The effect of nozzle geometry

Extensive studies of the effect of nozzle geometry were carried out by VOLGER, 1964. A VTOL model was equipped with various arrangements of interchangeable single or multiple, round or slotted jets, with and without jet deflection. The various nozzle geometries tested are shown in Figure 2.13. All configurations showed interference lift losses that increased with velocity ratio. For most jet arrangements, nose-up pitching moments due to jet interference occurred and increased with velocity ratio. The three configurations which suffered the least interference effect on the lift and pitching moment were numbers 2, 6 and 7. The reduced effect shown by the slotted jets was thought to be due to their more streamlined shape in cross section and the smaller planform area behind the jet.

An investigation was made by VOLGER & GOODSON, 1973 to obtain the aerodynamic characteristics of a fuselage model with various arrangements of elongated slots in the fuselage bottom to provide vertical lift. The model, which was almost square in cross section, represented the fuselage of a STOVL aircraft. It was powered by an air driven ejector with the intake on the upper surface of the fuselage. The model was equipped with various arrangements of nozzles which are shown in Figure 2.14. The aerodynamic lift of the fuselage at zero degrees angle of attack was zero. As velocity ratio was increased from zero (hover) to 0.4, all three configurations showed a reduction in the combined aerodynamic lift plus thrust. Moving the slots outward reduced the affected model area directly behind the jets, thereby reducing the interference effects between the model, jets and freestream. Yawing the slots either in-

ward or outward at the forward end resulted in a reduction in lift and an increase in nose-up pitching moments compared with the unyawed slots. Yawing the slots outward was less detrimental than inward. The effect of inclining the jet 20 degrees away from the plane of symmetry produced some lift improvement and a more nose-down pitching moment as a result of less interference between the freestream and the outward spreading jets. Any indicated benefit from inclining the jet would, however, be partially offset by the 6 percent loss in lift resulting from the inclination of the thrust axis. A combination of 10 degrees outward yaw of the slots and 10 degrees outward inclination gave less lift loss than configurations with or without angular deflections. Yaw appeared to affect the results more than inclination.

2.2.2.4 The relative location of wing and jet

As regards jet position relative to the wing, rearward location of the jet exit naturally tends to alleviate the lift loss and the nose-up pitching moments arising from jet interference, since the surface extent aft of the jet exit is reduced. WILLIAMS & WOOD, 1966, found evidence to suggest that with multiple jets the velocity ratio range over which the lift loss occurs can be much reduced and the subsequent lift augmentation much increased by the adoption of a span-wise row arrangement towards the rear of the wing instead of a close cluster.

The effect of sweeping the wings aft on a four jet VTOL configuration were examined by OTIS, 1962. Two wing positions were tested (Figure 2.15), one with 25 degrees leading edge sweep and the other with 75 degrees. The forward nozzles were placed under the leading edge of the inboard wing section (fixed geometry) and the rear nozzles were under the trailing edge of this section. With the wing in the low-sweep position, the lift loss was less than 50 percent of that generated in the highly-swept position. This appears to be due to the position of the wing area relative to the jets in these two positions. The low-sweep wing had no wing area behind the rear nozzles whereas the highly-swept wing had nearly all the wing area behind the rear nozzles.

In order to investigate the effect of jet position more systematically, a generalised study of jet positions from several wing chord lengths ahead to several wing chord lengths behind an unswept wing was reported by HAMMOND & MCLEMORE, 1967. In this investigation, an aspect ratio 6, unswept, untapered wing-fuselage model equipped with a 30 percent chord slotted Fowler flap was used. Two jets, one on either side of the fuselage, were positioned at about 25 percent semi-span and at the various longitudinal and vertical positions shown by the 'plus' marks in Figure 2.16. The jets were mounted independently of the wing so that only the aerodynamic forces and interference effects were measured on the wing. The data show that with the jet exits on the wing chord plane, considerable jet interference was experienced even with the jet as far as four wing chords ahead of the wing. Favourable interference effects, however, were encountered with the jets beneath and behind the 50

percent chord point of the wing and the interference effects are most favourable for positions closest to the flap. These favourable interference increments were believed to be due to the action of the jet in helping the flap achieve its full lift potential. Another slightly different configuration [HAMMOND & MCLEMORE, 1967], this time with jets operating simultaneously both in front of and behind the wing, indicated an overall favourable interference lift effect, again indicating the importance of configuration geometry on the jet interference lift and moment characteristics. These findings agree well with those of MARGASON & GENTRY, 1968, SCHULTZ & VIEHWEGER, 1974 and NANGIA, 1994.

WINSTON *et al*, 1975, report on a configuration which was tested to determine the optimum jet exit location from an induced lift standpoint. The general results are illustrated in Figure 2.17. The model was tested with the lift/cruise jets in three longitudinal positions as shown. The plot of total lift to thrust ratio as a function of velocity ratio illustrates the lift improvement obtained by successive aft movement of the jet exits towards the wing trailing edge.

The evolution of the Harrier II aircraft included the addition of a supercritical aerofoil section, an increase in wing area and span, and a change from plain 50 degree trailing edge flaps to larger single-slotted flaps with 60 degrees of deflection. As a result of these modifications the lift coefficient of the Harrier II was increased over the original design by an increment of 0.7 up to angles of attack of 12 degrees [KOTANSKY, 1984]. As an example of the sensitivity of STOVL aircraft performance to small changes in the powered lift system configuration consider the scarf on the forward nozzles. On the Harrier II with the slotted trailing edge flap, the scarfed forward nozzle flow interacted with the wing undersurface and inboard pylon at transitional forward speeds causing a flow separation upstream of the flap. Removal of the scarf directed the forward jet to a position further below the wing and produced a C_L increment of approximately 0.2 [KOTANSKY, 1984].

2.2.2.5 The effect of nozzle vector angle, δ_j

Wind tunnel tests carried out on a one-sixth scale model of the Kestrel (XV-6A) [MARGASON *et al*, 1972] measured the effect of vectoring the nozzles on the incremental lift and pitching moment at a range of velocity ratios and angles of attack. At zero degrees angle of attack, increasing nozzle vector angle to a more vertical position, increased the lift loss and nose-up pitching moment. This agrees well with the work of FÜTTERER & HARMS, 1967 and KRENZ & BARCHE, 1967.

2.2.2.6 Lift improvement devices (LIDs)

SPREEMAN, 1960, noted that in one full-scale flight investigation, deflecting the trailing-edge flaps reduced the losses in lift and nose-up pitching moments. The

beneficial effect of the flaps on this configuration can be attributed to positive pressures being built up in front of the flap on the lower surface.

The alleviation of unfavourable jet interference effects was shown possible by WILLIAMS & WOOD, 1966 with the addition of stream-wise fences to the lower surface of the airframe, along the sides of the jet exit. The geometry of the fence was found to be important. The depth of the fence should be at least one jet diameter and the stream-wise length at least two jet diameters so as to extend forward of the jet exit as well as bounding the sides. Flow visualisation suggested that the fences reduced the initial curvature of the jet, thus increasing the penetration of the jet plume and delaying the growth of the trailing vortex flows. This was consistent with the apparent negligible effect of the fences at low velocity ratios, where the rate of deflection of the jet is inherently small. The effect of the fences on a simple fuselage model was excellent, reducing maximum transitional lift loss from 27 percent to 7 percent.

2.2.3 Interference effects between jet(s) and intake(s)

The question of the applicability of the principle of superposition to the problems of exit interference effects and intake interference effects in combination has often been raised; that is, can the jet-induced effects be measured on one model and the intake-effects on another and the results simply added to determine the characteristics of the total configuration? KUHN & MCKINNEY, 1965 concluded that the answer was yes. They tested a simple lift-jet fuselage model which had separate jet and intake simulation. Within the accuracy of the data there was little or no interference effect. The lift engine and intake had only small mass flow rates, however, and were installed in a large fuselage. BRADBURY, 1981, comments that on VTOL models in the transition phase of flight the intake interference effects are generally not sufficiently important to warrant modelling the intake flows.

Intake interference effects were observed by MARGASON & GENTRY, 1968. Their five-jet VTOL configuration had three lift engines simulated in the forward portion of the fuselage ahead of the wing and two lift/cruise engines with deflected thrust simulated in the rear portion of the fuselage near the wing trailing edge (see Figure 2.18). The inlets of the lift engines were on the upper surface of the fuselage and those of the lift/cruise engines were on the side of the forward portion of the fuselage. With the inlets closed, the model showed increments of lift loss and nose-up pitching moments. Opening the inlets added an increment to the nose-up pitching moment but did not affect the lift loss as shown in Figure 2.18.

WINSTON, 1970 found similar results with a six-jet V/STOL model. Here, four lift engines and two lift/cruise engines were simulated. The intake flow produced a constant positive lift increment and an increasing nose-up pitching moment as veloc-

ity ratio was increased. At a fixed velocity ratio, the longitudinal interference increments due to intake flow were constant over a range of angles of attack.

An investigation carried out by MINECK & MARGASON, 1973 and MINECK & SCHWENDERMANN, 1973 determined some interference effects between the jets and intakes on a STOVL aircraft. The model tested is shown in Figures 2.19 and 2.20 and was a vectored thrust VSTOL fighter configuration equipped with one lift-jet and two vectored thrust engine simulators. The lift-jet simulator, located in the fuselage, was a simple convergent nozzle without an external air intake. The lift-jet exhausted 90 degrees from the horizontal plane and was located on the centre-line of the fuselage bottom 76.7 mm ($1.34d_n$) forward of the model moment reference centre which was at the wing quarter-chord point. The vectored-thrust engine simulators, mounted in removable fuselage-supported nacelles, were of the ejector type which induced intake flow. The vectored-thrust jets could be set 26.7 mm ($0.29d_n$) forward or 186.2 mm ($2.0d_n$) aft of the moment reference centre and could also be vectored at angles of 0, 45 and 90 degrees from the horizontal. The model was equipped with a series of pressure tappings. The port wing was tapped from leading to trailing edge at intervals of 5 percent chord and at 25.0, 38.7, 52.4 and 80.0 percent semi-span. The fuselage had 22 unequally spaced pressure tappings ranging from 13.0 to 73.2 percent of the fuselage length and at distances of 0.00 mm, 31.75 mm ($0.56d_n$) and 50.80 mm ($0.89d_n$) from the fuselage centre-line. Finally there were 11 pressure tappings on the port nacelle upper surface and 8 on the lower surface. Two tappings from each surface were located inside the intake lip. Tests were carried out at velocity ratios of 0.1, 0.2 and 0.3.

In general, without thrust* and zero degrees angle of attack, the pressure coefficients on the upper and lower surfaces of the wing had similar distributions, but with thrust and zero degrees angle of attack, the pressure coefficients on the lower surface were more negative than on the upper surface. With thrust and zero degrees angle of attack, the wing was operating at a negative local angle of attack because of the jet-induced downwash.

In addition to inducing a downwash on the wing, the vectored-thrust jet exhaust induced a region of negative pressure coefficients on the lower surface of the wing. The low pressure region was larger and the pressure coefficients more negative for the front vectored-thrust nozzles than for the rear vectored-thrust nozzles. These induced effects decreased with increasing velocity ratio and increasing span-wise distance from the jet.

To determine the effect of intake flow, the vectored-thrust configurations were tested with both intakes closed using elliptical plugs. Examination of the force and moment

---

* *'Without Thrust' refers to conditions with no jet exhaust flow. Conversely 'With Thrust' refers to the jet exhaust flow simulated by compressed air. The intake flow is not necessarily represented in these cases.*

data for the intake open and intake closed indicated that closing the intakes decreased the angle of attack by approximately 2 degrees. Hence, with intakes closed, the wing must be operated at an angle of attack between 1 and 2 degrees greater to obtain the same section lift coefficient obtained with the intakes open. With the intakes closed, there appears to have been no jet flow either and so it is not known whether the change in angle of attack is attributable purely to intake flow, jet flow or a combination of both.

For all configurations without power, the pressures on the fuselage were very close to the freestream static pressure. With thrust, the lift-jet-induced large negative pressure coefficients on the bottom of the fuselage with the peak negative pressure coefficients decreasing slightly with increasing angle of attack. Also, the blockage due to the jet caused a region of positive pressure coefficients upstream of the jet. With thrust, the vectored-thrust jets induced a region of negative pressure coefficients which decreased with increasing angle of attack and increasing effective velocity ratio.

For the vectored-thrust jets without thrust, the pressure distribution on the nacelles showed the same trends as an aerofoil would through a range of angles of attack with large negative pressure coefficients near the leading edge of the upper surface and positive pressure coefficients on the lower surface. The addition of thrust changed the pressure coefficients near the nacelle. To determine the effect of intake flow, the intakes were again closed with elliptical plugs. The plugs prevented the large negative pressure coefficients on the upper surface up to the stall angle of attack. The maximum negative C_p on the upper surface with the intakes closed was -0.641 at an angle of attack of 12 degrees compared with -1.641 at the same angle of attack and an effective velocity ratio of 0.3. Once more, it is not known whether these effects may be caused by intake flow, jet flow or a combination of both. Analysis of the stagnation point on the intake upper and lower surfaces clearly shows a difference between the vectored-thrust jets on and off. With intake flow off and jet flow off, the stagnation point on the upper lip does not change with angle of attack. However, with intake and jet flow on, the stagnation point moves inside the upper lip as the angle of attack is increased. The stagnation point on the lower lip for both configurations moves from inside the lip to outside as angle of attack is increased. With intake and jet flow on, however, the stagnation point is nearer the outside of the lip for any given angle of attack.

Data for the VAK 191B described by HAFTMANN, 1981 showed a consistent discrepancy between the lift loss measured in flight and the lift loss measured on a wind tunnel model. The full-size aircraft had a transitional lift loss 4 to 10 percent greater than the wind tunnel model and a nose-up pitching moment 5 to 8 percent higher. This was explained by differences in the jet conditions between full-size and wind tunnel model. The wind tunnel model, however, used a free flow intake with

no suction simulated. There is the possibility that jet/intake interference was responsible for the measured differences.

As more complex STOVL aircraft designs were developed, it became increasingly apparent that the argument for separate jet and intake testing on STOVL aircraft was not valid. The term 'close-coupled aerodynamics' has become increasingly popular in describing the engine/airframe designs and operating conditions in which the air intake and nozzle system flows create significant interferences with respect to each other and/or which, when combined, create interferences to airframe surfaces differing from the sum of the individual interferences. HARRIS *et al*, 1991 suggested that aircraft designs, in which the distance from the intake face to the front nozzle relative to the diameter of the compressor face is less than 3, will undoubtedly feature close-coupled aerodynamics. Whereas for designs in which this ratio is greater than 8 the aerodynamics can generally be considered to be uncoupled. Evidence to support this all-encompassing statement is not, however, provided. In the intermediate range it is likely that coupled aerodynamics will arise in a significant proportion of the overall operating envelope of the aircraft. Close-coupled aerodynamics will also arise if vectored or deflected jets are located close to the wing or control surfaces or when intake airflows result in significant interferences at control or lifting surface locations. Nearly all STOVL designs will fall into the category of close-coupled aerodynamics and therefore the need for full flow-field model representations using simulators with 'live' inlet and exhaust flows is evident. As far as the author is aware the discrepancy between simultaneous and separate jet and intake testing on a STOVL aircraft has not been quantified.

This section has discussed the aerodynamic interference effects encountered by a STOVL aircraft in transition out of ground effect characterised by a lift loss and a nose-up pitching moment. The effects appear to be highly configuration-dependent particularly with complex models. It has been shown that there is some disagreement as to the significance of testing combined jet and intake models although in more recent years, the importance of investigating close-coupled jet/intake systems has been highlighted. Undoubtedly the design of STOVL aircraft has a great influence on the observed interference effects and some work relating to STOVL aircraft design has been covered by WILES, 1965, TAPE *et al.*, 1983 and CURTIS, 1992.

2.3 STOVL aircraft in ground effect

Operation in ground effect is an important STOVL design condition but it is not directly relevant to the current project. A brief summary of the main aerodynamic phenomena associated with operating a STOVL aircraft in ground effect are included here for completeness.

2.3.1 Jet impingement

Jet impingement gives rise to noise and ground erosion problems. Ground erosion is the destructive effect of the jet(s) on the surface below the aircraft. The magnitude of the erosion is dependent on the jet exit temperature, dynamic pressure, duration of impingement as well as the properties of the ground [BARCHE, 1974]. STOVL aircraft noise is important for a number of reasons: survivability, ground crew safety, and public acceptability during peace-time operations [KNOWLES & BRAY, 1991]. As well as the usual sources of noise associated with supersonic jets (shear noise, shock noise etc.) STOVL aircraft potentially suffer additional problems associated with jet impingement.

2.3.2 Wall jet flows

When hovering in ground effect, the lift losses due to entrainment can be considerably greater than out of ground effect, particularly for the single jet case. When the jet impinges on the ground it is turned outward and forms a wall jet which flows radially outwards from the impingement point. This radial wall jet becomes the primary entrainment mechanism and draws ambient air through the gap between the edge of the planform and the wall jet. The sub-ambient pressures induced on the configuration are lower near the edge than toward the centre of the planform. These pressures decrease as the aircraft nears the ground, therefore causing an increase in the lift loss as altitude is reduced.

2.3.3 Fountain flows between multiple jets

When two or more jets are installed, the wall jets flowing radially from the impingement point of adjacent jets meet on a stagnation line midway between the jets (if they are of equal strength) and are directed upwards in a fountain flow. The impingement of this fountain flow on the underside of the aircraft creates a lift force which at least partially offsets the wall jet-generated 'suckdown'. In addition, when three or more jets are used, a fountain core is generated at the centroid of the jet pattern where the fan shaped fountain from each pair of adjacent jets meet. This fountain core usually creates a significantly stronger lift increment than that created by a two-jet fountain.

2.3.4 The ground vortex

When an aircraft is operating at transition speeds in ground effect a ground vortex is formed by the action of the freestream opposing and rolling up the wall jet flowing forward from the impingement point of the lift-jet(s). Suction pressures are induced on the ground as well as the lower surface of the aircraft. Under low freestream to jet velocity ratios, the ground vortex can be well forward of the aircraft. When two jets are located side by side, the interaction of their respective wall jets creates a

stronger wall jet which penetrates the ground vortex and forms a forward vortex pair.

2.3.5 Hot gas ingestion

Hot gas ingestion is a serious problem for jet-lift STOVL aircraft because a thrust loss occurs as a result of elevated engine inlet temperatures. Another reason for concern is that the engine compressor may stall as a result of the very rapid rise in inlet temperature or a non uniform temperature distribution about the engine compressor face. There are three main causes of hot gas ingestion.

1. Near-field effects, caused by fountain flows generated by multiple jets.
2. Mid-field effects, caused by buoyancy of the hot gases detaching from the wall jet.
3. Far-field effects, caused by the stagnation of the wall jet by a head wind (the ground vortex).

Extensive studies of STOVL aircraft in ground effect have been covered by;

TOLHURST & KELLY, 1966; BARCHE, 1981; AGARWAL, 1986; FLUK, 1987; KNOTT, 1987; KUHN, 1987; MILFORD, 1987; STEWART, 1987; MCGUIRK *et al.*, 1990; MCLEAN *et al.*, 1990; BRAY, 1992; TAFTI & VANKA, 1992; WILSON, 1995; KIRKHAM, 1996; KNOWLES, 1996 and MYSZKO, 1997.

2.4 Summary

This chapter has reviewed previous work carried out on STOVL interference effects relevant to the current research topic. Two main operational environments encountered by STOVL aircraft have been discussed: hovering out of ground effect and transition out of ground effect. The former has included the fluid mechanics of an isolated free jet and the interference effects caused by such a jet when combined with simple and more complex fuselage/wing arrangements. On the subject of transition out of ground effect, the discussion has followed a similar format. Firstly, the characteristics of a free jet in a cross-flow were explained. The discussion then moved on to cover interference effects on simple and more complex jet-lift aircraft in transition, paying particular attention to any studies involving intake simulation. Finally, for completeness, a brief summary of the main aerodynamic phenomena associated with operating a STOVL aircraft in ground effect have been presented.

As far as can be determined, no previous experimental work has been carried out specifically to study and quantify mutual interference effects between jet(s) and intake(s) on a STOVL aircraft.

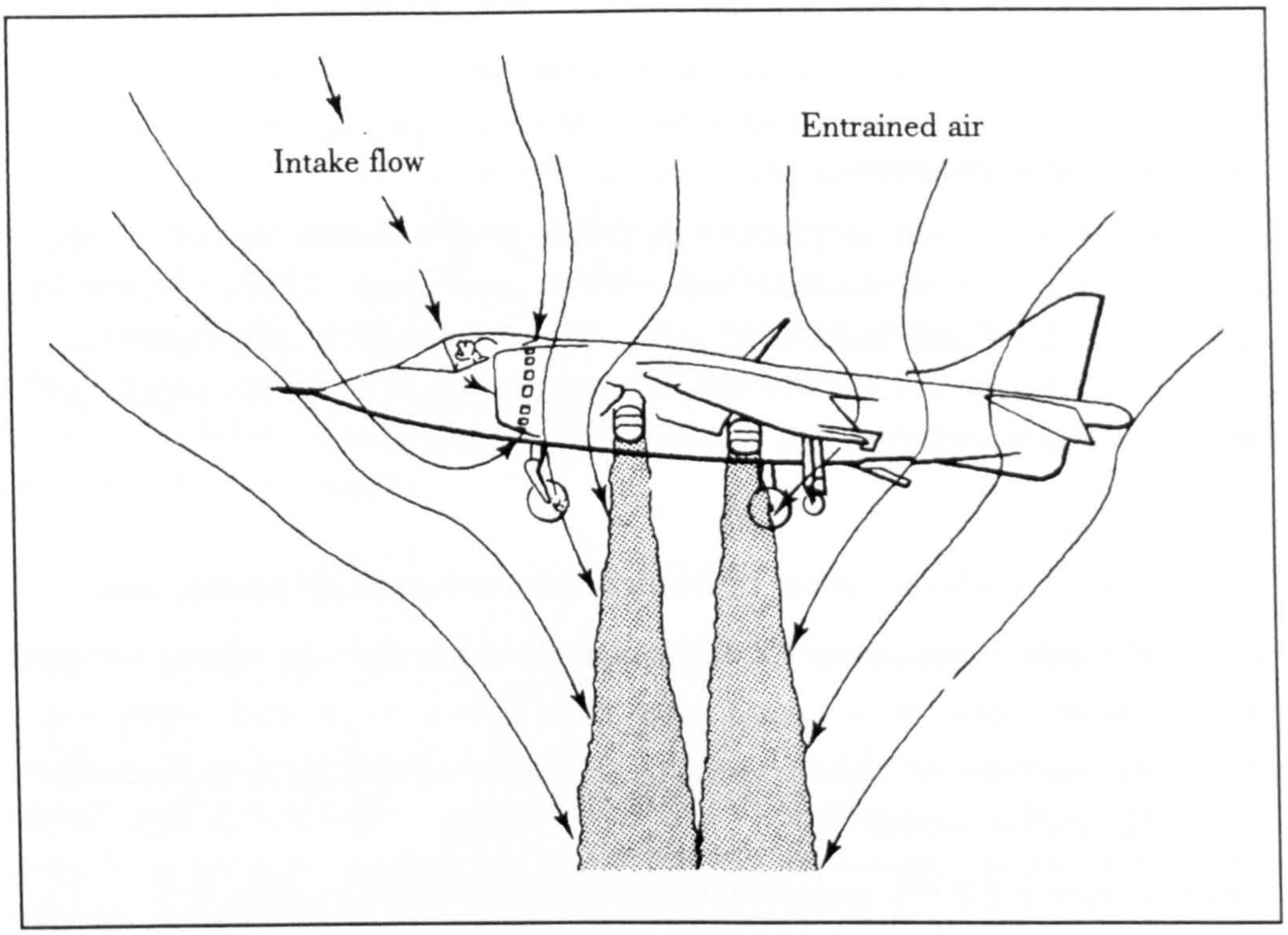

Figure 2.1 *- The flow-field surrounding a STOVL aircraft in hover.*

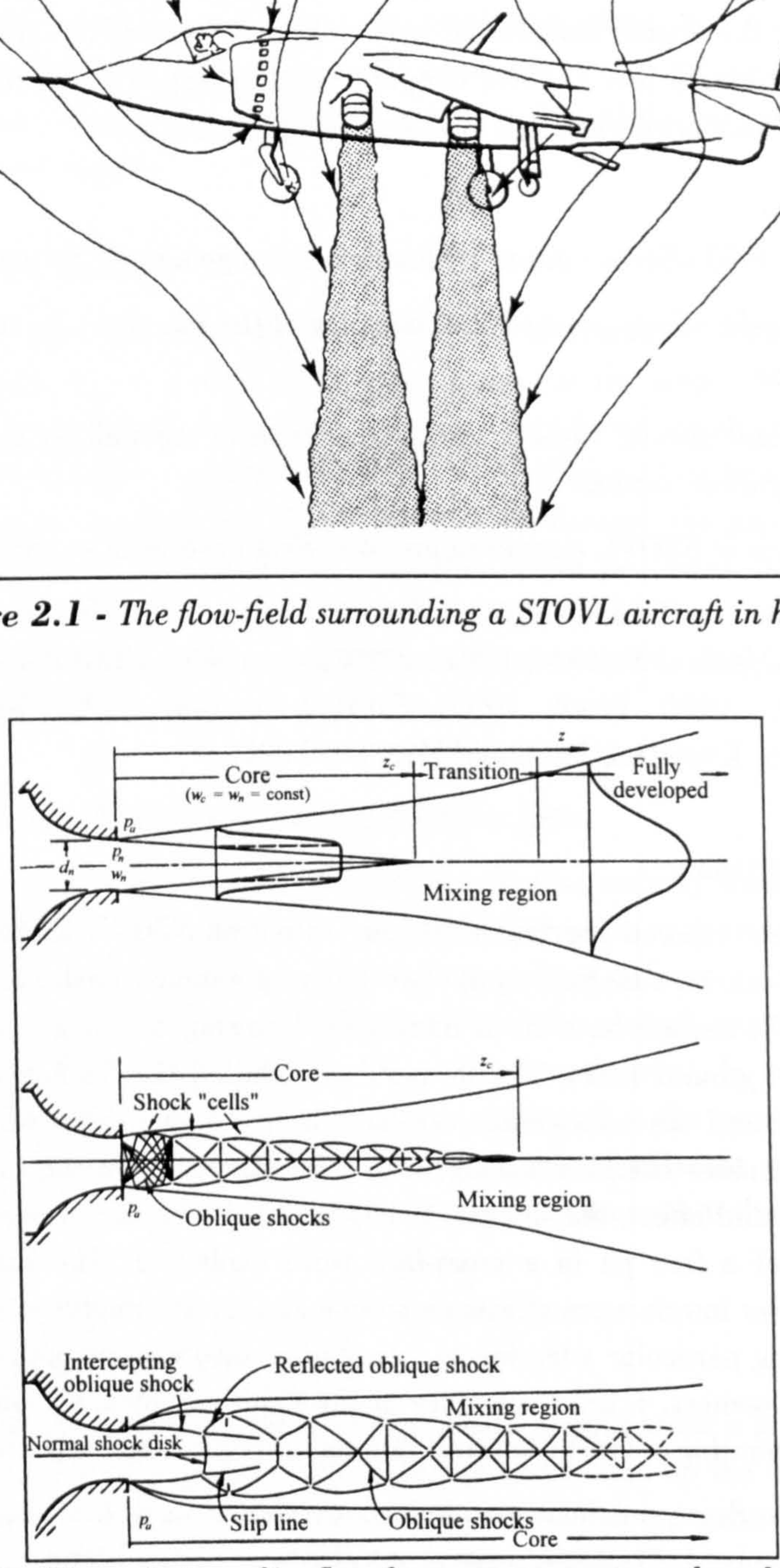

Figure 2.2 *- The variation of jet flow from a convergent nozzle; subsonic jet (top), moderately underexpanded jet (middle) and highly underexpanded jet (bottom) (DONALDSON & SNEDEKER, 1971).*

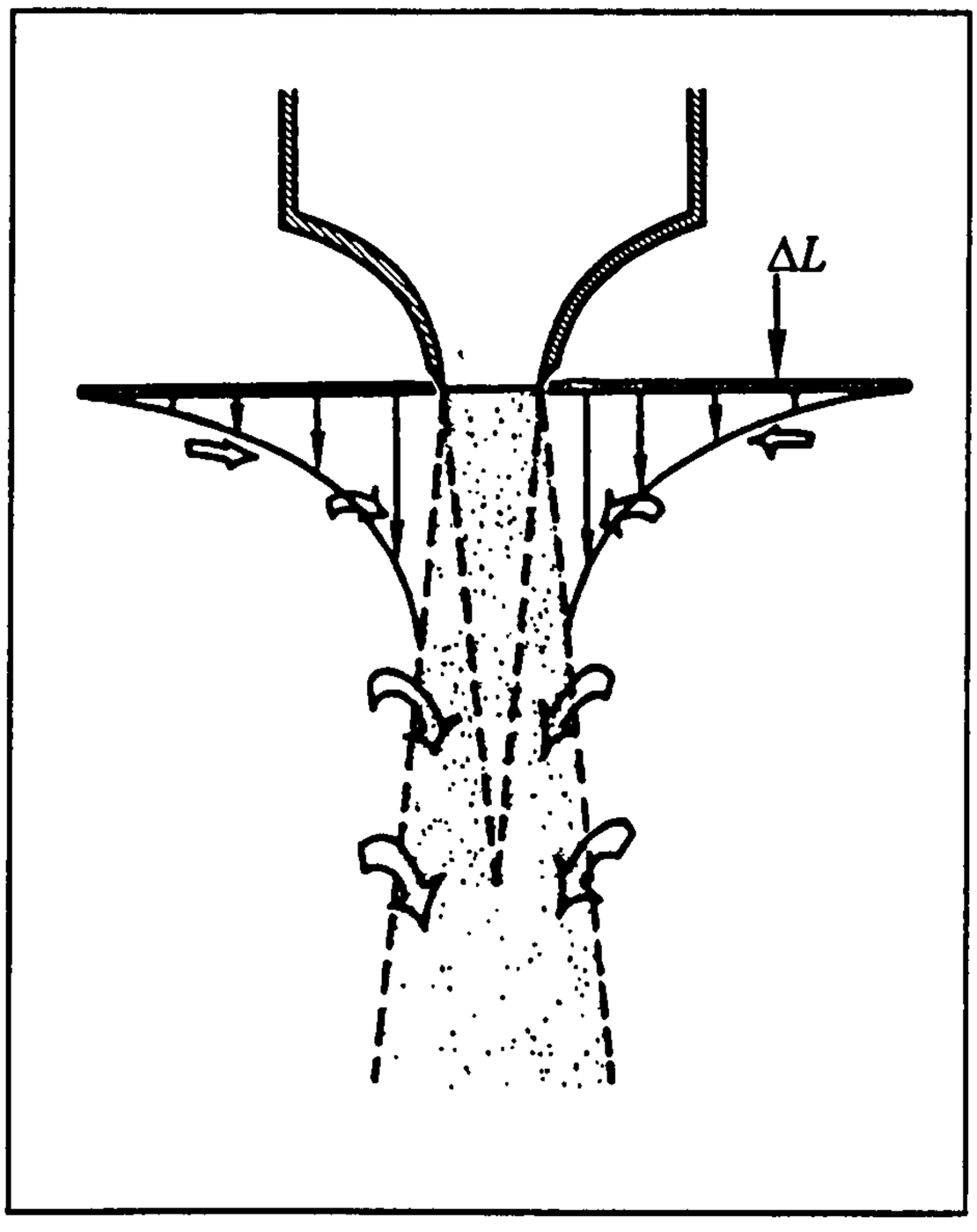

***Figure 2.3** - The lift loss generated on a flat plate by a single nozzle (WILLIAMS & WOOD, 1966).*

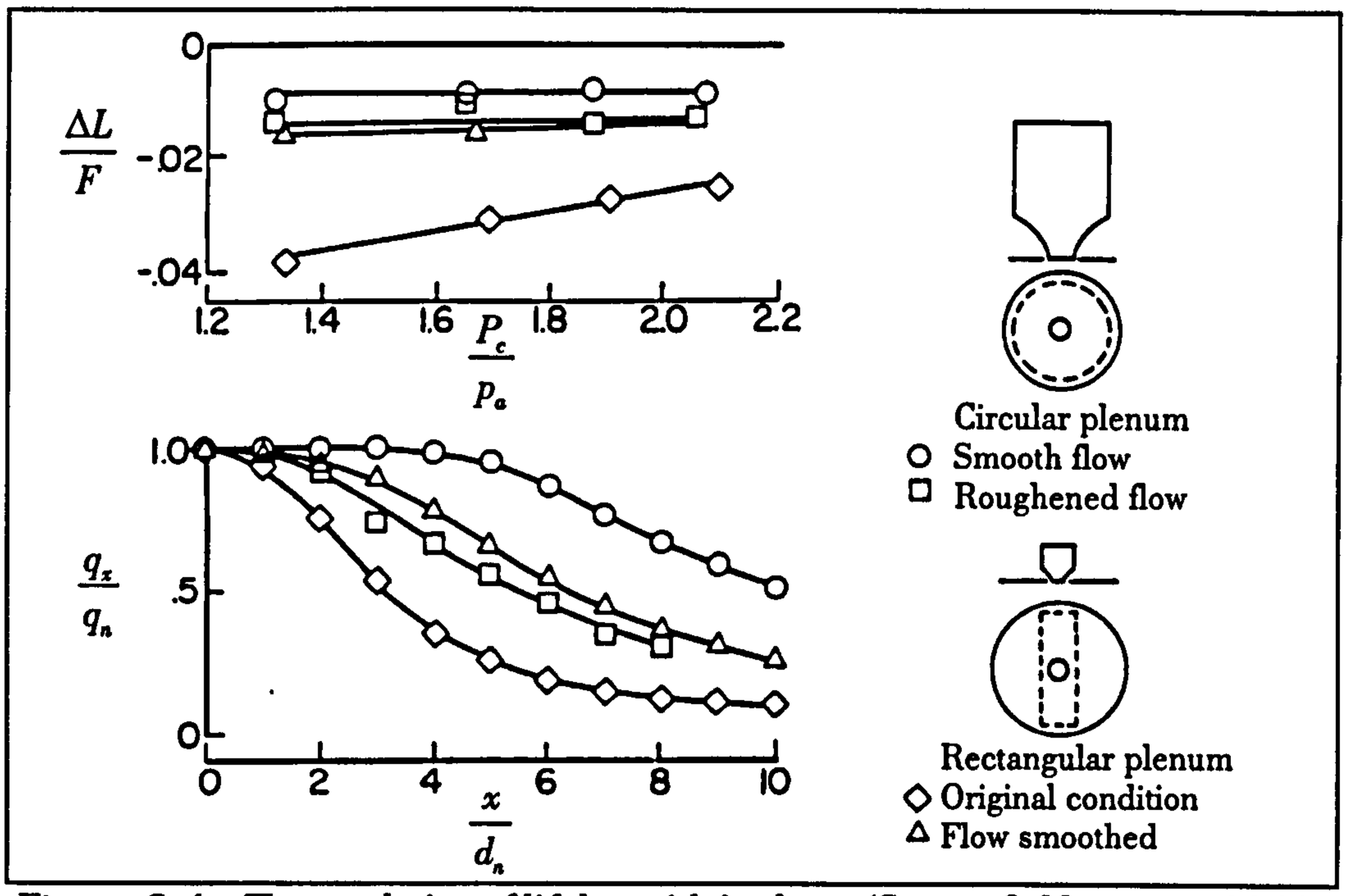

***Figure 2.4** - The correlation of lift loss with jet decay (GENTRY & MARGASON, 1966).*

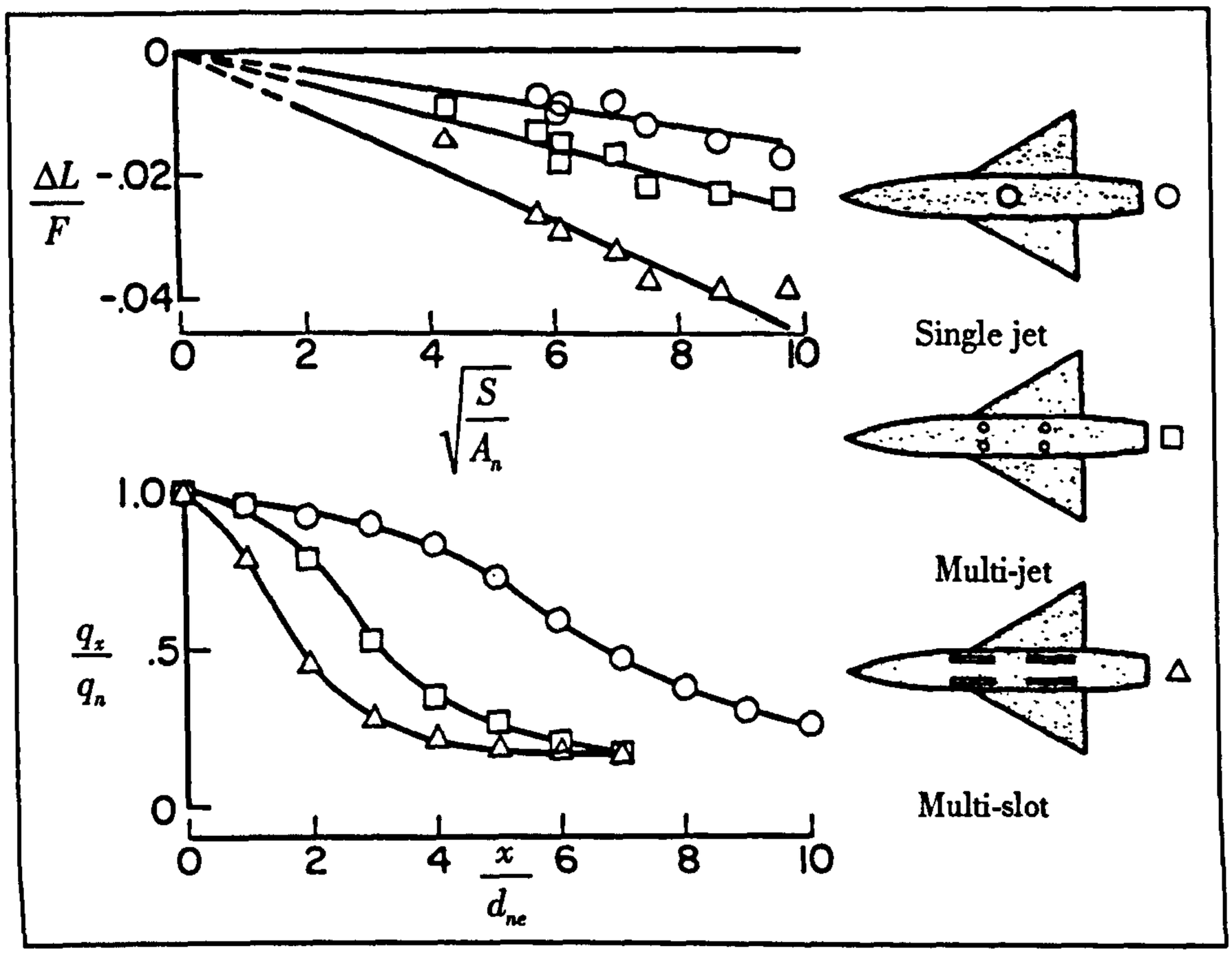

***Figure 2.5** - The effect of jet configuration on lift loss and jet decay (GENTRY & MARGASON, 1966).*

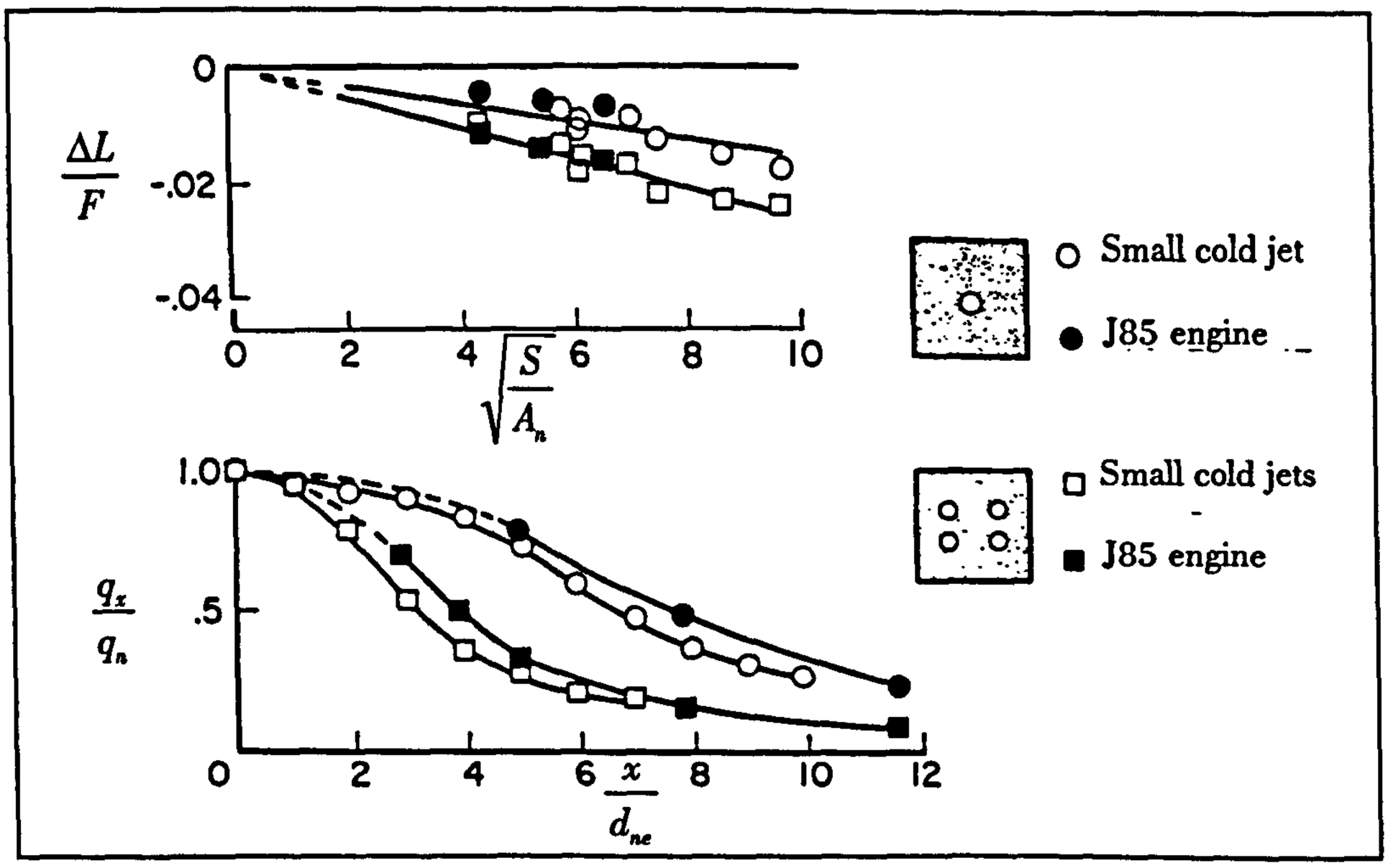

***Figure 2.6** - Comparison of small scale with large scale lift loss data (MCLEMORE, 1966).*

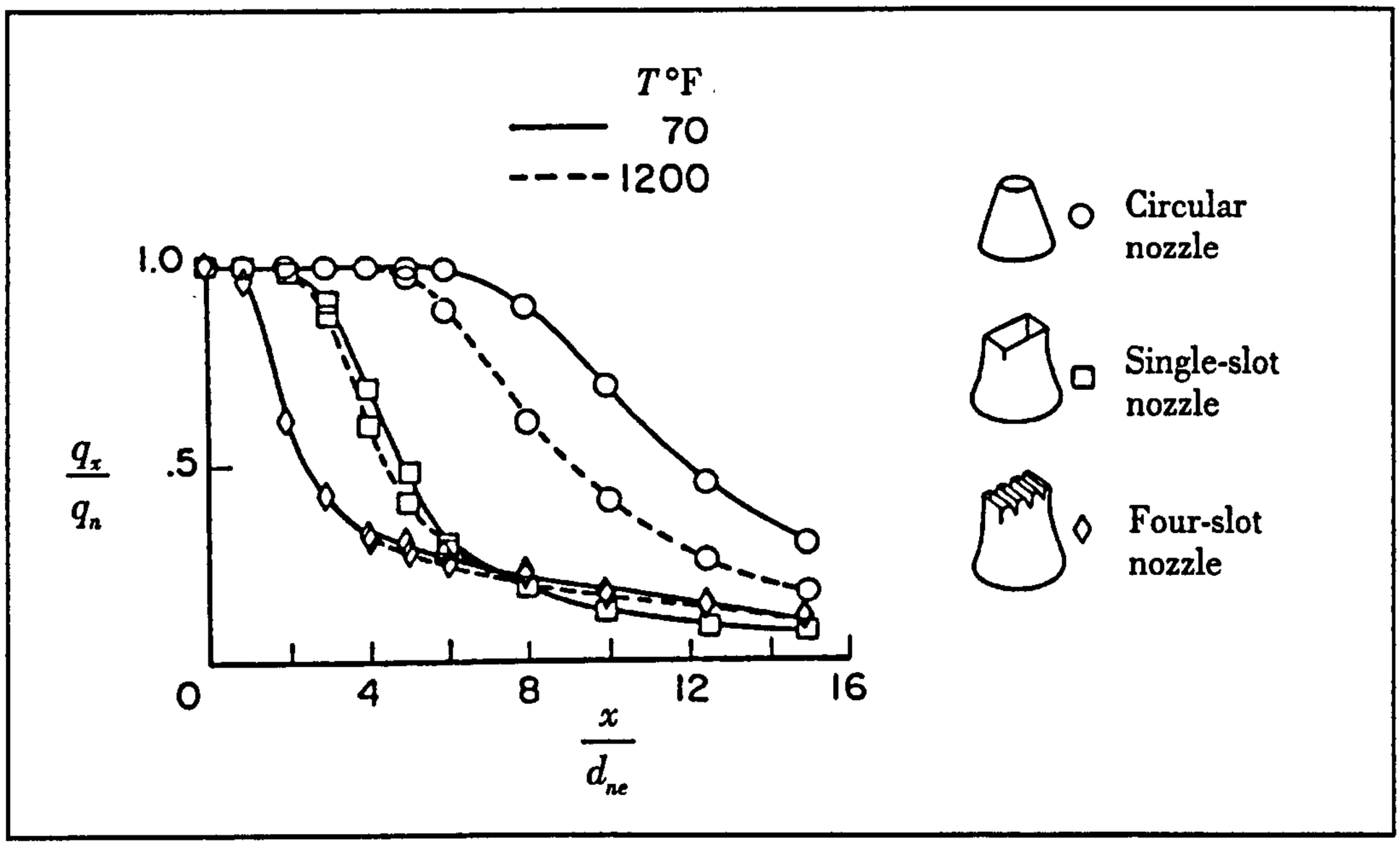

***Figure 2.7** - The effect of temperature and nozzle configuration on jet decay (HAMMOND, 1966).*

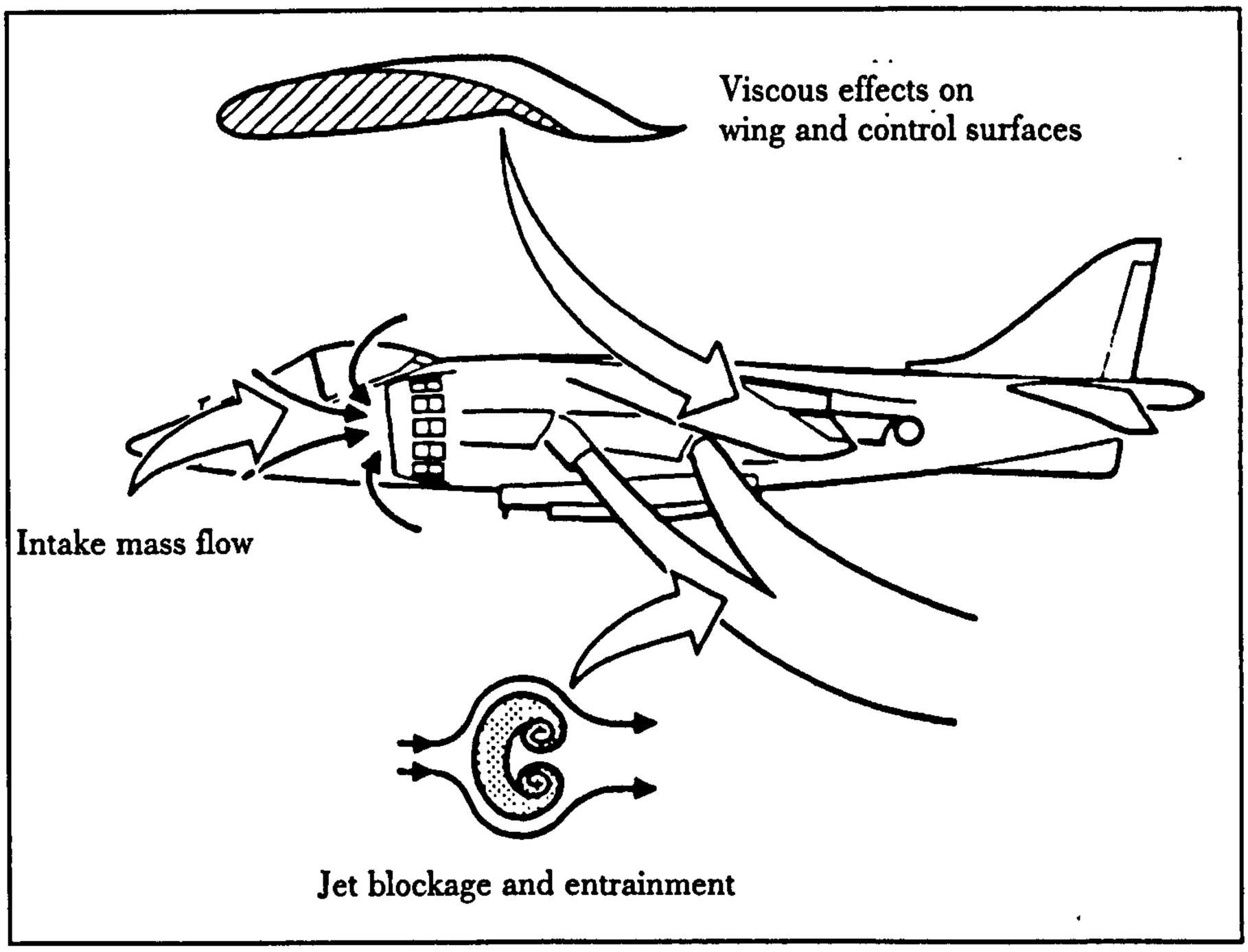

***Figure 2.8** - The flow-field about a STOVL aircraft in transition out of ground effect.*

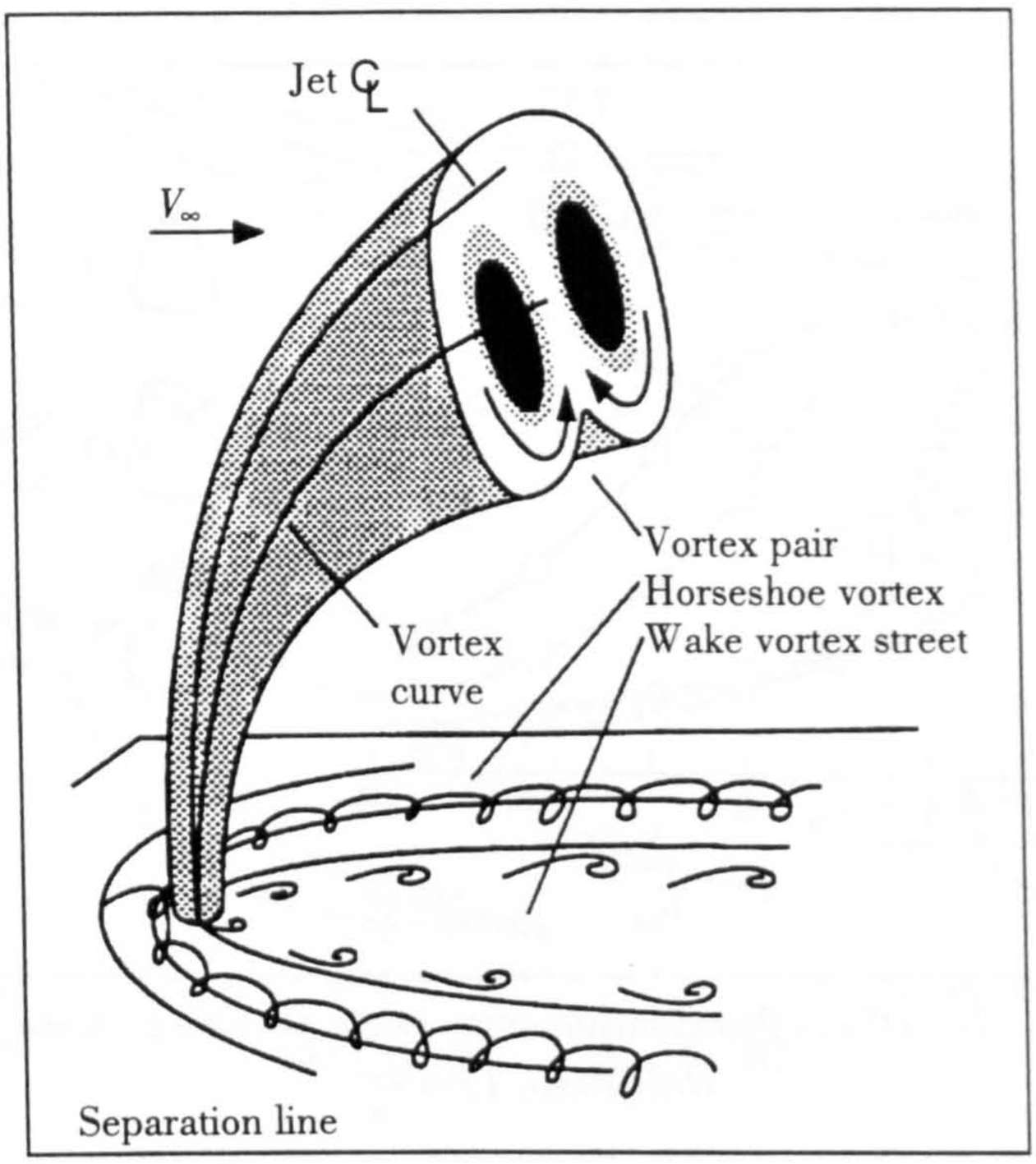

Figure 2.9 *- Sketch of the vortex systems associated with a jet in cross-flow (MARGASON, 1993).*

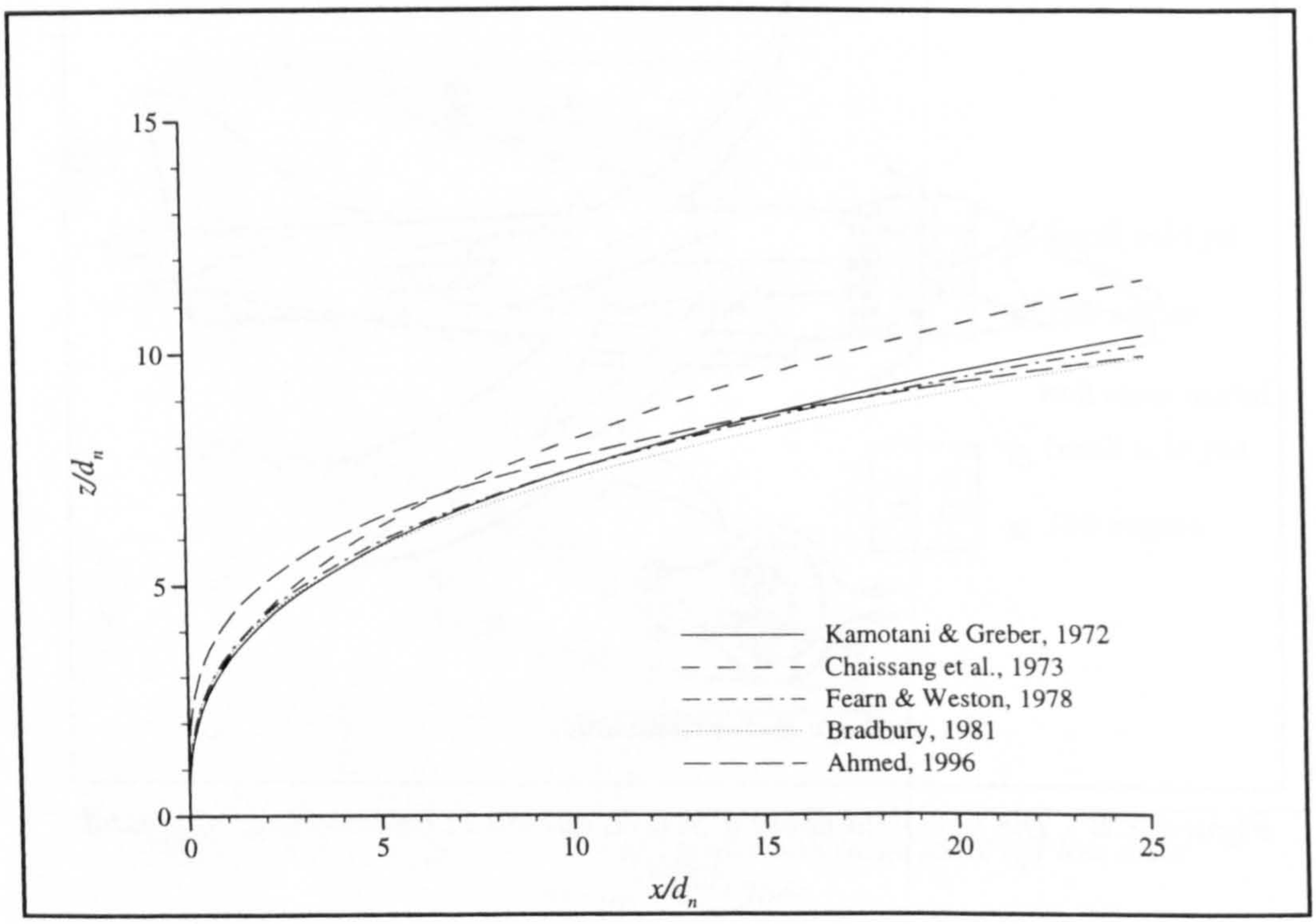

Figure 2.10 *- Comparison of predicted jet in cross-flow trajectories ($\delta_j = 90°$, $V_e = 0.25$).*

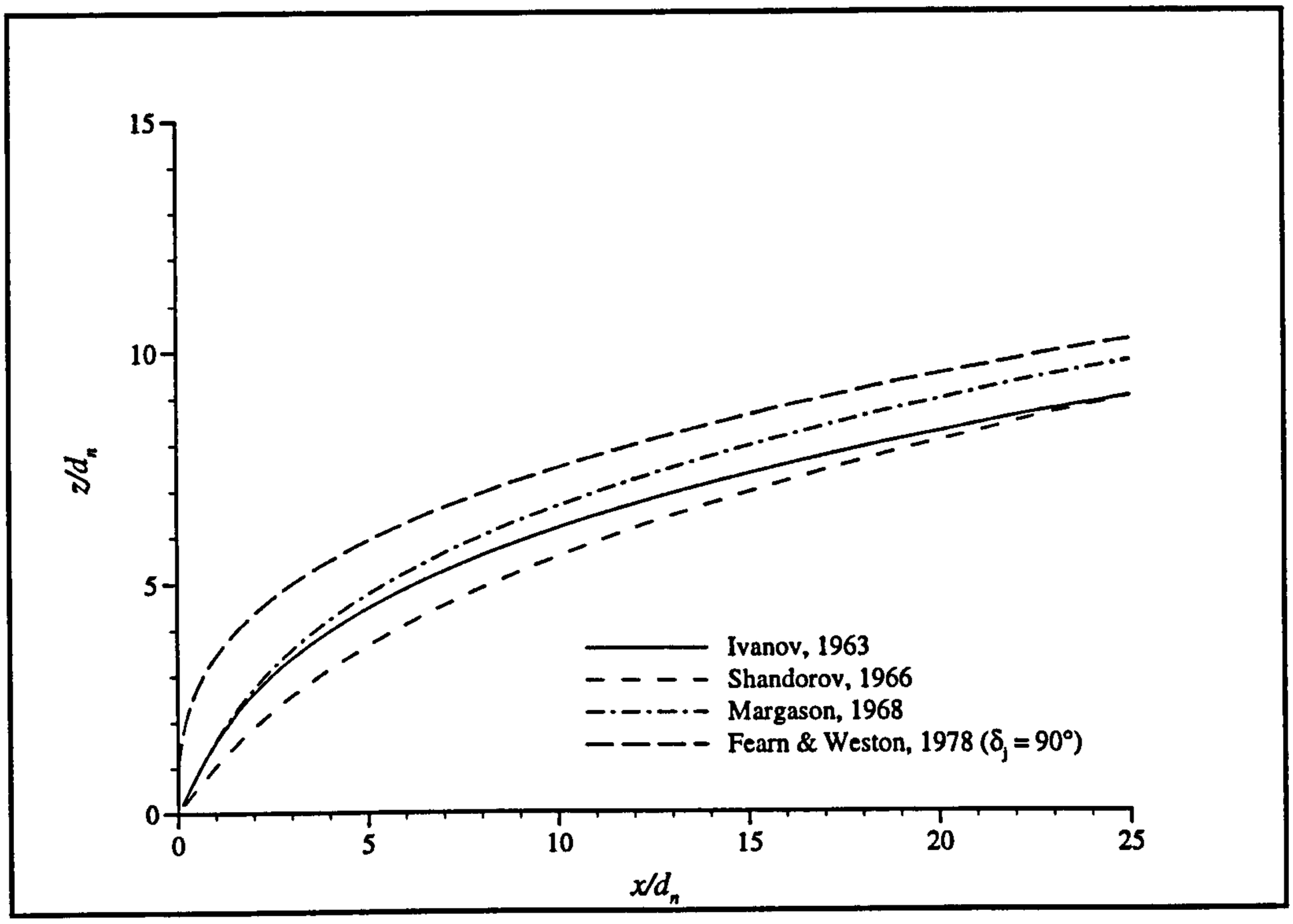

***Figure 2.11** - Comparison of predicted jet in cross-flow trajectories ($\delta_j = 60°$, $V_e = 0.25$).*

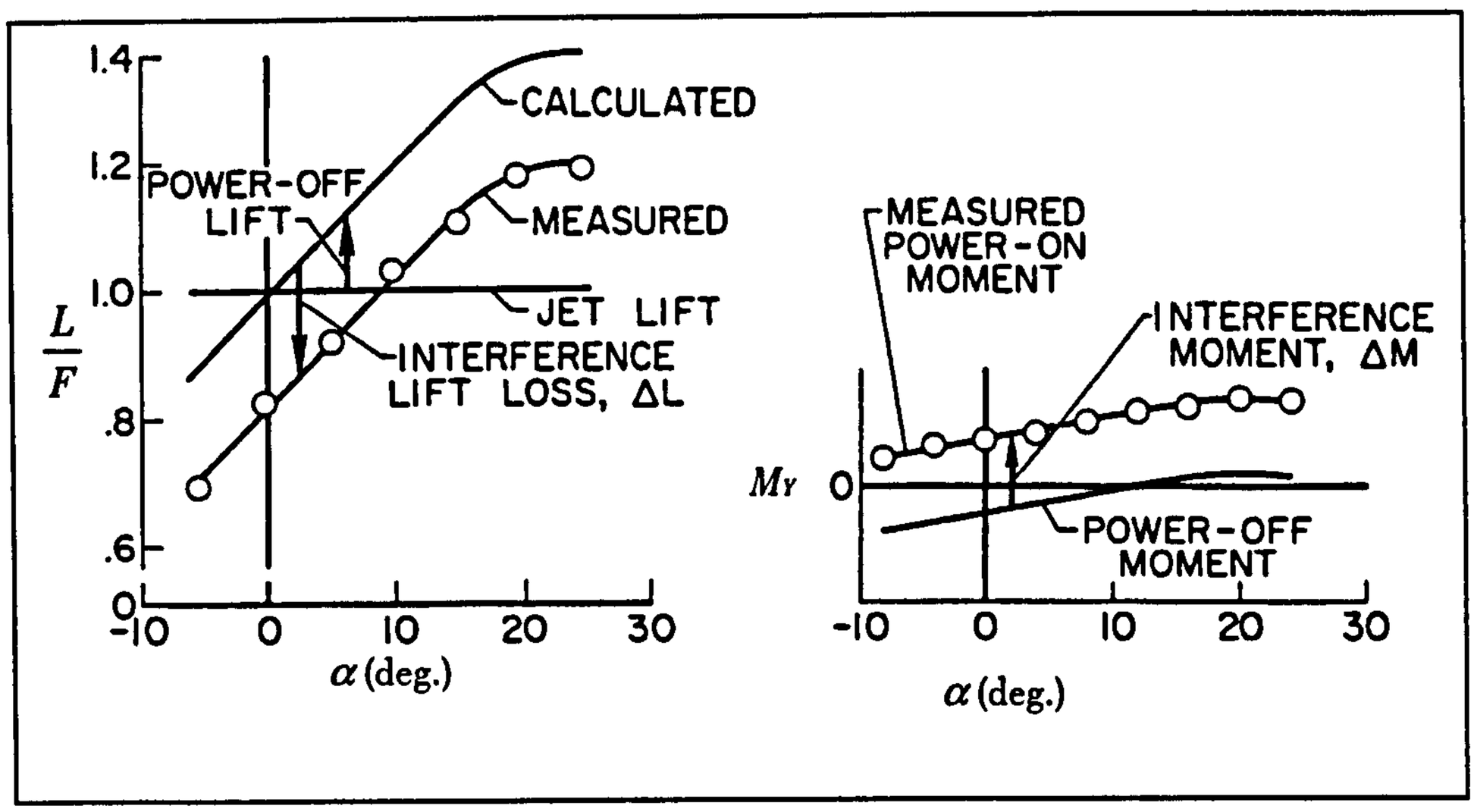

***Figure 2.12** - Jet interference in transition flight (MARGASON, 1966).*

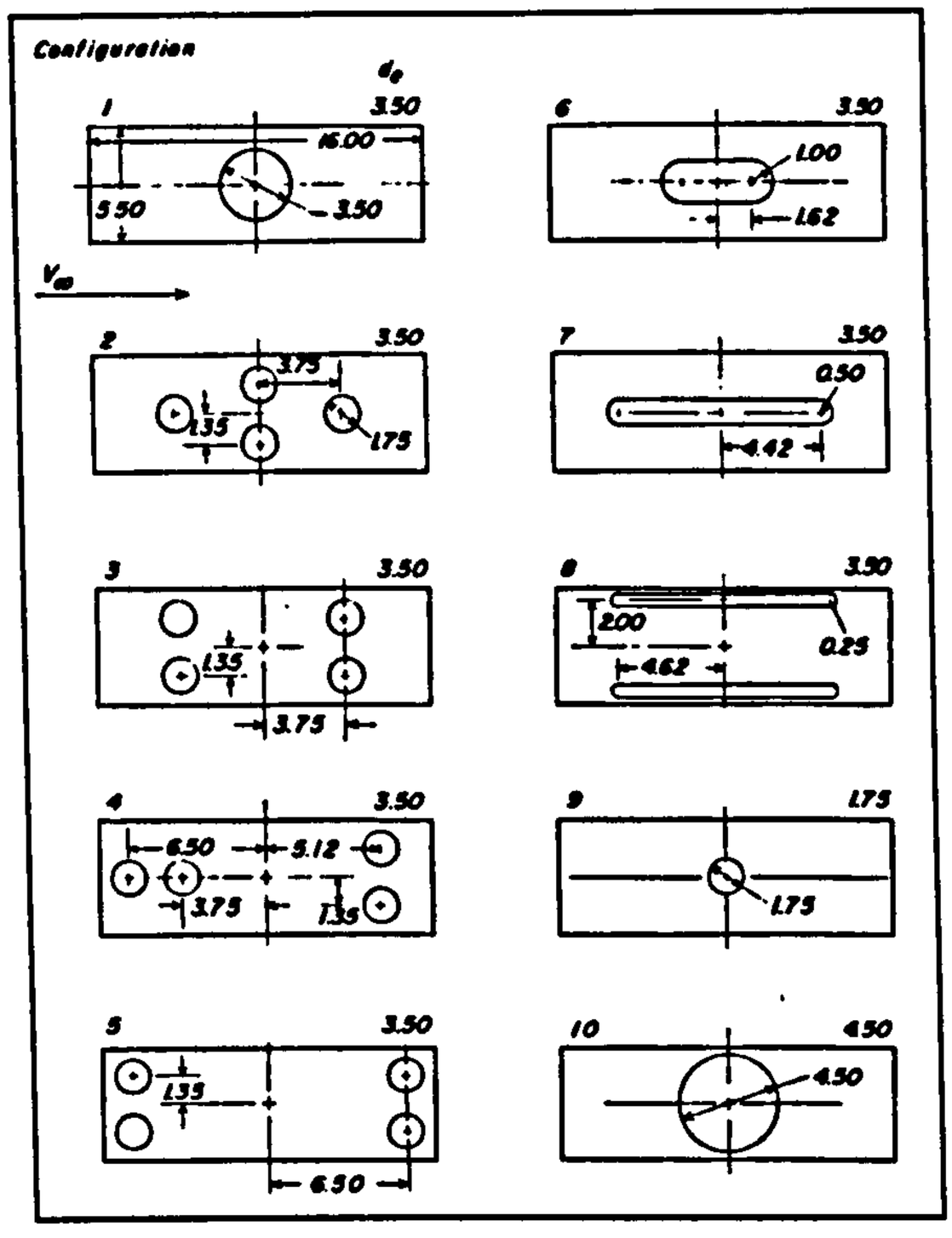

***Figure 2.13** - The various nozzle configurations tested by VOLGER, 1964*

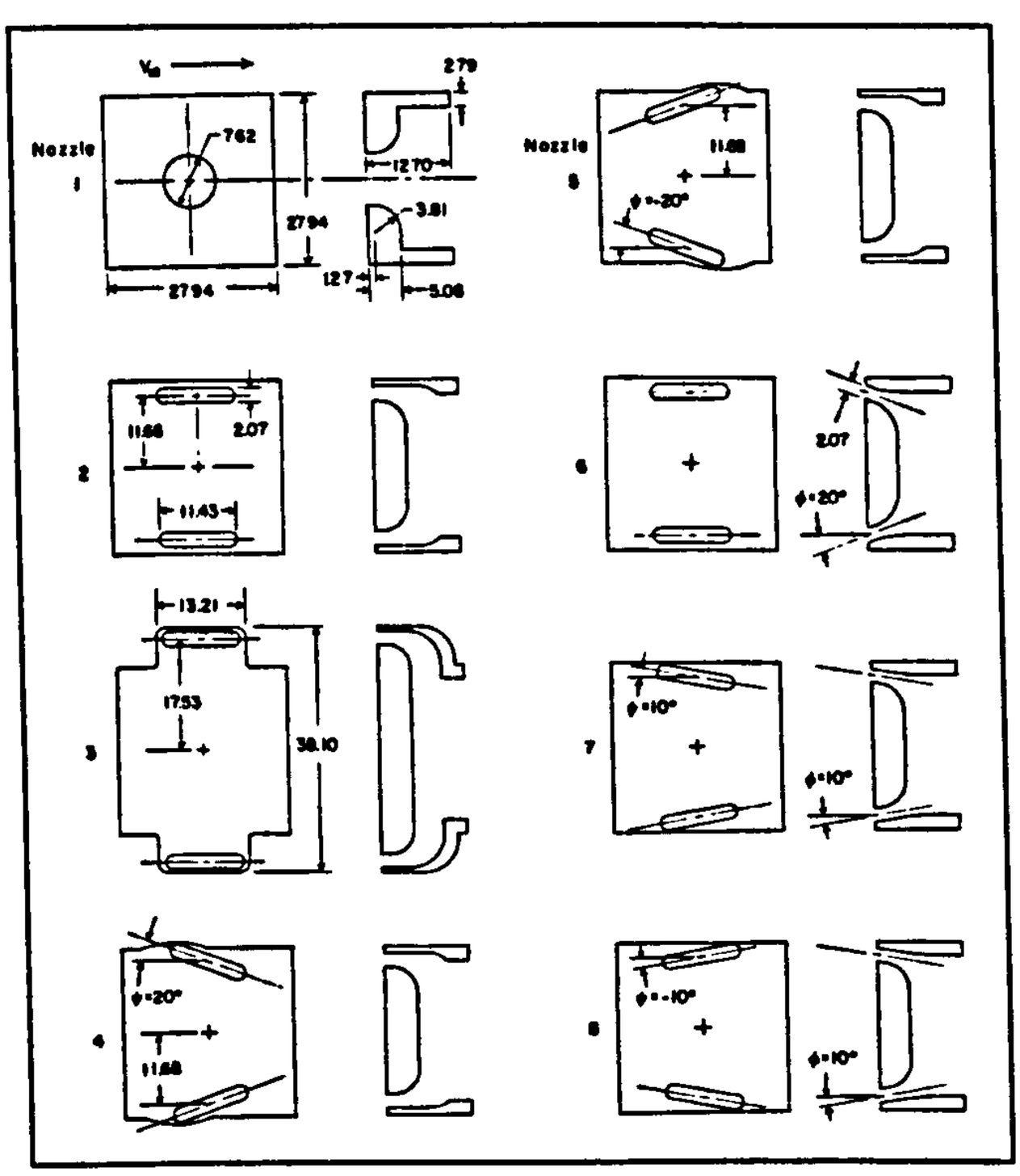

***Figure 2.14** - Bottom views and lateral sections of nozzle configurations investigated by VOLGER & GOODSON, 1973.*

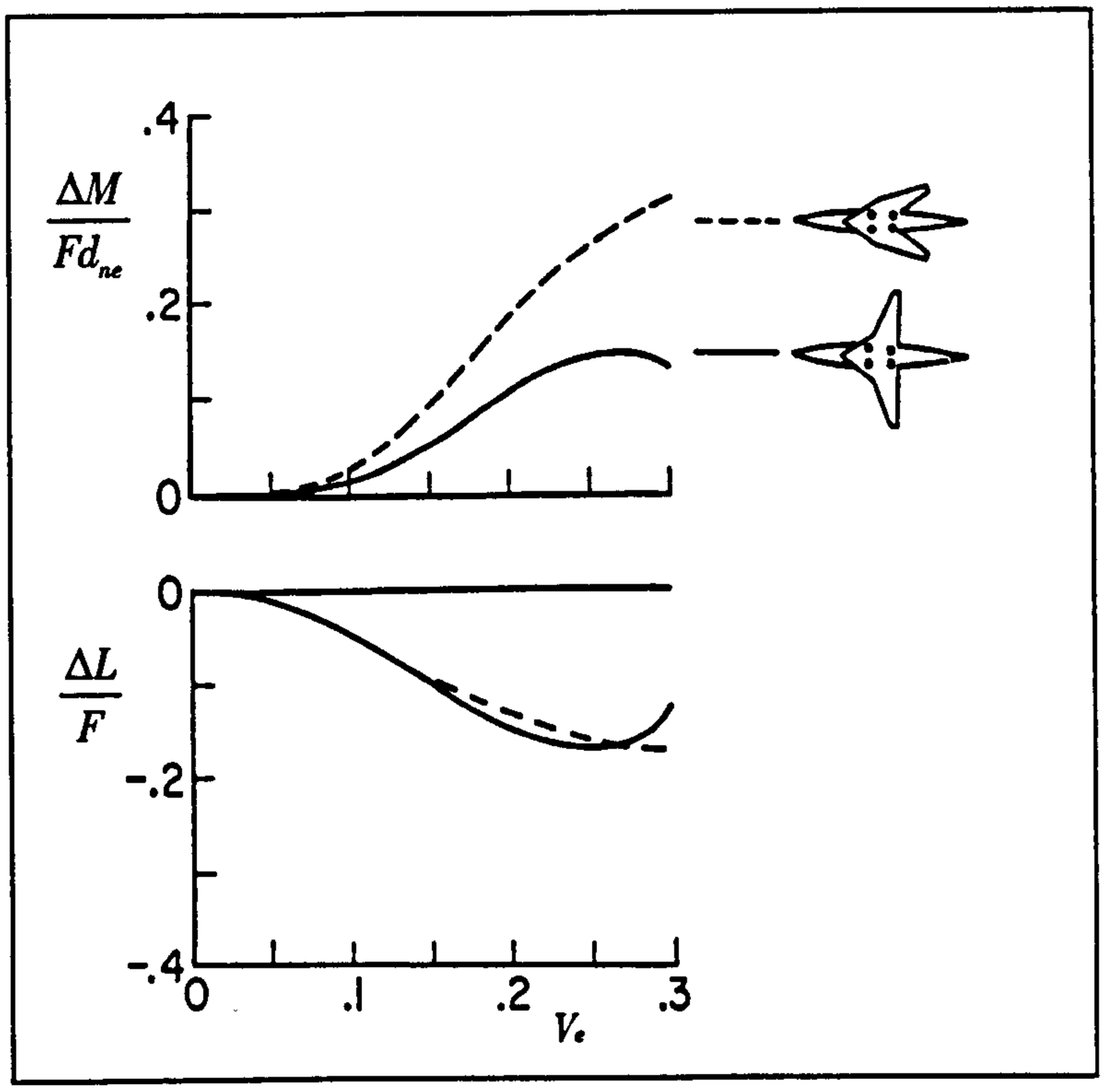

***Figure 2.15** - The effect of wing planform on lift and pitching moment (OTIS, 1962).*

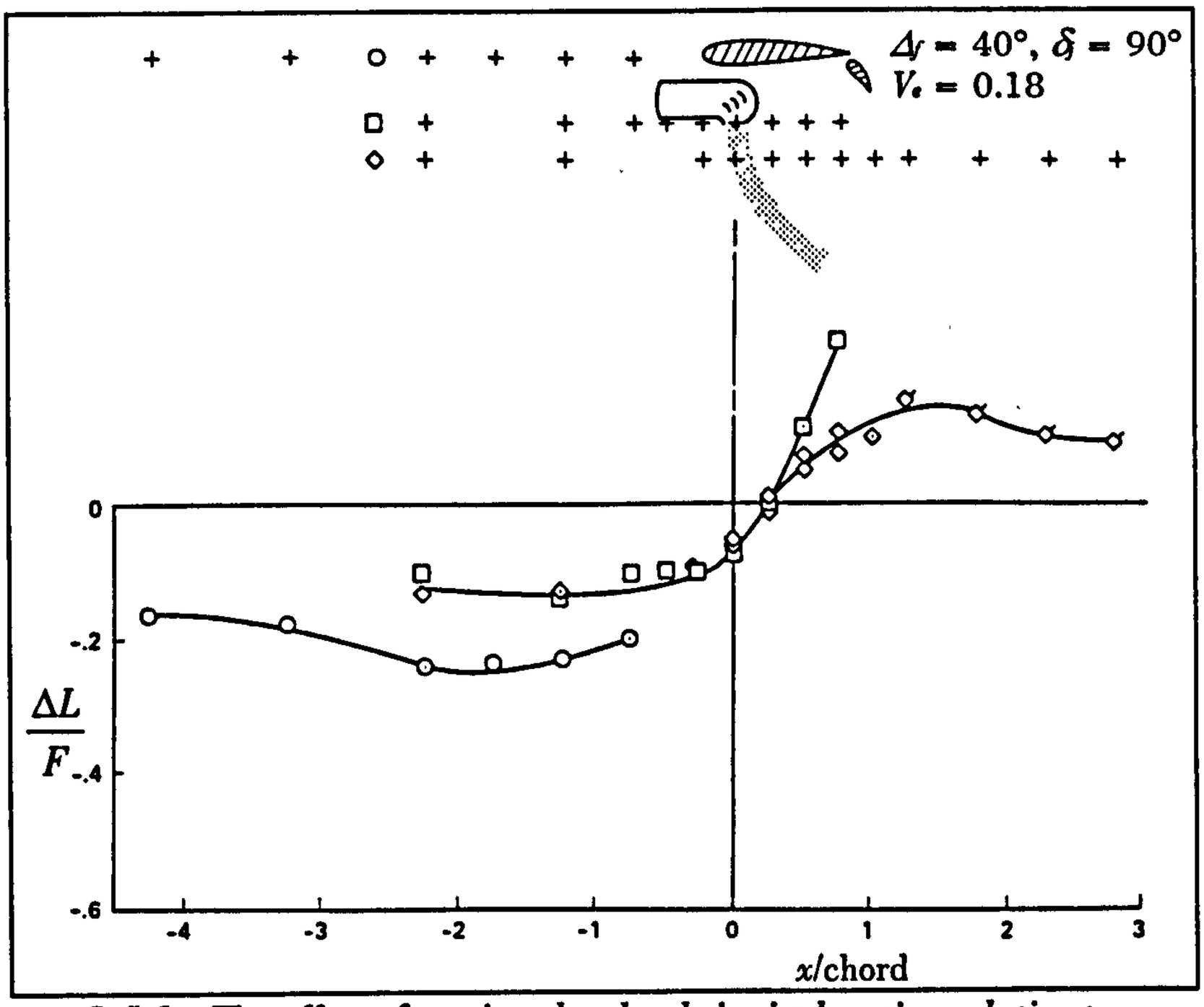

***Figure 2.16** - The effect of varying the chordwise jet location relative to a nearby wing on the induced lift (HAMMOND & MCLEMORE, 1967).*

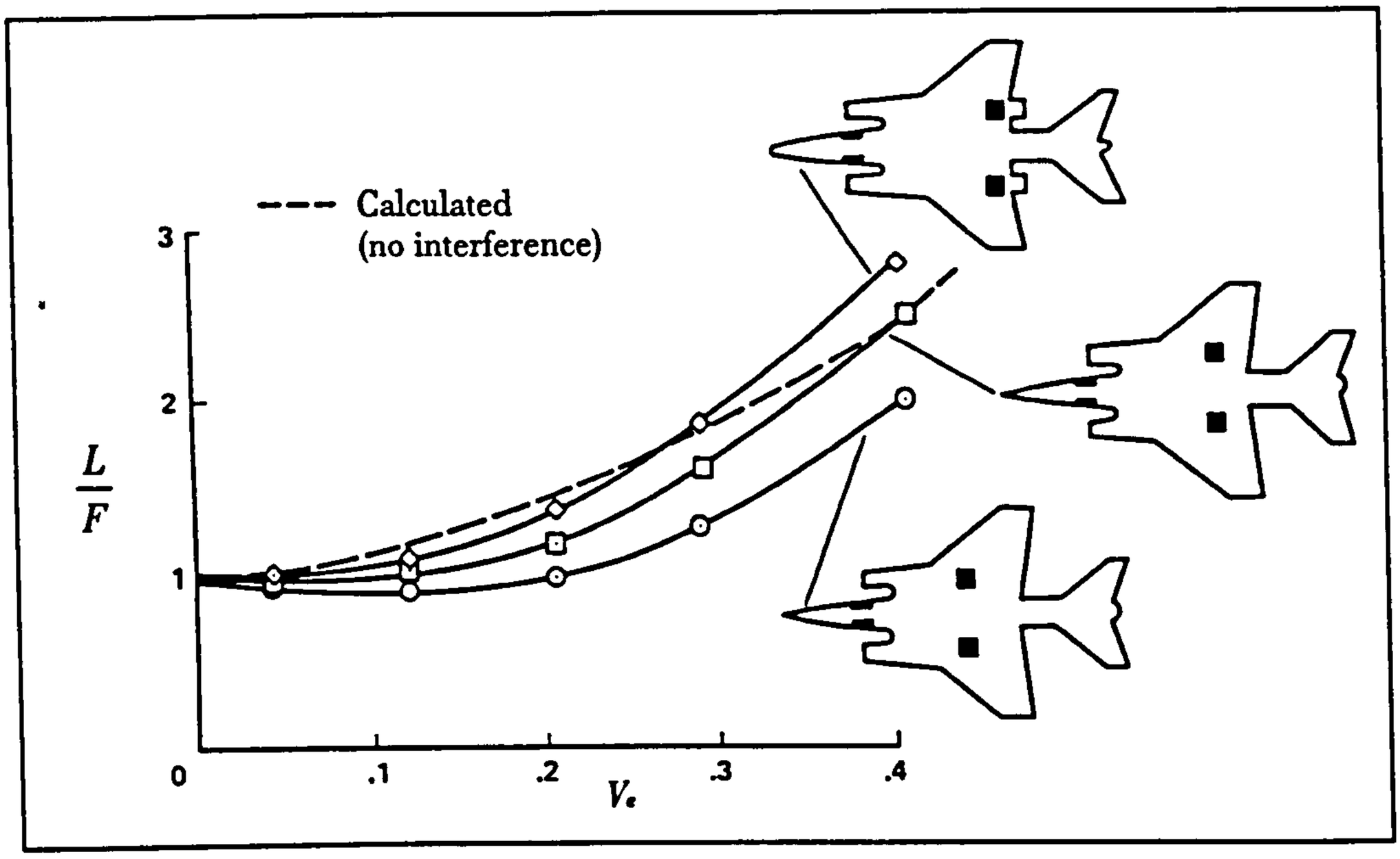

***Figure 2.17** - The effect of chordwise location of deflected lift/cruise jets relative to the wing tailing edge on the total lift for a supersonic combat lift plus lift/cruise VSTOL aircraft configuration (WINSTON et al., 1975).*

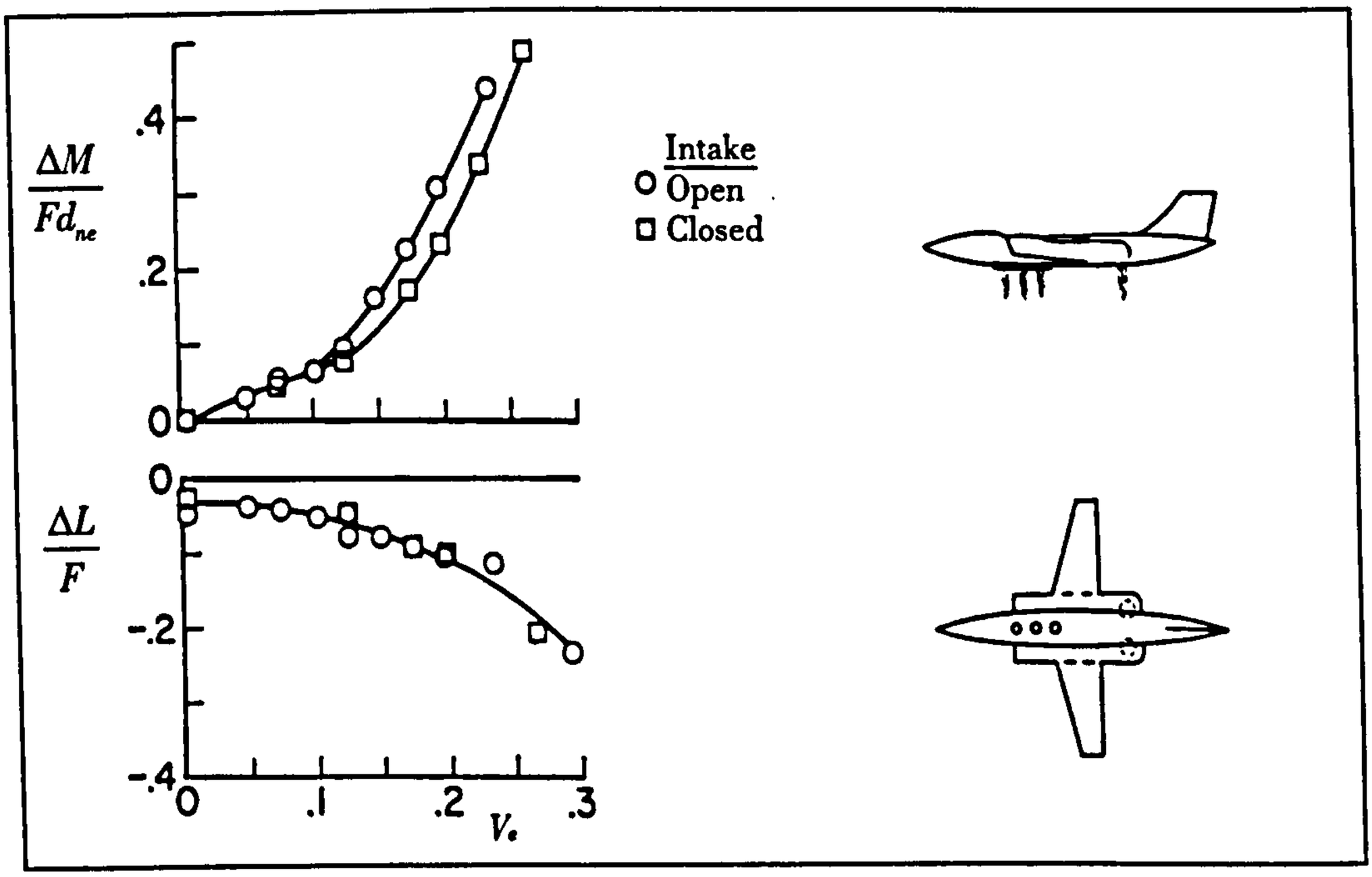

***Figure 2.18** - The effect of inlet flow on a STOVL model out of ground effect (MARGASON & GENTRY, 1968).*

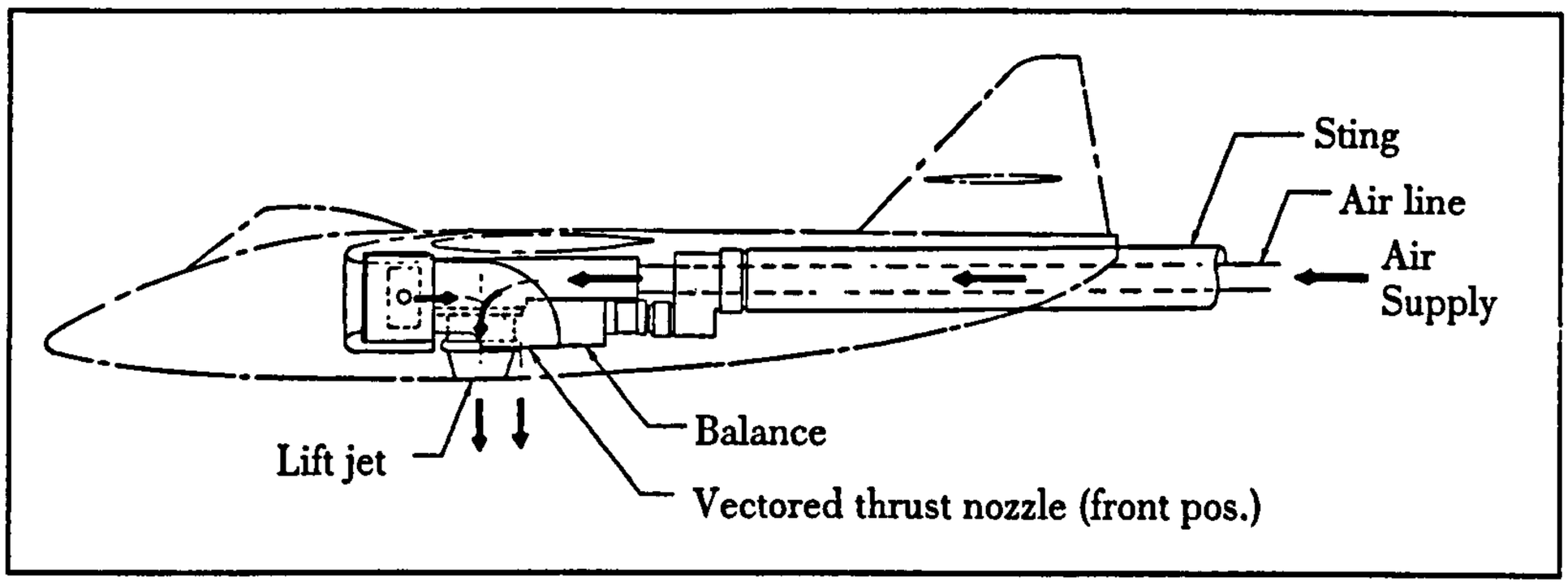

***Figure 2.19** - Side view of the high pressure air system used by MINECK & SCHWENDERMANN, 1973 to simulate thrust.*

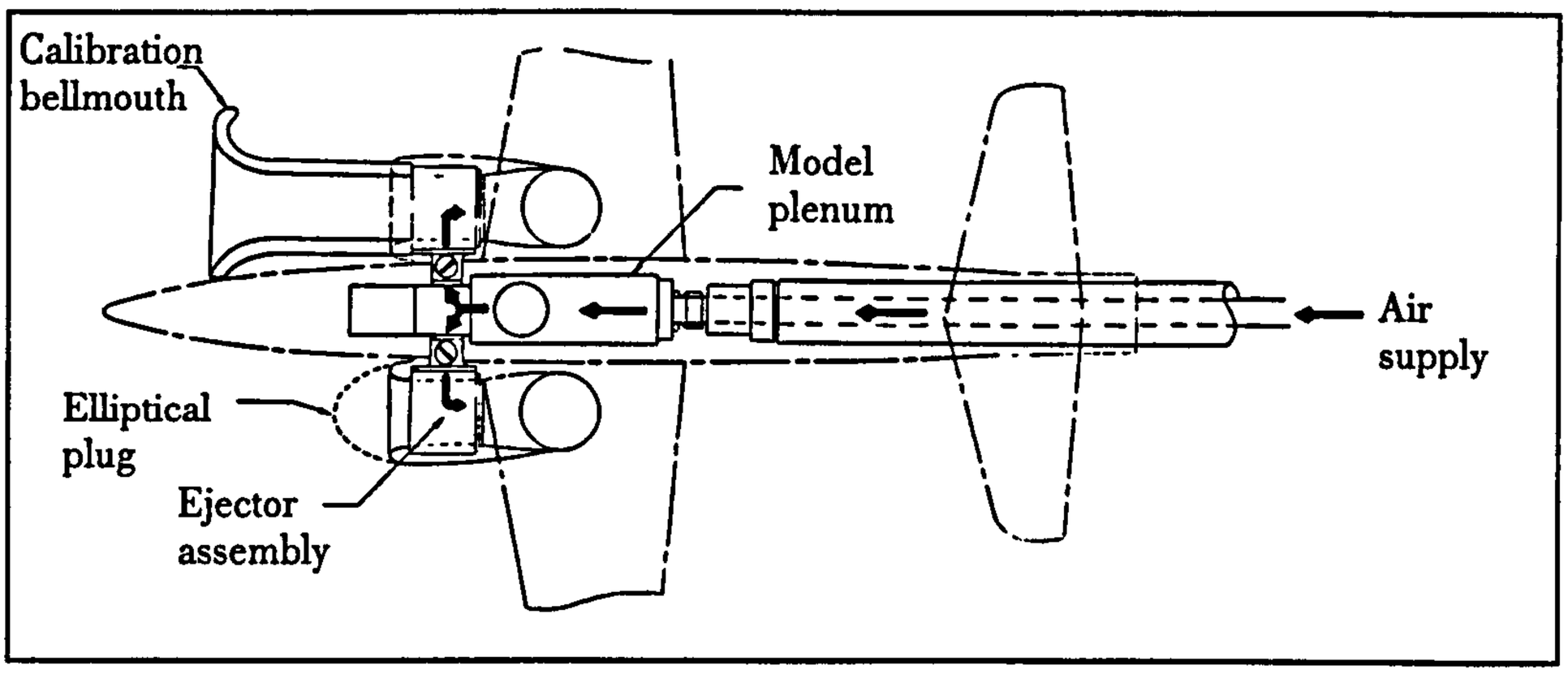

***Figure 2.20** - Top view of the high pressure air system used by MINECK & SCHWENDEMANN, 1973 to simulate thrust.*

3 Experimentation

In this chapter the design of a wind tunnel model providing jet and intake simulation on a generic STOVL aircraft is described. The development of the associated experimental facilities is discussed and the experimental programme then outlined. The chapter concludes with an analysis of the experimental errors. The results obtained from these experiments will be discussed in Chapter Four.

3.1 Design and construction of the wind tunnel model

Chapter One outlined the main aim of the current research which was to determine the significance (if any) of the mutual interference between jet and intake flows on a generic jet-lift STOVL aircraft. In Chapter Two it was established that, although previous STOVL research has looked at jet/intake interference, the results obtained so far are inconclusive. It was, therefore, necessary to carry out a series of experiments systematically to investigate and quantify these interference effects. The results of the experiments would determine if the practice of linearly adding the results from isolated jet and intake tests is valid for STOVL aircraft.

A test vehicle was needed to investigate the jet/intake interference effects. From the outset it was felt that the model should be entirely generic and therefore no attempt was made to model an existing STOVL aircraft. The model selected was a tail-less, shoulder-wing design of approximately 1 metre span with a single, vectored lift-jet and rectangular, side-mounted intakes. Within the time-scale and funding available, it was not possible to design a fully-metric wind tunnel model with simultaneous jet and intake simulation. The aircraft forces, therefore, were to be inferred from surface pressure data on the wings and intakes. The essential requirements for the wind tunnel model were as follows.

- A single, convergent jet nozzle at a fixed vector angle which could be moved longitudinally relative to the wing and intakes.
- Tests to be conducted at three nozzle pressure ratios: NPR = 2.0, 3.0 and 4.0.
- A constant jet mass flow rate across the NPR range, equivalent to a 25.4 mm (1 inch) diameter nozzle at a NPR of 2.0.
- Side-mounted 'powered' intakes with pressure tappings around the lips.
- A wing with flaps and a suitable aerofoil section, pressure-tapped around the root.
- Tests to be conducted out of ground effect at a variety of wind tunnel speeds.

If time permitted, it was also desirable to conduct the following tests.

- Provide a low pressure ratio jet (NPR = 1.5) with 50% more mass flow than above, to simulate a remote lift-fan (see Figure 1.8).
- Tests to be conducted at a variety of pressure ratios (NPR = 1.5, 2.0, 3.0 and 4.0) with a constant nozzle area to investigate the effect of varying jet mass flow rate. The 25.4 mm (1 inch) diameter nozzle was chosen for this.

3.1.1 Jet simulation

Four alternative ways of simulating in the wind tunnel the air flow through the lift-jet were investigated. The first of these was the use of a small axial-flow fan driven by an electric motor. It soon became apparent, however, that a fan and motor arrangement of the size which could be fitted into the model would not be able to provide sufficient mass flow rate nor the high pressure required.

The second alternative was to use a model aircraft gas turbine. These are generally of the centrifugal type and are often based on commercial vehicle turbo-chargers. An engine was identified* which was able to produce a greater mass flow rate than the electric motor driven fan but still fell short of the figure required. Such an engine also introduced a number of environmental problems including the introduction of heat and combustion products into the wind tunnel air flow, excessive noise and potential dangers from fire or turbine failure.

It was decided that the best way to power the lift-jet would be through the use of compressed air which is a 'clean' power source. The use of an ejector was an attractive proposition as this would have provided both jet and intake flows with a single unit. This was, however, eventually discounted on the grounds of cost and complexity of design. Previous STOVL jet work at RMCS had also used compressed air but the jet(s) was (were) powered directly by the compressed air and a suitable supply was already in existence. The distribution of compressed air to one of three nozzle positions required the use of a settling chamber.

The settling chamber chosen was based on a design proposed and built by POWER, 1989 at RMCS and subsequently used extensively by BRAY, 1992, WILSON, 1995 and MYSZKO, 1997. In order to maximise any jet/intake interference effects, it was desirable to keep the intake separation as small as possible implying a narrow settling chamber. The minimum width of the settling chamber was determined by the 63.5 mm (2½ inch) diameter compressed air supply pipe.

The settling chamber was made up of four sections. The top plate (Figure 3.1) was constructed of 10 mm steel plate which had a threaded collar welded to it. This connected the settling chamber to the 63.5 mm (2½ inch) semi-flexible compressed air supply pipe. The second and third sections (Figures 3.2 and 3.3) formed the volume of the settling chamber, which was approximately 1.5×10^{-3} m^3. They were machined from a solid block of aluminium with 20 mm-thick walls. The wall of the second section was drilled to accommodate a brass total pressure probe for monitoring the settling chamber total pressure. The bottom section (Figure 3.4) was again machined from solid aluminium and had fittings for the three nozzle positions. The nozzles screwed into the fittings and were vectored aft 60 degrees to the horizontal. The settling chamber was fitted with baffles and filter material between sections one

---

* *JPX T-240 centrifugal gas turbine engine, Westbury Products UK.*

and two, and two and three. This, it was hoped, would provide an evenly-distributed flow through the chamber and prevent particulates from eroding the internal surface of the nozzle.

3.1.2 Jet nozzles

A single jet nozzle was provided, representing the forward lift-jet of a STOVL aircraft, vectored aft 60 degrees to the horizontal. This vector angle was chosen as being typical of a STOVL aircraft in transitional flight. The nozzle could be located in one of three positions relative to the wing and intakes as determined by the settling chamber; 90 mm (approximately $2d_{ie}$) aft of the intake plane (in line with the wing root leading edge); in the same plane as the intake; or 90 mm ahead of the intake plane (see Figure 3.22).

Four nozzle pressure ratios were to be tested. Three of these simulated a lift-jet of nozzle pressure ratio (NPR) 2.0, 3.0 and 4.0 respectively. The fourth simulated a lift-fan of pressure ratio 1.5. The mass flow rate through the lift-jet nozzles was kept constant, requiring nozzles with different areas. The base-line for the lift-jet mass flow rate was a 25.4 mm (1 inch) nozzle at a NPR of 2.0. The mass flow rate through a choked convergent nozzle is given by Equation 3.1.

$$\dot{m} = \frac{AP}{\sqrt{T}}\sqrt{\frac{\gamma}{R}\left(\frac{2}{\gamma+1}\right)^{\frac{\gamma+1}{\gamma-1}}} \tag{3.1}$$

where in this case:

$A = A_n$

$P = P_c \quad = 202650$ Pa.

$T = T_c \quad = 288$ K.

For a nozzle of 25.4 mm (1 inch) diameter and a NPR of 2.0, the mass flow rate, $\dot{m}$ is 0.245 kgs^{-1}. Keeping the mass flow rate constant and solving for A_n, gives the required nozzle diameters of 20.74 mm and 17.96 mm at NPRs of 3.0 and 4.0 respectively.

A nozzle with an NPR of 1.5 passing 50 percent more mass flow rate was also required, to simulate a remote lift-fan. During the design of this nozzle, a mistake was made in the calculation of the jet exit area. Equation 3.1 was used, giving a nozzle exit diameter of 35.92 mm whereas the expression for an unchoked nozzle (Equation 3.2) should have been used.

$$\dot{m} = \sqrt{\frac{\gamma}{R}}\frac{AP}{\sqrt{T}}\frac{M}{\left[1+\left(\frac{\gamma-1}{2}\right)M^2\right]^{\frac{\gamma+1}{2(\gamma-1)}}} \tag{3.2}$$

This gives a jet nozzle exit diameter of 36.73 mm. If the smaller nozzle were run at an NPR of 1.5, this would give an error of 4.34 percent in the required mass flow rate. This is clearly unacceptable and so the 35.92 mm nozzle was run at an NPR of 1.586 to maintain the required mass flow rate. The tests were run at constant NPR, so a slight variation in mass flow rate was expected due to changing ambient conditions. A summary of the jet nozzle diameters required for different NPRs is given in Table 3.1 below.

***Table 3.1** - Nozzle diameters for various NPRs.*

NPR	1.5	1.586*	2.0	3.0	4.0
$\dot{m}$ ***(kgs^{-1})***	0.367	0.367	0.245	0.245	0.245
d_n ***(mm)***	36.73	35.92	25.4	20.74	17.96

The jet nozzles were of a simple convergent design. The nozzle convergence had a length equal to one quarter of the exit diameter and an angle of 10 degrees. In order to keep the nozzle blockage as consistent as possible, the outer diameter was kept constant. This did mean, however, that the external nozzle taper angle changed between the different sizes. Drawings for the four jet nozzles used are given in Figures 3.5 to 3.8. Figure 3.9 shows a photograph of one of these jet nozzles. A set of spacers, which adapt the exit hole in the settling chamber to that of the nozzle were also made and these are shown in Figure 3.10. With only one nozzle being used at a time, plugs were required to block off the other two exits and these are shown in Figure 3.11.

3.1.3 Intakes

It was assumed that the STOVL configuration being represented would have vectoring lift-jets arranged in tandem and that the rearmost jet would not produce a significant interference effect compared with the front one. Thus, only one vectoring lift-jet was simulated, but the intakes had to 'suck' enough air for both jets.

The intakes were required to have an inlet Mach number such that their effect on the jet flow would be similar to full scale and there should still be an acceleration of freestream air into the intake at the maximum wind tunnel velocity during testing (30 ms^{-1}). Any deflection of this capture streamtube by the jet would be indicated by a change in the pressure distribution around the intake lips. An intake throat velocity of at least three times the wind tunnel maximum velocity was desirable. An inlet Mach number of 0.3 was therefore chosen. Using Equation 3.2 with the following parameters:

---

* *This column shows the actual nozzle used for lift-fan testing.*

$M = M_i$ = 0.3

$P = P_i$ = 101325 Pa

$T = T_i$ = 288 K

$\dot{m} = \dot{m}_i$ = 0.489 kgs^{-1}

gave an area of 2.062×10^{-3} m^2 per intake. This was approximated to 2.0×10^{-3} m^2, thus giving an exact known intake area. Choosing an intake with a 2:1 aspect ratio and parallel sides, this translated to a height of 63.2 mm and a width of 31.6 mm. An elliptical lip section was chosen with an aspect ratio of 3:1. A boundary layer diverter was fitted to the intake to try to prevent the fuselage boundary layer from being ingested into the intake.

The rectangular cross-section aided construction and the installation of static pressure tappings. There are 46 static pressure tappings of 0.5 mm diameter located on the centre-line of the starboard upper and lower, inner and outer surfaces. Hole diameters below 0.5 mm result in large response times and the holes are easily blocked by dust in the flow. Larger holes, however, are less accurate because of the amount of distortion they introduce into the flow-field [ARTS *et al.*, 1994].

Due to manufacturing limitations, the intakes were made in two halves, split along the horizontal axis. Drawings for the intakes are given in Figures 3.12 to 3.15. Figure 3.16 shows the intakes and the ducting which takes the intake air along the side of the fuselage to the rear of the model, combining to form a single circular exit. Figure 3.17 shows the intake 'plugs' which divert the airflow around the intakes for tests without intakes 'sucking' (model configurations 'A' and 'B' - see Section 3.3).

The shape of the intake plugs was decided upon after consultation with Dr Bruce of DERA (Farnborough). An elliptical shape is often used as a standard intake fairing for semi-circular intakes. For the rectangular intakes on the test model, the intake fairing was chosen to be a two-dimensional ellipse of aspect ratio 3:1. This intake fairing does not necessarily represent the most appropriate 'no intake' simulation but was designed to represent the type of intake fairing used on wind tunnel models where intake simulation is not provided. It is possible that a mutual interference between the jet and fairing might exist. This would probably take the form of a change in the jet entrainment flow-field. This was expected to be small although, due to insufficient time during the test programme, it was not possible to confirm this with measurements. The interference between the intake fairing and the jet was therefore assumed to be zero. Figure 3.18 shows the starboard intake with the boundary layer diverter installed and a jet nozzle in the forward position.

3.1.4 Wing

The wing span of the model was limited by the size of the wind tunnel working section. The width of the wind tunnel jet, which is elliptical in section, is 1.5 metres. A

wing span of 1 metre was therefore chosen for the model. The aerofoil section selected was a NACA 1408. The 8 percent thickness to chord ratio was representative of high subsonic speed aircraft and a 1 percent camber was chosen to give some lift at zero incidence. A plain flap was included with a hinge-line at 75 percent chord. The flap extends from 30 percent to 70 percent semi-span and can be deflected up to 50 degrees. A flap setting of 45 degrees was chosen for the tests. This is similar to that used by the Harrier in short take-off configuration. A total of 33 static pressure tappings, at spacings of approximately 5 percent chord, were set into the wing upper and lower surfaces at 25 percent semi-span, just outboard of the wing root, but inboard of the flap root. Space limitations, and the difficulties of routing the tubing through the flap hinge precluded it from being pressure tapped. The pressure tappings were again 0.5 mm in diameter.

Originally, the intention was to make the wing from aluminium, but the RMCS workshop was unable to perform the three-dimensional machining required. The use of an external contractor to build an aluminium wing proved too costly. It was therefore decided that the author's aero-modelling knowledge would be used to build the wing (Figure 3.19). It was constructed from a core of high density expanded polystyrene foam. Two sets of aluminium tip and root templates were made by the RMCS workshop to the aerofoil section used, one set for cutting the core and the other set for finishing the wing skin. The core templates were tack-glued to a block of the foam and the wing core was cut using a hot-wire cutter. The core templates were then removed. The foam core was then grooved at 25 percent and 75 percent chord top and bottom. Kevlar strands soaked in epoxy resin were then laid into the grooves and allowed to harden. These created the front and rear wing spars. Two hardwood blocks were then set into the wing root at the spar locations. When drilled and tapped these would provide locations for fixing the wing to the fuselage.

The leading and trailing edges were then added along with the root and tip balsa sections. The wing was then skinned with 1.5 mm balsa and given a final sanding, using the skin templates to maintain the correct aerofoil shape. Next, the static pressure tappings were set into the starboard wing at the locations shown. Finally the wing was finished in two-part epoxy resin and fine fibre-glass cloth. The pressure tappings were then opened up. When the pressure tappings were checked it was discovered that some were blocked. If the blockage could not be cleared the tube for the tappings had to be cut out of the wing and re-fitted. Figure 3.20 shows the starboard wing and pressure tappings. The flap is shown in the test position of 45 degrees.

3.1.5 Fuselage

The fuselage was approximately square in cross-section and constructed from 3 mm marine ply and 1.5 mm balsa. It connects together all the components described above to form a tail-less aircraft. The nose was made from the same foam as was

used for the wing. The nose was shaped by hand since no automated machining was available which could generate the complex blending required. The profile is a blending of a rectangular section to a circular section.

The tubing for the pressure tappings was routed into the fuselage from the wing and intakes, out of the top and through a corrugated flexible duct. The duct was fixed to the back of the compressed air supply pipe and carried the pressure tapping tubing out of the tunnel working section to the Scani-Valves (described later). Part of the duct for the tubing can be seen in Figure 3.18.

Access panels were fitted to the model on the upper and lower surfaces of the fuselage. The upper surface panels provided access to the wing mounting bolts, the fuselage-to-settling chamber mounting bolts and the connections for the pressure tapping tubing. The lower surface panels provided access to the three vectored nozzle positions on the settling chamber.

The fuselage was finished with epoxy resin in the same way as the wing to provide a smooth durable surface. The model took approximately six months to complete. A general layout of the model is shown in Figures 3.21 and 3.22.

3.2 Experimental facilities

This section describes the development of the experimental facilities which was necessary before the start of the current experimentation. Although the wind tunnel area had already been used for the study of high-speed jets, a number of modifications and additions had to be made to the facilities before the current testing could commence. This mainly regarded the wind tunnel speed-control and compressed air pressure-control systems. As will be seen later, this delayed the start of experimentation somewhat.

3.2.1 Wind tunnel

All tests were carried out in a return flow, open-jet wind tunnel at RMCS. This section describes the general layout of the tunnel, the method by which the tunnel was speed controlled using a 286-based computer, and the calibration of the tunnel for testing purposes.

3.2.1.1 Description

A general layout of the tunnel is shown in Figure 3.23. The tunnel cross-section is basically a rectangular octagon changing to a circular section for the four-bladed, fixed-pitch hardwood fan, which is 1.59 m (62.75 inches) in diameter. The contraction ratio used is approximately 3.3 and a gauze screen is fitted at the outlet from the fourth corner, supported around the periphery by springs. From a regular octagon at this point, the duct expands to an irregular octagon at the commencement of

the contraction. The elliptical nozzle is obtained by fairing the 1.52 m (5 foot) by 1.14 m (3.75 foot) circumscribing octagon. The overall dimensions of the elliptical nozzle are therefore 1.52 m by 1.14 m (5 foot by 3.75 foot) The contraction and nozzle section of the tunnel is mounted on a rotating gear assembly which enables the nozzle major axis to be fixed in an upright or horizontal position depending on the type and geometry of model being tested. For the tests carried out, a horizontal position was chosen to enable a reasonable-size wing span model to be used. The working section is 2.13 m (7 foot) long and the maximum wind tunnel air velocity is approximately 32 ms^{-1} with a 'clean' test section.

3.2.1.2 Speed control hardware

The tunnel was powered by a 56 kW (75 h.p.) electric motor running at 1460 rpm and driving through a Dowty 'Dowmatic' Hydrostatic transmission incorporating a servo-operated swash plate. This controls the flow of hydraulic fluid to the motor located in the fan fairing, providing a means of speed control. At some point prior to the current research, the servo had been replaced by a remotely-operated manual control system (Figure 3.24). A small control box housed two buttons for increasing or decreasing the tunnel speed. The control box was linked to an RS 4-phase unipolar stepper motor drive board which provided power to the actuator and simple control functions such as direction and speed. Two 'end stop' micro-switches prevented the operator from exceeding the travel on the hydraulic fluid control valve by cutting the power to the linear actuator. The control box disabled the appropriate micro-switch in order to bring the control valve off the micro-switch, e.g., if the 'over-speed' micro-switch had been activated then pressing the 'decrease speed' button will disable the switch, enabling the wind tunnel speed to be reduced. This system required the operator to be present during the tests to set a particular tunnel speed manually and, at best, tunnel dynamic pressure could only be maintained to ± 5 percent.

An automated speed control driven by a computer was therefore needed. The ideal solution was to replace the existing hydraulic drive and motor arrangement with a modern thyristor-controlled d.c. motor and drive combination which would then be controlled directly by computer. At the time, this was deemed too expensive and time consuming, so an alternative was sought. It was decided that the simplest form of control would be to have a computer operate the actuator. Figure 3.25 shows a flow diagram for the automated control system. The output from the CIL S-block links in to the RS stepper motor drive board (the S-block providing the control signal and the RS board providing the power signal) this enabled the computer to move the actuator, thus changing the wind speed in the tunnel.

For the computer actually to control the speed, it required information about the wind tunnel dynamic pressure. This was read by a Furness Controls FCO34 differential strain gauge pressure transducer, outputting a voltage between 0 V and 5 V

over a pressure range of 0 mm to 100 mm w.g. with a claimed accuracy of ±1 percent of reading. The output voltage from the pressure transducer was read by a four-input 12-bit CIL 'mini-pod' analogue to digital converter (ADC). This reads voltages from 0 V to 4.096 V, giving a theoretical resolution of ±1 mV (±0.1962 Pa). A k-type thermocouple reads the air temperature in the tunnel.

3.2.1.3 Calibration

Good calibration of the wind tunnel was essential for accurate results. All the data collected were in the form of pressures which needed to be converted to pressure coefficients, requiring an accurate value for dynamic pressure. The calibration of the wind tunnel dynamic pressure was based on a method suggested by KUENSTNER *et al.*, 1992 for open-jet wind tunnels. Two pressure tappings were located in the roof of the tunnel settling chamber, either side of the centre-line and linked together using some PVC tubing. Two more pressure tappings were situated in the roof of the tunnel nozzle, again either side of the centre-line. The free stream dynamic pressure, q_∞ was determined by Equation 3.3 as follows:

$$q_\infty = (p_{ts} - p_{tn})k_{t1} + k_{t2} \tag{3.3}$$

A Pitot static probe, mounted in the working section of the wind tunnel, and connected to the FCO34 pressure transducer, was used to read q_∞. An FCO44* pressure transducer was used to read $(p_{ts} - p_{tn})$. A graph showing the calibration is given in Figure 3.26. From this, k_{t1} was found to be 0.808 and k_{t2} was +4.942 Pa. Once the calibration coefficients were known, they could be used in the wind tunnel control software.

With the test model in the tunnel, the undisturbed static pressure of the flow could no longer be determined directly. It could, however, be related to a flow equivalent pressure, the tunnel nozzle static pressure, p_{tn}. In general static pressure coefficient C_p is defined as

$$C_p = \frac{p - p_\infty}{q_\infty} \tag{3.4}$$

A static pressure offset, k_p was introduced by adding and subtracting p_{tn}.

$$C_p = \frac{p - p_\infty + p_{tn} - p_{tn}}{q_\infty} \tag{3.5}$$

$$\therefore \quad C_p = \frac{p - p_{tn}}{q_\infty} - \frac{p_\infty - p_{tn}}{q_\infty} \tag{3.6}$$

---

* *This is identical to the FCO34 but can read negative differential pressures.*

$$\therefore \qquad C_p = \frac{p - p_m}{q_\infty} - k_p \qquad (3.7)$$

A graph showing the calibration line for k_p is given in Figure 3.27 and was determined to be -0.122.

3.2.1.4 Speed control software

The software which set and maintained the wind tunnel speed was written in FORTRAN 77. A flow chart showing the main structure of the program is given in Figure 3.28. When the user inputted a required wind tunnel speed, the computer estimated the number of steps to move the linear actuator and then moved it. It then read the new dynamic pressure and adjusted the actuator accordingly. The computer could set and maintain a constant dynamic pressure to an accuracy of ± 0.25 percent over a range of 50 Pa to 600 Pa. The time taken to establish an 'in tolerance' dynamic pressure was approximately 60 seconds.

3.2.1.5 Wind tunnel interference

The interference between the model and the wind tunnel should be considered. The main interference effect is on the measured lift coefficient. For a lifting wing in a closed wind tunnel, the lift-induced downwash is impeded by the tunnel walls causing the streamlines around the wing to be flattened. The result is an effective reduction in induced drag and incidence. A correction must therefore be applied to the measured drag and incidence. As an example, an Auster wing (NACA 23012 aerofoil section) of 1.11 m span tested in the RMCS closed wind tunnel (1.52 m by 0.91 m) requires an incidence correction of about 1.0 C_L degrees. This gives approximately a 1 degree increase in the measured incidence at stall. The opposite effect is generated by an open-jet wind tunnel. In this case the wind tunnel air flow is less than the infinitely large stream upon which the aircraft acts in free air. It is easier for the lift-induced downwash generated by a wing to deflect the constant pressure boundary of the wind tunnel flow than an equivalent streamline in free air. In this case a correction should be applied which reduces the measured drag and incidence. This correction, however, is typically an order of magnitude smaller than that needed in a closed tunnel.

For STOVL aircraft, the situation is complicated further by the lifting jet(s). Not only does the interference between the wind tunnel airflow and the model need to be considered but also the interference between the wind tunnel airflow and the direct lift system (in this case the compressed air jet). Although several experimental studies have been made of wind tunnel interference on STOVL configurations, there are no generally accepted correction factors. MASKELL, 1966 concluded that if the overall performance of a particular STOVL aircraft depended on the mutual interference between the different lifting elements and their associated flow-fields, then

there was little prospect of deriving adequate wind tunnel corrections until the nature of the interference was better understood. Although there has been significant progress in the understanding of STOVL interference effects in the past 30 years, it is the author's belief that there is still insufficient understanding of the aforementioned interference effects to enable an accurate mathematical model describing wind tunnel/model interference for a STOVL jet-lift configuration. HEYSON, 1978 in addition advises caution in the use of open-jet wind tunnel corrections with STOVL models. Firstly, the wind tunnel jet boundaries are shifted due to the presence of the model and jet(s) and secondly for STOVL aircraft at low speeds, the jet velocities may be larger than the freestream velocities (as is the case here). Both effects, states HEYSON, will invalidate the use of classical open-jet wind tunnel corrections. There are as yet, however, no alternative theories as to the treatment of these problems.

The blockage effect of the model on the wind tunnel flow was taken into account by the calibration of the wind tunnel and its control software. The calibration technique automatically compensated for changes in blockage (due to difference in jet deflection for example), maintaining a constant wind tunnel dynamic pressure. The wing lift and jet interference on the wind tunnel airflow is expected to be small but this was not checked and therefore should be borne in mind when interpreting the present results. The experiments reported here were not, however, necessarily concerned with reproducing free flight conditions, merely with correctly identifying, and quantifying, a possible mutual interference effect which would otherwise be overlooked in separate (usually closed) wind tunnel tests. As a consequence of this discussion the effect of wind tunnel interference will be neglected from the test results although the reader should be aware that in reality a wind tunnel interference will most probably exist.

3.2.2 Compressed air supply

3.2.2.1 Description

As mentioned earlier, a substantial compressed air supply system was already in place to power the lift-jet. The compressed air was supplied by two 261 kW (350 h.p.) Howden rotary screw compressors which could be run in parallel or series and supply up to 0.9 kgs^{-1} at 7 bar gauge (series) or 1.8 kgs^{-1} at 4 bar gauge (parallel). This enabled all tests to be run continuously. The air was fully dried and passed through a 34 m^3 storage vessel, which acted as a heat sink, before entering the laboratory. This meant that the air entering the wind tunnel model settling chamber was at ambient temperature.

3.2.2.2 Pressure control hardware

It was required that the nozzle pressure ratio should be kept as constant as possible. A pressure control system was already in place to control the compressed air to the jet nozzle. A schematic diagram showing the pressure control hardware is shown in Figure 3.29. Figure 3.30 shows the control system with pressure transducers and emergency stop button.

The compressed air from the storage tank entered the laboratory via a 127 mm (5 inch) diameter pipe, reducing to 63.5 mm (2½ inch) diameter, and into Regulator 1. Regulators 1 and 2 were of the pressure-operated type. The control pressure was supplied by a Bristol compressor. Regulator 1 was used to step the supply pressure down from 7 bar gauge to 4 bar gauge. Regulator 2 was operated by a Watson-Smith 101X electropneumatic converter. This device output a pressure proportional to a supplied voltage and had a maximum input pressure of 8 bar gauge. The voltage was supplied by a CIL O-block 16-bit digital to analogue converter (DAC) with a range of 0 V to 5 V.

The settling chamber pressure was read using a Druck PDCR 810 pressure transducer with a pressure range of 0 bar to 3.5 bar gauge. The output from the pressure transducer was in the range 0 V to 100 mV. This was then amplified by 50 using a CIL B-block to give an output range of 0 V to 5 V. Atmospheric pressure was read using a Setra model 270 pressure transducer with a 0 V to 5 V output and a range of 800 mbar to 1100 mbar absolute. All voltages were read using two four-channel CIL 16-bit analogue to digital converters (ADC) to be processed by the pressure control and data acquisition software. There were also three k-type thermocouples to measure the ambient, settling chamber and wind tunnel air temperatures.

3.2.3 Additional instrumentation

The large number of pressure tappings in the model meant that it was uneconomical to attach a pressure transducer to each one and so two 48-port mechanical scanning valves supplied by Scani-Valve Ltd. were used. The first Scani-Valve had the 46 intake pressures as its inputs and the output went to the first input of the second Scani-Valve. Inputs 2 to 34 of the second Scani-Valve were used for the wing pressures with the output going to a Furness Controls FCO14 micromanometer. This is a multi-range device with full-scale readings of 10 mm, 100 mm and 1000 mm w.g. The intake pressures were read on the 1000 mm scale and the wing pressures were measured on the 100 mm scale. Unfortunately, the micromanometer had no means by which the scale could be switched by computer and so it had to be done manually by the researcher. The Scani-Valves were driven by a CIL R-block relay via a Scani-Valve controller and power supply. The Scani-Valves were equipped with encoders which returned a logic signal which was dependent on the position of the Scani-Valve. This enabled the control and data acquisition software to check the

position of the Scani-Valves and determine if they had failed to move when requested.

An emergency stop system was developed which could be operated by the computer or the operator. When activated, it would stop the wind tunnel and turn off the compressed air to the nozzle.

3.2.4 Pressure control and data acquisition software

Statistical analysis may be used to determine the number of sample points required for a given accuracy and probability. The measured mean value of static pressure, $\hat{\bar{p}}$ (true value $\bar{p}$), will statistically fall within the interval

$$\bar{p} - z_{\alpha/2}\sigma\left[\hat{\bar{p}}\right] < \hat{\bar{p}} < \bar{p} + z_{\alpha/2}\sigma\left[\hat{\bar{p}}\right] \tag{3.8}$$

on a normal distribution curve with a probability of $(1-\alpha)$ percent. For a 99 percent confidence level $(z_{\alpha/2} = 2.57)$, the likely error in the mean is given by

$$\frac{\hat{\bar{p}}}{\bar{p}} = 1 \pm 2.57 \frac{\sigma\left[\hat{\bar{p}}\right]}{\bar{p}} \tag{3.9}$$

It may be shown that

$$\frac{\sigma\left[\hat{\bar{p}}\right]}{\bar{p}} = \frac{1}{\sqrt{N}} \frac{\sigma_p}{\bar{p}} \tag{3.10}$$

where N is the number of sample points and $\frac{\sigma_p}{\bar{p}}$ is the turbulence intensity in static pressure. Substituting Equation 3.10 into 3.9, gives

$$\frac{\hat{\bar{p}}}{\bar{p}} = 1 \pm 2.57 \frac{1}{\sqrt{N}} \frac{\sigma_p}{\bar{p}} \tag{3.11}$$

The number of sample points chosen, N, was 5000. The turbulence intensity is difficult to estimate but was assumed not to exceed 10 percent. Substituting these values into Equation 3.11 gives a theoretical error in the mean of ± 0.36 percent with a 99 percent confidence level. To evaluate the sample frequency, the integral time-scale must be estimated. The time-scale was chosen to be the time taken for a fluid particle to cross the pressure tapping at the lowest freestream velocity tested (10 ms^{-1}), giving a time-scale of 0.5 ms. Samples separated by two or more time-scales give statistically independent samples [BRUUN, 1995] and so the sample interval used was 1 ms (a frequency of 1 kHz).

The control software was based on the same design as that used to control the wind tunnel speed (Figure 3.31 shows a flow diagram) and can maintain an NPR to a tolerance of ±0.25 percent. The NPR and wind tunnel dynamic pressure were monitored whilst the micromanometer pressure transducer was being sampled thus en-

suring that the tolerance was maintained throughout the sample period. The total sample time for a data set was only 395 seconds (6.6 minutes), however total elapsed time taken for a data set at an NPR of 1.586 was approximately 30 minutes and increased steadily to 120 minutes for an NPR of 4.0. This was mainly due to the pressure control software, which had greater difficulty maintaining a high NPR than a low one.

3.2.5 Pressure loss through the intake and ducting

It was decided that the simplest way to provide the intake suction was to connect the circular outlet from the model to a centrifugal fan. Before a fan could be purchased, an estimate was required of the likely pressure drop through the model intake ducting and any pipe-work connecting the model to the fan. Figures 3.32 and 3.33 show the wind tunnel model mounted ready for testing to commence. The support struts, compressed air supply pipe and intake ducting can all be seen clearly.

3.2.5.1 Wind tunnel model

A small centrifugal fan was already available but could not provide the desired intake mass flow rate. Using this fan a pressure loss of 0.27 m w.g. was measured through the model intake ducting for an inlet dynamic head of 0.17 m w.g.

Atmospheric conditions on the day gave an air density of 1.20 kgm^{-3} at a temperature of 293 K. Using the mass flow rate equation:

$$\dot{m} = \rho A V \tag{3.12}$$

$$\dot{m} = 1.2 \times 0.004 \times \sqrt{\frac{2 \times 0.17 \times 1000 \times 9.81}{1.2}} = 0.253\,\mathrm{kgs^{-1}}$$

The required mass flow rate is 0.489 kgs^{-1} and from Darcy's equation:

$$h_w = \frac{32\dot{m}^2 fl}{\pi^2 d^5 g \rho_a \rho_w} \tag{3.13}$$

the pressure loss is proportional to the square of the mass flow rate. Therefore the pressure loss through the model at the required mass flow rate is expected to be:

$$h_w = 0.27 \times \left(\frac{0.489^2}{0.253^2}\right) = 1.008\,\mathrm{m}$$

The pressure losses through the duct-work from the model to the fan were then determined theoretically.

3.2.5.2 90 degree bend, diameter 65 mm

A 65 mm diameter, 90 degree bend was fitted to the exit of the model intake ducting. This turned the flow perpendicular to the wind tunnel free stream. The pressure

loss through this component was determined to be 0.15 times the dynamic head for a bend radius to duct diameter, r/d of 2.0 [AIRSCREW COMPANY, 1961]. Through the bend, the velocity is obtained from Equation 3.12 and was determined to be 122.8 ms^{-1}. This gave a dynamic head of 0.922 m w.g. and hence the pressure loss through the bend would be 0.138 m w.g.

3.2.5.3 Straight duct, diameter 65 mm

A 1 m straight duct of 65 mm diameter was fitted after the 90 degree bend. This brought the intake air out of the tunnel working section and into the inner section of the wind tunnel circuit where the centrifugal fan was to be situated. From Equation 3.13, the pressure loss down this length of duct can be determined. The friction coefficient f is 0.005 [MASSEY, 1970] for a Reynolds number of 5.5×10^5 (based on the duct diameter) and a relative roughness k/d of 0.001. The pressure loss is therefore 0.284 m w.g.

3.2.5.4 Conical diffuser, 65 mm to 225 mm diameter

A conical diffuser with a 5 degree half angle was to be fitted to the end of the 65 mm diameter straight duct. This increased the duct area to that of the fan inlet. From AIRSCREW COMPANY, 1961, the pressure loss was determined to be 0.118 times the diffuser inlet dynamic head. This gave a diffuser pressure loss of 0.109 m w.g.

3.2.5.5 90 degree bend, 225 mm diameter

Another 90 degree bend was required to turn the ducting towards the fan inlet, the centre-line of which was parallel to the tunnel free stream. The pressure loss can be determined using the same method as for the 65 mm bend. This time $r/d = 1.0$ giving a pressure loss of 0.26 times the dynamic head. The velocity at this section, however, was relatively low at 10.2 ms^{-1}. Hence the pressure loss was only 0.002 m w.g.

3.2.5.6 Straight duct, diameter 225 mm

A straight duct of 225 mm diameter and 1.2 m long connected the intake ducting to the fan inlet. The pressure loss down this section can be determined from Equation 3.13. Assuming the same friction coefficient as that used for the 65 mm diameter duct, the pressure loss was 0.001 m w.g.

3.2.5.7 Total pressure loss

The total pressure loss for the whole system was therefore 1.542 m (61 inches) w.g. With this value and the required volume flow rate of 0.4 m^3s^{-1} (850 cfm), a suitable

fan was bought. The fan was supplied by Woodcock and Wilson Ltd. of Huddersfield and the specifications are as follows:

Duty: 0.61 m^3s^{-1} (1300 cfm) @ 2.0 m (79 inch) w.g. suction.

Size: 1.0 m (39.5 inch) diameter.

Speed: 2950 rpm (direct drive).

Power: 30 kW 3-phase constant speed a.c. motor.

The diffuser and the 225 mm diameter ducting were made from galvanised steel and supplied by KRF Metal Fabrications Ltd. of Bristol. The 65 mm diameter ducting was standard domestic drainpipe.

3.2.6 Estimation of the intake mass flow rate

Approximately 3.5 m of 225 mm diameter ducting (also supplied by KRF Ltd.) was attached to the fan outlet to take the intake air from the fan exit and away from the wind tunnel working section. Measurement of the mass flow rate through the fan was done using a Pitot-static rake placed on the outlet of this ducting. The rake was positioned in four orientations (horizontal, vertical and two 45 degree positions) so as to obtain a good average of the dynamic pressure distribution across the outlet. The dynamic pressure was then integrated circumferentially to obtain the volume flow rate. This was determined to be 0.39 m^3s^{-1}. Based on temperature measurements of the air exiting the duct, the density was 1.103 kgm^{-3}, giving a mass flow rate of 0.43 kgs^{-1}. This is slightly below the value of 0.489 kgs^{-1} required but was considered to be acceptably close. The theoretical intake mean velocity was therefore almost 100 ms^{-1}.

3.3 Experimental programme

This section describes the experimental programme which was required to enable identification of the jet/intake interference effects which were discussed in Chapter Two. In order to try to isolate the effects of the jet and intakes, four model configurations were tested:

A - intakes faired, jet off;

B - intakes faired, jet on;

C - intakes 'powered', jet off;

D - intakes 'powered', jet on.

Configuration A provided the datum case. Configuration B, when compared with Configuration A, showed the effect of the jet on the wing C_p distribution and the intake outer surface pressures. Configuration C, when compared with Configuration A, showed the effect of the intake on the wing C_p distribution. Configuration D, when

compared with Configuration C, showed the effect of the jet on the intake flow and by comparison with Configuration A showed the combined effect of jet and intake flows on the wing C_p distribution. Table 3.2 shows the full test matrix.

***Table 3.2** - Test matrix.*

		Wind Tunnel Standard Velocity (ms^{-1})								
		10			***20***			***30***		
		Nozzle Position			***Nozzle Position***			***Nozzle Position***		
NPR	***Configuration***	***1***	***2***	***3***	***1***	***2***	***3***	***1***	***2***	***3***
n/a	A		✓			✓			✓	
n/a	C		✓			✓			✓	
1.586	B	✓	✓	✓	✓	✓	✓	✓	✓	✓
1.586	D	✓	✓	✓	✓	✓	✓	✓	✓	✓
2.0	B	✓	✓	✓	✓	✓	✓	✓	✓	✓
2.0	D	✓	✓	✓	✓	✓	✓	✓	✓	✓
3.0	B	✓	✓	✓	✓	✓	✓	✓	✓	✓
3.0	D	✓	✓	✓	✓	✓	✓	✓	✓	✓
4.0	B	✓	✓	✓	✓	✓	✓	✓	✓	✓
4.0	D	✓	✓	✓	✓	✓	✓	✓	✓	✓
A = Intakes faired, jet off.					C = Intakes 'sucking', jet off.					
B = Intakes faired, jet on.					D = Intakes 'sucking', jet on.					

Only one test run was required for Configurations A and C at each wind tunnel velocity. This was because no jet nozzle was needed for these tests, hence nozzle position and NPR were not applicable. With these jet 'off' configurations, the nozzle was replaced by a blank, leaving the lower surface of the fuselage flush. By comparison, the nozzles protruded slightly below the fuselage (see Figures 3.18, 3.22, 3.32 and 3.33).

Two phases to the tests were carried out. Phase 1 was run with the following parameters.

- NPRs of 2.0, 3.0 and 4.0 (constant mass flow rate, variable nozzle areas).
- Three different nozzle positions (forward, centre and rearward).
- Wind tunnel standard air velocities of 10, 20 and 30 ms^{-1}.
- Out of ground effect (the model was 1.5 m from the tunnel floor).

Phase 2 was a more extensive programme. In the first part (Phase 2a), the tests conducted under Phase 1 were repeated. In addition, the low NPR lift-fan nozzle was also tested. In the second part of Phase 2 (Phase 2b), tests were carried out

with a fixed nozzle area to investigate the effect of varying mass flow rate. The Phase 2 test programme was therefore as follows.

- NPRs of 2.0, 3.0 and 4.0 (constant mass flow rate, variable area nozzle).
- An NPR of 1.586 with 50 percent more mass flow rate than above.
- NPRs of 1.586, 2.0, 3.0 and 4.0 at constant area (the 25.4 mm (1 inch) nozzle was chosen for this purpose).
- Wind tunnel standard air velocities of 10, 20 and 30 ms^{-1}.
- Out of ground effect.

The tests were completed over a period of four months and took approximately 300 hours of wind tunnel time to complete.

3.4 Error analysis

This section discusses the errors likely to be present in the measurements of the static pressures on the wind tunnel model. The errors in the measured data were introduced by a number of factors including the variability of the flow-field measured as well as the instrumentation and the model positioning.

As has already been stated, all tests were conducted at a nominal zero degree wing incidence. Since this research was interested in differences relative to a datum, the absolute value of the incidence was of a lesser importance. What was important was the consistency in the wing incidence between one test and another. The model was removed from the wind tunnel between the Phase 1 and Phase 2 tests and also when changing the model intake configuration. Although the wing incidence was nominally the same for all cases, there will be some error in wing incidence between them. The model pitch incidence was set using a cross-spirit-level. The smallest change in inclination which was detectable to the naked eye was a 1 in 640 slope. This is equivalent to an angular change of 0.1 degrees. The two-dimensional lift curve slope, a_{2d} for the NACA 1408 aerofoil used was 0.11 per degree [ABBOTT & VON DOENHOFF, 1959]. The error in root section lift coefficient, $C_{l\,(root)}$ would therefore be a minimum of 0.01. Another possible error could have been caused by the thrust of the jet. It was thought that this might be sufficient to change the incidence of the model. Measurement of the model incidence with and without the jet running showed no measurable change in incidence due to jet operation. This confirmed the rigidity of the multi-strut support arrangement.

Fluctuations in the wind tunnel dynamic pressure had a direct influence on the measured static pressure. The tolerance on the wind tunnel control software was set to ±0.25 percent. Another source of error in the measured static pressures was the accuracy of the micromanometer. Furness Controls quote a non-linearity error of ±1.0 percent of the reading. Variations in NPR of 0.25 percent were thought to

have an insignificant effect on the static pressure readings. If there were a significant variation in ambient temperature during a run then this would cause the pressure transducer zeros to drift. Ambient temperature during a data set did not change by more than 3 °C. The quoted temperature drift for all pressure transducers was 0.04 percent per degree Celsius. A maximum error of ±0.12 percent could therefore be encountered. The maximum theoretical error in static pressure was therefore ±1.5 percent.

When integrated, the C_p distributions would also therefore contain an error of ±1.5 percent. The combination of C_p distributions to obtain force coefficients would compound this error to ±3.0 percent for $C_{l\,(root)}$ and ±6.0 percent for C_{ni}. These are, however, the maximum errors and in reality they should be much smaller than this.

3.5 Summary

In order to investigate the mutual jet/intake interference effects, described in Chapter 2, a test vehicle was needed. The model selected was a tail-less, shoulder-wing design of approximately 1 metre span with a single, vectored lift-jet and rectangular, side-mounted intakes. The aircraft forces were to be inferred from surface pressure data on the wings and intakes.

The first part of this chapter has described the design and construction of the wind tunnel model. This has included a method by which the airflow through the lift-jet was simulated using compressed air; the design and construction of the jet nozzles; the design and construction of the wing and intakes, including pressure tappings; and the design and construction of the fuselage.

Experiments were to be carried out in the RMCS open-jet wind tunnel. Before testing could commence, however, a number of modifications and additions had to be made to the existing high-speed jet research facilities. The second part of this chapter has discussed the development of the existing experimental facilities to enable the chosen test programme, described in the third part of the chapter, to be carried out.

Finally an estimation has been made of the errors likely to be present in the measurement of the static pressures obtained from the wing and intake pressure tappings on the wind tunnel model.

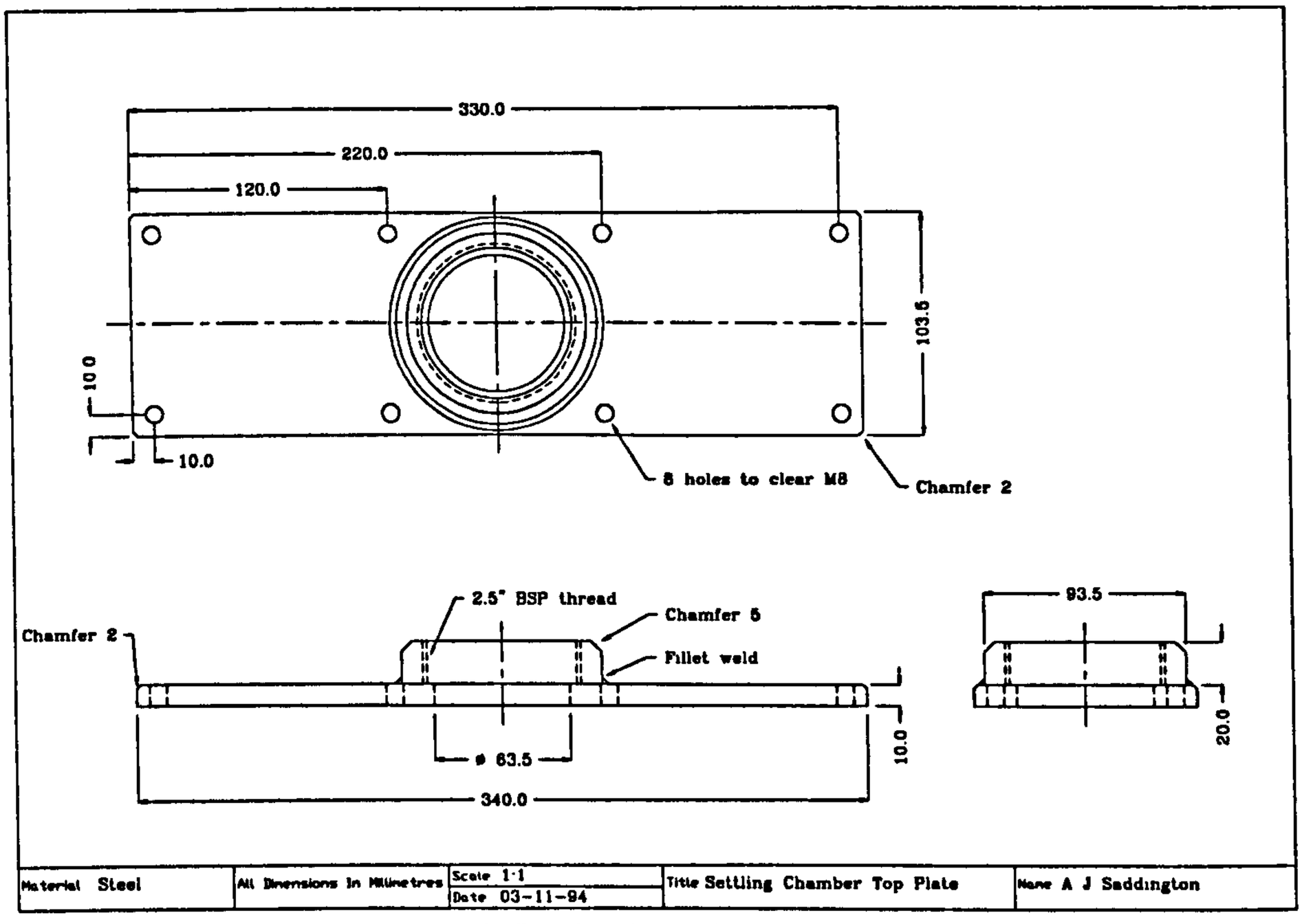

***Figure 3.1** - Settling chamber top plate.*

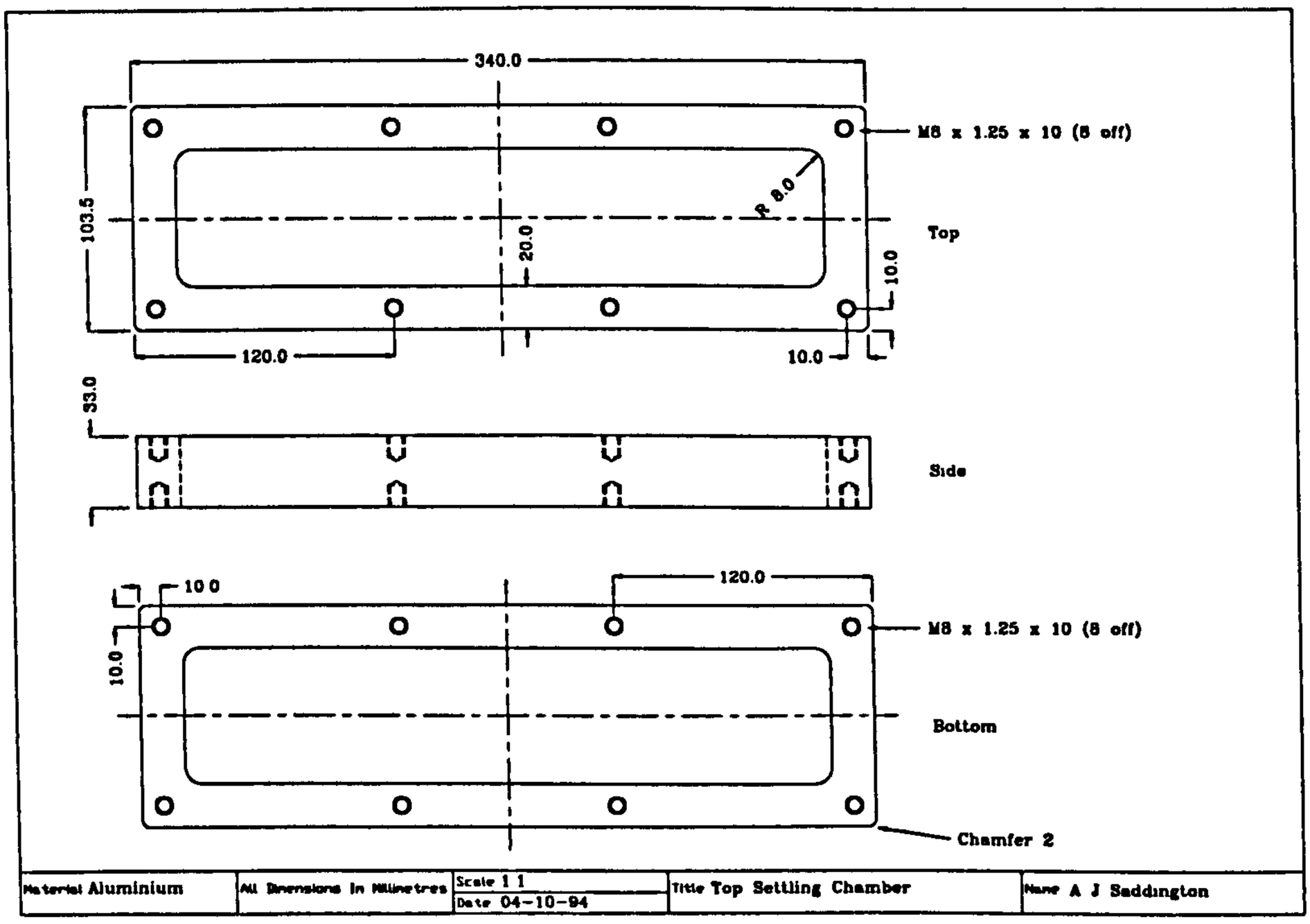

***Figure 3.2** - Settling chamber upper section.*

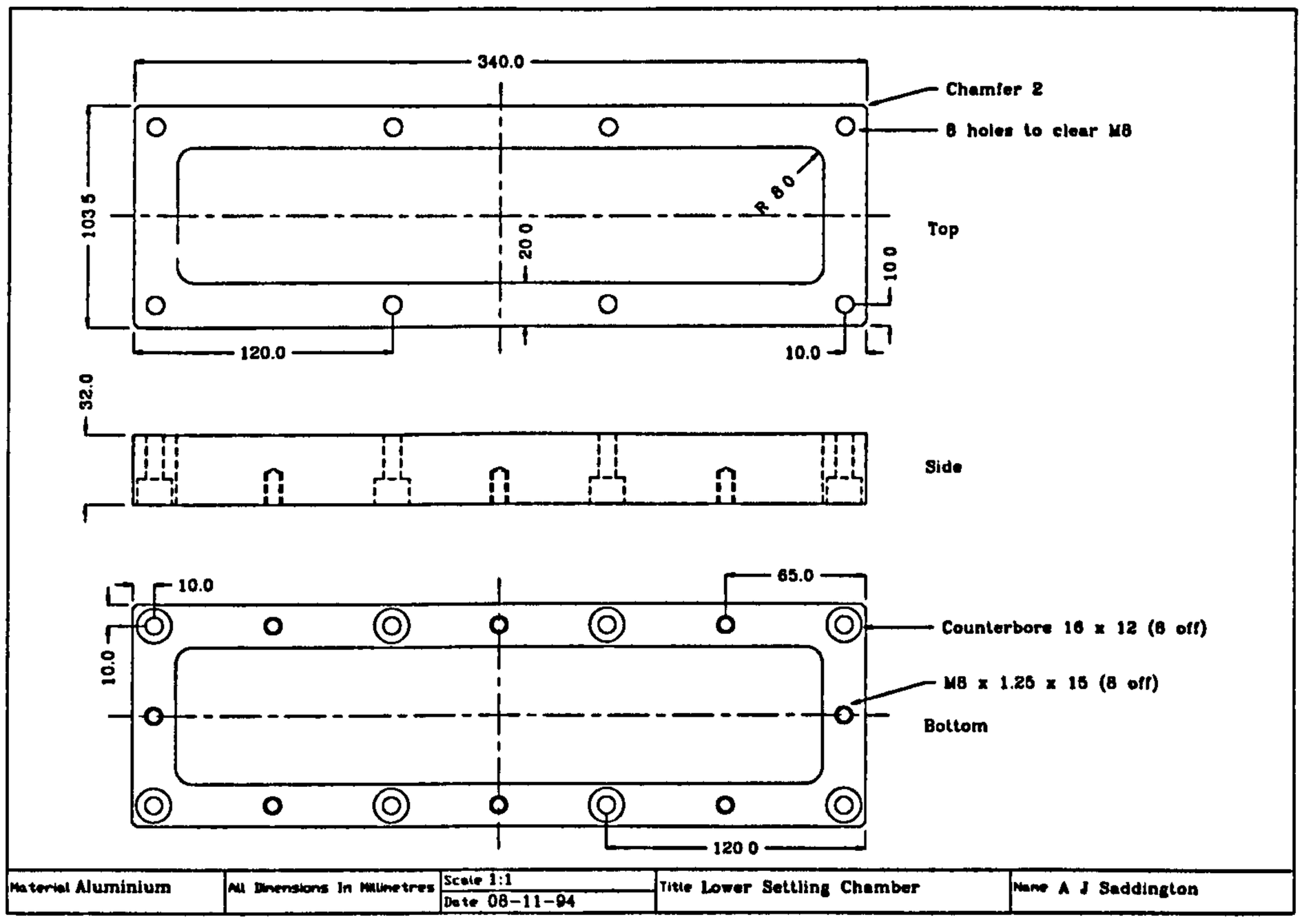

***Figure 3.3** - Settling chamber lower section.*

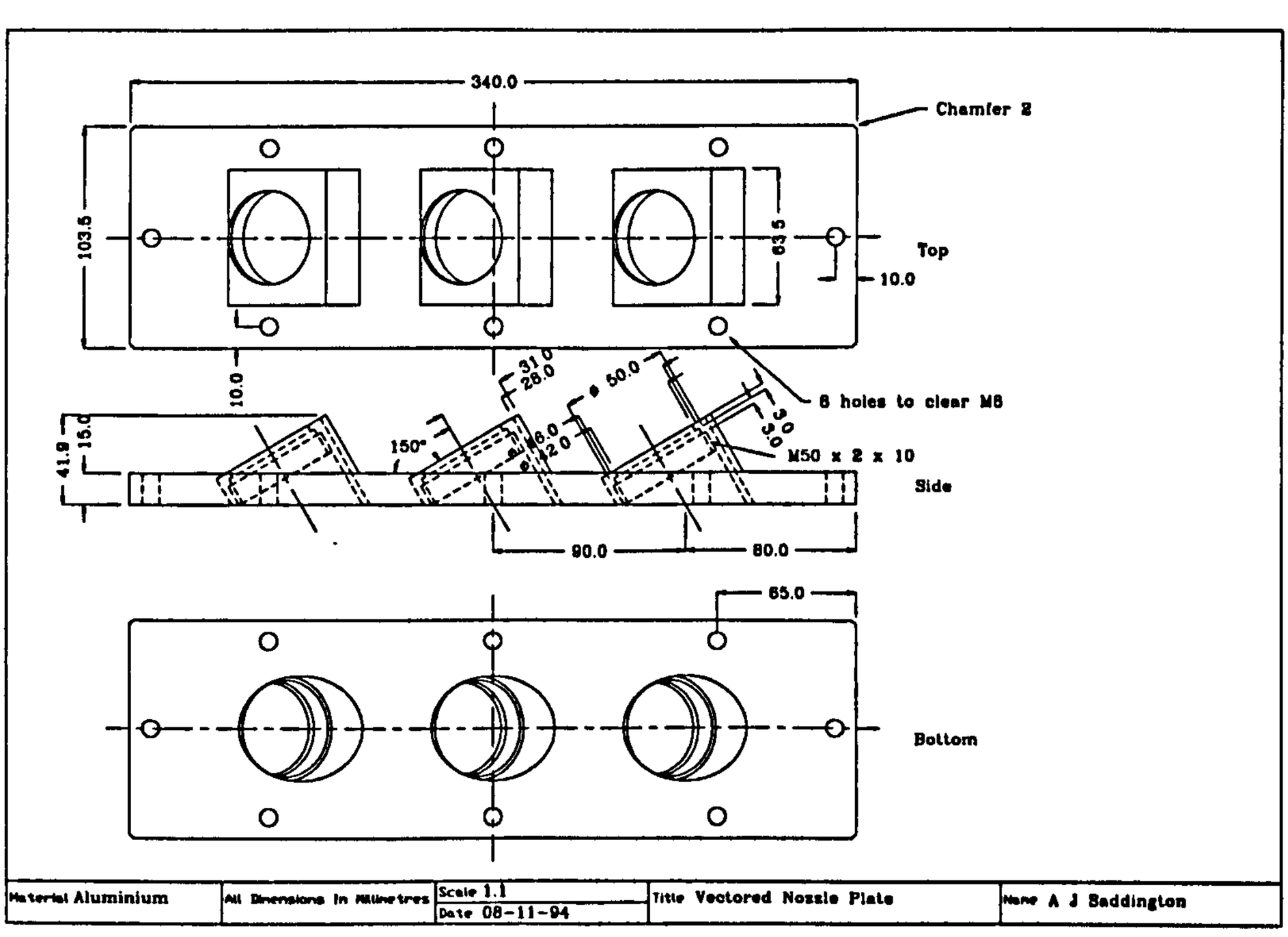

***Figure 3.4** - Settling chamber bottom plate.*

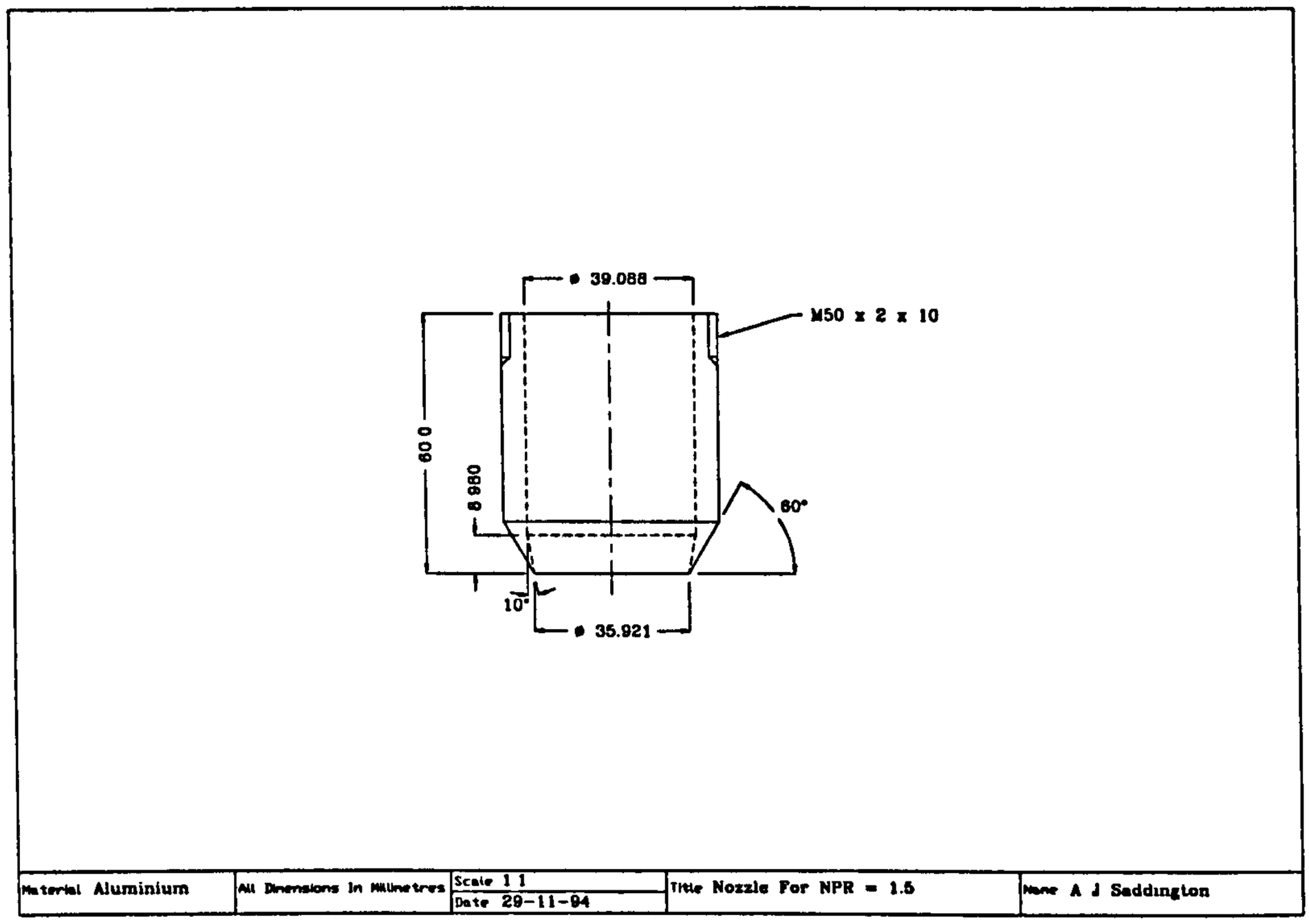

***Figure 3.5** - Nozzle for tests at NPR = 1.586.*

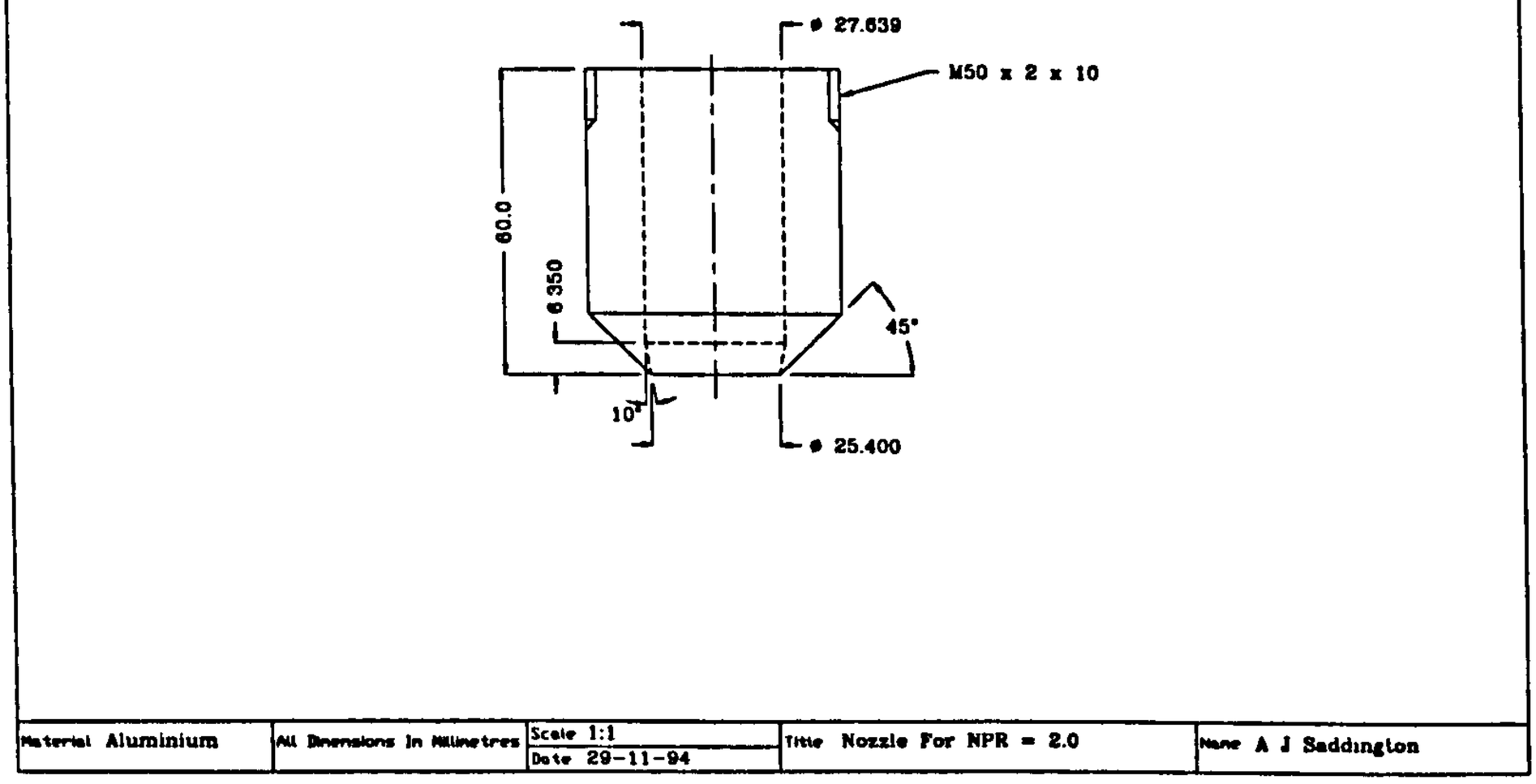

***Figure 3.6** - Nozzle for tests at NPR = 2.0.*

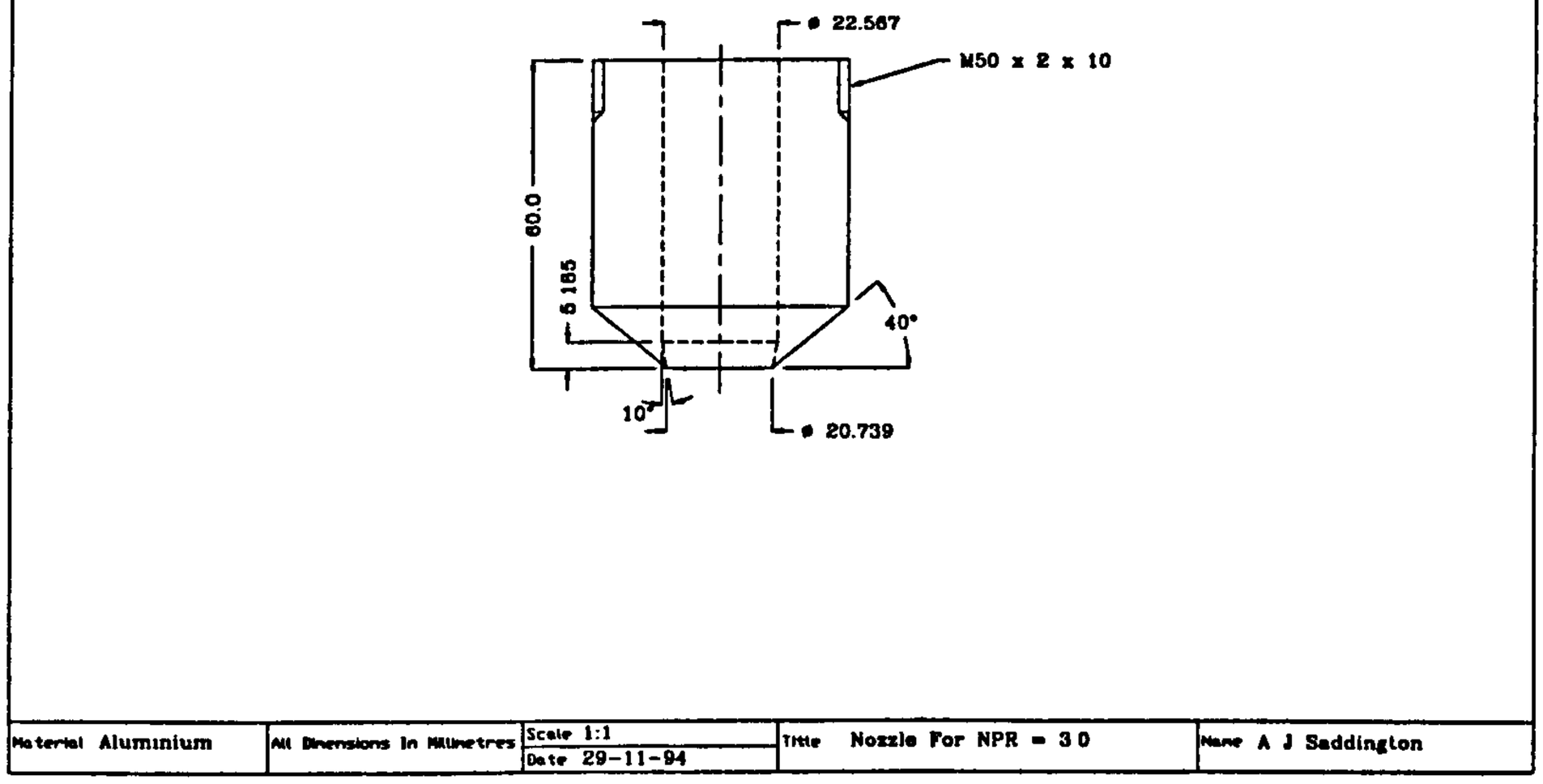

***Figure 3.7** - Nozzle for tests at NPR = 3.0.*

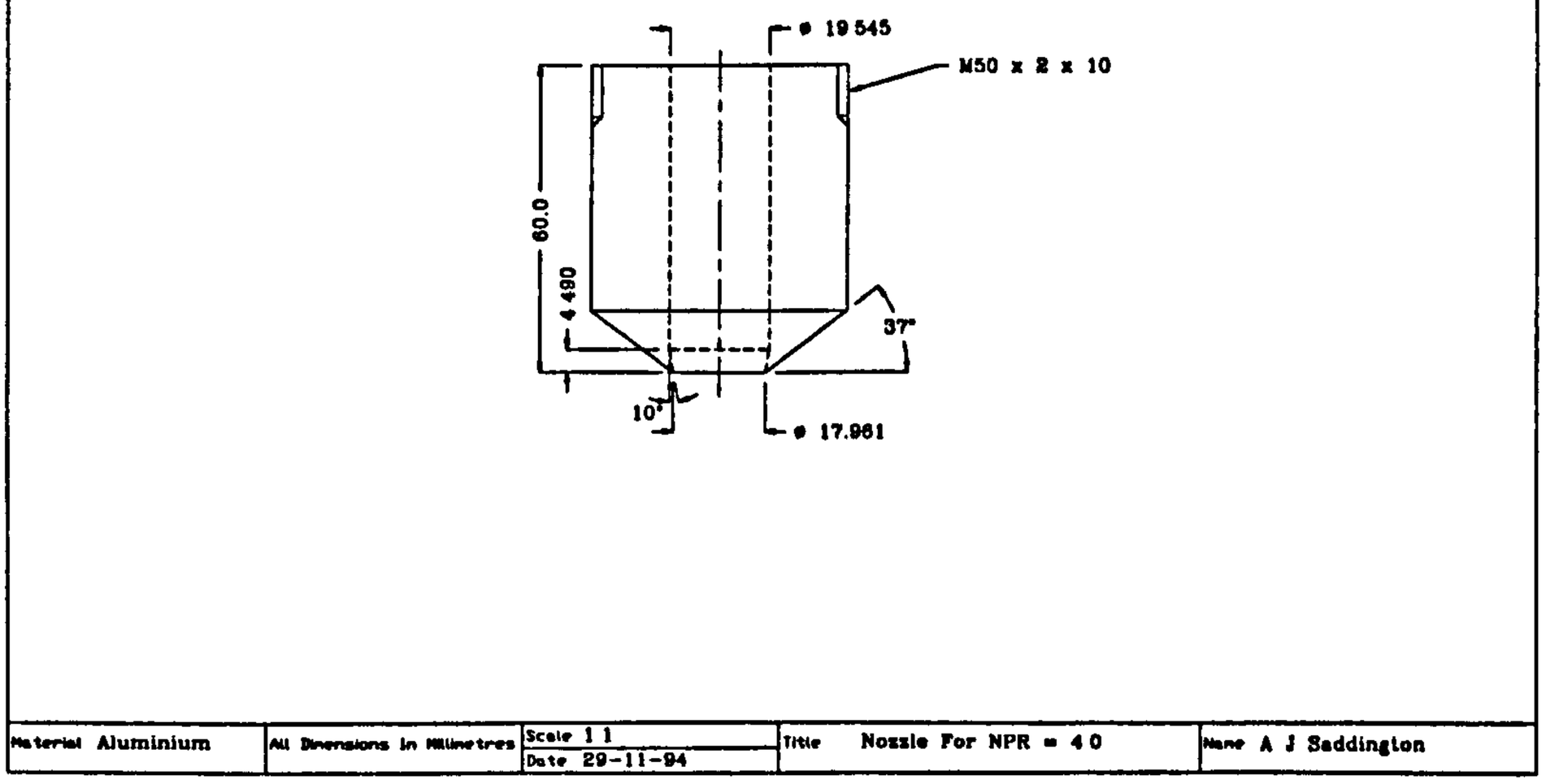

***Figure 3.8** - Nozzle for tests at NPR = 4.0.*

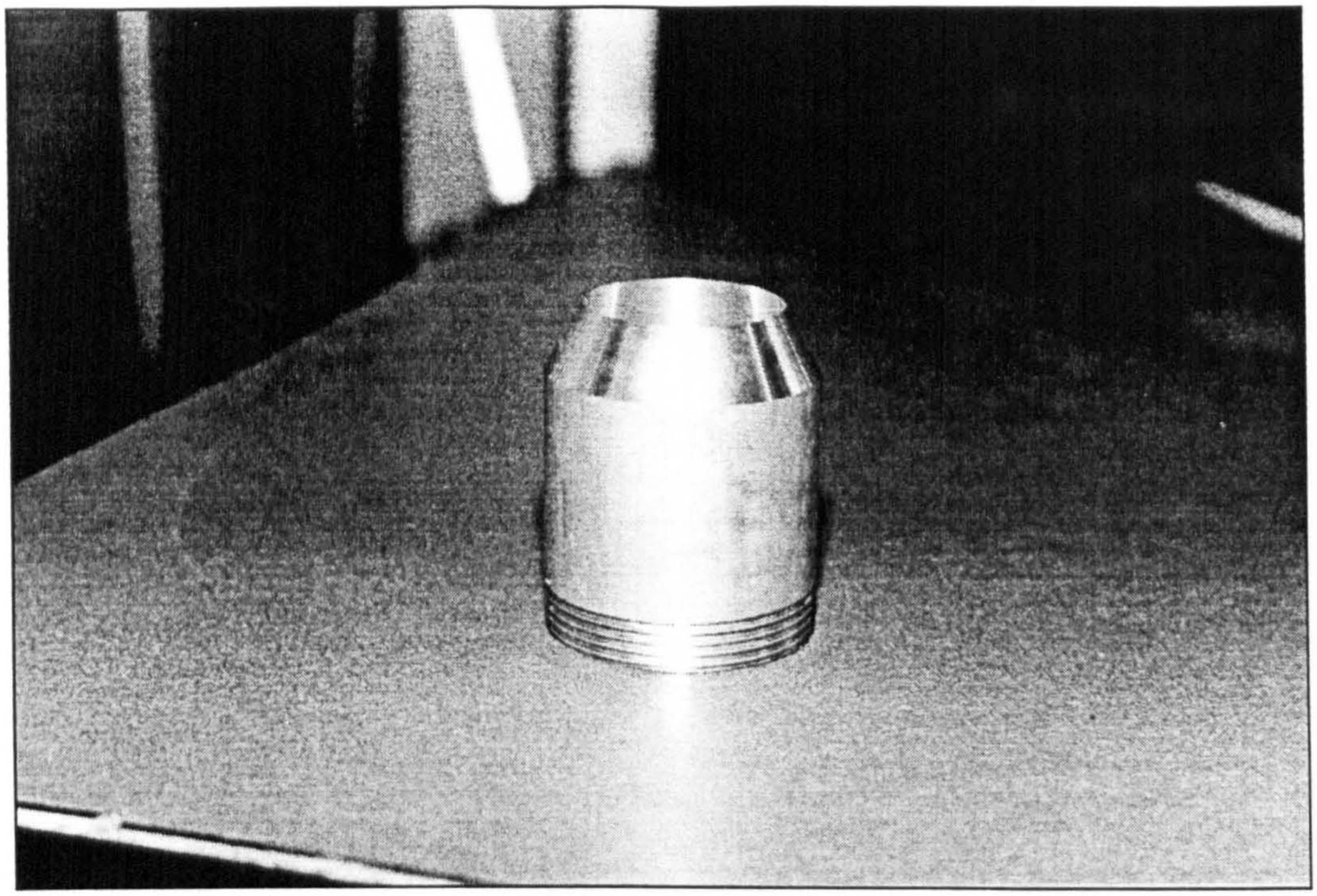

***Figure 3.9** - A typical jet nozzle (NPR = 2.0) used on the wind tunnel model.*

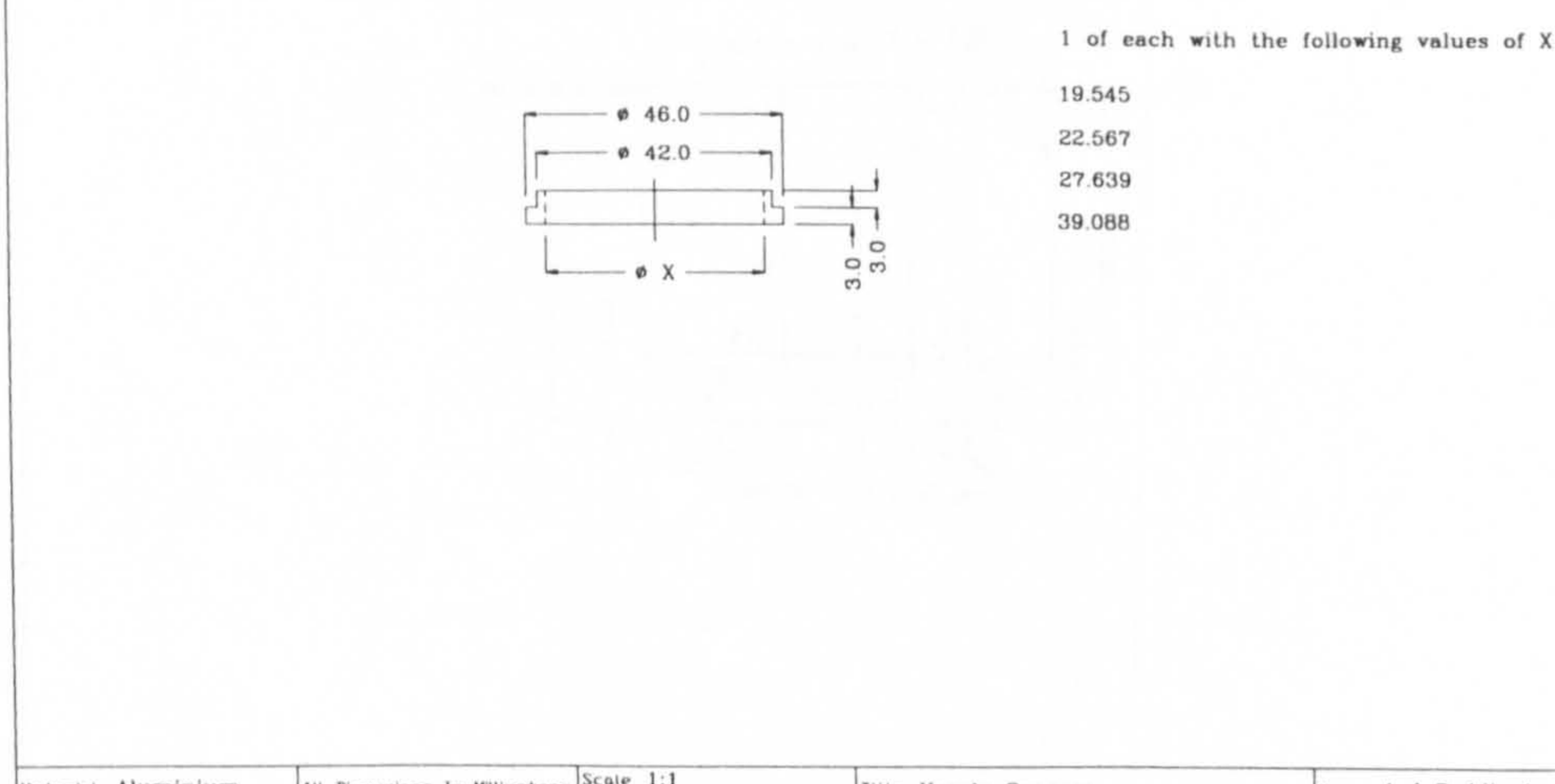

***Figure 3.10** - Nozzle spacers.*

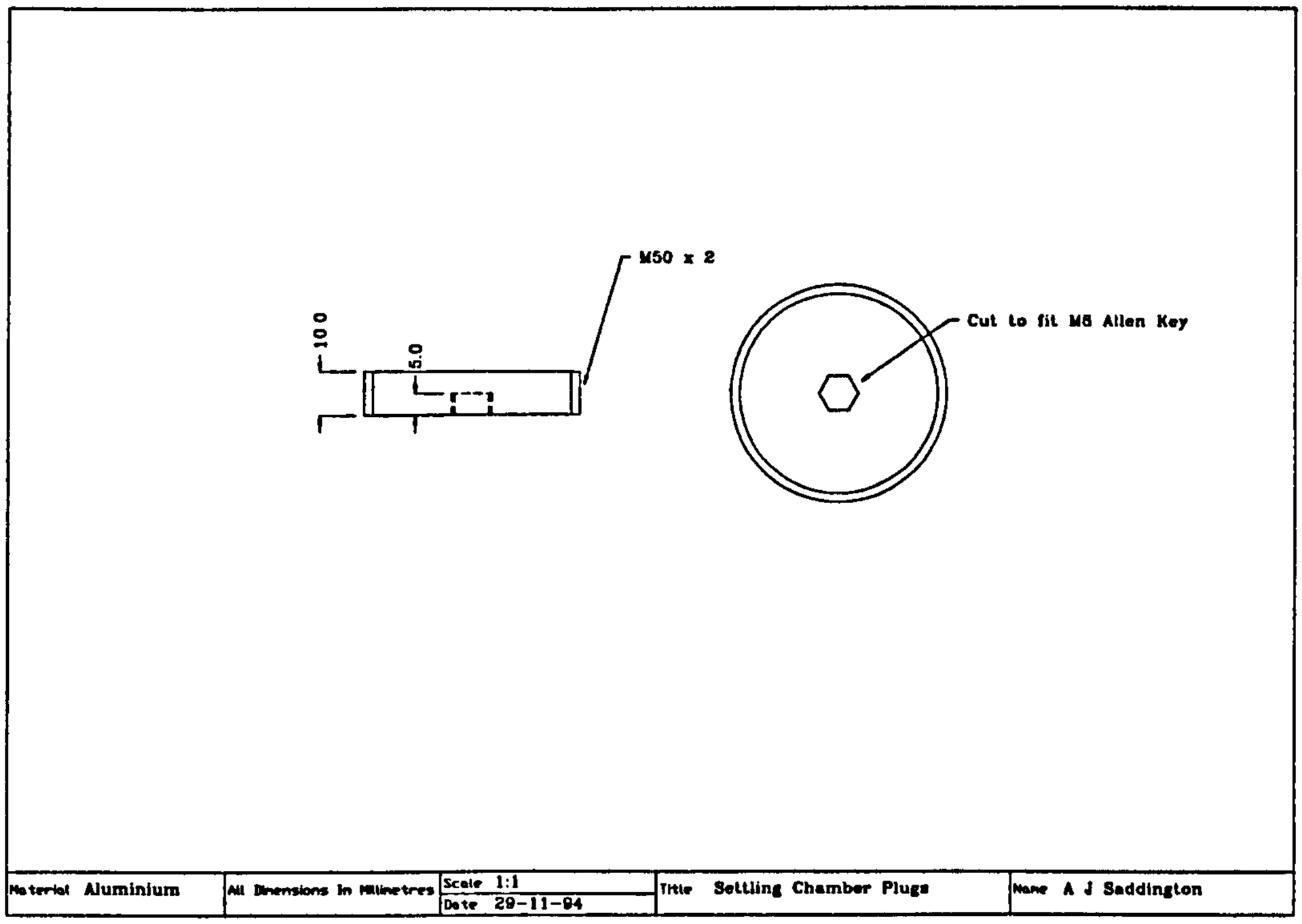

***Figure 3.11** - Settling chamber plug.*

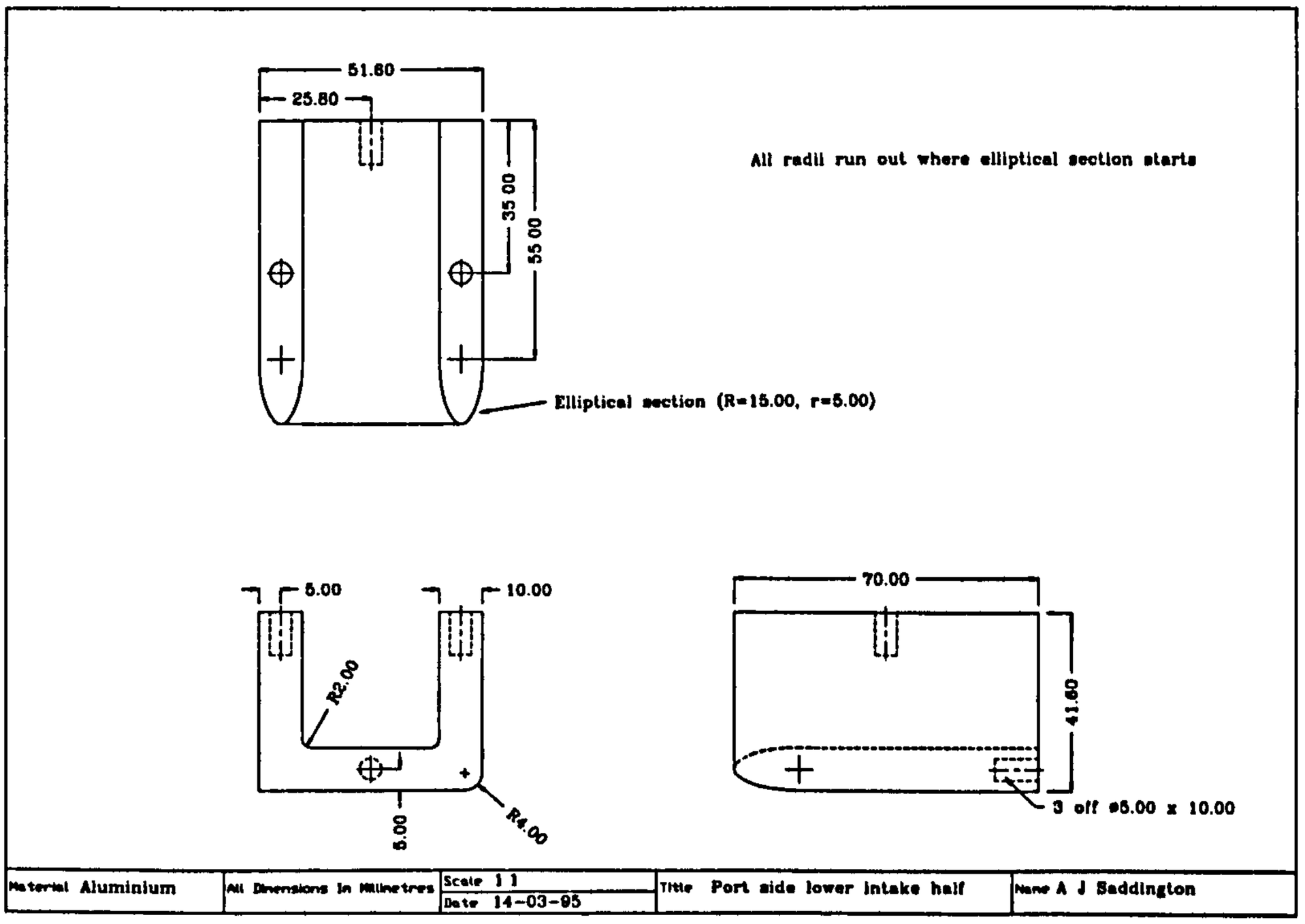

***Figure 3.12** - Port intake, lower half.*

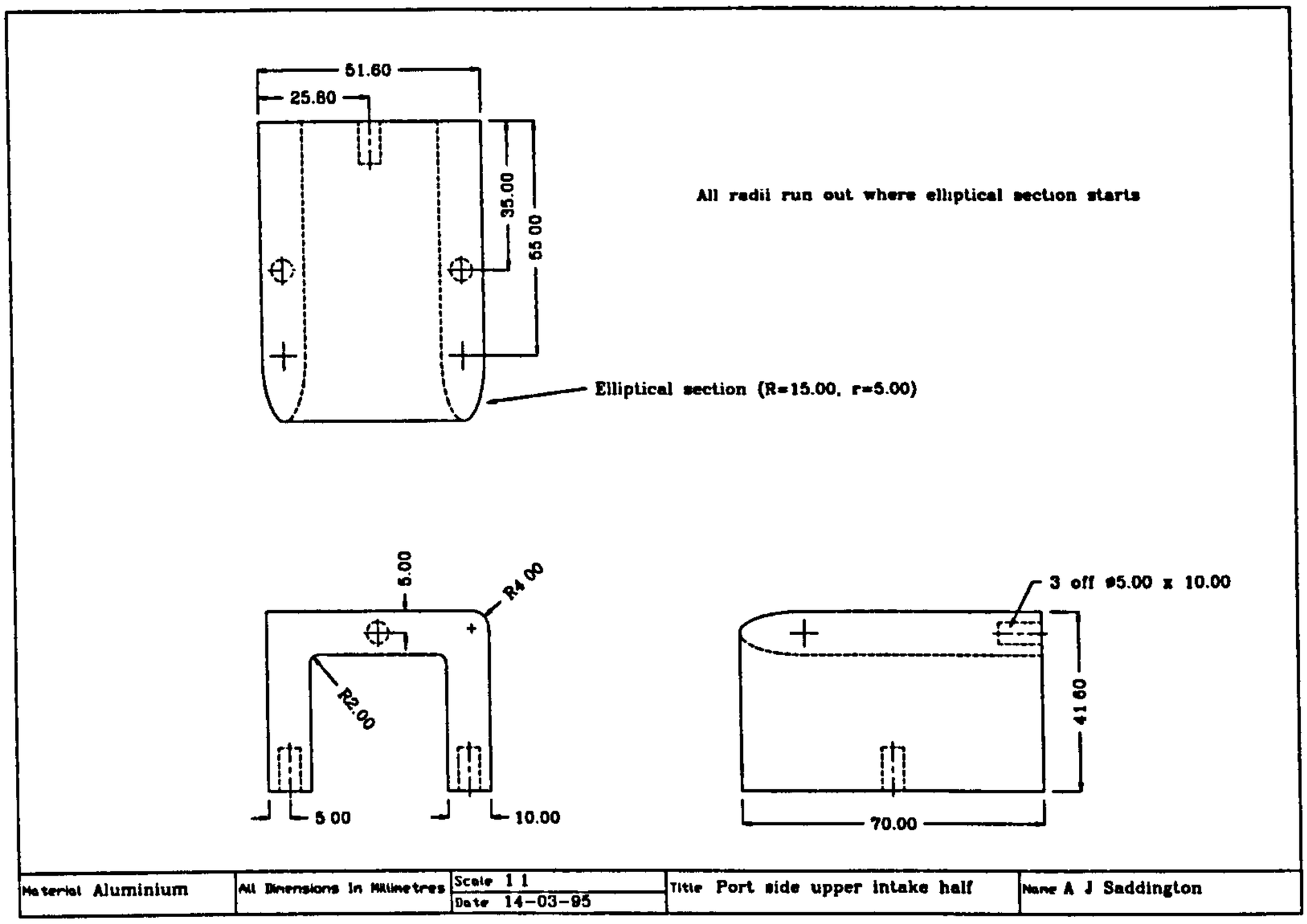

***Figure 3.13** - Port intake, upper half.*

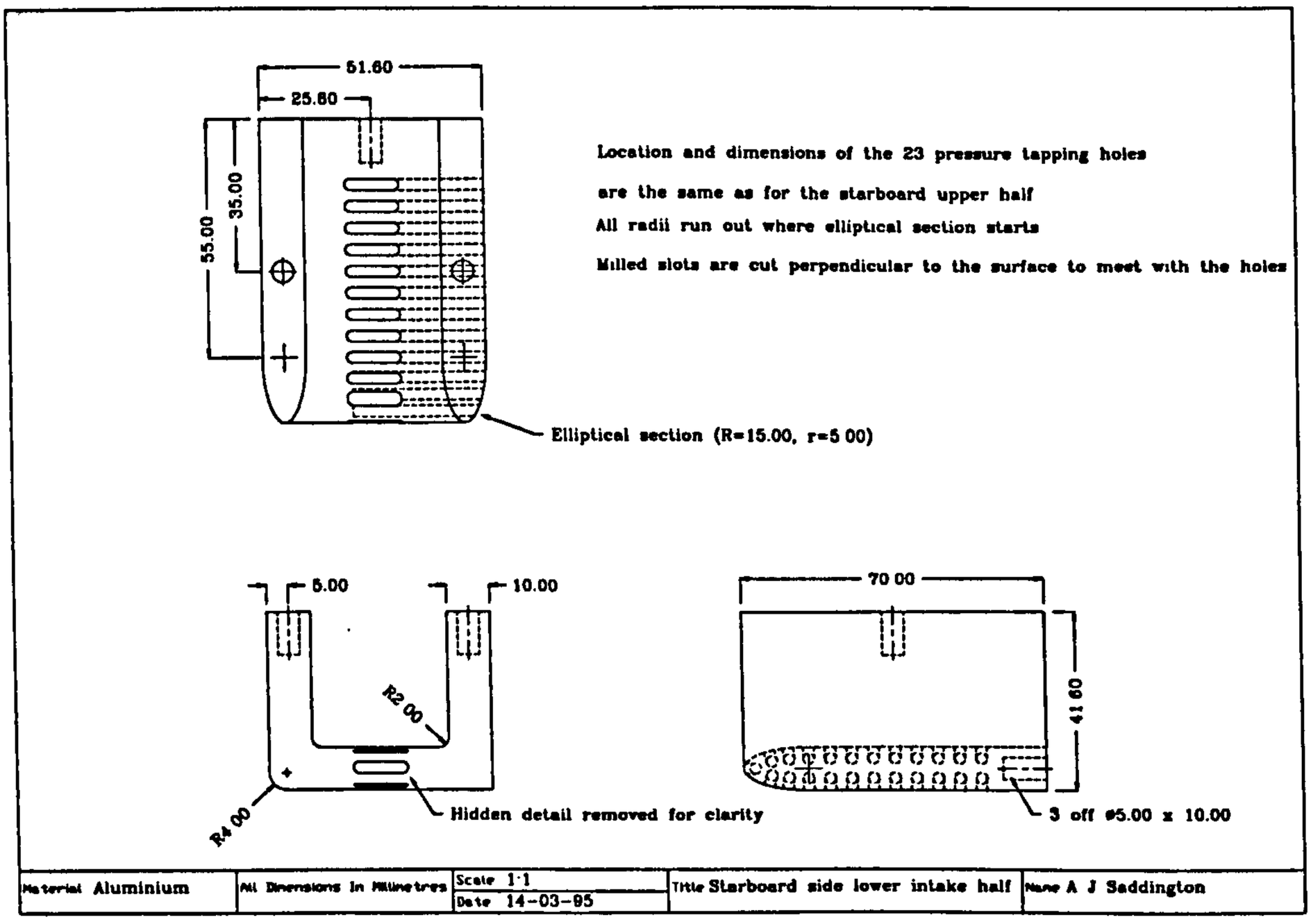

***Figure 3.14** - Starboard intake, lower half.*

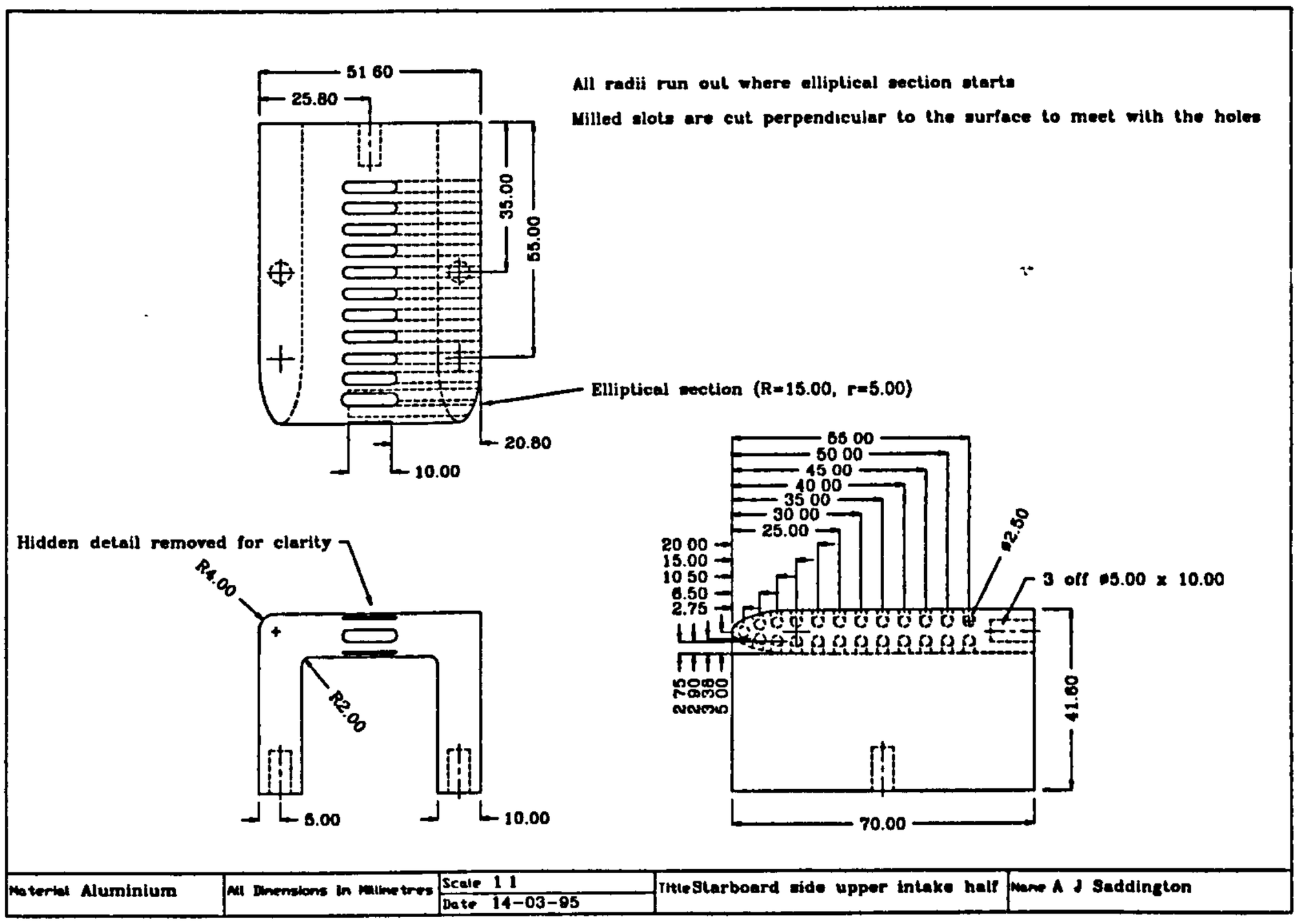

***Figure 3.15** - Starboard intake, upper half.*

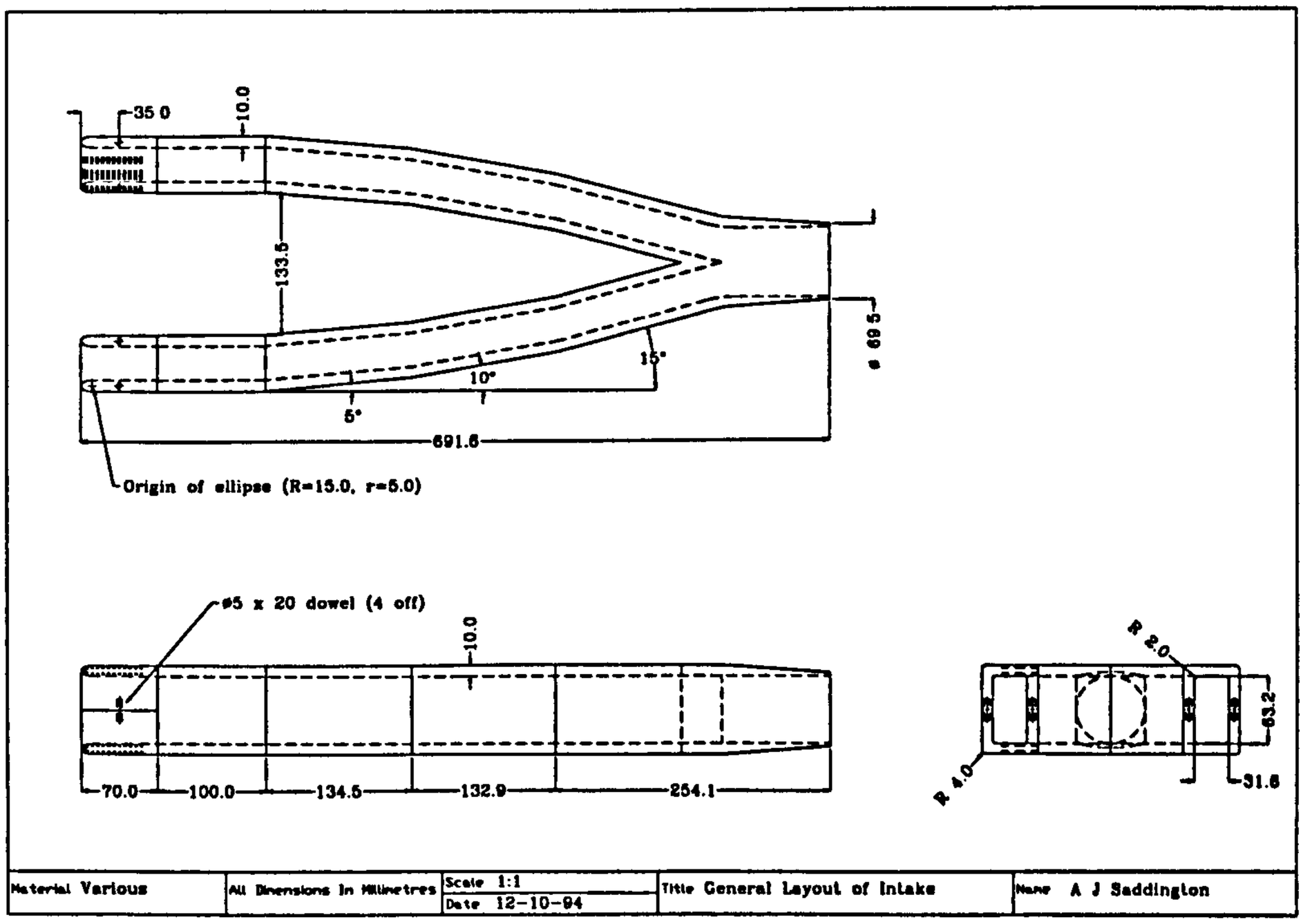

***Figure 3.16** - General layout of intake ducting.*

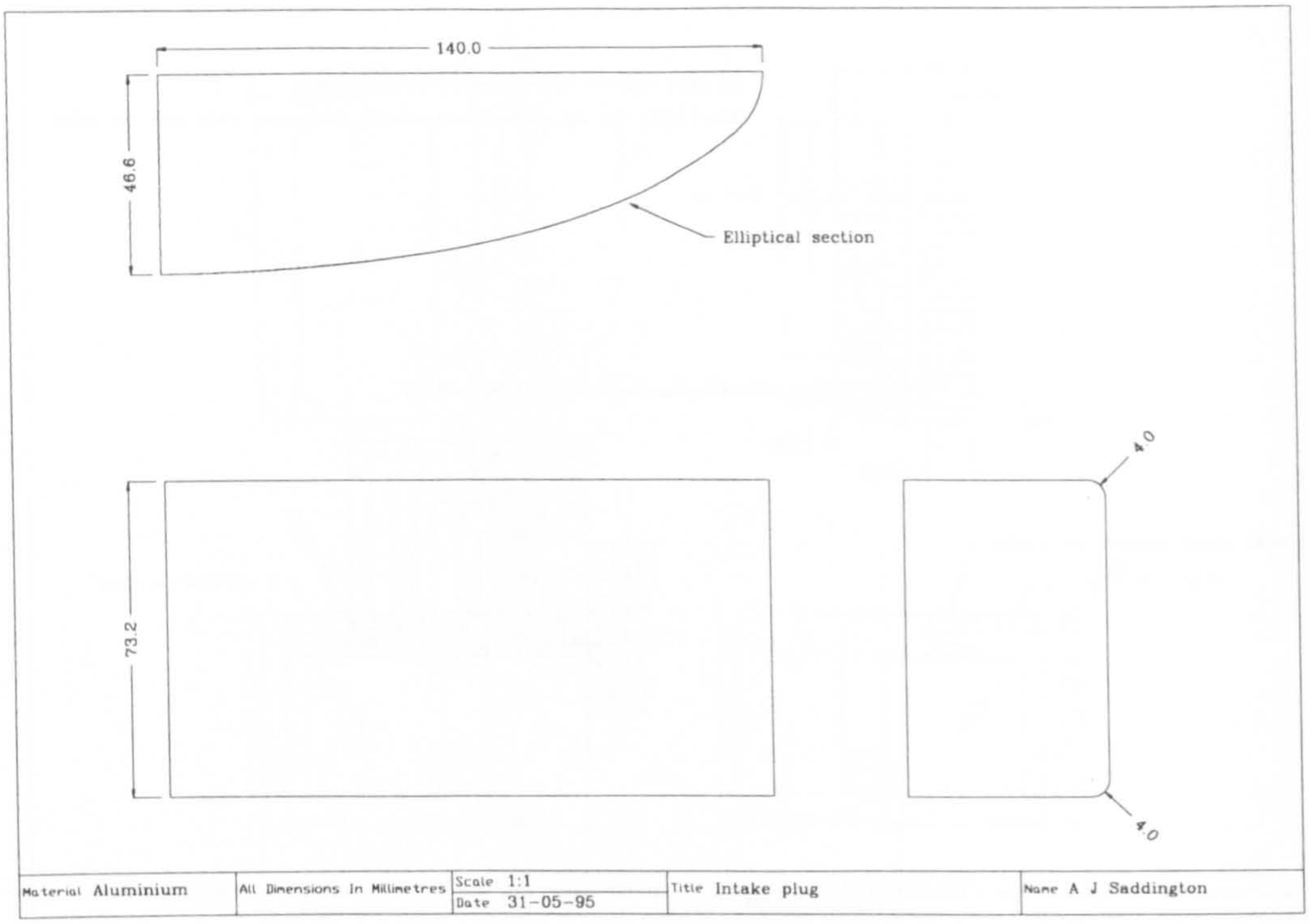

***Figure 3.17** - Intake plug.*

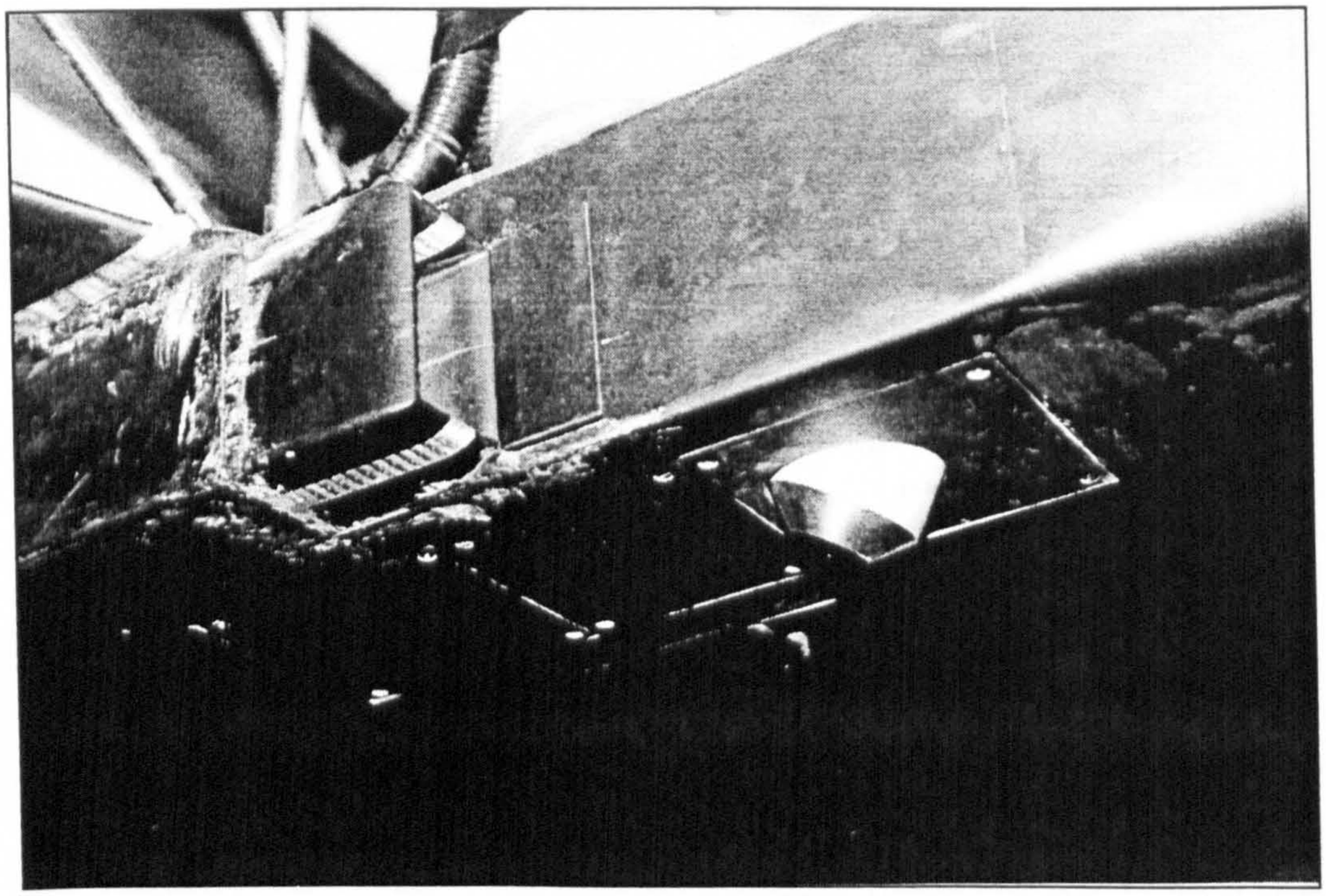

***Figure 3.18** - The wind tunnel model showing a jet nozzle in the forward position and the starboard intake. The intake pressure tappings can clearly be seen.*

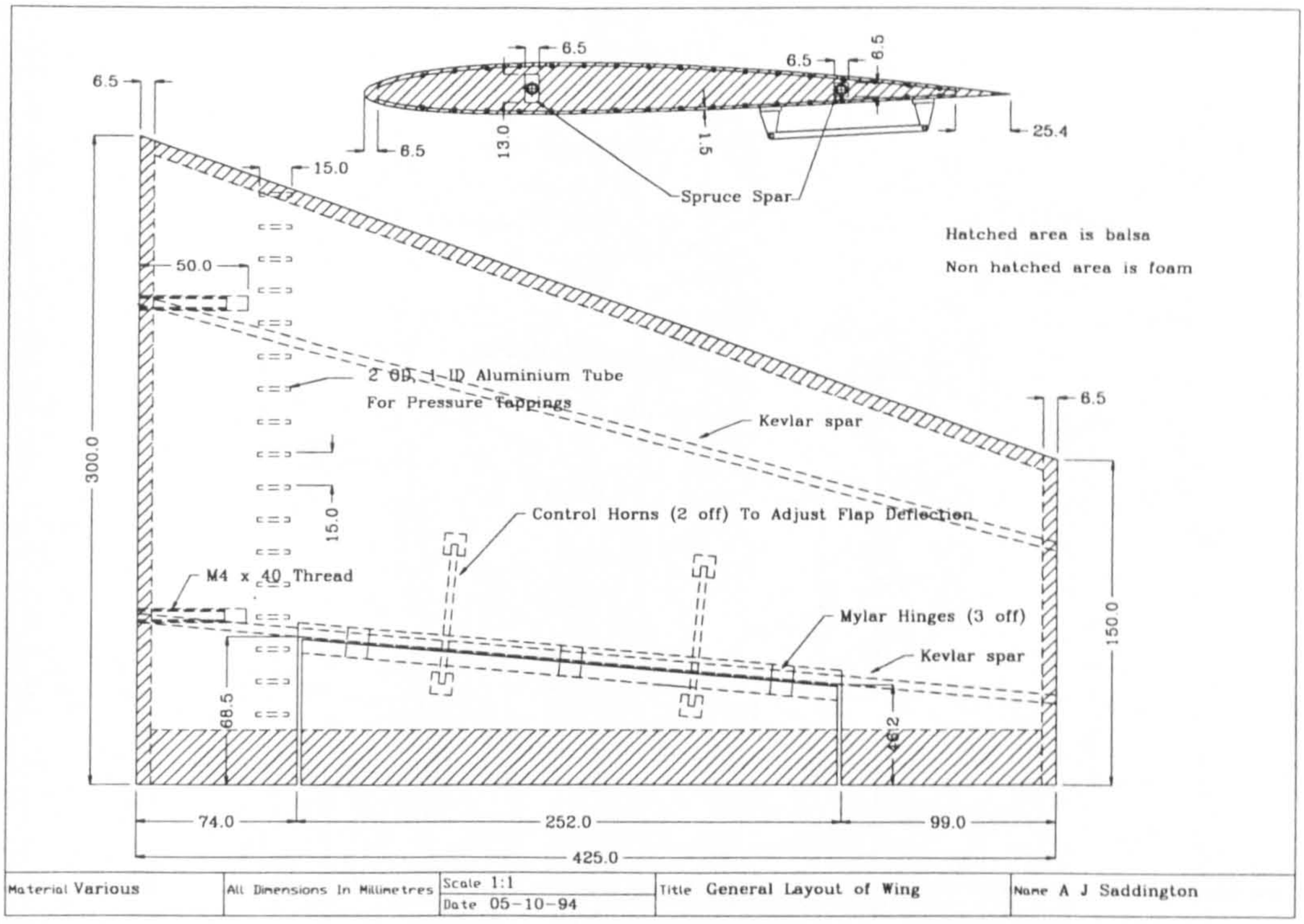

Figure 3.19 *- General layout of the starboard wing.*

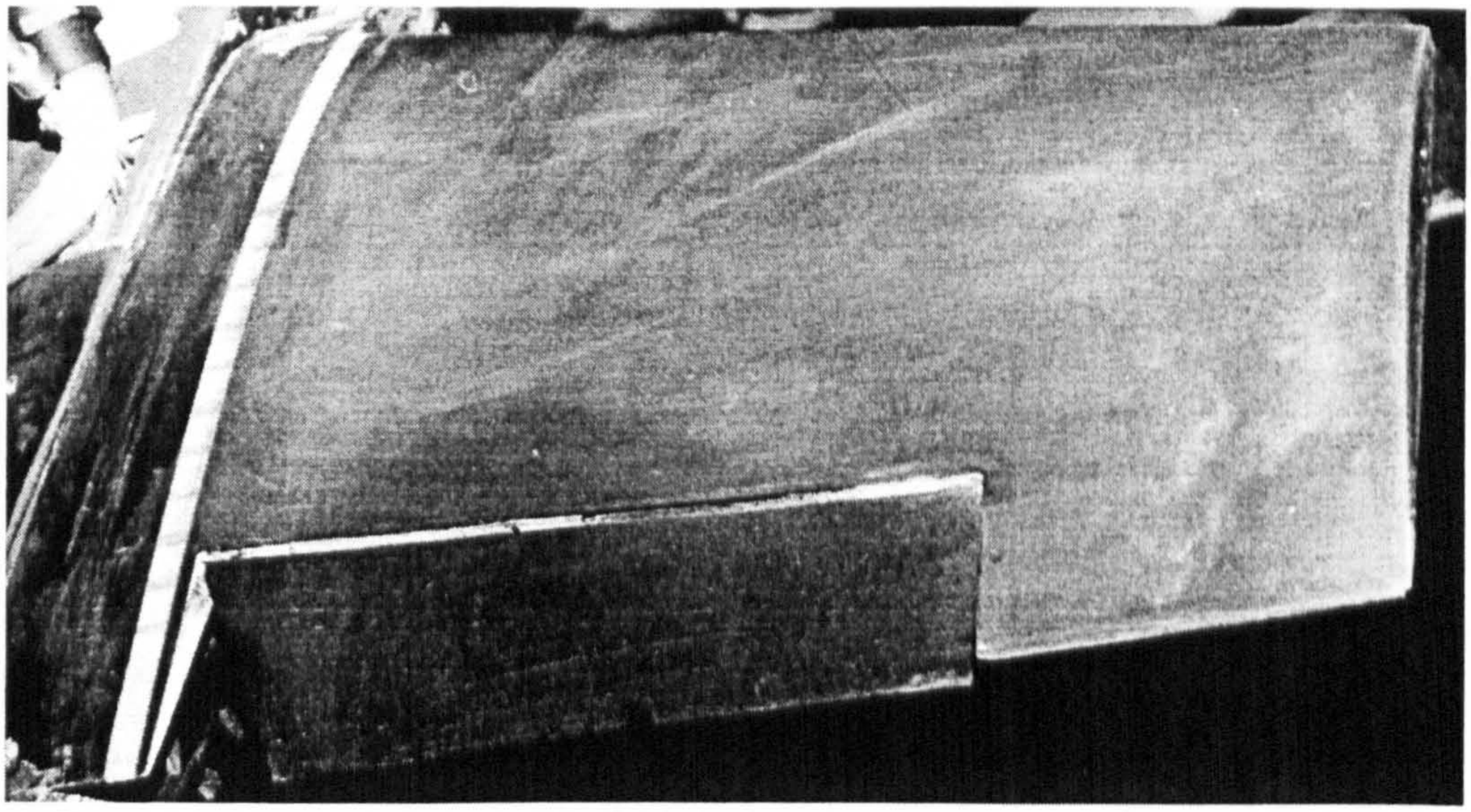

Figure 3.20 *- Starboard wing showing upper surface pressure tappings and flap.*

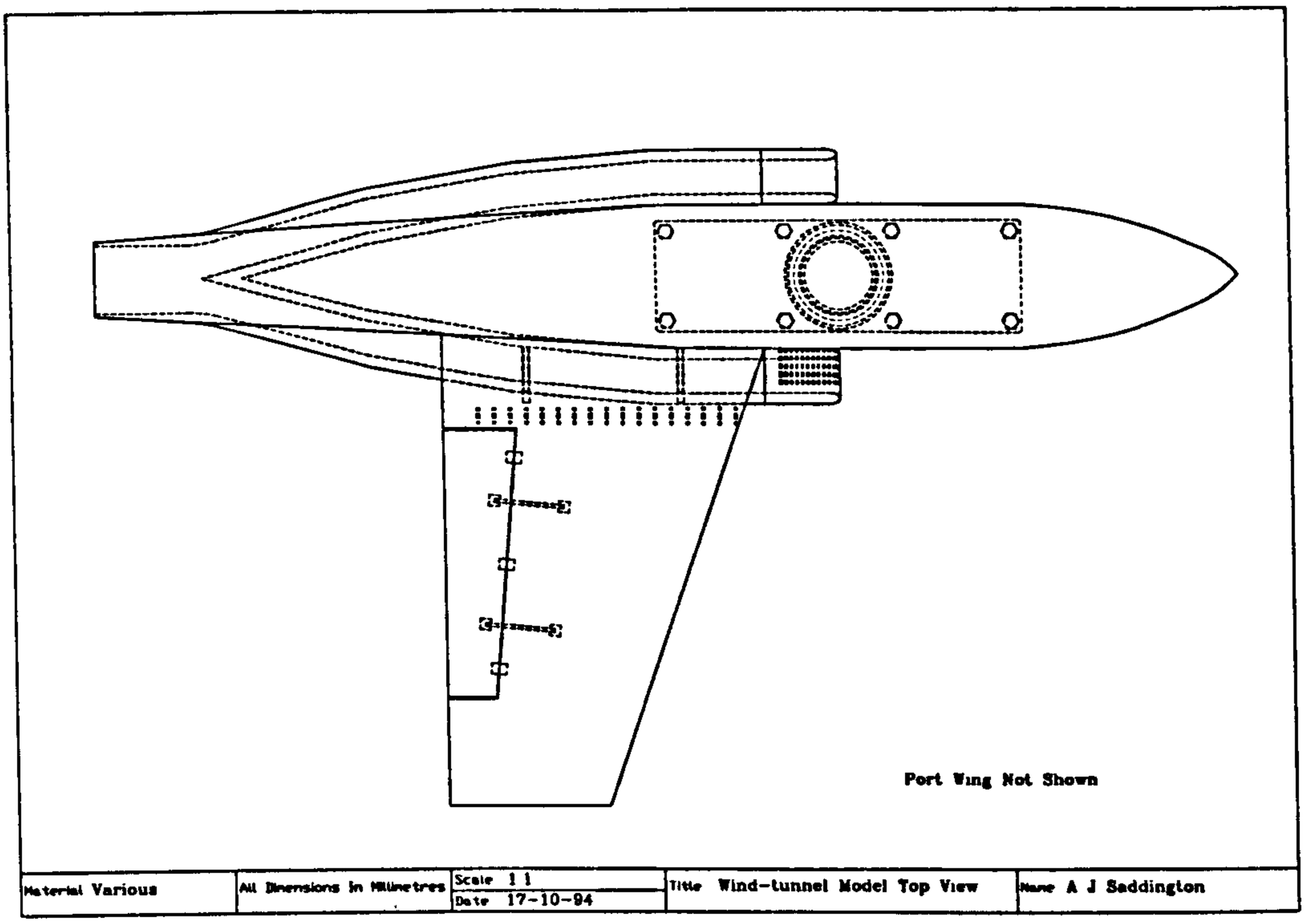

***Figure 3.21** - Top view of the wind tunnel model.*

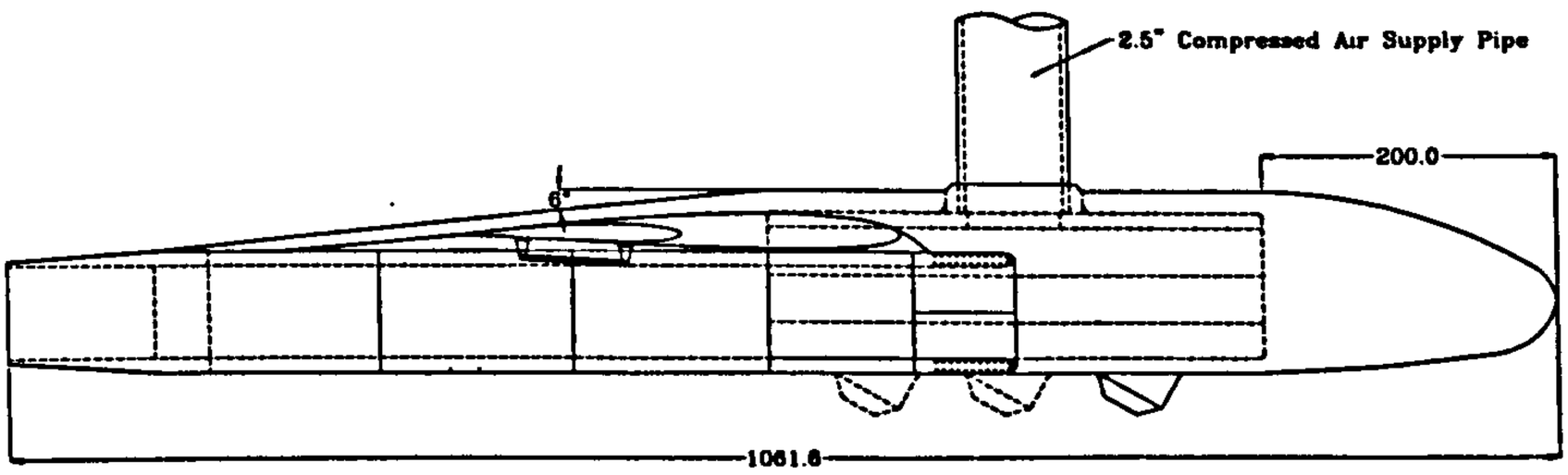

***Figure 3.22** - Side view of the wind tunnel model.*

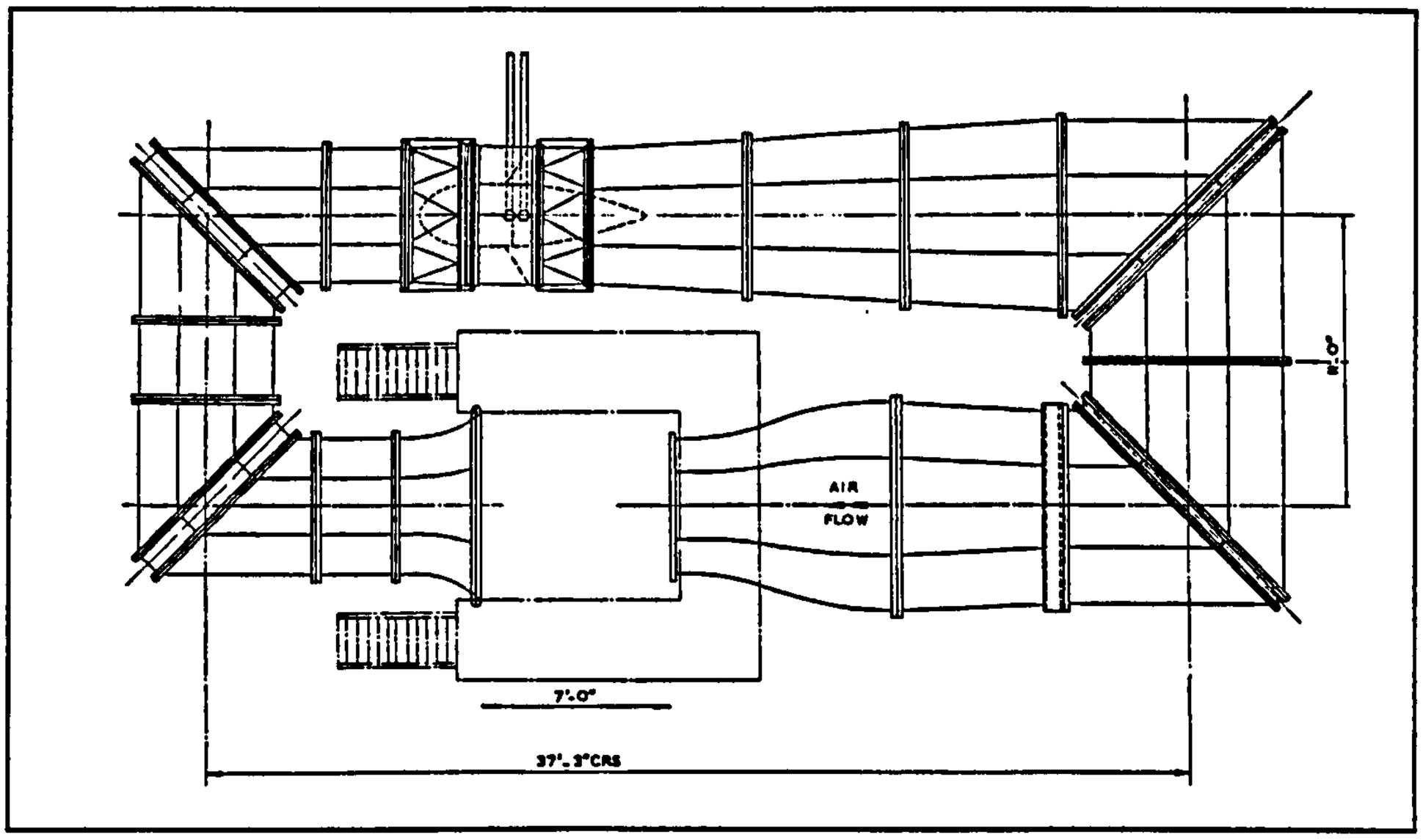

***Figure 3.23** - RMCS 5 foot by 3.75 foot open-jet wind tunnel.*

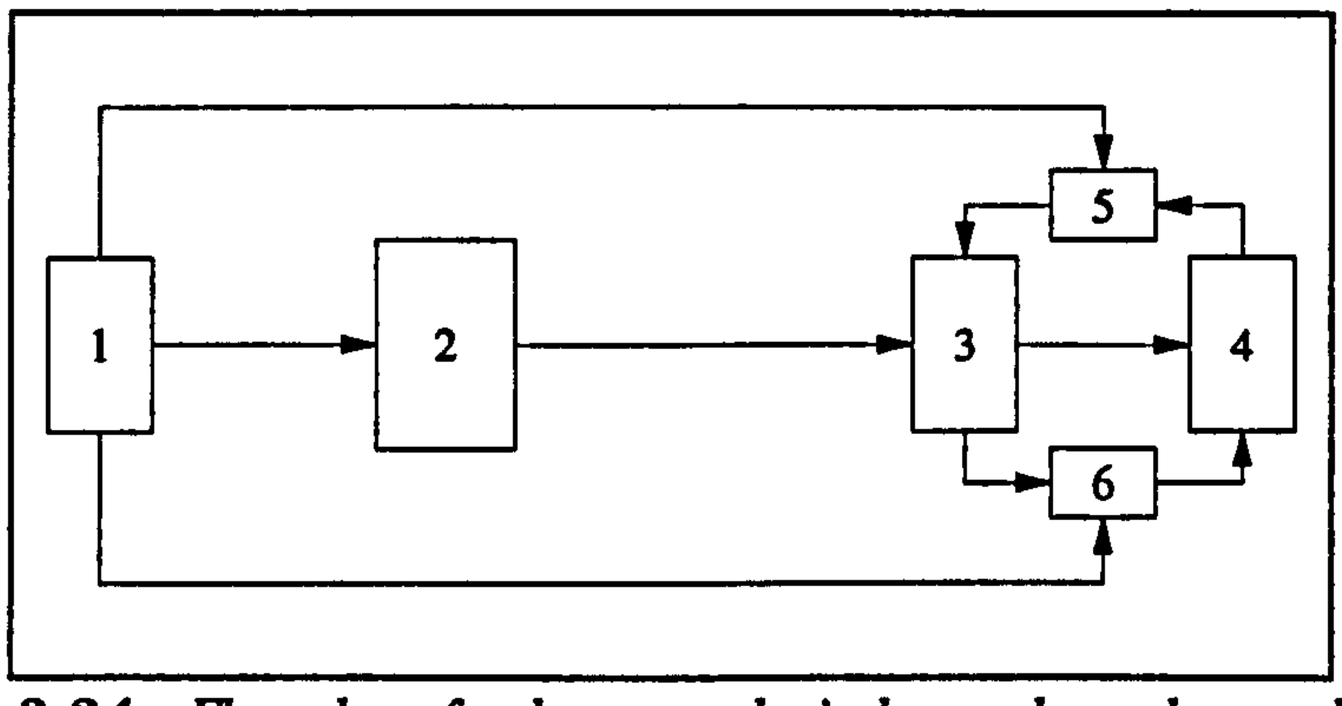

***Figure 3.24** - Flow chart for the manual wind tunnel speed control system.*

1. Manual control box with 'increase speed' and 'decrease speed ' buttons.
2. RS 4-phase unipolar stepper motor drive board.
3. Linear actuator.
4. Hydraulic fluid control valve for Dowmatic drive.
5. Over-speed micro-switch.
6. Under-speed micro-switch.

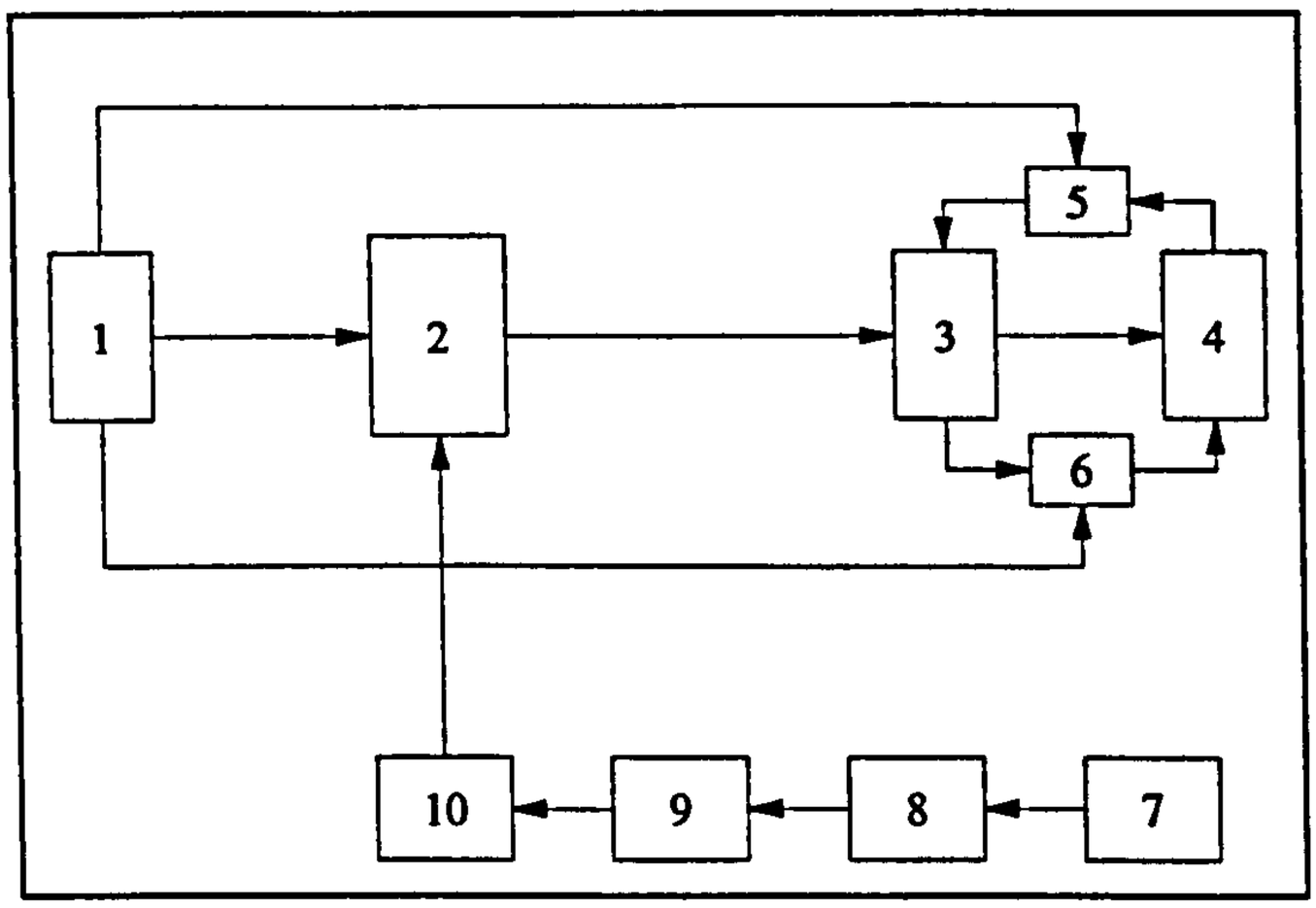

***Figure 3.25** - Flow chart for combined manual and computer-operated wind tunnel speed control system.*

1. - 6. As Figure 3.24 above.

7. Furness Controls FCO34 differential pressure transducer.

8. CIL mini-pod 8-channel, 12-bit digital to analogue converter.

9. Viglen 286-based PC with CIL alpha 01 controller card.

10. CIL S-block 4-phase unipolar stepper motor controller card.

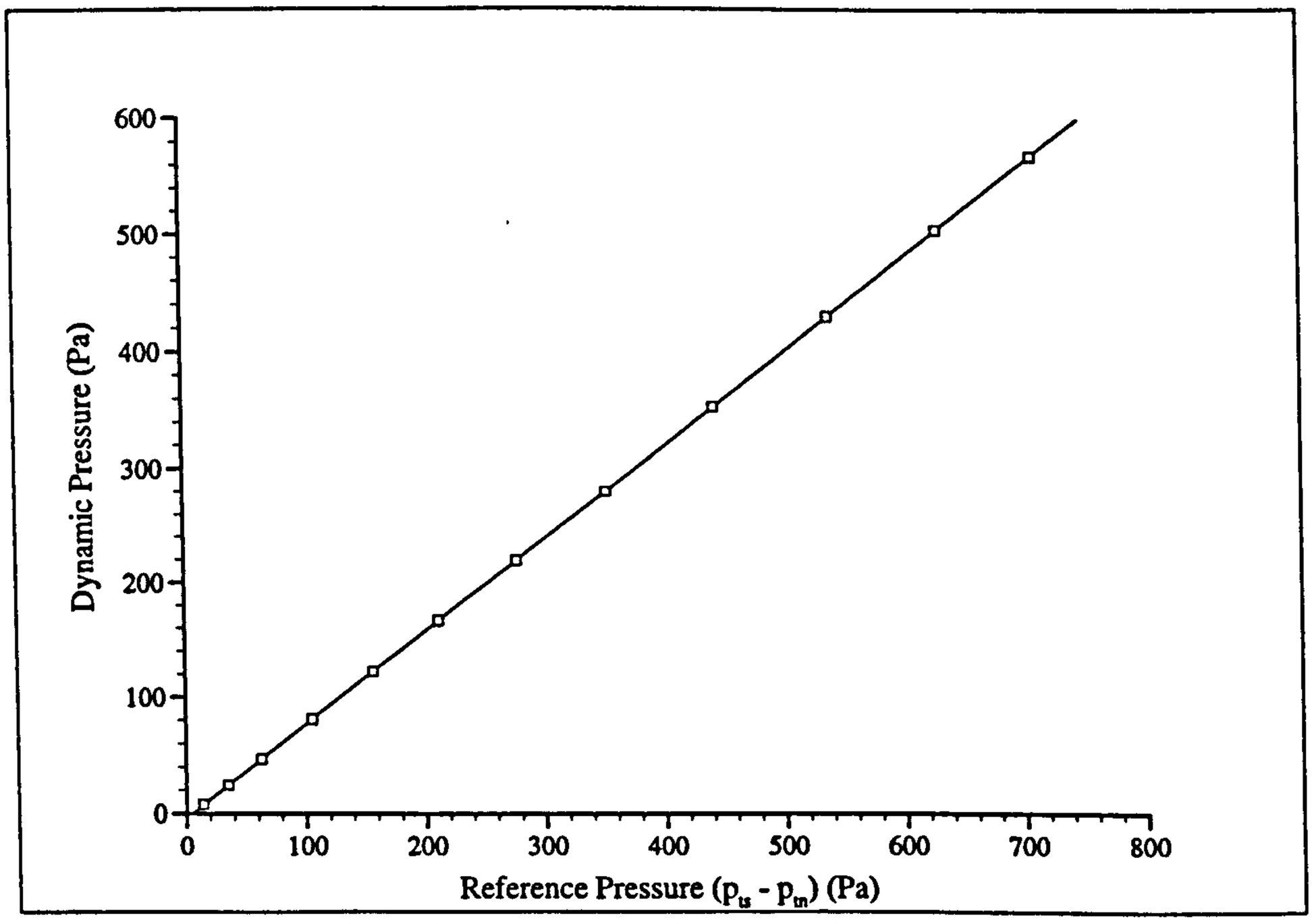

***Figure 3.26** - Calibration of wind tunnel reference pressure (p_{ts} - p_{tn}).*

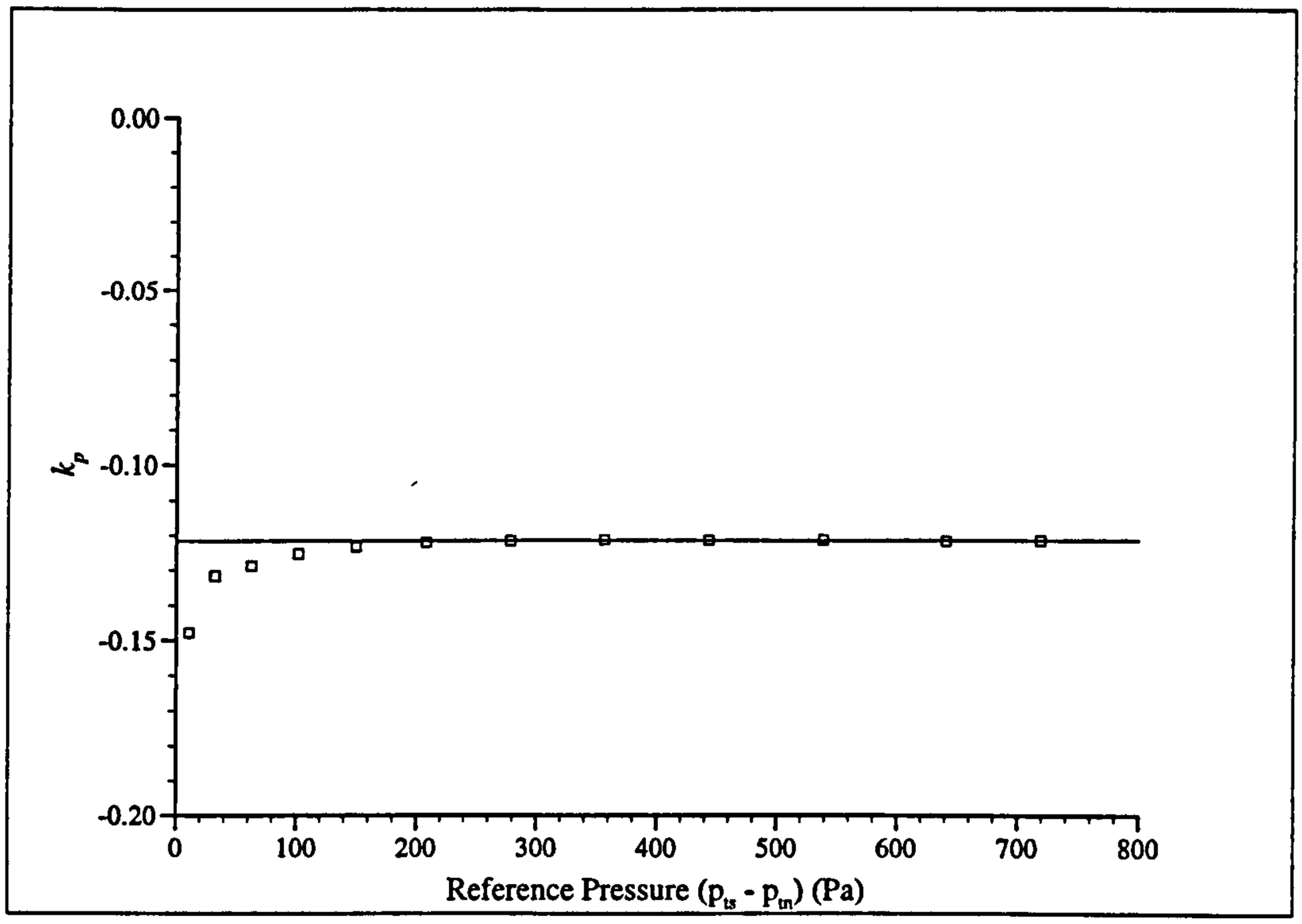

***Figure 3.27** - Determination of static pressure offset, k_p.*

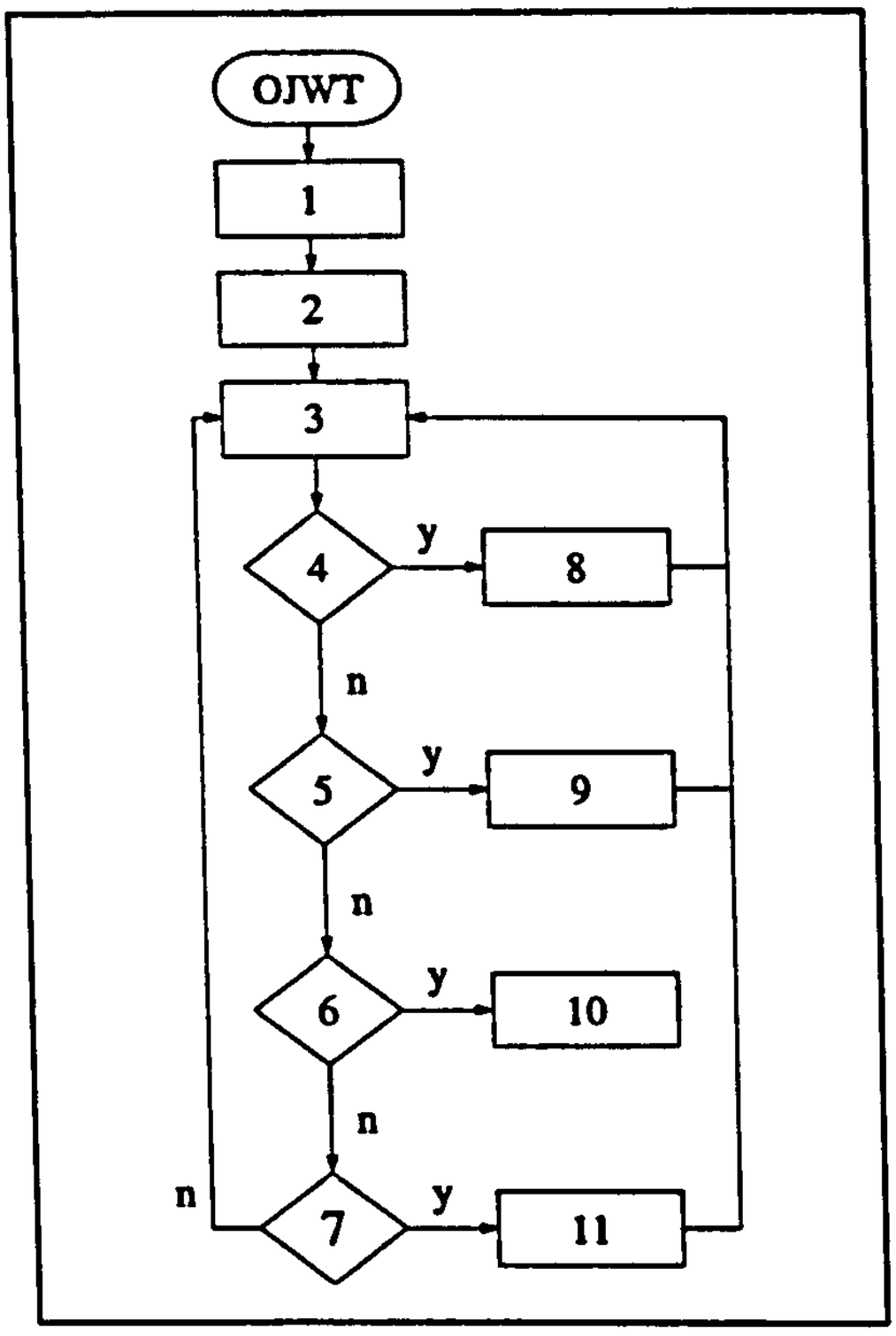

***Figure 3.28** - Schematic of the wind tunnel speed control software.*

1. Initialise system parameters.
2. Set-up screen display.
3. Get keyboard command.
4. Is the command 'set speed' ?
5. Is the command 'zero pressure transducer' ?
6. Is the command 'exit' ?
7. Is the 'maintain speed' flag set ?
8. Set tunnel speed to required value, set 'maintain speed' flag and update the screen display.
9. Get pressure transducer zero voltage offset and update the screen display.
10. Exit program.
11. Maintain tunnel speed to required value and update the screen display.

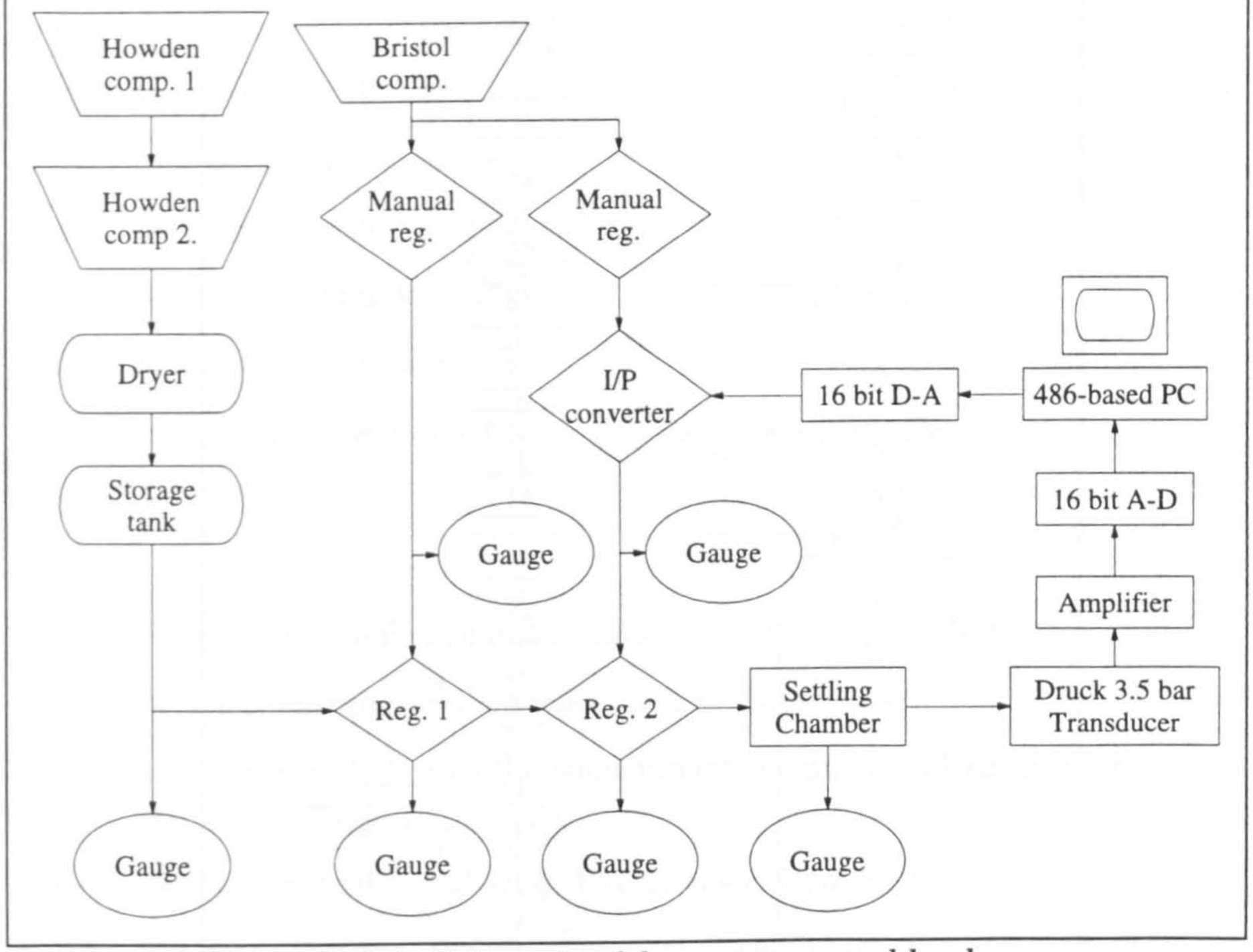

Figure 2.29 - *Schematic of the pressure control hardware.*

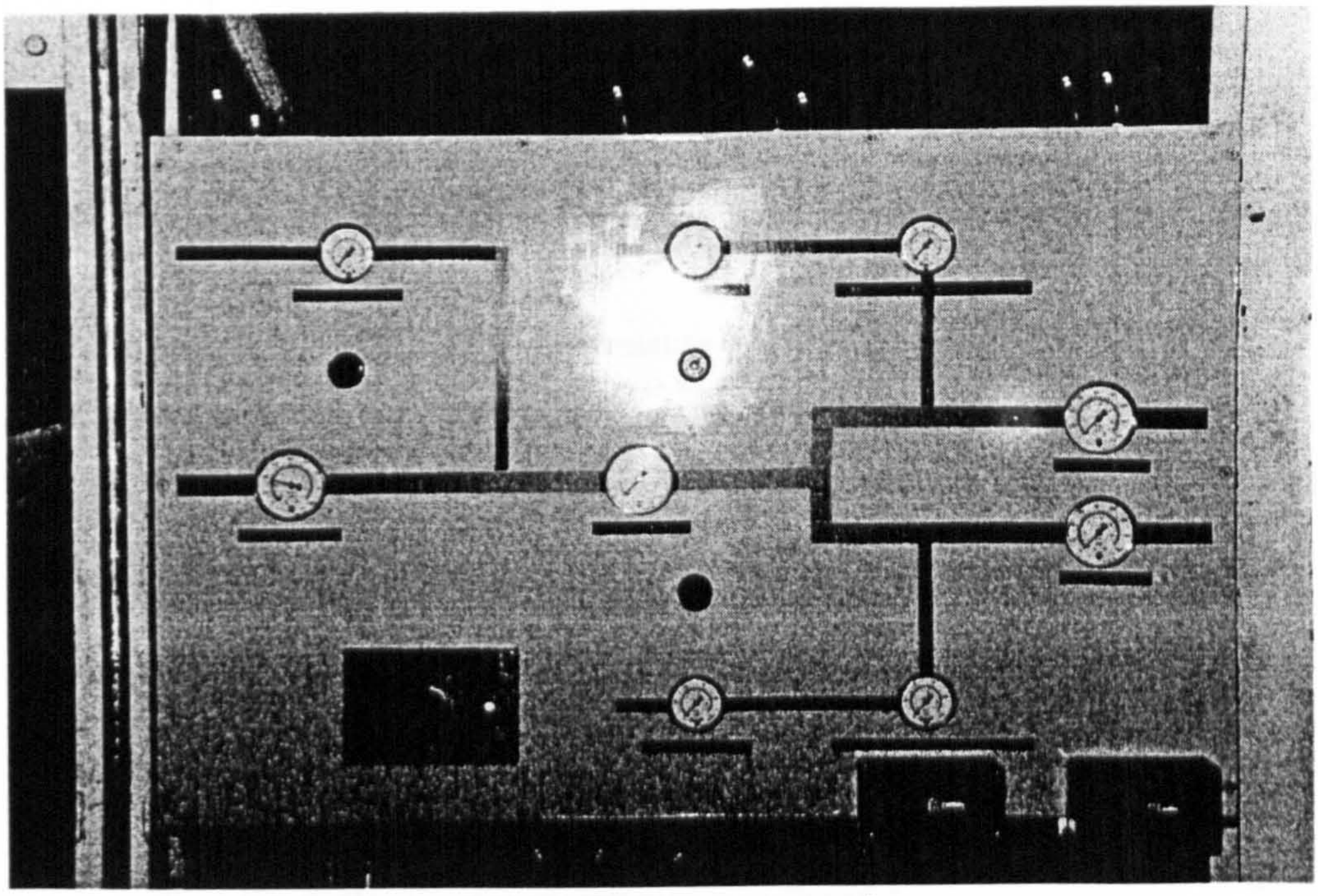

Figure 3.30 - *The pressure control system.*

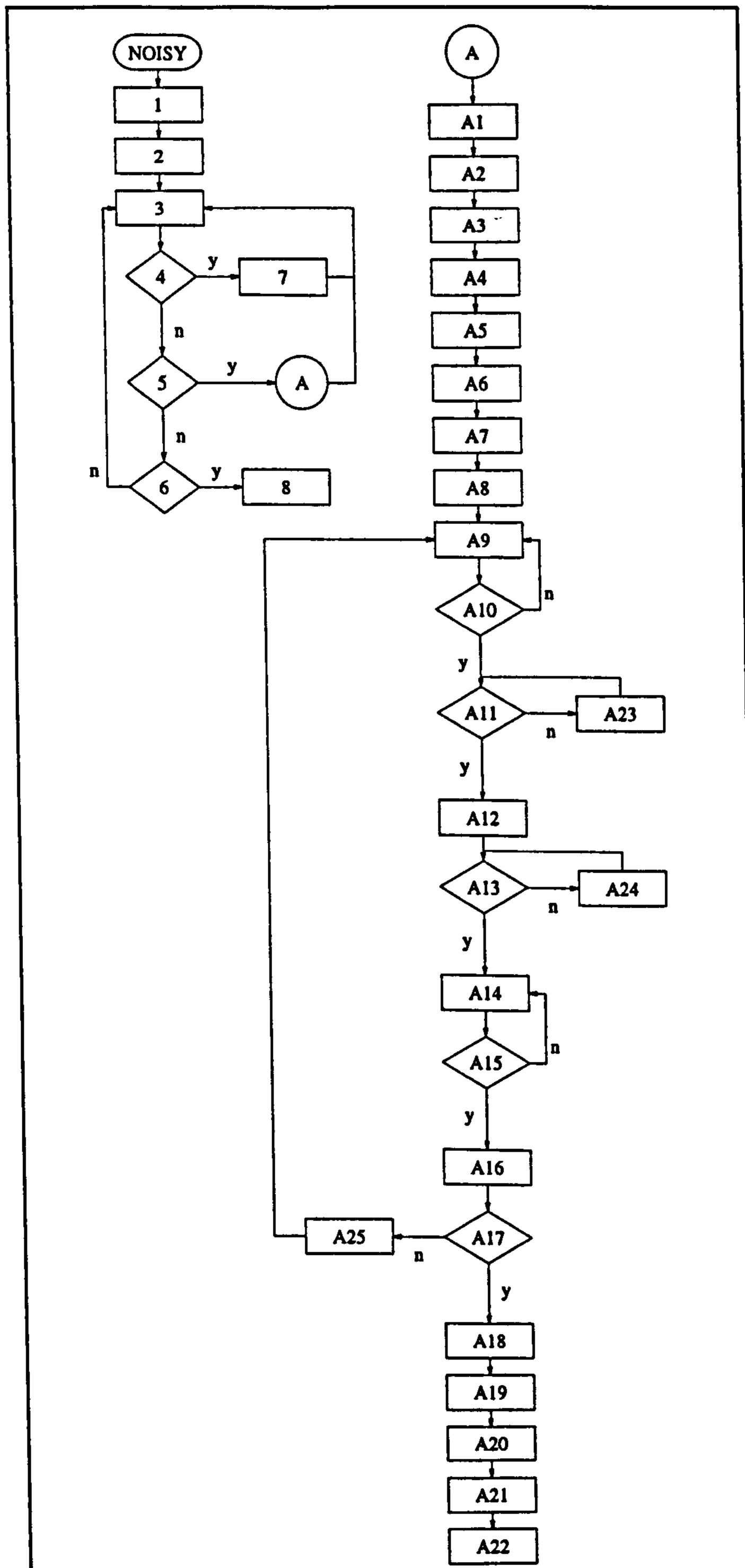

***Figure 3.31** - Schematic of the pressure control and data acquisition software (see key below).*

1. Initialise system parameters.
2. Set-up screen display.
3. Get keyboard command.
4. Is the command 'home Scani-Valves' ?
5. Is the command 'take data set' ?
6. Is the command 'exit' ?
7. Set Scani-Valves to their home positions and update the screen display.
8. Exit program.

A1. Set settling chamber pressure transducer zero voltage offset.

A2. Initialise micromanometer pressure transducer parameters.

A3. Open comm. link with the wind tunnel computer and get current set dynamic pressure.

A4. Get required NPR and set it. Update the screen display.

A5. Set Scani-Valves to their home positions and update the screen display.

A6. Open result file and write header information.

A7. Read the current time and date and write to the result file.

A8. Read atmospheric, settling chamber and wind tunnel temperatures and write to the result file.

A9. Open comm. link with the wind tunnel computer and get current 'in tolerance' status.

A10. Is the wind tunnel dynamic pressure within tolerance ?

A11. Is the NPR within tolerance ?

A12. Sample the micromanometer pressure transducer and maintain the current NPR setting.

A13. Has the NPR gone out of tolerance whilst sampling the micromanometer pressure transducer ?

A14. Open comm. link with the wind tunnel computer and get current 'in tolerance status.

A15. Has the wind tunnel dynamic pressure gone out of tolerance whilst sampling the micromanometer pressure transducer ?

A16. Write the sample data point to the result file and update the screen display.

A17. Have all the pressure tappings been sampled ?

A18. Read atmospheric, settling chamber and wind tunnel temperatures and write to the result file.

A19. Read the current time and date and write to the result file.

A20. Close the result file.

A21. Set the Scani-Valves to their home positions.

A22. Return

A23. Wait for NPR to come into tolerance.

A24. Wait for NPR to come into tolerance.

A25. Step appropriate Scani-Valve to next position.

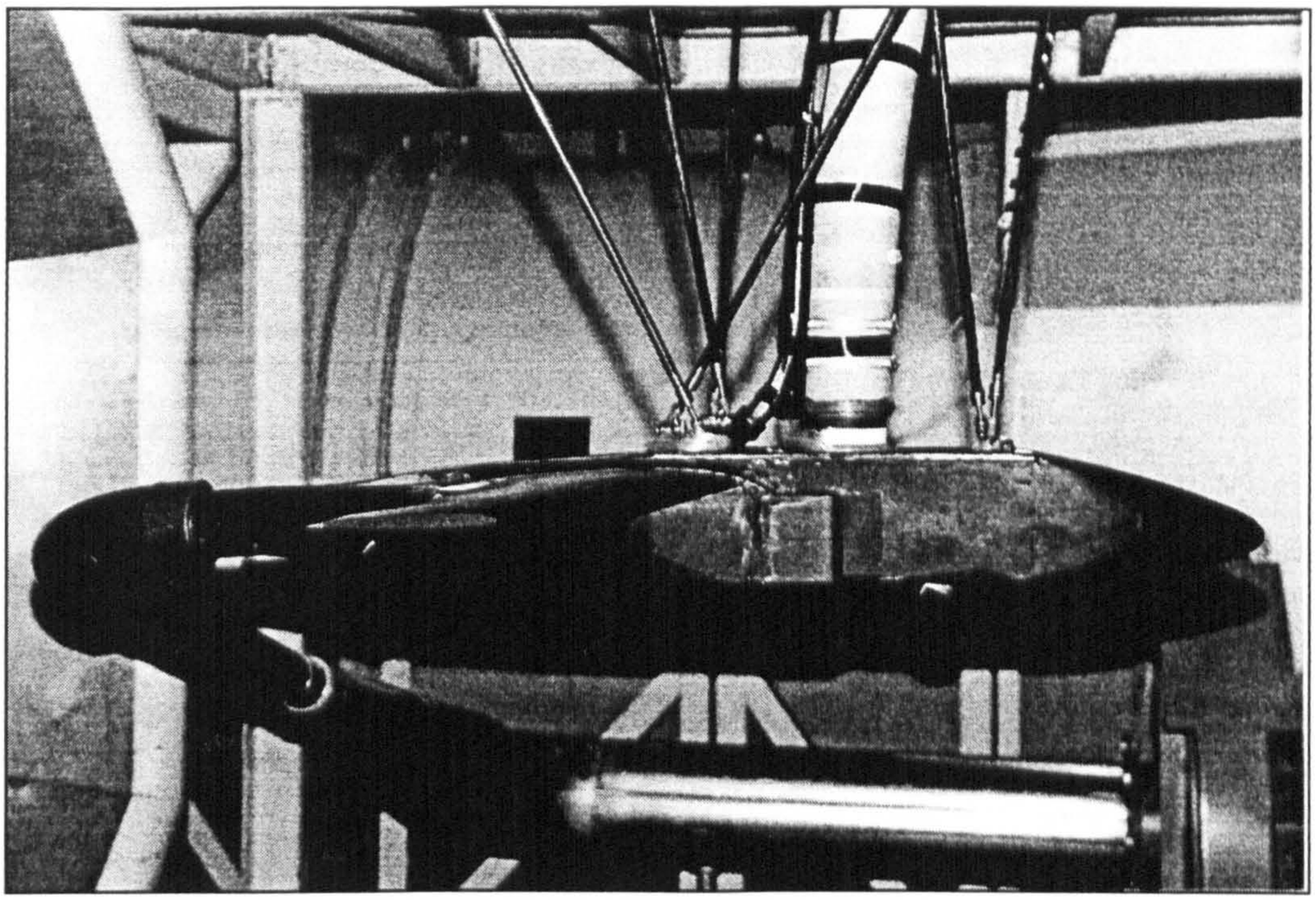

Figure 3.32 - *Side view of the wind tunnel model showing the support struts, compressed air supply pipe and intake ducting.*

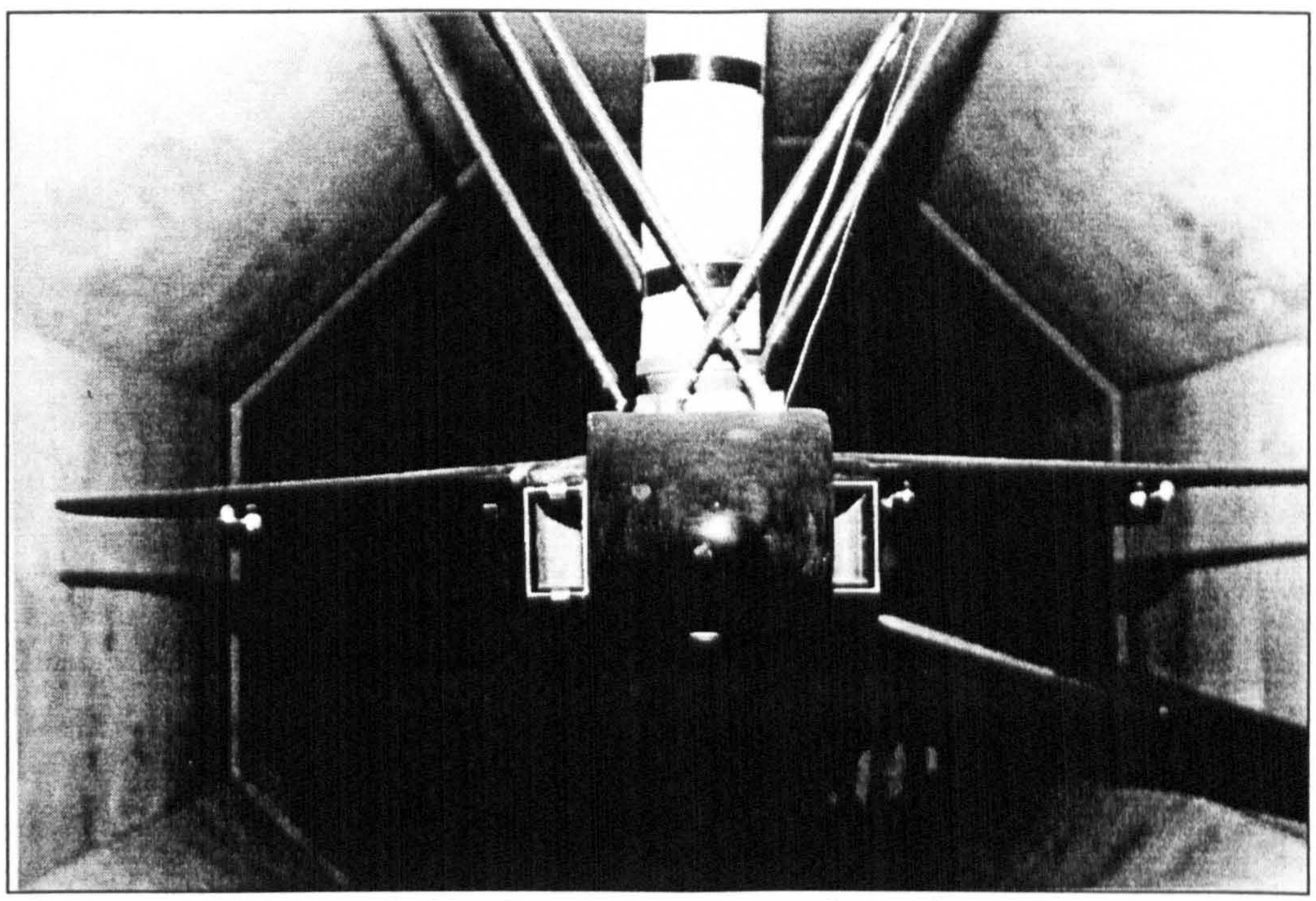

Figure 3.33 - *Front view of the wind tunnel model.*

4 Experimental Results

In this chapter the results of the experimental work are presented and discussed. Where possible, comparisons have been drawn between these results and similar past research.

4.1 Experimental procedure

This section describes the procedure used to set-up the model in the wind tunnel and gives an overview of the routine to obtain a single data set.

The settling chamber was mounted centrally in the working section of the open-jet wind tunnel using six support struts and set to zero degrees pitch and roll using a cross spirit level. The wind tunnel model, with the appropriate intake configuration for the test, was then located onto the settling chamber and secured in place. The compressed air supply pipe and the intake suction pipe were then connected to the top of the settling chamber and the rear of the fuselage respectively. The intake suction pipe was left connected even when intake suction was not required to maintain the consistency of the model configuration. Next, the 1.6 mm inside diameter PVC tubing was connected from the pressure tappings to the appropriate ports on the Scani-Valves and from these on to the Furness Controls FCO14 micromanometer. The total pressure probe in the settling chamber was then connected to the Druck pressure transducer. Finally the correct nozzle configuration was set for the particular test. A typical data set procedure is described below.

1. The Furness Controls FCO34 pressure transducer, which was used to measure the dynamic pressure, was zeroed in the wind tunnel control software.
2. The wind tunnel was then run up to the required dynamic pressure for testing.
3. The pressure control and data acquisition software was then run. The FCO14 micromanometer, which was used to measure the static pressures on the model, was also zeroed.
4. The centrifugal compressor, used for intake suction, was started if necessary.
5. The settling chamber pressure required for the particular test run was then set. For each static pressure reading on the model the software maintained the required settling chamber pressure and checked the wind tunnel dynamic pressure. The static pressure data were collected sequentially and stored in a result file. Further details of the control and data acquisition software are given in Section 3.2.

At the end of the run, the compressed air to the nozzle was automatically switched off. The wind tunnel and centrifugal compressor were then stopped by the researcher. The model configuration was then changed and testing continued.

The modular nature of the wind tunnel model enabled swift configuration changes to be made without the need to remove the model from the wind tunnel. The model,

however, did have to be removed from the tunnel (leaving just the settling chamber) to enable the intake configuration to be changed.

4.1.1 Changes introduced following the Phase 1 experiments

The Phase 2a experiments were a repeat of the Phase 1 experiments but with the addition to the test programme of tests at an NPR of 1.586. The Phase 2a tests were then repeated using a constant nozzle area (the 25.4 mm diameter nozzle was used) to ascertain the effect of varying mass flow rate. These tests were designated Phase 2b.

Some minor modifications were also made to improve the instrumentation and the control and data acquisition software. During the Phase 1 experiments it was noted that when the Scani-Valves switched across a large pressure difference, there was a significant time delay before the pressure in the interconnecting tube between the Scani-Valve and the pressure transducer had equalised. As a consequence, the sample pressures were in error. The magnitude of this error is not known. It did, however, result in the tendency to underestimate peak pressures. A three second delay was found to be sufficient to allow the pressure to equalise before sampling commenced and this modification was implemented in the data acquisition software prior to Phase 2 testing.

In addition, the 12-bit digital to analogue converter (DAC) was replaced by a 16-bit one. This provided a greater resolution for controlling the settling chamber pressure.

4.2 Schlieren photography

During the Phase 1 experiments, a Schlieren optical system was set up to look at the flow from the jet nozzles. Photographs of the jet efflux at NPRs of 2.0, 3.0 and 4.0 are shown in Figures 4.1, 4.2 and 4.3 respectively. At an NPR of 2.0 the jet is just visible. At higher NPRs the pictures clearly show the shock structure in the jet which is a result of the moderate underexpansion. Observation of the Schlieren image during a particular test run showed that the shock structure was very stable with no visible changes. This indicated that the tolerance on NPR was sufficient to eliminate any variation in shock structure during a particular test run. It was hoped that the Schlieren system might have been able to show the jet deflecting under high cross-flow velocities, but this was not the case. There was no evidence of any jet deflection nor any identifiable change in the shock structure between zero and maximum cross-flow velocity. This was probably due to the fact that the Schlieren system was only able to show the first three to five nozzle diameters (depending on the NPR). In this region of the jet structure there would be little or no jet deflection at the cross-flow velocities used.

4.3 Repeatability

Before the commencement of the Phase 1 and Phase 2 experiments, the repeatability of the recorded data was checked. A single test run was repeated three times in quick succession and the data compared. It was found that the wing and intake recorded static pressures fell just within the 1.5 percent error band estimated in Section 3.4.

As already mentioned, in between the Phase 1 and Phase 2 tests, the model and settling chamber were removed from the wind tunnel. This introduced an error in setting up the settling chamber incidence which in Section 3.4 was estimated to be no less than 0.1 degrees. Comparison of the Phase 1 and Phase 2 $C_{l\,(root)}$ data for the intake faired, jet off (datum) condition indicated that the Phase 2 tests were conducted at an incidence approximately 0.2 degrees greater than the Phase 1 tests. This indicates the importance of accurately setting up the model incidence.

4.4 Data reduction

A FORTRAN 77 program was written to read particular groups of result files and calculate the pressure coefficients. This program then created a Tecplot V7 ASCII data file containing the pressure coefficients and the non-dimensional co-ordinates of the wing and intake pressure tappings. On the wing pressure distribution curves, a C_p value of 0.0 at x/chord = 1.0 was added to the recorded data. This enabled the pressure distributions to be integrated to give $C_{l\,(root)}$ for the wing upper and lower surfaces. The intake pressure distributions were also integrated to give an intake normal force coefficient, C_{ni}. Graphs showing all the wing and intake pressure distributions can be found in the Cranfield University internal reports, SADDINGTON, 1996 (Phase 1) and SADDINGTON, 1997 (Phase 2). Some of these graphs will be used in the following sections to describe the various jet- and intake-related interference effects.

The effective velocity ratios for all the tests carried out are calculated in Appendix A. The Phase 1 raw C_p data are tabulated in Appendix B. The Phase 2a data (tests with nominally constant nozzle mass flow rate) are tabulated in Appendix C and the Phase 2b data (tests with constant nozzle area) in Appendix D.

4.5 Presentation of results

Referring to the test matrix (Table 3.2), the results were categorised as described below.

- Configuration A provided the datum wing pressure distribution case.
- Configuration B, when compared with Configuration A, showed the effect of the jet on the wing C_p distribution.

- Configuration C, when compared with Configuration A, showed the effect of the intake on the wing C_p distribution.
- Configuration D, when compared with Configuration C showed the effect of the jet on the intake pressure distributions.
- Configuration D, when compared with Configuration A showed the combined effect of the jet and intake flows on the wing C_p distribution.

Finally, the important comparison was made between the two methods of determining the total interference effect of the jet and intakes on the wing:

1. the linear addition of Configuration B and C results;
2. the Configuration D results.

The following sections discuss the effect of the different model configurations, described in Section 3.3 on the wing and intake pressure distributions and their associated forces. In addition, the effect of parameter changes within a particular model configuration are also presented.

4.6 The effect of the jet on the wing

In general, the jet entrainment appeared to introduce a localised velocity component into the cross-flow. As a consequence of the 60 degree jet vector angle, the jet-induced entrainment added a horizontal (freestream) and vertical velocity component into the flow-field around the aircraft. The jet-induced downwash and locally increased freestream dynamic pressure altered the wing root upper and lower surface C_p distributions. In general the result was a reduction in upper surface suction and an increase in lower surface suction. The changes were found to be influenced to a greater or lesser extent by all of the configuration variables; effective velocity ratio, NPR, nozzle area and longitudinal nozzle location. In all cases the jet operation was detrimental to the aerodynamic performance of the wing and resulted in wing root sectional lift losses, $\Delta C_{l\,(root)}$ of between -0.042 (-17.5%) and -0.234 (-89.4%) depending on the model configuration. The latter corresponds to an effective reduction in wing root incidence of over 2 degrees. Figure 4.4 shows the main jet-induced interference effects on the wing which have been described above.

It should be noted that the lift coefficient changes quoted are root sectional values. Since the influence of the jet diminishes as span-wise distance from the jet increases, the changes in $C_{l\,(root)}$ will be greater than those for the wing as a whole. The span-wise extent of the jet influence for the particular configuration tested is not known, but SPREEMAN, 1960 suggested that it may extend from 5 to 10 nozzle diameters. If the higher figure were chosen, then for the configuration tested, jet-induced interference effects would extend to between 35 percent and 75 percent semi-span, depending on the nozzle diameter chosen.

The jet-induced changes in wing root sectional lift coefficient, $C_{l\,(root)}$ are given in Tables 4.1, 4.2 and 4.3. Table 4.1 presents the Phase 1 data, whilst Tables 4.2 and 4.3 show the Phase 2a and Phase 2b data respectively.

Care should be taken when interpreting the percentage changes since at first sight they may appear to be alarmingly high. This is due to the relatively low datum $C_{l\,(root)}$ values. As a consequence, the percentage changes were somewhat higher than for a STOVL aircraft in transition, where $C_{l\,(root)}$ values would be expected to be greater. As has previously been observed, [MARGASON, 1966] the induced lift loss due to jet operation is generally thought to be independent of angle of attack, and therefore although the percentage changes will vary as the datum $C_{l\,(root)}$ is increased, the absolute changes should remain approximately the same. The results should, therefore, provide a good indication of the expected change in $C_{l\,(root)}$ for a similar STOVL aircraft configuration in transition.

Although the various interference effects for the particular aircraft under investigation are known quantitatively, it is not known how they would differ for a substantially different STOVL configuration. In Chapter 2, the effects of small changes in model configuration were shown to influence the flow-field around a STOVL aircraft. The configuration of the aircraft under investigation, although generic and with features common to many STOVL aircraft, could not represent all possible configurations simultaneously. Side-mounted intakes feature on the Harrier, Yak-38, Yak-141 and two of the original three JSF proposals (a chin-mounted intake was chosen for the Boeing JSF). All these aircraft have shoulder-mounted wings and with the exception of the Harrier and Boeing JSF, all use a centrally-located forward lifting jet or jets. It is expected, therefore, that the interference effects measured on the STOVL aircraft under investigation should be similar to those encountered on other current STOVL aircraft designs.

The following sections discuss the influence of the jet on the wing root pressure distribution and $C_{l\,(root)}$ values in more detail. The effect of variations in effective velocity ratio, NPR, nozzle area and nozzle position are also presented. For the purpose of this discussion, the Phase 2 data set will be used since it is more comprehensive and theoretically more accurate. The trends and comments are also applicable to the Phase 1 data.

4.6.1 The influence of effective velocity ratio, V_e

This section describes the influence of varying effective velocity ratio at constant NPR and nozzle position on the wing upper and lower surface pressure distributions. Comparisons are drawn with the data of MINECK & MARGASON, 1973.

4.6.1.1 Wing upper surface

Figure 4.5 presents the wing upper surface pressure distribution at an NPR of 1.586 with the nozzle in its forward position. The graph shows the pressure distribution at four different velocity ratios. Note that a velocity ratio of infinity is the jet-off (datum) condition. It is immediately clear that as velocity ratio is reduced from infinity the pressure distribution on the forward section of the wing upper surface is changed. The suction pressures forward of the mid-chord point are reduced, reducing the upper surface lift contribution. This effect is caused by the entrainment flow-field of the jet inducing a localised downwash. The downwash adds a vertical velocity component to the freestream and effectively reduces the angle of attack of the wing (see Figure 4.4). As effective velocity ratio is reduced, the relative magnitude of the ratio between downwash velocity and freestream velocity increases and as a consequence, the induced change in angle of attack increases with reducing velocity ratio.

An additional point to note is the pressure coefficient on the leading edge of the wing. With the jet off, the C_p value is 0.92, indicating that this pressure tapping is very near the forward stagnation point. With the jet blowing, however, the C_p value at this point reduces to 0.84 at an effective velocity ratio of 0.105, 0.79 at $V_e = 0.070$ and 0.67 at $V_e = 0.035$. This provides evidence that the forward stagnation point on the wing has shifted around the leading edge towards the upper surface and is consistent with a reduction in angle of attack.

Comparisons are drawn between these results and the wing pressure distribution on a V/STOL fighter aircraft tested by MINECK & MARGASON, 1973. Unfortunately, direct comparisons of the data are not possible, due to differences in the aircraft configuration (e.g. different aerofoil sections) and operating parameters (different NPR and velocity ratios), but comparisons of the trends can nevertheless be made. The configuration of MINECK & MARGASON'S aircraft was, in general, quite similar to the configuration of the author's model. It had a single, vertically-mounted, convergent nozzle lift-jet, located centrally in the fuselage underside, in line with the wing leading edge. The jet exit velocity was constant at around 200 ms^{-1} (an NPR of approximately 1.25). The model had a high-mounted wing (NACA 63A010 section) with four chord-wise rows of static pressure tappings at 25.0 percent, 38.7 percent, 52.4 percent and 80.0 percent semi-span. For their particular configuration, tests were conducted at four effective velocity ratios (including infinity) and 9 different wing incidences. For the purposes of comparison, however, only tests at zero degrees incidence will be considered here.

Figure 4.6 shows the upper surface pressure distribution on the wing at 25 percent semi-span (the same as the author's model). There are fewer pressure tappings and the data show a little more scatter but nevertheless the trends are the same. The data show a jet-induced interference resulting in a reduction in the suction pressures

on the wing upper surface. The greatest reduction in upper surface suction is at the lowest velocity ratio, in agreement with the author's data. The C_p values on the wing leading edge are also changed due to the jet interference, indicating a shift in the forward stagnation position.

Figure 4.7 shows the upper surface pressure distribution on the wing of MINECK & MARGASON'S aircraft at 80 percent semi-span. A jet-induced interference is still evident, even at this span-wise position (a little over 7 nozzle diameters). Varying effective velocity ratio influences the pressure distribution although the effect is obviously lessened. This would tend to confirm SPREEMAN'S, 1960 data that the jet influence extends span-wise to between 5 and 10 nozzle diameters.

4.6.1.2 Wing lower surface

Figure 4.8 shows the wing lower surface pressure distribution at an NPR of 1.586 with the nozzle in its forward position. On this surface a jet-induced 'suckdown' effect is immediately apparent. The suction pressures on the forward section of the wing lower surface are greatly increased by the operation of the jet. As with the upper surface, the effect is greatest at low velocity ratios due to the increased ratio of jet-induced downwash velocity to freestream velocity. By comparing this surface with the upper one, it is also evident that the lower surface provides a greater contribution towards the wing root sectional lift loss, $\Delta C_{l\,(root)}$ than does the upper surface.

Comparisons between these data and those of MINECK & MARGASON, 1973 can again be drawn. Figures 4.9 and 4.10 show the lower surface pressure distribution on their configuration at 25 percent and 80 percent semi-span respectively. A jet-induced 'suckdown' is again evident, particularly at 25 percent semi-span. The interference effect does, however, extend to the 80 percent semi-span position. As with the author's model, the lower surface of the wing shows more jet-induced interference than the upper surface.

4.6.1.3 The net effect

Integration of the wing upper and lower surface pressure distributions enables the calculation of the wing root sectional lift coefficient, $C_{l\,(root)}$. It is found that in general the same trend is observed, namely as effective velocity ratio is reduced, the jet-induced aerodynamic interference on the wing root sectional lift coefficient increases. Note that this is an indication of the change in aerodynamic lift and should therefore not be interpreted as representing the change in total lift on the aircraft (i.e. aerodynamic lift plus jet thrust lift). Section 2.2.2.1 describes the effect of effective velocity ratio on the total aircraft lift.

As an example of the trend observed, Figure 4.11 shows the variation in $\Delta C_{l\,(root)}$ (as a percentage of the datum $C_{l\,(root)}$) with effective velocity ratio at different NPRs and with the nozzle in its forward position. For a particular NPR, $\Delta C_{l\,(root)}$ becomes less

negative as effective velocity ratio is increased. This is due to the reduced downwash angle through which the jet interference changes the freestream velocity. If the jet-induced downwash were constant for a particular NPR then $\Delta C_{l\,(root)}$ would vary linearly with V_e. This is not the case, however, particularly for high NPRs. The reason for this is that the topology of the jet also changes with variations in velocity ratio. As V_e is increased the jet deflects more, resulting in an increased horizontal velocity component being introduced into the freestream and a reduced downwash. This is confirmed by data from the CFD-predicted downwash flow-field (see Chapter 6 for more details). Figure 4.12a shows the predicted downwash flow-field for an NPR of 1.5 and four different effective velocity ratios. The graph shows the change in downwash velocity, w with freestream distance, y from the nozzle exit. Figure 4.12b shows the associated co-ordinate system used for the jet in cross-flow CFD work. As effective velocity ratio is increased the peak downwash velocity decreases. The results are the same for the other NPRs modelled. This means that $C_{l\,(root)}$ does not vary linearly with V_e. MINECK & MARGASON'S data also show the same non-linear trend of C_l with V_e.

For MINECK & MARGASON'S aircraft, jet-induced interference resulted in an effective reduction in wing incidence (at 25 percent semi-span) of 0.4, 0.8 and 1.5 degrees at the three velocity ratios quoted. This is a similar range to that observed with the author's model.

In general, varying effective velocity ratio at different nozzle positions gave the same trends as discussed above, although the magnitudes of the pressures and hence sectional lift coefficients were slightly different. These results will not, therefore, be discussed further here. The reader is referred to Tables 4.1 to 4.3 for further details.

4.6.2 The influence of NPR (constant nominal mass flow rate)

This section discusses the effect of varying NPR, with a constant nozzle position and freestream dynamic pressure, on the wing upper and lower surface pressure distributions. These tests were conducted with a nominally constant mass flow rate (for NPRs of 2.0, 3.0 and 4.0), i.e. as the NPR was increased, the nozzle area was reduced. This was achieved by having different diameter nozzles for each of the three NPRs tested. Also included in this section is the low NPR, high mass flow rate nozzle. This had 50 percent more mass flow rate than the other nozzles but operated at an NPR of only 1.586.

4.6.2.1 Wing upper surface

Figure 4.13 shows the effect of varying NPR on the wing upper surface pressure distribution for a constant freestream dynamic pressure of 61.3 Pa (see Appendix A for equivalent standard velocity). Due to the relative magnitude of the entrainment flow-field between the jet and the freestream, this dynamic pressure should, there-

fore, provide the best indication of any NPR-related effects. Note that an NPR of 1.0 is the jet-off (datum) condition. There is a jet-induced interference, which has already been discussed above. Increasing NPR appears to increase the jet interference on the wing upper surface. This is thought to be due to the increase in jet velocity as NPR is increased. This effect, however, almost completely disappears at the two higher freestream dynamic pressures and therefore appears to be of significance only at low freestream dynamic pressures.

4.6.2.2 Wing lower surface

On the lower surface of the wing (Figure 4.14) there is a strong 'suckdown' interference induced by the jet. As with the upper surface, however, there is little change in pressure distribution with changes in NPR. At higher freestream dynamic pressures the jet-induced interference is lessened (because of the smaller downwash angle). At these higher freestream velocities, the pressure distributions at the different NPRs become almost indistinguishable.

4.6.2.3 The net effect

The wing upper and lower surface pressure distributions were integrated to give a net change in wing root sectional lift coefficient $\Delta C_{l\,(root)}$. As an example of the trends, consider Figure 4.15. At the lowest freestream dynamic pressure (61.3 Pa), there was a slight trend towards an increasing sectional lift loss with increasing NPR. At the intermediate freestream dynamic pressure, the opposite applied, $\Delta C_{l\,(root)}$ became less negative with increasing NPR. At the highest freestream dynamic pressure, there was no discernible trend brought about by changes in NPR.

An explanation for the small influence NPR had can be found by examining some of the numerical modelling data for a round vectored jet in cross-flow (see Chapter 6 for more details). Figure 4.16 shows the change in downwash velocity, w with freestream distance, y from the nozzle exit (see Figure 4.12b) for the four NPRs* and a freestream dynamic pressure of 61.3 Pa. The plot is taken at a distance, z of 0.125 m below the nozzle. The graph shows that, with the exception of a small band between y = 0.04 m and y = 0.08 m, the downwash velocity is essentially independent of NPR. With a constant nozzle area, a higher NPR jet would be expected to have a larger entrainment flow-field due to the increased peak velocity in the jet. By reducing the nozzle area, however, the flow-field of the higher NPR jet is effectively shrunk (see Figure 4.12b). The result is that the flow-field and hence downwash velocity for all the NPRs is approximately the same at almost any given dis-

* *Although the k-ε turbulence model is limited in its ability to handle compressibility effects (discussed in Chapter 6) it was not felt that these limitations would undermine this result.*

tance from the nozzle exit. This is supported by the results of SHUMPERT & TIBBETTS, 1969 (see Section 2.1.2.2).

It is believed that the small changes in wing upper and lower surface pressure distribution with NPR are due to the influence of the small band of different downwash velocities between y = 0.04 m and y = 0.08 m caused by the different NPR jets. As freestream dynamic pressure is increased, the downwash velocity decreases due to the greater jet deflection. The reason that the NPR effect quickly diminishes with increasing freestream dynamic pressure is the non-linear relationship between aerodynamic lift loss and effective velocity ratio. This effect was discussed in Section 4.6.1. Figures 4.17 and 4.18 show the variation in $C_{l\,(root)}$ with NPR for the centre and rearward nozzle positions. Again, varying NPR appears to show no consistent trend on the wing lift loss.

4.6.3 The influence of NPR (constant nozzle area)

As already stated above, tests were also conducted with a constant nozzle area. The 25.4 mm diameter nozzle was used for all the NPRs tested; i.e. 1.586, 2.0, 3.0 and 4.0. This section describes the effect of varying NPR with a constant nozzle area on the wing root sectional pressure distribution. Nozzle position and freestream dynamic pressure were kept constant.

4.6.3.1 Wing upper surface

Figure 4.19 shows the wing upper surface pressure distribution for the five different NPRs at a freestream dynamic pressure of 61.3 Pa. From the graph, it is clear that as NPR is increased, the jet-induced interference on the pressure distribution increases also. The effect of the jet is to reduce the suction pressures on the forward section of the wing up to about the 50 percent chord point, although for an NPR of 4.0, the wing pressure distribution is changed all the way back to the trailing edge. There are also relatively large changes in the leading edge static pressures, indicating a significant shift in the forward stagnation point.

Examining the CFD-predicted downwash flow-field (Figure 4.20) for this particular set of NPRs indicates why NPR has such a strong effect with a constant nozzle area. The graph is plotted from the same data as Figure 4.16 but this time the freestream distance, y (see Figure 4.12b), has been non-dimensionalised with nozzle diameter, d_n and the results are for a distance of $5d_n$ below the nozzle exit plane rather than 0.125 m. This eliminates the nozzle diameter effect. The CFD results show that the downwash induced by the jet varies greatly depending on the NPR specified* (at constant nozzle area). The higher the NPR, the higher the entrainment velocities and hence the higher the downwash velocity at a given distance from the nozzle exit.

---

* *See footnote on previous page..*

There is a distinct difference in the downwash velocity at different NPRs up to a freestream distance of approximately $10d_n$ (equivalent to 254 mm with the nozzle diameter used for the experimental tests). Contrast this with the small distance (40 mm or so) over which the downwash velocities differed in Figure 4.16 and the small difference in magnitude of these velocities. As freestream dynamic pressure is increased, the NPR effect lessens due to the reduction in downwash angle and downwash velocity. An NPR effect can, however, still be seen in the pressure distributions at the highest freestream dynamic pressure (551 Pa).

4.6.3.2 Wing lower surface

Figure 4.21 shows a plot of the wing lower surface pressure distribution. There is the usual jet-induced 'suckdown' effect present. The effect of varying NPR can also be seen on the graph. Increasing NPR increases the suction pressures forward of the 75 percent chord point, reducing the overall lift on the wing. As with the upper surface, the higher the NPR, the greater the jet-induced interference.

4.6.3.3 The net effect

Upper and lower surface pressure distributions were again integrated to give the wing root sectional lift coefficient, $C_{l\,(root)}$. Figure 4.22 shows the effect of varying NPR for three freestream dynamic pressures with the nozzle in its forward position. At the lowest freestream dynamic pressure (61.3 Pa), there is a strong NPR effect. At the highest freestream dynamic pressure (551 Pa), the NPR effect is reduced, as expected, but still evident. At the intermediate freestream dynamic pressure (245 Pa), however, there is an unexpected deviation from the trend. NPRs 3.0 and 4.0 give less change in $C_{l\,(root)}$ than at 551 Pa freestream dynamic pressure. At first glance, these could be considered to be spurious points, but this phenomenon is also evident at the centre nozzle position (Figure 4.23), although not at the rearward one (Figure 4.24). It is difficult to hypothesise the cause of this effect and at present no explanation can be found.

4.6.4 The influence of nozzle position

This section describes the effect of varying nozzle position at constant NPR and constant freestream dynamic pressure on the wing upper and lower surface pressure distributions.

4.6.4.1 Wing upper surface

Figure 4.25 shows the upper surface pressure distribution for an NPR of 1.586 and a freestream dynamic pressure of 61.3 Pa. Changing the nozzle position had a small influence on the pressure distribution. For this particular case, the rearward position appears to be the best and in fact gives a slight lift enhancement to the upper sur-

face when compared with the datum. The forward and centre positions show a slight reduction in upper surface suction and similar pressure distributions to one another.

The reason for the differences is thought to be the relative location of the jet entrainment flow-field and the wing. With the nozzle in its forward and centre positions, the entrainment flow-field is quite well ahead of the wing leading edge and this is shown by the reduction in suction pressures on the forward section of the wing. With the nozzle in its rearward position, however, the entrainment flow-field will be partially above the wing. Not only is there a vertical velocity component induced by the jet, but a horizontal one as well. This may be increasing the local freestream dynamic pressure and hence increasing the upper surface suction pressures.

As already noted, NPR and freestream dynamic pressure influence the location of the entrainment flow-field, and it was expected that these parameters would influence the trend with nozzle position. Figure 4.26 shows the pressure distribution on the upper surface of the wing at an NPR of 4.0 and a freestream dynamic pressure of 61.3 Pa. At these test conditions the trend with nozzle position is slightly different to that seen in Figure 4.25. The centre and rearward nozzle positions give more upper surface suction than the datum condition, whilst the forward nozzle position shows significantly less upper surface suction.

In general, it appears that the forward nozzle position gives the lowest upper surface suction and the rearward the highest. This is due to the location of the jet entrainment flow-field. The effect of the centre nozzle position is somewhere in between the other two. The relative magnitude of the lift loss for the three nozzle positions is, however, also dependent on NPR and freestream dynamic pressure.

4.6.4.2 Wing lower surface

On the lower surface of the wing (Figure 4.27) the effect of nozzle location described above is easier to see. Again, there is the usual jet-induced 'suckdown' effect. The pressure distributions for the forward and centre nozzle positions are almost identical, as with the upper surface. The rearward nozzle position gives increased lower surface suction due to the jet-induced increased local freestream dynamic pressure over the wing lower surface.

At the highest NPR (Figure 4.28) the lower surface pressure distribution follows the same trend as the upper surface. The centre and rearward positions give much increased lower surface suction pressures whilst the forward nozzle position shows much less jet interference.

4.6.4.3 The net effect

The net effect of the interferences described above is a relatively small change in $C_{l\,(root)}$ with changes in nozzle position. The increased upper and lower surface suc-

tions observed with the nozzle in its rearward position tend to cancel one another. Figure 4.29 shows the variation in $\Delta Cl_{(root)}$ with nozzle position for different NPRs at a freestream dynamic pressure of 61.3 Pa. In general, the data show that the forward nozzle position is the best (in terms of giving the lowest lift loss), then the centre, with the rearward position giving the highest sectional lift loss. It is not anticipated that this trend (of lift loss with nozzle position) will continue since, as discussed in Section 2.2.2.4, lift increases can be induced with nozzle positions near the wing trailing edge. With the freestream dynamic pressure increased to 245 Pa (Figure 4.30), there is almost no change in $Cl_{(root)}$ with changes in nozzle position. At the highest freestream dynamic pressure, 551 Pa (Figure 4.31) the rearward nozzle position proves to be the best, but only just. The Phase 2b data (constant nozzle area) shows similar trends.

Comparisons can be drawn with the data of HAMMOND & MCLEMORE, 1967. The details of their experiment have already been discussed in Section 2.2.2.4. Their jet was positioned approximately 0.45 chord lengths below the wing centre-line, compared with approximately 0.35 chord lengths for the author's model. HAMMOND & MCLEMORE found that varying the longitudinal nozzle position up to two chord lengths ahead of the wing leading edge did not significantly influence the interference lift loss. As already stated here, this was also found to be the case with the author's model especially at high freestream dynamic pressures.

4.7 The effect of the intakes on the wing

The changes in wing root sectional lift coefficient, $Cl_{(root)}$ due to the operation of the intake suction system are given in Tables 4.4 and 4.5. Table 4.4 shows the Phase 1 data and Table 4.5 the Phase 2 data. Note that there is no distinction here between Phases 2a and 2b because these tests did not involve the jet nozzles.

4.7.1 Wing upper surface

Figure 4.32 shows the wing upper surface pressure distribution with the intakes faired and with the intakes 'sucking'. The intake flow reduces the suction pressures on the upper surface of the wing, forward of the 50 percent chord point, and slightly increases them aft of the 50 percent chord point. The overall effect is that the wing upper surface lift contribution is reduced. The reason for the change is the presence of the intake flow. With the intakes faired, the airflow over the upper surface of the wing is relatively unobstructed by any part of the airframe. With the intakes 'sucking', however, the intake capture streamtube deflects the flow ahead of the wing which changes the local direction of the freestream air flowing over the wing upper surface. This results in the observed changes (see Figure 4.34).

Visualisation, of the flow around the intake and wing leading edge, using a tuft probe, indicated that the intake introduced a downward velocity component into the

freestream ahead of and above the wing upper surface. This is because the intake is lower than the wing. At a freestream dynamic pressure of 61.3 Pa, the capture area ratio of the intake is approximately 10 and so this effect is quite noticeable. As the freestream dynamic pressure is increased, the capture area of the intake decreases, becoming 5 at 245 Pa and 3.3 at 551 Pa. This results in a smaller change in flow direction into the intake. Hence, the intake interference reduces with increasing freestream dynamic pressure.

4.7.2 Wing lower surface

On the lower surface of the wing (Figure 4.33), the effect of the intake flow is more marked than on the wing upper surface. With the intakes 'sucking', the suction pressures over most of the lower surface of the wing are more positive, increasing the lift on the wing. With the intakes faired, the freestream air is accelerated by the fairing before passing over the wing lower surface. With the fairing removed, this acceleration is no longer present. Most of the air which would be diverted around the intake and under the wing is now being sucked into it (see Figure 4.34). As a result, the air flowing under the wing is of a lower velocity. This is thought to be the main reason for the difference between the two cases. There will also be a capture streamtube deflection effect similar to that on the upper surface. As with the upper surface, increasing freestream dynamic pressure reduces the intake faired/'sucking' differences.

4.7.3 The net effect of the intake on the wing

Integrating the upper and lower surface pressure distributions to obtain $C_{l\,(root)}$ shows that with the intakes 'sucking' the upper surface lift contribution is reduced at all freestream dynamic pressures. The percentage reduction is highest at the lowest freestream dynamic pressure. On the lower surface, the intakes 'sucking' condition gives a lift enhancement which is greater than the reduction on the upper surface. The net effect is that the wing generates more aerodynamic lift with the intakes 'sucking' than with the intakes faired. At a freestream dynamic pressure of 61.3 Pa, the effective increase in wing incidence due to intake suction is approximately 0.5 degrees. With the freestream dynamic pressure at 245 Pa the increase in wing incidence is 0.2 degrees and only 0.1 degrees at 551 Pa freestream dynamic pressure.

In their investigation of the pressure distribution on a V/STOL fighter, MINECK & MARGASON, 1973 did not record the pressures on the wing of the model with and without intake flow. Comparisons cannot, therefore, be drawn between their work and the results described in this section. MINECK & SCHWENDEMANN, 1973, using the same wind tunnel model, determined from force and moment data that the effect of intake plugs was effectively to reduce the wing angle of attack by 1 to 2 degrees. The intakes, however, were of the unpowered free-flow type. Considering that

the intakes on their model were proportionately larger than on the author's model, the 0.5 degree increase in wing root incidence recorded here would seem reasonable.

4.8 The effect of the jet on the intake flow

In order to determine the extent to which the jet alters the intake flow, the pressure distributions around the intake lips were examined. In general the jet entrainment introduces a localised velocity component into the freestream which appears to deflect the intake capture streamtube. The changes were found to be influenced to some extent by all the configuration variables, namely effective velocity ratio, NPR, nozzle area and longitudinal nozzle location. The pressure distributions were then integrated to give an intake normal force coefficient, C_{ni}. This provides an indication of the changes in airload seen by the intake due to jet operation.

The changes in C_{ni} are given in Tables 4.6 (Phase 1), 4.7 (Phase 2a) and 4.8 (Phase 2b). Negative values indicate a net downward load on the intake. The datum case was determined from model Configuration C. The following sections describe in more detail the effect of the jet on the four intake surface pressure distributions, lower outer, lower inner, upper inner and upper outer.

4.8.1 Lower outer surface

Figure 4.35 shows a typical intake lower outer surface* pressure distribution for the forward nozzle position. In this case the freestream dynamic pressure is 551 Pa. With the jet off, the C_p values on the majority of the lower outer surface of the intake were approximately zero. This is typical of the pressure distribution on a flat surface at zero degrees incidence to the freestream. Nearer the intake lip, the static pressure increases until the stagnation point is reached which, although not clearly captured on the graph, is nevertheless on the outer surface of the intake. This indicates that even at the highest freestream dynamic pressure, the intake is operating at a high level of suction, consistent with a STOVL aircraft operating at high power levels and low forward speed.

With the jet blowing, the C_p values on the lower outer surface of the intake are substantially more negative than with the jet off, of the order of -0.25 C_p. The lower pressure coefficients are caused by the action of the jet entraining ambient air, increasing the local air velocity over the intake lower surface, and thereby inducing a suction pressure on that surface. The jet-induced suction pressures on the intake lower surface decrease with increasing distance, x from the intake highlight. This is due to the increased distance away from the jet entrainment flow-field. It is likely that the stagnation point on the lower half of the intake is also shifted, but the

* *See Figure 4.47 for identification of intake surfaces and summary of jet-induced effects.*

magnitude of the change is difficult to ascertain from the pressure distribution data. Interpolation of the data to determine the location of the stagnation position was considered unworkable due to the high pressure gradients around the stagnation point area. As a consequence, there will be an error in the derived intake normal force coefficient, C_{ni} but this error is not thought to affect the overall results significantly. Figure 4.35 also shows the effect of changing NPR for constant nozzle mass flow rate. Increasing NPR reduces the jet-induced interference on the intake lower surface. This is a different effect to the one observed on the wing where increasing NPR with a constant nozzle mass flow rate has no significant effect on the pressure distributions. There is, however, an additional explanation, the effect of which is particularly strong for the STOVL aircraft tested. Very close to the nozzle exit, the jet may be unchanged by the freestream and as a consequence behaves in a similar manner to a solid cylinder in a cross-flow. Freestream air flowing around the jet will be accelerated increasing the local freestream air velocity. The 'blockage' will be larger, and hence the velocities higher at the pressure tapping locations, as the diameter of the nozzle is increased. The nozzle 'blockage' effect was not evident on the wing pressure distribution. This was probably due to the increased span-wise and vertical distance of the wing pressure tappings away from the jet nozzle compared with the intake tappings.

Figure 4.36 shows the same operating conditions as the previous graph except that the nozzle is now in the centre position. The effect of the jet operation is very similar to that with the forward nozzle position. The suction pressures induced by the jet over the whole of the lower surface of the intake are almost constant. With this nozzle position, the jet is situated very close to the intake pressure tappings and hence its influence is seen equally by all the pressure tappings. As with the forward nozzle position, the jet 'blockage' effect is also present and to a similar strength.

With the nozzle in the rearward position (Figure 4.37), the effect of the jet is less evident, as would be expected with the nozzle located behind the intake. The induced suction pressures are less negative than with the forward or centre nozzle positions and there is no evidence of the jet 'blockage' effect.

With a constant nozzle area and varying NPR, the effect of the jet on the intake lower outer surface pressure distribution is similar to that described above but with some notable differences. These tests eliminated the varying diameter which gave rise to the jet 'blockage' effect described above. With the nozzle in the forward position (Figure 4.38), varying NPR had little effect on the pressure distribution. This would tend to suggest that for this particular nozzle position the jet 'blockage' effect described above is the dominating influence on the intake lower outer surface pressures. At lower freestream dynamic pressures NPR does have an effect and, as would be expected, the higher the NPR, the more negative the pressures on the intake lower outer surface. At the centre and forward nozzle positions, Figures 4.39

and 4.40 respectively, the effect of increasing NPR is much clearer. The higher the NPR, the more jet-induced interference there is on the intake surface.

The results from these and the constant nozzle mass flow rate tests would tend to indicate that the jet-induced interference on the aircraft is determined by a combination of nozzle (and hence initial jet) diameter and NPR.

4.8.2 Lower inner and upper inner surfaces

Figure 4.41 shows the intake lower inner surface pressure distribution for the forward nozzle position and a freestream dynamic pressure of 61.3 Pa. The effect of jet operation is to reduce the suction pressures over almost the entire intake surface by approximately 3 C_p, depending on the NPR. Near the intake lip, the difference is greater, and on the intake highlight the reduction is of the order of 20 C_p. The jet induces a downward velocity component into the intake flow, moving the stagnation point on the lower surface of the intake further round from the lower outer surface towards the highlight. This means that less acceleration of the intake air takes place around the lower intake lip as shown by the less negative pressures in the graph. For the constant mass flow rate tests shown, the higher the NPR, the less the jet-induced interference on this intake surface. This is consistent with the lower outer surface discussed above.

On the upper inner surface (Figure 4.42) the effect is similar, except that in this case the jet interference results in an increase in the suction pressures around the intake lip. The increase in suction pressures on this surface is smaller than the decrease observed on the lower inner surface because the jet interference is stronger near the lower surface.

4.8.3 Upper outer surface

On the upper outer surface of the intake (Figure 4.43), there is a small jet-induced interference. The effect of the jet is to decrease the positive pressures on the surface of the intake. The higher the NPR, the greater the jet-induced interference. This is most likely due to the higher downwash velocity at higher NPRs. The interference effect is much smaller than for the lower outer surface due to the greater distance between the upper surface of the intake and the jet. Nozzle mass flow rate does not appear to influence the interference effect. Figure 4.44 shows that with the constant nozzle area tests (Phase 2b), the jet-induced interference is almost identical to the Phase 2a tests.

Some comparisons can be made between the data obtained from the author's model and those of MINECK & MARGASON, 1973. Figure 4.45 shows the intake upper outer surface pressure distribution on the author's STOVL configuration for the rearward nozzle position and an NPR of 1.586; this is the nearest comparable configuration to the one tested by MINECK & MARGASON. The data show that as effective velocity

ratio is reduced, the jet-induced interference on the intake surface increases. This is in agreement with MINECK & MARGASON'S data (Figure 4.46).

The jet-induced interference effects described above are summarised for all four intake surfaces in Figure 4.47.

4.8.4 The net effect of the jet on the intake flow

The pressure distributions on all four of the intake surfaces were integrated to give an intake normal force coefficient, C_{ni}. These were then summed to give the net pressure force acting on the intake (negative indicating a downward force). Figure 4.48 shows the variation in C_{ni} for the three nozzle positions and a freestream dynamic pressure of 61.3 Pa. It is immediately clear that the jet-induced interference on the intake varies with nozzle position. The forward nozzle shows the greatest change in C_{ni}, then the centre, with the rearward position showing the least. With nominally constant mass flow rate, varying NPR gave no identifiable trend in C_{ni}. This was especially evident at the higher freestream dynamic pressures (Figures 4.49 and 4.50). In these figures the effect of different nozzle positions is also particularly clear.

With regard to the constant nozzle area tests, Figure 4.51 shows the variation in C_{ni} with NPR for the three nozzle positions and a freestream dynamic pressure of 61.3 Pa. Increasing NPR increases the downward force on the intake due to the higher downwash velocity which has been shown to exist in the entrainment flowfield. At the higher freestream dynamic pressures of 245 Pa (Figure 4.52) and 551 Pa (Figure 4.53), however, the NPR effect is not evident.

4.9 Comparison of separate and simultaneous jet and intake testing

This section compares the effect on $\Delta C_{l\,(root)}$ of jet operation alone, jet and intakes operating separately and jet and intakes operating simultaneously. The jet-induced changes in wing root sectional lift coefficient, $C_{l\,(root)}$, for the combined jet and intake tests are given in Tables 4.9, 4.10 and 4.11. Table 4.9 shows the Phase 1 results, with Tables 4.10 and 4.11 showing the Phase 2a and Phase 2b results respectively.

With both the jet blowing and the intakes 'sucking', the expectation might be that the wing upper and lower surface pressure distributions would be some combination of the isolated jet and intake configurations (B and C) described above, and this is indeed the case. In general, the wing shows less-negative $\Delta C_{l\,(root)}$ values with the jet blowing and intakes 'sucking' than with the jet blowing and intakes faired. If no mutual interference existed between the jet and intakes then the combined effect of the two would simply be obtained by the linear addition of the results from the isolated jet and intake configurations. If there is a mutual interference effect, however,

then there would be a discrepancy between these results and the $\Delta C_{l\,(root)}$ values obtained with the jet and intakes operating simultaneously.

Analysis of the data from simultaneous jet/intake testing shows that the numerical sum of the interference effects on the $C_{l\,(root)}$ values generated by the jet and intake tested separately, is not the same as with the jet and intakes in operation together. The effects appear, therefore, to be adding non-linearly. The discrepancy is the jet/intake mutual interference, in particular the effect of the jet on the intake flow.

Comparisons of the effect of testing the jet and intakes separately and simultaneously are given in Tables 4.12 (Phase 1), 4.13 (Phase 2a) and 4.14 (Phase 2b). In general, the results show that obtaining the overall wing root sectional lift loss, $\Delta C_{l\,(root)}$ from simultaneous jet and intake testing, gives a greater lift loss than by summing the values from separate jet and intake testing. The difference varies depending on the test parameters, but for the STOVL aircraft tested, was determined to be as high as 0.08 $C_{l\,(root)}$ (equivalent to a change of 0.75 degrees in wing root incidence).

The combined effect of separate jet and intake testing is to shift the wing root interference lift loss, caused by the jet, a fixed amount, which was determined by the Configuration C tests. This method of determining the wing lift loss only takes into consideration the effect of freestream dynamic pressure on the results and not NPR or nozzle position. In the following sections, the effect of varying the three operating parameters, V_e, NPR and nozzle position are discussed.

4.9.1 The influence of effective velocity ratio, V_e

Figure 4.54 shows the wing root sectional lift loss for an NPR of 1.586 and the nozzle in the forward position. With the jet operating alone, increasing effective velocity ratio reduces the lift loss. This trend has already been described in Section 4.6.1. The 'jet and intake separate' line is obtained by adding the appropriate intake interference effect to the jet-only data. With the jet and intakes operating together, the result is somewhat different, particularly at low effective velocity ratios.

Regarding the forward nozzle position (Figure 4.54), the discrepancy in lift loss is greatest at the lowest effective velocity ratio (0.035), the difference being over 17 percent (0.045 $C_{l\,(root)}$). This is because the jet-induced interference on the intake flow increases with reducing velocity ratio as described in Section 4.8.1. As effective velocity ratio is increased, the jet-induced interference on the intake reduces and so the difference between the two methods of obtaining the wing lift loss is also reduced. Even at the highest velocity ratio of 0.105 there is still a detectable difference, although it is smaller (3 percent $C_{l\,(root)}$). At the centre and rearward nozzle positions (Figures 4.55 and 4.56) the trend is similar i.e. the discrepancy is greatest at low velocity ratios and reduces as the velocity ratio increases.

With all three nozzle positions shown, the wing root sectional lift loss with jet and intakes operating together is similar to the jet-only case at high effective velocity ratios. In this instance it appears that the lift-enhancing effect of the intake is cancelled by the jet-induced interference on the intake. Whether this trend with V_e will continue is not known. It is conceivable that at even higher freestream dynamic pressures, the lift loss with jet and intakes operating separately may be greater than the jet on its own. To confirm this possibility, however, it would be necessary to conduct testing at higher freestream dynamic pressures (assuming that the NPRs remain the same). Unfortunately this is not possible with the facilities available.

4.9.2 The influence of NPR (constant nominal mass flow rate)

The effect of varying NPR at constant nozzle mass flow rate is shown in Figure 4.57 for the forward nozzle position and a freestream dynamic pressure of 245 Pa. The 'jet-only' and 'jet and intake separate' plots are parallel, separated by the intake lift enhancement determined from the Configuration C tests. The simultaneous jet and intake test falls neatly between the two and, with the exception of some slight deviation gives a constant difference of approximately 4 percent $C_{l\,(root)}$. This is as expected since it has already been shown in Section 4.6.2 that varying NPR at constant nozzle mass flow rate has little or no influence on the jet-induced interference on the intake flow. The same is true of the centre (Figure 4.58) and rearward (Figure 4.59) nozzle positions.

4.9.3 The influence of NPR (constant nozzle area)

Figure 4.60 shows the effect of varying NPR with a constant nozzle area and a freestream dynamic pressure of 551 Pa. As NPR is increased, the lift loss on the wing (jet-only tests) increases. This has been described previously in Section 4.6.3. Again the effect of separate jet and intake testing is to add a constant offset to this data. With the jet and intakes operating simultaneously, the wing lift loss falls between the two and follows the same trend. As with the constant mass flow rate case, the effect of the jet on the intake follows the same NPR trend as the effect of the jet on the wing and so, whether taken separately or together, the trend with NPR is the same. Figures 4.61 and 4.62 show the centre and rearward nozzle positions respectively. Here, again, the trend and differences are similar.

4.9.4 The influence of nozzle position

The effect of nozzle position is shown in Figure 4.63 for an NPR of 1.586 and a freestream dynamic pressure of 61.3 Pa. This graph shows quite clearly one of the shortfalls of testing the jet and intakes separately. As already mentioned, the $C_{l\,(root)}$ increment added to the jet-only tests does not vary with nozzle position because it is obtained from the two jet-off configurations. The jet-induced interference on the in-

take is greatest at the forward nozzle position and decreases as the nozzle is moved further aft. This was described in Section 4.8.4. This trend is reflected in Figure 4.63 where, at the forward nozzle position, the discrepancy between separate and simultaneous intake testing is quite large, 17 percent $Cl_{(root)}$, reducing to 13 percent for the centre nozzle position and 9 percent for the rearward position.

At higher freestream dynamic pressures, the jet-induced interference on the intake is smaller. The consequence of this is also apparent in Figures 4.64 and 4.65 where nozzle position does not seem to have such a strong influence on the difference between separate and simultaneous jet and intake testing.

4.10 Summary

4.10.1 The effect of the jet on the wing

In general, the jet entrainment appeared to introduce a localised velocity component into the cross-flow which altered the wing upper and lower surface pressure distributions. The changes were found to be influenced to a greater or lesser extent by all of the configuration parameters, namely effective velocity ratio, NPR and longitudinal jet location. The following observations were made.

- The jet-induced lift loss on $Cl_{(root)}$ varied between -0.042 and -0.234. The latter is equivalent to a reduction in wing root incidence of over 2 degrees.
- Increasing effective velocity ratio reduced the jet-induced $\Delta Cl_{(root)}$ increments for constant NPR and nozzle position. The variation was non-linear.
- Varying NPR with a constant nozzle mass flow rate showed no consistent effect on $\Delta Cl_{(root)}$.
- Increasing NPR with a constant nozzle area increased the jet-induced $\Delta Cl_{(root)}$ increment, particularly at low freestream dynamic pressures.
- Nozzle position showed a small influence on $\Delta Cl_{(root)}$. Its effect was dependent on the particular combination of NPR and freestream dynamic pressure.

4.10.2 The effect of the intakes on the wing

The effect of the intakes on the wing was to create a 'lift enhancement'. This was due to the intake flow altering the local velocity and direction of the freestream air ahead of the wing. At the lowest freestream dynamic pressure tested (61.3 Pa) the lift enhancement was equivalent to a 0.5 degree increase in wing incidence. As freestream dynamic pressure was increased the lift-enhancing effect reduced becoming 0.2 degrees at 245 Pa and 0.1 degrees at 551 Pa.

4.10.3 The effect of the jet on the intakes

Jet-induced interference introduced a velocity component into the freestream which affected the intake flow as well as the airflow over the wing. This created a download on the intakes which was determined from the intake static pressure distributions. The following observations were made.

- The largest change in intake normal force coefficient C_{ni} occurred at the lowest freestream dynamic pressure and reduced with increasing dynamic pressure.
- Increasing NPR at constant nozzle mass flow rate did not affect the value of C_{ni} for a particular nozzle position and freestream dynamic pressure.
- Increasing NPR with a constant nozzle area increased ΔC_{ni}, particularly at the lowest freestream dynamic pressure.
- Jet-induced interference on the intake was greatest for the forward nozzle position, followed by the centre and rearward positions. The difference between C_{ni} at the centre position and the two positions either side was approximately the same i.e. the effect decreased linearly with nozzle position.

4.10.4 The effect of the jet and the intakes on the wing

In general, with the jet and intakes operating simultaneously, the $\Delta Cl_{(root)}$ values for a particular set of model parameters were lower than for the jet-only configuration. The trends observed on the wing pressure distributions with the jet-only configuration were very similar. The numerical sums of the $\Delta Cl_{(root)}$ values obtained from separate jet and intake configurations, however, were not the same as the $\Delta Cl_{(root)}$ values obtained with simultaneous jet and intake testing. The discrepancy between the two methods is due to the jet-induced interference on the intake flow. This brings into question the applicability of separate jet and intake testing for STOVL aircraft.

4.10.5 Comparison between separate and simultaneous jet and intake testing

In general, there was a discrepancy between the $\Delta Cl_{(root)}$ values obtained from separate and simultaneous intake testing. The discrepancy between the two methods was found to be dependent on all the model configuration parameters. The following observations were made.

- The discrepancy varied between approximately -0.08 and 0.0 $\Delta Cl_{(root)}$ depending on the model configuration and test parameters. This is equivalent to nearly 0.75 degrees change in wing root incidence.

- The discrepancy was found to be greatest at the lowest effective velocity ratios but was still evident at the highest ones.
- Both methods of determining the combined interference effect of the jet and intakes on the wing followed the same trend with NPR (for both the constant mass flow rate and constant nozzle area tests). The discrepancy, therefore, was reasonably constant for variations in NPR.
- At the lowest freestream dynamic pressure tested (61.3 Pa) the discrepancy was greatest at the forward nozzle position and reduced as the nozzle was moved further aft. At the two higher freestream dynamic pressures, the discrepancy was greatest at the centre nozzle position.

***Table 4.1** - Effect of the jet on the wing, Phase 1 results.*

NPR	*Nozzle Pos.*	q_∞	V_e	$\int C_{p\,(upper)}$	$\int C_{p\,(lower)}$	$C_{l\,(root)}$	$\Delta C_{l\,(root)}$	$\Delta C_{l\,(root)}$ %
1.0	n/a	61.27	∞	-0.268438	-0.040620	0.227818	n/a	n/a
2.0	Forward	61.27	0.029	-0.269639	-0.134976	0.134663	-0.093	-40.89
3.0	Forward	61.27	0.023	-0.265671	-0.132616	0.133055	-0.095	-41.60
4.0	Forward	61.27	0.020	-0.261027	-0.135907	0.125120	-0.103	-45.08
2.0	Centre	61.27	0.029	-0.263744	-0.134540	0.129204	-0.099	-43.29
3.0	Centre	61.27	0.023	-0.266027	-0.139022	0.127005	-0.101	-44.25
4.0	Centre	61.27	0.020	-0.296432	-0.166309	0.130123	-0.098	-42.88
2.0	Rearward	61.27	0.029	-0.283910	-0.158308	0.125602	-0.102	-44.87
3.0	Rearward	61.27	0.023	-0.290626	-0.173451	0.117175	-0.111	-48.57
4.0	Rearward	61.27	0.020	-0.292933	-0.175893	0.117040	-0.111	-48.63
1.0	n/a	245.10	∞	-0.293664	-0.060556	0.233108	n/a	n/a
2.0	Forward	245.10	0.057	-0.273382	-0.113570	0.159812	-0.073	-31.44
3.0	Forward	245.10	0.047	-0.275028	-0.110270	0.164758	-0.068	-29.32
4.0	Forward	245.10	0.040	-0.285153	-0.104803	0.180350	-0.053	-22.63
2.0	Centre	245.10	0.057	-0.281411	-0.127282	0.154129	-0.079	-33.88
3.0	Centre	245.10	0.047	-0.282334	-0.122527	0.159807	-0.073	-31.45
4.0	Centre	245.10	0.040	-0.289276	-0.118455	0.170821	-0.062	-26.72
2.0	Rearward	245.10	0.057	-0.294016	-0.121368	0.172648	-0.060	-25.94
3.0	Rearward	245.10	0.047	-0.294238	-0.128155	0.166083	-0.067	-28.75
4.0	Rearward	245.10	0.040	-0.291262	-0.126408	0.164854	-0.068	-29.28
1.0	n/a	551.40	∞	-0.298247	-0.076296	0.221951	n/a	n/a
2.0	Forward	551.40	0.086	-0.279423	-0.122607	0.156816	-0.065	-29.35
3.0	Forward	551.40	0.070	-0.268656	-0.119988	0.148668	-0.073	-33.02
4.0	Forward	551.40	0.061	-0.269604	-0.117486	0.152118	-0.070	-31.46
2.0	Centre	551.40	0.086	-0.282874	-0.126573	0.156301	-0.066	-29.58
3.0	Centre	551.40	0.070	-0.274399	-0.120970	0.153429	-0.069	-30.87
4.0	Centre	551.40	0.061	-0.275286	-0.122460	0.152826	-0.069	-31.14
2.0	Rearward	551.40	0.086	-0.294413	-0.123356	0.171057	-0.051	-22.93
3.0	Rearward	551.40	0.070	-0.286836	-0.125345	0.161491	-0.060	-27.24
4.0	Rearward	551.40	0.061	-0.282225	-0.123935	0.158290	-0.064	-28.68

***Table 4.2** - Effect of the jet on the wing, Phase 2a results (constant nozzle mass flow rate).*

NPR	Nozzle Pos.	q_∞	V_∞	$\int C_{p\,(upper)}$	$\int C_{p\,(lower)}$	$C_{l\,(root)}$	$\Delta C_{l\,(root)}$	$\Delta C_{l\,(root)}$ %
1.0	n/a	61.27	∞	-0.293126	-0.031739	0.261387	n/a	n/a
1.586	Forward	61.27	0.035	-0.294357	-0.140532	0.153825	-0.108	-41.15
2.0	Forward	61.27	0.029	-0.279006	-0.127512	0.151494	-0.110	-42.04
3.0	Forward	61.27	0.023	-0.257014	-0.120031	0.136983	-0.124	-47.59
4.0	Forward	61.27	0.020	-0.262193	-0.131887	0.130306	-0.131	-50.15
1.586	Centre	61.27	0.035	-0.284930	-0.134731	0.150199	-0.111	-42.54
2.0	Centre	61.27	0.029	-0.252008	-0.103584	0.148424	-0.113	-43.22
3.0	Centre	61.27	0.023	-0.256551	-0.136268	0.120283	-0.141	-53.98
4.0	Centre	61.27	0.020	-0.358991	-0.211974	0.147017	-0.114	-43.76
1.586	Rearward	61.27	0.035	-0.324231	-0.191206	0.133025	-0.128	-49.11
2.0	Rearward	61.27	0.029	-0.304253	-0.168989	0.135264	-0.126	-48.25
3.0	Rearward	61.27	0.023	-0.305370	-0.191985	0.113385	-0.148	-56.62
4.0	Rearward	61.27	0.020	-0.335416	-0.217876	0.117540	-0.144	-55.03
1.0	n/a	245.10	∞	-0.305598	-0.051170	0.254428	n/a	n/a
1.586	Forward	245.10	0.070	-0.297138	-0.122713	0.174425	-0.080	-31.44
2.0	Forward	245.10	0.057	-0.280548	-0.109077	0.171471	-0.083	-32.61
3.0	Forward	245.10	0.047	-0.284264	-0.101811	0.182453	-0.072	-28.29
4.0	Forward	245.10	0.040	-0.285161	-0.096130	0.189031	-0.065	-25.70
1.586	Centre	245.10	0.070	-0.292210	-0.112864	0.179346	-0.075	-29.51
2.0	Centre	245.10	0.057	-0.284364	-0.109176	0.175188	-0.079	-31.14
3.0	Centre	245.10	0.047	-0.287450	-0.108053	0.179397	-0.075	-29.49
4.0	Centre	245.10	0.040	-0.311598	-0.117321	0.194277	-0.060	-23.64
1.586	Rearward	245.10	0.070	-0.312962	-0.130251	0.182711	-0.072	-28.19
2.0	Rearward	245.10	0.057	-0.301195	-0.116302	0.184893	-0.070	-27.33
3.0	Rearward	245.10	0.047	-0.301508	-0.119159	0.182349	-0.072	-28.33
4.0	Rearward	245.10	0.040	-0.305746	-0.121944	0.183802	-0.071	-27.76
1.0	n/a	551.40	∞	-0.308091	-0.067150	0.240941	n/a	n/a
1.586	Forward	551.40	0.105	-0.305560	-0.127217	0.178343	-0.063	-25.98
2.0	Forward	551.40	0.086	-0.291987	-0.114266	0.177721	-0.063	-26.24
3.0	Forward	551.40	0.070	-0.287103	-0.108698	0.178405	-0.063	-25.95
4.0	Forward	551.40	0.061	-0.284926	-0.102053	0.182873	-0.058	-24.10
1.586	Centre	551.40	0.105	-0.307267	-0.132419	0.174848	-0.066	-27.43
2.0	Centre	551.40	0.086	-0.299975	-0.117660	0.182315	-0.059	-24.33
3.0	Centre	551.40	0.070	-0.291757	-0.111333	0.180424	-0.061	-25.12
4.0	Centre	551.40	0.061	-0.298409	-0.110129	0.188280	-0.053	-21.86
1.586	Rearward	551.40	0.105	-0.315173	-0.129487	0.185686	-0.055	-22.93
2.0	Rearward	551.40	0.086	-0.308429	-0.116651	0.191778	-0.049	-20.40
3.0	Rearward	551.40	0.070	-0.302227	-0.114676	0.187551	-0.053	-22.16
4.0	Rearward	551.40	0.061	-0.302967	-0.114186	0.188781	-0.052	-21.65

***Table 4.3** - Effect of the jet on the wing, Phase 2b results (constant nozzle area).*

NPR	Nozzle Pos.	q_∞	V_∞	$\int C_{p\,(upper)}$	$\int C_{p\,(lower)}$	$C_{l\,(wing)}$	$\Delta C_{l\,(wing)}$	$\Delta C_{l\,(wing)}$ %
1.0	n/a	61.27	∞	-0.293126	-0.031739	0.261387	n/a	n/a
1.586	Forward	61.27	0.035	-0.291824	-0.107962	0.183862	-0.078	-29.66
2.0	Forward	61.27	0.029	-0.279006	-0.127512	0.151494	-0.110	-42.04
3.0	Forward	61.27	0.023	-0.262271	-0.147867	0.114404	-0.147	-56.23
4.0	Forward	61.27	0.020	-0.216078	-0.165105	0.050973	-0.210	-80.50
1.586	Centre	61.27	0.035	-0.309167	-0.124490	0.184677	-0.077	-29.35
2.0	Centre	61.27	0.029	-0.252008	-0.103584	0.148424	-0.113	-43.22
3.0	Centre	61.27	0.023	-0.265379	-0.169107	0.096272	-0.165	-63.17
4.0	Centre	61.27	0.020	-0.236463	-0.191151	0.045312	-0.216	-82.66
1.586	Rearward	61.27	0.035	-0.292295	-0.132896	0.159399	-0.102	-39.02
2.0	Rearward	61.27	0.029	-0.304253	-0.168989	0.135264	-0.126	-48.25
3.0	Rearward	61.27	0.023	-0.249265	-0.177761	0.071504	-0.190	-72.64
4.0	Rearward	61.27	0.020	-0.301422	-0.273632	0.027790	-0.234	-89.37
1.0	n/a	245.10	∞	-0.305598	-0.051170	0.254428	n/a	n/a
1.586	Forward	245.10	0.070	-0.298982	-0.110308	0.188674	-0.066	-25.84
2.0	Forward	245.10	0.057	-0.280548	-0.109077	0.171471	-0.083	-32.61
3.0	Forward	245.10	0.047	-0.288863	-0.106435	0.182428	-0.072	-28.30
4.0	Forward	245.10	0.040	-0.289045	-0.118891	0.170154	-0.084	-33.12
1.586	Centre	245.10	0.070	-0.306075	-0.112324	0.193751	-0.061	-23.85
2.0	Centre	245.10	0.057	-0.284364	-0.109176	0.175188	-0.079	-31.14
3.0	Centre	245.10	0.047	-0.297135	-0.120926	0.176209	-0.078	-30.74
4.0	Centre	245.10	0.040	-0.299618	-0.125354	0.174264	-0.080	-31.51
1.586	Rearward	245.10	0.070	-0.305341	-0.107610	0.197731	-0.057	-22.28
2.0	Rearward	245.10	0.057	-0.301195	-0.116302	0.184893	-0.070	-27.33
3.0	Rearward	245.10	0.047	-0.295976	-0.123371	0.172605	-0.082	-32.16
4.0	Rearward	245.10	0.040	-0.306613	-0.134189	0.172424	-0.082	-32.23
1.0	n/a	551.40	∞	-0.308091	-0.067150	0.240941	n/a	n/a
1.586	Forward	551.40	0.105	-0.304246	-0.112075	0.192171	-0.049	-20.24
2.0	Forward	551.40	0.086	-0.291987	-0.114266	0.177721	-0.063	-26.24
3.0	Forward	551.40	0.070	-0.285055	-0.118628	0.166427	-0.075	-30.93
4.0	Forward	551.40	0.061	-0.277305	-0.119838	0.157467	-0.083	-34.64
1.586	Centre	551.40	0.105	-0.308950	-0.111114	0.197836	-0.043	-17.89
2.0	Centre	551.40	0.086	-0.299975	-0.117660	0.182315	-0.059	-24.33
3.0	Centre	551.40	0.070	-0.290120	-0.119317	0.170803	-0.070	-29.11
4.0	Centre	551.40	0.061	-0.285883	-0.126642	0.159241	-0.082	-33.91
1.586	Rearward	551.40	0.105	-0.308960	-0.110162	0.198798	-0.042	-17.49
2.0	Rearward	551.40	0.086	-0.308429	-0.116651	0.191778	-0.049	-20.40
3.0	Rearward	551.40	0.070	-0.298695	-0.111801	0.186894	-0.054	-22.43
4.0	Rearward	551.40	0.061	-0.293912	-0.118469	0.175443	-0.065	-27.18

***Table 4.4** - Effect of the intake on the wing, Phase 1 results.*

q_∞	*Intakes 'Sucking' ?*	$\int C_{p\,(upper)}$	$\int C_{p\,(lower)}$	$C_{l\,(root)}$	$\Delta C_{l\,(root)}$	$\Delta C_{l\,(root)}$ %
61.27	no	-0.268438	-0.040620	0.227818	n/a	n/a
61.27	yes	-0.261585	0.058249	0.319834	0.092	40.39
245.1	no	-0.293664	-0.060556	0.233108	n/a	n/a
245.1	yes	-0.301325	-0.015833	0.285492	0.052	22.47
551.4	no	-0.298247	-0.076296	0.221951	n/a	n/a
551.4	yes	-0.306600	-0.048801	0.257799	0.036	16.15

***Table 4.5** - Effect of the intake on the wing, Phase 2 results.*

q_∞	*Intakes 'sucking' ?*	$\int C_{p\,(upper)}$	$\int C_{p\,(lower)}$	$C_{l\,(root)}$	$\Delta C_{l\,(root)}$	$\Delta C_{l\,(root)}$ %
61.27	no	-0.293126	-0.031739	0.261387	n/a	n/a
61.27	yes	-0.277825	0.039636	0.317461	0.056	21.45
245.10	no	-0.305598	-0.051170	0.254428	n/a	n/a
245.10	yes	-0.295046	-0.018151	0.276895	0.022	8.83
551.40	no	-0.308091	-0.067150	0.240941	n/a	n/a
551.40	yes	-0.303229	-0.052088	0.251141	0.010	4.23

Table 4.6 - Effect of the jet on the intake, Phase 1 results.

NPR	Nossle Pos.	q_∞	V_∞	$\int C_p$ (upper, rear)	$\int C_p$ (upper, front)	$\int C_p$ (lower, rear)	$\int C_p$ (lower, front)	C_M	ΔC_M	ΔC_M %
1.0	n/a	61.27	∞	-8.640020	-93.794596	-90.232771	-4.016147	1.062048	n/a	n/a
2.0	Forward	61.27	0.029	-5.886572	-95.581567	-90.517151	-5.230743	-4.408587	-5.471	-515.10
3.0	Forward	61.27	0.023	-6.087599	-96.304160	-90.547758	-5.260955	-4.929758	-5.992	-564.17
4.0	Forward	61.27	0.020	-5.973103	-95.945191	-89.832776	-5.152346	-5.291658	-6.354	-598.25
2.0	Centre	61.27	0.029	-5.616624	-95.016860	-89.981842	-5.317860	-4.736254	-5.798	-545.95
3.0	Centre	61.27	0.023	-5.814219	-96.049010	-90.643066	-5.318912	-4.910637	-5.973	-562.37
4.0	Centre	61.27	0.020	-5.901283	-96.360832	-90.447831	-5.298559	-5.310277	-6.372	-600.00
2.0	Rearward	61.27	0.029	-5.447213	-94.756615	-90.623593	-5.628955	-4.314764	-5.377	-506.27
3.0	Rearward	61.27	0.023	-5.548796	-95.230489	-90.554666	-5.550521	-4.677548	-5.740	-540.43
4.0	Rearward	61.27	0.020	-5.801165	-94.599634	-90.103513	-5.480381	-4.175337	-5.237	-493.14
1.0	n/a	245.10	∞	-1.300668	-22.596435	-21.481062	-0.468619	-0.283324	n/a	n/a
2.0	Forward	245.10	0.057	-0.747610	-23.075351	-21.381399	-0.680049	-1.626391	-1.343	474.04
3.0	Forward	245.10	0.047	-0.781315	-22.942048	-21.158002	-0.658205	-1.660936	-1.378	486.23
4.0	Forward	245.10	0.040	-0.812791	-22.971664	-21.129514	-0.625017	-1.654376	-1.371	483.92
2.0	Centre	245.10	0.057	-0.682292	-22.443009	-21.058791	-0.778999	-1.480925	-1.198	422.70
3.0	Centre	245.10	0.047	-0.737317	-22.616153	-21.167489	-0.772564	-1.483911	-1.201	423.75
4.0	Centre	245.10	0.040	-0.821022	-22.773304	-21.187114	-0.752526	-1.517694	-1.234	435.67
2.0	Rearward	245.10	0.057	-0.669162	-22.289162	-21.199578	-0.745617	-1.166039	-0.883	311.56
3.0	Rearward	245.10	0.047	-0.723513	-22.450809	-21.214450	-0.747090	-1.259936	-0.977	344.70
4.0	Rearward	245.10	0.040	-0.777669	-22.178335	-20.918425	-0.728654	-1.210895	-0.928	327.39
1.0	n/a	551.40	∞	-0.235506	-9.388807	-8.779503	-0.123377	-0.497175	n/a	n/a
2.0	Forward	551.40	0.086	-0.105235	-9.474633	-8.641997	-0.263060	-0.990461	-0.493	99.22
3.0	Forward	551.40	0.070	-0.120504	-9.412377	-8.626848	-0.243424	-0.908449	-0.411	82.72
4.0	Forward	551.40	0.061	-0.104881	-9.367325	-8.595649	-0.215219	-0.882014	-0.385	77.41
2.0	Centre	551.40	0.086	-0.087761	-9.268309	-8.657855	-0.314652	-0.837345	-0.340	68.42
3.0	Centre	551.40	0.070	-0.096393	-9.291824	-8.738390	-0.297721	-0.754762	-0.258	51.81
4.0	Centre	551.40	0.061	-0.094779	-9.241374	-8.683277	-0.286297	-0.749615	-0.252	50.77
2.0	Rearward	551.40	0.086	-0.073421	-9.276497	-8.790382	-0.213409	-0.626103	-0.129	25.93
3.0	Rearward	551.40	0.070	-0.087646	-9.193156	-8.765250	-0.217744	-0.558004	-0.061	12.23
4.0	Rearward	551.40	0.061	-0.086478	-9.173510	-8.753497	-0.215537	-0.549072	-0.052	10.44

Table 4.7 - Effect of the jet on the intake, Phase 2a results (constant nozzle mass flow rate).

NPR	Nozzle Pos.	q_∞	V_∞	$\int C_{p\,(\text{upper outside})}$	$\int C_{p\,(\text{upper inside})}$	$\int C_{p\,(\text{lower inside})}$	$\int C_{p\,(\text{lower outside})}$	C_m	ΔC_m	ΔC_m %
1.0	n/a	61.27	∞	-5.245497	-96.525740	-93.997853	-6.060346	-3.342736	n/a	n/a
1.586	Forward	61.27	0.035	-5.587912	-95.558089	-89.720606	-4.957730	-5.207301	-1.865	-35.81
2.0	Forward	61.27	0.029	-5.758332	-95.848345	-90.008795	-5.118690	-5.199908	-1.857	-35.66
3.0	Forward	61.27	0.023	-5.917406	-96.068978	-89.727157	-5.032647	-5.457062	-2.114	-40.60
4.0	Forward	61.27	0.020	-6.176365	-97.806566	-91.628938	-5.235947	-5.237210	-1.894	-36.38
1.586	Centre	61.27	0.035	-5.740915	-96.641319	-91.512358	-5.474520	-4.862566	-1.520	-29.19
2.0	Centre	61.27	0.029	-5.574731	-94.963955	-89.806318	-5.338679	-4.921585	-1.579	-30.32
3.0	Centre	61.27	0.023	-5.775924	-97.619074	-92.142301	-5.337666	-5.038515	-1.696	-32.57
4.0	Centre	61.27	0.020	-5.970036	-97.407793	-91.600531	-5.289658	-5.126884	-1.784	-34.26
1.586	Rearward	61.27	0.035	-5.254492	-93.990767	-90.045464	-5.446615	-4.137426	-0.795	-15.26
2.0	Rearward	61.27	0.029	-5.307751	-93.380647	-89.283978	-5.454572	-4.243490	-0.901	-17.30
3.0	Rearward	61.27	0.023	-5.541524	-95.689004	-91.049790	-5.452128	-4.549818	-1.207	-23.18
4.0	Rearward	61.27	0.020	-5.757216	-95.017296	-90.318131	-5.476304	-4.418253	-1.076	-20.65
1.0	n/a	245.10	∞	-0.593817	-22.067514	-21.237803	-0.698446	-0.934340	n/a	n/a
1.586	Forward	245.10	0.070	-0.685345	-22.797189	-20.974588	-0.652533	-1.789789	-0.855	-91.56
2.0	Forward	245.10	0.057	-0.696468	-22.789058	-20.958691	-0.645962	-1.779861	-0.846	-90.49
3.0	Forward	245.10	0.047	-0.723601	-22.809350	-20.924547	-0.606776	-1.767978	-0.834	-89.22
4.0	Forward	245.10	0.040	-0.844256	-23.337535	-21.390251	-0.641865	-1.744893	-0.811	-86.75
1.586	Centre	245.10	0.070	-0.650701	-22.521544	-21.175989	-0.797894	-1.492748	-0.558	-59.76
2.0	Centre	245.10	0.057	-0.664770	-22.358785	-20.957550	-0.771582	-1.508047	-0.574	-61.40
3.0	Centre	245.10	0.047	-0.723523	-22.895106	-21.408794	-0.773768	-1.536557	-0.602	-64.45
4.0	Centre	245.10	0.040	-0.774030	-22.826071	-21.294444	-0.750569	-1.508166	-0.574	-61.42
1.586	Rearward	245.10	0.070	-0.620306	-21.987137	-20.898444	-0.725619	-1.194006	-0.260	-27.79
2.0	Rearward	245.10	0.057	-0.628973	-21.921995	-20.781573	-0.718562	-1.230011	-0.296	-31.64
3.0	Rearward	245.10	0.047	-0.695712	-22.298793	-21.040196	-0.746642	-1.309527	-0.375	-40.16
4.0	Rearward	245.10	0.040	-0.737557	-22.256326	-20.907476	-0.727891	-1.339184	-0.405	-43.33
1.0	n/a	551.40	∞	-0.023488	-9.176780	-8.762906	-0.148607	-0.538993	n/a	n/a
1.586	Forward	551.40	0.105	-0.068716	-9.326865	-8.506819	-0.267101	-1.018431	-0.479	-88.95
2.0	Forward	551.40	0.086	-0.086246	-9.337307	-8.473900	-0.252669	-1.029830	-0.491	-91.07
3.0	Forward	551.40	0.070	-0.109026	-9.346613	-8.486674	-0.224716	-0.975629	-0.437	-81.01
4.0	Forward	551.40	0.061	-0.121525	-9.499794	-8.660844	-0.215822	-0.933247	-0.394	-73.15
1.586	Centre	551.40	0.105	-0.065260	-9.269348	-8.687337	-0.336875	-0.853626	-0.315	-58.37
2.0	Centre	551.40	0.086	-0.075313	-9.258611	-8.661998	-0.303736	-0.825036	-0.286	-53.07
3.0	Centre	551.40	0.070	-0.092952	-9.433744	-8.856222	-0.295420	-0.779990	-0.241	-44.71
4.0	Centre	551.40	0.061	-0.099282	-9.384528	-8.802641	-0.285521	-0.768126	-0.229	-42.51
1.586	Rearward	551.40	0.105	-0.056736	-9.113240	-8.641377	-0.212563	-0.627690	-0.089	-16.46
2.0	Rearward	551.40	0.086	-0.064843	-9.115056	-8.611990	-0.207400	-0.645623	-0.107	-19.78
3.0	Rearward	551.40	0.070	-0.077976	-9.214947	-8.760218	-0.217119	-0.593872	-0.055	-10.18
4.0	Rearward	551.40	0.061	-0.086633	-9.189998	-8.717516	-0.216362	-0.602211	-0.063	-11.73

Table 4.8 - Effect of the jet on the intake, Phase 2b results (constant nozzle area).

NPR	Nozzle Pos.	q_∞	V_∞	$\int C_p$	$\int C_p$	$\int C_p$	$\int C_p$	C_m	ΔC_m	ΔC_m %
1.0	n/a	61.27	∞	-5.245497	-96.525740	-93.997853	-6.060346	-3.342736	n/a	n/a
1.586	Forward	61.27	0.035	-5.545875	-94.607436	-89.852869	-5.248097	-4.456789	-1.114	-33.33
2.0	Forward	61.27	0.029	-5.758332	-95.848345	-90.008795	-5.118690	-5.199908	-1.857	-55.56
3.0	Forward	61.27	0.023	-6.047529	-96.078455	-89.060944	-4.906438	-5.876420	-2.534	-75.80
4.0	Forward	61.27	0.020	-6.361711	-97.506338	-89.316725	-4.731671	-6.559573	-3.217	-96.23
1.586	Centre	61.27	0.035	-5.595924	-96.739083	-92.271614	-5.600589	-4.472134	-1.129	-33.79
2.0	Centre	61.27	0.029	-5.574731	-94.963955	-89.806318	-5.338679	-4.921585	-1.579	-47.23
3.0	Centre	61.27	0.023	-6.019421	-97.806704	-91.222798	-5.272244	-5.836729	-2.494	-74.61
4.0	Centre	61.27	0.020	-6.402161	-98.302060	-90.816938	-5.132357	-6.215318	-2.873	-85.94
1.586	Rearward	61.27	0.035	-5.501545	-96.658968	-92.692077	-5.818256	-4.283602	-0.941	-28.15
2.0	Rearward	61.27	0.029	-5.307751	-93.380647	-89.283978	-5.454572	-4.243490	-0.901	-26.95
3.0	Rearward	61.27	0.023	-5.823181	-97.338998	-92.006415	-5.529836	-5.039238	-1.697	-50.75
4.0	Rearward	61.27	0.020	-6.134312	-98.033833	-91.897857	-5.391722	-5.393386	-2.051	-61.35
1.0	n/a	245.10	∞	-0.593817	-22.067514	-21.237803	-0.698446	-0.934340	n/a	n/a
1.586	Forward	245.10	0.070	-0.651755	-22.462850	-20.741389	-0.635164	-1.704870	-0.771	-82.47
2.0	Forward	245.10	0.057	-0.696468	-22.789058	-20.958691	-0.645962	-1.779861	-0.846	-90.49
3.0	Forward	245.10	0.047	-0.740094	-22.764137	-20.790347	-0.607265	-1.840961	-0.907	-97.03
4.0	Forward	245.10	0.040	-0.816349	-23.116281	-20.935338	-0.597445	-1.962039	-1.028	-109.99
1.586	Centre	245.10	0.070	-0.664068	-22.681522	-21.398536	-0.782694	-1.401612	-0.467	-50.01
2.0	Centre	245.10	0.057	-0.664770	-22.358785	-20.957550	-0.771582	-1.508047	-0.574	-61.40
3.0	Centre	245.10	0.047	-0.696588	-22.673125	-21.122720	-0.764780	-1.618597	-0.684	-73.23
4.0	Centre	245.10	0.040	-0.768909	-23.109775	-21.471114	-0.779657	-1.649409	-0.715	-76.53
1.586	Rearward	245.10	0.070	-0.651899	-22.667798	-21.565416	-0.762993	-1.213476	-0.279	-29.88
2.0	Rearward	245.10	0.057	-0.628973	-21.921995	-20.781573	-0.718562	-1.230011	-0.296	-31.64
3.0	Rearward	245.10	0.047	-0.703025	-22.664757	-21.364907	-0.763518	-1.360343	-0.426	-45.59
4.0	Rearward	245.10	0.040	-0.767527	-22.716568	-21.344237	-0.763815	-1.368619	-0.434	-46.48
1.0	n/a	551.40	∞	-0.023488	-9.176780	-8.762906	-0.148607	-0.538993	n/a	n/a
1.586	Forward	551.40	0.105	-0.064725	-9.313119	-8.512477	-0.243434	-0.979351	-0.440	-81.70
2.0	Forward	551.40	0.086	-0.086246	-9.337307	-8.473900	-0.252669	-1.029830	-0.491	-91.07
3.0	Forward	551.40	0.070	-0.110639	-9.521526	-8.616752	-0.245477	-1.039612	-0.501	-92.88
4.0	Forward	551.40	0.061	-0.123634	-9.618031	-8.639270	-0.233482	-1.088609	-0.550	-101.97
1.586	Centre	551.40	0.105	-0.065515	-9.430812	-8.901232	-0.293395	-0.757460	-0.218	-40.53
2.0	Centre	551.40	0.086	-0.075313	-9.258611	-8.661998	-0.303736	-0.825036	-0.286	-53.07
3.0	Centre	551.40	0.070	-0.094623	-9.445019	-8.836086	-0.316780	-0.831090	-0.292	-54.19
4.0	Centre	551.40	0.061	-0.117005	-9.512885	-8.846091	-0.335084	-0.884873	-0.346	-64.17
1.586	Rearward	551.40	0.105	-0.051632	-9.436362	-9.005557	-0.200666	-0.579839	-0.041	-7.58
2.0	Rearward	551.40	0.086	-0.064843	-9.115056	-8.611990	-0.207400	-0.645623	-0.107	-19.78
3.0	Rearward	551.40	0.070	-0.090355	-9.416145	-8.917964	-0.238480	-0.646306	-0.107	-19.91
4.0	Rearward	551.40	0.061	-0.086222	-9.407879	-8.907200	-0.234466	-0.648923	-0.110	-20.40

***Table 4.9** - Effect of the jet and intake on the wing, Phase 1 results.*

NPR	*Nozzle Pos.*	q_∞	V_e	$\int C_{p\,(upper)}$	$\int C_{p\,(lower)}$	$C_{l\,(root)}$	$\Delta C_{l\,(root)}$	$\Delta C_{l\,(root)}$ %
1.0	n/a	61.27	∞	-0.268438	-0.040620	0.227818	n/a	n/a
2.0	Forward	61.27	0.029	-0.190908	-0.001280	0.189628	-0.038	-16.76
3.0	Forward	61.27	0.023	-0.181733	-0.019795	0.161938	-0.066	-28.92
4.0	Forward	61.27	0.020	-0.165795	-0.006818	0.158977	-0.069	-30.22
2.0	Centre	61.27	0.029	-0.173039	-0.020036	0.153003	-0.075	-32.84
3.0	Centre	61.27	0.023	-0.217977	-0.069063	0.148914	-0.079	-34.63
4.0	Centre	61.27	0.020	-0.153435	-0.013955	0.139480	-0.088	-38.78
2.0	Rearward	61.27	0.029	-0.189406	-0.019560	0.169846	-0.058	-25.45
3.0	Rearward	61.27	0.023	-0.183647	-0.034936	0.148711	-0.079	-34.72
4.0	Rearward	61.27	0.020	-0.274390	-0.143798	0.130592	-0.097	-42.68
1.0	n/a	245.10	∞	-0.293664	-0.060556	0.233108	n/a	n/a
2.0	Forward	245.10	0.057	-0.272087	-0.077131	0.194956	-0.038	-16.37
3.0	Forward	245.10	0.047	-0.263834	-0.072032	0.191802	-0.041	-17.72
4.0	Forward	245.10	0.040	-0.284909	-0.084703	0.200206	-0.033	-14.11
2.0	Centre	245.10	0.057	-0.279969	-0.104346	0.175623	-0.057	-24.66
3.0	Centre	245.10	0.047	-0.274943	-0.095335	0.179608	-0.054	-22.95
4.0	Centre	245.10	0.040	-0.284632	-0.103538	0.181094	-0.052	-22.31
2.0	Rearward	245.10	0.057	-0.291993	-0.100242	0.191751	-0.041	-17.74
3.0	Rearward	245.10	0.047	-0.281578	-0.100476	0.181102	-0.052	-22.31
4.0	Rearward	245.10	0.040	-0.284532	-0.097886	0.186646	-0.046	-19.93
1.0	n/a	551.40	∞	-0.298247	-0.076296	0.221951	n/a	n/a
2.0	Forward	551.40	0.086	-0.293121	-0.112411	0.180710	-0.041	-18.58
3.0	Forward	551.40	0.070	-0.286351	-0.098753	0.187598	-0.034	-15.48
4.0	Forward	551.40	0.061	-0.281747	-0.089147	0.192600	-0.029	-13.22
2.0	Centre	551.40	0.086	-0.294994	-0.121219	0.173775	-0.048	-21.71
3.0	Centre	551.40	0.070	-0.294591	-0.105718	0.188873	-0.033	-14.90
4.0	Centre	551.40	0.061	-0.281013	-0.094527	0.186486	-0.035	-15.98
2.0	Rearward	551.40	0.086	-0.301833	-0.112971	0.188862	-0.033	-14.91
3.0	Rearward	551.40	0.070	-0.301596	-0.102974	0.198622	-0.023	-10.51
4.0	Rearward	551.40	0.061	-0.292037	-0.094479	0.197558	-0.024	-10.99

***Table 4.10** - Effect of the jet and intake on the wing, Phase 2a results (constant nozzle mass flow rate).*

NPR	*Nozzle Pos.*	q_∞	V_e	$\int C_{p\,(upper)}$	$\int C_{p\,(lower)}$	$C_{l\,(root)}$	$\Delta C_{l\,(root)}$	$\Delta C_{l\,(root)}$ %
1.0	n/a	61.27	∞	-0.293126	-0.031739	0.261387	n/a	n/a
1.586	Forward	61.27	0.035	-0.254551	-0.089826	0.164725	-0.097	-36.98
2.0	Forward	61.27	0.029	-0.261129	-0.070202	0.190927	-0.070	-26.96
3.0	Forward	61.27	0.023	-0.225132	-0.089943	0.135189	-0.126	-48.28
4.0	Forward	61.27	0.020	-0.261535	-0.088198	0.173337	-0.088	-33.69
1.586	Centre	61.27	0.035	-0.270016	-0.097373	0.172643	-0.089	-33.95
2.0	Centre	61.27	0.029	-0.284605	-0.077483	0.207122	-0.054	-20.76
3.0	Centre	61.27	0.023	-0.291279	-0.124213	0.167066	-0.094	-36.08
4.0	Centre	61.27	0.020	-0.276514	-0.111716	0.164798	-0.097	-36.95
1.586	Rearward	61.27	0.035	-0.317365	-0.151213	0.166152	-0.095	-36.43
2.0	Rearward	61.27	0.029	-0.262266	-0.084855	0.177411	-0.084	-32.13
3.0	Rearward	61.27	0.023	-0.297822	-0.148788	0.149034	-0.112	-42.98
4.0	Rearward	61.27	0.020	-0.263730	-0.133732	0.129998	-0.131	-50.27
1.0	n/a	245.10	∞	-0.305598	-0.051170	0.254428	n/a	n/a
1.586	Forward	245.10	0.070	-0.277109	-0.084657	0.192452	-0.062	-24.36
2.0	Forward	245.10	0.057	-0.271086	-0.083838	0.187248	-0.067	-26.40
3.0	Forward	245.10	0.047	-0.255919	-0.064356	0.191563	-0.063	-24.71
4.0	Forward	245.10	0.040	-0.291080	-0.090645	0.200435	-0.054	-21.22
1.586	Centre	245.10	0.070	-0.286859	-0.096911	0.189948	-0.064	-25.34
2.0	Centre	245.10	0.057	-0.278625	-0.090670	0.187955	-0.066	-26.13
3.0	Centre	245.10	0.047	-0.291060	-0.089960	0.201100	-0.053	-20.96
4.0	Centre	245.10	0.040	-0.287731	-0.083004	0.204727	-0.050	-19.53
1.586	Rearward	245.10	0.070	-0.290254	-0.091861	0.198393	-0.056	-22.02
2.0	Rearward	245.10	0.057	-0.276491	-0.079723	0.196768	-0.058	-22.66
3.0	Rearward	245.10	0.047	-0.298114	-0.097554	0.200560	-0.054	-21.17
4.0	Rearward	245.10	0.040	-0.279577	-0.080370	0.199207	-0.055	-21.70
1.0	n/a	551.40	∞	-0.308091	-0.067150	0.240941	n/a	n/a
1.586	Forward	551.40	0.105	-0.287183	-0.105516	0.181667	-0.059	-24.60
2.0	Forward	551.40	0.086	-0.280499	-0.105179	0.175320	-0.066	-27.24
3.0	Forward	551.40	0.070	-0.268044	-0.093217	0.174827	-0.066	-27.44
4.0	Forward	551.40	0.061	-0.269569	-0.089100	0.180469	-0.060	-25.10
1.586	Centre	551.40	0.105	-0.299259	-0.123680	0.175579	-0.065	-27.13
2.0	Centre	551.40	0.086	-0.289020	-0.110546	0.178474	-0.062	-25.93
3.0	Centre	551.40	0.070	-0.286508	-0.099477	0.187031	-0.054	-22.37
4.0	Centre	551.40	0.061	-0.283441	-0.096400	0.187041	-0.054	-22.37
1.586	Rearward	551.40	0.105	-0.303851	-0.120134	0.183717	-0.057	-23.75
2.0	Rearward	551.40	0.086	-0.293664	-0.106982	0.186682	-0.054	-22.52
3.0	Rearward	551.40	0.070	-0.288177	-0.096746	0.191431	-0.050	-20.55
4.0	Rearward	551.40	0.061	-0.287088	-0.098234	0.188854	-0.052	-21.62

***Table 4.11** - Effect of the jet and intake on the wing, Phase 2b results (constant nozzle area).*

NPR	*Nozzle Pos.*	q_∞	V_∞	$\int C_{p\,(upper)}$	$\int C_{p\,(lower)}$	$C_{l\,(root)}$	$\Delta C_{l\,(root)}$	$\Delta C_{l\,(root)}$ %
1.0	n/a	61.27	∞	-0.293126	-0.031739	0.261387	n/a	n/a
1.586	Forward	61.27	0.035	-0.242099	-0.037477	0.204622	-0.057	-21.72
2.0	Forward	61.27	0.029	-0.261129	-0.070202	0.190927	-0.070	-26.96
3.0	Forward	61.27	0.023	-0.242690	-0.122741	0.119949	-0.141	-54.11
4.0	Forward	61.27	0.020	-0.216527	-0.150486	0.066041	-0.195	-74.73
1.586	Centre	61.27	0.035	-0.201362	-0.006831	0.194531	-0.067	-25.58
2.0	Centre	61.27	0.029	-0.284605	-0.077483	0.207122	-0.054	-20.76
3.0	Centre	61.27	0.023	-0.201139	-0.118061	0.083078	-0.178	-68.22
4.0	Centre	61.27	0.020	-0.220280	-0.201350	0.018930	-0.242	-92.76
1.586	Rearward	61.27	0.035	-0.265258	-0.059213	0.206045	-0.055	-21.17
2.0	Rearward	61.27	0.029	-0.262266	-0.084855	0.177411	-0.084	-32.13
3.0	Rearward	61.27	0.023	-0.251364	-0.161869	0.089495	-0.172	-65.76
4.0	Rearward	61.27	0.020	-0.274328	-0.255410	0.018918	-0.242	-92.76
1.0	n/a	245.10	∞	-0.305598	-0.051170	0.254428	n/a	n/a
1.586	Forward	245.10	0.070	-0.261012	-0.069091	0.191921	-0.063	-24.57
2.0	Forward	245.10	0.057	-0.271086	-0.083838	0.187248	-0.067	-26.40
3.0	Forward	245.10	0.047	-0.272656	-0.080876	0.191780	-0.063	-24.62
4.0	Forward	245.10	0.040	-0.271507	-0.087987	0.183520	-0.071	-27.87
1.586	Centre	245.10	0.070	-0.279363	-0.077866	0.201497	-0.053	-20.80
2.0	Centre	245.10	0.057	-0.278625	-0.090670	0.187955	-0.066	-26.13
3.0	Centre	245.10	0.047	-0.256731	-0.073437	0.183294	-0.071	-27.96
4.0	Centre	245.10	0.040	-0.273614	-0.083319	0.190295	-0.064	-25.21
1.586	Rearward	245.10	0.070	-0.285132	-0.076519	0.208613	-0.046	-18.01
2.0	Rearward	245.10	0.057	-0.276491	-0.079723	0.196768	-0.058	-22.66
3.0	Rearward	245.10	0.047	-0.282493	-0.100109	0.182384	-0.072	-28.32
4.0	Rearward	245.10	0.040	-0.279309	-0.100408	0.178901	-0.076	-29.69
1.0	n/a	551.40	∞	-0.308091	-0.067150	0.240941	n/a	n/a
1.586	Forward	551.40	0.105	-0.282039	-0.094800	0.187239	-0.054	-22.29
2.0	Forward	551.40	0.086	-0.280499	-0.105179	0.175320	-0.066	-27.24
3.0	Forward	551.40	0.070	-0.268743	-0.102537	0.166206	-0.075	-31.02
4.0	Forward	551.40	0.061	-0.261217	-0.101724	0.159493	-0.081	-33.80
1.586	Centre	551.40	0.105	-0.290492	-0.097598	0.192894	-0.048	-19.94
2.0	Centre	551.40	0.086	-0.289020	-0.110546	0.178474	-0.062	-25.93
3.0	Centre	551.40	0.070	-0.269500	-0.100445	0.169055	-0.072	-29.84
4.0	Centre	551.40	0.061	-0.279880	-0.119713	0.160167	-0.081	-33.52
1.586	Rearward	551.40	0.105	-0.291889	-0.090391	0.201498	-0.039	-16.37
2.0	Rearward	551.40	0.086	-0.293664	-0.106982	0.186682	-0.054	-22.52
3.0	Rearward	551.40	0.070	-0.282146	-0.105032	0.177114	-0.064	-26.49
4.0	Rearward	551.40	0.061	-0.266732	-0.094480	0.172252	-0.069	-28.51

***Table 4.12** - Comparison of the effect of testing jet and intakes separately, Phase 1 results.*

NPR	Nozzle Pos.	q_∞	V_∞	(Jet and intakes separate)		(Jet and intakes together)		(Difference)	
				$\Delta C_{l_{(nose)}}$	$\Delta C_{l_{(nose)}}$ %	$\Delta C_{l_{(nose)}}$	$\Delta C_{l_{(nose)}}$ %	$\Delta C_{l_{(nose)}}$	$\Delta C_{l_{(nose)}}$ %
2.0	Forward	61.27	0.029	-0.001	-0.50	-0.038	-16.76	-0.037	-16.26
3.0	Forward	61.27	0.023	-0.003	-1.21	-0.066	-28.92	-0.063	-27.71
4.0	Forward	61.27	0.020	-0.011	-4.69	-0.069	-30.22	-0.058	-25.53
2.0	Centre	61.27	0.029	-0.007	-2.90	-0.075	-32.84	-0.068	-29.94
3.0	Centre	61.27	0.023	-0.009	-3.86	-0.079	-34.63	-0.070	-30.77
4.0	Centre	61.27	0.020	-0.006	-2.49	-0.088	-38.78	-0.083	-36.28
2.0	Rearward	61.27	0.029	-0.010	-4.48	-0.058	-25.45	-0.048	-20.97
3.0	Rearward	61.27	0.023	-0.019	-8.18	-0.079	-34.72	-0.060	-26.55
4.0	Rearward	61.27	0.020	-0.019	-8.24	-0.097	-42.68	-0.078	-34.44
2.0	Forward	245.10	0.057	-0.021	-8.97	-0.038	-16.37	-0.017	-7.40
3.0	Forward	245.10	0.047	-0.016	-6.85	-0.041	-17.72	-0.025	-10.87
4.0	Forward	245.10	0.040	0.000	-0.16	-0.033	-14.11	-0.033	-13.95
2.0	Centre	245.10	0.057	-0.027	-11.41	-0.057	-24.66	-0.031	-13.25
3.0	Centre	245.10	0.047	-0.021	-8.97	-0.054	-22.95	-0.033	-13.98
4.0	Centre	245.10	0.040	-0.010	-4.25	-0.052	-22.31	-0.042	-18.07
2.0	Rearward	245.10	0.057	-0.008	-3.46	-0.041	-17.74	-0.033	-14.28
3.0	Rearward	245.10	0.047	-0.015	-6.28	-0.052	-22.31	-0.037	-16.03
4.0	Rearward	245.10	0.040	-0.016	-6.81	-0.046	-19.93	-0.031	-13.12
2.0	Forward	551.40	0.086	-0.029	-13.20	-0.041	-18.58	-0.012	-5.39
3.0	Forward	551.40	0.070	-0.037	-16.87	-0.034	-15.48	0.003	1.39
4.0	Forward	551.40	0.061	-0.034	-15.31	-0.029	-13.22	0.005	2.09
2.0	Centre	551.40	0.086	-0.030	-13.43	-0.048	-21.71	-0.018	-8.28
3.0	Centre	551.40	0.070	-0.033	-14.72	-0.033	-14.90	0.000	-0.18
4.0	Centre	551.40	0.061	-0.033	-14.99	-0.035	-15.98	-0.002	-0.99
2.0	Rearward	551.40	0.086	-0.015	-6.78	-0.033	-14.91	-0.018	-8.13
3.0	Rearward	551.40	0.070	-0.025	-11.09	-0.023	-10.51	0.001	0.58
4.0	Rearward	551.40	0.061	-0.028	-12.53	-0.024	-10.99	0.003	1.54

Table 4.13 - *Comparison of the effect of testing jet and intakes separately, Phase 2a results (constant nozzle mass flow rate).*

NPR	Nozzle Pos.	q_∞	V_∞	(Jet and intakes separate)		(Jet and intakes combined)		(Difference)	
				$\Delta C_{I_{(front)}}$	$\Delta C_{I_{(front)}}$ %	$\Delta C_{I_{(front)}}$	$\Delta C_{I_{(front)}}$ %	$\Delta C_{I_{(front)}}$	$\Delta C_{I_{(front)}}$ %
1.586	Forward	61.27	0.035	-0.051	-19.70	-0.097	-36.98	-0.045	-17.28
2.0	Forward	61.27	0.029	-0.054	-20.59	-0.070	-26.96	-0.017	-6.37
3.0	Forward	61.27	0.023	-0.068	-26.14	-0.126	-48.28	-0.058	-22.14
4.0	Forward	61.27	0.020	-0.075	-28.70	-0.088	-33.69	-0.013	-4.99
1.586	Centre	61.27	0.035	-0.055	-21.09	-0.089	-33.95	-0.034	-12.87
2.0	Centre	61.27	0.029	-0.057	-21.76	-0.054	-20.76	0.003	1.00
3.0	Centre	61.27	0.023	-0.085	-32.53	-0.094	-36.08	-0.009	-3.55
4.0	Centre	61.27	0.020	-0.058	-22.30	-0.097	-36.95	-0.038	-14.65
1.586	Rearward	61.27	0.035	-0.072	-27.66	-0.095	-36.43	-0.023	-8.78
2.0	Rearward	61.27	0.029	-0.070	-26.80	-0.084	-32.13	-0.014	-5.33
3.0	Rearward	61.27	0.023	-0.092	-35.17	-0.112	-42.98	-0.020	-7.81
4.0	Rearward	61.27	0.020	-0.088	-33.58	-0.131	-50.27	-0.044	-16.69
1.586	Forward	245.10	0.070	-0.058	-22.61	-0.062	-24.36	-0.004	-1.75
2.0	Forward	245.10	0.057	-0.060	-23.77	-0.067	-26.40	-0.007	-2.63
3.0	Forward	245.10	0.047	-0.050	-19.46	-0.063	-24.71	-0.013	-5.25
4.0	Forward	245.10	0.040	-0.043	-16.87	-0.054	-21.22	-0.011	-4.35
1.586	Centre	245.10	0.070	-0.053	-20.68	-0.064	-25.34	-0.012	-4.66
2.0	Centre	245.10	0.057	-0.057	-22.31	-0.066	-26.13	-0.010	-3.81
3.0	Centre	245.10	0.047	-0.053	-20.66	-0.053	-20.96	-0.001	-0.30
4.0	Centre	245.10	0.040	-0.038	-14.81	-0.050	-19.53	-0.012	-4.72
1.586	Rearward	245.10	0.070	-0.049	-19.36	-0.056	-22.02	-0.007	-2.67
2.0	Rearward	245.10	0.057	-0.047	-18.50	-0.058	-22.66	-0.011	-4.16
3.0	Rearward	245.10	0.047	-0.050	-19.50	-0.054	-21.17	-0.004	-1.67
4.0	Rearward	245.10	0.040	-0.048	-18.93	-0.055	-21.70	-0.007	-2.78
1.586	Forward	551.40	0.105	-0.052	-21.75	-0.059	-24.60	-0.007	-2.85
2.0	Forward	551.40	0.086	-0.053	-22.01	-0.066	-27.24	-0.013	-5.23
3.0	Forward	551.40	0.070	-0.052	-21.72	-0.066	-27.44	-0.014	-5.72
4.0	Forward	551.40	0.061	-0.048	-19.87	-0.060	-25.10	-0.013	-5.23
1.586	Centre	551.40	0.105	-0.056	-23.20	-0.065	-27.13	-0.009	-3.93
2.0	Centre	551.40	0.086	-0.048	-20.10	-0.062	-25.93	-0.014	-5.83
3.0	Centre	551.40	0.070	-0.050	-20.88	-0.054	-22.37	-0.004	-1.49
4.0	Centre	551.40	0.061	-0.042	-17.62	-0.054	-22.37	-0.011	-4.75
1.586	Rearward	551.40	0.105	-0.045	-18.70	-0.057	-23.75	-0.012	-5.05
2.0	Rearward	551.40	0.086	-0.039	-16.17	-0.054	-22.52	-0.015	-6.35
3.0	Rearward	551.40	0.070	-0.043	-17.93	-0.050	-20.55	-0.006	-2.62
4.0	Rearward	551.40	0.061	-0.042	-17.42	-0.052	-21.62	-0.010	-4.20

***Table 4.14** - Comparison of the effect of testing jet and intakes separately, Phase 2b results (constant nozzle area).*

NPR	Nozzle Pos.	q_∞	V_∞	(Jet and intakes separate)		(Jet and intakes together)		(Difference)	
				$\Delta C_{I(nose)}$	$\Delta C_{I(nose)}$ %	$\Delta C_{I(nose)}$	$\Delta C_{I(nose)}$ %	$\Delta C_{I(nose)}$	$\Delta C_{I(nose)}$ %
1.586	Forward	61.27	0.035	-0.021	-8.21	-0.057	-21.72	-0.035	-13.51
2.0	Forward	61.27	0.029	-0.054	-20.59	-0.070	-26.96	-0.017	-6.37
3.0	Forward	61.27	0.023	-0.091	-34.78	-0.141	-54.11	-0.051	-19.33
4.0	Forward	61.27	0.020	-0.154	-59.05	-0.195	-74.73	-0.041	-15.69
1.586	Centre	61.27	0.035	-0.021	-7.89	-0.067	-25.58	-0.046	-17.68
2.0	Centre	61.27	0.029	-0.057	-21.76	-0.054	-20.76	0.003	1.00
3.0	Centre	61.27	0.023	-0.109	-41.72	-0.178	-68.22	-0.069	-26.50
4.0	Centre	61.27	0.020	-0.160	-61.21	-0.242	-92.76	-0.082	-31.55
1.586	Rearward	61.27	0.035	-0.046	-17.57	-0.055	-21.17	-0.009	-3.61
2.0	Rearward	61.27	0.029	-0.070	-26.80	-0.084	-32.13	-0.014	-5.33
3.0	Rearward	61.27	0.023	-0.134	-51.19	-0.172	-65.76	-0.038	-14.57
4.0	Rearward	61.27	0.020	-0.178	-67.92	-0.242	-92.76	-0.065	-24.85
1.586	Forward	245.10	0.070	-0.043	-17.01	-0.063	-24.57	-0.019	-7.55
2.0	Forward	245.10	0.057	-0.060	-23.77	-0.067	-26.40	-0.007	-2.63
3.0	Forward	245.10	0.047	-0.050	-19.47	-0.063	-24.62	-0.013	-5.15
4.0	Forward	245.10	0.040	-0.062	-24.29	-0.071	-27.87	-0.009	-3.58
1.586	Centre	245.10	0.070	-0.038	-15.02	-0.053	-20.80	-0.015	-5.79
2.0	Centre	245.10	0.057	-0.057	-22.31	-0.066	-26.13	-0.010	-3.81
3.0	Centre	245.10	0.047	-0.056	-21.91	-0.071	-27.96	-0.015	-6.05
4.0	Centre	245.10	0.040	-0.058	-22.68	-0.064	-25.21	-0.006	-2.53
1.586	Rearward	245.10	0.070	-0.034	-13.45	-0.046	-18.01	-0.012	-4.55
2.0	Rearward	245.10	0.057	-0.047	-18.50	-0.058	-22.66	-0.011	-4.16
3.0	Rearward	245.10	0.047	-0.059	-23.33	-0.072	-28.32	-0.013	-4.99
4.0	Rearward	245.10	0.040	-0.060	-23.40	-0.076	-29.69	-0.016	-6.28
1.586	Forward	551.40	0.105	-0.039	-16.01	-0.054	-22.29	-0.015	-6.28
2.0	Forward	551.40	0.086	-0.053	-22.01	-0.066	-27.24	-0.013	-5.23
3.0	Forward	551.40	0.070	-0.064	-26.69	-0.075	-31.02	-0.010	-4.33
4.0	Forward	551.40	0.061	-0.073	-30.41	-0.081	-33.80	-0.008	-3.39
1.586	Centre	551.40	0.105	-0.033	-13.66	-0.048	-19.94	-0.015	-6.28
2.0	Centre	551.40	0.086	-0.048	-20.10	-0.062	-25.93	-0.014	-5.83
3.0	Centre	551.40	0.070	-0.060	-24.88	-0.072	-29.84	-0.012	-4.96
4.0	Centre	551.40	0.061	-0.072	-29.68	-0.081	-33.52	-0.009	-3.85
1.586	Rearward	551.40	0.105	-0.032	-13.26	-0.039	-16.37	-0.008	-3.11
2.0	Rearward	551.40	0.086	-0.039	-16.17	-0.054	-22.52	-0.015	-6.35
3.0	Rearward	551.40	0.070	-0.044	-18.20	-0.064	-26.49	-0.020	-8.29
4.0	Rearward	551.40	0.061	-0.055	-22.95	-0.069	-28.51	-0.013	-5.56

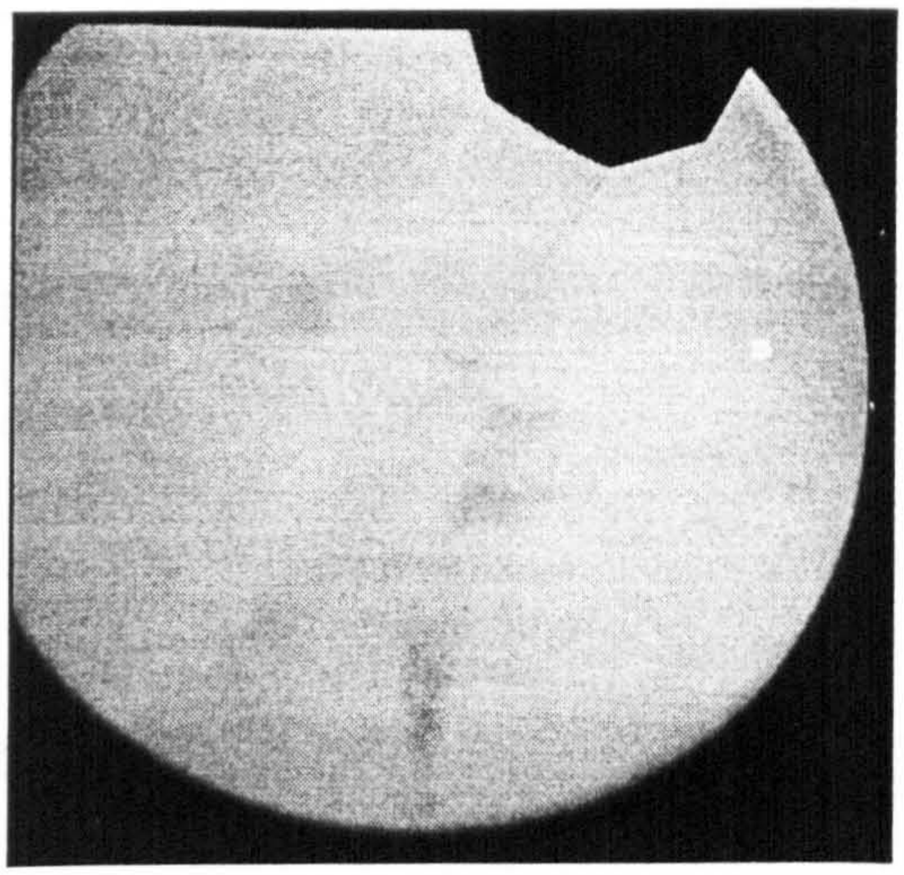

Figure 4.1 - *The vectored jet at an NPR of 2.0.*

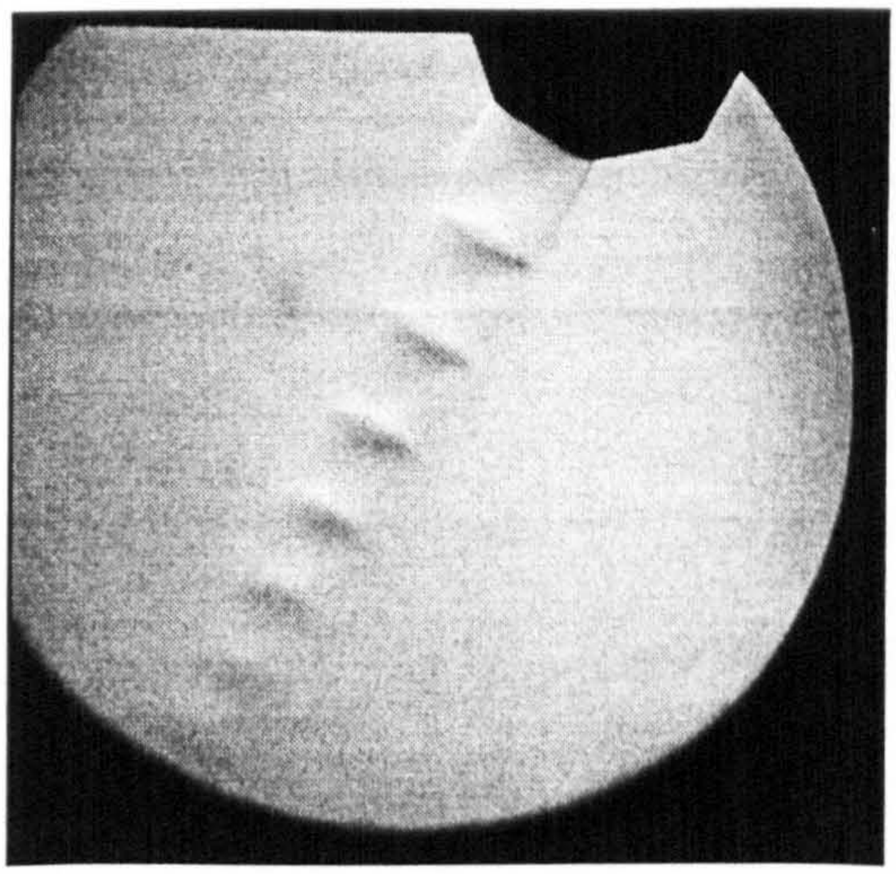

Figure 4.2 - *The vectored jet at an NPR of 3.0.*

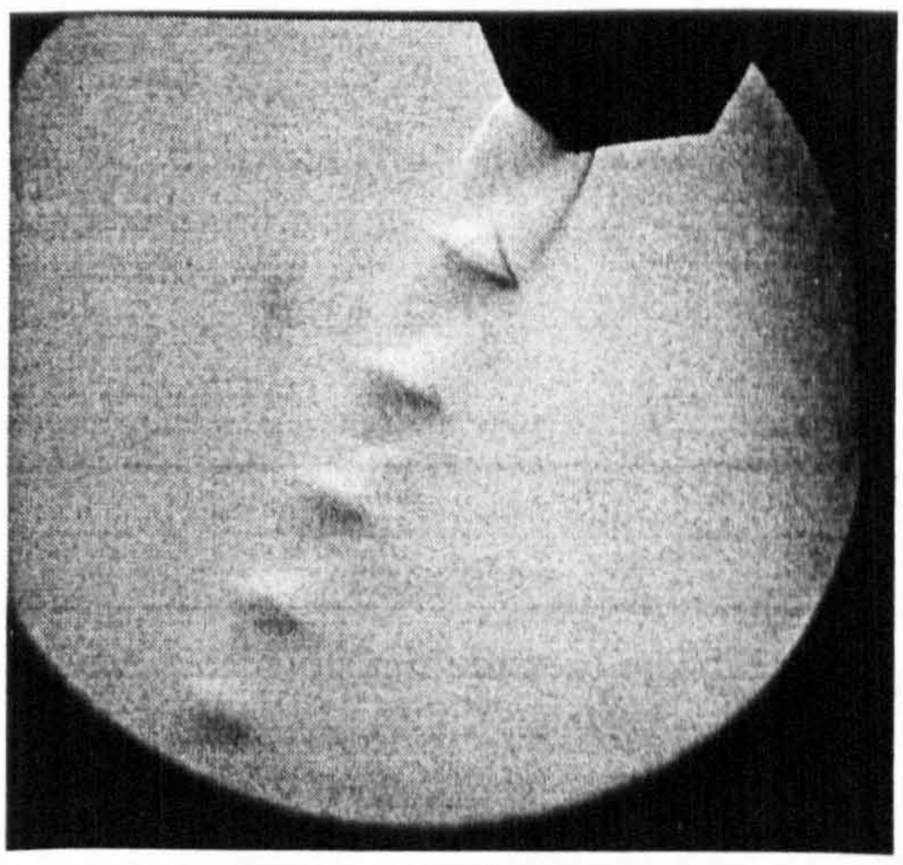

Figure 4.3 - *The vectored jet at an NPR of 4.0.*

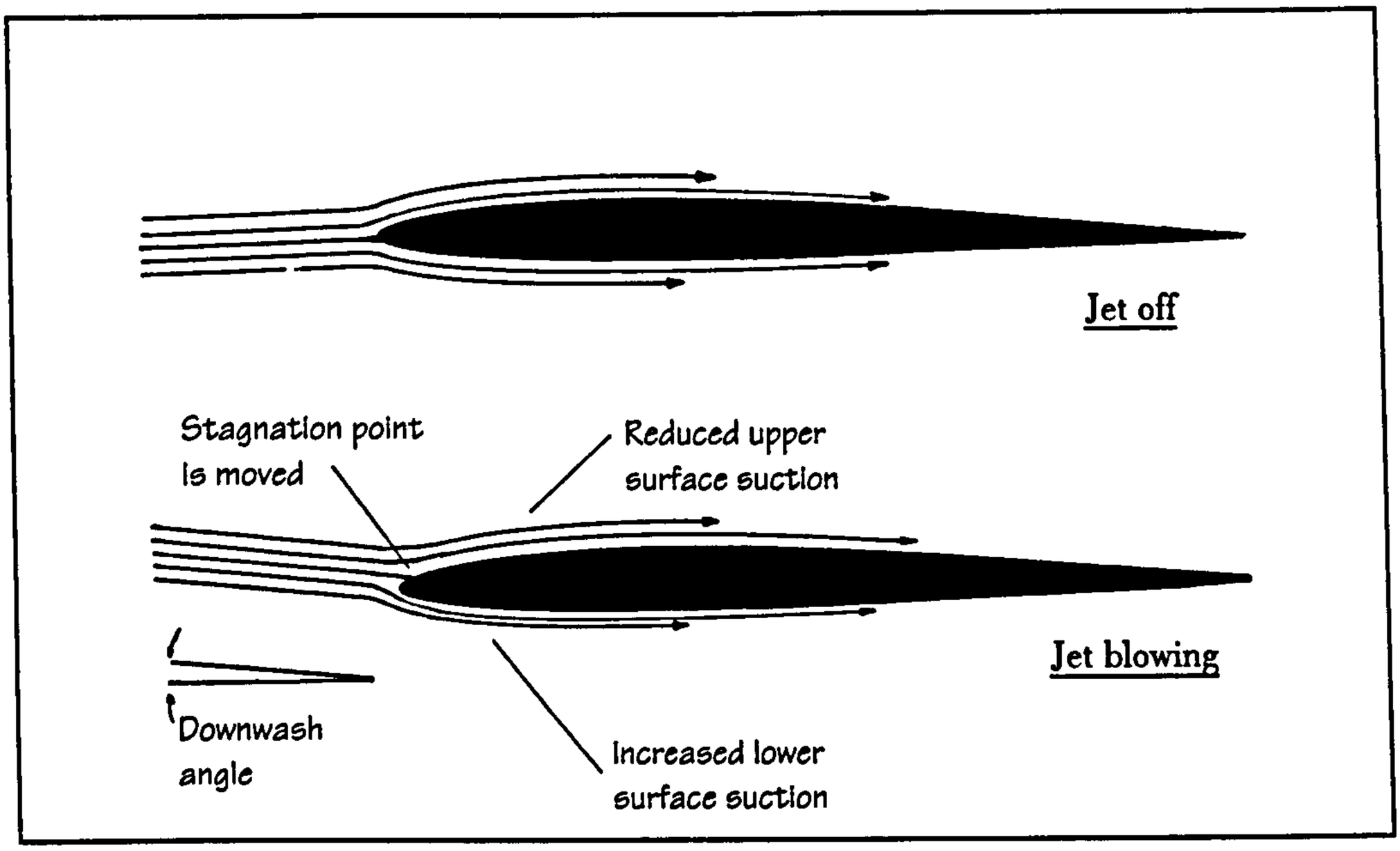

***Figure 4.4** - Sketch showing the main jet-induced interference effects on the wing.*

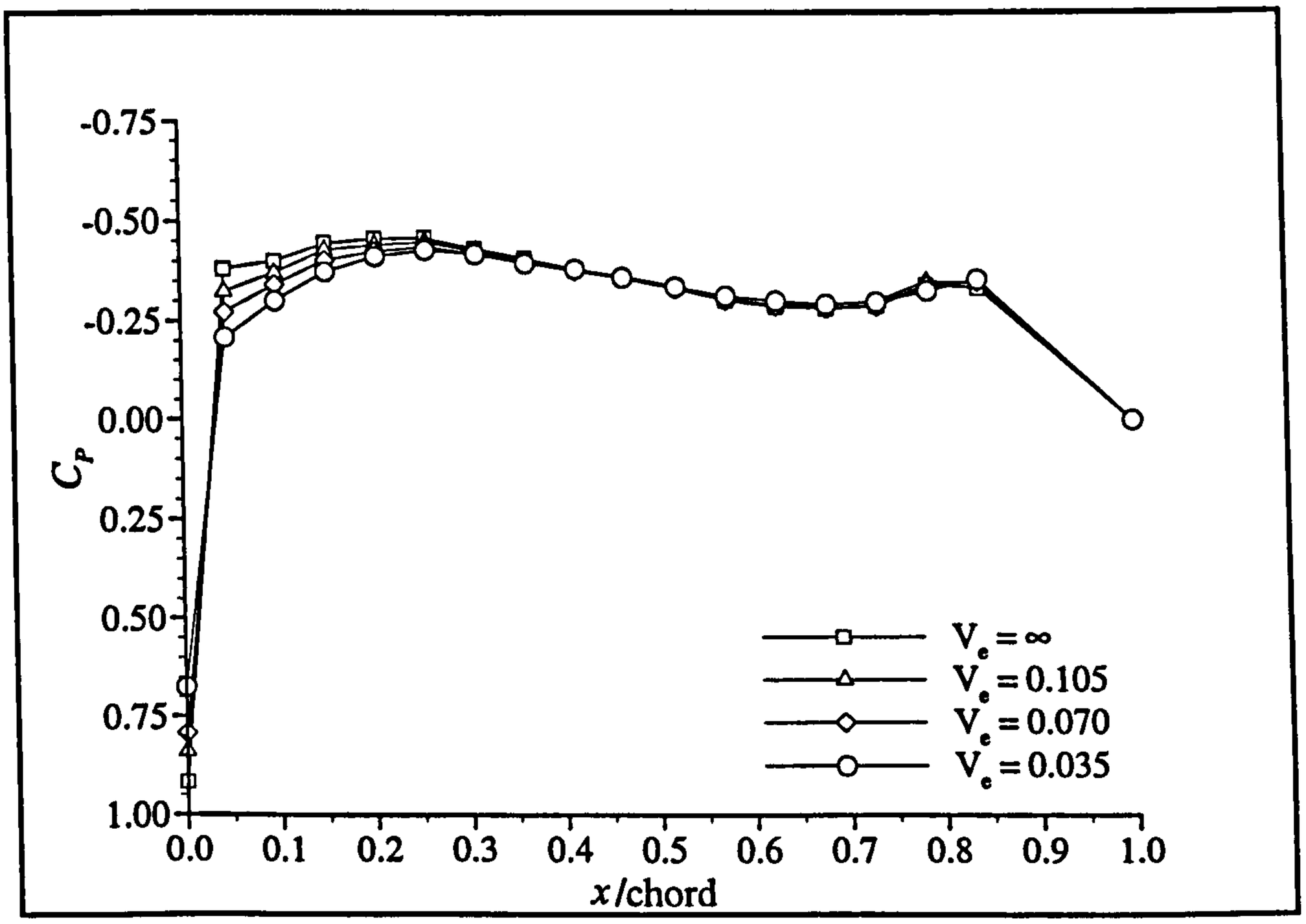

***Figure 4.5** - Wing upper surface pressure distribution, intakes faired, forward nozzle position, NPR = 1.586 (Phase 2a data).*

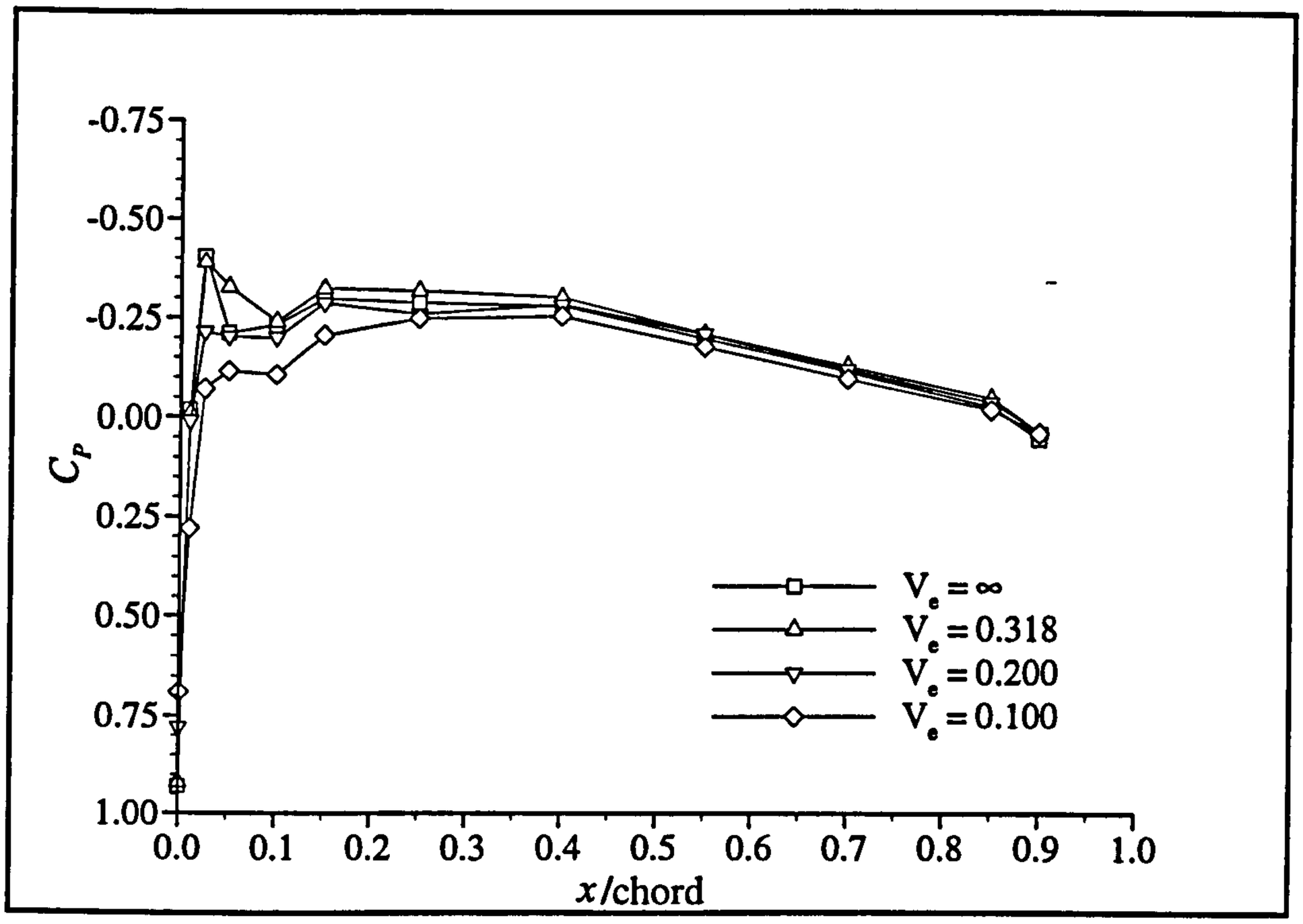

***Figure 4.6** - Wing upper surface pressure distribution on a V/STOL fighter at 25% semi-span (MINECK & MARGASON, 1973).*

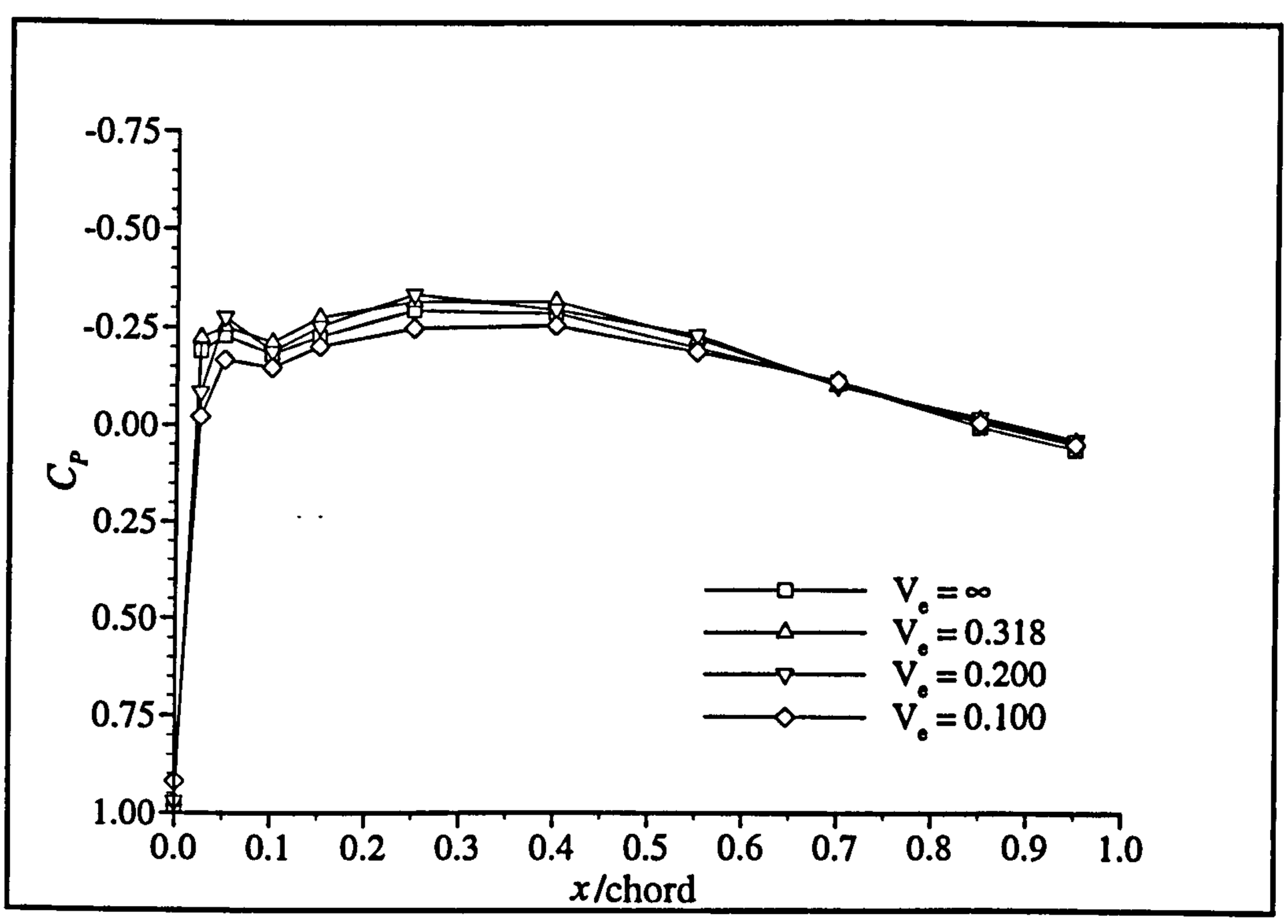

***Figure 4.7** - Wing upper surface pressure distribution on a V/STOL fighter at 80% semi-span (MINECK & MARGASON, 1973).*

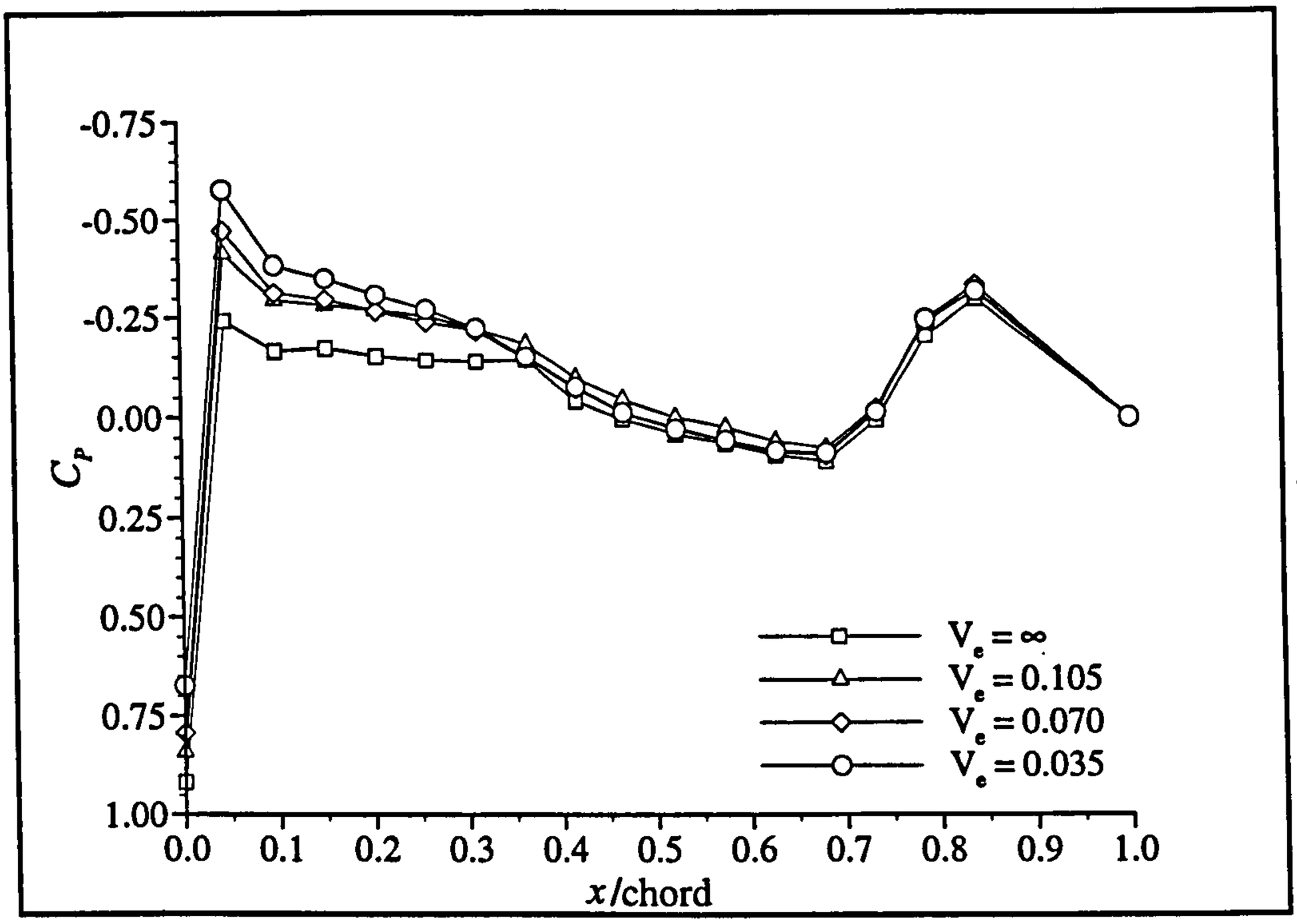

***Figure 4.8** - Wing lower surface pressure distribution, intakes faired, forward nozzle position, NPR = 1.586 (Phase 2a data).*

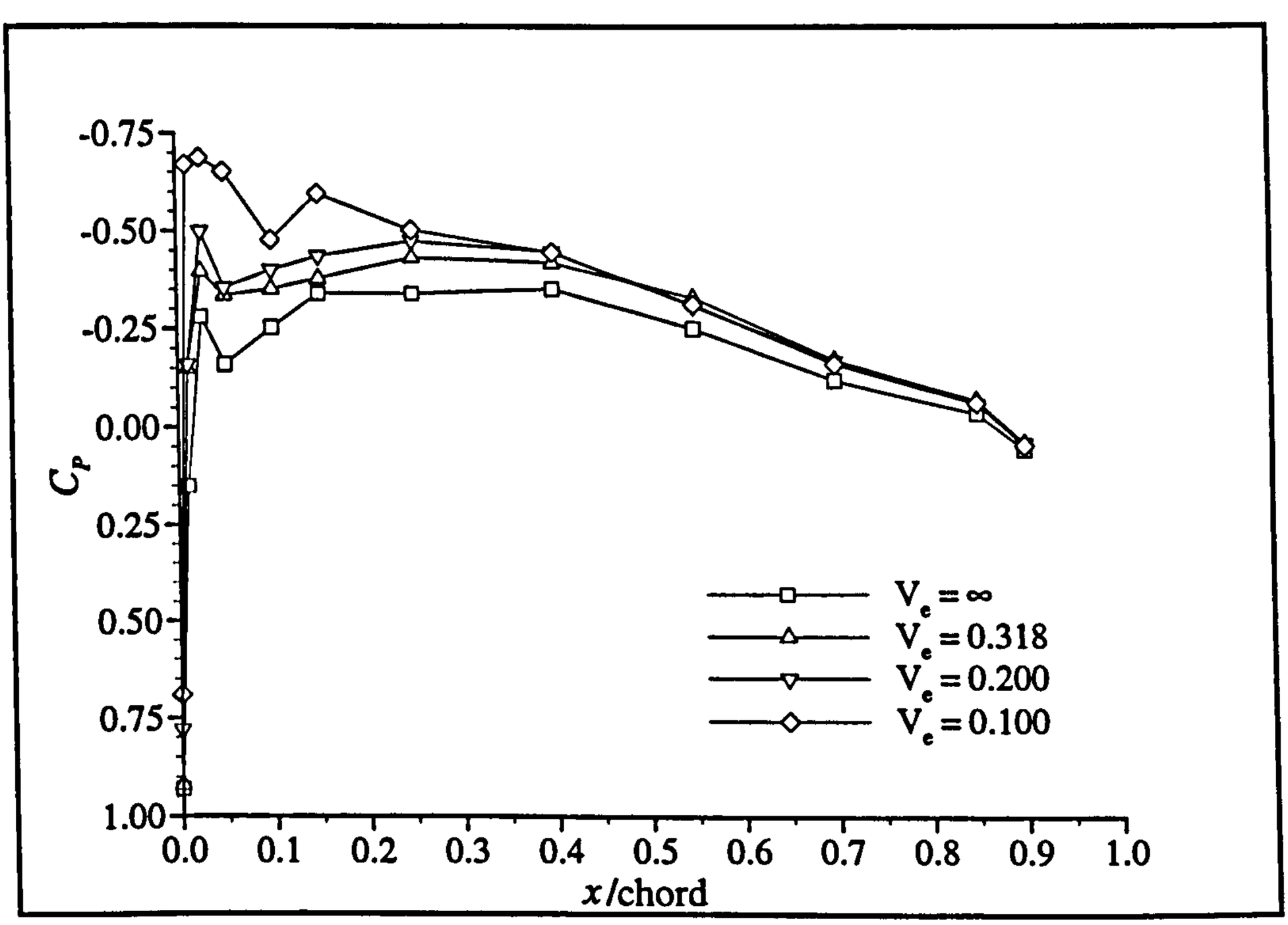

***Figure 4.9** - Wing lower surface pressure distribution on a V/STOL fighter at 25% semi-span (MINECK & MARGASON, 1973).*

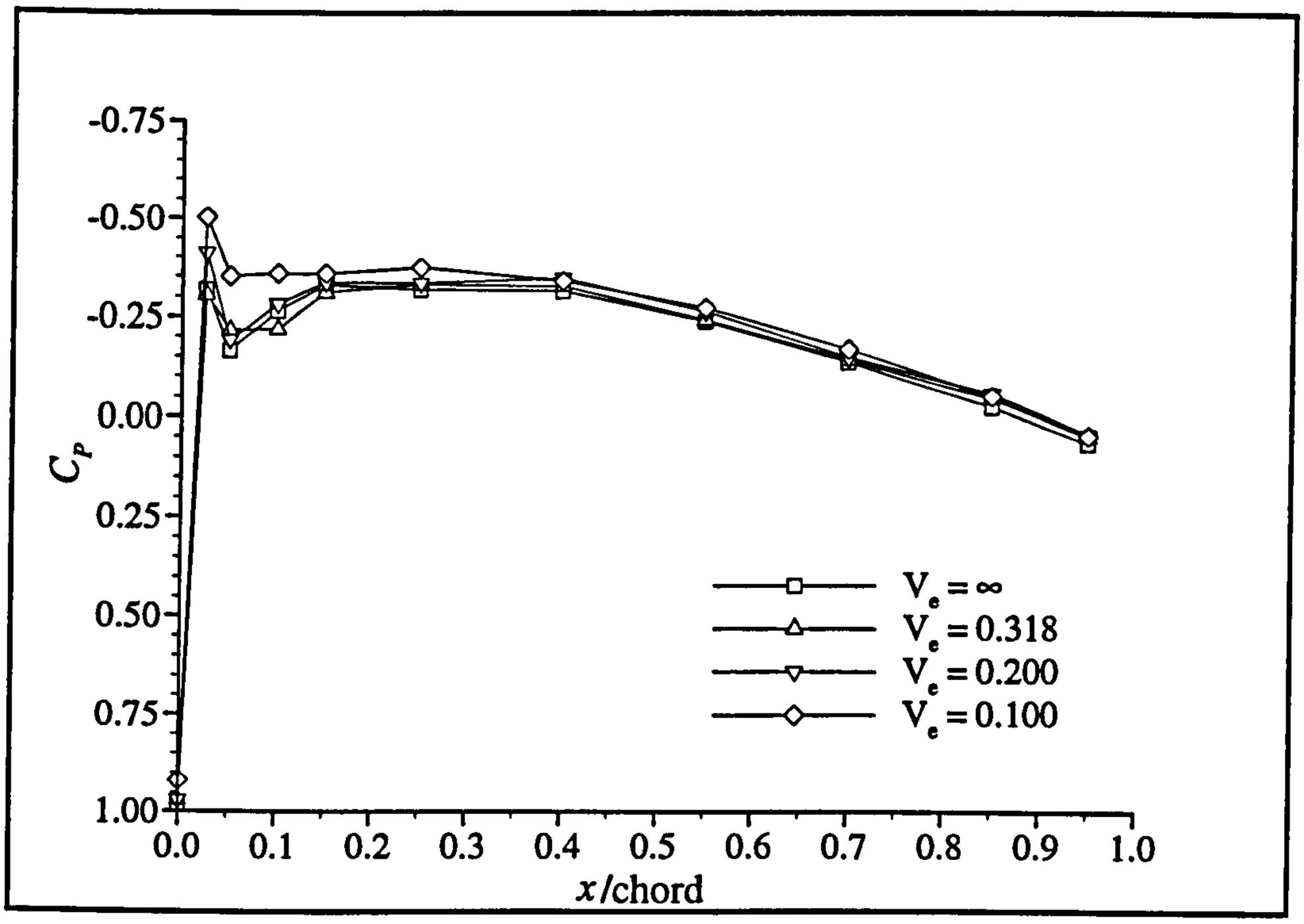

***Figure 4.10** - Wing lower surface pressure distribution on a V/STOL fighter at 80% semi-span (MINECK & MARGASON, 1973).*

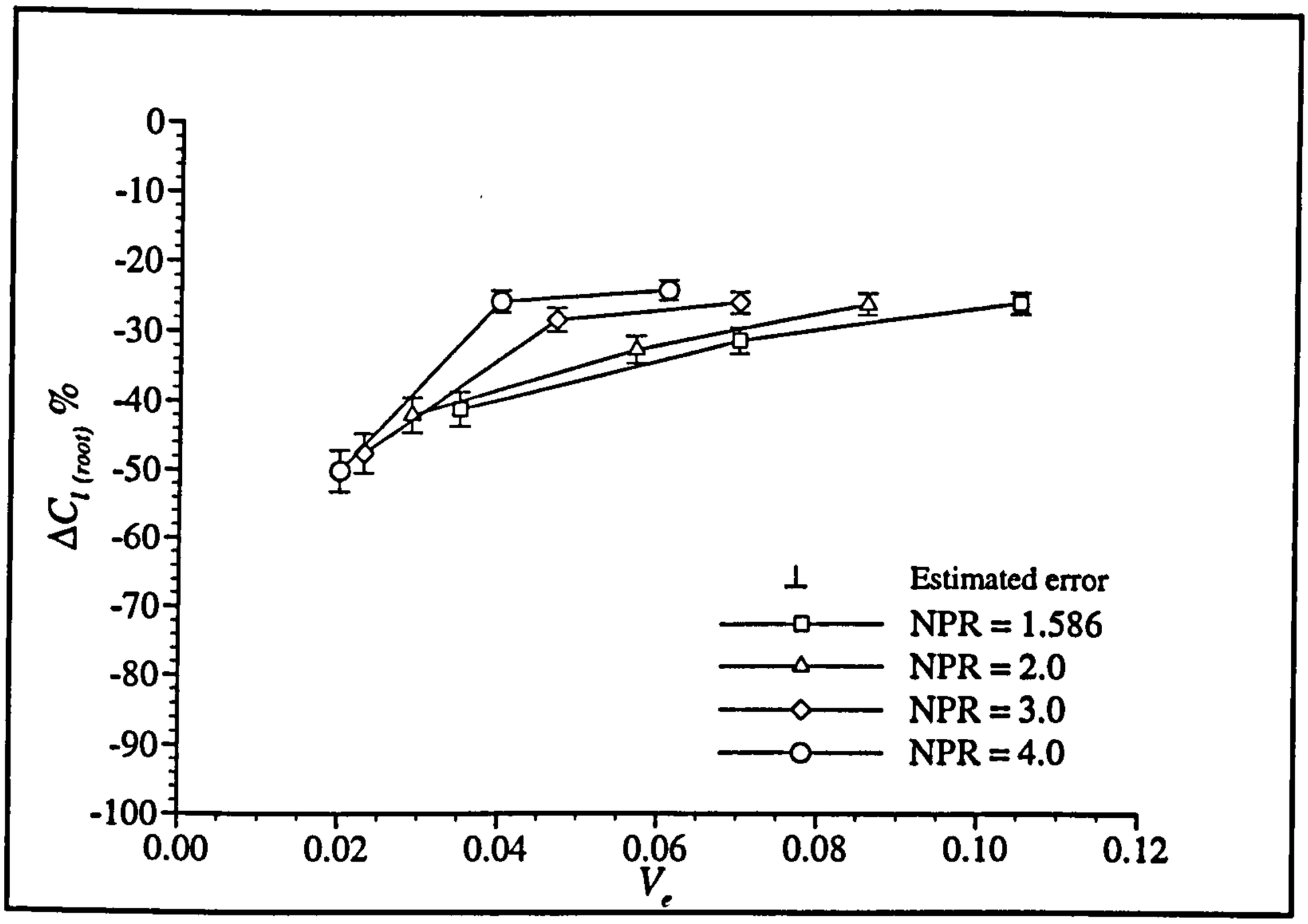

***Figure 4.11** - Variation in $C_{l\,(root)}$ with effective velocity ratio for four different NPRs, intakes faired, forward nozzle position (Phase 2a data).*

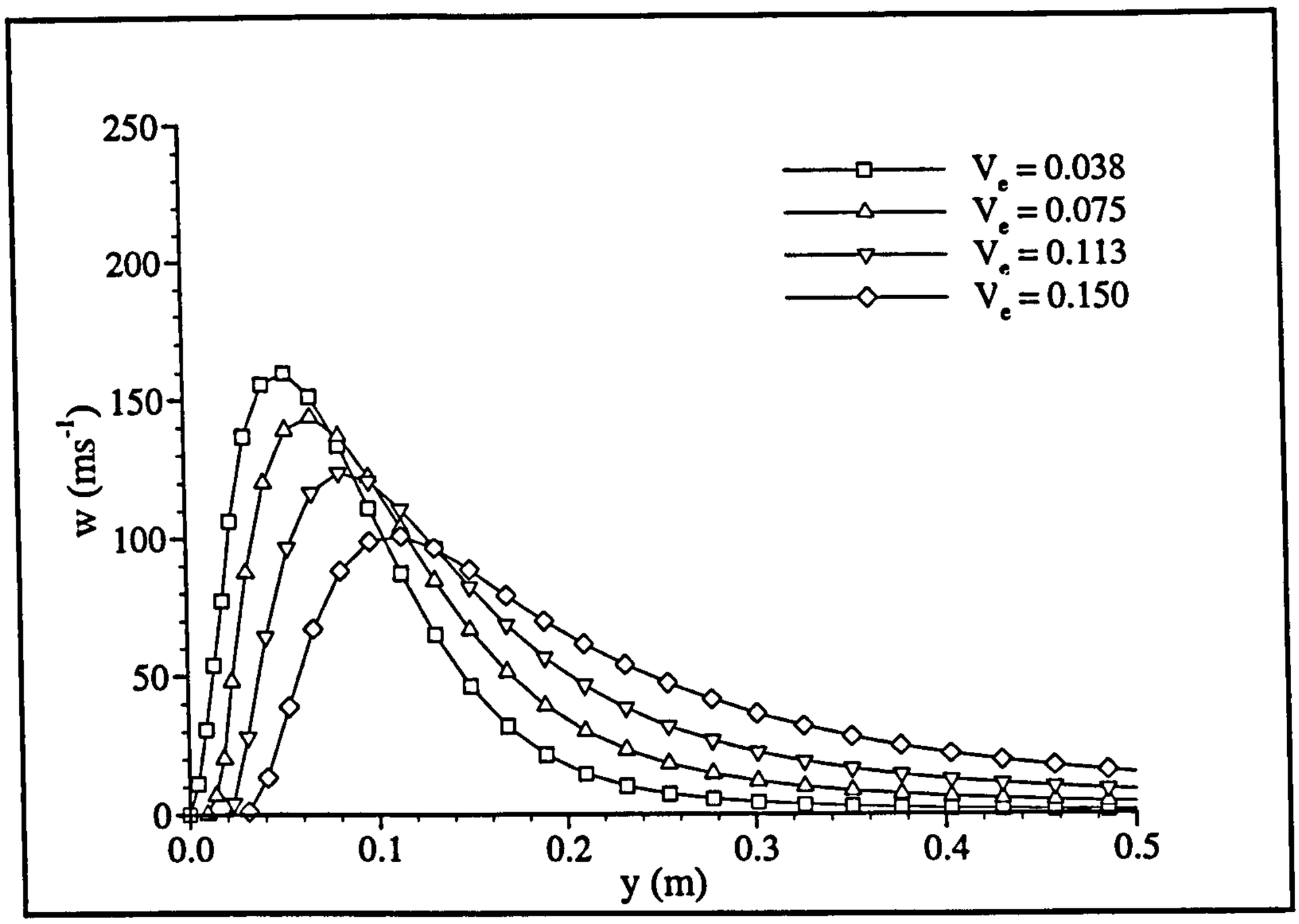

***a** - Downwash velocity 0.125 m below nozzle exit, NPR = 1.5.*

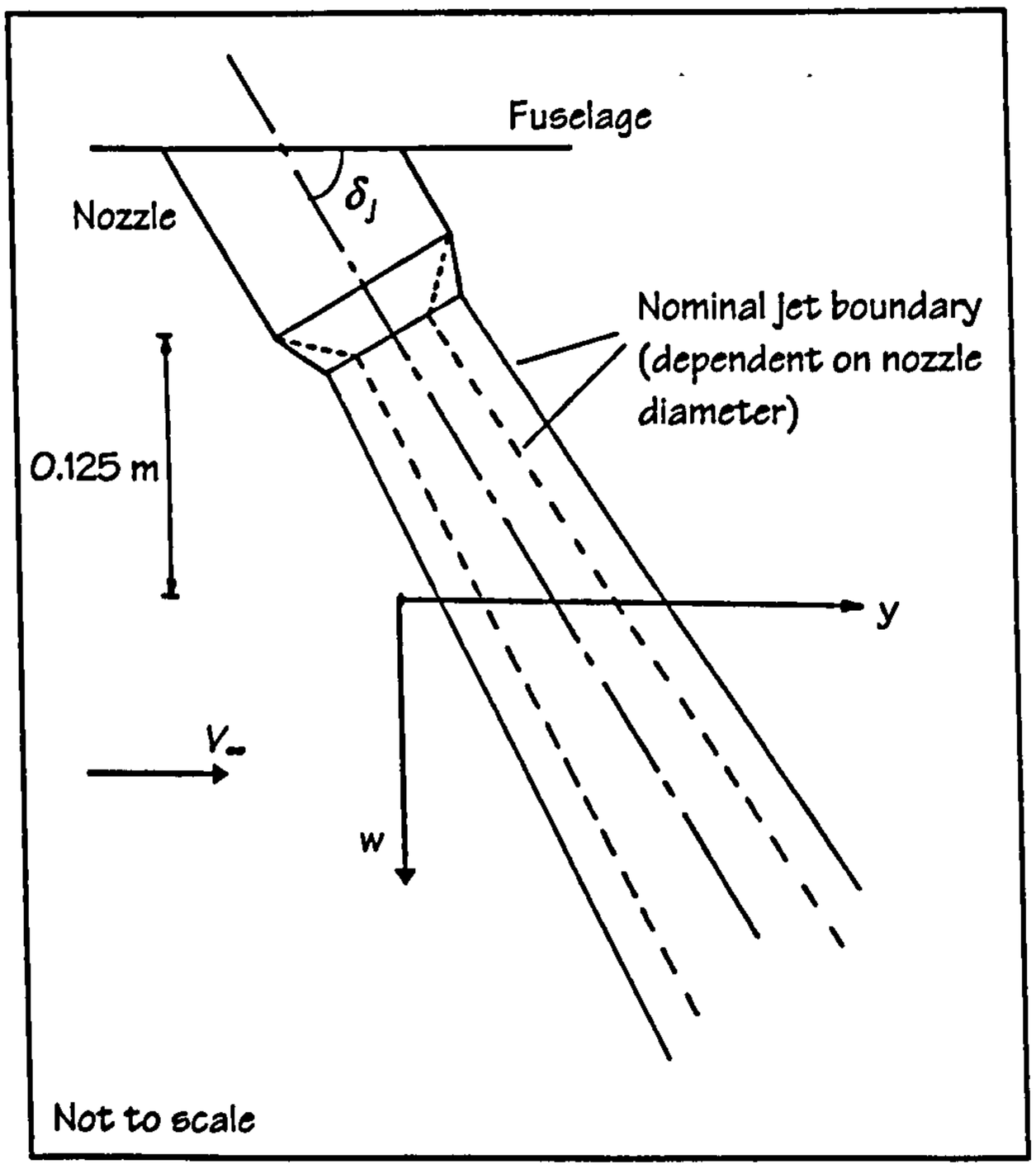

***b** - Sketch of the co-ordinate system used showing the effect of nozzle diameter.*

***Figure 4.12** - CFD-predicted flow-field for a round jet vectored 60 degrees.*

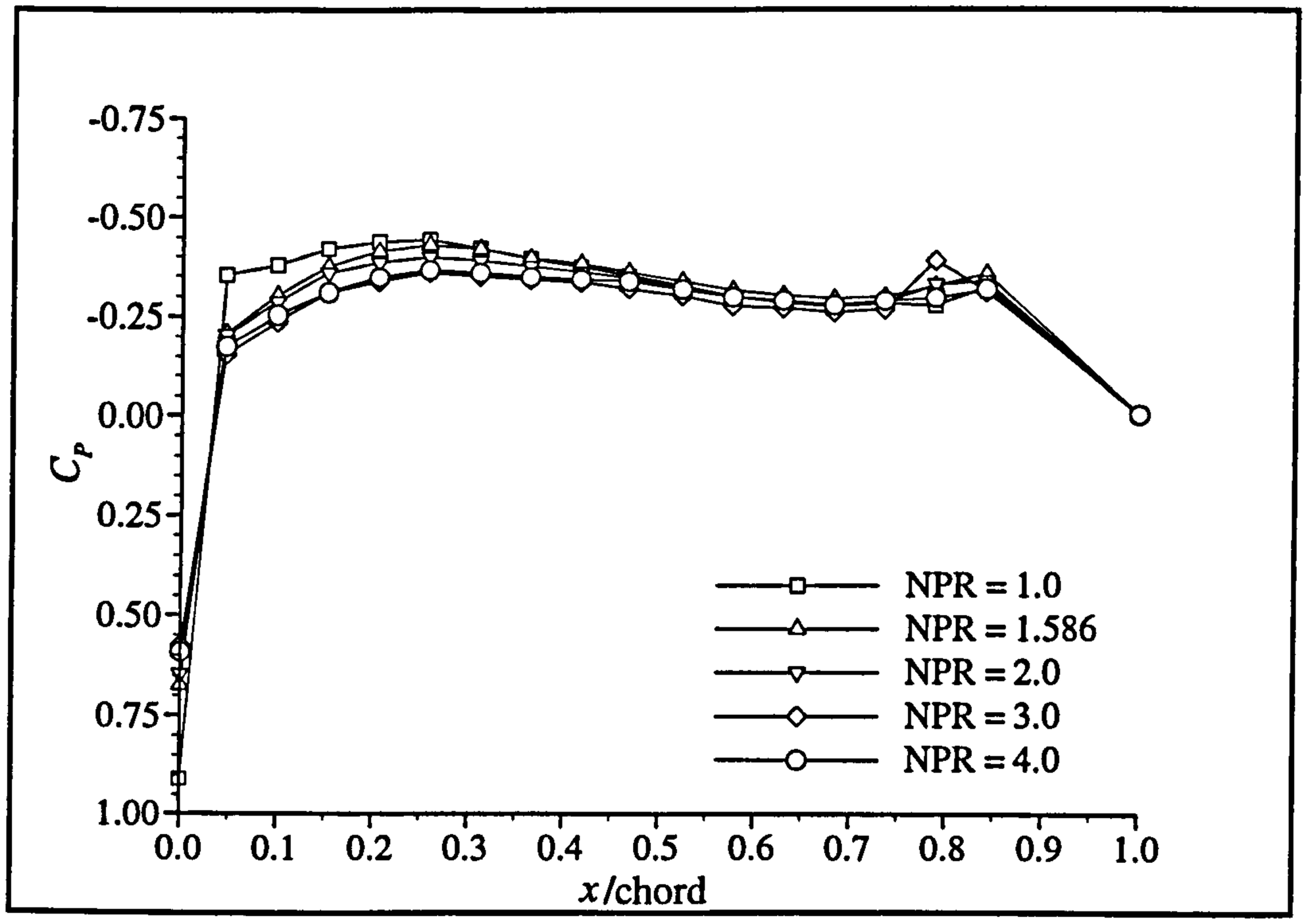

***Figure 4.13** - Wing upper surface pressure distribution, intakes faired, forward nozzle position, q_∞ = 61.3 Pa (Phase 2a data).*

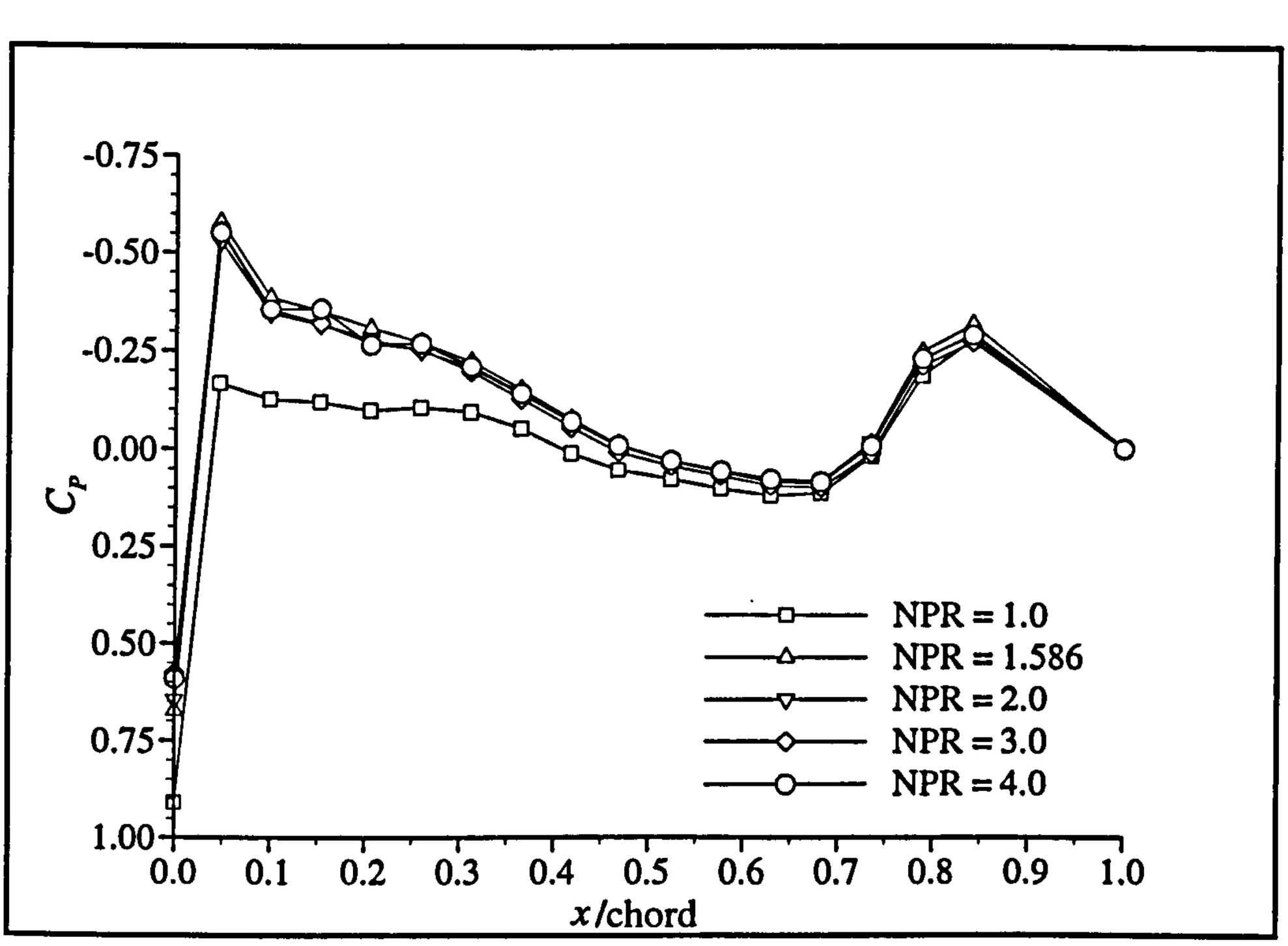

***Figure 4.14** - Wing lower surface pressure distribution, intakes faired, forward nozzle position, q_∞ = 61.3 Pa (Phase 2a data).*

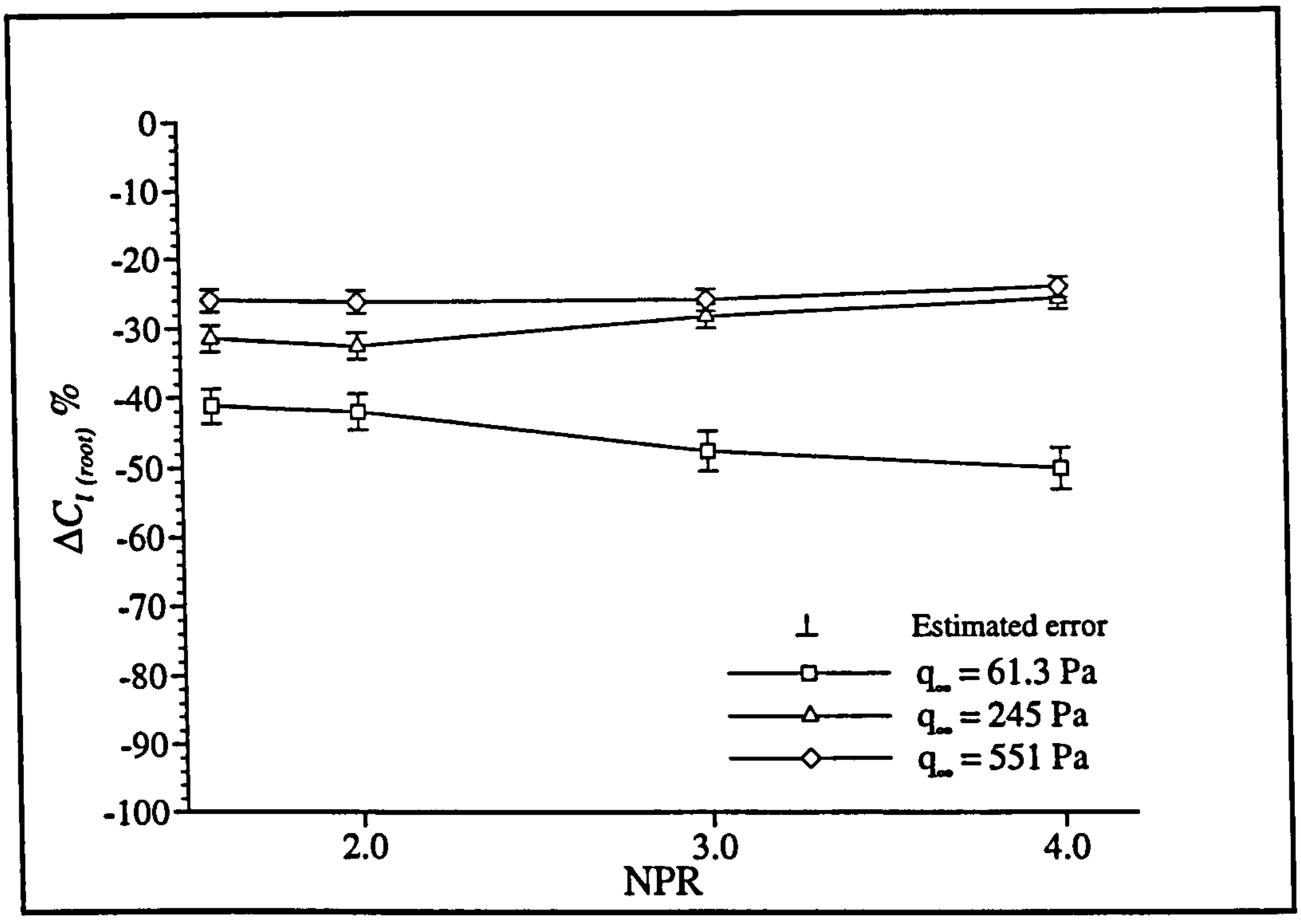

***Figure 4.15** - Variation in $C_{l\,(root)}$ with NPR for three different freestream dynamic pressures, intakes faired, forward nozzle position (Phase 2a data).*

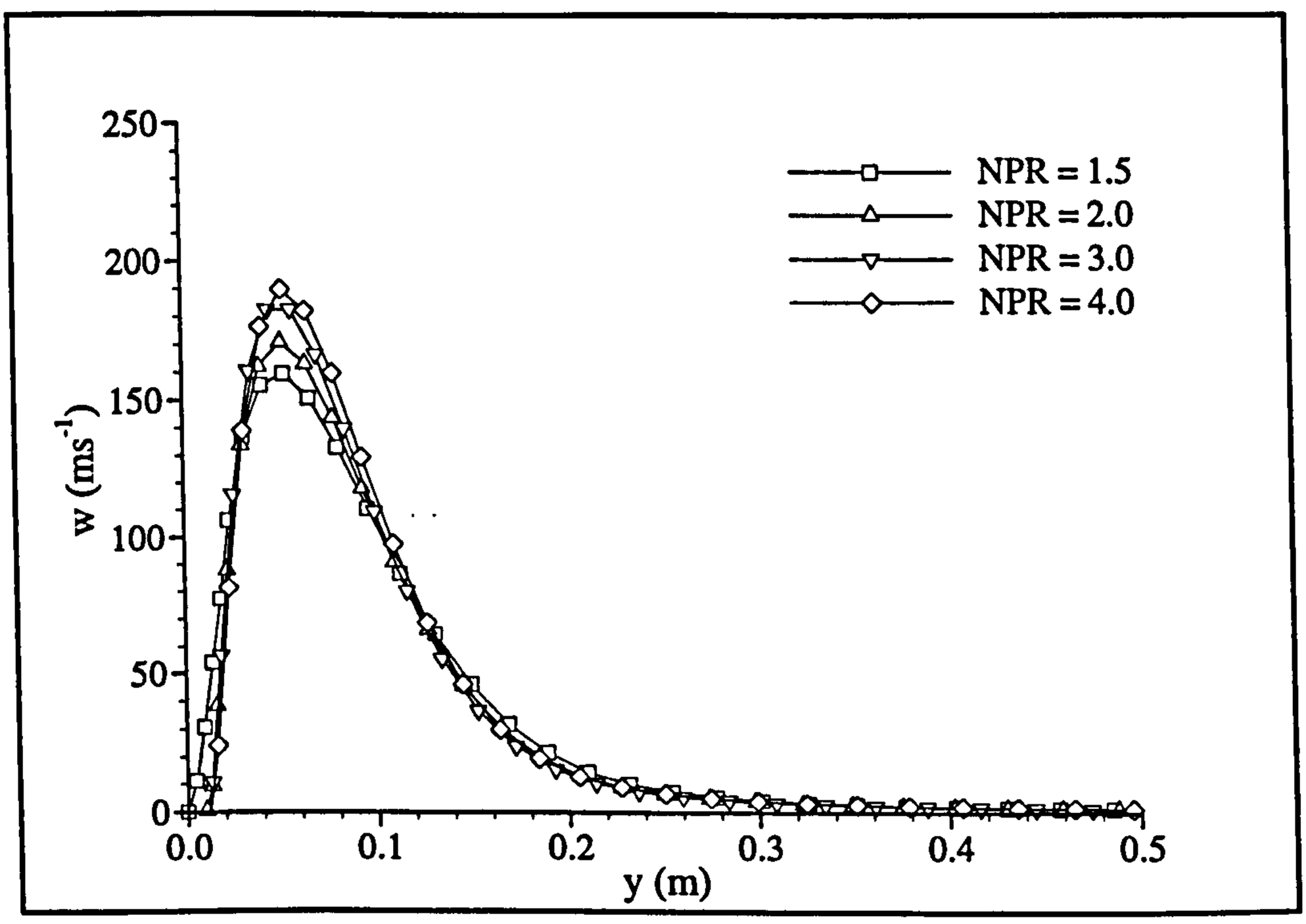

***Figure 4.16** - CFD-predicted downwash for a round jet vectored 60 degrees, 0.125 m below nozzle exit, q_∞ = 61.3 Pa (constant nozzle mass flow rate).*

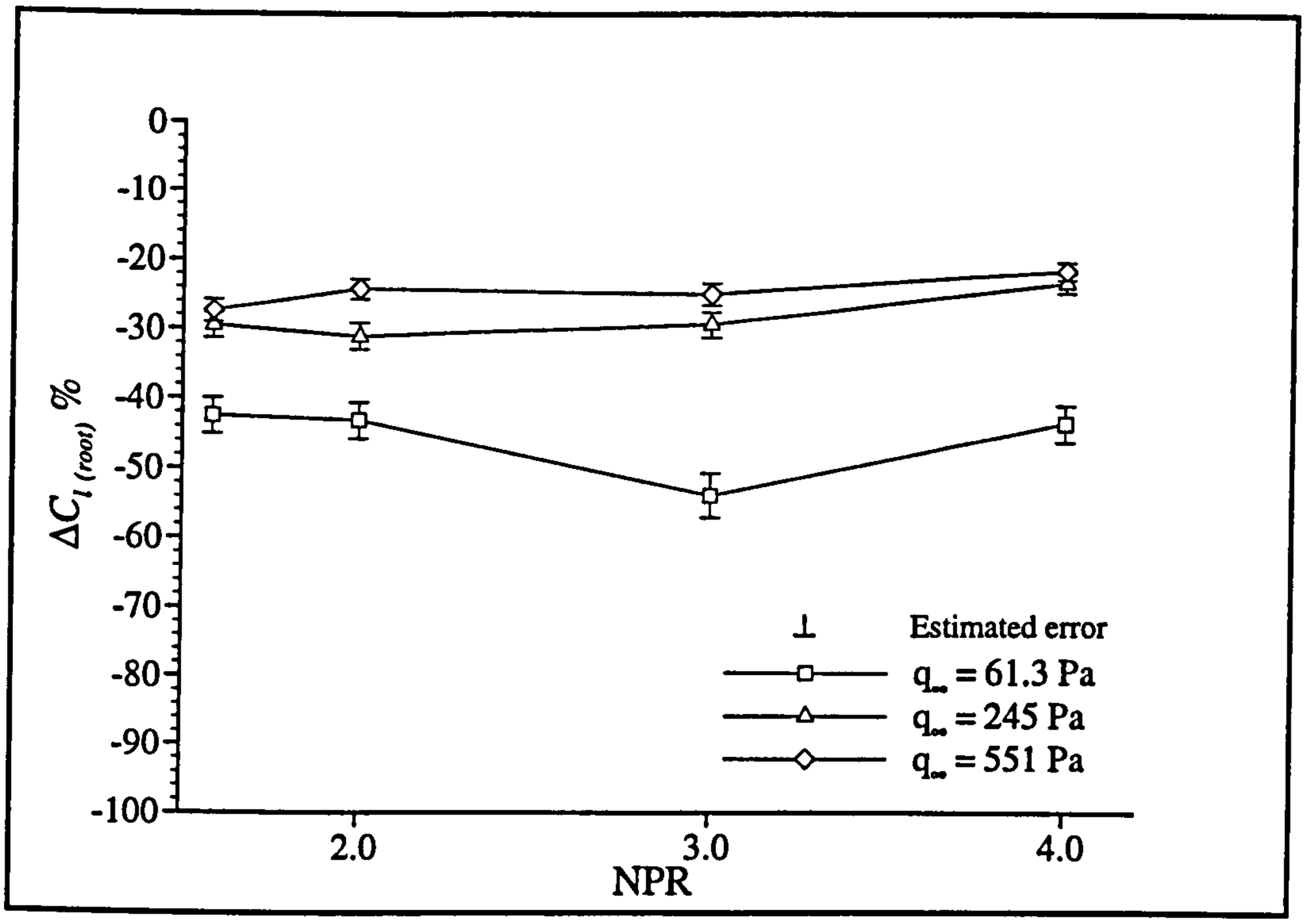

***Figure 4.17** - Variation in $C_{l\,(root)}$ with NPR for three different freestream dynamic pressures, intakes faired, centre nozzle position (Phase 2a data).*

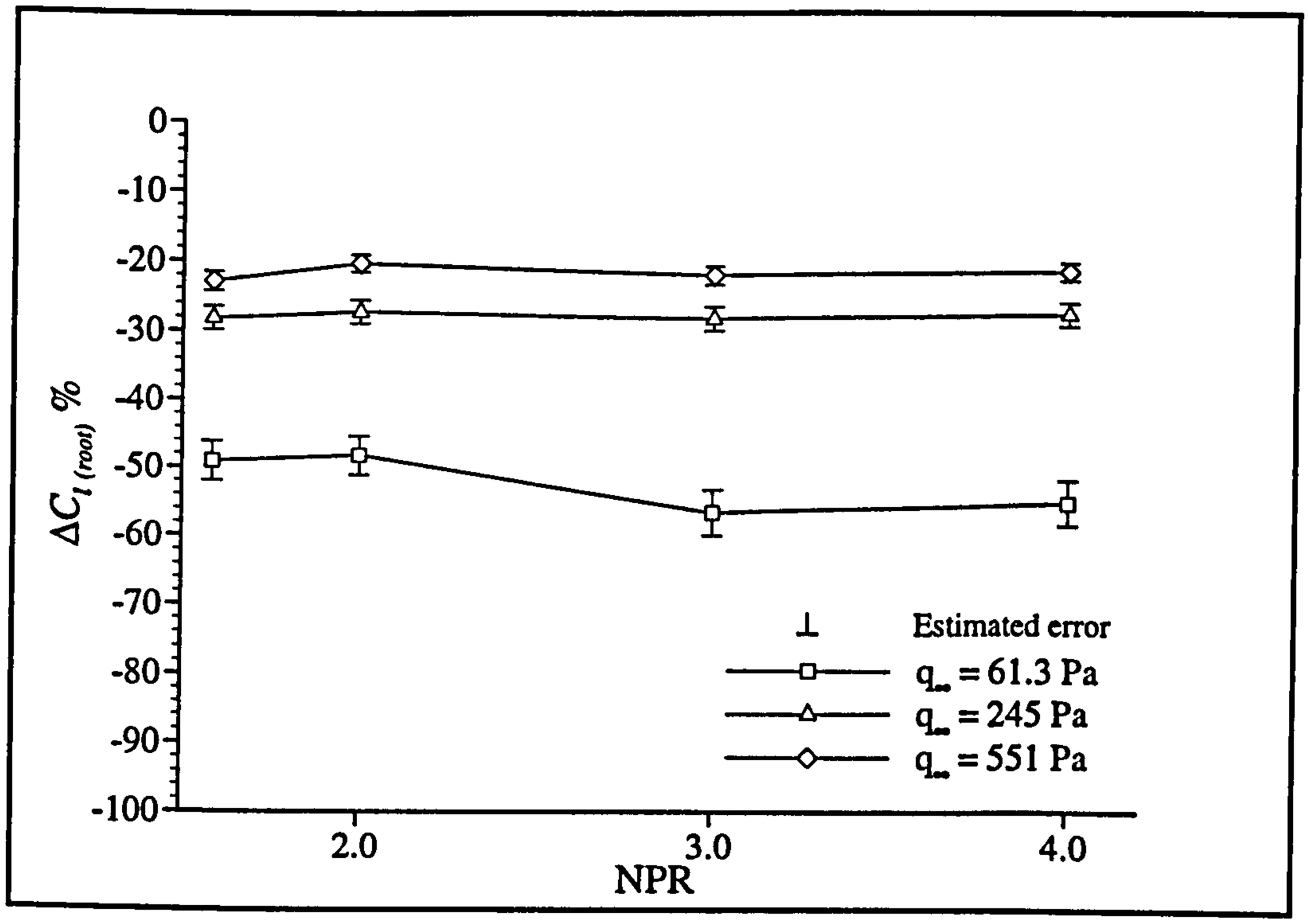

***Figure 4.18** - Variation in $C_{l\,(root)}$ with NPR for three different freestream dynamic pressures, intakes faired, rearward nozzle position (Phase 2a data).*

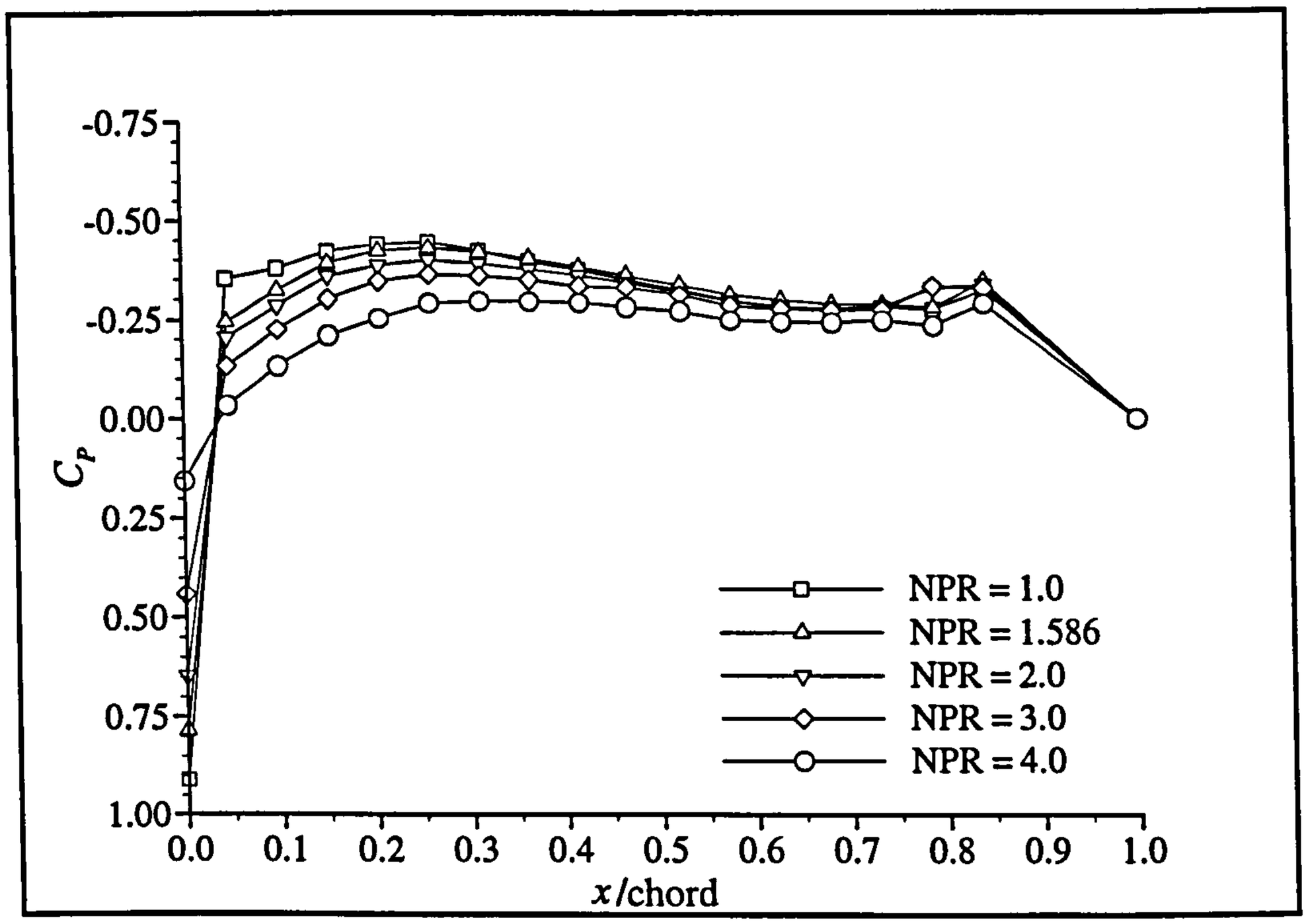

***Figure 4.19** - Wing upper surface pressure distribution, intakes faired, forward nozzle position, q_∞ = 61.3 Pa (Phase 2b data).*

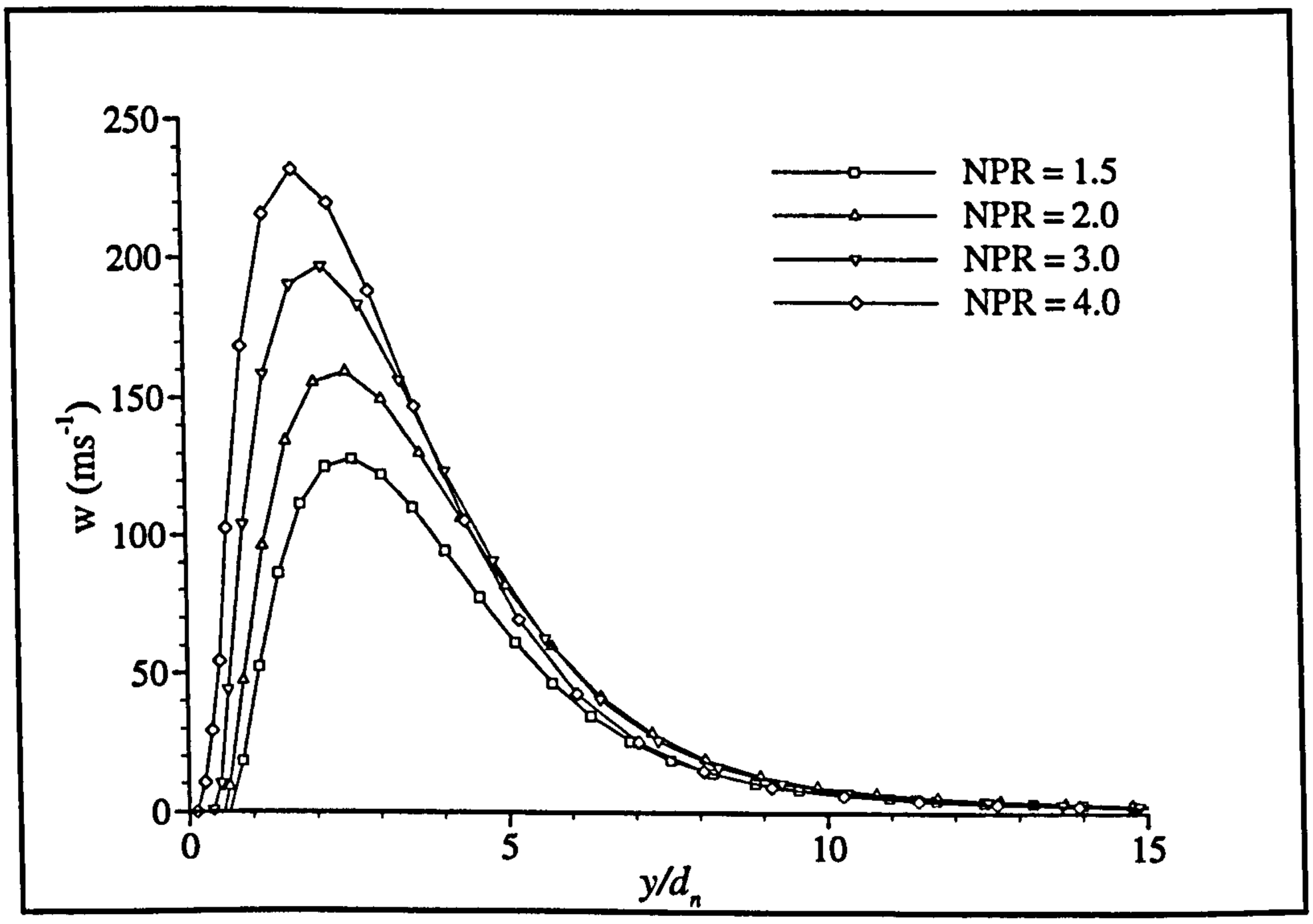

***Figure 4.20** - CFD-predicted downwash for a round jet vectored 60 degrees, 5 d_n below nozzle exit, q_∞ = 61.3 Pa (constant nozzle area).*

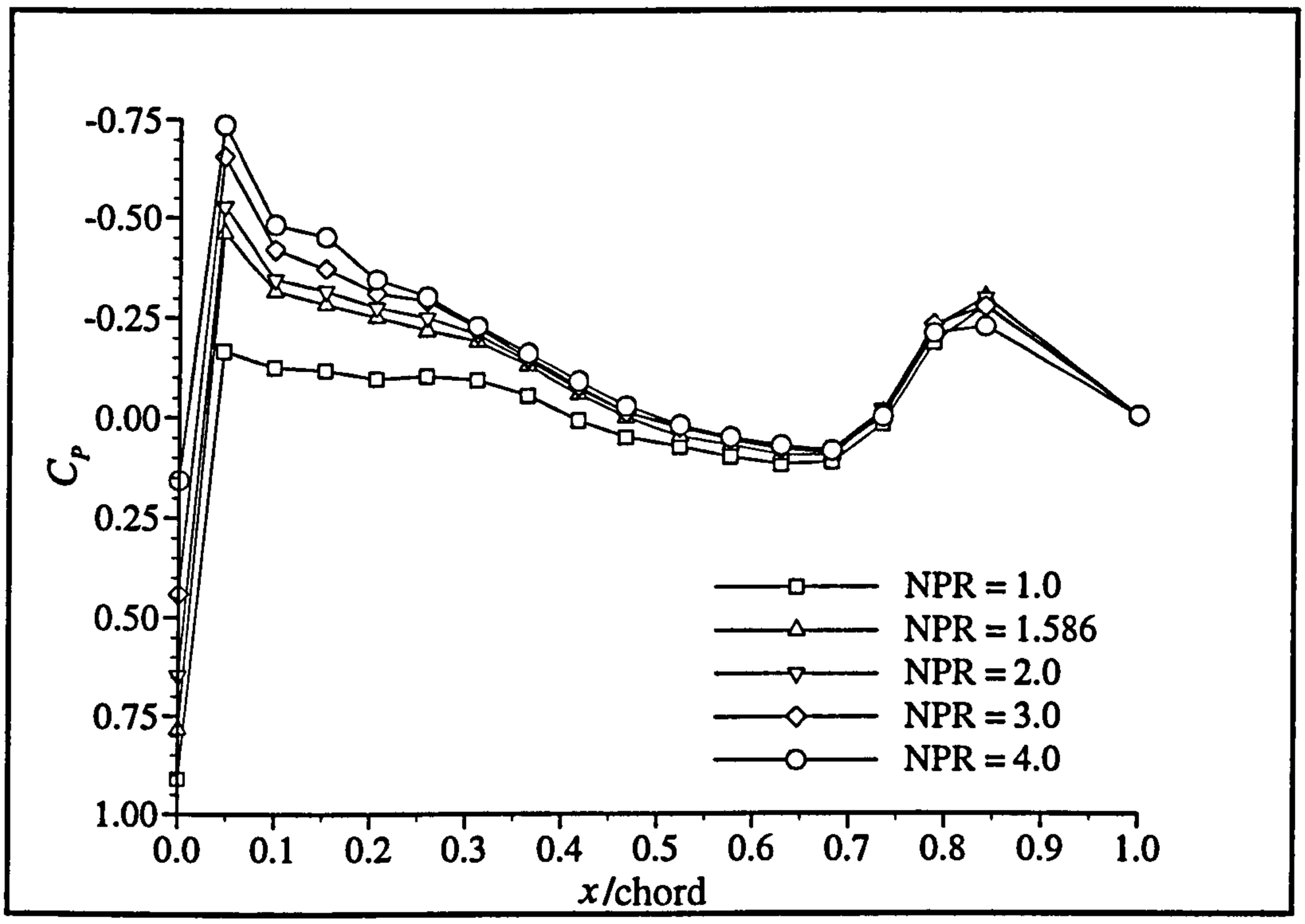

***Figure 4.21** - Wing lower surface pressure distribution, intakes faired, forward nozzle position, q_∞ = 61.3 Pa (Phase 2b data).*

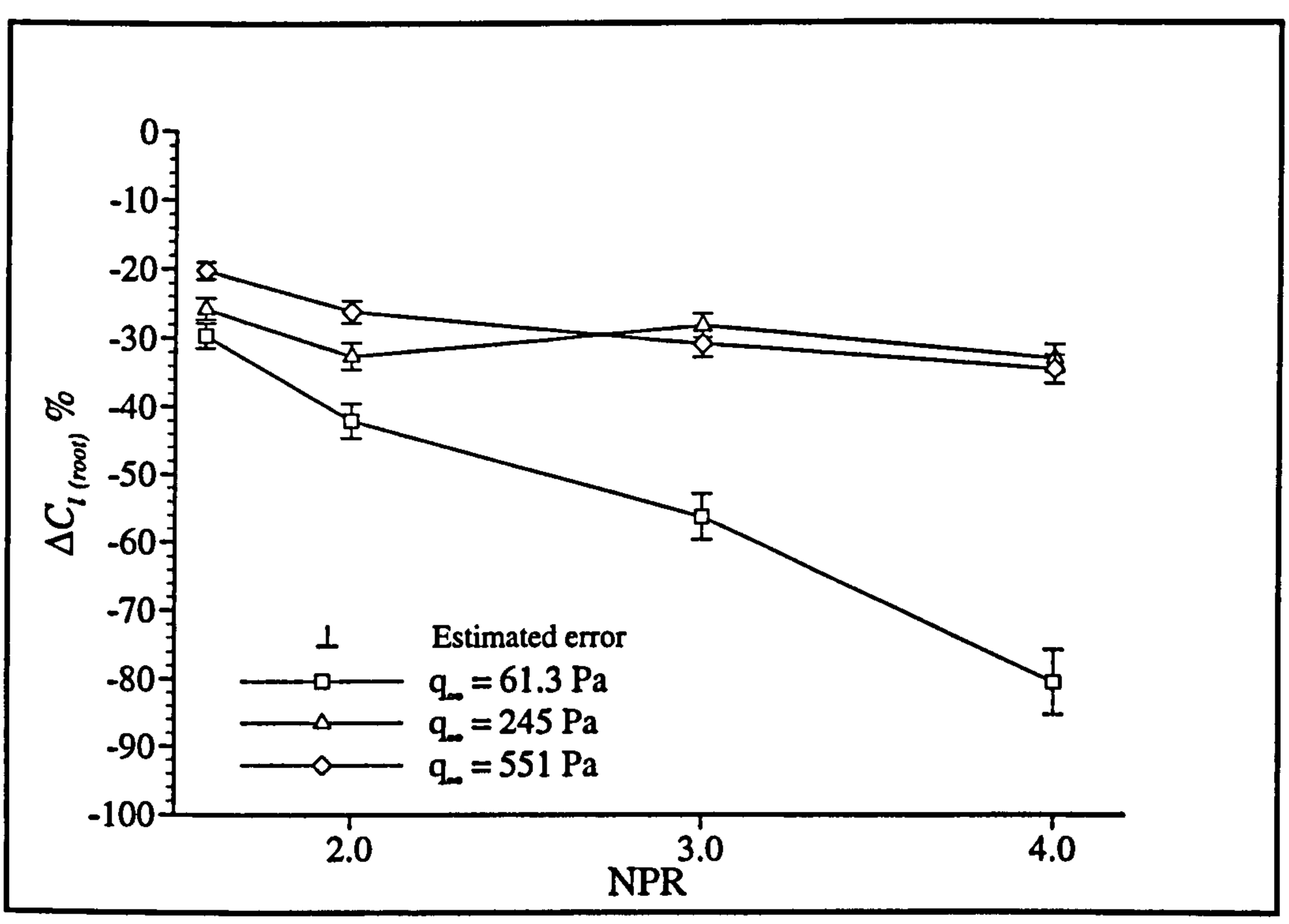

***Figure 4.22** - Variation in $C_{l\,(root)}$ with NPR for three different freestream dynamic pressures, intakes faired, forward nozzle position (Phase 2b data).*

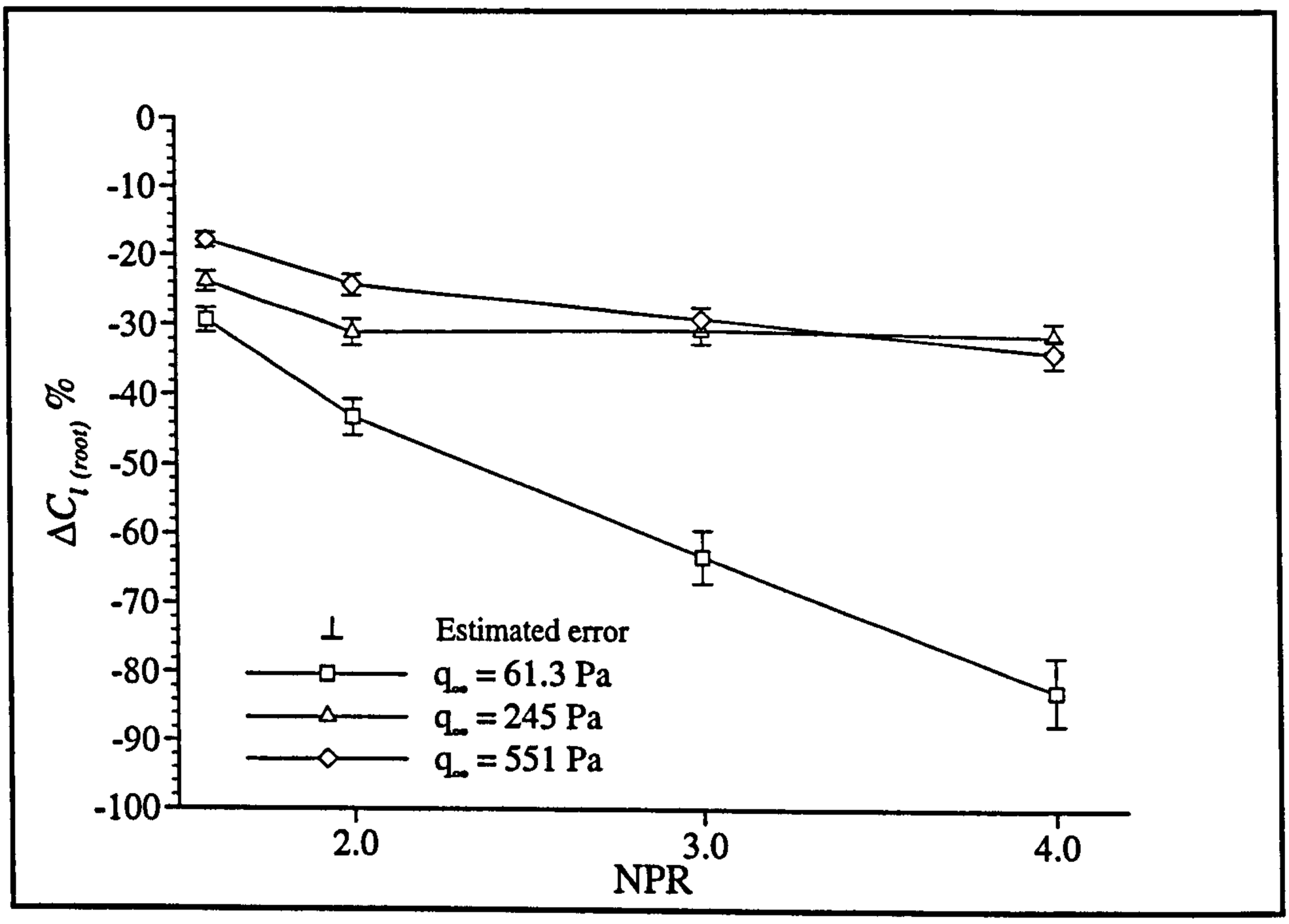

***Figure 4.23** - Variation in $C_{l\,(root)}$ with NPR for three different freestream dynamic pressures, intakes faired, centre nozzle position (Phase 2b data).*

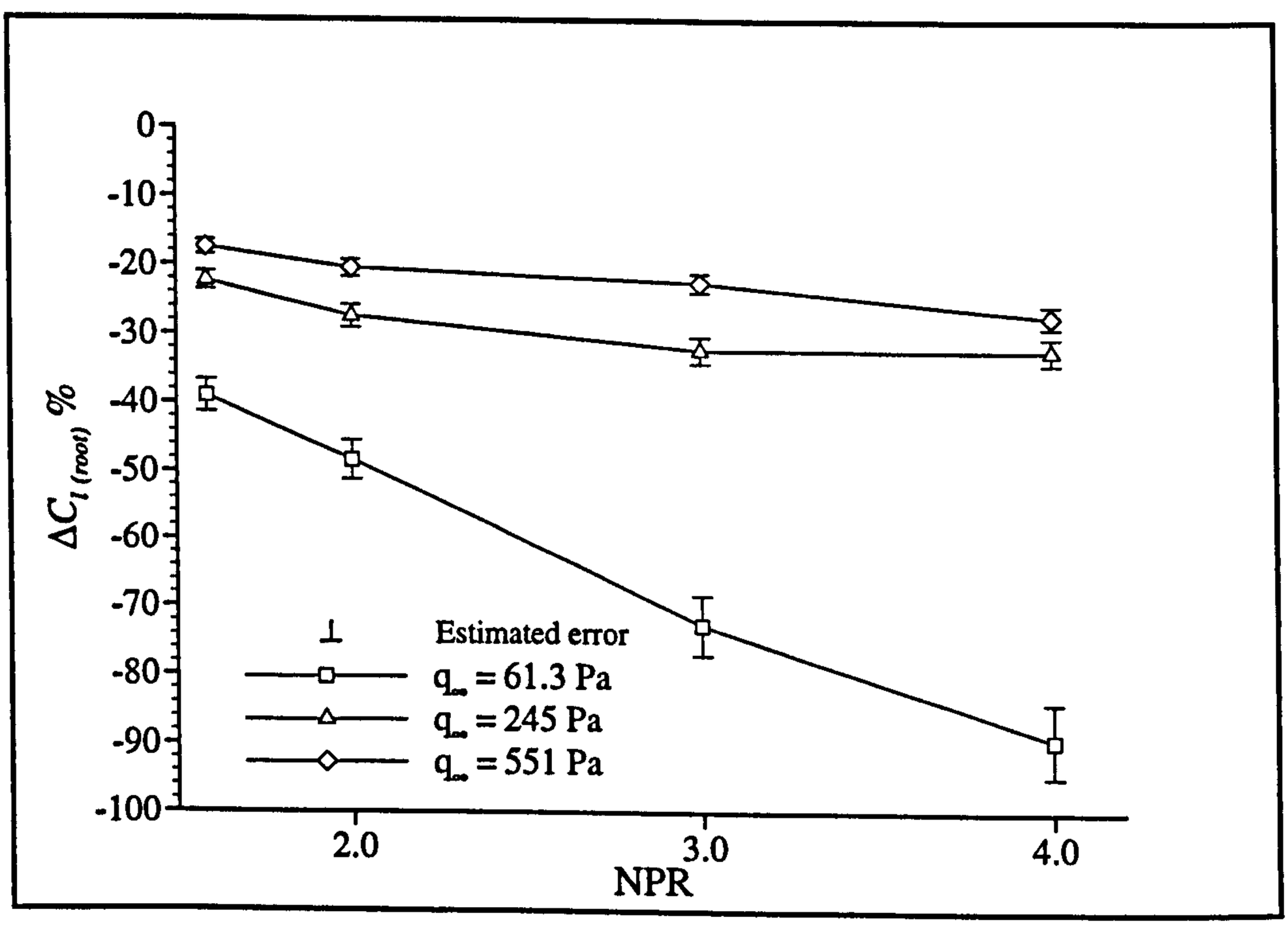

***Figure 4.24** - Variation in $C_{l\,(root)}$ with NPR for three different freestream dynamic pressures, intakes faired, rearward nozzle position (Phase 2b data).*

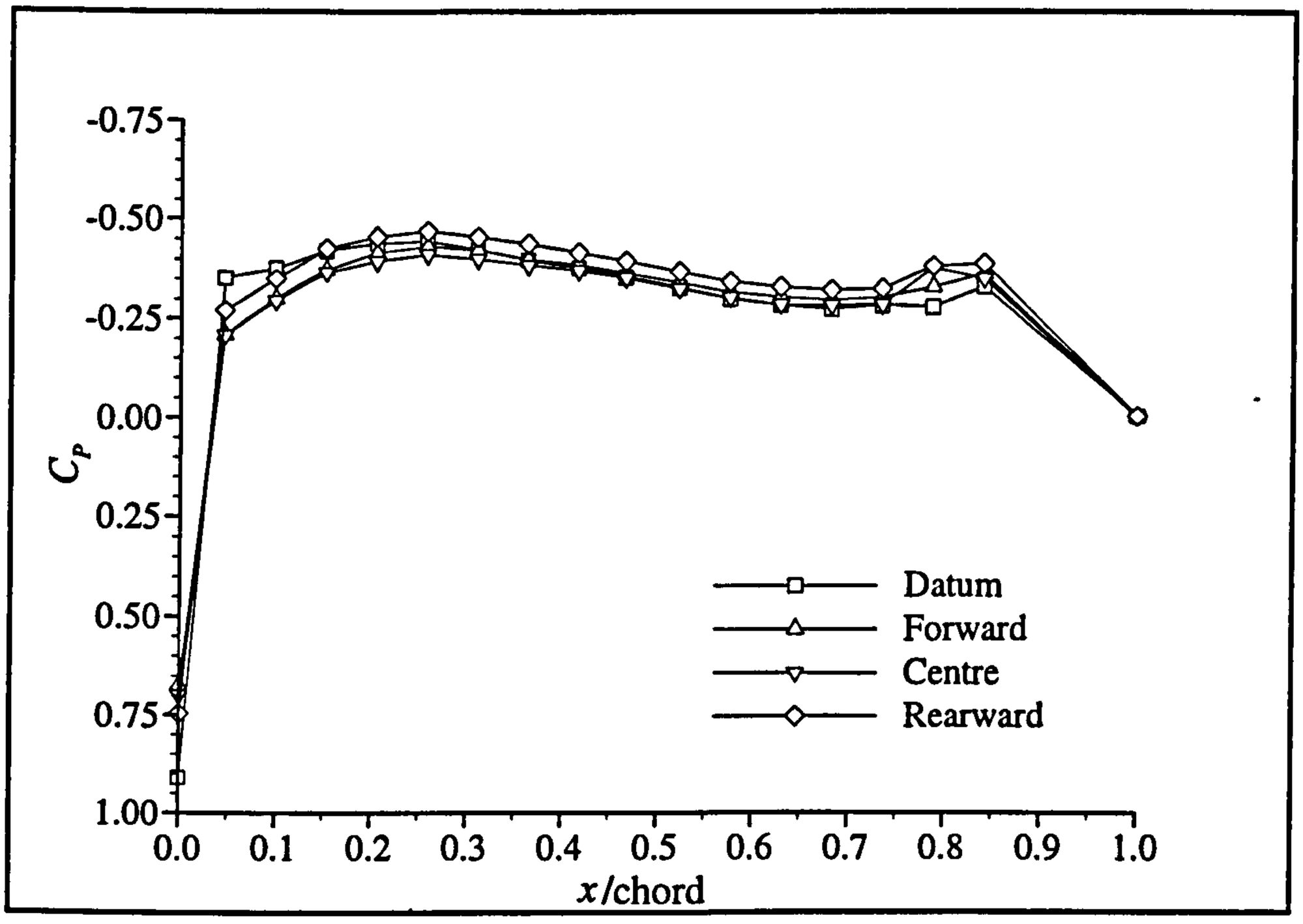

***Figure 4.25** - Wing upper surface pressure distribution, intakes faired, NPR = 1.586, q_∞ = 61.3 Pa (Phase 2a data).*

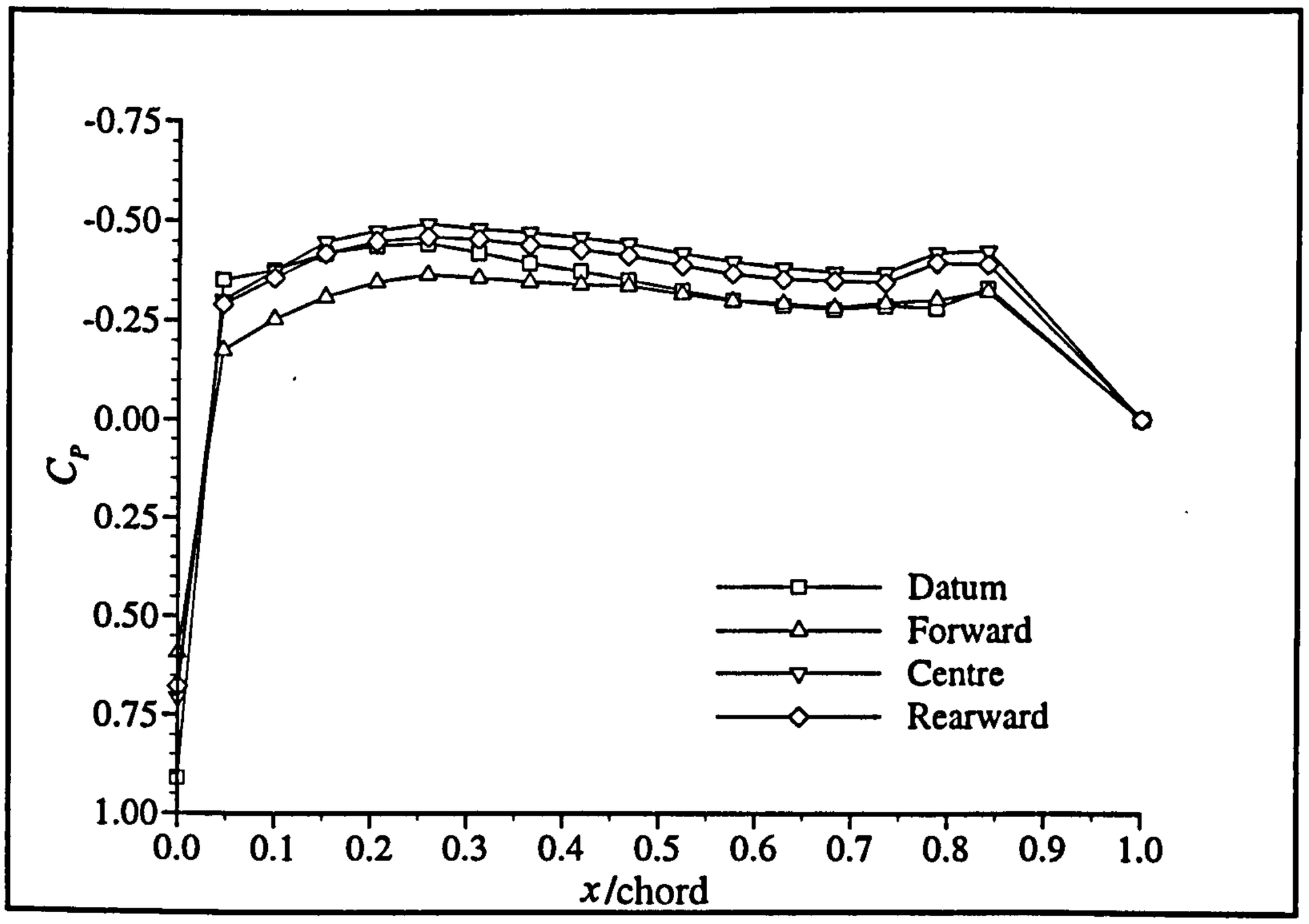

***Figure 4.26** - Wing upper surface pressure distribution, intakes faired, NPR = 4.0, q_∞ = 61.3 Pa (Phase 2a data).*

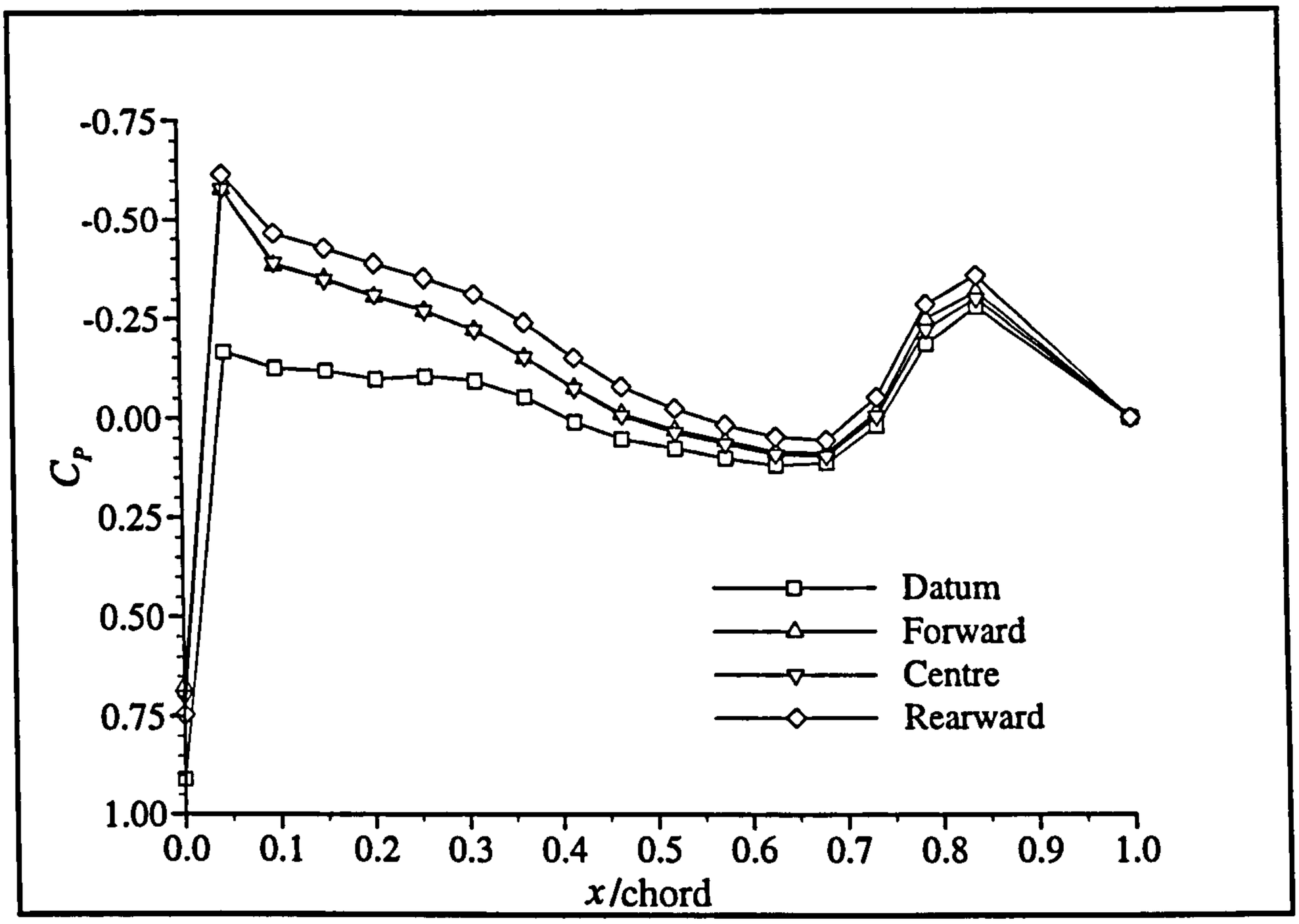

***Figure 4.27** - Wing lower surface pressure distribution, intakes faired, NPR = 1.586, q_∞ = 61.3 Pa (Phase 2a data).*

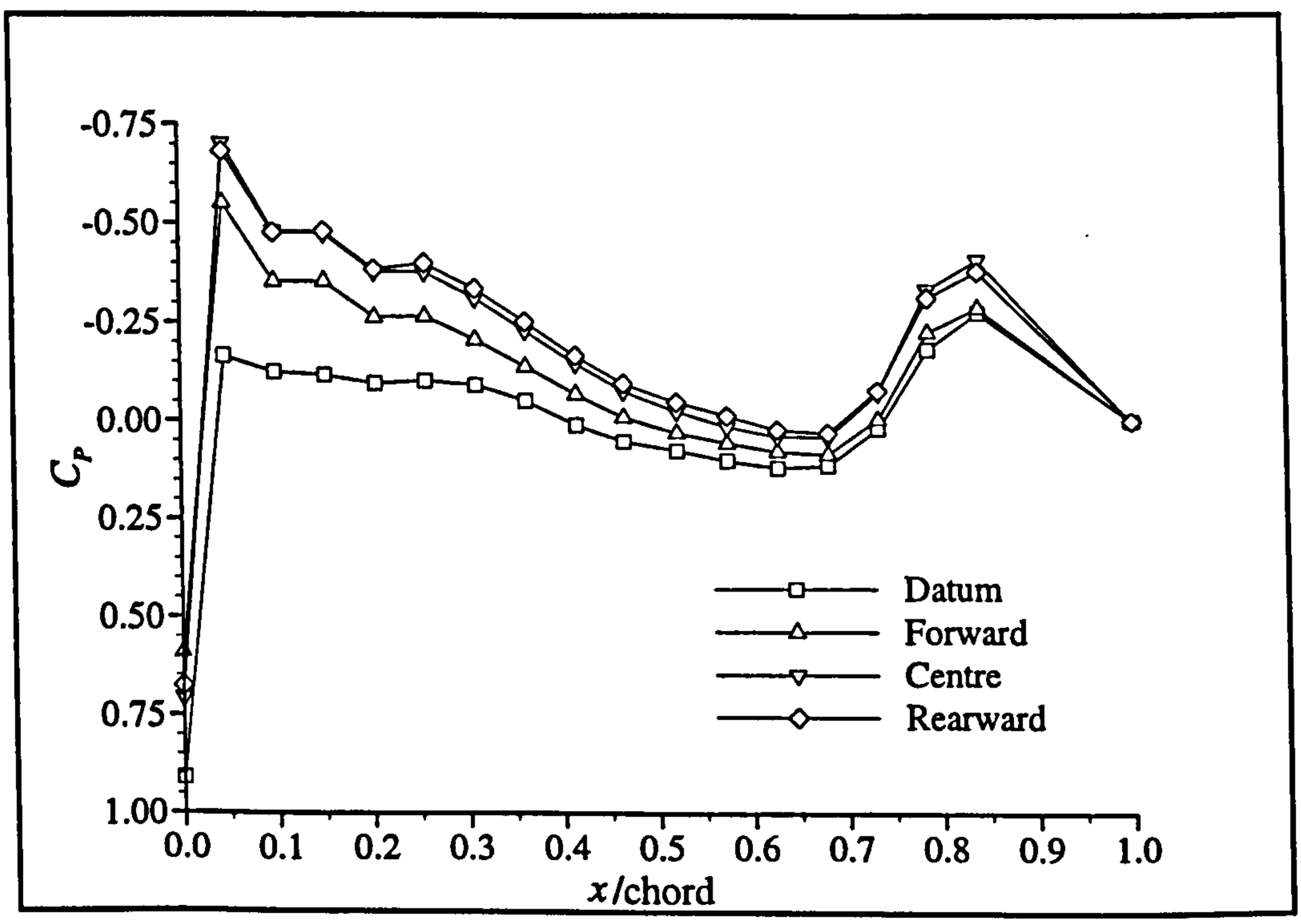

***Figure 4.28** -Wing lower surface pressure distribution, intakes faired, NPR = 4.0, q_∞ = 61.3 Pa (Phase 2a data).*

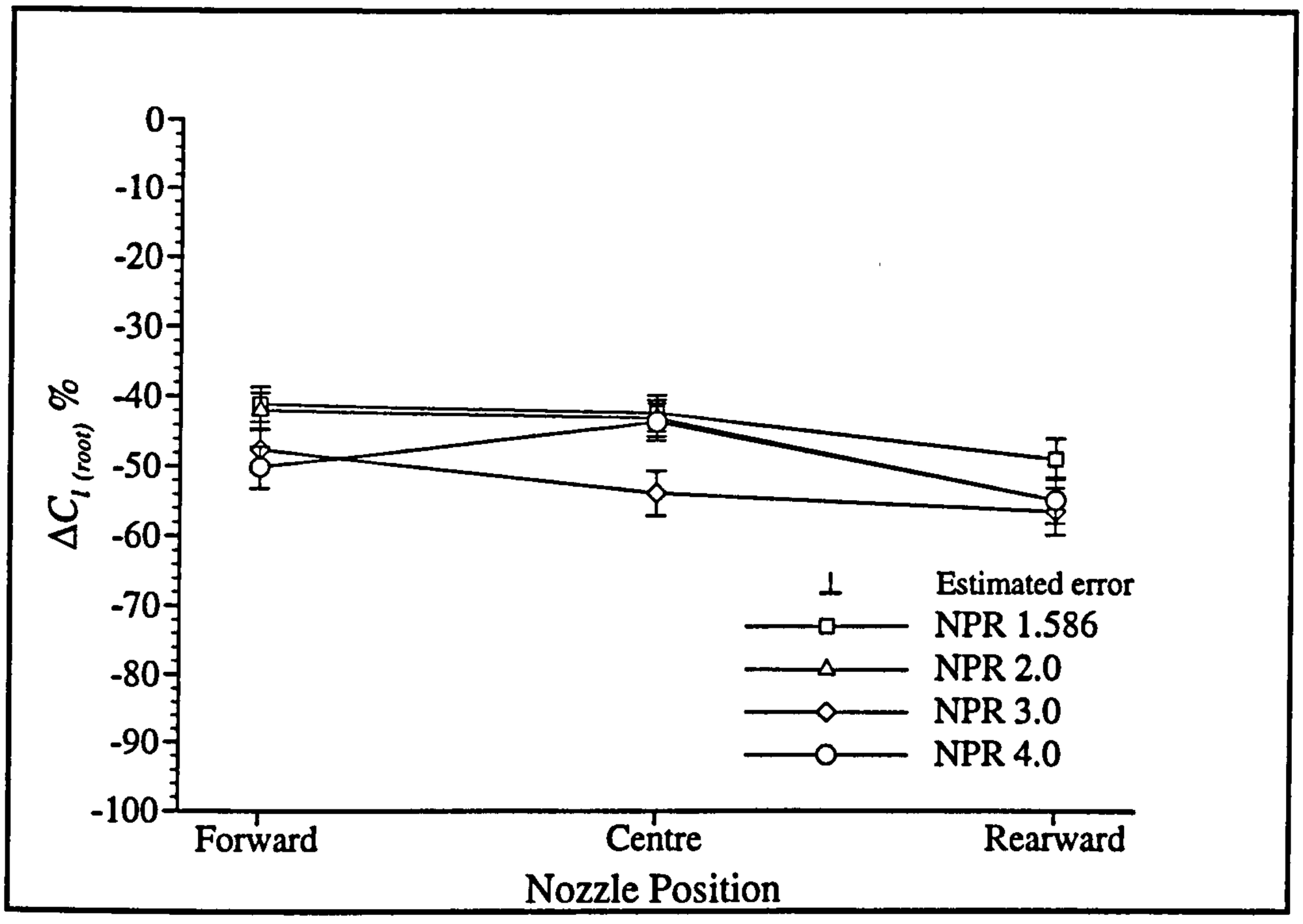

***Figure 4.29** - Variation in $C_{l\,(root)}$ with nozzle position for four different NPRs, intakes faired, q_∞ = 61.3 Pa (Phase 2a data).*

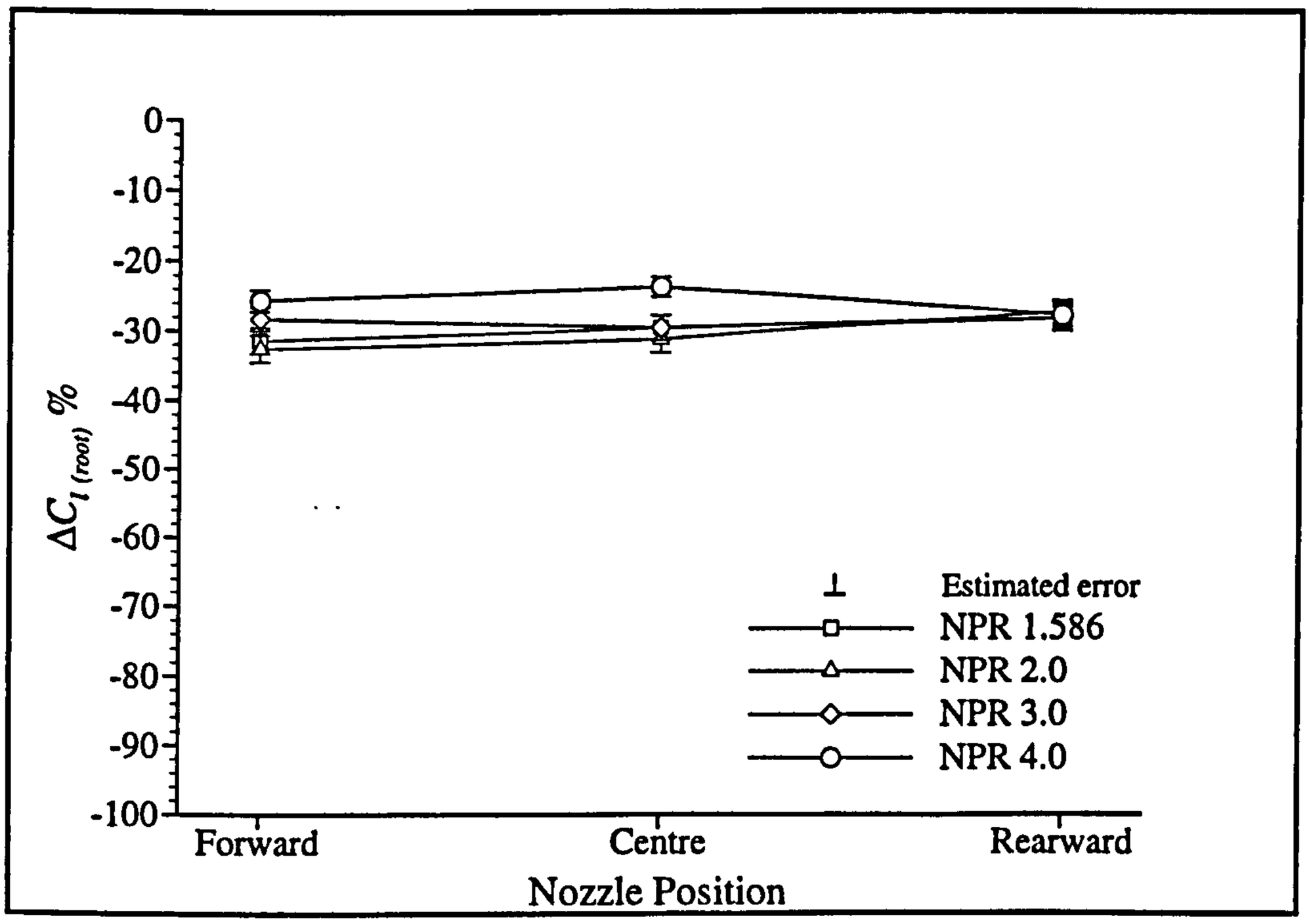

***Figure 4.30** - Variation in $C_{l\,(root)}$ with nozzle position for four different NPRs, intakes faired, q_∞ = 245 Pa (Phase 2a data).*

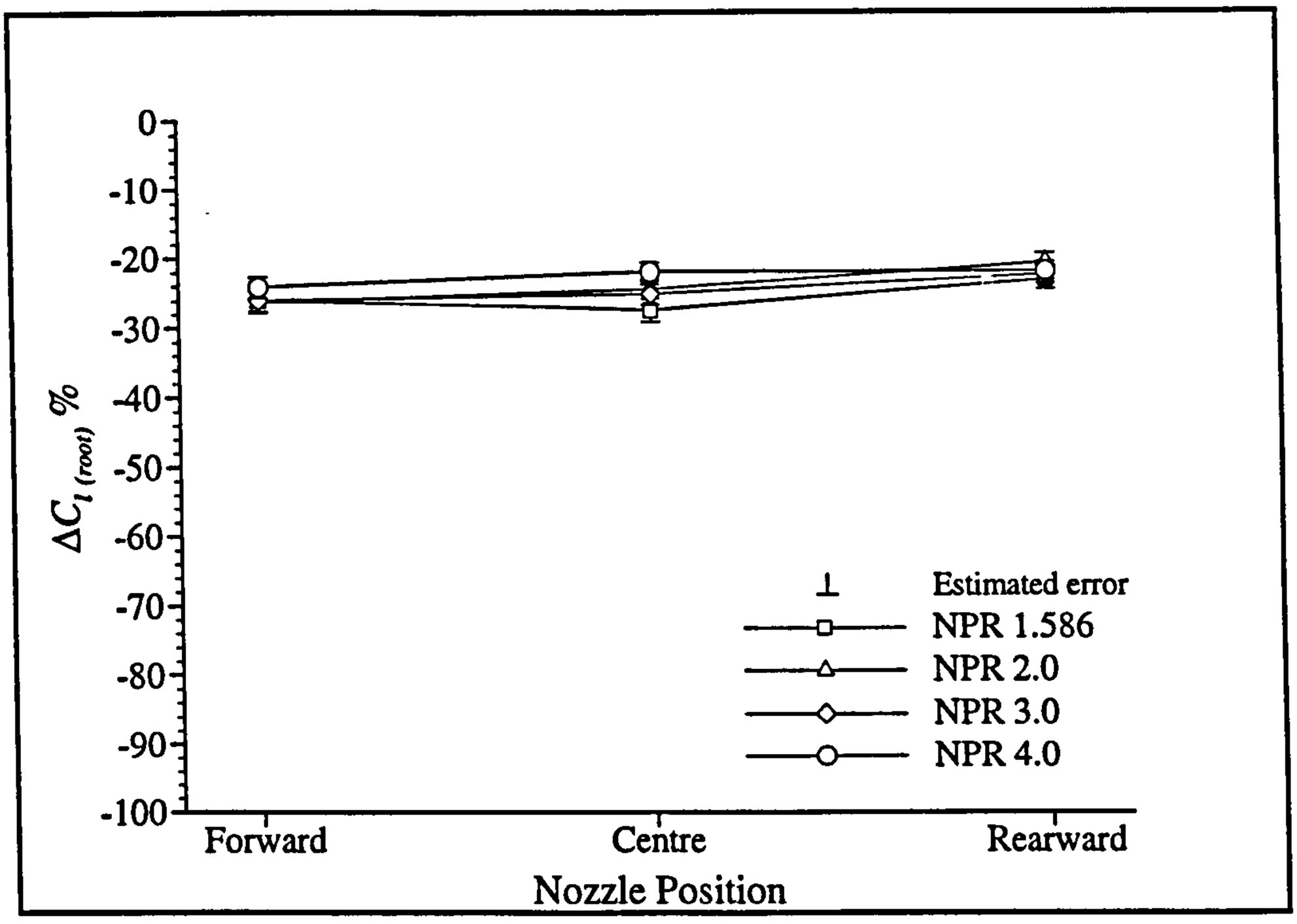

***Figure 4.31** - Variation in $C_{l\,(root)}$ with nozzle position for four different NPRs, intakes faired, q_∞ = 551 Pa (Phase 2a data).*

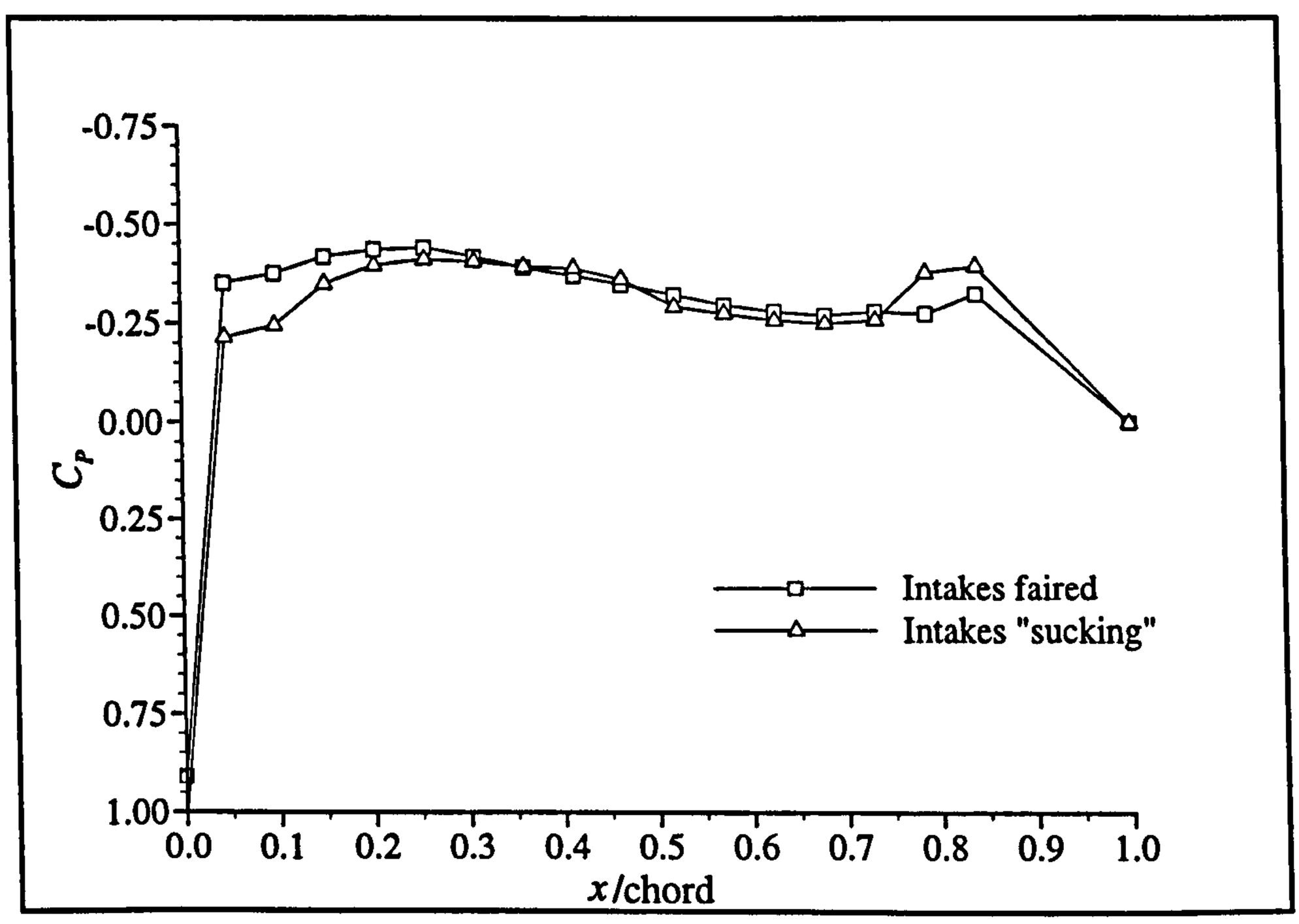

***Figure 4.32** - Wing upper surface pressure distribution, jet off, q_∞ = 61.3 Pa (Phase 2 data).*

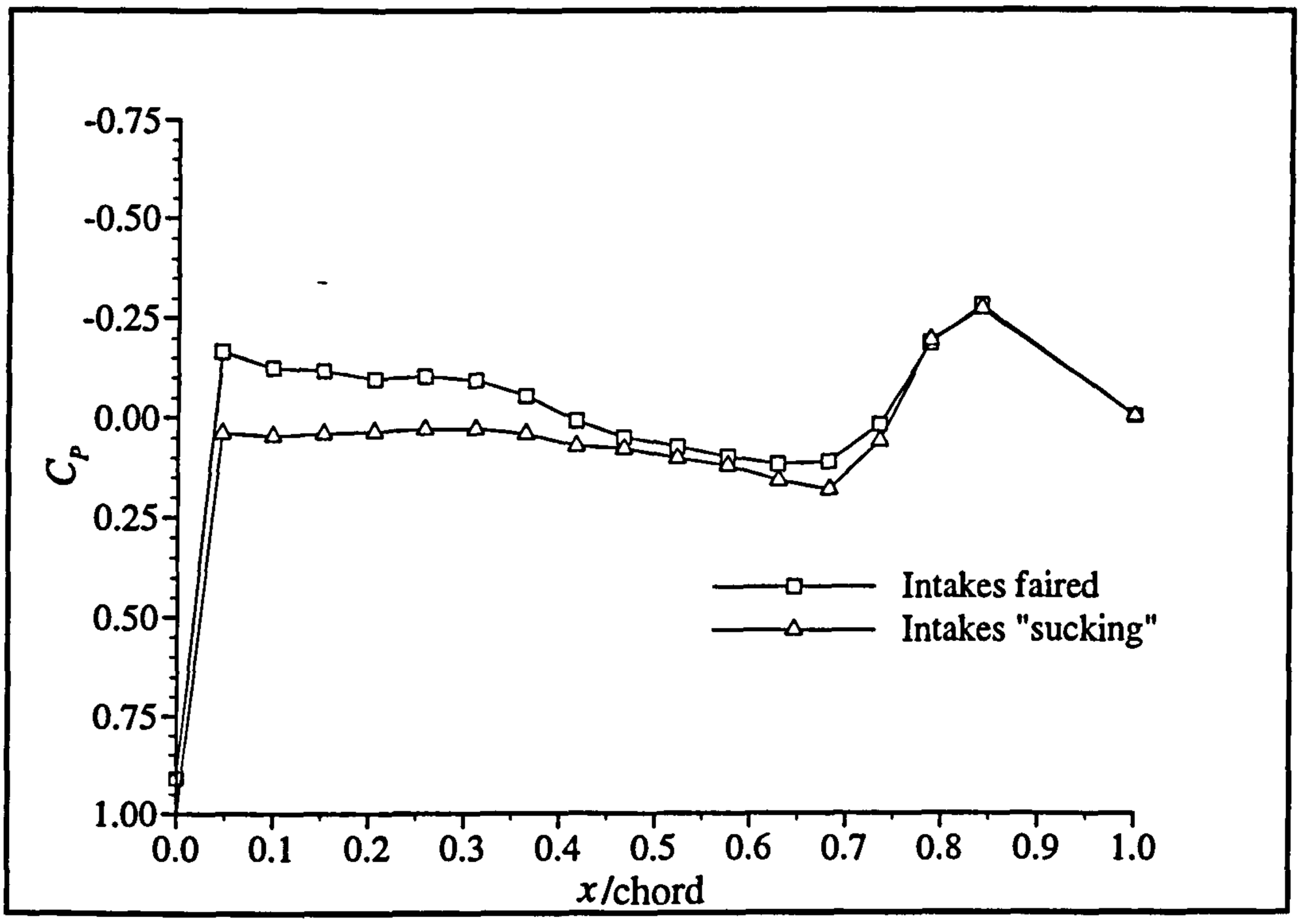

***Figure 4.33** - Wing lower surface pressure distribution, jet off, q_∞ = 61.3 Pa, (Phase 2 data).*

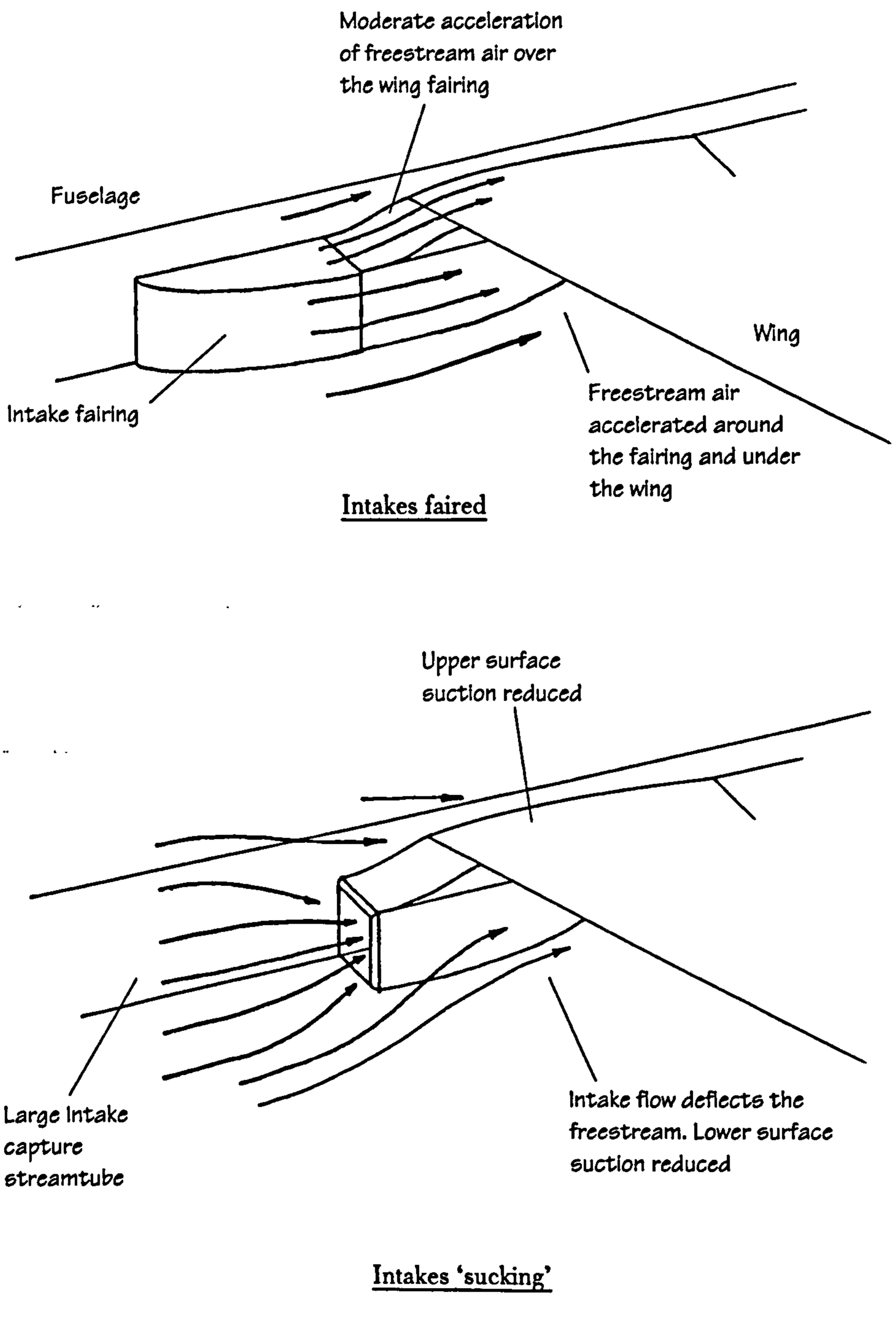

***Figure 4.34** - Sketch of the observed intake/wing interference effects.*

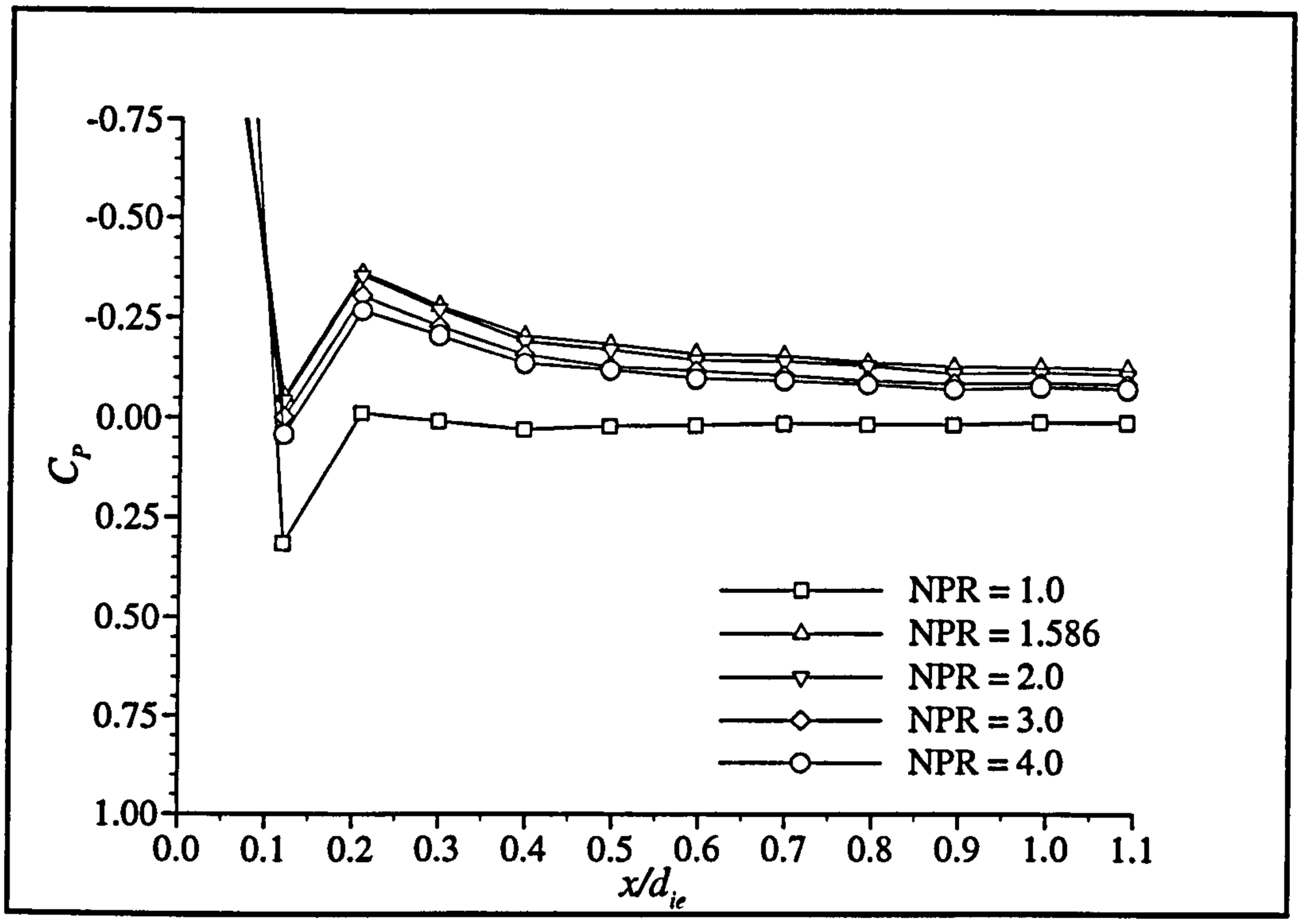

***Figure 4.35** - Intake lower outer surface pressure distribution, intakes 'sucking', forward nozzle position, q_∞ = 551 Pa (Phase 2a data).*

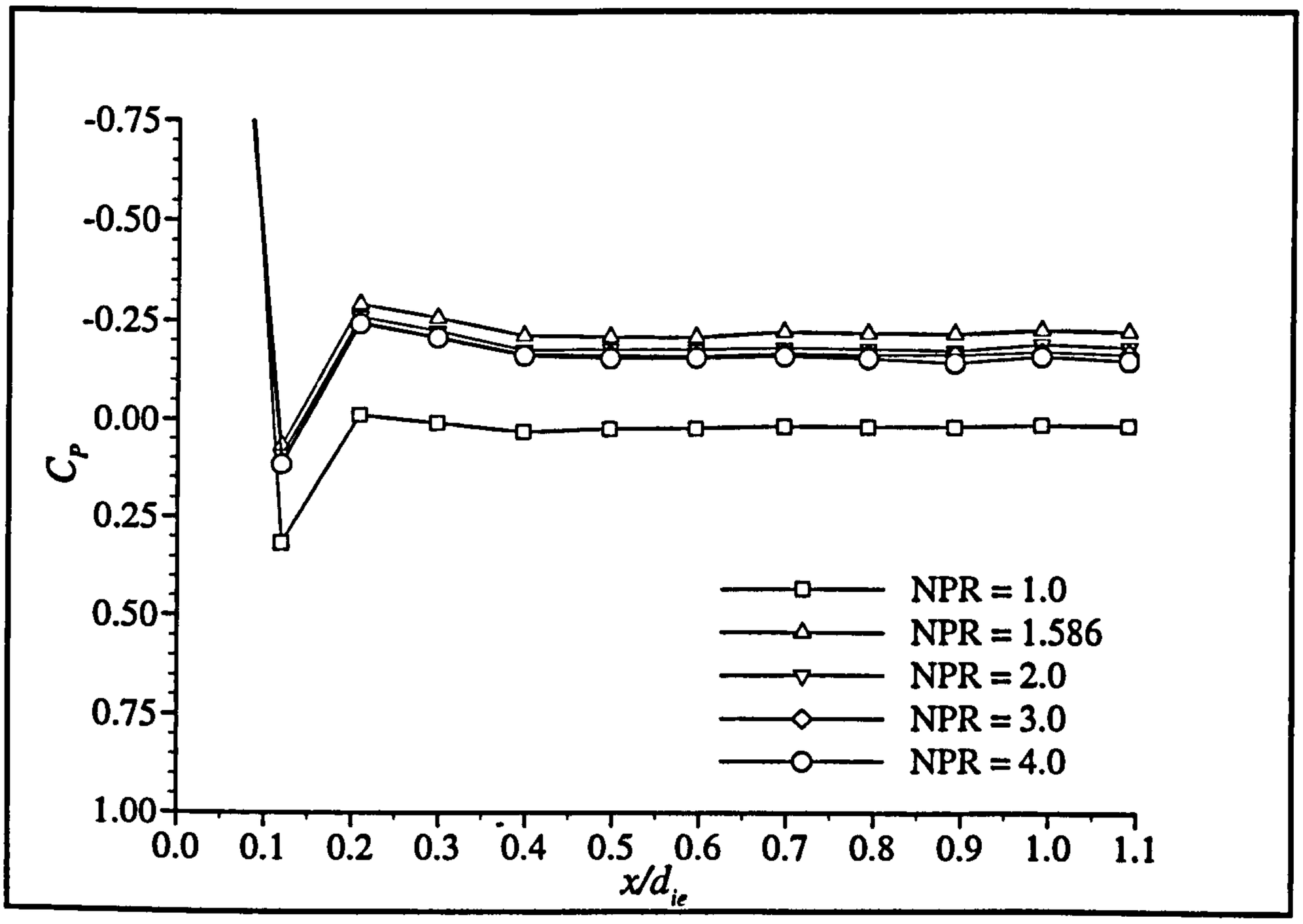

***Figure 4.36** - Intake lower outer surface pressure distribution, intakes 'sucking', centre nozzle position, q_∞ = 551 Pa (Phase 2a data).*

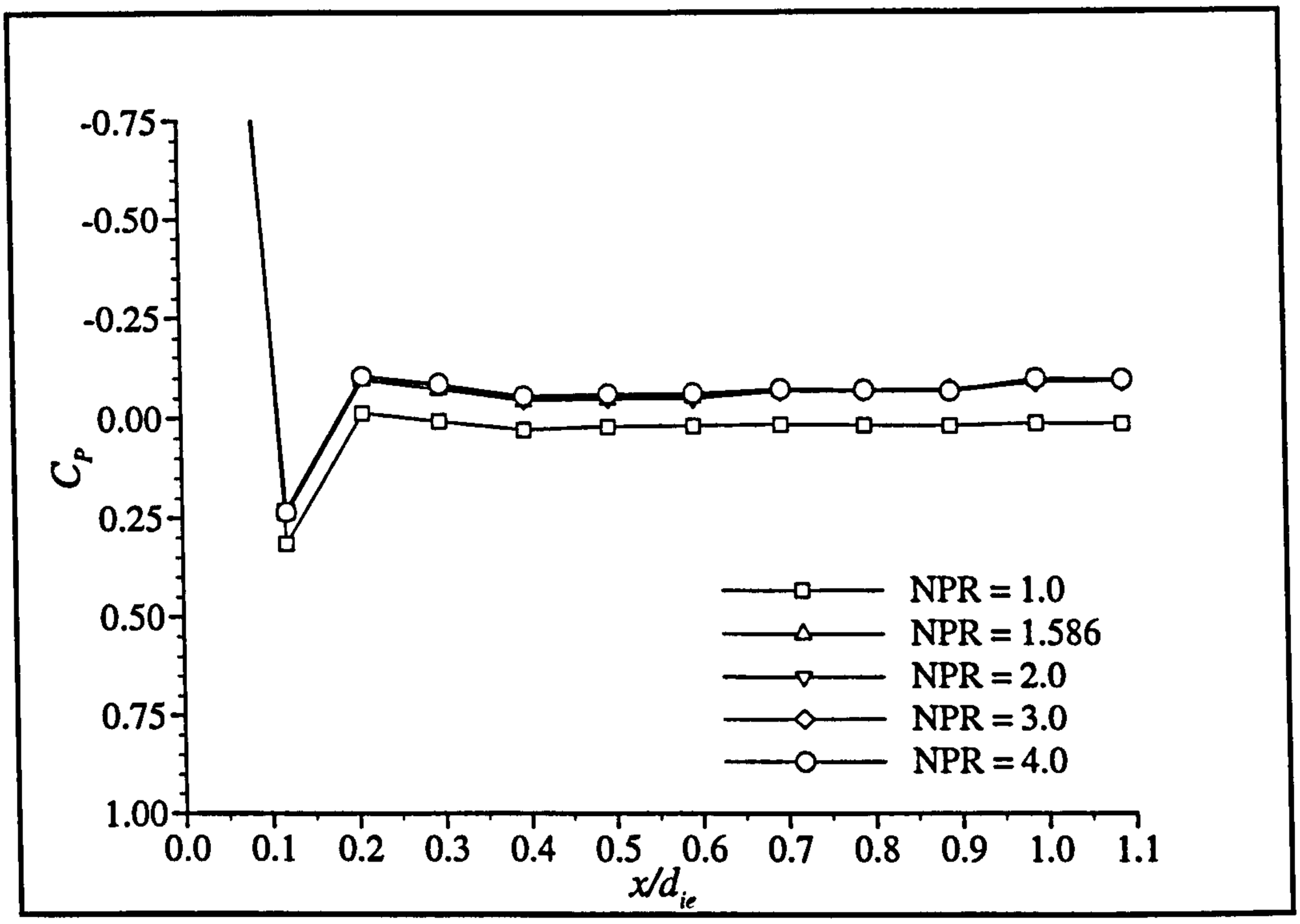

***Figure 4.37** - Intake lower outer surface pressure distribution, intakes 'sucking', rearward nozzle position, q_∞ = 551 Pa (Phase 2a data).*

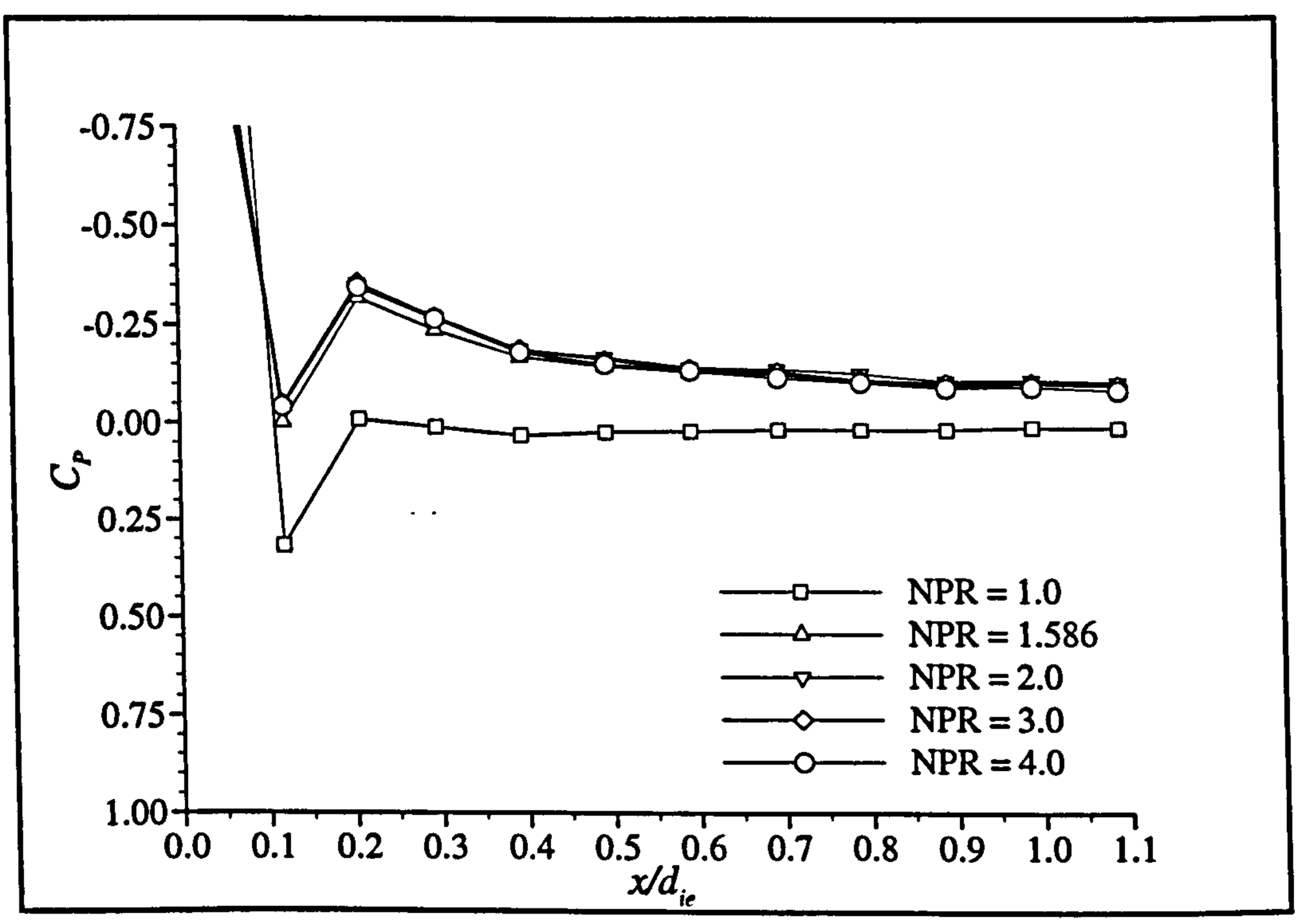

***Figure 4.38** - Intake lower outer surface pressure distribution, intakes 'sucking', forward nozzle position, q_∞ = 551 Pa (Phase 2b data).*

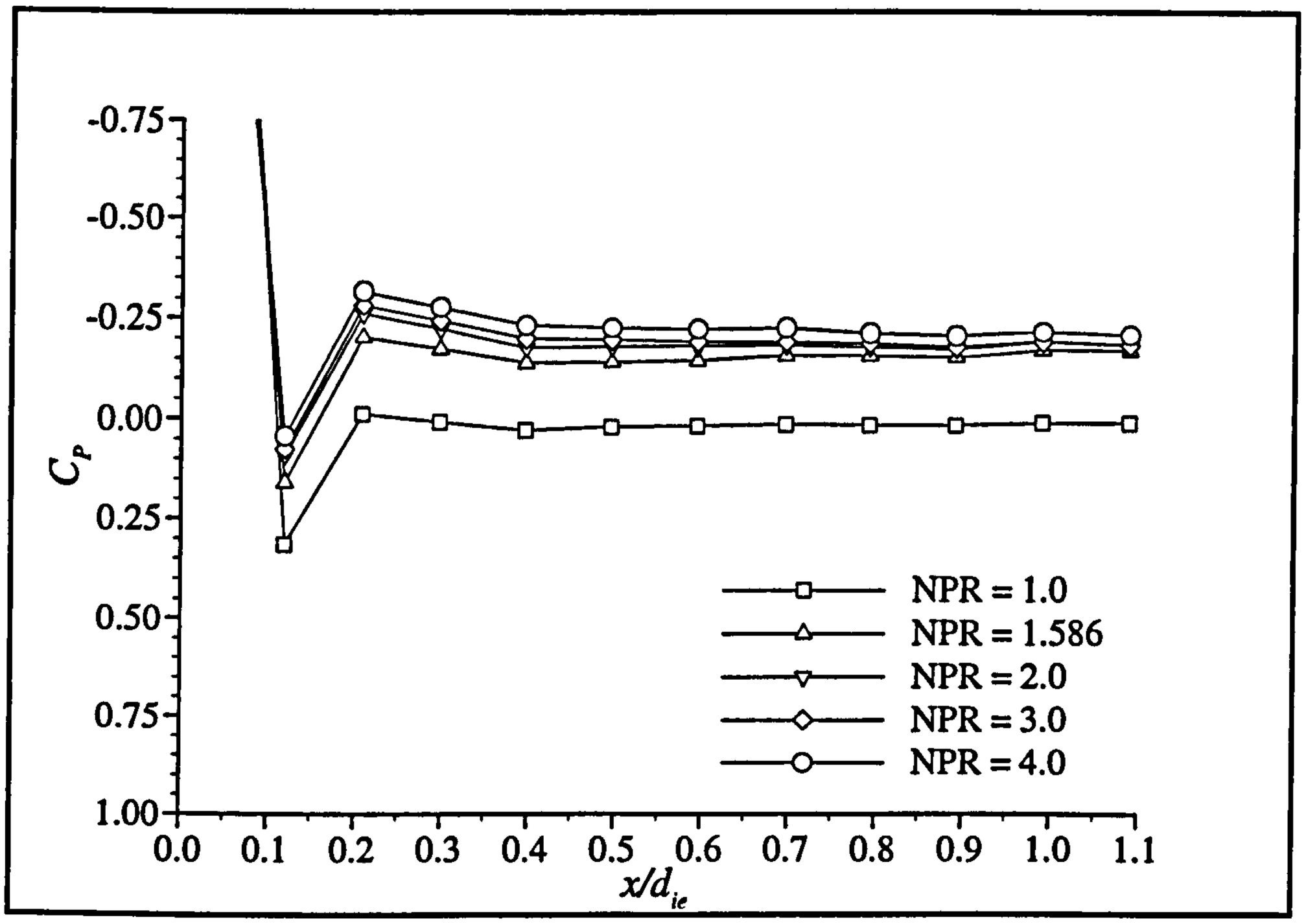

***Figure 4.39** - Intake lower outer surface pressure distribution, intakes 'sucking', centre nozzle position, q_∞ = 551 Pa (Phase 2b data).*

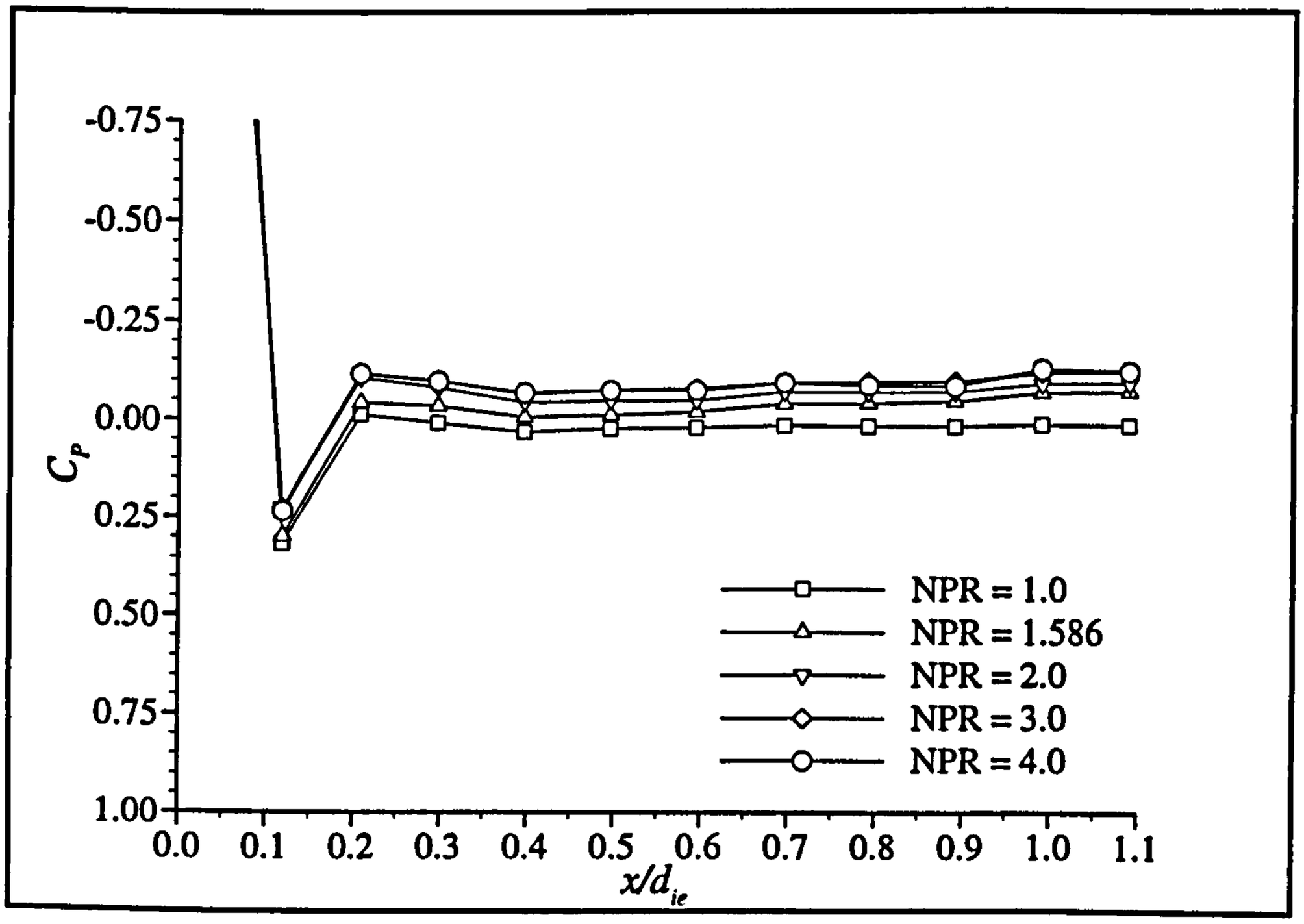

***Figure 4.40** - Intake lower outer surface pressure distribution, intakes 'sucking', rearward nozzle position, q_∞ = 551 Pa (Phase 2b data).*

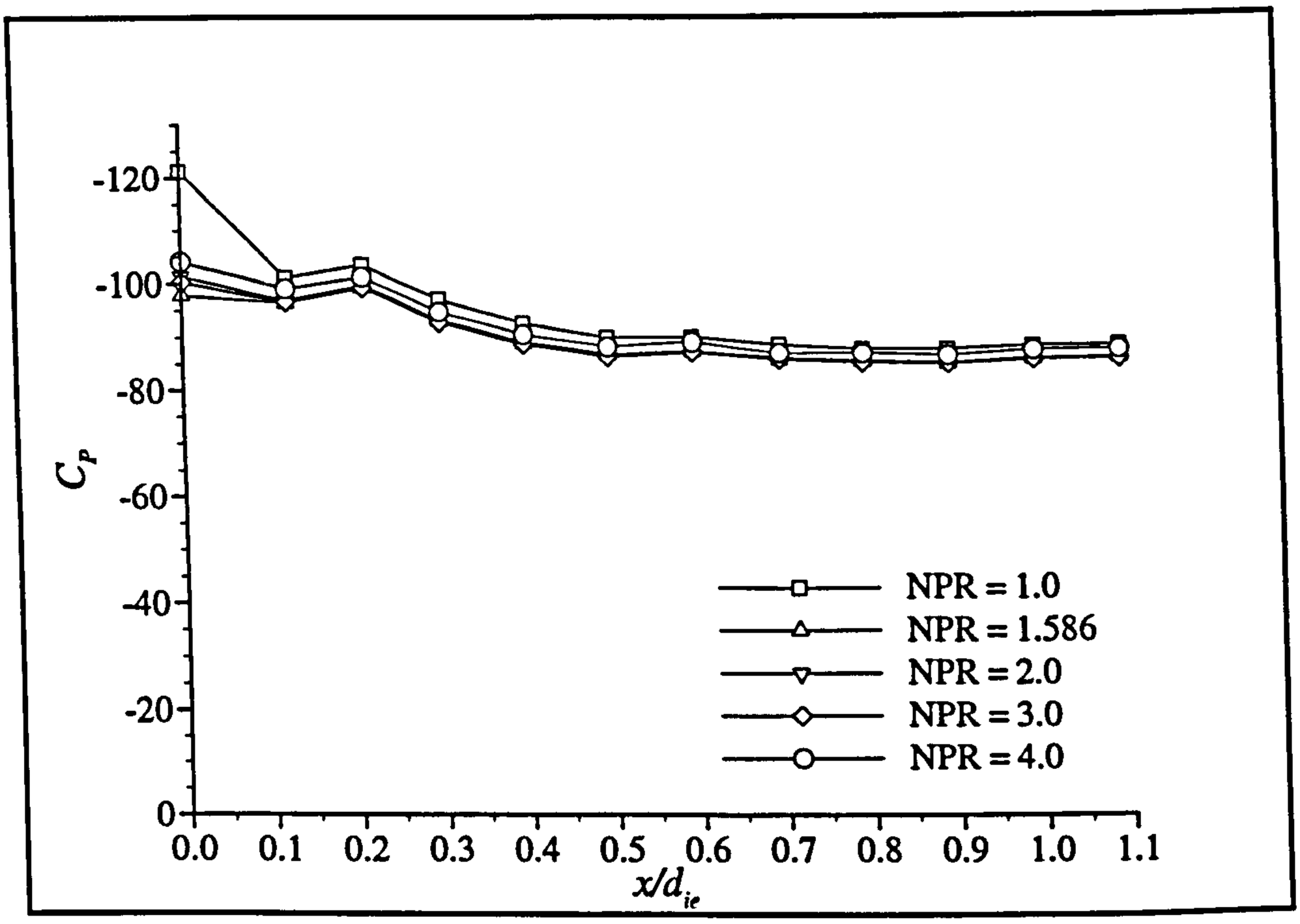

***Figure 4.41** - Intake lower inner surface pressure distribution, intakes 'sucking', forward nozzle position, q_∞ = 61.3 Pa (Phase 2a data).*

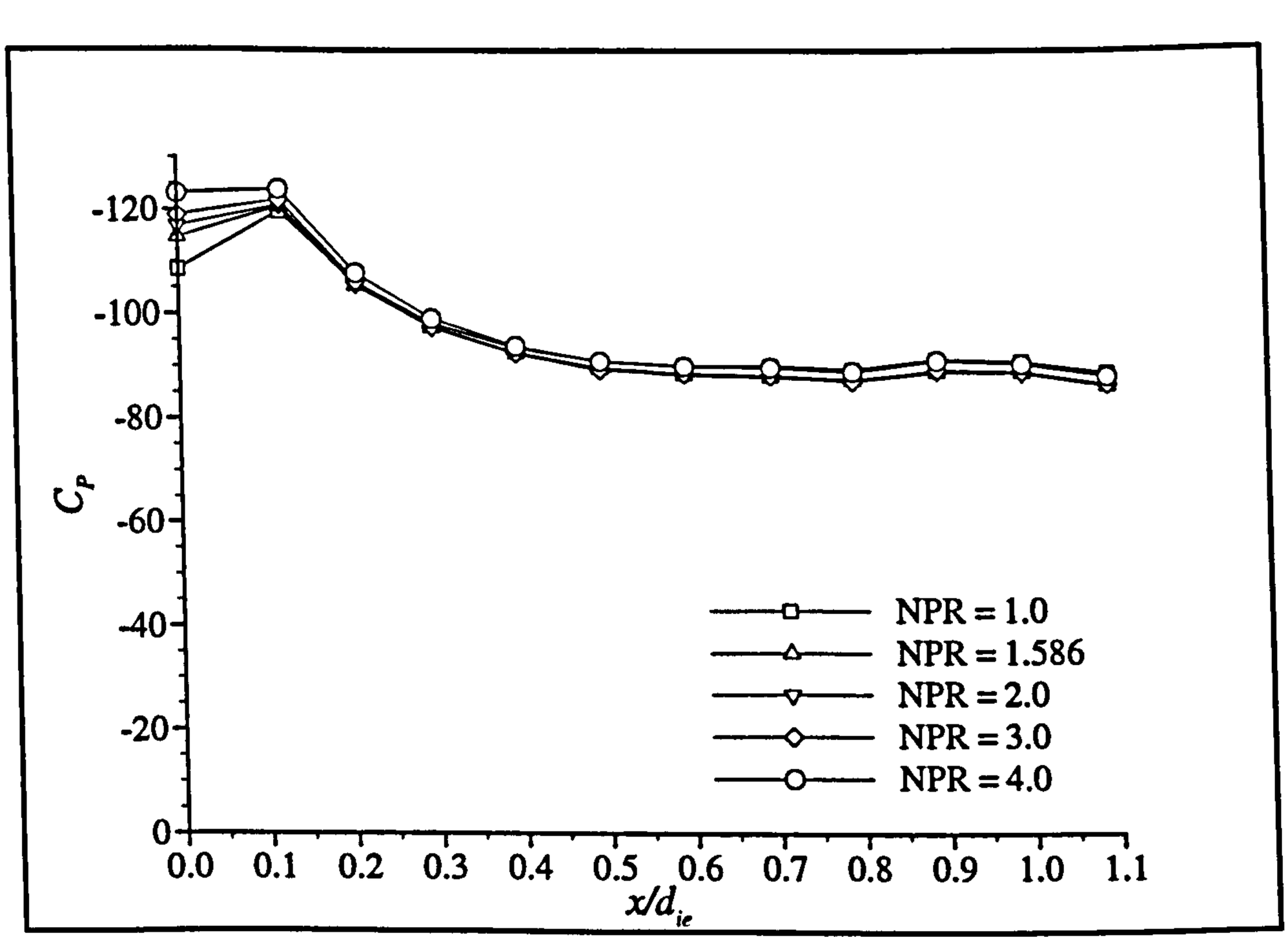

***Figure 4.42** - Intake upper inner surface pressure distribution, intakes 'sucking', forward nozzle position, q_∞ = 61.3 Pa (Phase 2a data).*

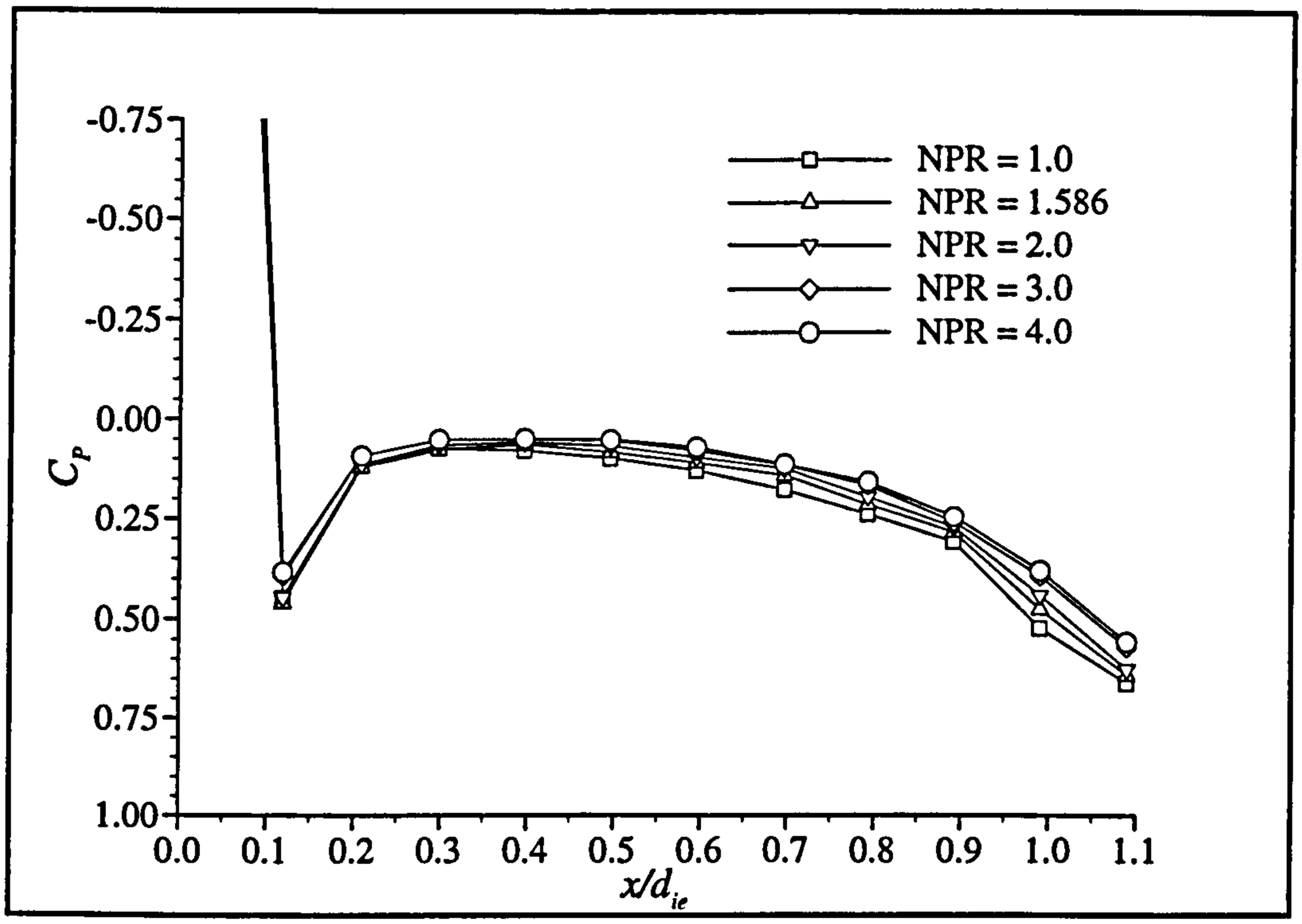

***Figure 4.43** - Intake upper outer surface pressure distribution, intakes 'sucking', forward nozzle position, q_∞ = 551 Pa (Phase 2a data).*

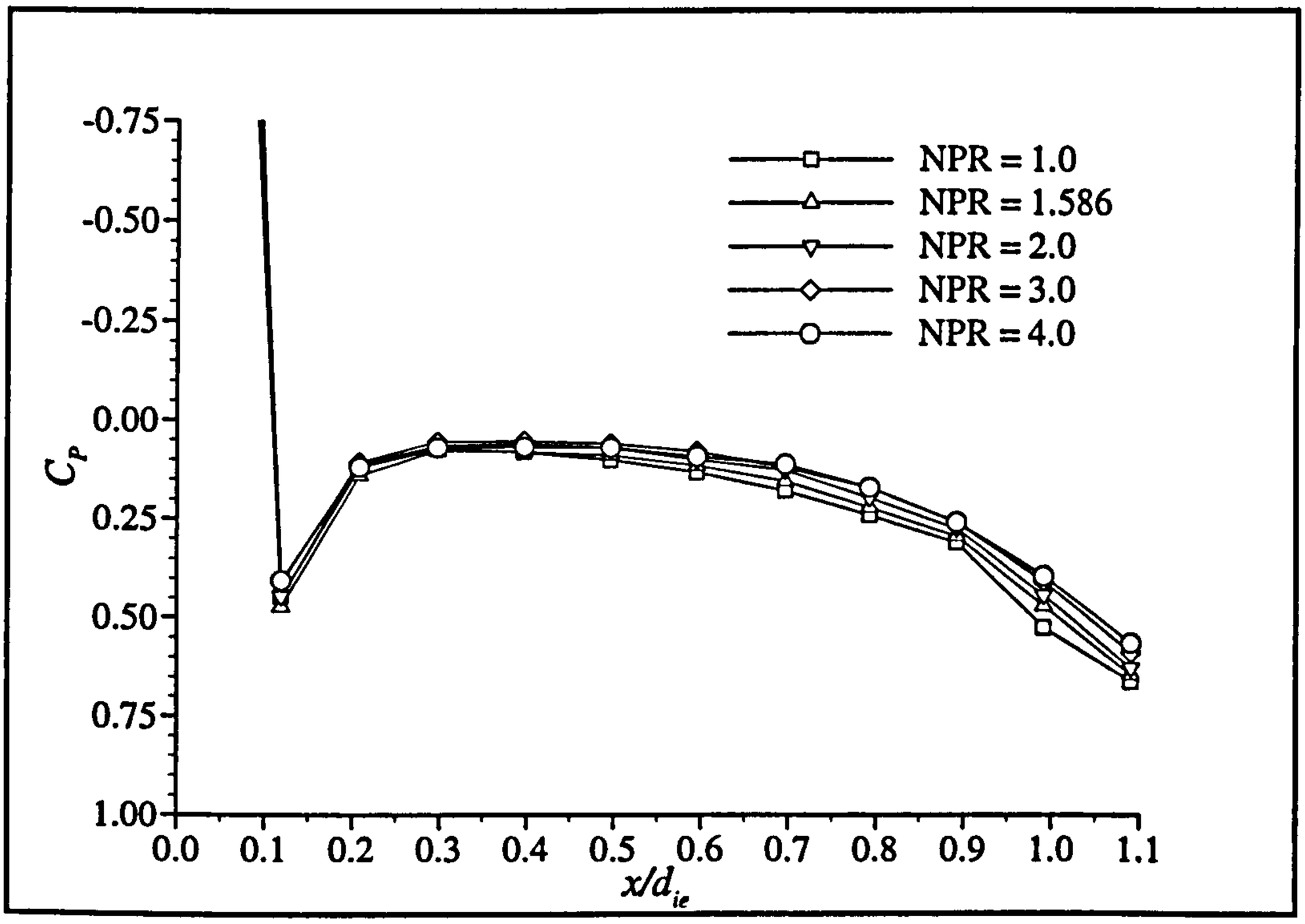

***Figure 4.44** - Intake upper outer surface pressure distribution, intakes 'sucking', forward nozzle position, q_∞ = 551 Pa (Phase 2b data).*

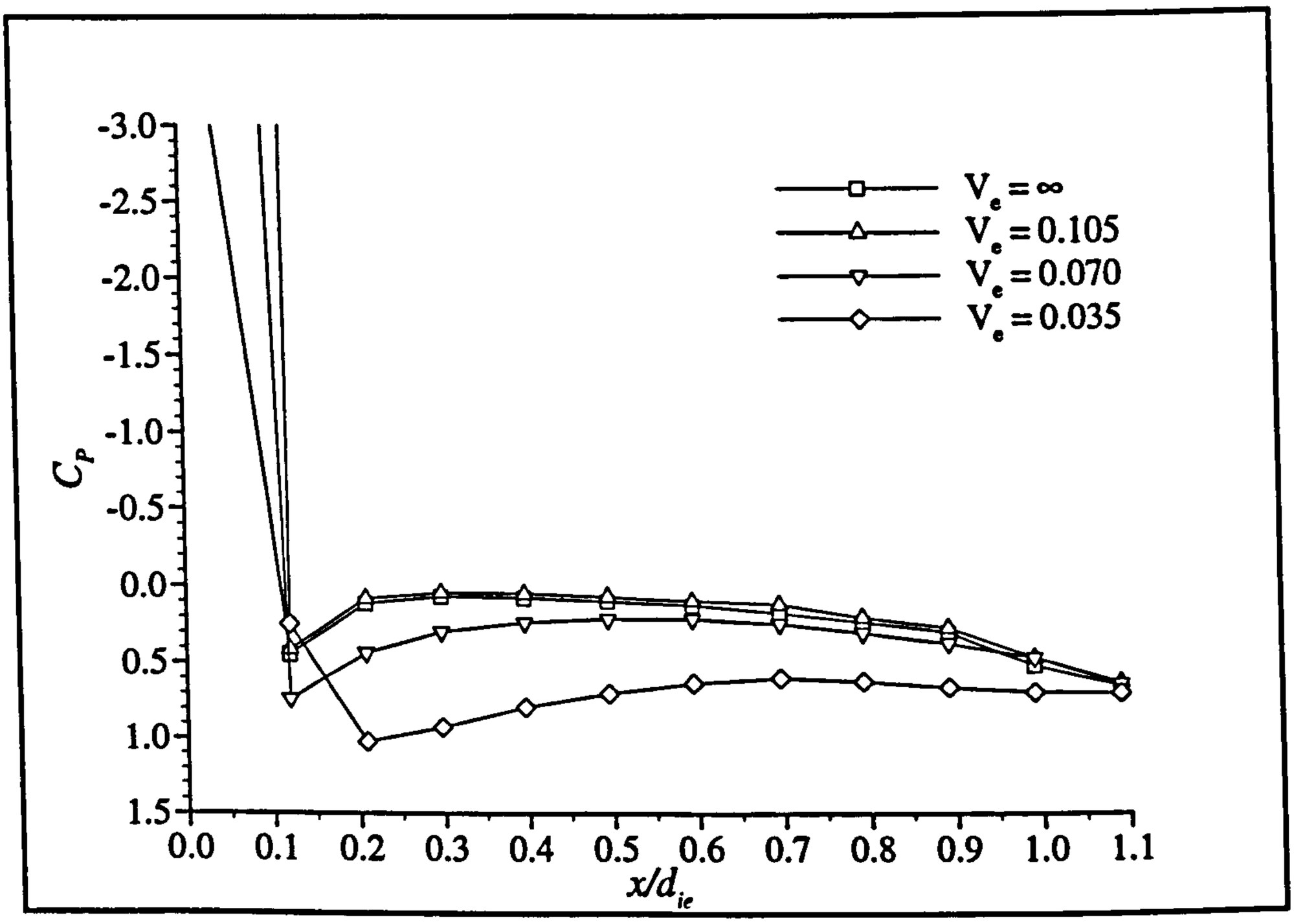

***Figure 4.45** - Intake upper outer surface pressure distribution, intakes 'sucking', rearward nozzle position, NPR = 1.586 (Phase 2a data).*

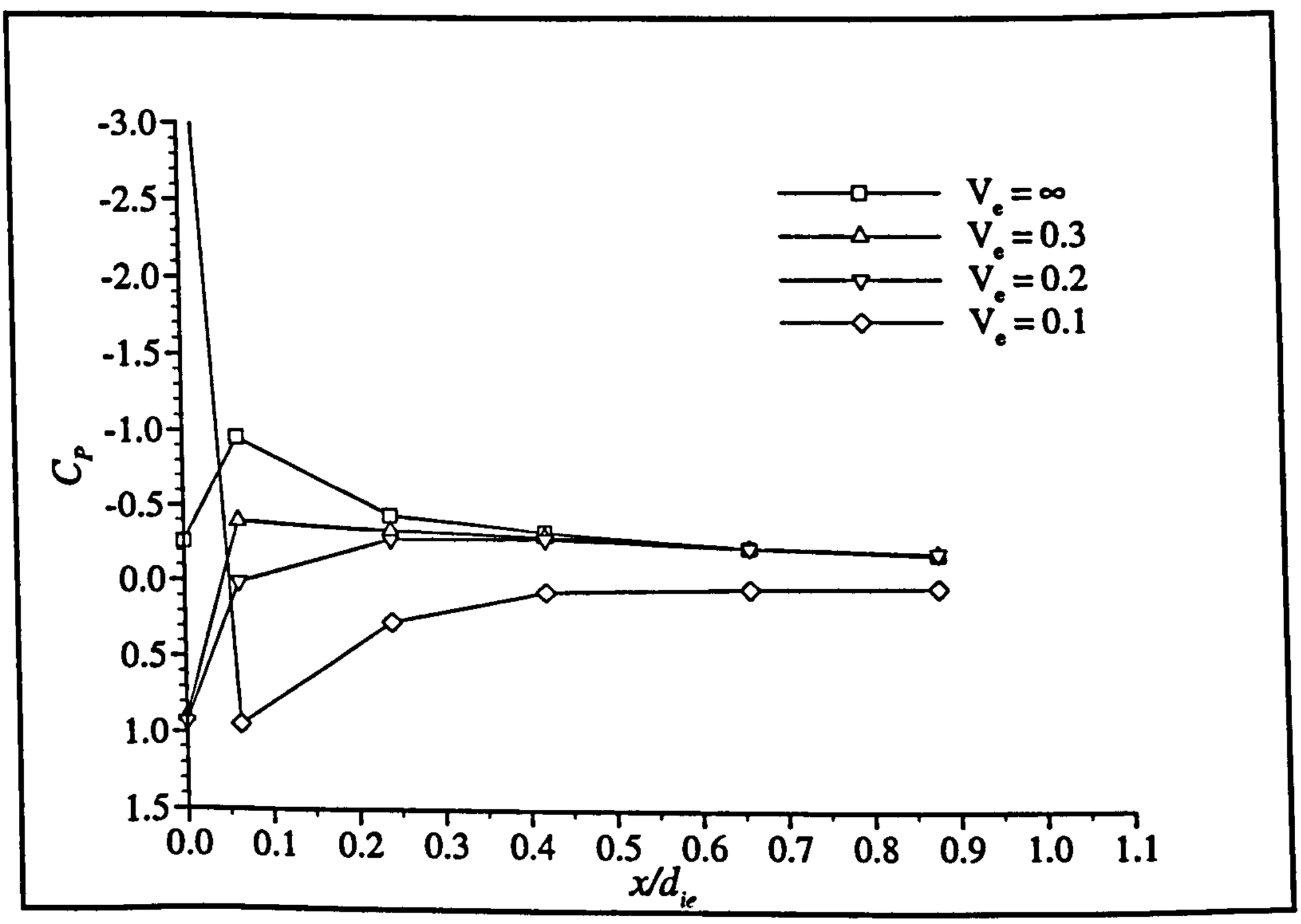

***Figure 4.46** - Intake upper outer surface pressure distribution on a V/STOL fighter (MINECK & MARGASON, 1973).*

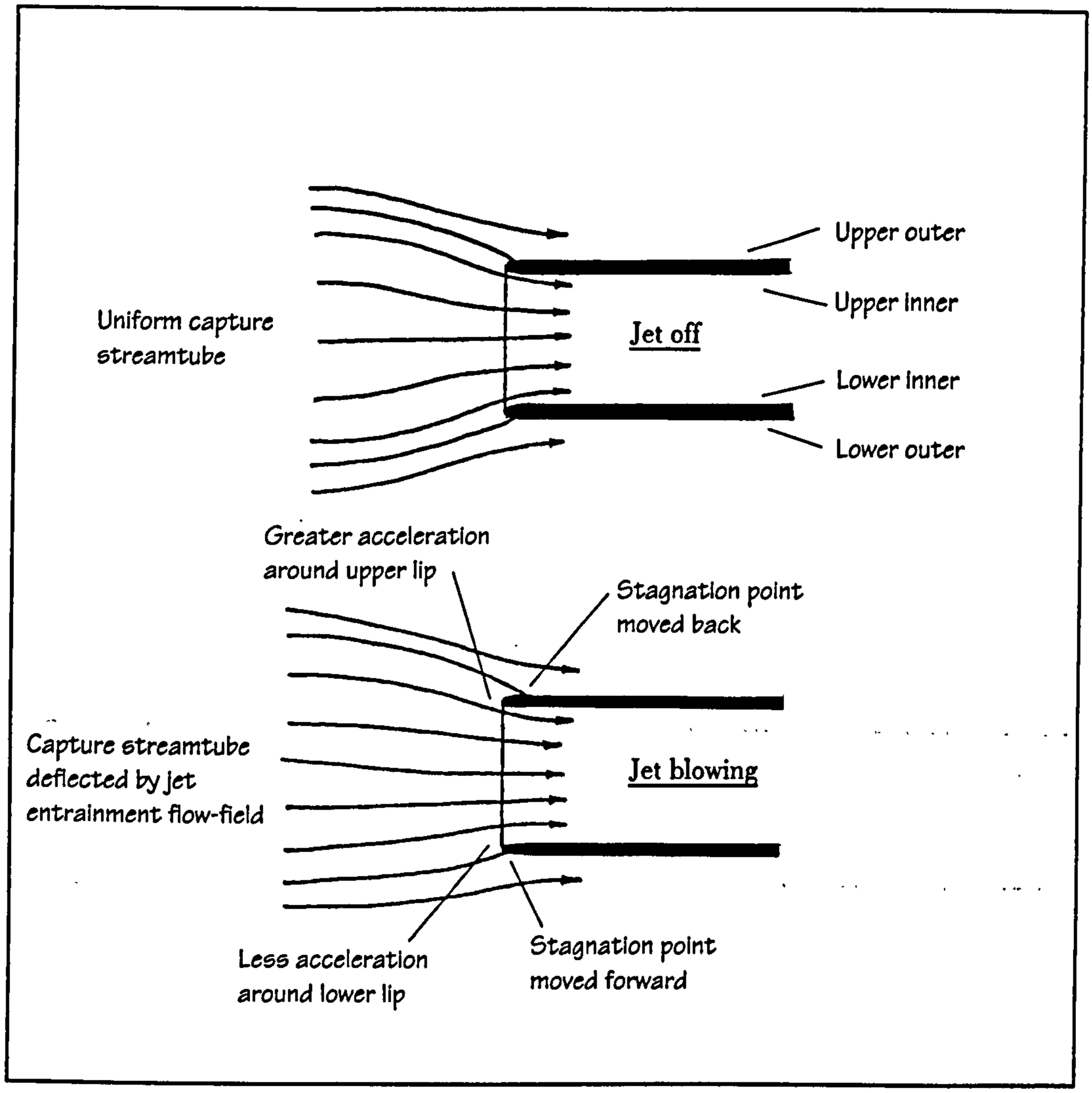

***Figure 4.47** - Sketch of the jet-induced interference effects on the intake.*

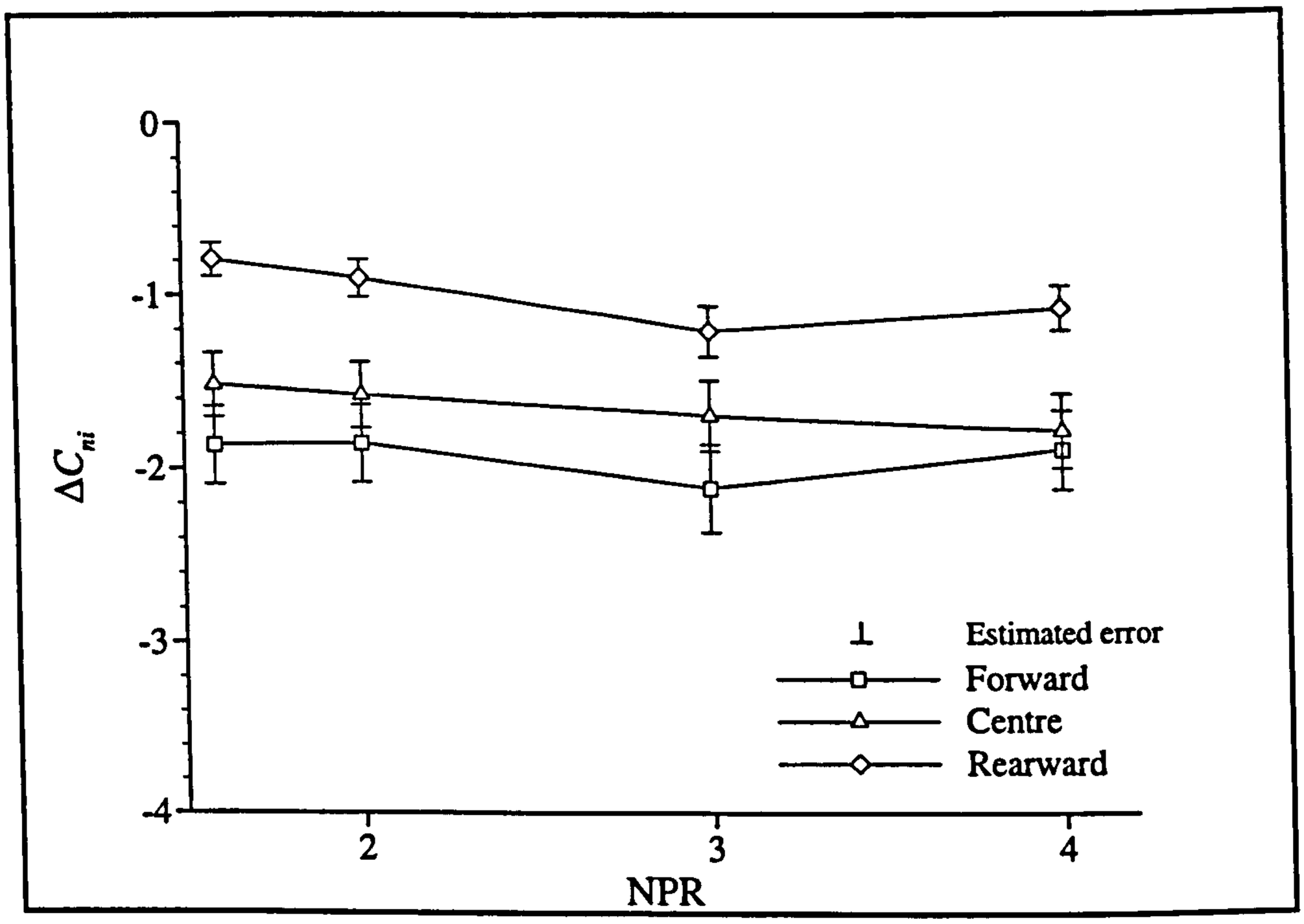

***Figure 4.48** - Variation in C_{ni} with NPR for three nozzle positions, q_∞ = 61.3 Pa (Phase 2a data).*

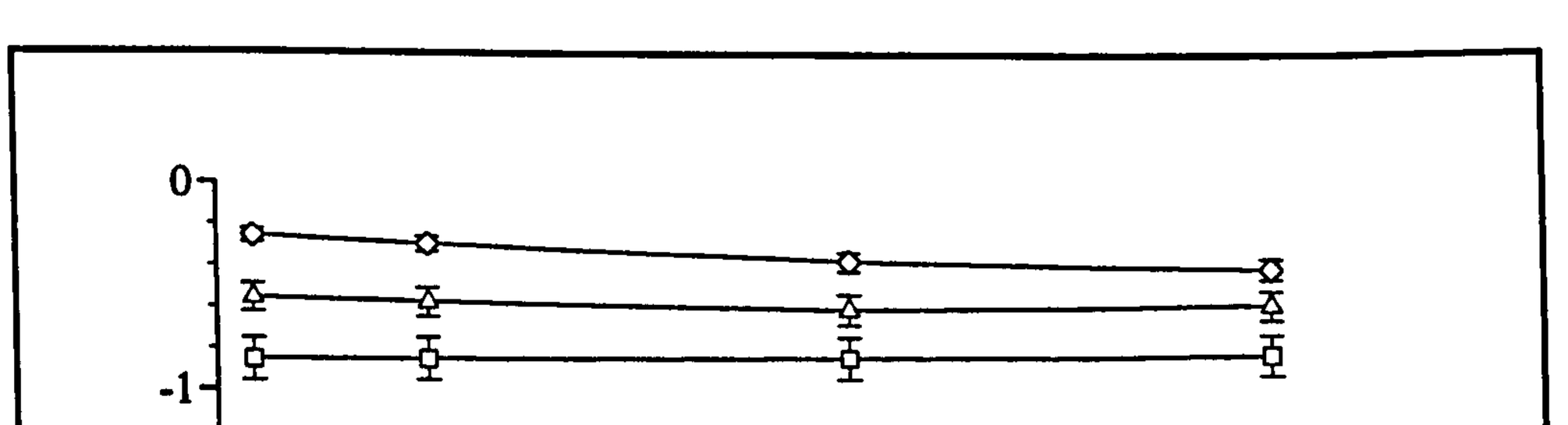

***Figure 4.49** - Variation in C_{ni} with NPR for three nozzle positions, q_∞ = 245 Pa (Phase 2a data).*

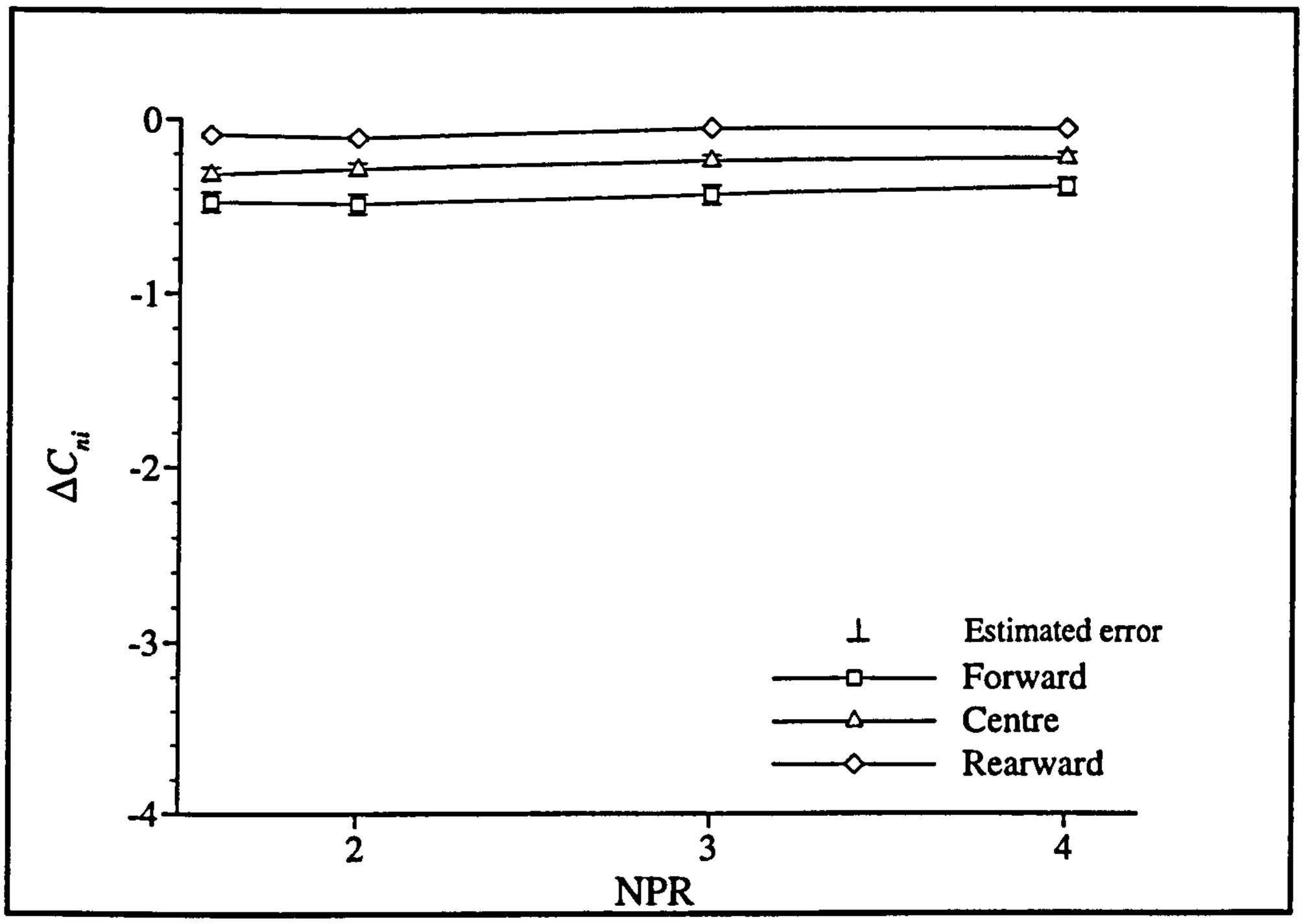

***Figure 4.50** - Variation in C_{ni} with NPR for three nozzle positions, q_∞ = 551 Pa (Phase 2a data).*

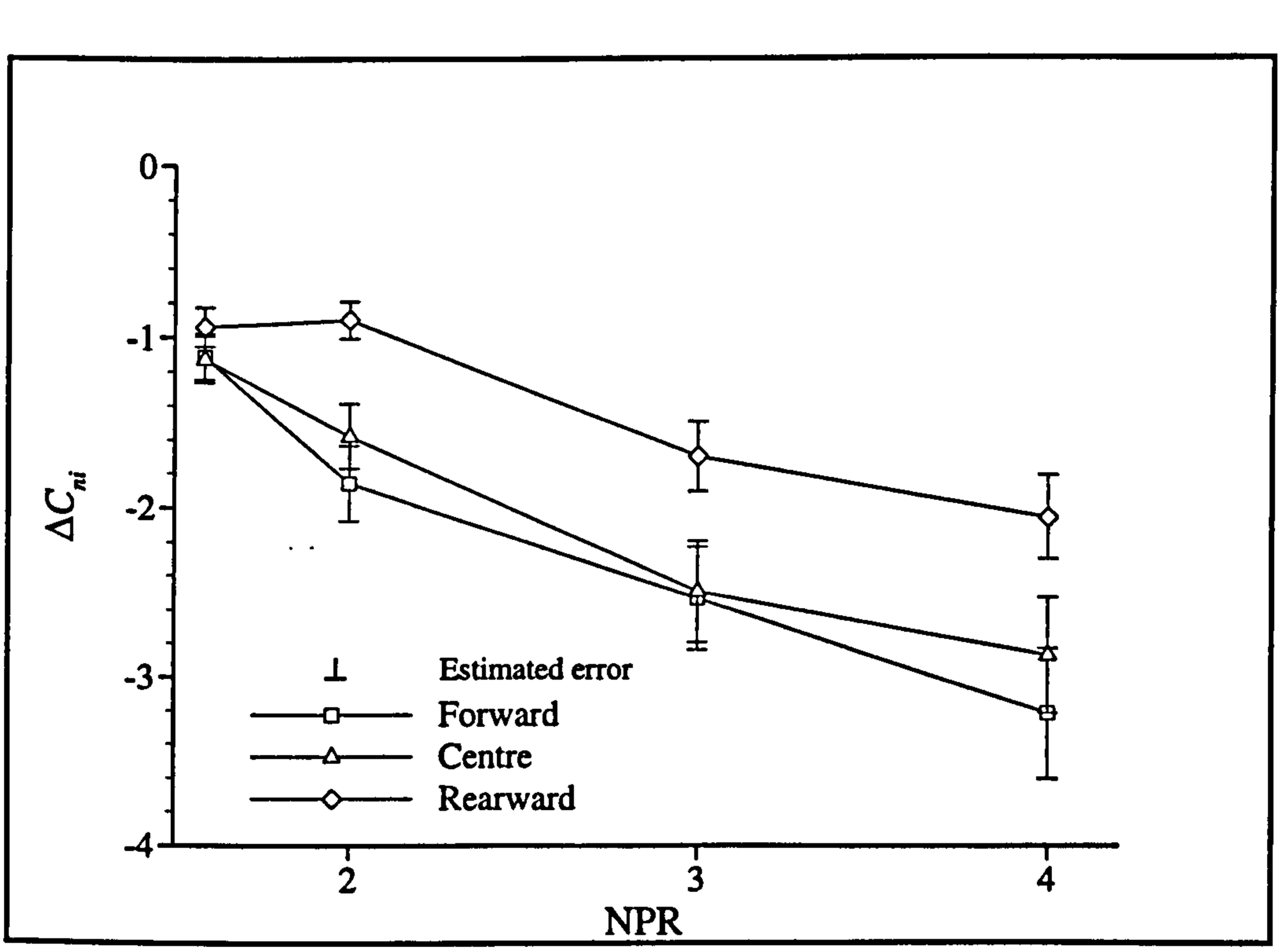

***Figure 4.51** - Variation in C_{ni} with NPR for three nozzle positions, q_∞ = 61.3 Pa (Phase 2b data).*

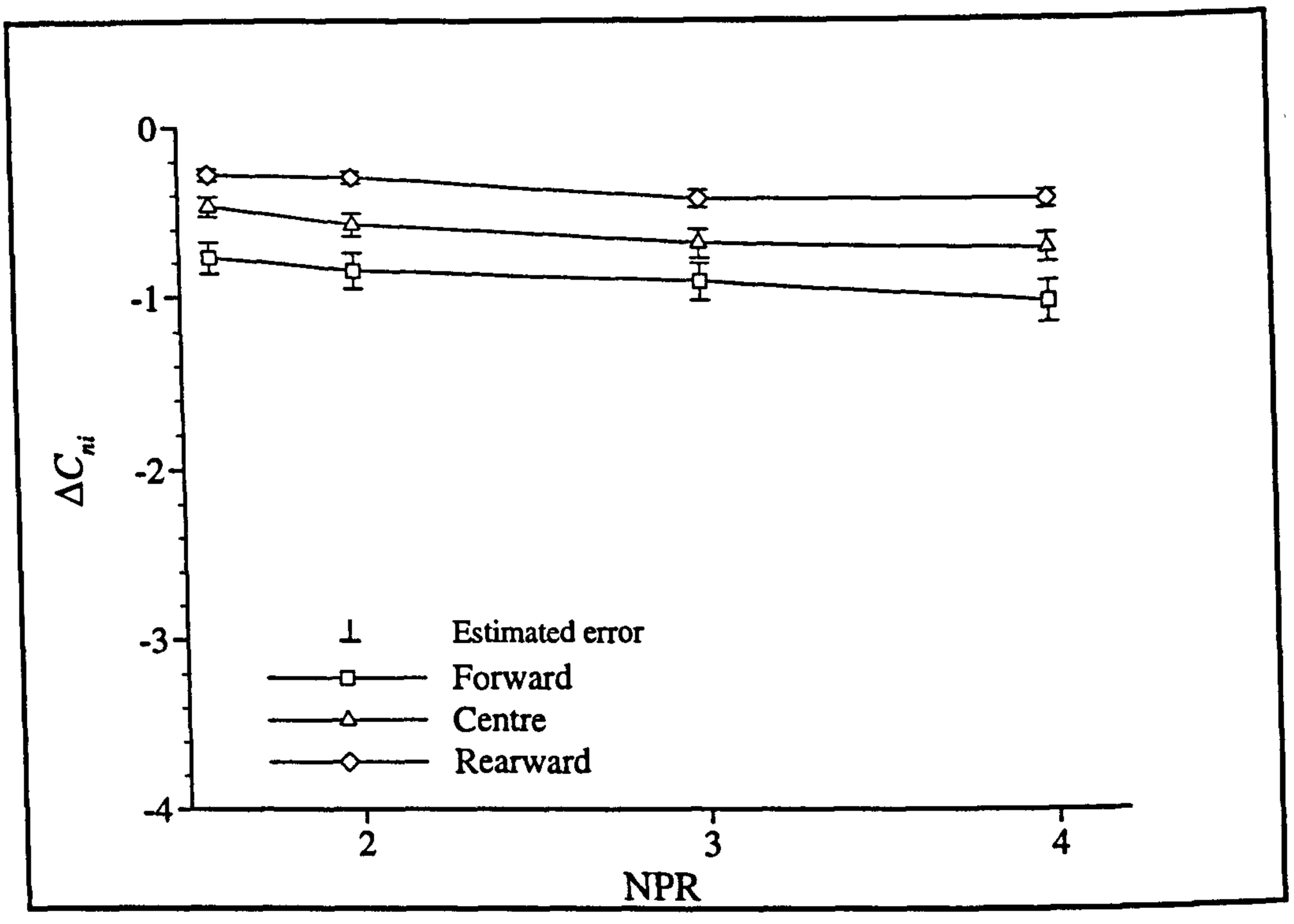

***Figure 4.52** - Variation in C_{ni} with NPR for three nozzle positions, $q_\infty = 245$ Pa (Phase 2b data).*

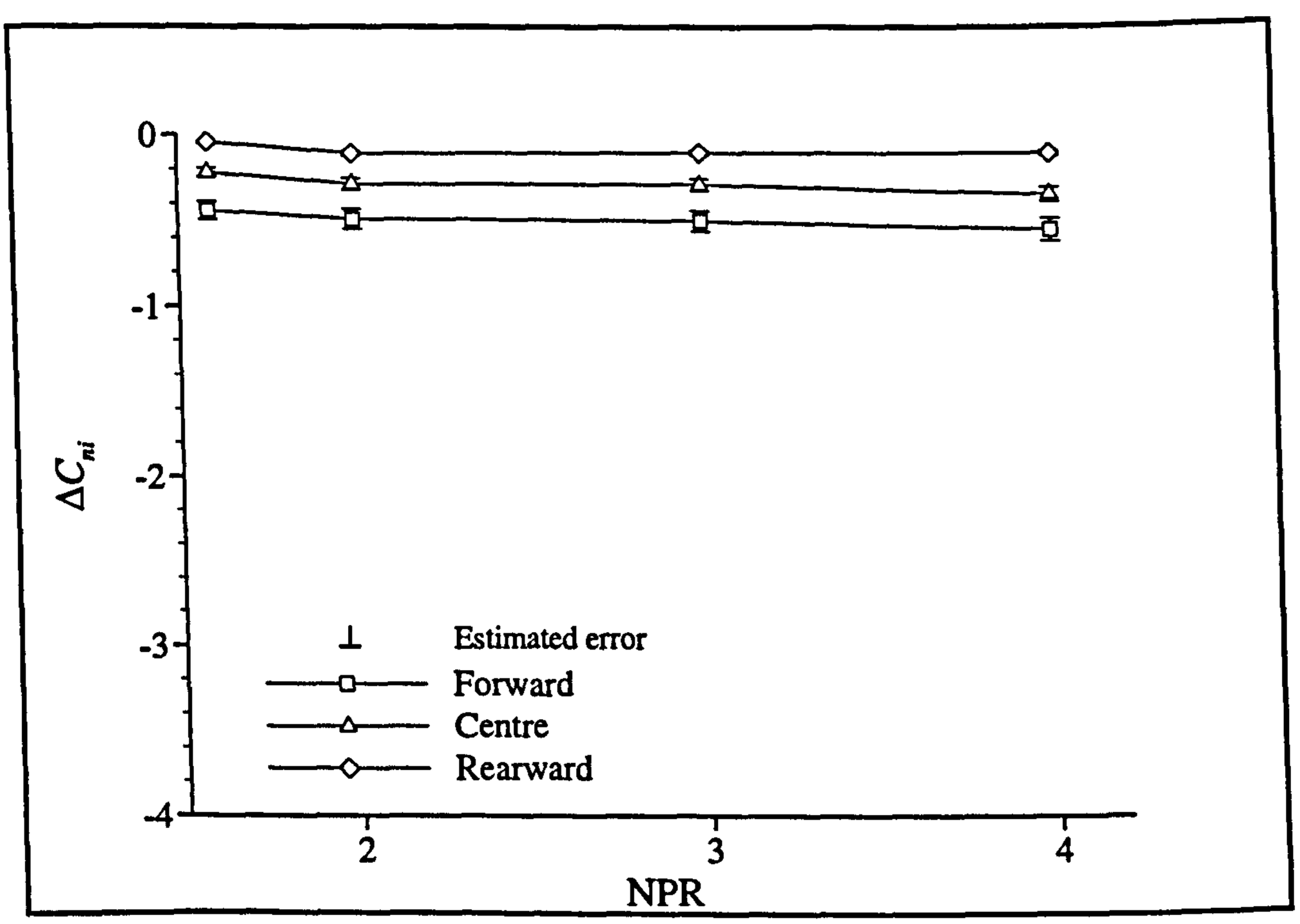

***Figure 4.53** - Variation in C_{ni} with NPR for three nozzle positions, $q_\infty = 551$ Pa (Phase 2a data).*

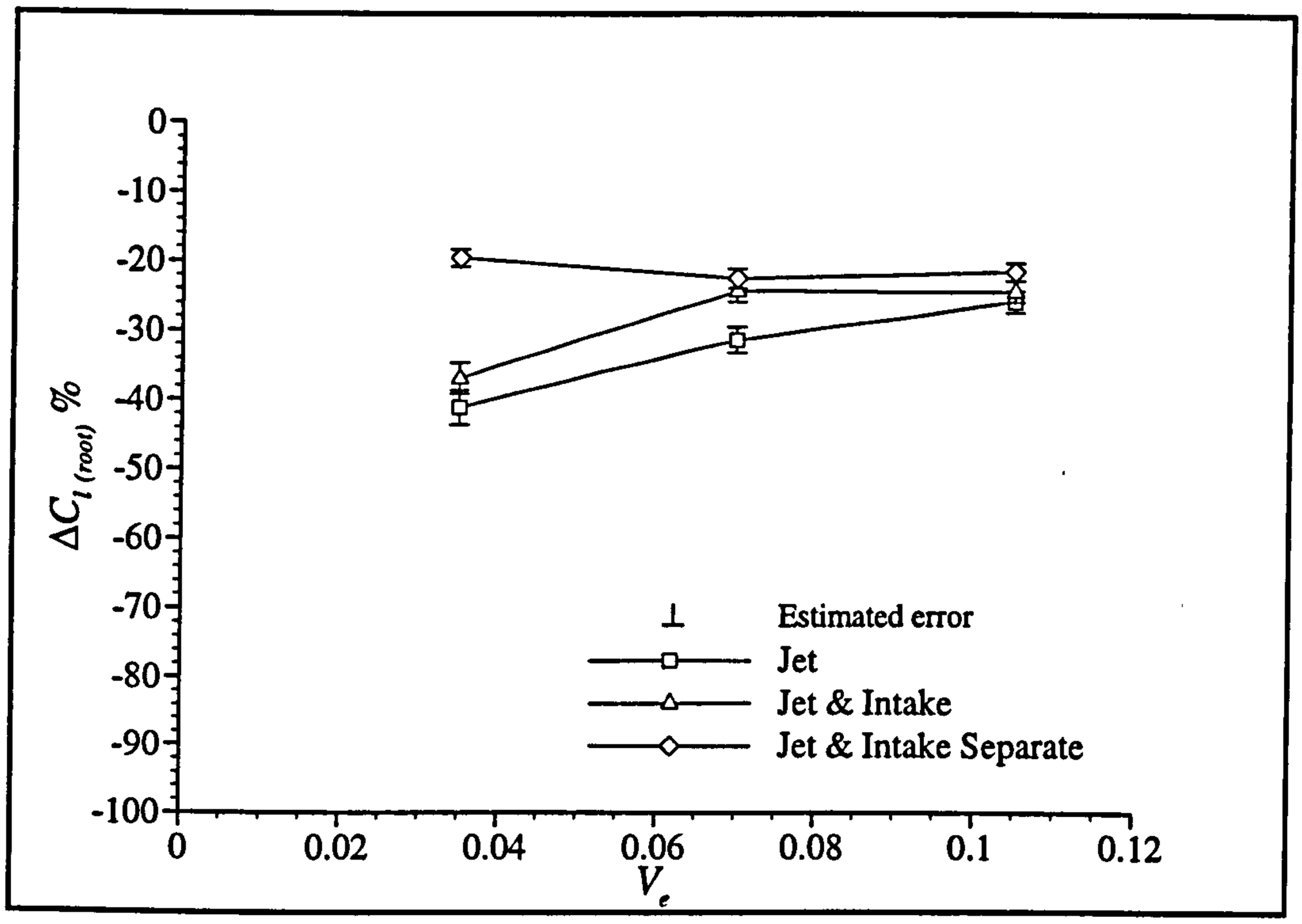

***Figure 4.54** - Effect of separate jet and intake testing on $\Delta C_{l\,(root)}$, forward nozzle position, NPR = 1.586 (Phase 2a data).*

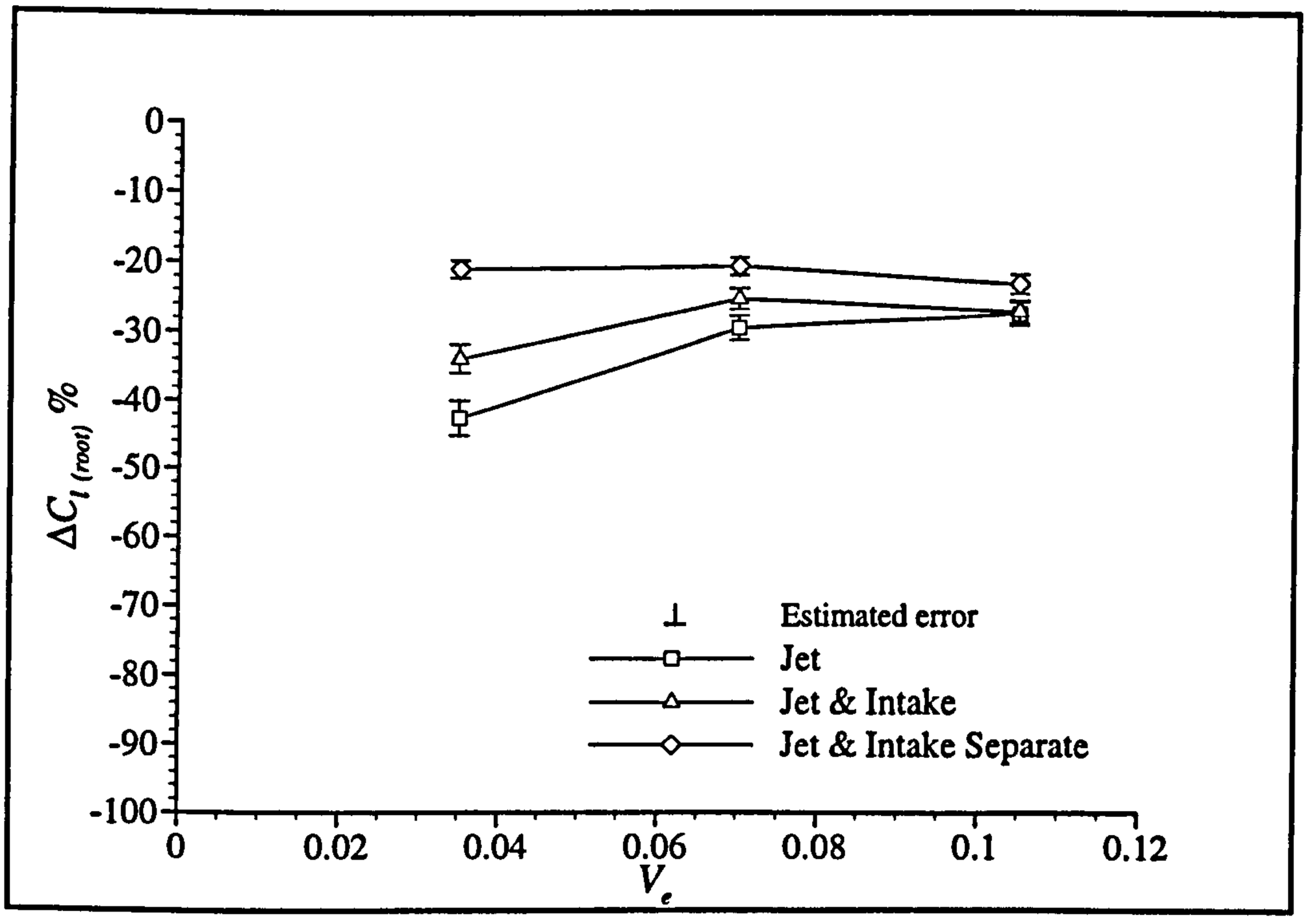

***Figure 4.55** - Effect of separate jet and intake testing on $\Delta C_{l\,(root)}$, centre nozzle position, NPR = 1.586 (Phase 2a data).*

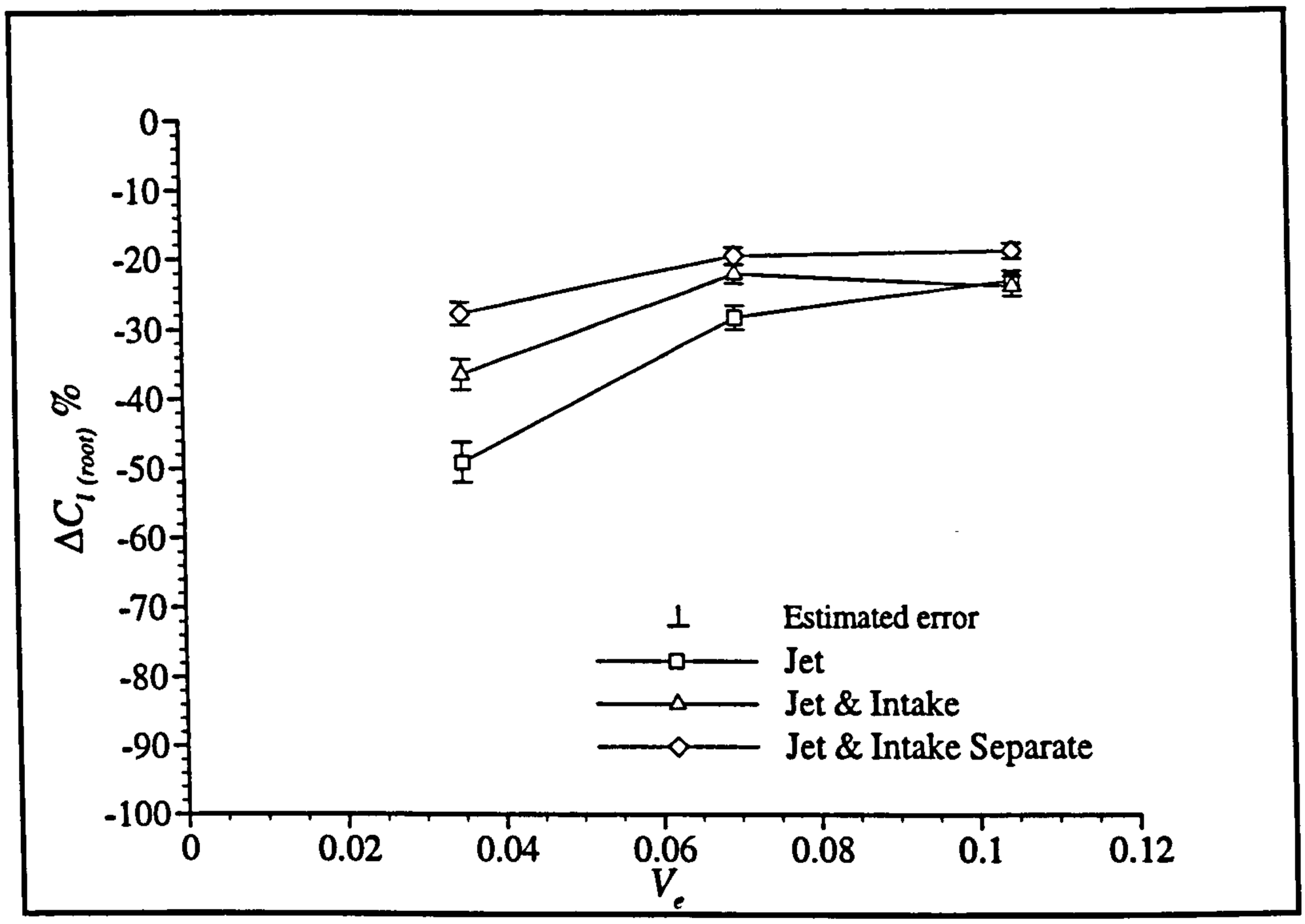

***Figure 4.56** - Effect of separate jet and intake testing on $\Delta C_{l\,(root)}$, rearward nozzle position, NPR = 1.586 (Phase 2a data).*

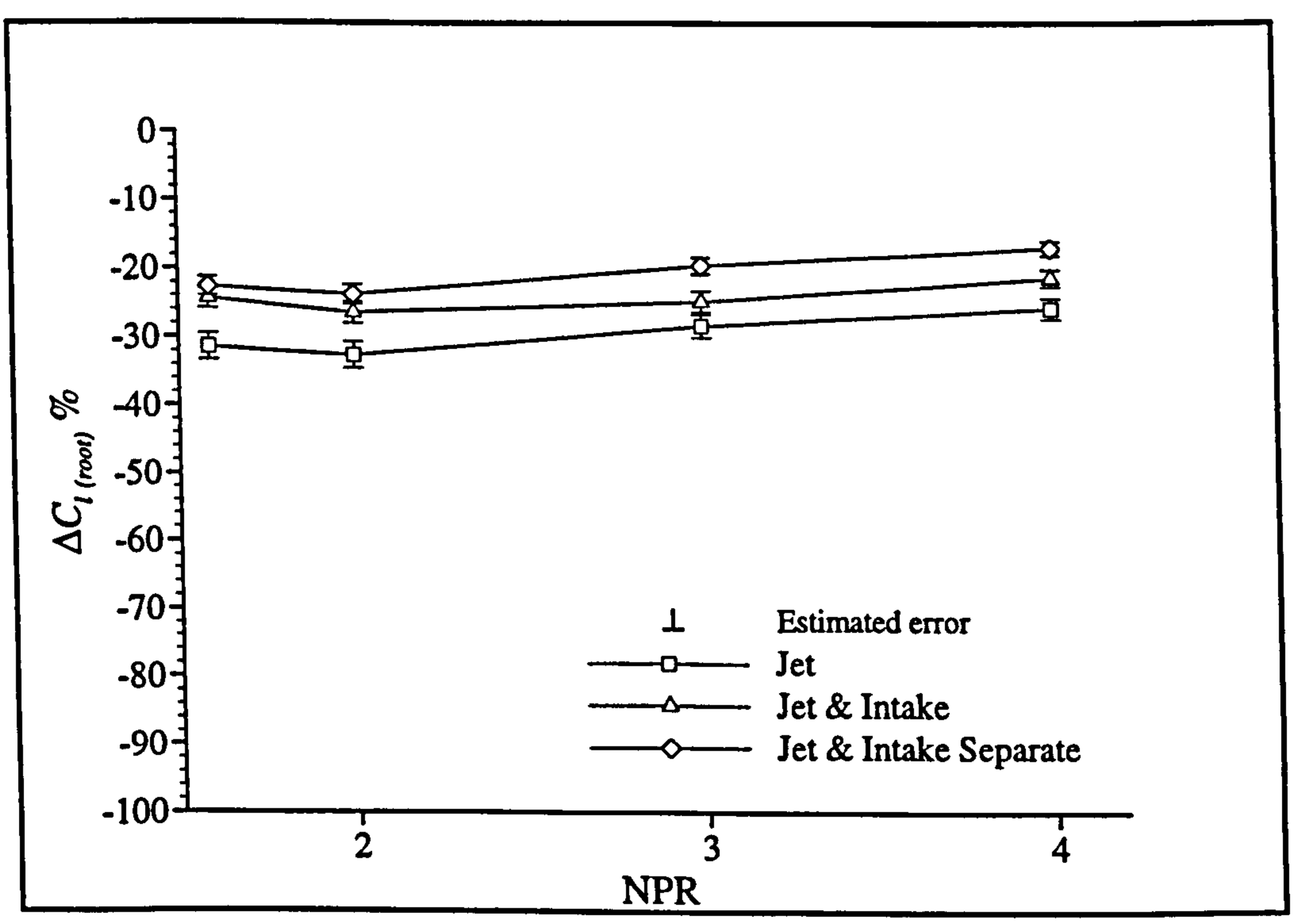

***Figure 4.57** - Effect of separate jet and intake testing on $\Delta C_{l\,(root)}$, forward nozzle position, q_∞ = 245 Pa (Phase 2a data).*

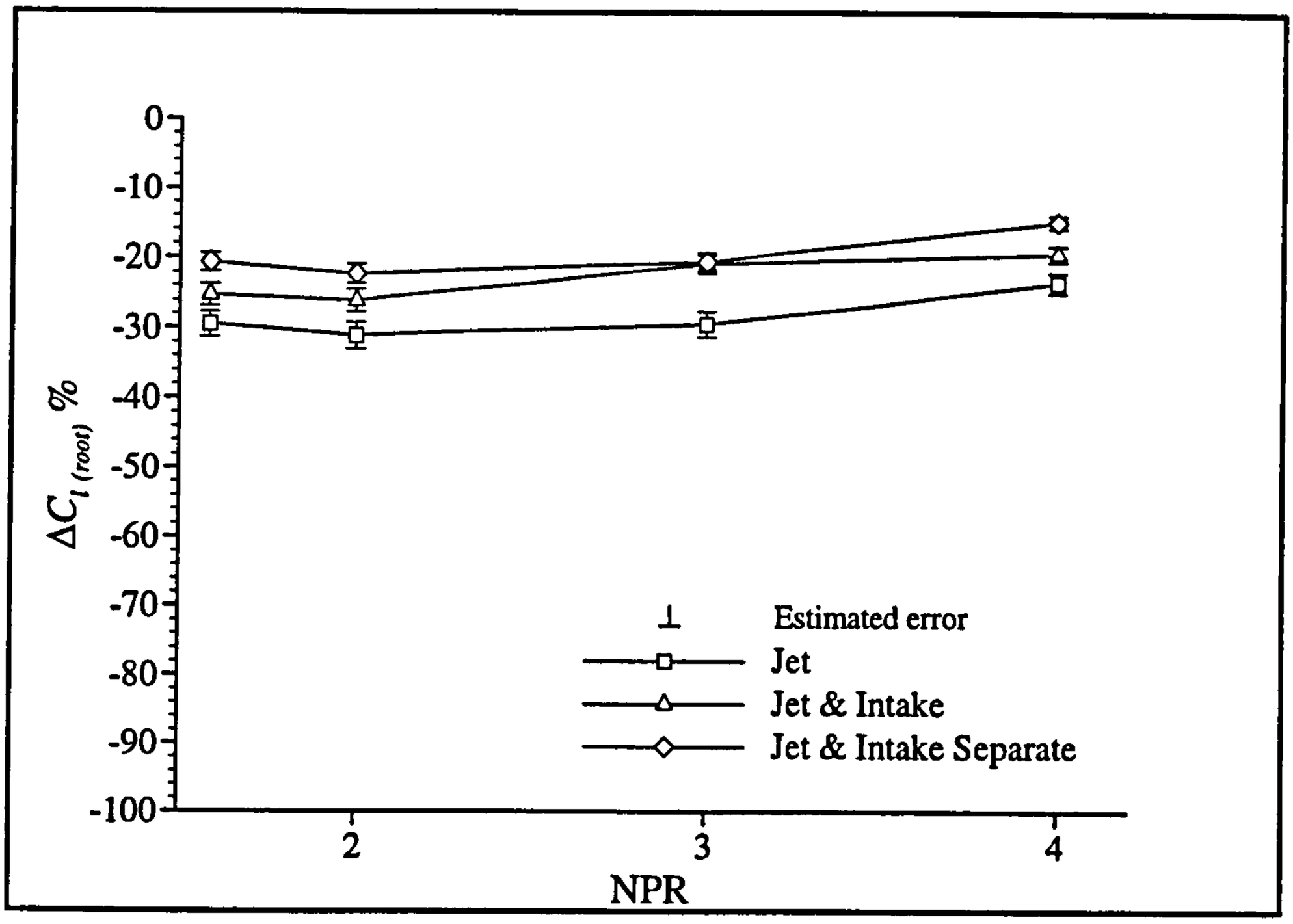

***Figure 4.58** - Effect of separate jet and intake testing on $\Delta C_{l\,(root)}$, centre nozzle position, q_∞ = 245 Pa (Phase 2a data).*

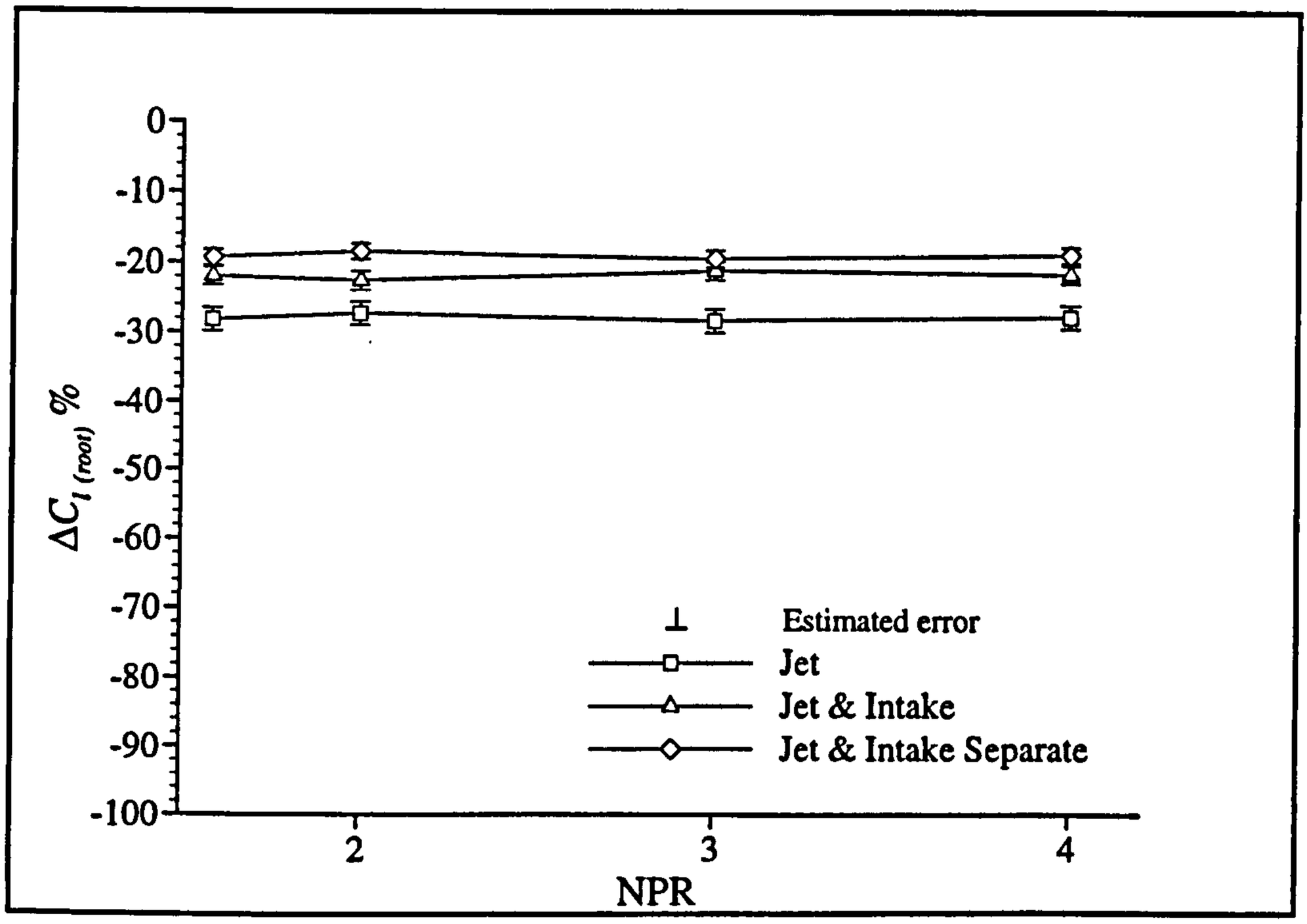

***Figure 4.59** - Effect of separate jet and intake testing on $\Delta C_{l\,(root)}$, rearward nozzle position, q_∞ = 245 Pa (Phase 2a data).*

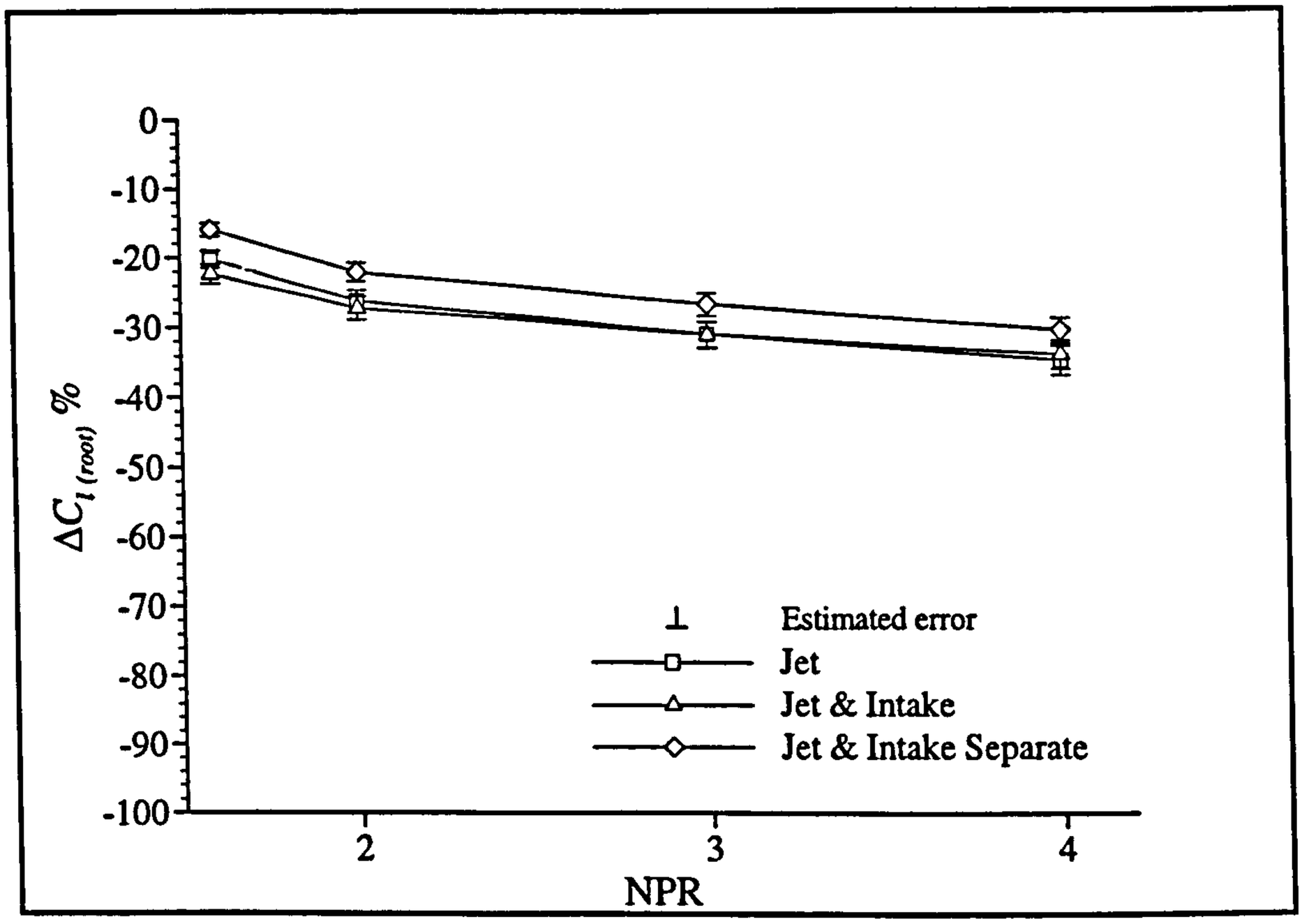

***Figure 4.60** - Effect of separate jet and intake testing on $\Delta C_{l\,(root)}$, forward nozzle position, q_∞ = 551 Pa (Phase 2b data).*

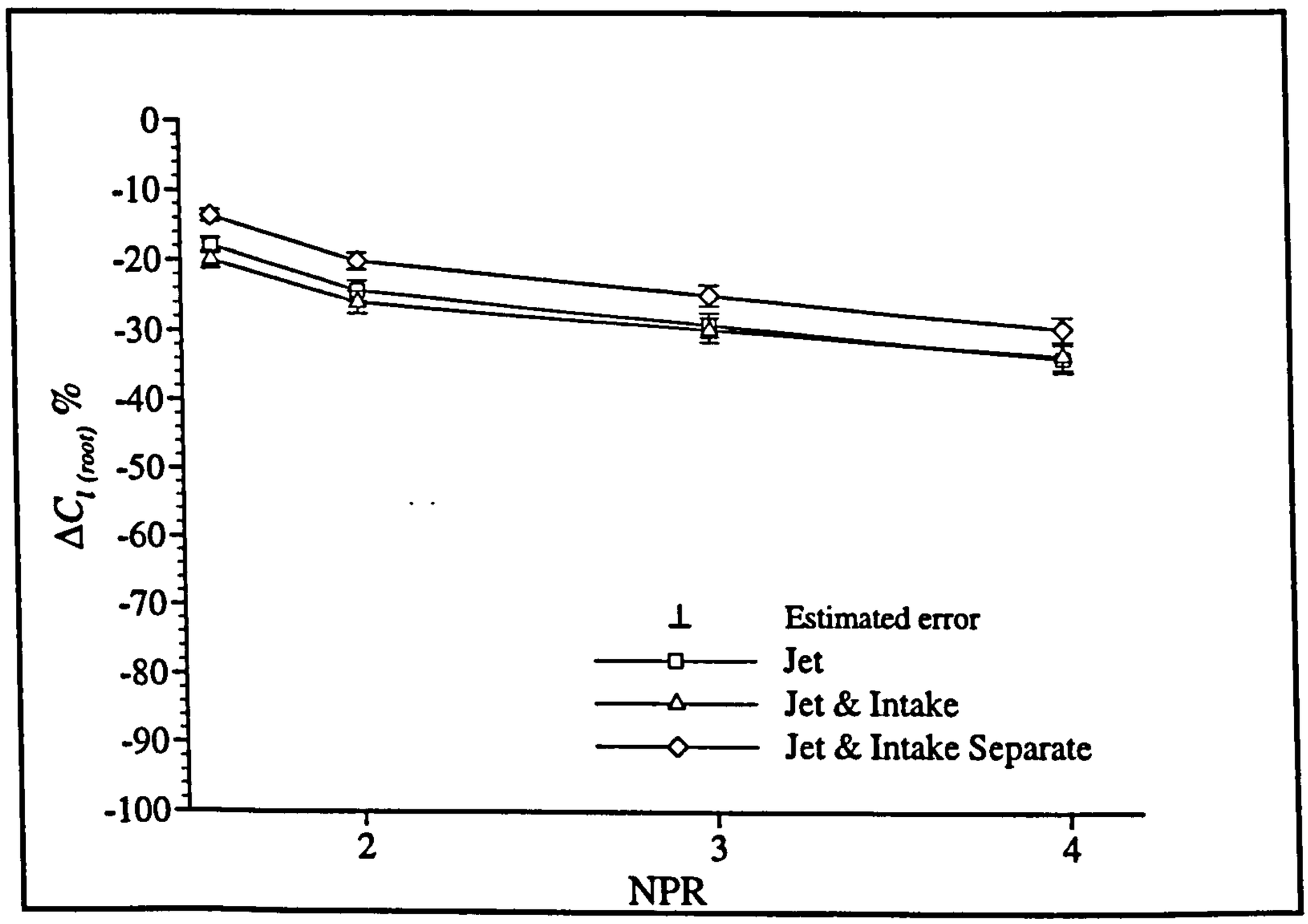

***Figure 4.61** - Effect of separate jet and intake testing on $\Delta C_{l\,(root)}$, centre nozzle position, q_∞ = 551 Pa (Phase 2b data).*

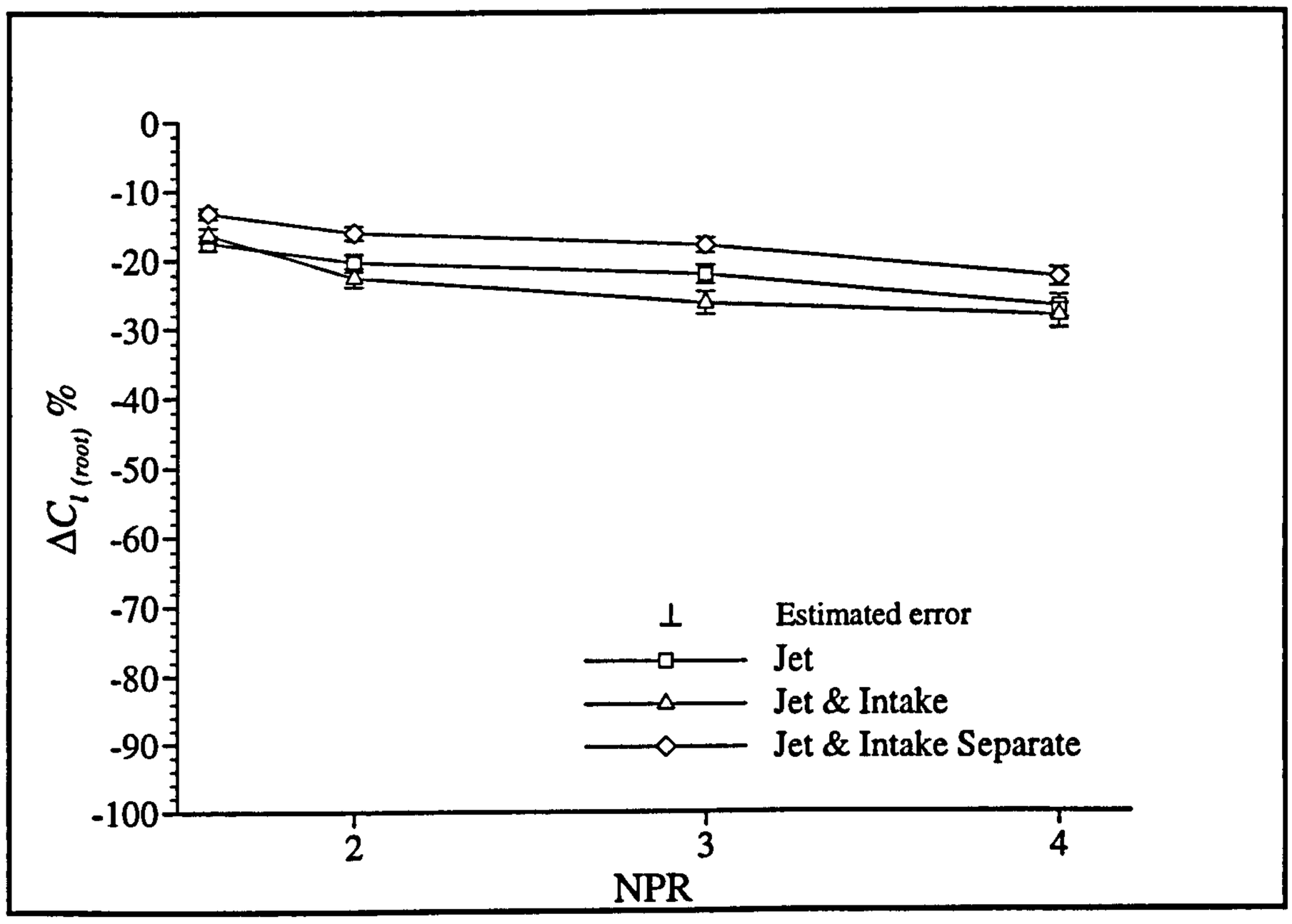

***Figure 4.62** - Effect of separate jet and intake testing on $\Delta C_{l\,(root)}$, rearward nozzle position, q_∞ = 551 Pa (Phase 2b data).*

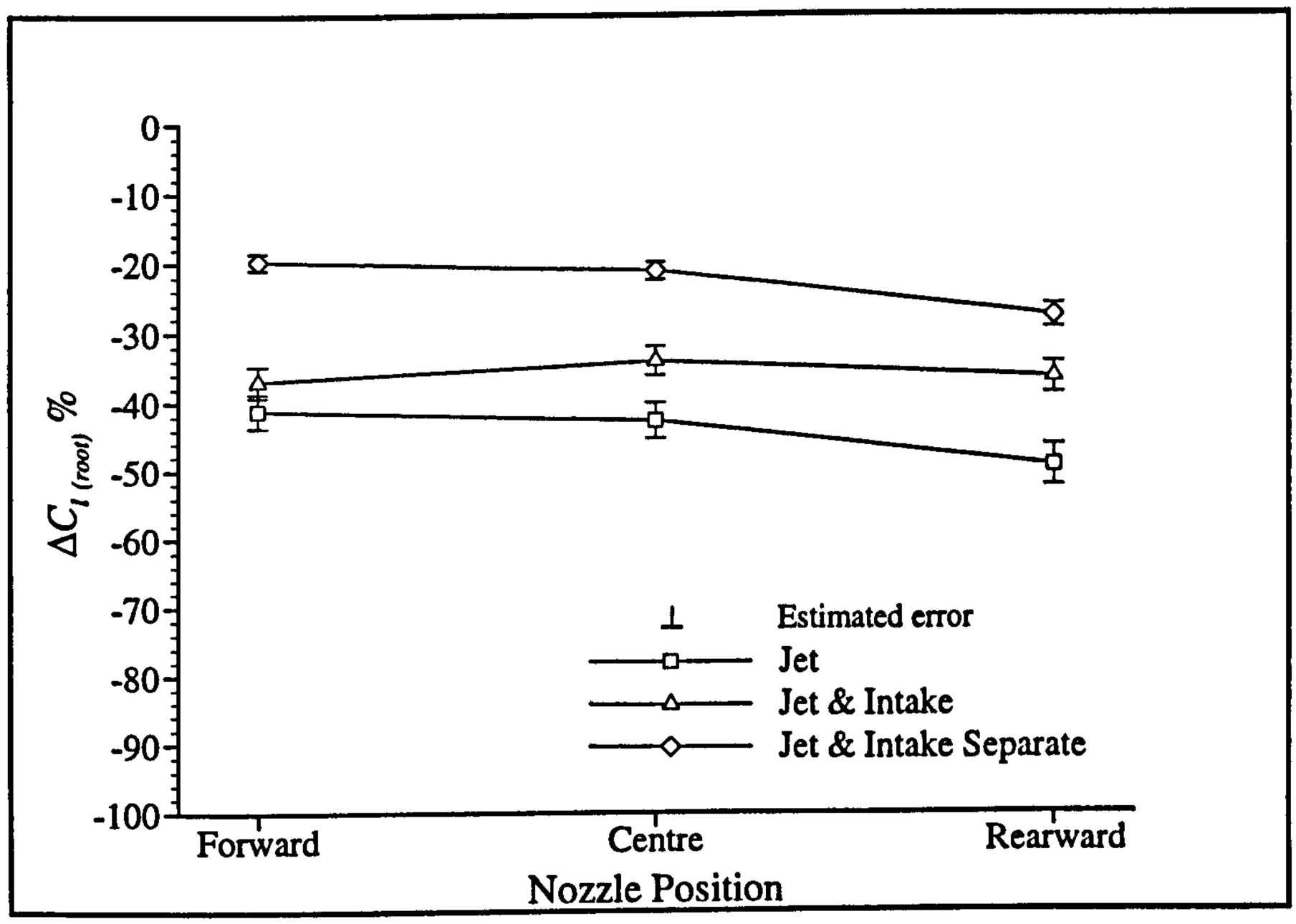

***Figure 4.63** - Effect of separate jet and intake testing on $\Delta C_{l\,(root)}$, NPR = 1.586, q_∞ = 61.3 Pa (Phase 2a data).*

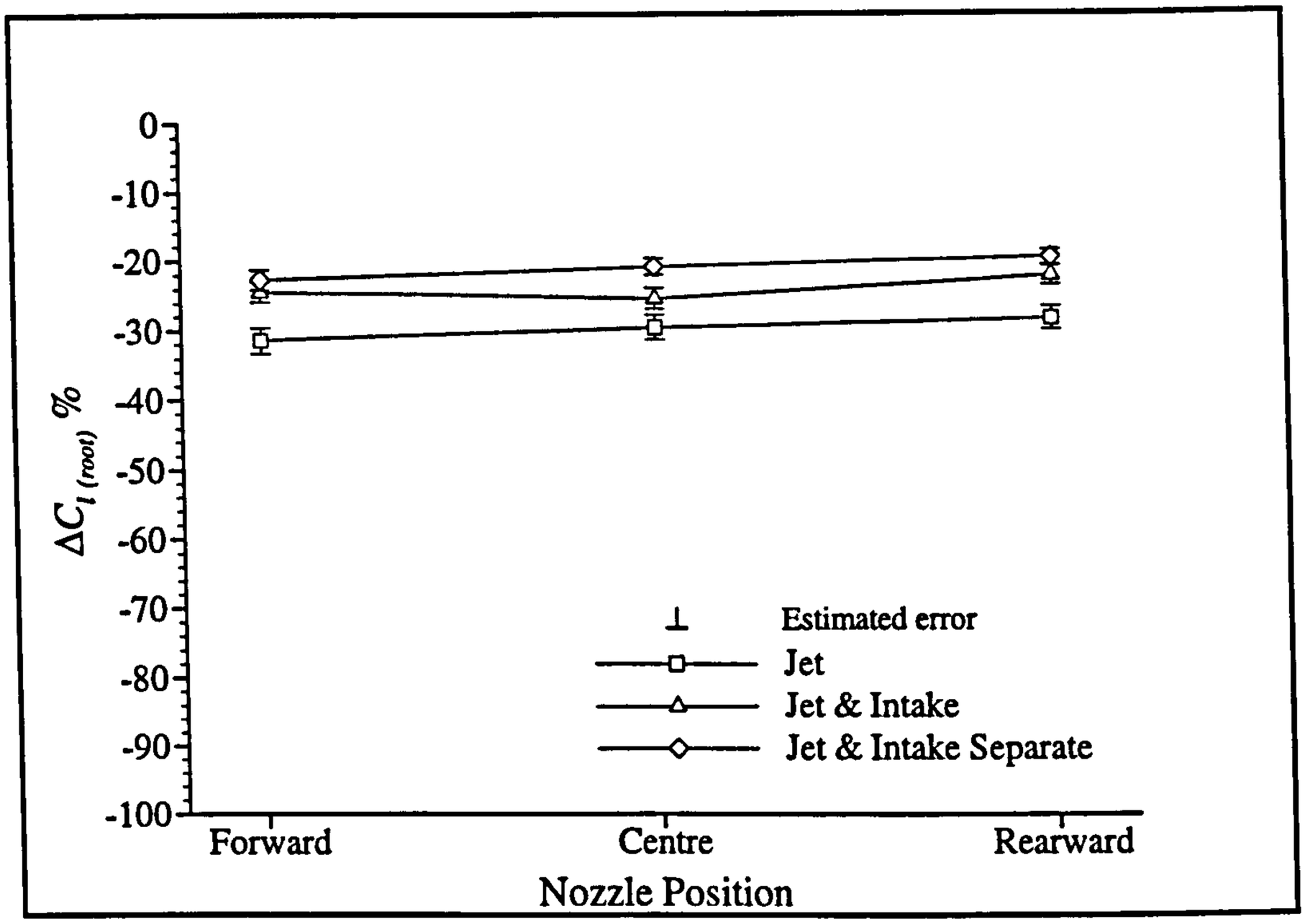

***Figure 4.64** - Effect of separate jet and intake testing on $\Delta C_{l\,(root)}$, NPR = 1.586, q_∞ = 245 Pa (Phase 2a data).*

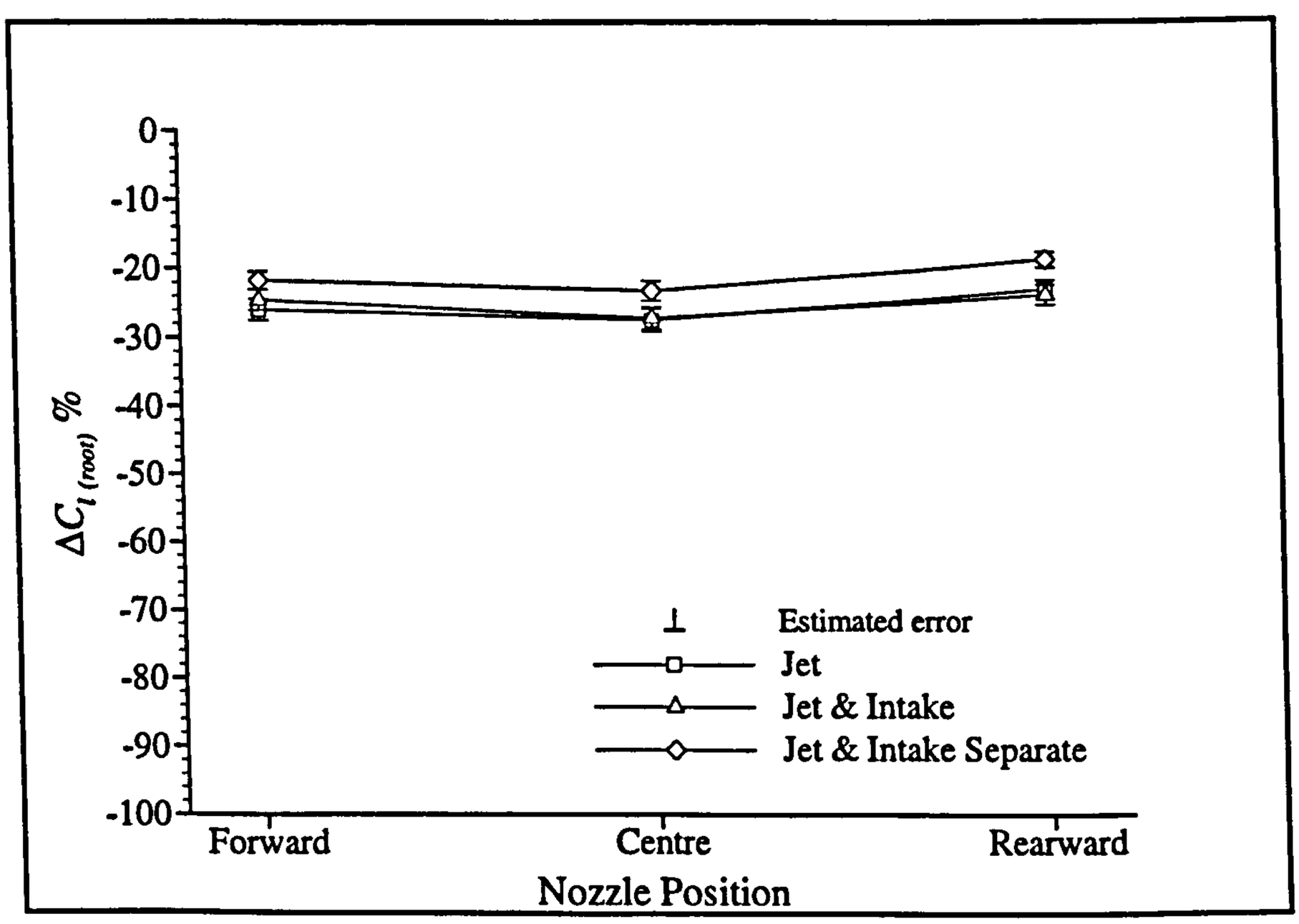

***Figure 4.65** - Effect of separate jet and intake testing on $\Delta C_{l\,(root)}$, NPR = 1.586, q_∞ = 551 Pa (Phase 2a data).*

5 Numerical Modelling

The numerical modelling undertaken during this project used the commercially-available PHOENICS computational fluid dynamics (CFD) code. This chapter presents the fundamental equations for fluid flow and describes how CFD is used to solve these equations. Previous PHOENICS work relevant to the current research area is also discussed.

5.1 Introduction

In aerodynamics, the flows of practical relevance are almost always turbulent, especially close to solid surfaces. This means that the fluid motion is highly random, unsteady and three-dimensional. Due to these complexities, the turbulent motion and heat and mass-transfer associated with it are extremely difficult to describe and thus to predict theoretically. The exact equations describing the turbulent motion are known (the Navier-Stokes equations), and numerical procedures are available to solve these equations, but the processing speed and storage capacity of present-day computers is still not sufficient to provide a solution for anything other than the most basic flow problems.

5.2 Turbulence

TAYLOR & VON KARMAN (see WILCOX, 1994) proposed the following definition of turbulence: 'Turbulence is an irregular motion which in general makes its appearance in fluids, gaseous or liquid, when they flow past solid surfaces or even when neighbouring streams of the same fluid flow past or over one another'. It is characterised by the presence of a large range of fluctuating length and time scales. The irregular nature of turbulence is in contrast to laminar motion, so called because historically the fluid was imagined to flow in smooth laminae or layers. Virtually all flows of engineering interest are turbulent.

Turbulent flows always occur when the Reynolds number is large and develop as an instability of laminar flow. To analyse the stability of laminar flows, virtually all methods begin by linearising the equations of motion. For a real (i.e. viscous) fluid, the instabilities result from the interaction between the Navier-Stokes equation's non-linear inertial terms and viscous terms. The interaction is very complex because it is rotational, three-dimensional and time-dependent. The strongly rotational nature of turbulence is linked to its three-dimensionality. Stretching of vortex lines is required to maintain the ever-present fluctuating vorticity in a turbulent flow. Vortex stretching is absent in two-dimensional flows so that turbulence must be three-dimensional. This inherent three-dimensionality means that there are no satisfactory two-dimensional approximations and this is one of the reasons why turbulence is difficult to model.

The time-dependent nature of turbulence also contributes to the difficulty of solving the governing equations. This additional complexity goes beyond the introduction of an additional dimension. Turbulence is characterised by random fluctuations preventing a deterministic approach to the problem. Instead, statistical approaches must be used. At first sight, this approach is not really a problem since for most applications the flow properties of interest would normally be integrated over time to determine time-averages. However, time-averaging leads to statistical correlations in

the equations of motion that cannot be determined analytically. This is the classical closure problem.

In principle, the time-dependent, three-dimensional Navier-Stokes equations contain all of the physics of a given turbulent flow. That this is true follows from the fact that turbulence is a continuum phenomenon. Turbulence consists of a continuous range of length-scales ranging from smallest to largest. The smallest length-scales are generally several orders of magnitude smaller than the largest, the latter being of the same order of magnitude as the dimension of the object about which the fluid is flowing. Turbulence features a cascading process whereby, as the turbulence decays, its kinetic energy transfers from larger eddies to smaller ones. Ultimately, the smallest eddies dissipate into heat through the action of molecular viscosity. Thus turbulent flows are always dissipative in nature. Another important feature of turbulence is its enhanced diffusivity. Turbulent diffusion greatly enhances the transfer of mass, momentum and energy. Apparent stresses develop in turbulent flows that are several orders of magnitude larger than in corresponding laminar flows.

The following sections describe the governing equations of fluid flow and mainly summarise the works of SCHLICHTING, 1960, CEBECI & SMITH, 1974, RODI, 1984 and WILCOX, 1994. It is important to analyse the principal equations used in numerical modelling before embarking on an explanation of the way in which numerical modelling was used to determine flow-fields of interest.

5.3 The governing equations

In the general case of three-dimensional motion, the velocity field is specified by the vector

$$\mathbf{V} = u\mathbf{i} + v\mathbf{j} + w\mathbf{k} \tag{5.1}$$

where u, v and w are the three orthogonal components describing the motion of the fluid with pressure p, density ρ, temperature T and viscosity μ. For the determination of these seven quantities there exist seven equations; the continuity equation (conservation of mass), the three equations of motion (conservation of momentum), the thermodynamic equation of state, the energy equation and the empirical viscosity equation. All the equations expressed here are in tensor notation. For an explanation of this refer to RODI, 1984 or WILCOX, 1994.

The equation of continuity expresses the fact that for a unit volume there is a balance between the masses entering and leaving per unit time, and the change in density. This leads to the equation

$$\underbrace{\frac{\partial \rho}{\partial t}}_{\substack{\text{rate of change} \\ \text{of mass}}} + \underbrace{\frac{\partial (\rho u_i)}{\partial x_i}}_{\text{net mass flux}} = 0 \tag{5.2}$$

If the fluid is incompressible then the continuity equation may be simplified to

$$\rho \frac{\partial u_i}{\partial x_i} = 0 \tag{5.3}$$

The equations of motion are derived from Newton's Second Law, which states that the product of mass and acceleration is equal to the sum of the external forces acting throughout the mass of the body (gravitational forces) and forces acting on the boundary (pressure and friction). In the general case of three-dimensional motion, three momentum equations are derived, one for each orthogonal component. These are more commonly known as the Navier-Stokes equations.

$$\underbrace{\frac{\partial(\rho u_i)}{\partial t}}_{\substack{\text{rate of change}\\ \text{of mass flux}}} + \underbrace{\frac{\partial(\rho u_i u_j)}{\partial x_j}}_{\substack{\text{net momentum}\\ \text{flux}}} = \underbrace{-\frac{\partial p}{\partial x_i}}_{\text{pressure force}} + \underbrace{\mu \frac{\partial^2 u_i}{\partial x_j \partial x_j} + \frac{1}{3}\mu \frac{\partial^2 u_j}{\partial x_i \partial x_j}}_{\text{friction force}} + \underbrace{S_i}_{\text{body force}} \tag{5.4}$$

If the fluid is incompressible, then the Navier-Stokes equations may also be simplified, becoming

$$\rho\left[\frac{\partial u_i}{\partial t} + \frac{\partial(u_i u_j)}{\partial x_j}\right] = -\frac{\partial p}{\partial x_i} + \mu \frac{\partial^2 u_i}{\partial x_j \partial x_j} + S_i \tag{5.5}$$

From thermodynamics the equation of state is obtained which combines pressure p, density ρ and temperature T, and which for a perfect gas has the form

$$p = \rho R T \tag{5.6}$$

If the flow is not isothermal, it is necessary to make use of the energy equation which uses the First Law of thermodynamics to draw up a balance between heat and mechanical energy. The result is a differential equation for the temperature distribution and which has the form

$$\underbrace{\frac{\partial(\rho h)}{\partial t}}_{\text{internal energy}} + \underbrace{\frac{\partial(\rho h u_i)}{\partial x_i}}_{\text{heat convection}} = \underbrace{\frac{\partial p}{\partial t} + \frac{\partial(p u_i)}{\partial x_i}}_{\substack{\text{compression/}\\ \text{expansion work}}} - \underbrace{\kappa \frac{\partial^2 T}{\partial x_i \partial x_i}}_{\text{heat conduction}} + \underbrace{\Phi}_{\text{friction heat}} \tag{5.7}$$

where Φ denotes the dissipation function.

$$\Phi = \tau_{ij} \frac{\partial u_i}{\partial x_j} \tag{5.8}$$

For incompressible flows, there is no compression or expansion work and so the first two terms on the right-hand side are zero.

The final equation of the system is given by the viscosity equation. For temperatures below 3000 K the viscosity of air is independent of pressure and in this range, the viscosity is given by Sutherland's Law:

$$\mu = 1.458 \times 10^{-6} \frac{T^{1.5}}{T + 110.4} \tag{5.9}$$

5.4 The closure problem

As already stated, turbulence consists of random fluctuations of the various flow properties in a fluid. At present, the individual motion of all the fluid particles cannot be determined and so a statistical method has to be used to determine the average motion of the fluid particles. The procedure described here is that introduced by REYNOLDS, 1895 in which all fluid quantities are expressed as the sum of mean and fluctuating components. The non-linearity of the Navier-Stokes equation leads to the appearance of momentum fluxes that act as apparent stresses throughout the flow. These momentum fluxes in turn cannot be determined. If equations for these stresses are then derived the resulting equations contain additional unknown quantities. This is the closure problem, which will be discussed further below.

5.5 Reynolds averaging

In general, Reynolds averaging assumes a variety of forms involving either an integral or summation. The most common form involves time-averaging.

The instantaneous quantity $\phi(t)$ is expressed as the sum of a mean component, $\overline{\phi}$ and a fluctuating component ϕ'. Hence

$$\left.\begin{aligned} u &= \overline{u} + u' \\ v &= \overline{v} + v' \\ w &= \overline{w} + w' \\ p &= \overline{p} + p' \end{aligned}\right\} \tag{5.10}$$

The time average or mean of any quantity $\phi(t)$ is taken as

$$\overline{\phi} = \lim_{\Delta t \to \infty} \frac{1}{\Delta t} \int_{t_0}^{t_0 + \Delta t} \phi(t)\,\mathrm{d}t \tag{5.11}$$

where Δt is the time step interval. For a steady state simulation, $\Delta t \to \infty$. The time average of the mean component is obviously equal to itself. Also the time average of any fluctuating component is zero since the flow is considered to be steady-state.

5.5.1 Time-averaging the incompressible equations

Initially the time-averaging will be applied to an incompressible isothermal fluid, such that the time average of Equations 5.3 and 5.5 need only be considered. For the continuity equation, substituting for the mean and fluctuating velocity components gives

$$\rho \frac{\partial(\overline{u}_i + u_i')}{\partial x_i} = 0 \tag{5.12}$$

Now time-averaging gives

$$\rho \frac{\partial \overline{u}_i}{\partial x_i} = 0 \tag{5.13}$$

Note, therefore that the Reynolds average of the incompressible continuity equation is the same as the instantaneous form but with the instantaneous velocity components replaced with time-averaged ones. Similarly, the Navier-Stokes equations can be treated in the same way. Substituting for the mean and fluctuating velocity components, gives

$$\rho\left[\frac{\partial(\overline{u}_i + u_i')}{\partial t} + \frac{\partial(\overline{u}_i + u_i')(\overline{u}_j + u_j')}{\partial x_j}\right] = -\frac{\partial(\overline{p} + p')}{\partial x_i} + \mu\left[\frac{\partial^2(\overline{u}_i + u_i')}{\partial x_j \partial x_j}\right] \tag{5.14}$$

Now time-averaging gives

$$\rho\left[\frac{\partial \overline{u}_i}{\partial t} + \frac{\partial(\overline{u}_i \overline{u}_j)}{\partial x_j} + \frac{\partial(\overline{u_i' u_j'})}{\partial x_j}\right] = -\frac{\partial \overline{p}}{\partial x_i} + \mu\left[\frac{\partial^2 \overline{u}_i}{\partial x_j \partial x_j}\right] \tag{5.15}$$

This can be rearranged into a more common form.

$$\rho\left[\frac{\partial \overline{u}_i}{\partial t} + \frac{\partial \overline{u}_i \overline{u}_j}{\partial x_j}\right] = -\frac{\partial \overline{p}}{\partial x_i} + \mu \frac{\partial^2 \overline{u}_i}{\partial x_j \partial x_j} - \rho \frac{\partial \overline{u_i' u_j'}}{\partial x_i} \tag{5.16}$$

The left hand side of Equation 5.16 is analogous with the left hand side of Equation 5.5 except that the instantaneous quantities have been replaced by their time-averaged ones. The same is also true of the first two terms on the right hand side. However, by time-averaging, additional terms known as Reynolds stresses have been introduced, which are products of the fluctuating components such as $\overline{u'v'}$. The fundamental problem created by time-averaging has now been introduced into the equations. Six unknown quantities have been produced as a result of time-averaging. However, no more additional equations have been created. So for general three-dimensional incompressible flow, there are four unknown mean flow properties (pressure and the three velocity components) plus the six Reynolds stress components, a total of ten. Clearly the system is not closed and no analytical solution can be found. This introduces the subject of turbulence modelling. The function of turbulence modelling is to devise approximations for the unknown correlations in terms of flow properties that are known so that a sufficient number of equations can be written. In making such approximations, the system of equations is closed.

5.6 Turbulence modelling

5.6.1 The Boussinesq eddy-viscosity

The oldest proposal for modelling the Reynolds stresses was developed by Boussinesq in 1877 and has become a significant part of most turbulence models. The eddy-viscosity concept assumes that the turbulent stresses are proportional to the mean velocity gradients. The coefficient of proportionality ν_t is called the eddy-viscosity. The Reynolds stresses are given by

$$\tau_{ij} \equiv -\rho\overline{u_i'u_j'} = \rho\nu_t\left[\frac{\partial\overline{u}_i}{\partial x_j}+\frac{\partial\overline{u}_j}{\partial x_i}\right]-\frac{2}{3}\rho k_t\delta_{ij} \tag{5.17}$$

where k is the turbulent kinetic energy given by

$$k=\frac{1}{2}\left(\overline{u'^2}+\overline{v'^2}+\overline{w'^2}\right) \tag{5.18}$$

and δ_{ij} is the Kronecker delta. A method is now required to describe the distribution of the eddy-viscosity.

5.6.2 Prandtl's mixing-length model

The first model to describe the distribution of the eddy-viscosity, and thus the first real turbulence model was suggested by PRANDTL, 1925 (see CEBECI & SMITH, 1974 and RODI, 1984) and is known as the Prandtl mixing-length hypothesis. The eddy-viscosity concept was conceived by presuming an analogy between the molecular motion and the turbulent motion. The turbulent eddies are thought of as lumps of fluid which, like molecules, collide and exchange momentum. The molecular viscosity is proportional to the average velocity and mean free path of the molecules. Accordingly the eddy viscosity is considered proportional to a velocity characterising the fluctuating motion and to a typical length of this motion which Prandtl called the 'mixing length'. The main success of the eddy viscosity concept was in the prediction of two-dimensional thin shear layers where the shear stress $\tau=-\rho\overline{u'v'}$ is the turbulent shear stress of prime importance. For this stress the relationship

$$\tau=\rho\nu_t\frac{\partial\overline{u}}{\partial y} \tag{5.19}$$

is obtained, where

$$\nu_t=l_m^2\left|\frac{\partial\overline{u}}{\partial y}\right| \tag{5.20}$$

For these simple flows, the mixing-length hypothesis has proved successful because l_m can be specified by simple empirical formulae in many situations. In free shear

layers, l_m is usually assumed to be constant across the layer and proportional to the local layer width δ[†]. The value of l_m/δ depends, however, on the type of flow being considered. Table 5.1 gives some examples

***Table 5.1** - Values of mixing length for free shear layers (RODI, 1985).*

Flow	*Plane mixing layer*	*Plane jet*	*Round jet*	*Radial jet*	*Plane wake*
l_m/δ	0.07	0.09	0.075	0.125	0.16

In flows of complexity greater than thin shear layers (e.g. an impinging jet), more than one turbulent stress component is of significance. The eddy viscosity is assumed to be a scalar quantity, however, this assumption of an isotropic eddy viscosity is a simplification which is of limited realism in complex flows. Therefore, different eddy viscosities are sometimes introduced for the turbulent momentum transport in different directions. In spite of these shortcomings, the eddy viscosity concept is still the basis of most turbulence models in use today.

5.6.3 One-equation models

In order to overcome the limitations of the mixing-length model, turbulence models were developed which account for the transport of turbulence quantities by solving differential transport equations for them. The velocity scale is no longer determined from the mean velocity gradients. Instead, the velocity fluctuations are characterised by the square-root of the turbulent kinetic energy. According to Equation 5.18, k is a direct measure of the intensity of the turbulence fluctuations in the three directions. The resulting equation describing the eddy-viscosity is

$$\nu_t = \sqrt{k}l \tag{5.21}$$

Note, however, that the length scale must still be specified.

5.6.4 Two-equation models

These models provide a method for determining the turbulent length-scale as well as the calculation of the velocity-scale. Consequently, two-equation models are described as 'complete' since they can be used with no prior knowledge of the turbulence structure. The most widely used two-equation model is the k-ε model. In the 'standard' k-ε model [LAUNDER & SHARMA, 1974], the equation describing the eddy viscosity is as follows:

[†] *δ is defined as the distance between points where the velocity differs from the free stream velocity by 1% of the maximum velocity difference across the layer. For symmetrical flows (e.g. round jets), δ is the distance from the symmetry axis to the 1% point at the outer edge.*

$$\nu_t = \frac{C_\mu k^2}{\varepsilon} \tag{5.22}$$

where ε is the rate of dissipation of turbulent kinetic energy. The two transport equations used for the solution of k and ε are

$$\frac{\partial k}{\partial t} + \overline{u}_i \frac{\partial k}{\partial x_i} = \frac{\partial}{\partial x_i}\left[\frac{\nu_t}{\sigma_k}\frac{\partial k}{\partial x_i}\right] + \nu_t \frac{\partial \overline{u}_i}{\partial x_j}\left[\frac{\partial \overline{u}_i}{\partial x_j} + \frac{\partial \overline{u}_j}{\partial x_i}\right] - \varepsilon \tag{5.23}$$

$$\frac{\partial \varepsilon}{\partial t} + \overline{u}_i \frac{\partial \varepsilon}{\partial x_i} = \frac{\partial}{\partial x_i}\left[\frac{\nu_t}{\sigma_\varepsilon}\frac{\partial \varepsilon}{\partial x_i}\right] + C_{1\varepsilon}\frac{\varepsilon}{k}\nu_t \frac{\partial \overline{u}_i}{\partial x_j}\left[\frac{\partial \overline{u}_i}{\partial x_j} + \frac{\partial \overline{u}_j}{\partial x_i}\right] - C_{2\varepsilon}\frac{\varepsilon^2}{k} \tag{5.24}$$

The constants, obtained from empirical data, are as follows:

***Table 5.2** - Coefficients in the 'standard' k-ε turbulence model (WILCOX, 1994).*

C_μ	$C_{\varepsilon 1}$	$C_{\varepsilon 2}$	σ_k	σ_ε
0.09	1.44	1.92	1.0	1.3

5.7 Compressibility effects

By definition, a compressible flow is one in which significant density changes occur, even when pressure changes are small. In addition to pressure and velocity fluctuations, changes in temperature and density must also be taken into account. If the standard time-averaging procedure is used for the compressible equations, then terms such as $\partial/\partial x\left(\overline{\rho' u'}\right)$ are generated. This indicates that a mean mass interchange occurs across the mean streamlines defined in terms of $\overline{u}$, $\overline{v}$, $\overline{w}$. It also indicates that the splitting of u, v, and w given by Equation 5.10 is not convenient, it is not consistent with the usual concept of a streamline [CEBECI & SMITH, 1974]. For that reason, the conventional time-averaging is replaced by the density-weighted-averaging procedure suggested by FAVRE, 1965.

The variable ϕ may be written as

$$\phi = \widetilde{\phi} + \phi'' \tag{5.25}$$

which is the sum of a mass-averaged component and a fluctuating component. Hence

$$\rho\phi = (\overline{\rho} + \rho')\left(\widetilde{\phi} + \phi''\right) \tag{5.26}$$

Time-averaging gives

$$\overline{\rho\phi} = \overline{\rho}\widetilde{\phi} \tag{5.27}$$

Note the important differences between the conventional averaging and Favre-averaging procedures. In conventional time-averaging, $\overline{\phi'} = 0$ and $\overline{\rho\phi'} \neq 0$. In Favre-averaging, $\overline{\phi''} \neq 0$ and $\overline{\rho\phi''} = 0$.

In order to mass-average the conservation equations, the various flow properties are decomposed as follows.

$$\left.\begin{aligned} u &= \tilde{u} + u'' & h &= \tilde{h} + h'' \\ v &= \tilde{v} + v'' & p &= \overline{p} + p' \\ w &= \tilde{w} + w'' & \rho &= \overline{\rho} + \rho' \\ T &= \tilde{T} + T'' \end{aligned}\right\} \tag{5.28}$$

Now taking the continuity equation (Equation 5.2) and substituting from Equation 5.27 gives

$$\frac{\partial(\overline{\rho} + \rho')}{\partial t} + \frac{\partial\left[(\overline{\rho} + \rho')(\tilde{u}_i + u_i'')\right]}{\partial x_i} = 0 \tag{5.29}$$

This can be time-averaged to give

$$\frac{\partial\overline{\rho}}{\partial t} + \frac{\partial(\overline{\rho}\tilde{u}_i)}{\partial x_i} = 0 \tag{5.30}$$

Equation 5.30 looks just like the incompressible mass conservation equation. In simplifying the compressibility effects, the momentum per unit volume is taken as the dependent variable instead of the velocity.

Taking the momentum equations (Equation 5.4), substituting for the instantaneous values and time-averaging gives

$$\frac{\partial(\overline{\rho}\tilde{u}_i)}{\partial t} + \frac{\partial\left(\overline{\rho}\tilde{u}_i\tilde{u}_j\right)}{\partial x_j} = -\frac{\partial\overline{p}}{\partial x_i} + \frac{\partial}{\partial x_j}\left[\overline{\tau}_{ij} - \overline{\rho u_i'' u_j''}\right] \tag{5.31}$$

With density-weighted averaging, the final equations have the same form term for term as the incompressible time-averaged equations but with two exceptions. Firstly, the viscous stresses τ_{ij} include fluctuations in viscosity and secondly, the Reynolds stresses include fluctuations in density.

The Favre-averaged energy equation can also be determined,

$$\frac{\partial\left(\overline{\rho}\tilde{h}\right)}{\partial t} + \frac{\partial\left(\overline{\rho}\tilde{h}\,\tilde{u}_i\right)}{\partial x_i} = \frac{\partial\overline{p}}{\partial t} + \frac{\partial(\overline{p}\tilde{u}_i)}{\partial x_i} - \kappa\frac{\partial^2\tilde{T}}{\partial x_i\partial x_i} - \frac{\partial\left(\overline{\rho h'' u_i''}\right)}{\partial x_i} + \overline{\Phi} \tag{5.32}$$

It must be remembered that while Favre-averaging eliminates density fluctuations from the averaged equations, it does not remove the effect that the density fluctuations have on the real physical turbulence. Consequently, Favre-averaging is a mathematical simplification, not a physical one.

5.7.1 Compressible-flow closure approximations

For turbulence models which use the Boussinesq approximation, closure approximations must be used which account for the mass-averaged form of the conservation equations. For zero, one and two-equation models the Boussinesq model may be modified for compressible flows, taking the form

$$\tau_{ij} \equiv -\overline{\rho u_i'' u_j''} = 2\overline{\rho}\nu_t\left[S_{ij} - \frac{1}{3}\frac{\partial \tilde{u}_k}{\partial x_k}\right] - \frac{2}{3}\overline{\rho}k\delta_{ij} \tag{5.33}$$

As with incompressible flows, the eddy-viscosity is then determined using a turbulence model. The most commonly used closure approximation for the turbulent heat-flux vector assumes that heat transfer is proportional to the mean temperature gradient, so that

$$\overline{\rho h'' u_i''} = -\frac{\overline{\rho}\nu_t c_P}{\mathrm{Pr}_t}\frac{\partial \tilde{T}}{\partial x_i} \tag{5.34}$$

For free shear layers, values of Pr_t of the order of 0.5 are used [WILCOX, 1994].

This is by no means an exhaustive account of turbulence modelling and closure methods. There are numerous other one- and two-equation turbulence models which have been developed over the years, but at their core the Boussinesq concept can still be found. In addition, more complex methods such as Reynolds Stress models and large eddy simulation (LES) are becoming more commonly used. These models, however, will not be discussed further here.

5.8 The PHOENICS program

The computational fluid dynamics (CFD) software used for numerical modelling in the present project is called PHOENICS which is an acronym for Parabolic, Hyperbolic or Elliptic Numerical Integration Code Series and is produced by Concentration, Heat and Momentum (CHAM) Ltd. It is a general purpose code for simulating single and multi-phase flow, heat transfer and chemical reaction phenomena. PHOENICS comprises two distinct programs called 'Satellite' and 'Earth'. Satellite is the pre-processor program which reads the user input file, known as a 'q1' file, and converts it into a form which the solver (Earth) can read. The q1 input file contains structured groups of code, numbered 1 to 24 written in the PHOENICS input language PIL. PIL is similar in appearance to FORTRAN but has special keywords and commands which are appropriate to CFD. Several examples of q1 files are given in Appendix E. These will be discussed in further detail in the next chapter.

5.8.1 Flow types

PHOENICS can solve flows which are parabolic, hyperbolic or elliptic. The distinction between these flows is shown in Figure 5.1 which depicts, for each case, the

domain of influence of a small disturbance. In parabolic flows, the disturbance has no effect upstream, and in the hyperbolic case the region of influence is restricted to the so called 'Mach cone'.

5.8.2 Grid types and arrangement

PHOENICS, like other CFD codes employs the concept of a 'grid', i.e. the flow domain is discretised into an array of finite grid 'cells' and 'nodes' in space and time. The grid may be Cartesian, polar-cylindrical or rectangular-curvilinear.

A Cartesian grid is composed of cells formed by the intersection of three sets of mutually perpendicular parallel planes on any one of which x, y or z is a constant. The intervals of x, y or z may be arbitrarily chosen.

A polar-cylindrical grid by contrast consists of cells formed by the intersection of:

- planes of constant z, perpendicular to the axis of rotation
- planes of constant x, which all pass through and thus intersect on that axis (so that x now represents an angular measurement not a linear one).
- concentric cylindrical surfaces, of constant radial co-ordinate y.

Once again the intervals of x, y or z may be arbitrarily chosen.

A rectangular-curvilinear grid is a rectangular grid which has been squeezed, stretched, bent and twisted in an arbitrary way. All the cells which were originally in contact with one another remain so, but their shapes may have changed considerably. Rectangular-curvilinear grids are often used for flow simulations in which it is desired that the grid should conform to the curved surface of some body, that they are often called 'body-fitted co-ordinates' or BFCs for short.

5.8.3 Solution algorithm

PHOENICS uses a 'finite-volume' numerical modelling form of the conservation equations. The finite-volume equations are derived by integration of the differential equations over control volumes (cells) which are of finite size and make up the domain under study. In the case of PHOENICS, the cells are topologically Cartesian, having six sides and eight corners. Within each cell is a grid node, for which the fluid property values are regarded as representative of the whole cell. Each cell communicates with its neighbours across the cell faces. Figure 5.2 shows a plan view of a single Cartesian cell with four of its neighbours. All scalar quantities (pressures, temperatures etc.) are evaluated by PHOENICS at the cell centres, shown by the locations P, N, S, E and W. Velocities, however, are evaluated for the cell wall locations, given by n, s, e and w. This method of determining the variables is known as the 'staggered grid' arrangement. Note that for the volume domain, the x-axis is from west to east, the y-axis is from south to north and the z-axis is from

low to high (perpendicular to the plane of Figure 5.2). PHOENICS computes imbalances in the Reynolds-averaged conservation equations for all of the volume elements. The code then systematically adjusts the associated flow variables (pressure, velocity etc.) until balances are sufficiently achieved for all volumes. The algorithm used by PHOENICS for solving the conservation equations is called 'SIMPLEST' and is based on the algorithm 'SIMPLE'. SIMPLE stands for Semi-Implicit Method for Pressure Linked Equations and was first suggested by PATANKAR & SPALDING, 1972. In an attempt to improve convergence, two modifications to SIMPLE were created, SIMPLER (see PATANKAR, 1980) which stands for SIMPLE Revised and SIMPLEST (see PATANKAR, 1981) which stands for SIMPLE ShorTened.

5.8.4 Operating system and versions

During development work, PHOENICS Versions 2.0, 2.1, 2.11 and 2.2 were used and initially run on a SUN SPARC 2 under the SUN operating system. This limited the work to simple two-dimensional problems. Later, an AXIL 420 (equivalent to a SUN SPARC 20) with the SOLARIS operating system was used. This enabled some three-dimensional calculations to be performed. For consistency, it was felt that all the results presented should be run on one version (Version 2.2). This did, however, necessitate re-running some of the earlier cases. For a more detailed explanation of PHOENICS, reference should be made to the PHOENICS manuals [CHAM, 1992] and SENIOR, 1997.

5.9 Previous PHOENICS modelling work

This section describes some previous numerical modelling of high speed, turbulent jet flows using the PHOENICS CFD code. A brief description of the more relevant modelling details are given below.

BRAY, 1992 modelled an axi-symmetric free jet using a polar cylindrical co-ordinate system and the k-ε turbulence model. The grid consisted of 24 cells in the y (radial) direction and 31 cells in the z (axial) direction. The third axis (circumferential) direction consisted of only one cell. This was considered a valid assumption based on the axisymmetry of the jet. Models were run for nozzle pressure ratios of 1.05, 1.2 and 1.25. In comparison with the experimental data of DONALDSON & SNEDEKER, 1971, BRAY found that the numerical model over-predicted the radial spreading of the free jet. The initial turbulence intensity of the jet was found to have a strong effect on the jet spreading rate and its centre-line axial velocity decay. As would be expected, the higher the initial turbulence intensity, the greater the spreading rate and the more rapid the decay. The ability of the numerical model to predict the correct decay rate could not be determined since the initial turbulence intensity of the jet used by DONALDSON & SNEDEKER was not known.

MYSZKO, 1997 also looked at free jet profiles and axial velocity decay using a grid geometry based on that of BRAY, 1992. The grid was the same two-dimensional, polar cylindrical grid but with 49 cells in the radial direction and 60 cells in the axial direction. MYSZKO, 1997 found similar results to those of BRAY, 1992 i.e. the k-ε turbulence model over-predicted the free jet spreading rate and hence the axial decay rate also. MYSZKO also implemented the 'Rodi correction' to the free jet which reduces its spreading rate by reducing the coefficients C_μ and $C_{\varepsilon 2}$ and hence the dissipation rate of turbulent kinetic energy. The implementation proved successful which is not surprising since RODI, 1984 developed the correction solely for this purpose. This correction was found to provide better agreement with MYSZKO's own experimental data.

WILSON, 1995 modelled a round jet in cross-flow using a polar cylindrical grid very similar to those used by BRAY, 1992 and MYSZKO, 1997. He found that the polar cylindrical grid was unsuitable for the modelling of a round jet in cross-flow because of the difficulty in defining the cross-flow boundary condition and ensuring that this boundary did not interfere with the solution domain.

It has been discovered by the author that in all of the above numerical modelling work a significant error was made in the input q1 file. In specifying the source of mass flow rate per unit area, the total density was used instead of the static density. This would provide increasing errors in the specification of jet mass flow rate as NPR was increased. The error in density, and hence mass flow rate would be proportional to the $NPR^{0.714}$. At low NPRs the error would be quite small (3.5 percent at an NPR of 1.05), but the error will increase as NPR is increased.

The effect on the results is difficult to determine. Effectively the jet exit conditions are unrealistic since there is a mismatch between density and pressure. A higher value of static density will increase the effective NPR of the jet and hence the exit velocity. This error was not present in the current work discussed in Chapter 6.

5.10 Summary

In this chapter, the subject of computational fluid dynamics numerical modelling has been introduced. It has been shown that when the conservation equations are simplified, either by means of time-averaging or Favre-averaging, additional unknown terms are created in the conservation equations. This leads to a closure problem and the introduction of turbulence modelling. A brief introduction to the CFD software used in this study (PHOENICS) has been presented. Finally, a brief review of some of the relevant previous numerical modelling work using PHOENICS has been presented. The results of the current CFD work will be described and discussed in the following chapter.

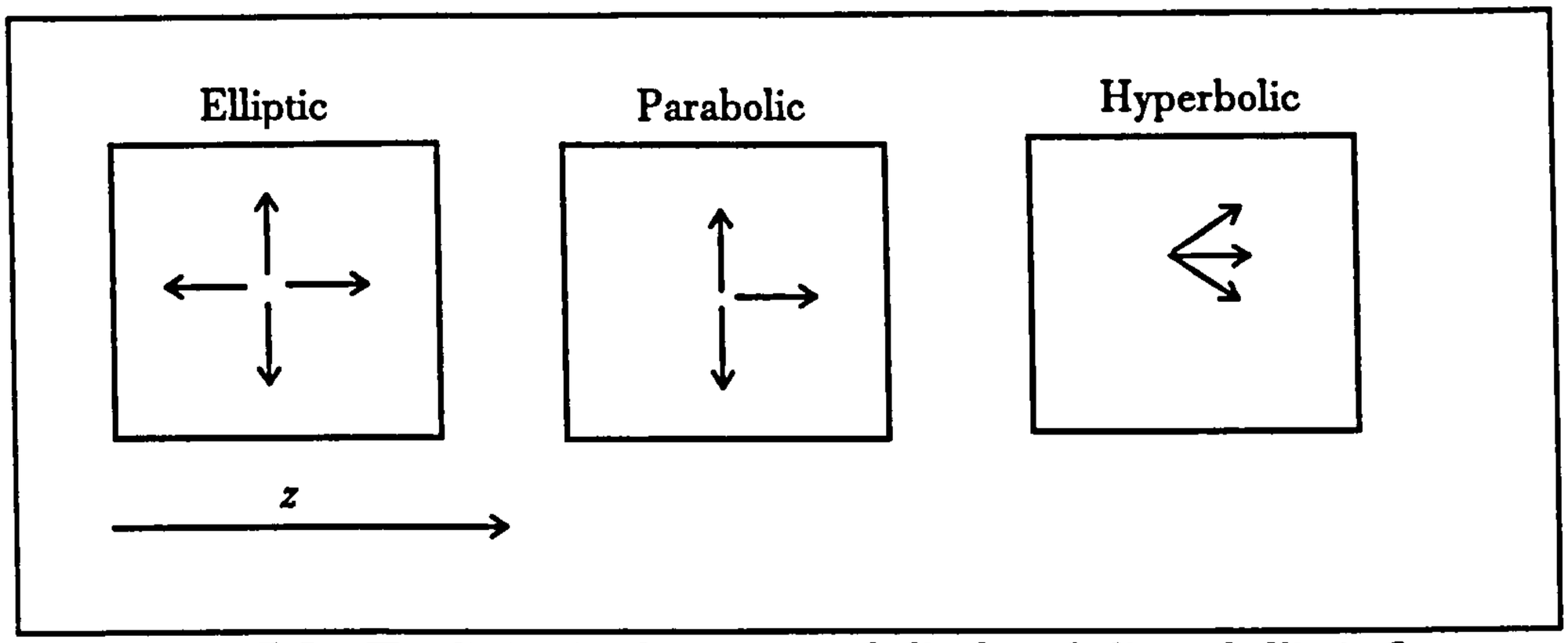

***Figure 5.1** - The distinction between parabolic, hyperbolic and elliptic flows.*

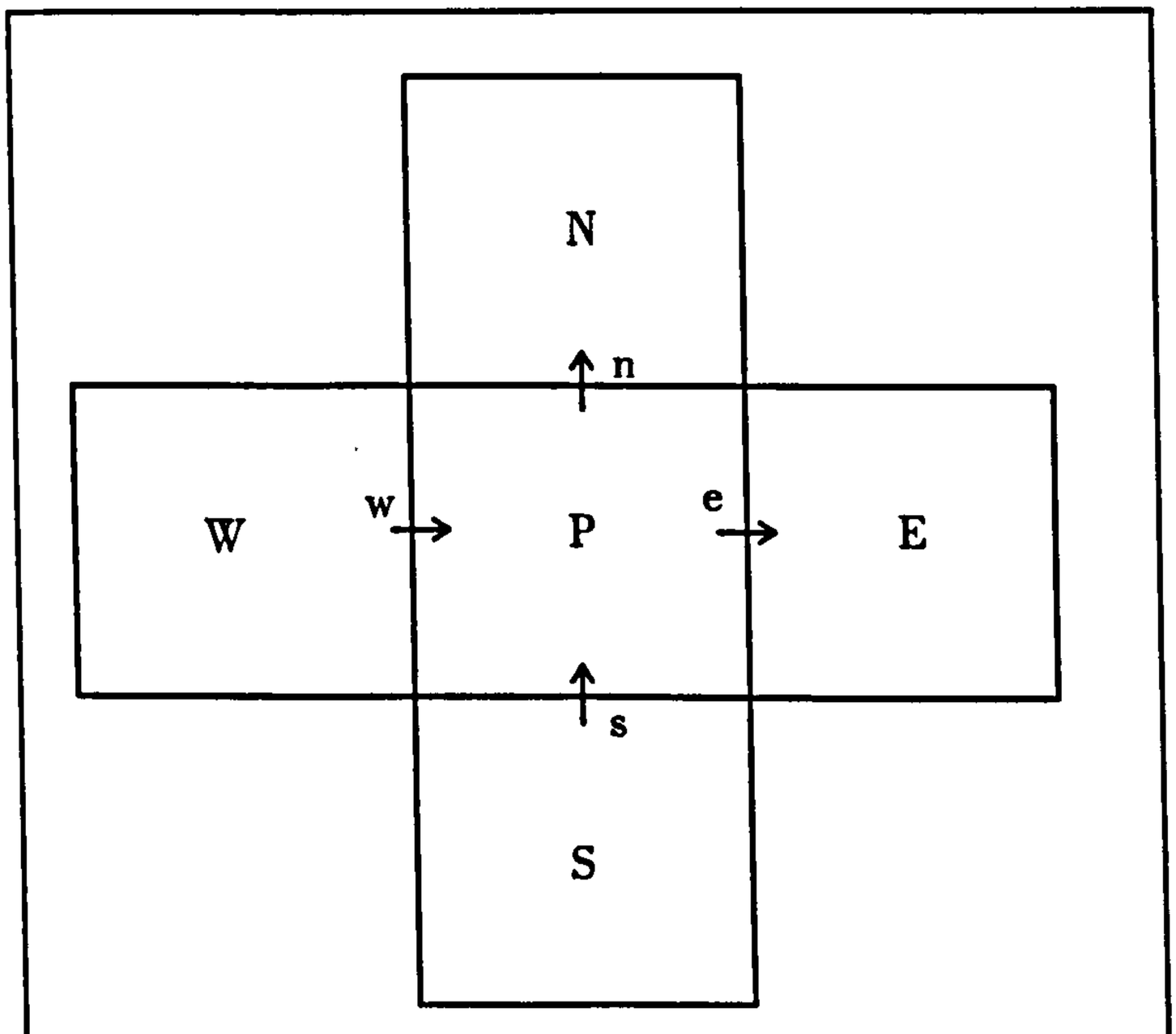

***Figure 5.2** - The staggered grid arrangement.*

6 Numerical Modelling Results

This chapter describes the numerical modelling carried out on flow-fields relevant to STOVL aircraft aerodynamics using the PHOENICS CFD software. Results are compared with previous numerical and experimental data.

6.1 Aim of the numerical modelling

The aim of the numerical modelling was to analyse some of the flow features which could not easily be visualised or measured with the wind tunnel model. It was immediately obvious that a simulation of the whole aircraft was not possible due to limitations in the grid generation capabilities of PHOENICS and the processing power required to generate a solution within a realistic time frame. Isolated components of the model, such as the wing, jet and intakes were, therefore, to be modelled. It was hoped that the CFD simulations would provide additional information which could help to explain some of the interference effects observed with the wind tunnel model. The results are presented in the following order:

- NACA 1408 aerofoil section;
- 'round' free jet;
- 'round' jet in a cross-flow.

After initial investigations it became apparent that no useful results for the intakes could be achieved in a form comparable with the experimental measurements. The number of grid cells required to define the intake lip geometry was too great to enable a solution with the computational resources available.

6.2 Convergence

Initially, convergence was checked by monitoring the variables at a point in the solution domain where the gradient of the variables was expected to be high. At the end of the run, these variables were checked to see if they had reached a steady value. However, this did not give an overall indication of the degree of convergence for the model. The point in the domain where the variables were checked was determined by the user and as such was open to error in judgement. A second method was therefore used which proved to be more satisfactory. PHOENICS has the facility to output the whole field residuals for all the variables as the solution progresses. The sum of the residuals in the conservation equations over the entire domain is normalised with the appropriate net flux for that variable and given as a percentage. When the residuals for all the variables were no longer seen to be decreasing, the solution was considered to be converged. For all the cases modelled, the residual errors in the flow variables were below 3 percent. The number of sweeps required was typically of the order of 5000. Figure 6.1 shows a typical plot for the convergence of the flow variables (in this case a three-dimensional jet in cross-flow).

6.3 NACA 1408 aerofoil

The aim of this simulation was to model the aerofoil used on the wind tunnel model. The grid domain was specified using the body-fitted grid facility which is available in PHOENICS. The simulation was run with freestream velocities of 10 ms^{-1}, 20 ms^{-1}, 30 ms^{-1} and 40 ms^{-1}. A sample q1 input file is given in Appendix E, Section E1.

6.3.1 Computational grid

The aerofoil tested had a chord of 0.3 m and was modelled at zero degrees incidence. The free-stream distance (z-direction) was set to 2.0 m and the transverse distance (y-direction) specified as 3.0 m. This was found to be necessary to prevent the boundary conditions from influencing the solution. The number of cells in the y direction is 101 and in the z direction is 90. Note that because PHOENICS is a finite volume code, the domain is only pseudo two-dimensional. The remaining direction therefore, in this case the x-direction, must have finite width and at least one cell. A magnified view of the grid structure around the aerofoil is shown in Figure 6.2. The grid expands away from the aerofoil towards the boundaries with a power law, b_y of 1.85 in the y-direction and b_z of 1.5 in the z-direction. The power law is given by the expression

$$b_x \log\left(\frac{i}{nx}\right) = \log\left(\frac{\Delta x}{x}\right) \tag{6.1}$$

where b_x is the power law in the x-direction based on the ith cell location which has a cumulative width Δx for a total domain width x with nx cells.

6.3.2 Flow conditions

The simulation was steady-state (STEADY=T), elliptic in nature (PARAB=F) and used the k-ε turbulence model (TURMOD=KEMODL). The solution was assumed to be incompressible and isothermal so values of ambient density (RHO1) and temperature (TMP1) were set constant at 1.225 kgm^{-3} and 288.15 K respectively. Also, the laminar kinematic viscosity (ENUL) was set to a constant value of 1.461×10^{-5}. The initial sources of turbulent kinetic energy and its dissipation rate were those suggested by CHAM for flows of this type and are given by Equations 6.2 and 6.3.

$$k = \left(\overline{V} \times Tu\right)^2 \tag{6.2}$$

$$\varepsilon = \frac{0.009k^2}{50\nu} \tag{6.3}$$

where $\overline{V}$ is the mean freestream velocity and Tu is the mean turbulence intensity, which was set to 3 percent.

6.3.3 Boundary conditions

Only two external boundary conditions were set, the upstream (low) and downstream (high) boundaries. The remaining four boundaries (north, south, east and west) were left undefined. PHOENICS then assumes that these are friction-less surfaces. The upstream (inlet) boundary condition was specified as follows:

- a uniform source of mass flow rate per unit area;
- a uniform source of velocity;
- a uniform source of turbulent kinetic energy;
- a uniform source of dissipation rate.

The downstream (outlet) boundary condition was specified as:

- a fixed pressure of zero relative to ambient pressure;
- the remaining flow variables were left unspecified. PHOENICS then sets these to the prevailing value in the particular cell throughout the solution procedure i.e. no additional sources (or sinks) of these flow variables are added at the boundary.

The aerofoil was specified as a friction blockage in the domain.

6.3.4 Results

Figure 6.3 shows a typical vector plot around the aerofoil. The PHOENICS-predicted pressure distribution was compared with a theoretical pressure distribution (Figure 6.4). The latter was determined from a potential flow panel code written at RMCS by Dr M. V. Finnis, validated for NACA 4-digit aerofoils. The two pressure distributions are similar although there are differences. Essentially the k-ε model predicts too little suction on the upper and lower surfaces of the aerofoil. This may be due to two main factors. Firstly, PHOENICS is not able to solve for pressures on the surface of a boundary, in this case the aerofoil. This will mean that the pressures plotted are those a finite distance away from the surface, in this case 1.5 mm. However, it is not thought that this small distance would account for the differences observed. Secondly, the standard k-ε model in PHOENICS uses a logarithmic law wall function to determine flow parameters close to a solid surface. The wall function is purely empirical and will almost certainly introduce inaccuracies into the solution. However, the magnitude of these inaccuracies is not known. A two-layer k-ε model was not successfully implemented due to convergence problems created by the very thin, high aspect ratio cells required in the laminar sub-layer. The presence of the boundary layer in the viscous k-ε solution may also be responsible for reducing the suction pressures on the aerofoil surface due to the effective change in surface curvature.

The forward stagnation point is also not captured by the PHOENICS prediction. This is probably due to insufficient numbers of grid cells in the area around the nose of the aerofoil producing a volume-averaged pressure in this area. Despite these differences, the sectional lift coefficient, C_l does show good agreement. The potential flow code predicts a C_l of 0.122 whilst PHOENICS predicts 0.116, a 5 percent difference. Variations in Reynolds number, between 2.0×10^5 and 8.0×10^5 (based on wing chord) did not have any effect on the results. This is attributed to the fact that the turbulence model does not account for variations in Reynolds number and merely assumes that any boundary layer will be turbulent irrespective of the calculated Reynolds number.

It was hoped that comparisons could be made with the experimental pressure distribution but this proved difficult because, although the pressure tappings on the wind tunnel model were not along a section containing the flap, they were, nevertheless, influenced by it. Although the computational model was developed into a constant chord three-dimensional wing, PHOENICS did not provide sufficient grid generation tools to enable a simulation of the wing used on the wind tunnel model. Neither could any other experimental data be found on the pressure distribution around a NACA 1408 aerofoil. An attempt was made to use this simple three-dimensional wing with a jet model to investigate jet/wing interactions. Problems were encountered, however, with the specification of an inlet boundary condition within the solution domain, i.e. not at its extremities. As a result of these difficulties, no further development work was carried out on the wing CFD model. It was subsequently disclosed that there was a bug in the PHOENICS software which prevented the correct specification of inlet boundary conditions within the solution domain. The bug was corrected in Version 2.2 of the software, however, by this stage time was short and attempts at modelling jet/wing interactions had been abandoned.

6.4 Round free jet

In his recommendations for future work, BRAY, 1992 suggested that work on the modelling of underexpanded free jets should be carried out with an aim to determining the ability of PHOENICS to handle supersonic flow. This fitted in well with the requirements of this project to look at underexpanded jets in cross-flow. The modelling of a round free jet was used as a precursor to later jet in cross-flow work. Simulations were run for varying NPRs (1.5, 2.0, 3.0 and 4.0) and nozzle diameters (36.73 mm, 25.40 mm, 20.74 mm and 17.96 mm respectively). These corresponded to the NPRs and diameters used on the wind tunnel model. The q1 file for an NPR of 1.5 is given in Appendix E, Section E2. In addition, tests at NPRs of 1.25 and 2.68 were made, to enable comparisons with the experimental data of DONALDSON & SNEDEKER, 1971.

6.4.1 Computational grid

Initial attempts at modelling a round free jet were made using a body fitted grid which distorted from an axisymmetric grid in the centre around the jet, to a rectangular outer boundary. Although a suitable grid was created, serious convergence problems occurred and a solution using a turbulence model was never generated. This was attributed to the very skewed cells surrounding the jet, which were a consequence of using the body fitted grid structure, and the very high velocity gradients in this area of the domain. Similar problems were encountered by MATSON, 1993. Consultations with user-support at CHAM failed to resolve the problem and all further use of a body fitted grid for this purpose was abandoned.

In light of this problem, it was decided to approximate the round jet onto a Cartesian grid structure, a technique used by other researchers when modelling round jets in cross-flows (for example INCE *et al.*, 1993). The final grid used is shown in Figure 6.5. Only half of the jet and surrounding domain was modelled since symmetry was imposed. The grid consisted of 24 cells in the x-direction, 88 cells in the y-direction and 60 cells in the z-direction and had dimensions of 0.5 m, 2.0 m and 1.5 m in these directions. This corresponded approximately to the dimensions of the working section of the open-jet wind tunnel used in the experimental work. The half-jet was approximated onto a uniform grid of 32 cells, 4 in the x-direction and eight in the y-direction (Figure 6.6). The grid density was reduced as the distance from the jet origin increased using a power law, such that the first cell away from the jet was the same width as those defining the jet. For the six NPRs tested, the nozzle diameters and grid expansion powers were as follows (Equation 6.1 explains the use of b_x etc.).

***Table 6.1** - Nozzle diameters and grid expansion powers used in the modelling of a free jet.*

NPR	d_n *(m)*	b_x	b_y	b_z
1.25, 1.5	0.03673	1.476	1.454	1.414
2.0, 2.68	0.02540	1.680	1.556	1.504
3.0	0.02074	1.749	1.612	1.554
4.0	0.01796	1.798	1.651	1.589

6.4.2 Flow conditions

The simulation was steady-state (STEADY=T), elliptic in nature (PARAB=F) and used the k-ε turbulence model (TURMOD=KEMODL). It involved changes in temperature, density and viscosity and these had to be taken into account within the model. Variations in static temperature are given by the equation

$$T = T_0 - \frac{V^2}{2c_p} \tag{6.4}$$

which was activated by use of the PIL command TMP1=GRND5. This invoked the equation

$$\texttt{TMP1}=(\texttt{TMP1A}-0.5(\texttt{U1}^2+\texttt{V1}^2+\texttt{W1}^2))/\texttt{TMP1B} \tag{6.5}$$

where TMP1A = c_pT_0 and TMP1B = c_p.

Changes in density were accounted for by the ideal gas law using RHO1=GRND5 which is given by the perfect gas equation:

$$\rho=\frac{p}{RT} \tag{6.6}$$

Again this has its associated PHOENICS equation

$$\texttt{RHO1}=\texttt{RHO1B}\times(\texttt{PRESS0}+\texttt{P1})/\texttt{TMP1} \tag{6.7}$$

The user is required to provide the parameter RHO1B which was set equal to $1/R$ for this work.

Finally, variations in viscosity were determined by Sutherland's Law

$$\mu=1.458\times10^{-6}\frac{T^{1.5}}{T+110.4} \tag{6.8}$$

which was set in PHOENICS by the statement ENUL=GRND6. In PHOENICS Equation 6.8 has the form

$$\texttt{ENUL}=(\texttt{ENULA}\times\texttt{TMP1}^{1.5}/(\texttt{TMP1}+\texttt{ENULB})/\texttt{RHO1} \tag{6.9}$$

where the parameters ENULA and ENULB correspond to the values 1.458×10^{-6} and 110.4 respectively.

The initial source of turbulent kinetic energy was as given in Equation 6.2, however, for these jet calculations it was based on jet exit velocity. The initial source of dissipation rate was again suggested by CHAM, and for high-speed jet flows is given by Equation 6.10:

$$\varepsilon=\frac{3}{7}\frac{k^{1.5}}{d_n} \tag{6.10}$$

6.4.3 Boundary conditions

Boundary conditions were specified for five of the six sides of the domain (north, south, high, low and west), the remaining side (east) was left as friction-less surface (plane of symmetry). The details are given below.

High - Jet

- A uniform source of mass flow rate per unit area.
- A uniform source of jet exit velocity.

- A uniform source of turbulent kinetic energy, (Tu = 3 percent).
- A uniform source of dissipation rate of turbulent kinetic energy.

The remainder of the high boundary was set as a friction surface to simulate a flat plate or fuselage underside.

Low

- This was set to a friction wall to simulate the laboratory floor.

South

- A fixed pressure of zero relative to ambient pressure.
- The remaining flow variables were left unspecified*.

North

- A fixed pressure of zero relative to ambient pressure.
- The remaining flow variables were left unspecified*.

West

- A fixed pressure of zero relative to ambient pressure.
- The remaining flow variables were left unspecified*.

6.4.4 Results

Tests were run for the six pressure ratios mentioned above. Figure 6.7 shows a typical vector plot through the centre-line of the jet. This clearly shows the entrainment flow-field created by the turbulent mixing of the free jet with ambient air and the associated jet spreading. Each run took approximately 7 days on the AXIL 420 machine. This was the only available computer with sufficient memory to run these calculations.

6.4.4.1 Velocity profiles in a subcritical jet

The development of a subcritical pressure ratio free jet, in this case an NPR of 1.25, is shown in detail in Figure 6.8. This is a graph of jet centre-line velocity, w normalised with local peak velocity, w_{max} against radial distance, r normalised with the jet's local half width, $y_{1/2}$. The graph shows the decay of the exit velocity profile as downstream distance, z is increased. The jet does not exhibit self-similarity in the outer half of the jet (i.e. $y > y_{1/2}$) until approximately 20 nozzle diameters below the jet exit in contrast to BRAY, 1992 and MYSZKO, 1997 who quote values of 7.32 d_n (for an NPR of 1.25) and 6.0 d_n (for an NPR of 1.05) respectively. However, the

* *See the downstream boundary condition in section 6.3.3.*

inner half of the jet does appear to exhibit self similarity within these distances. The differences may be due to the fact that the free jet velocity profiles calculated by the PHOENICS models of BRAY, 1992 and MYSZKO, 1997 are actually impinging jet models with the jet at a maximum height of 10 d_n above the ground plane. It may be that the presence of the ground plane is causing a premature development of the jet in these cases. In contrast, the ground plane specified in the author's PHOENICS free jet model is over 40 nozzle diameters below the nozzle exit plane.

Figures 6.9, 6.10 and 6.11 show the PHOENICS predicted velocity profiles at three non-dimensional distances downstream from the nozzle exit. The results are compared with those from the experiments of DONALDSON & SNEDEKER, 1971.

Very close to the nozzle exit (z/d_n = 1.96) the profiles are in good agreement (Figure 6.9). The experimental results show that there is a jet potential core present with a width of approximately 0.55 $y_{1/2}$. The numerical results predict a potential core of approximately 0.5 $y_{1/2}$. The numerically predicted jet width is, however, much larger than the experimental value (2.1 $y_{1/2}$ compared with 1.7 $y_{1/2}$). This is an overprediction of 23 percent and is a well-documented characteristic of the k-ε turbulence model when used for round jet flows (see for example WILCOX, 1994).

Slightly further downstream from the nozzle exit at z/d_n = 3.92, the experimental core width has reduced to approximately 0.3 $y_{1/2}$, although this is only an estimate due to the limited number of data points available in this region. The potential core in the numerical results has also reduced and is slightly less than the experimental results at approximately 0.25 $y_{1/2}$. Again the overall jet width is overpredicted by the k-ε turbulence model at around 2.7 $y_{1/2}$ compared with an experimental value of 2.0 $y_{1/2}$ (Figure 6.10).

Concerning the fully developed profiles (Figure 6.11), which experimentally occurred at downstream distances of 7.32 d_n and higher, there is very good agreement between these and the numerical results. The k-ε model predicts a slightly wider jet than experimental work would suggest. The overprediction of round jet width by the k-ε model are a well documented characteristic of this turbulence model and are discussed in more detail in Section 6.4.4.5 below.

In general the k-ε-predicted velocity profiles were very encouraging and showed better agreement with the experimental results than the numerical work of BRAY, 1992 despite his more accurate representation of the nozzle exit geometry (round rather than stepped). No investigation of the effect of initial jet turbulence intensity on the velocity profiles was performed since this had already been covered previously by BRAY, 1992.

6.4.4.2 Velocity profiles in an underexpanded jet

The development of an underexpanded free jet at an NPR of 2.68 is shown in Figure 6.12. Self-similarity in the outer part of the jet is not completely achieved until approximately 40 nozzle diameters downstream of the nozzle exit, although in the inner half of the jet it is achieved within 10 diameters. Figures 6.13, 6.14 and 6.15 show normalised velocity profiles for this particular pressure ratio, compared with the experimental data of DONALDSON & SNEDEKER, 1971.

At a downstream distance of z/d_n = 1.96, the velocity profiles are quite dissimilar (Figure 6.13). The experimental data show an inverted velocity profile which is consistent with the expansion of the jet after exiting the nozzle. The overall jet width is quite small at 1.4 $y_{1/2}$. The numerically-predicted velocity profile is very similar in shape to that of the subsonic jet. There is no indication of an inverted profile at this axial distance. Examination of the numerical data confirms that there is a slight inverted profile immediately after the nozzle exit (with a 3 percent centre-line velocity deficit) but this rapidly disappears as downstream distance is increased. The numerically predicted jet width at this point is excessively overpredicted.

Further downstream from the nozzle exit at z/d_n = 3.92, the results agree a little better but there is still excessive overprediction of the jet width (Figure 6.14). The experimental velocity profile is now more akin to that predicted numerically at z/d_n = 1.96. This suggests that the numerical model is predicting too rapid a centre-line velocity decay. This is confirmed in Section 6.4.4.3 below.

The self-similar profiles show good agreement (Figure 6.15) although not quite as well as the subsonic jet case. Unfortunately, the experimental data do not cover the outer jet region and so comparison with the numerical data in this region is not possible.

With nozzle pressure ratios of 1.5, 2.0, 3.0 and 4.0, the predicted velocity profiles were very similar to those described above. The only difference being the downstream distance required to achieve self-similarity. This is linked to the decay rate of the particular jet in question. Even at an NPR of 4.0, there was little evidence of the inverted velocity profile observed experimentally by DONALDSON & SNEDEKER, 1971.

6.4.4.3 Centre-line velocity decay

In Figure 6.16, non-dimensional jet centre-line velocity, w/w_n has been plotted against non-dimensional axial distance z/d_n downstream from the nozzle exit. Considering first the subsonic velocity decay (NPR = 1.25), the numerical results show an underprediction in the length of the jet potential core by approximately 35 percent and a higher decay rate. This is attributed to the turbulence intensity, Tu of the numerical jet which is probably higher than the turbulence intensity in the DONALDSON & SNEDEKER jet. With numerical modelling, it has been shown in the

past (BRAY, 1992 and MYSZKO, 1997) that the initial turbulence intensity, *Tu* specified for the jet has a strong influence on the potential core length and subsequent decay rate of a free jet. Unfortunately, the turbulence intensity for the jet used in the experimental work is not known, but these results would suggest that it is less than the three percent specified in the numerical model.

For the moderately underexpanded jet (NPR = 2.68), the effects of underexpansion are at once apparent. Both experimental and numerical results indicate a supersonic jet potential core. However, the results are in poor agreement with each other. The numerical results show a much more rapid expansion of the jet after exit from the nozzle. This is consistent with the differences observed in the velocity profiles discussed above. As with the subsonic jet, the potential core is much shorter than measured experimentally. Again this is attributed to the higher jet turbulence intensity. In addition, PHOENICS has the tendency to smear shocks. This will increase the dissipation of turbulence energy in the early part of the jet development. This is discussed in more detail below along with other shortcomings of the k-ε turbulence model.

The three data points which make up the experimental jet potential core are insufficient to isolate any form of shock structure. The numerical results also fail to show evidence of a shock system with the exception of the slight drop in centre-line axial velocity at z/d_n of approximately 1. It was felt that the grid density near the nozzle exit was sufficiently fine to capture shock effects, however the shock structure appears to be smeared. SMITH, 1996 reported similar difficulties. He attributed the problem to the first order upwind numerical solver used by PHOENICS. The shocks were smeared as a result of numerical diffusion. SMITH'S own software, PLUME based on PHOENICS, implemented a higher order numerical scheme which improved shock capture capabilities. Details of the scheme were not disclosed.

6.4.4.4 Free jet spreading rate

The spreading rate of a free jet is defined as the slope of the curve defining the change of $y_{1/2}$ with downstream distance from the nozzle exit plane and is shown in Figure 6.17. The graph shows the k-ε predicted spreading rate for an NPR of 1.25 as well as the spreading rates for DONALDSON & SNEDEKER'S experiments at NPRs of 1.25 and 2.68.

For the subsonic jet (NPR = 1.25), the k-ε model gives a constant spreading rate of approximately 0.1. For the same pressure ratio, DONALDSON & SNEDEKER, 1971 measured an initially lower spreading rate, up to $z/d_n = 24$, after which the spreading rate increased slightly. No explanation was given for this increase in spreading rate. WILCOX, 1994 quotes experimentally-measured values of between 0.086 and 0.095 for an incompressible jet. Clearly the k-ε model over-predicts the spreading

rate for an incompressible jet and this is well documented by many other researchers e.g. POPE, 1978 and RODI, 1984.

With regard to the underexpanded jet, the k-ε model predicted the same spreading rate as for the lower NPR jet to the extent that the two curves were indistinguishable. Examination of the other numerically-predicted free jet data for NPRs of 1.5, 2.0, 3.0 and 4.0 showed that the spreading rate was independent of nozzle pressure ratio. DONALDSON & SNEDEKER, 1971, however, measured a greater spreading rate for the NPR 2.68 jet than the NPR 1.25 jet. The accuracy of their data has to be questioned since there is strong evidence in recent years that this is not the case. PAPAMOSCHOU & ROSHKO, 1988, for example, have conducted experimental measurements which predict a lower spreading rate as NPR is increased.

6.4.4.5 Comments on the k-ε turbulence model

Over the years, corrections to the k-ε model have been proposed by some researchers to try to improve the prediction of a round free jet e.g. POPE, 1978 and RODI, 1972. The corrections apply empirically-derived modifications to the ε equation to compensate for the observed discrepancies in spreading rate. The corrections, however, are only applicable to incompressible round jet flows and should be used with caution. WILCOX, 1994, comments that the POPE correction has an adverse effect on the prediction of wall jets. MYSZKO, 1997 found similar problems when using the RODI correction. However good these corrections are at modifying the free jet flowfield, their application to other types of fluid flow cannot be endorsed. They should, therefore, be treated with caution.

More recently, ROBINSON *et al.*, 1995 proposed a unified turbulence model for incompressible shear flows. The turbulence model, which is called k-ζ (enstrophy), has a new equation for the dissipation rate of turbulent kinetic energy. It is shown that one set of constants reproduces growth rates and similarity profiles of velocity and shear stress for plane jets, round jets and wall jets. In general, agreement was well within the scatter of experimental data. Such a turbulence model is not currently available within PHOENICS.

Experimentally, it has been observed by PAPAMOSCHOU & ROSHKO, 1988 that the spreading rates of high speed shear layers and jets, in which compressibility effects are important, is less than those of incompressible shear layers. These researchers also observed that the spreading rate starts to reduce at Mach numbers of around 0.5, well before the onset of supersonic flow.

Using direct numerical simulations of turbulent shear flow, SARKAR, 1995 established that the reduced spreading rate was due to the 'stabilising' influence of compressibility in the high-speed regime. This was due to the reduced efficiency of turbulence production. In the free jet modelling work undertaken in this project, a re-

duction in free jet spreading rate was not observed using the standard k-ε model. Indeed, the spreading rate was found to be independent of NPR. The reason for this is that although the standard k-ε model includes variations in density, there are no explicit terms to account for compressibility [SARKAR & LAKSHMANAN, 1991]. These researchers proposed an additional compressibility term in the dissipation equation. The model is based on a low Mach number analysis of the compressible Navier-Stokes equations and was calibrated using direct numerical simulations of compressible isotropic turbulence. The implementation of the model showed much improved agreement with experimental data over the k-ε model.

Application of some or all of the theories described above was beyond the scope of this work and could form the basis of an entire research project in itself. It has been demonstrated, however, that the apparently simple task of modelling a compressible, turbulent, round jet is far from easy. Indeed it has kept numerous researchers occupied for many years and only now with the advent of direct numerical simulation are accurate solutions to the problem emerging.

6.5 Round jet in cross-flow

As a natural progression from the modelling of a free jet, it was a relatively simple procedure to add a cross-flow boundary condition to one face of the cuboid domain (in contrast to the polar cylindrical grid used by BRAY, 1992, WILSON, 1995 and MYSZKO, 1997). There were two main aims to the jet in cross-flow work. Firstly, the results would provide some idea of the likely flow-field surrounding the underside of the fuselage of the wind tunnel model, which is flat. This has been found to be useful in explaining some of the observed interference effects on the wind tunnel model. Secondly, the results have been compared with experimentally-derived trajectories for both subsonic and supersonic jets in cross-flow. An example of a jet in cross-flow q1 file is given in Appendix E, Section E.3.

6.5.1 Computational grid

The grids used for jet in cross-flow modelling were identical to those used with the free jet described in Section 6.4.1. This maintained some consistency between the two sets of computational runs. Again, there were four different grids, one for each of the four different nozzle sizes (36.73 mm, 25.40 mm, 20.74 mm and 17.96 mm) and associated pressure ratios (1.5, 2.0, 3.0 and 4.0). The power exponents, used to determine the non-uniformity of the grid spacing, were the same as those given in Table 6.1.

6.5.2 Flow conditions

Flow conditions were identical to those used for free jet modelling (see Section 6.4.2). The same techniques were used to take account of variations in density, temperature and viscosity.

6.5.3 Boundary conditions

The boundary conditions were the same as those used for free jet modelling with the exception of the south boundary which was redefined as a momentum source, having the following properties:

- a uniform source of mass flow rate per unit area;
- a uniform source of velocity;
- a uniform source of turbulent kinetic energy;
- a uniform source of dissipation rate.

6.5.4 Results

Calculations were performed for four NPRs (1.5, 2.0, 3.0 and 4.0), four cross-flow velocities (10 ms^{-1}, 20 ms^{-1}, 30 ms^{-1} and 40 ms^{-1}) and two vector angles (60 degrees and 90 degrees). This gave a total of 32 cases which are summarised in Table 6.2 below. Run times were the same as for the free jet work, approximately 7 days each.

6.5.4.1 Jet trajectories (δ_j = 90 degrees)

The co-ordinates of the jet centre-line, denoted by the locus of maximum velocity, were interpolated from velocity and co-ordinate data in the PHOENICS results files. Figure 6.18 compares the numerically-predicted subsonic jet trajectories with the empirical correlation of FEARN & WESTON, 1978. In general, the jet trajectories agree reasonably well (considering the variation between different correlations - see Figure 6.22, discussed later). At the very low velocity ratio of 0.038, PHOENICS predicts too much jet deflection. As the velocity ratio is increased to 0.075, the agreement is better, but as the velocity ratio is increased further, the numerical model under-predicts the jet deflection. The reason for this is believed to be a combination of two effects. At low cross-flow velocities, the deflection of the jet is thought to be dominated by the viscous mixing of the jet with the freestream in much the same way as for a free jet. As already mentioned, the k-ε model overpredicts the spreading rate of a free jet. This increased viscous mixing is responsible for the over-prediction of jet deflection at low velocity ratios.

***Table 6.2** - Test matrix for jet in cross-flow numerical modelling*

NPR	V_∞	V_e	δ_j
1.5	10.0	0.038	60, 90
1.5	20.0	0.075	60, 90
1.5	30.0	0.113	60, 90
1.5	40.0	0.150	60, 90
2.0	10.0	0.029	60, 90
2.0	20.0	0.057	60, 90
2.0	30.0	0.086	60, 90
2.0	40.0	0.114	60, 90
3.0	10.0	0.023	60, 90
3.0	20.0	0.047	60, 90
3.0	30.0	0.070	60, 90
3.0	40.0	0.093	60, 90
4.0	10.0	0.020	60, 90
4.0	20.0	0.040	60, 90
4.0	30.0	0.061	60, 90
4.0	40.0	0.081	60, 90

At relatively high velocity ratios, the jet deflection is dominated by the mixing effect of the contra-rotating vortex pair. It is believed that it is this part of the jet in cross-flow structure which the numerical model is failing to predict sufficiently. This would result in the observed underprediction of the jet deflection as shown in Figure 6.18. Jet trajectories for NPRs of 2.0, 3.0 and 4.0 are shown in Figures 6.19, 6.20 and 6.21 respectively. There is very little change in the observed effects. The jet trajectory is again too low at low velocity ratios and too high at higher velocity ratios. The best agreement with FEARN & WESTON'S data is at a velocity ratio of approximately 0.06. Recalling Equation 2.9, it should be remembered that none of the empirically-derived correlations for the free jet trajectory contain an NPR term, but merely reflect changes in effective velocity ratio.

Figure 6.22 compares the trajectory of one particular jet (NPR 2.0, V_e = 0.057) with several experimentally derived empirical equations. For this particular effective velocity ratio, the numerical model shows very good agreement. Curiously, the numerically-predicted free jet trajectory shows the worst agreement with the correlation of AHMED, 1996. This is the only correlation presented for supersonic jets. The reason for this is thought to be the inability of the k-ε turbulence model to cope with supersonic flow and shock structures mentioned already.

Regarding the contra-rotating vortex pair, Figures 6.23 to 6.26, show velocity contours for three vertical planes through the jet. There is evidence of two vortices, particularly in Figure 6.26, but their size and intensity compared with experimental results is not known. It is the author's belief that the underprediction of jet deflec-

tion is due to inadequacies in the k-ε turbulence model which are failing adequately to define the contra-rotating vortex pair.

6.5.4.2 Jet trajectories (δ_j = 60 degrees)

Figure 6.27 presents the same jet and cross-flow conditions as Figure 6.18 but with the jet vector angle now set at 60 degrees. The trajectories are compared with the empirical correlation of IVANOV, 1963. Similar trends are indicated to those observed with a 90 degree vector angle, i.e. too much deflection at low velocity ratios and too little at higher velocity ratios. Figure 6.28 compares one particular trajectory (NPR 2.0, V_r = 0.057) with the trajectory correlations of three researchers. The agreement is good for this particular velocity ratio. For the remaining 60 degree vector cases the trends were the same and so no further discussion of these results is presented.

6.6 Summary

Numerical modelling work using the PHOENICS CFD code and the k-ε turbulence model has been performed. Results have been obtained for a NACA 1408 aerofoil, a round free jet at subcritical and underexpanded nozzle pressure ratios and a round jet in cross-flow with the same jet conditions. The results generated by the numerical modelling have been compared with available experimental data and showed reasonable agreement within the limitations of the turbulence model used. The following points have been made regarding the numerical modelling work.

- The suction pressures on an aerofoil modelled using the body-fitted co-ordinate system were underpredicted. The sectional lift coefficient, C_l, however, agreed with potential flow theory to within 5 percent.
- The k-ε turbulence model was found to over-predict the spreading rate and hence the centre-line velocity decay of a round free jet. Variations in NPR were found to have no effect on free jet spreading rate.
- PHOENICS tended to smear the shock structure of an underexpanded jet. The near-field velocity profiles showed poor agreement with experimental data.
- The centre-line trajectory of a round jet in cross-flow showed reasonably good agreement with established empirical correlations for the range of velocity ratios tested. The numerical model, however, predicted too much deflection at low velocity ratios and too little at higher ones.
- The results from the round free jet in cross-flow calculations were used in Chapter 4 to support discussion of some of the experimental results.

- The inability to model anything more complicated than an isolated aerofoil or free jet was disappointing. The work to model wing/jet and intake/jet combinations failed to achieve a satisfactory solution for these flow-field problems.

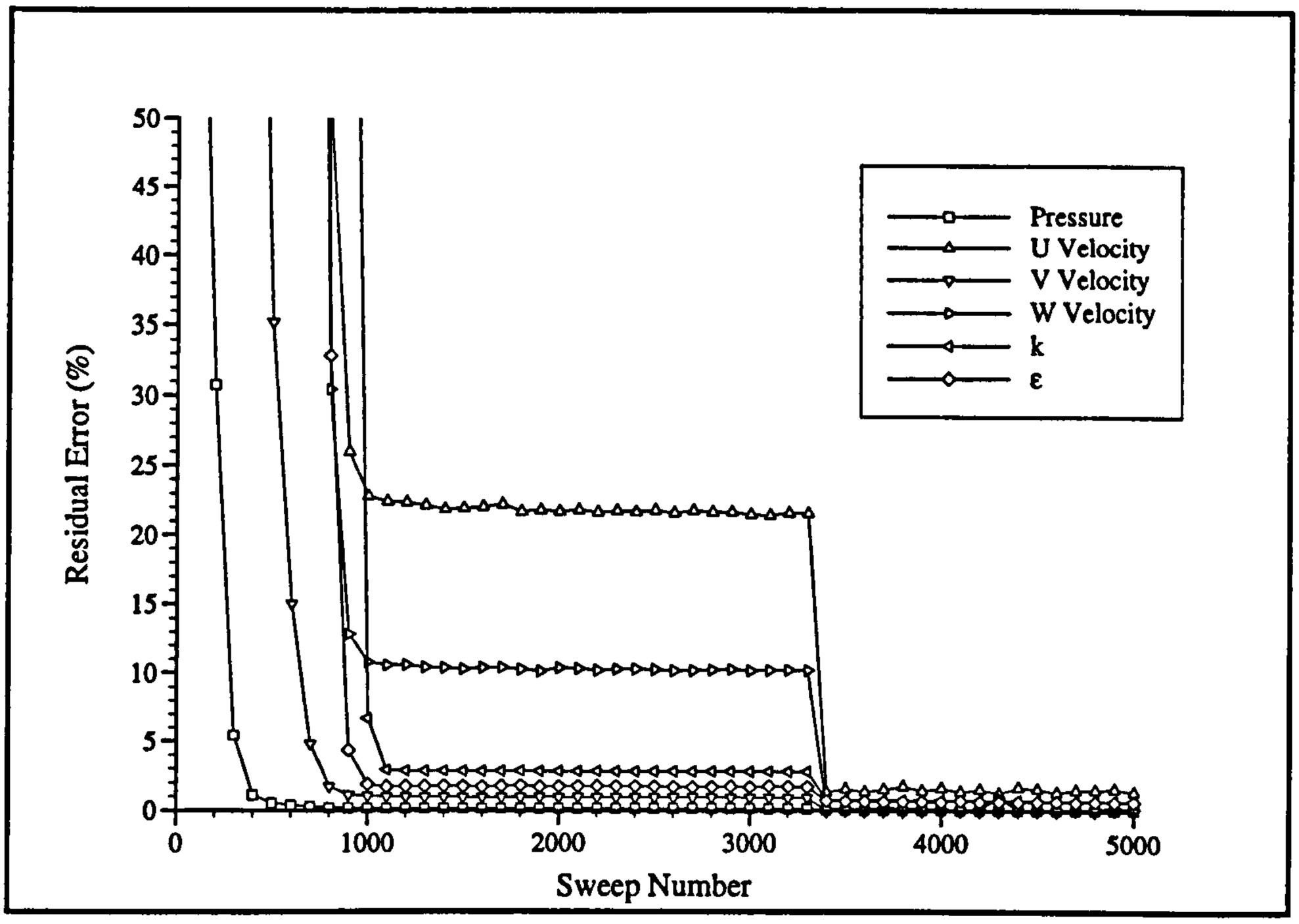

***Figure 6.1** - Typical convergence of k-ε solved variables.*

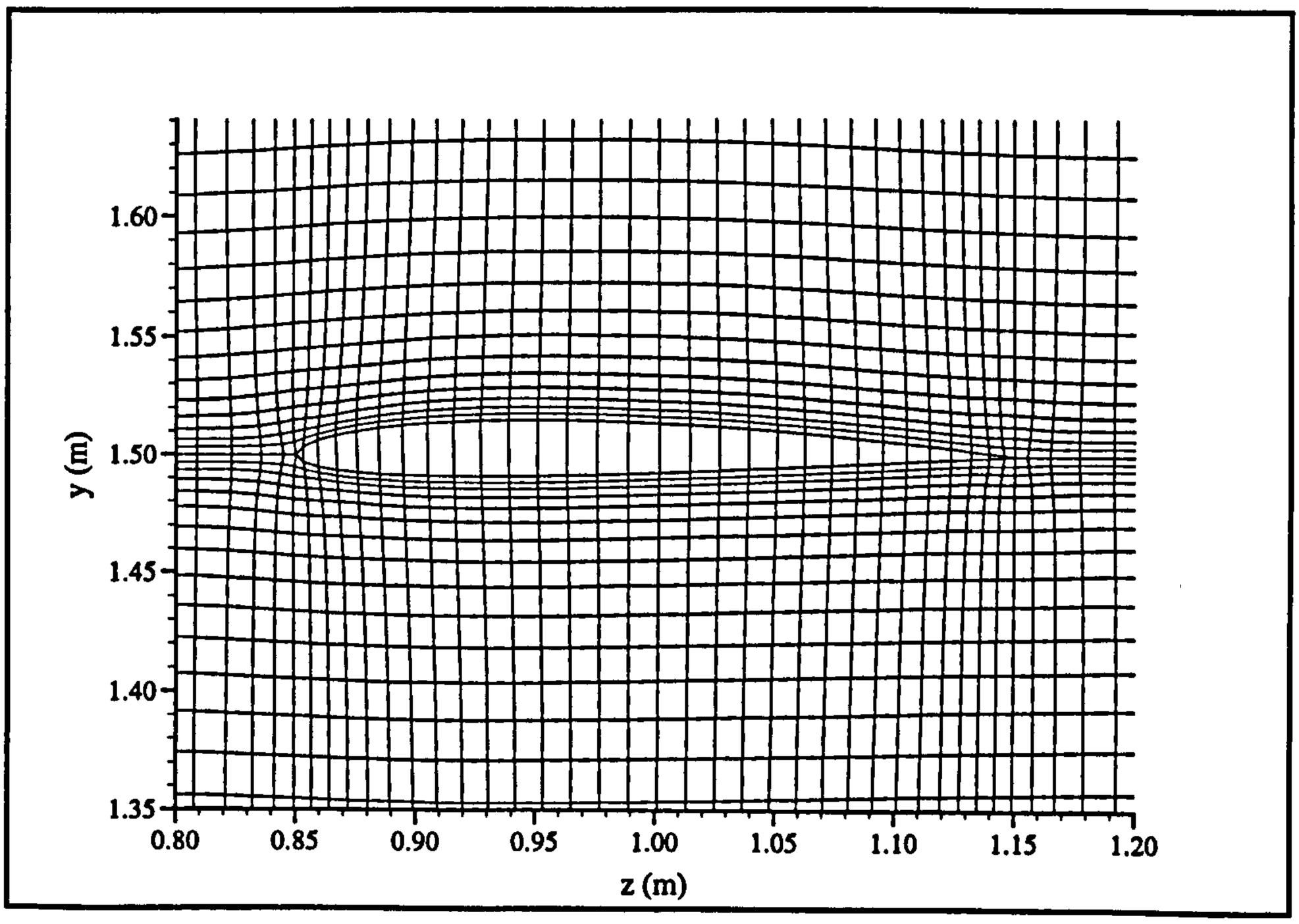

***Figure 6.2** - Body-fitted grid for NACA 1408 aerofoil.*

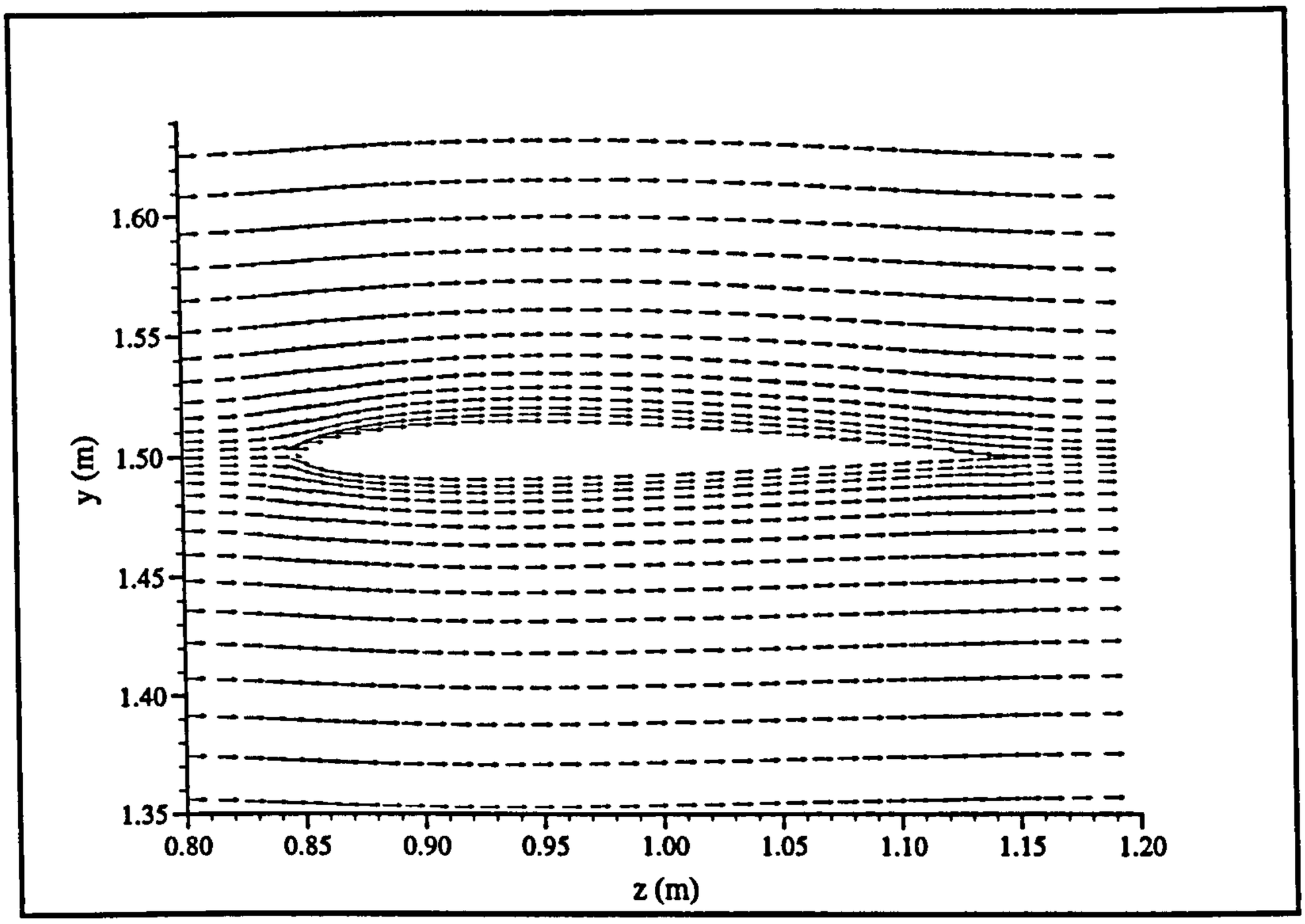

***Figure 6.3** - Typical vector plot for the NACA 1408 aerofoil.*

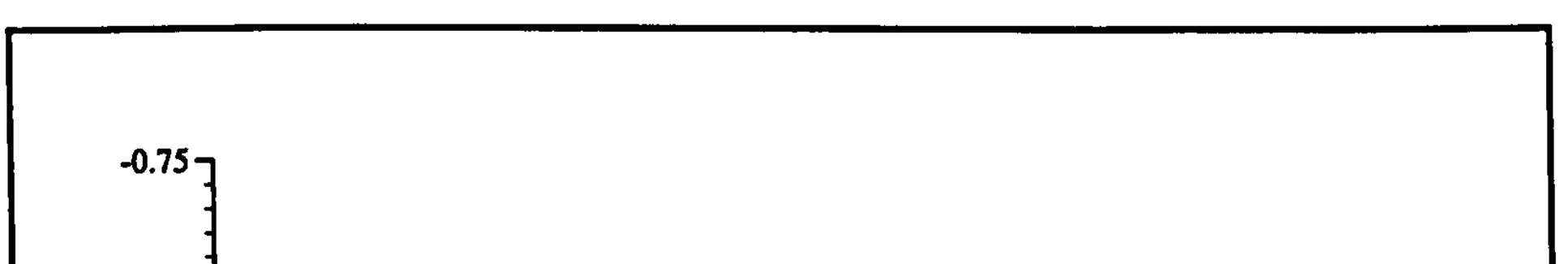

***Figure 6.4** - Comparison of surface pressure distribution on NACA 1408 aerofoil.*

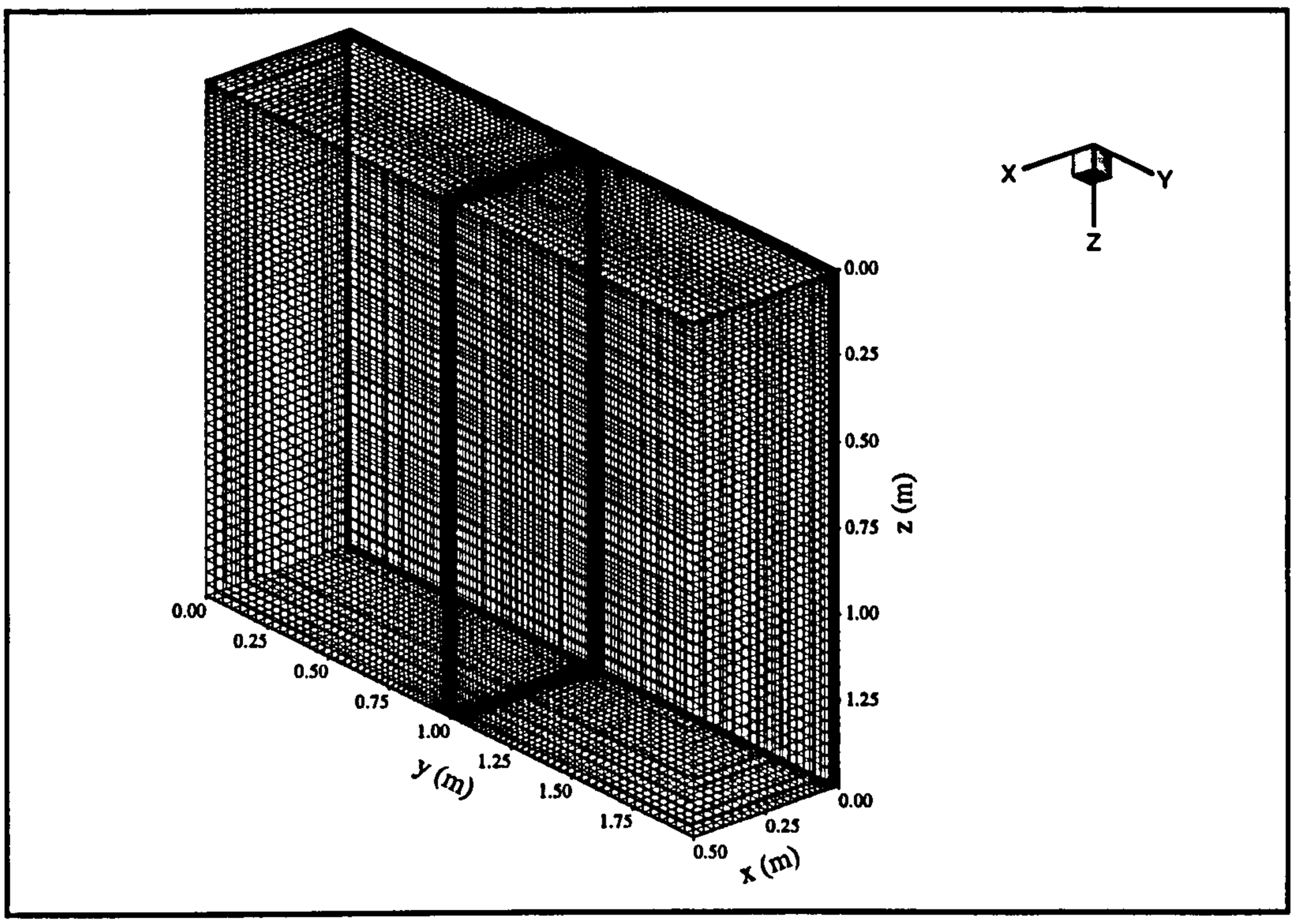

Figure 6.5 *- The Cartesian grid used for free jet and jet in cross-flow modelling.*

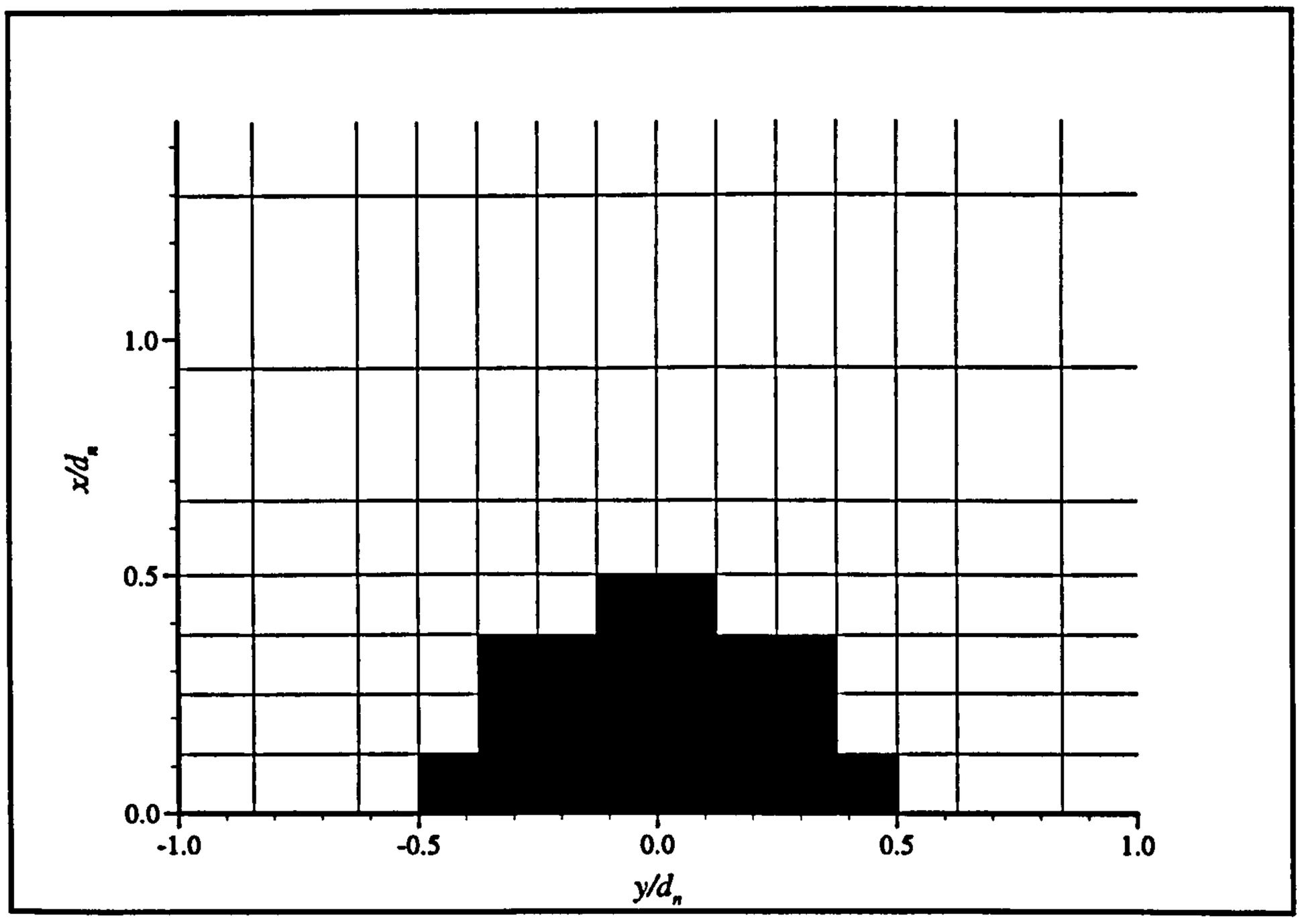

Figure 6.6 *- Close-up of the grid structure around the nozzle exit showing the cells used to approximate the round jet onto a Cartesian grid.*

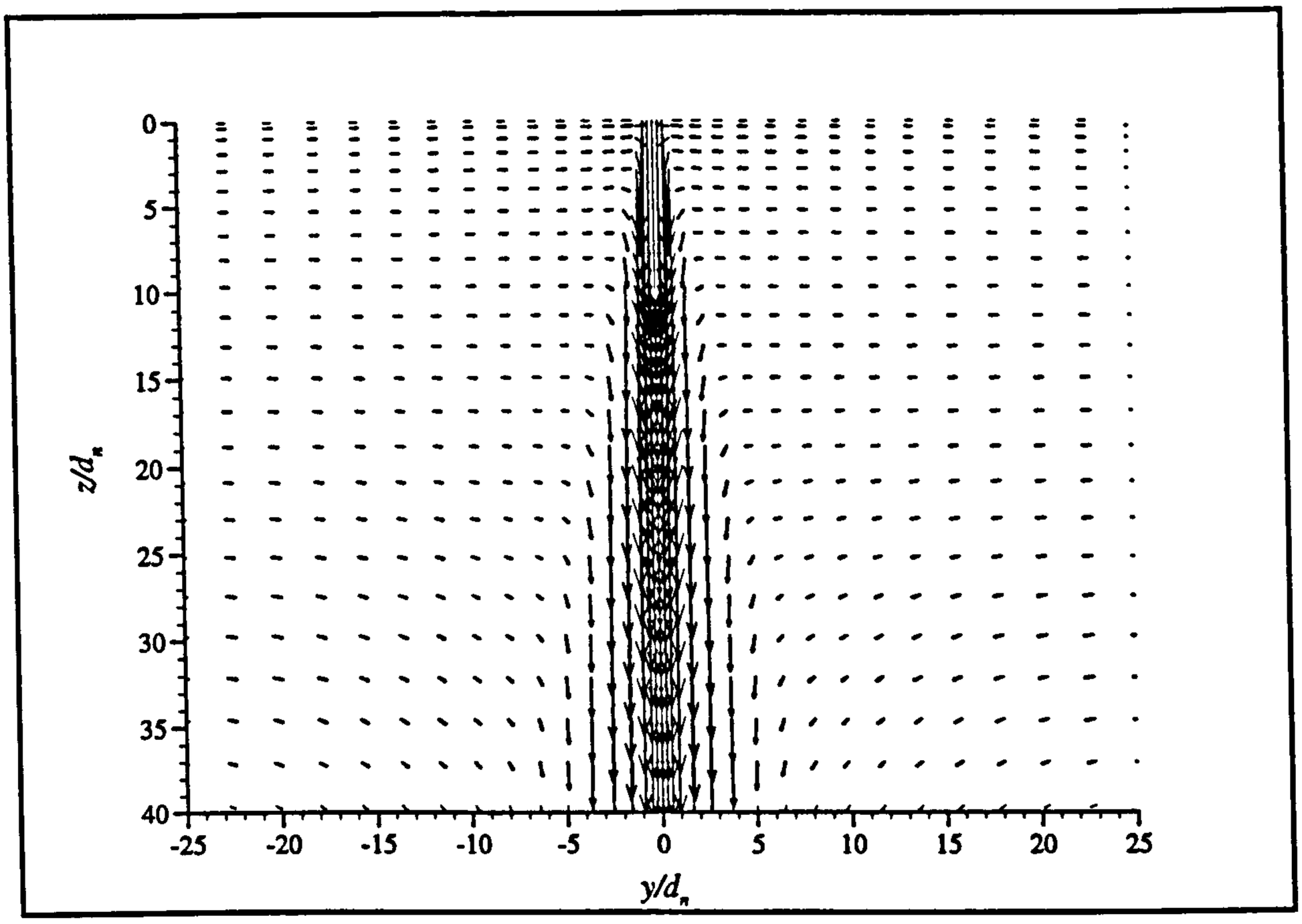

***Figure 6.7** - Typical free jet centre-line velocity vector plot showing entrainment mixing (NPR = 1.25).*

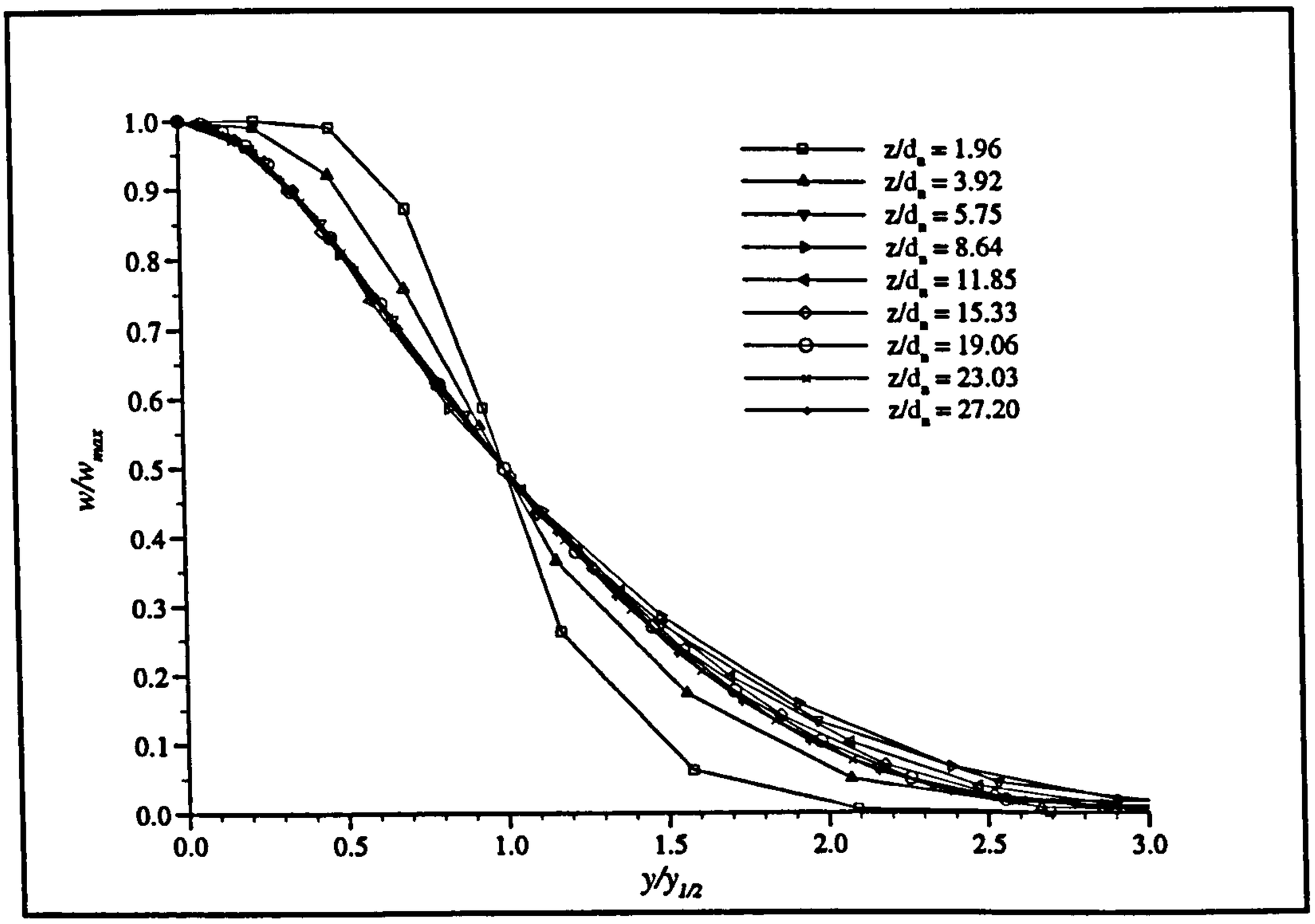

***Figure 6.8** - Selected non-dimensional subsonic free jet velocity profiles, showing the decay of the round jet to a self-similar profile (NPR = 1.25).*

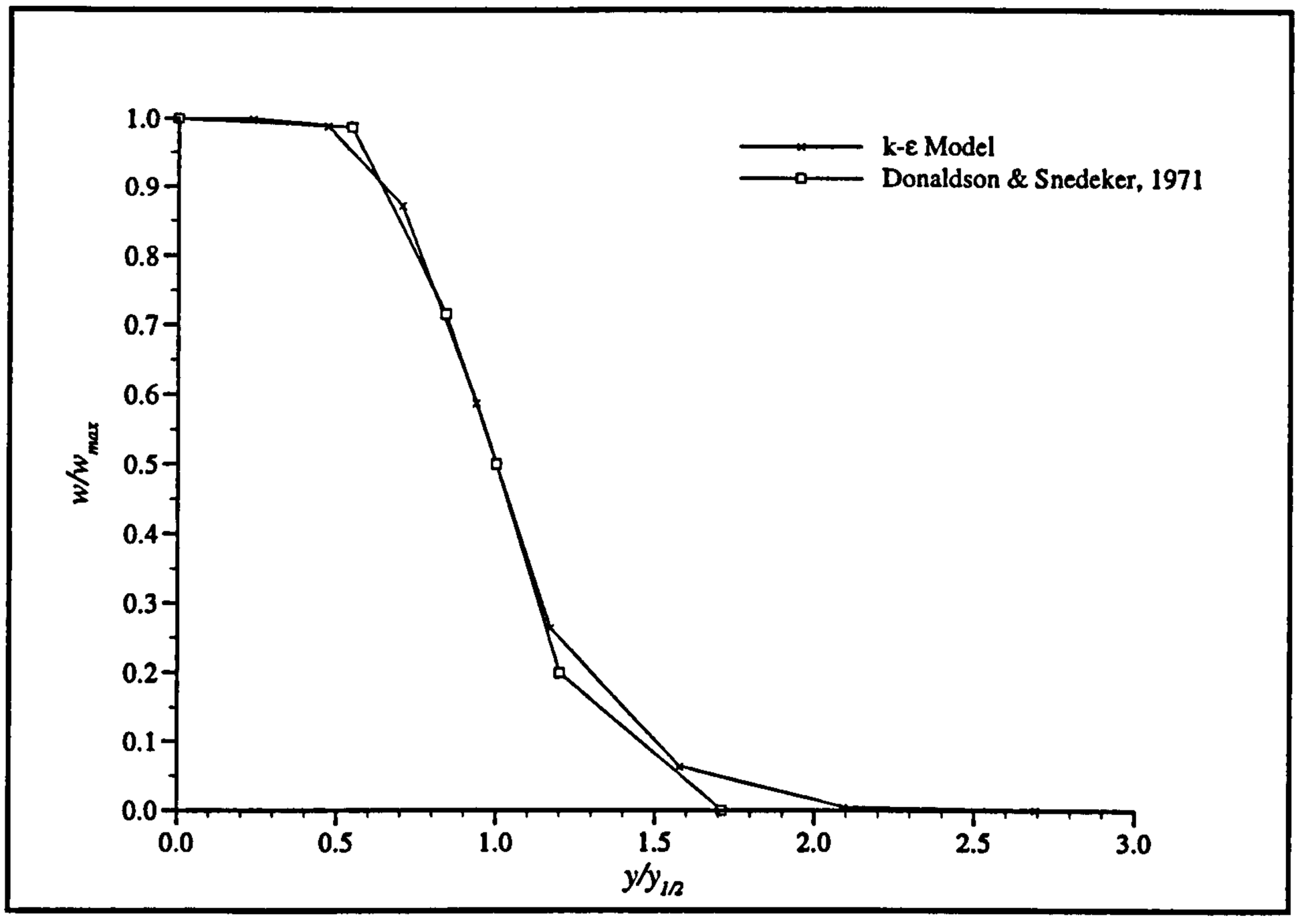

***Figure 6.9** - Normalised subsonic free jet velocity profiles (NPR = 1.25, z/d_n = 1.96).*

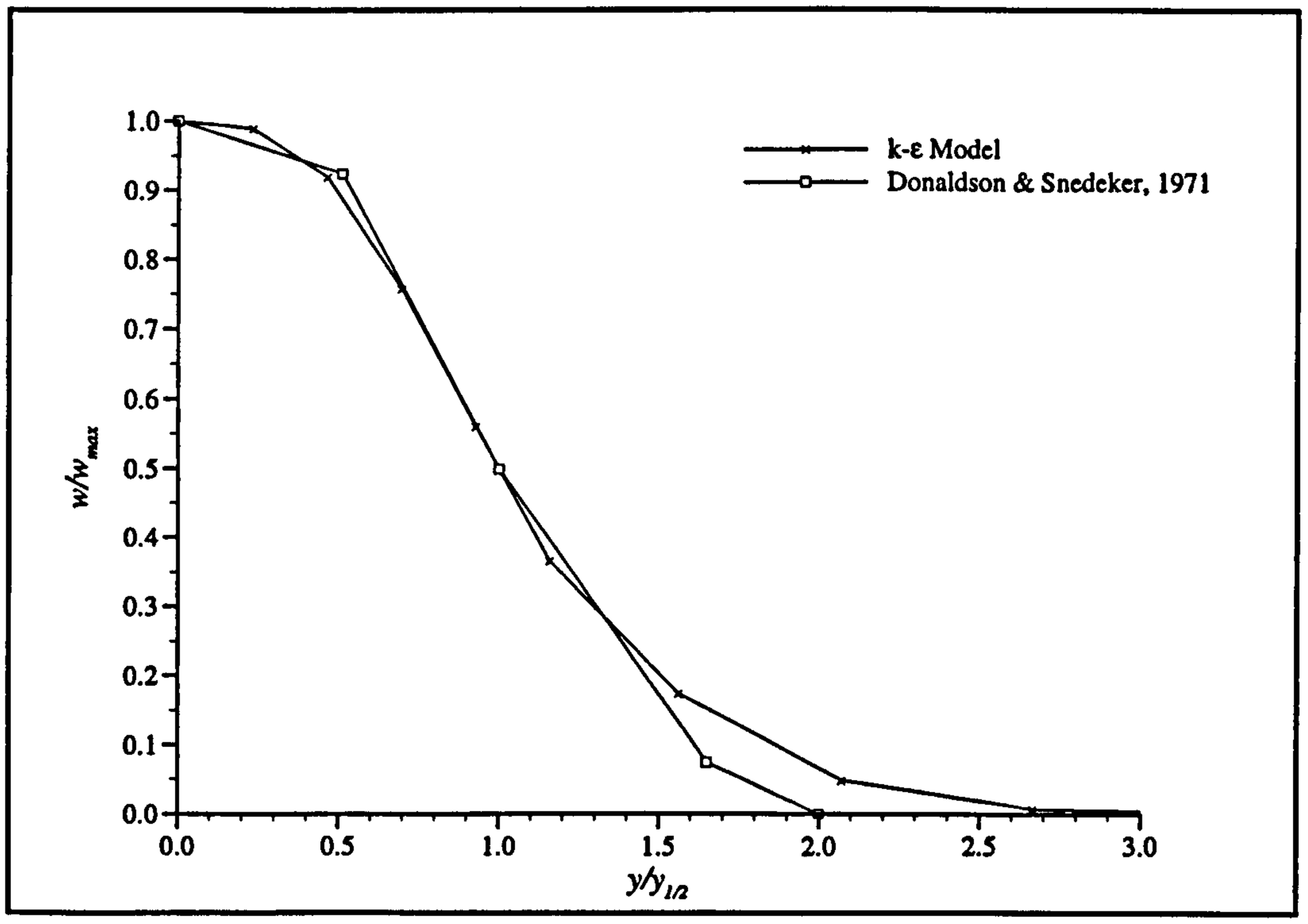

***Figure 6.10** - Normalised subsonic free jet velocity profiles (NPR = 1.25, z/d_n = 3.92).*

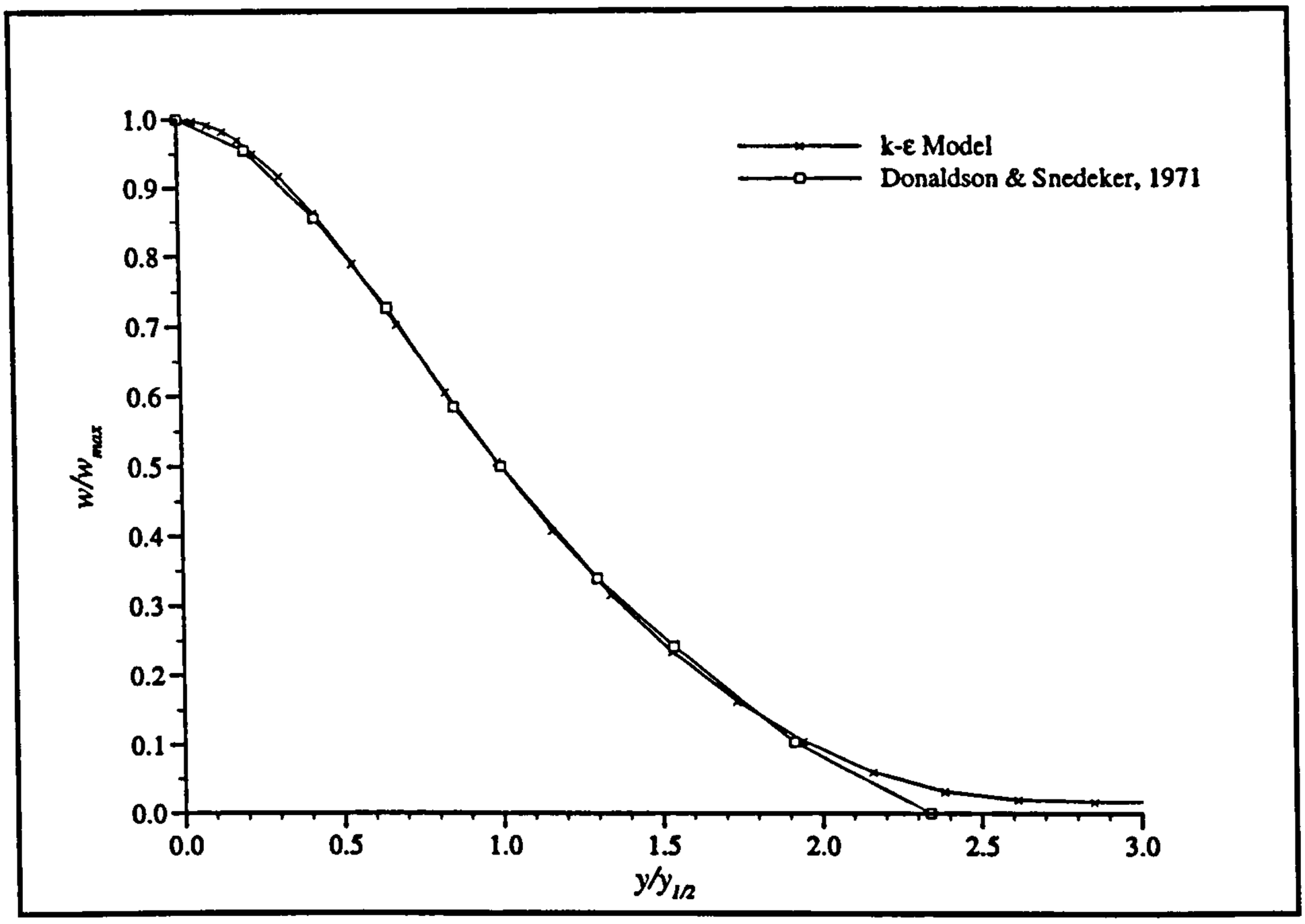

***Figure 6.11** - Normalised subsonic free jet velocity profiles (NPR = 1.25, z/d_n = self similar).*

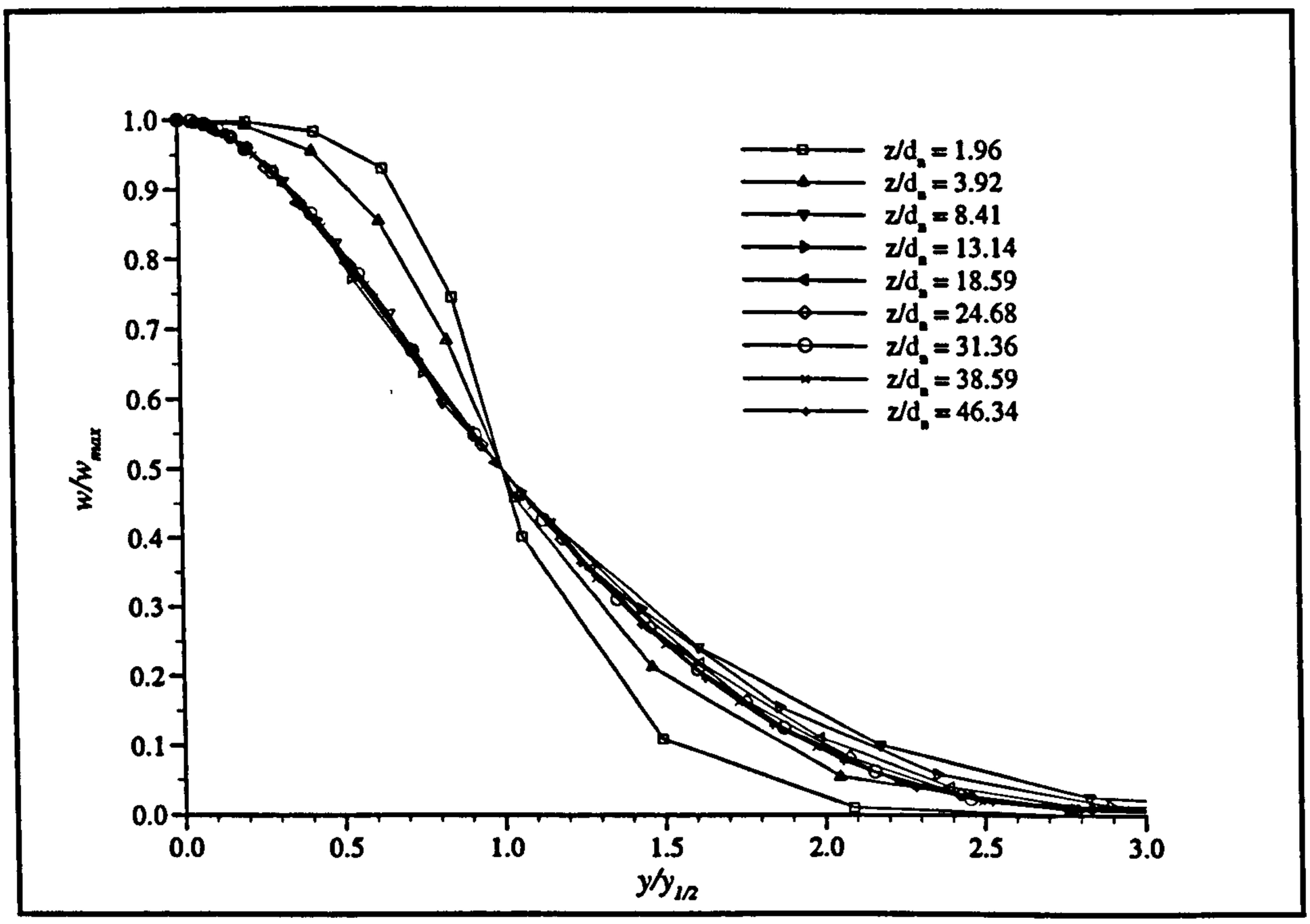

***Figure 6.12** - Selected non-dimensional underexpanded free jet velocity profiles showing the decay of the round jet to a self-similar profile (NPR = 2.68).*

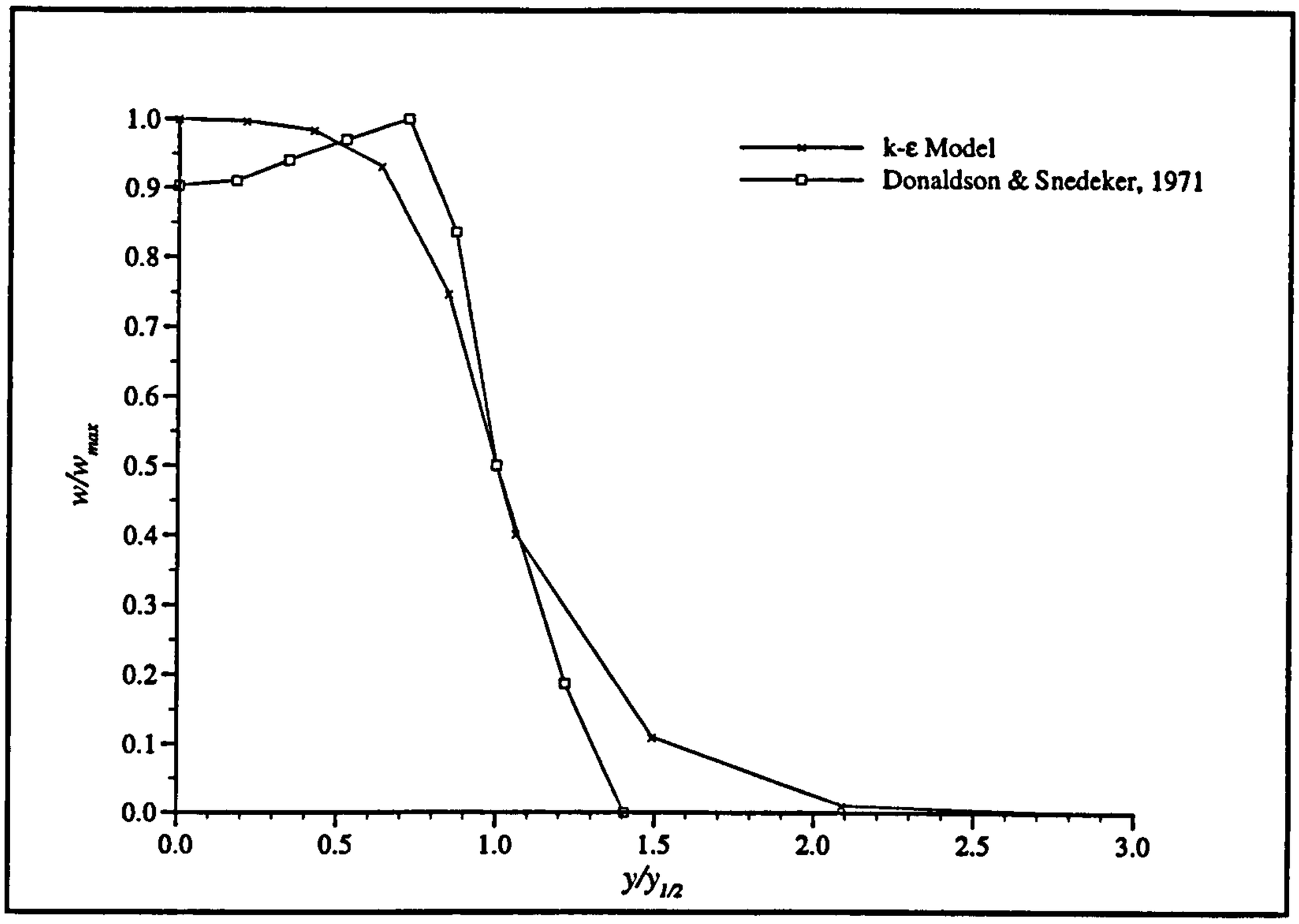

***Figure 6.13** - Normalised underexpanded free jet velocity profiles (NPR = 2.68, z/d_n = 1.96).*

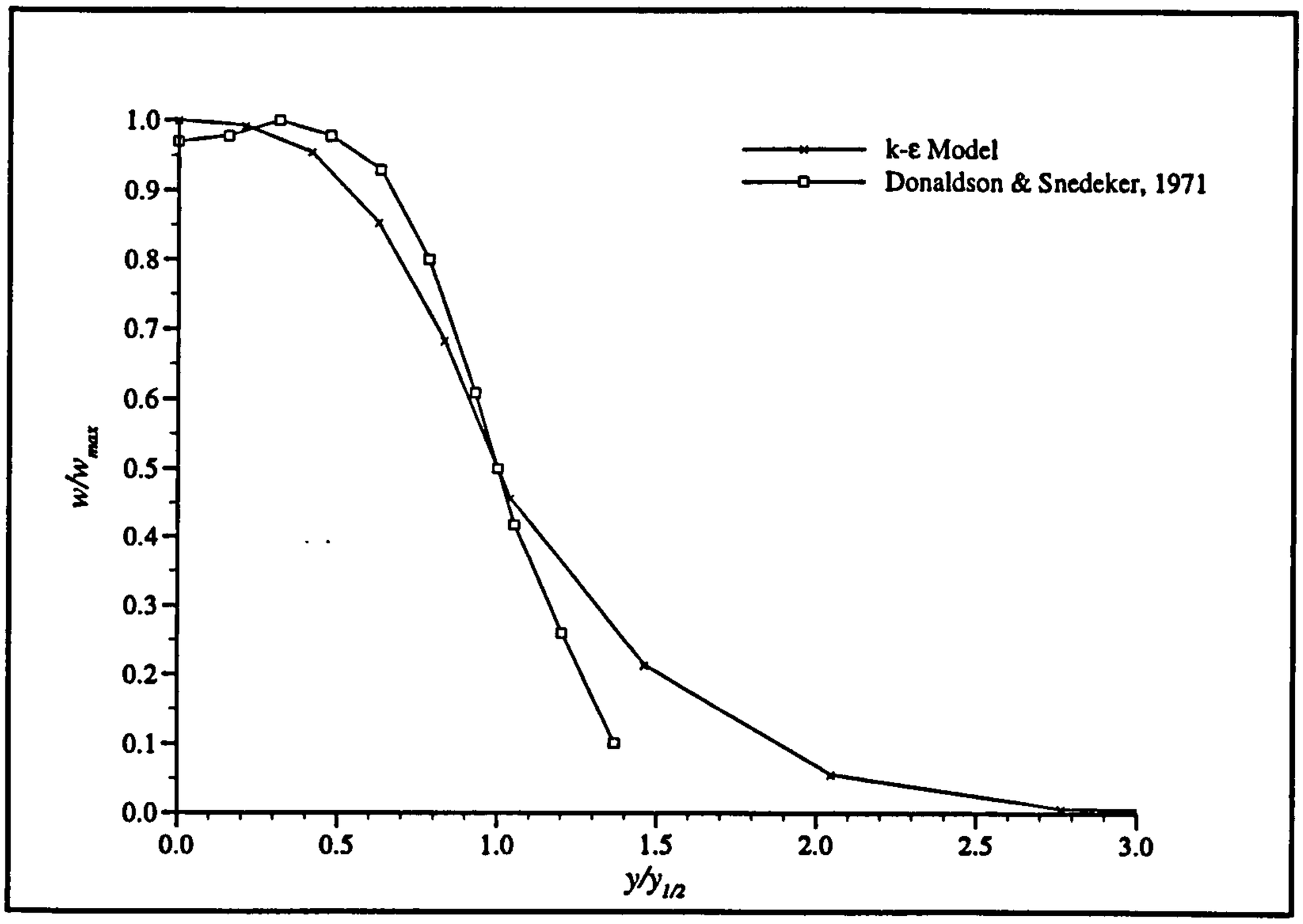

***Figure 6.14** - Normalised underexpanded free jet velocity profiles (NPR = 2.68, z/d_n = 3.92).*

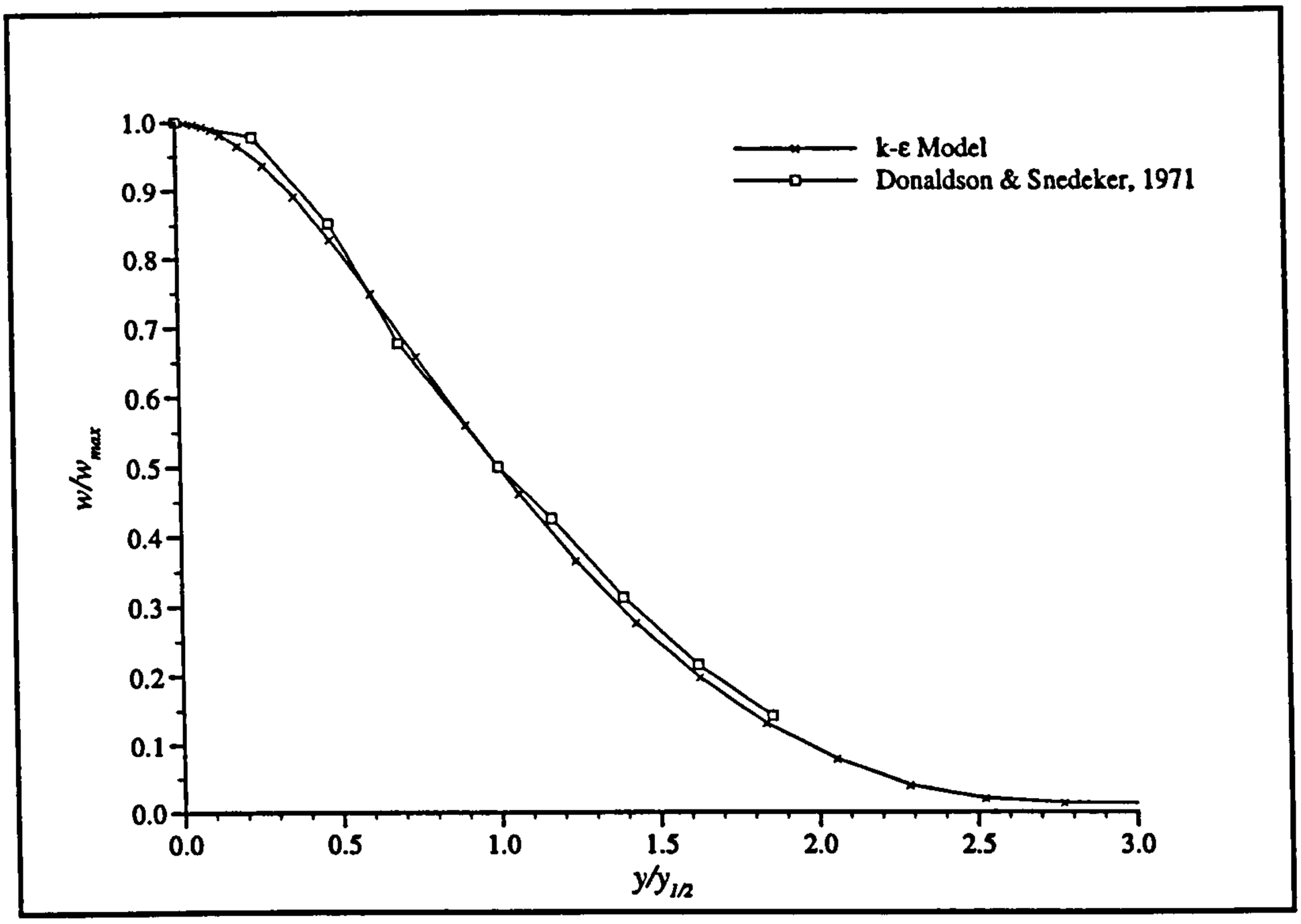

***Figure 6.15** - Normalised underexpanded free jet velocity profiles (NPR = 2.68, z/d$_n$ = self similar).*

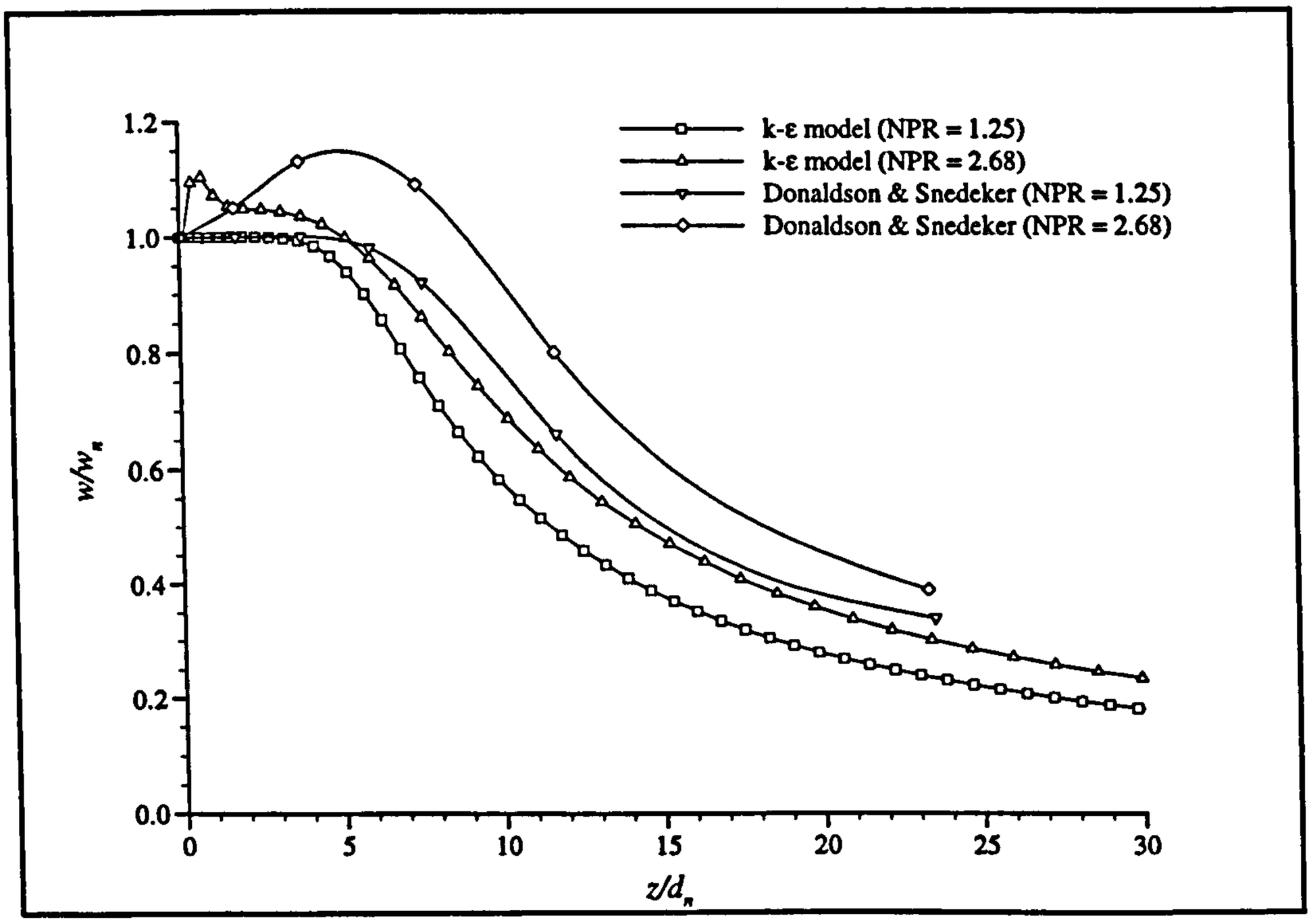

***Figure 6.16** - Comparison of k-ε predicted and experimental round-jet centre-line velocity decay.*

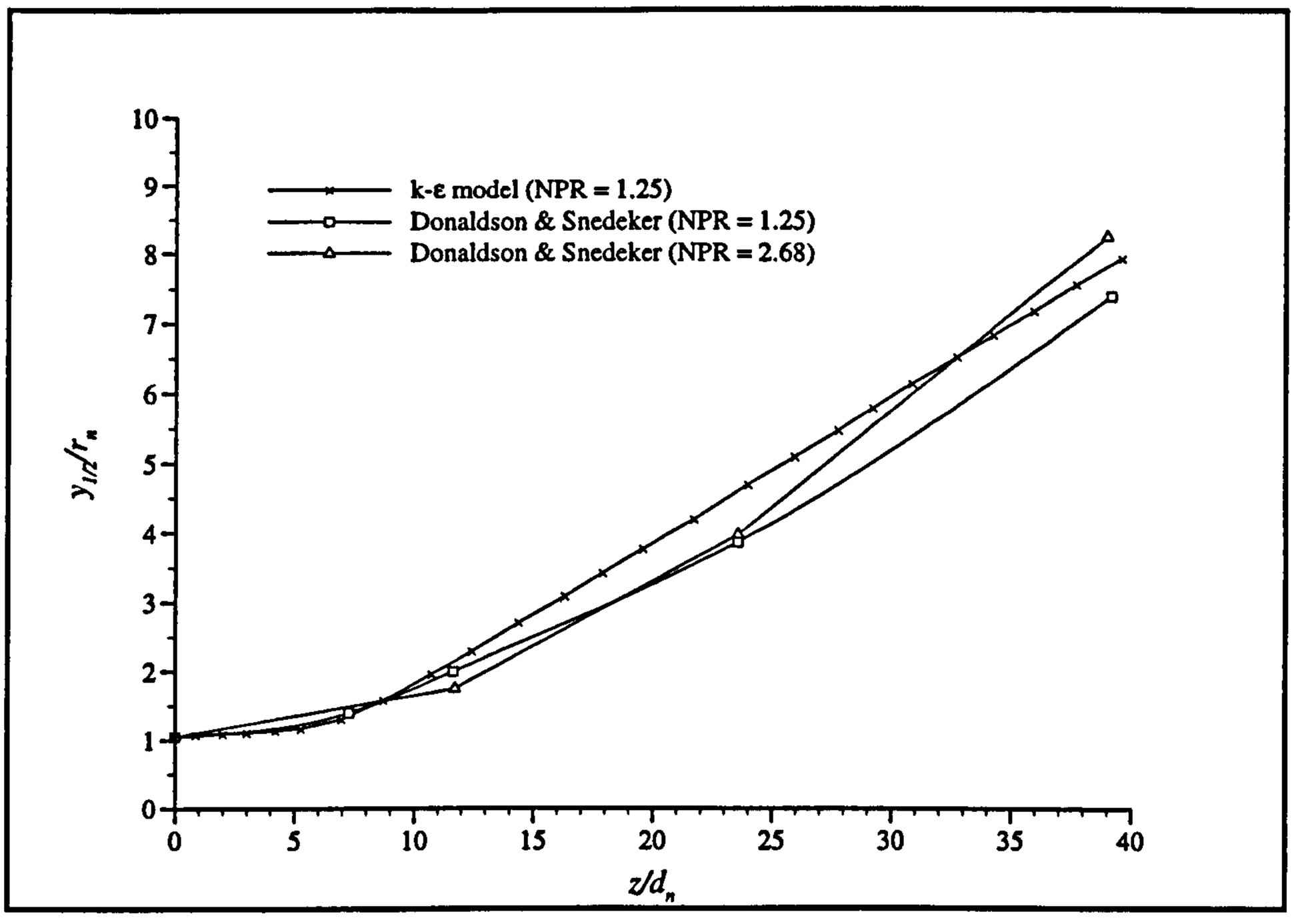

***Figure 6.17** - Comparison of k-ε predicted and experimental free jet spreading rate.*

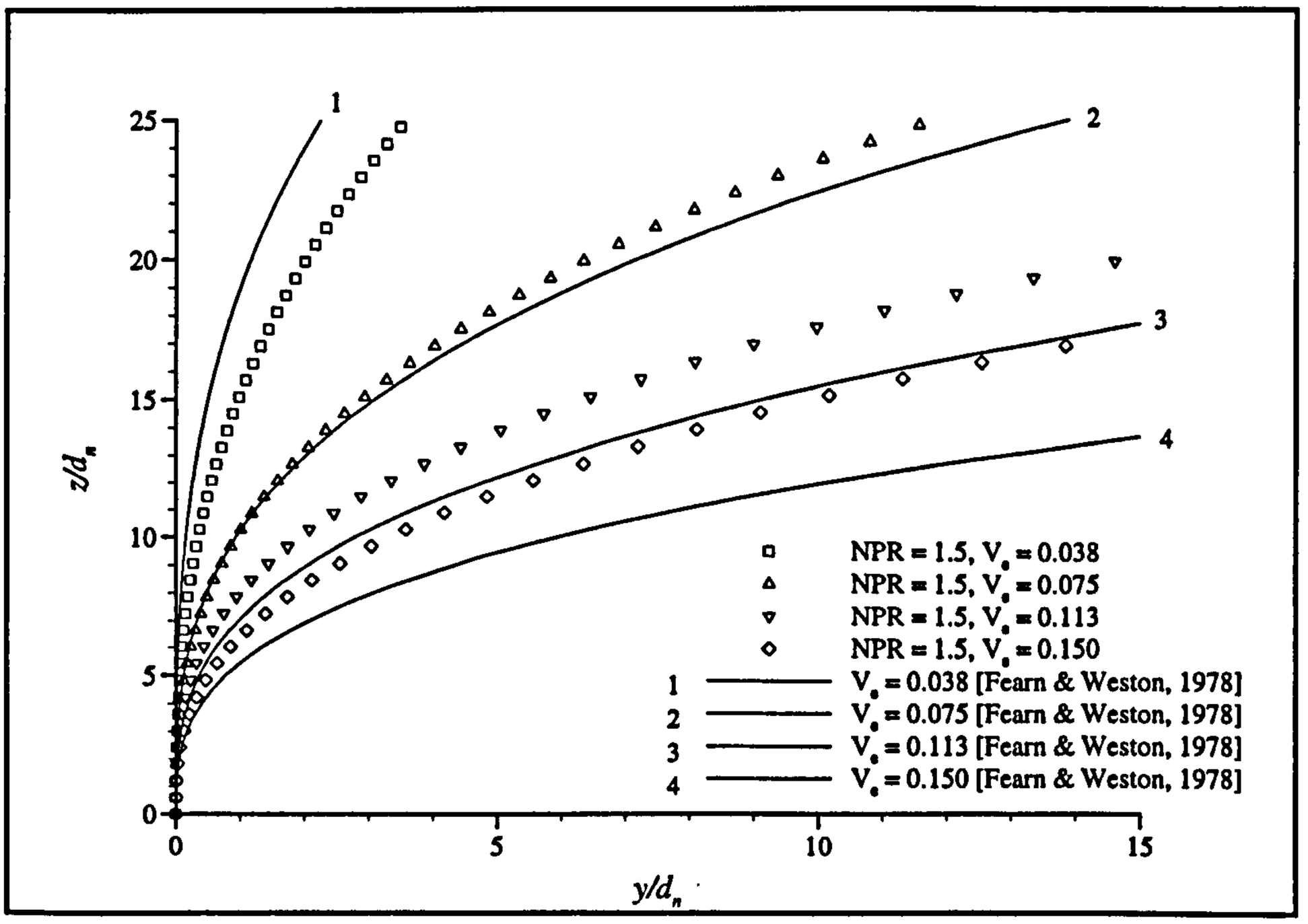

***Figure 6.18** - k-ε predicted round jet trajectories for an NPR of 1.5 (symbols) compared with FEARN & WESTON, 1978 (δ_j = 90 degrees).*

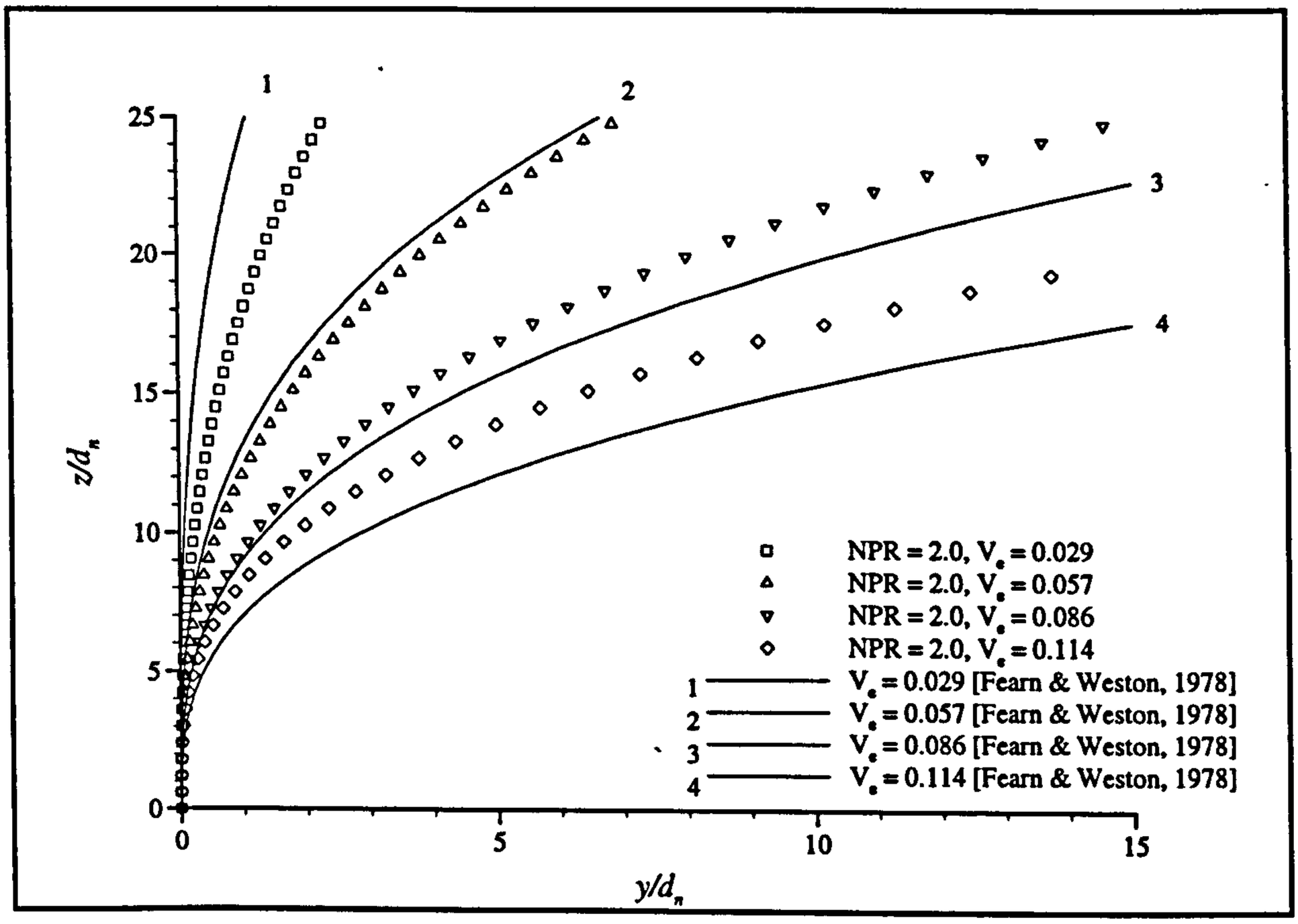

***Figure 6.19** - k-ε predicted round jet trajectories for an NPR of 2.0 (symbols) compared with FEARN & WESTON, 1978 (δ_j = 90 degrees).*

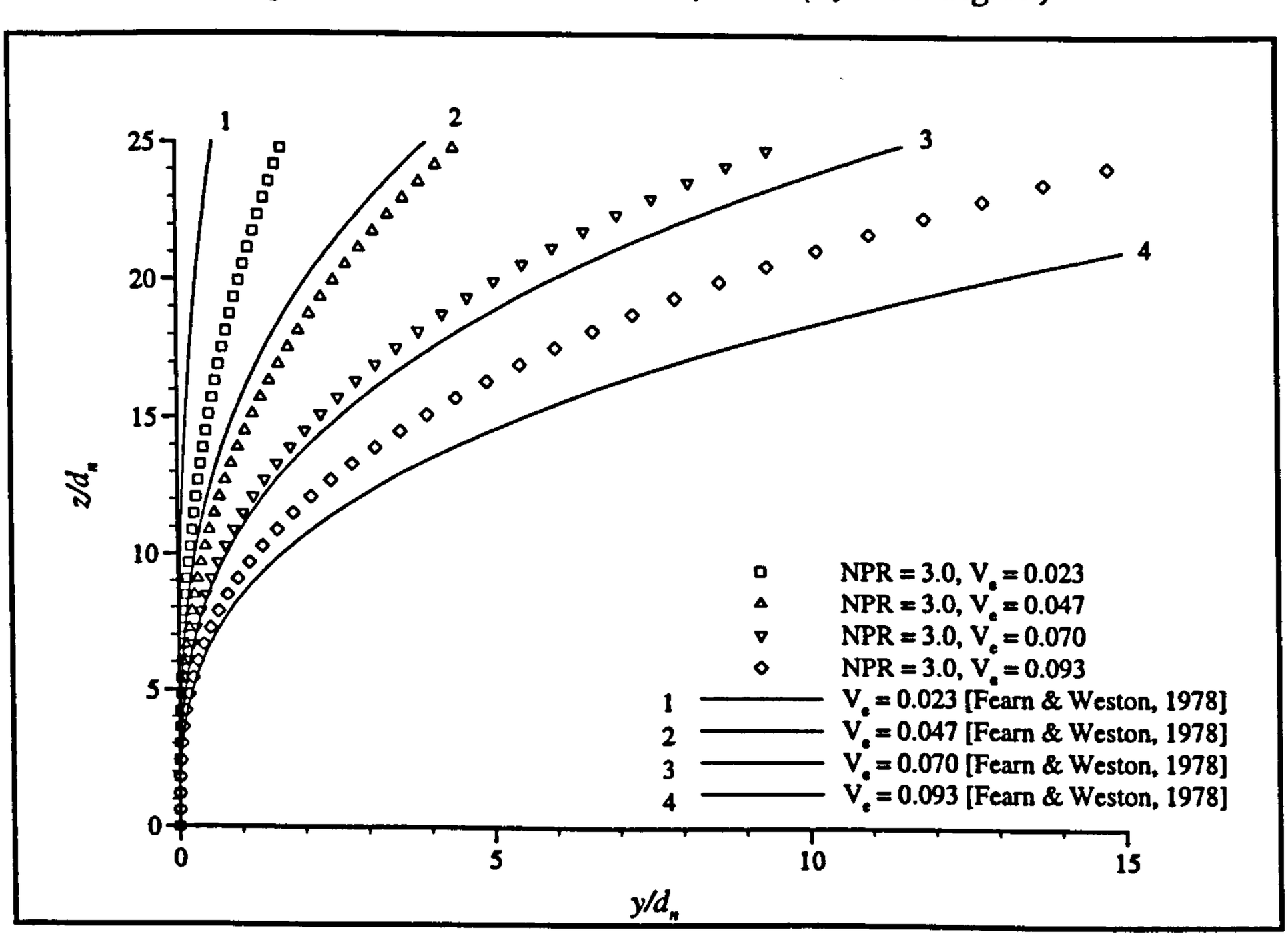

***Figure 6.20** - k-ε predicted round jet trajectories for an NPR of 3.0 (symbols) compared with FEARN & WESTON, 1978 (δ_j = 90 degrees).*

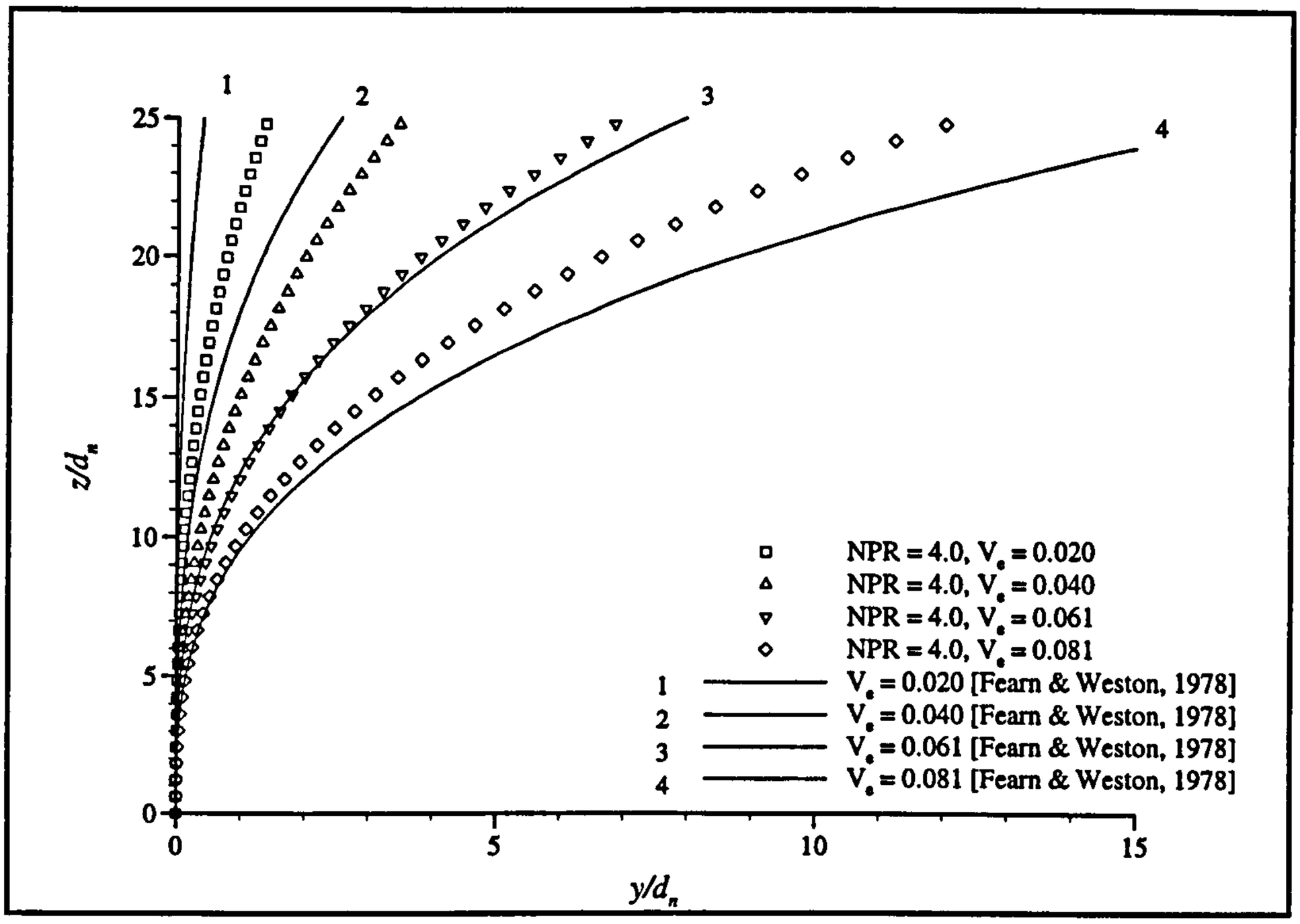

Figure 6.21 *- k-ε predicted round jet trajectories for an NPR of 4.0 (symbols) compared with FEARN & WESTON, 1978 (δ_j = 90 degrees).*

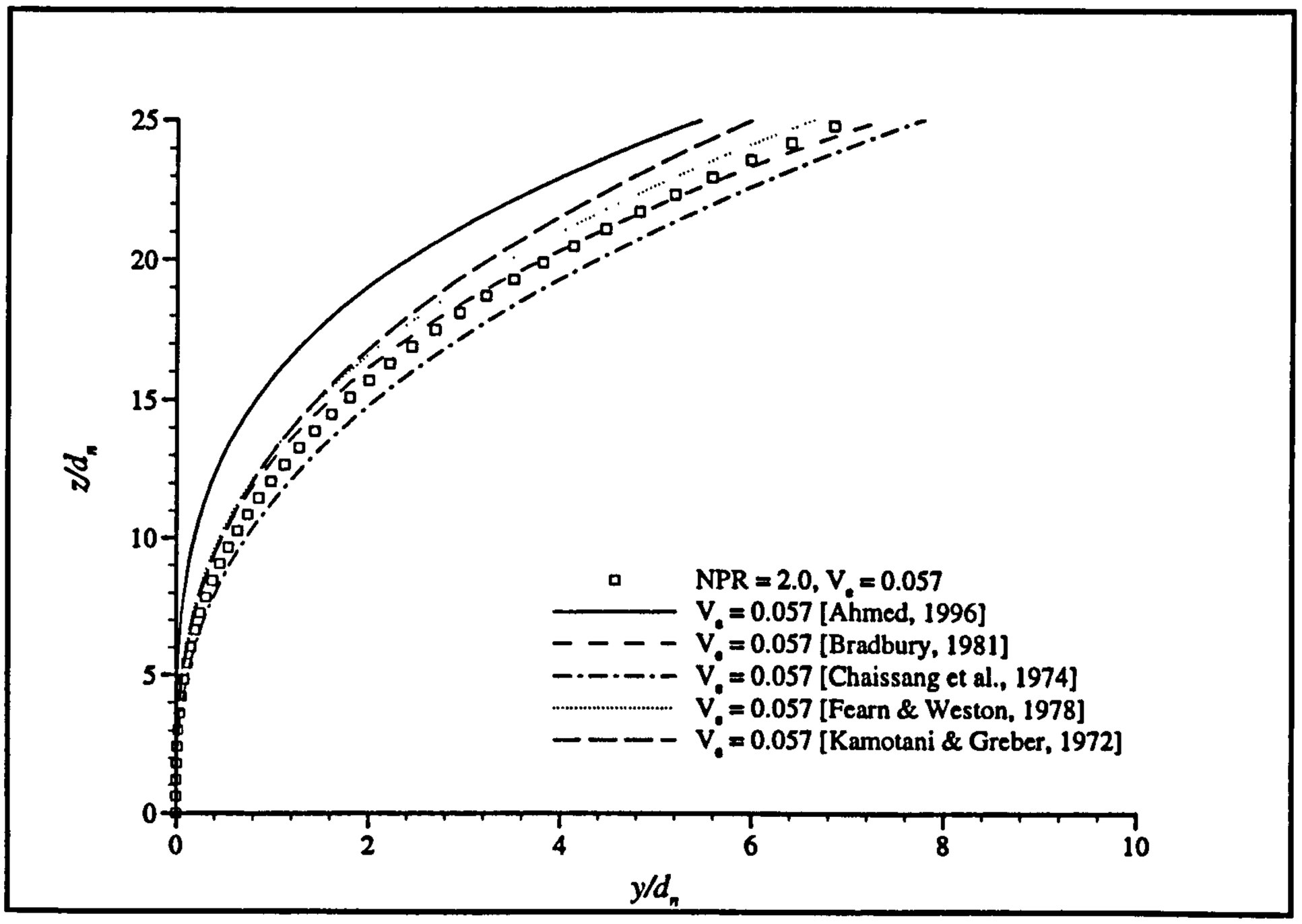

Figure 6.22 *- Comparison of k-ε predicted jet trajectory (symbol) with selected empirical correlations (δ_j = 90 degrees).*

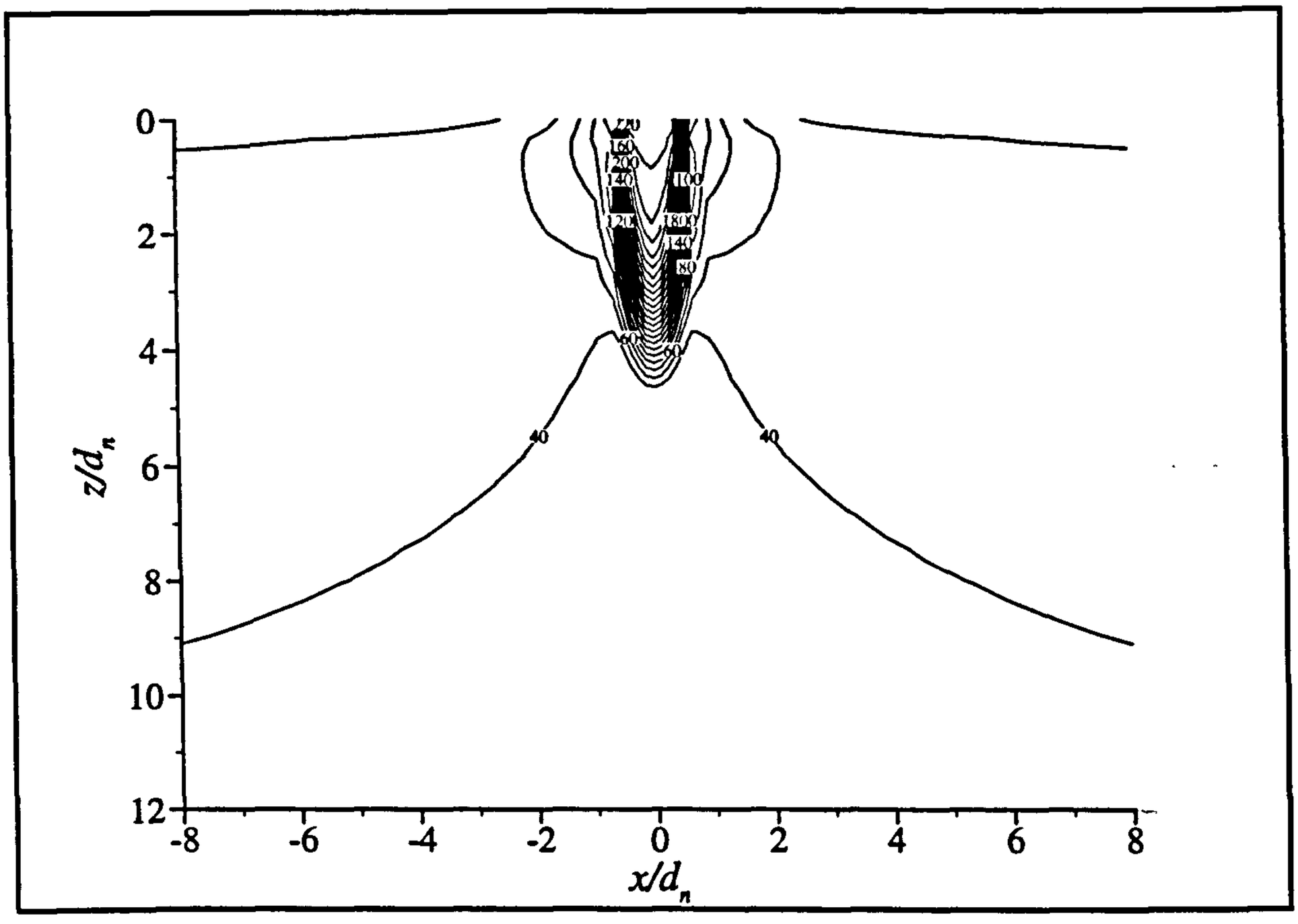

***Figure 6.23** - Velocity contours through a round jet in a cross-flow (V_r = 0.150, δ_j = 90 degrees, y/d_n = 0.0).*

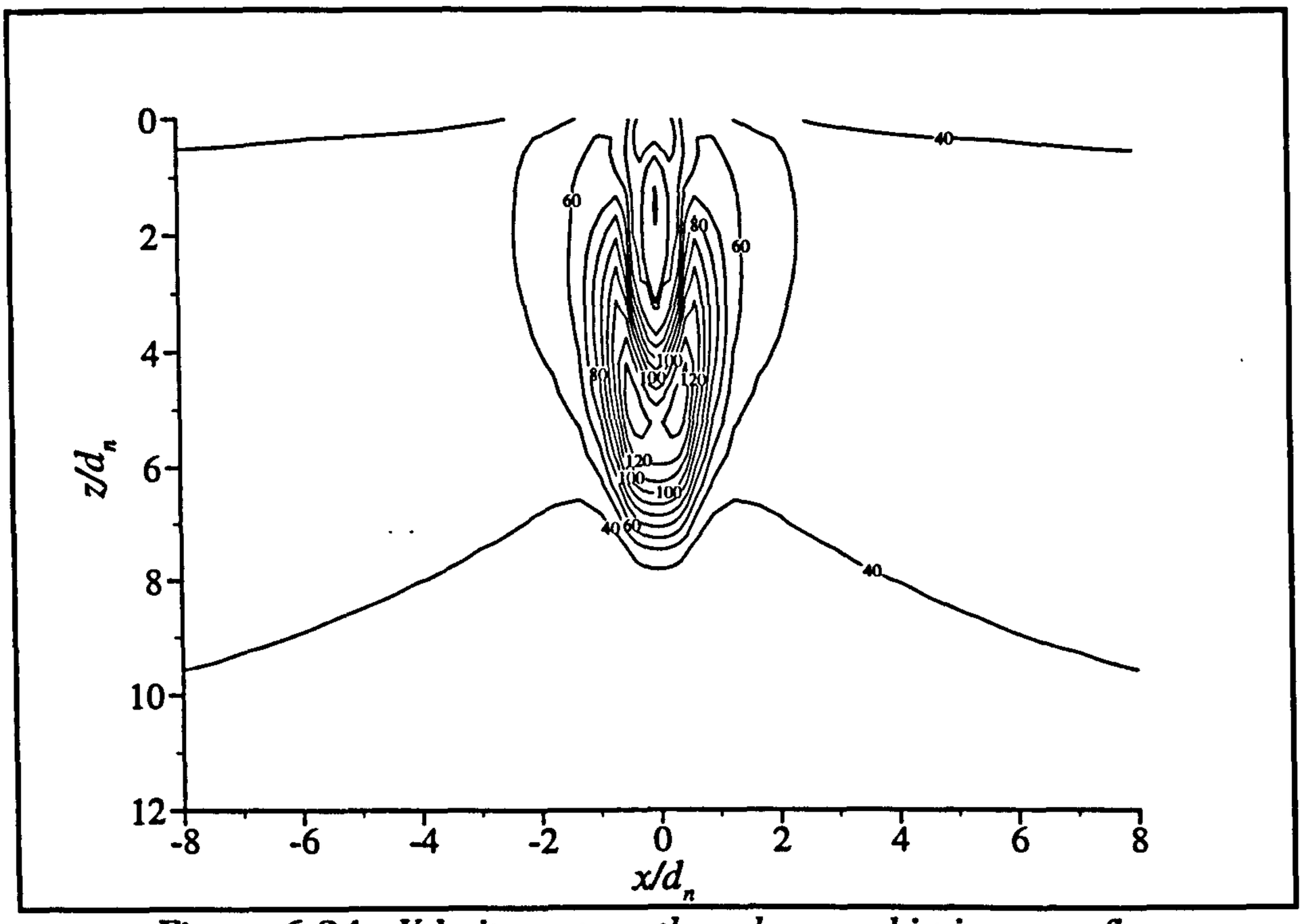

***Figure 6.24** - Velocity contours through a round jet in a cross-flow (V_r = 0.150, δ_j = 90 degrees, $y/d_n \approx 1.0$).*

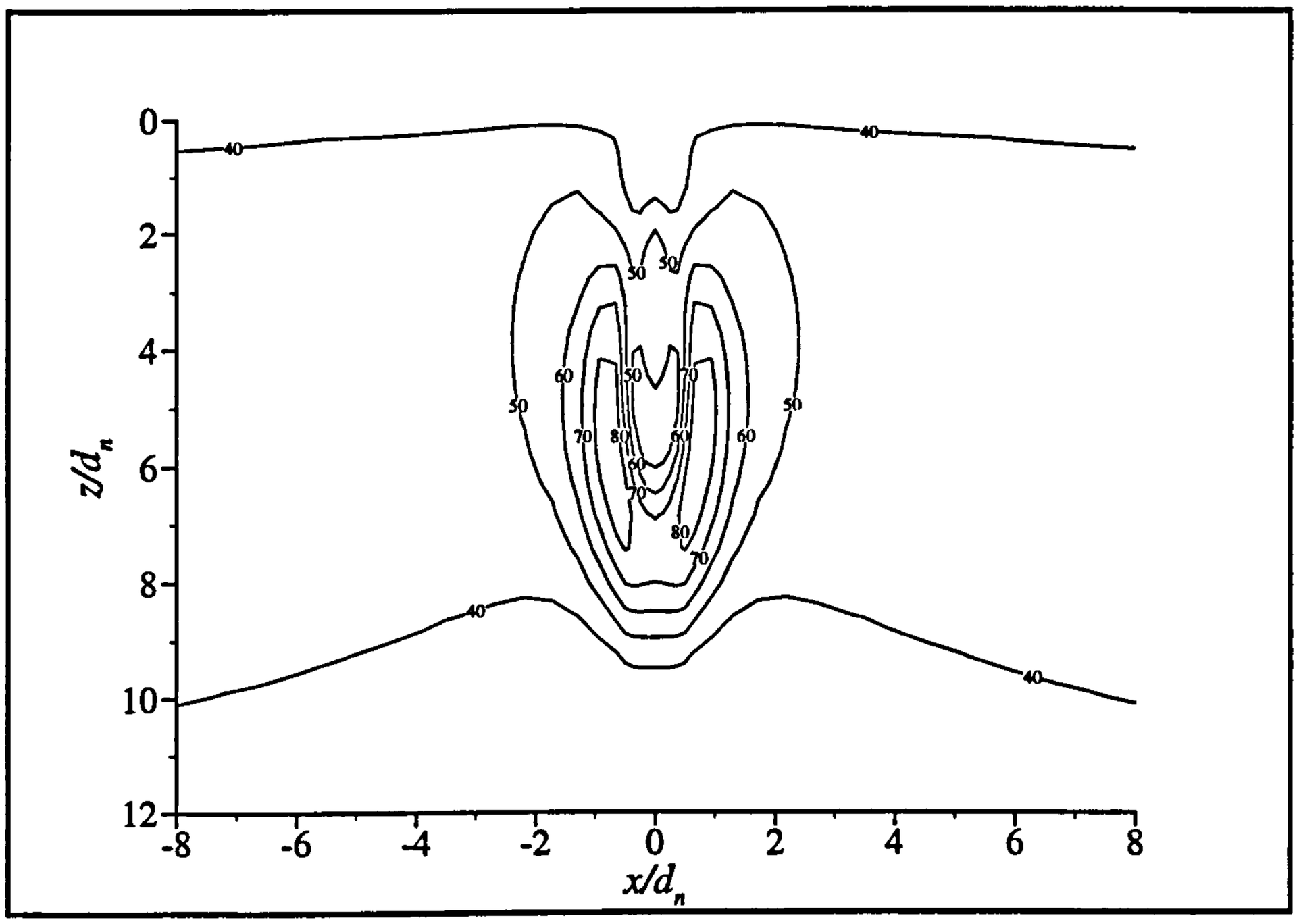

Figure 6.25 - *Velocity contours through a round jet in a cross-flow (V_r = 0.150, δ_j = 90 degrees, $y/d_n \approx 1.5$).*

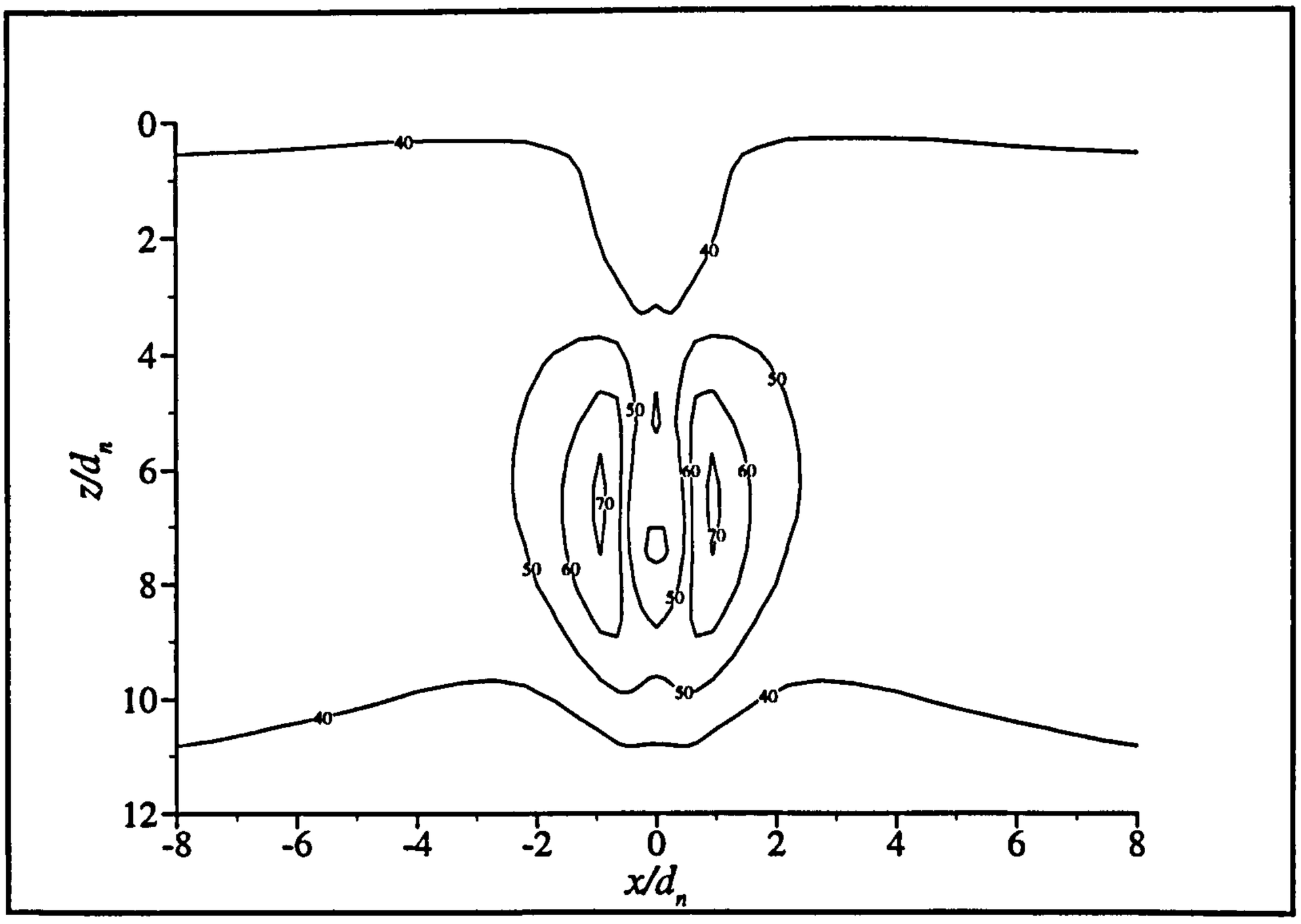

Figure 6.26 - *Velocity contours through a round jet in a cross-flow (V_r = 0.150, δ_j = 90 degrees, $y/d_n \approx 2.0$).*

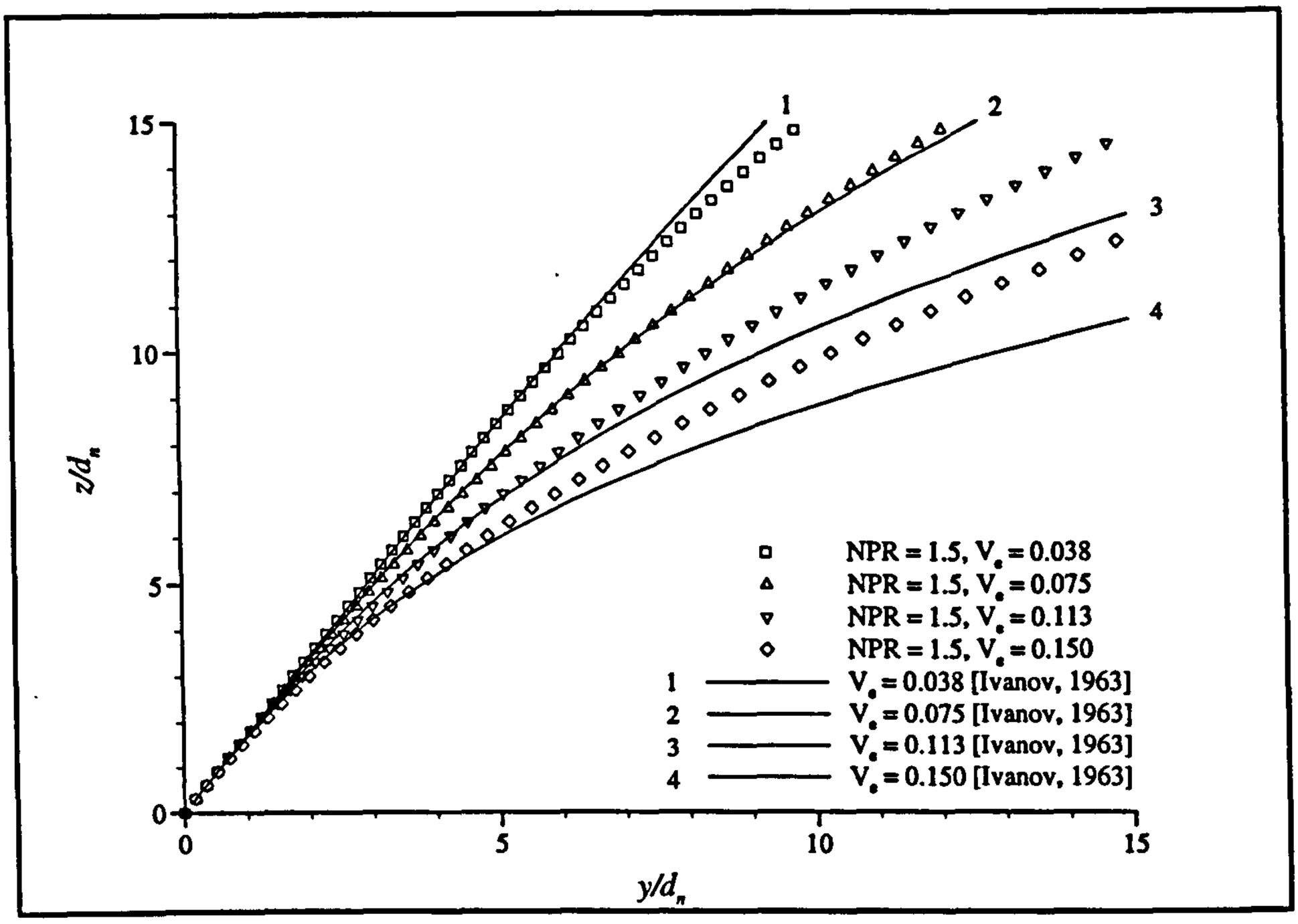

***Figure 6.27** - k-ε predicted round jet trajectories for an NPR of 1.5 (symbols) compared with IVANOV, 1963 (δ_j = 60 degrees).*

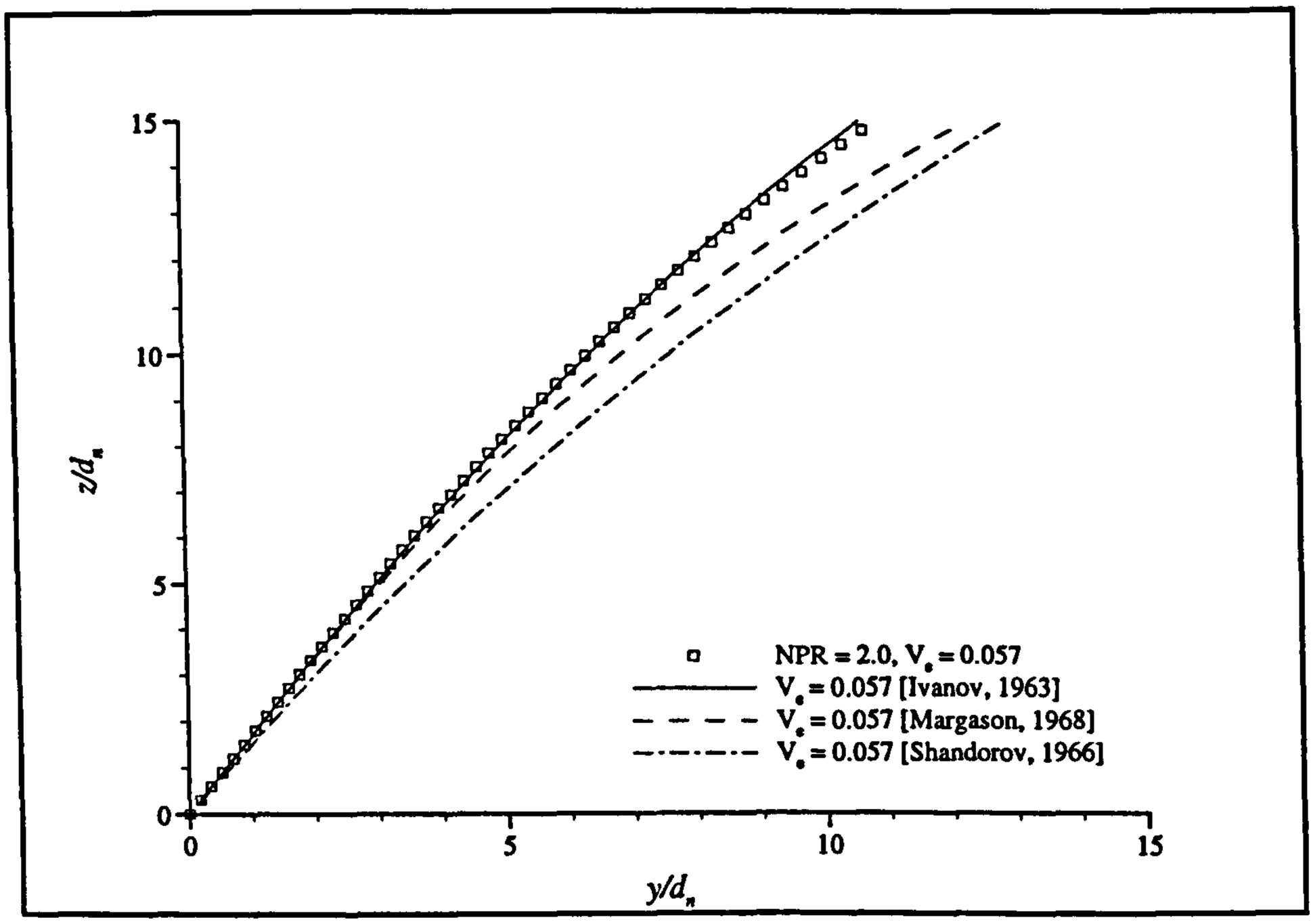

***Figure 6.28** - Comparison of k-ε predicted jet trajectory (symbol) with selected empirical correlations (δ_j = 60 degrees).*

7 Management Aspects of Wind Tunnel Project Work

This chapter encompasses the management aspects of the research project. The commercial justification for carrying out the research is first described. The overall project management, focusing on time and cost aspects, is discussed together with an analysis of the likely impact of the research findings for DERA Farnborough.

Based on these findings, a scenario is developed which calls for the procurement of a new large-scale, low-speed wind tunnel for the European aerospace industry. A brief review of existing low-speed European wind tunnels is presented, highlighting the need for a larger wind tunnel with a Reynolds number capability of 20 million. Design proposals are put forward for two low-speed wind tunnels, one atmospheric and the other pressurised, and estimates are made of their construction and operating costs.

The decision-making process for capital investment decisions is then discussed followed by a review and critical analysis of appraisal methods which could be used in the financial evaluation of a wind tunnel construction project. This includes traditional and modern 'discounted' methods. Following on from this, some of the broader non-financial considerations in the decision-making process are discussed.

Finally the chapter looks at the application of these evaluation tools to a wind tunnel construction project and the company which would operate it.

7.1 Commercial justification for the research

The cost of the development of new combat aircraft is now so expensive that it has become increasingly prohibitive for a single country to fund a major aircraft project on its own. Some exceptions do exist, most notably the USA, Russia, France and Sweden but even they are now looking for partners. The UK and USA have combined efforts with the development of the JSF. Russia looks increasingly to Western countries for financial support and commercial backing for its new aircraft projects. BAe has teamed up with SAAB to develop and market an export version of the latter's Gripen. Hence, in recent years we have seen new military and commercial aircraft built under consortia through international co-operation, particularly in Western Europe. With the cost of such aircraft running into billions of pounds any modifications to the aircraft configuration are extremely expensive and get more so as the project continues into the flight test stage.

It is important, therefore, to obtain early in the development of a new aircraft as thorough an understanding as possible of the aerodynamics and handling characteristics. The aerodynamics of STOVL aircraft are especially difficult to predict due to the complex nature of the flow-field surrounding such aircraft particularly in the transition from hover to wing-borne flight or vice versa. Over the past 40 years, aviation history has seen numerous failed STOVL projects which have not behaved as expected during transition. It is therefore worth putting considerable effort into investigating potential aerodynamic problems which STOVL aircraft may encounter, particularly during the transition phase of flight. One of the areas of concern is the mutual interference between the jets and intakes. It has already been shown earlier in this document that for the particular STOVL aircraft configuration tested such a mutual interference does exist. This questions the interpretation of data obtained from isolated jet and intake testing.

It is important that time and costs should be effectively managed throughout a project and the next section describes how these two variables were monitored throughout the current project duration.

7.2 Project management

7.2.1 Project time schedule

At the start of this project, a time schedule was drawn up (Figure 7.1). It was intended that the schedule be flexible, but most importantly, it defined specific deliverables and time boundaries which were to be adhered to as closely as possible. The project schedule was updated annually to reflect changes in the duration of certain deliverables whilst maintaining that all the research should be completed on time. The actual time schedule is given in Figure 7.2. No major problems were encoun-

tered during the research; however, there were some noticeable differences between the original schedule and the actual one. The setting up of the experimental facilities lasted longer than was expected and the start of collecting experimental data was delayed by one year. This was due in part to the delay in setting up the wind tunnel facilities but also due to difficulty obtaining wind tunnel time. Two other research projects also required the use of the wind tunnel. Initially six months was scheduled for the CFD work but it quickly became apparent that very little could be covered within such a short time. The CFD work was therefore extended. Figure 7.3 shows a Gantt chart for the project. The critical path is 1, 2, 3, 7, 9, 10, 11, 12, 13, 14.

7.2.2 Project costs

At the end of February 1997, the project was operating within budget. Table 7.1 shows the income and expenditure for the project up to that point. Between then and the end of the project (September 1997) there were only relatively minor items of expenditure which were more than matched by the final income payments. Thus, the project was completed well within budget.

***Table 7.1** - Income and expenditure for the project (February 1997).*

Item	*Credit (£)*	*Debit (£)*	*Balance (£)*
Fees for EngD	18,785.00		18,785.00
Inter campus transfers	5,708.62		24,493.62
Books, magazines and periodicals		42.60	24,451.02
Technical supplies and services		1,510.53	22,940.49
Equipment repairs, servicing and maintenance		579.27	22,361.22
Furniture, fixtures and fittings		71.12	22,290.10
Equipment other than computing		10,397.82	11,892.28
Computing hardware and software		6,628.85	5,263.43
Travel and subsistence		1,644.38	3,619.05
Hospitality		52.86	3,566.19
Conference fees		144.49	3,421.70
Library charges		10.20	3,411.50
Reprographics charges		98.55	3,312.95
Photographics charges		33.82	3,279.13
Stationary stores charges		168.68	3,110.45
Postal charges		9.16	3,101.29
Internal cross charges		1,760.00	1,341.29
Fax charges		0.79	1,340.50

7.3 Analysis of the likely impact on DERA Farnborough

DERA is funded by the MoD to carry out research in support of equipment purchases for the Armed Forces. It also has formal links with British Aerospace (BAe) to ensure that research programmes are complementary. If in the opinion of DERA, this project demonstrates a strong enough need for full jet and intake simulation on JSF models in transition, then more research funding might become available for the development of an improved, larger scale, combined jet/intake model. DERA Farnborough is well placed to develop such a model if required. Currently, the present project has little commercial importance to DERA, but it does have some strategic importance. Based on the knowledge gained carrying out this research project, DERA Farnborough could establish a competitive advantage in the STOVL wind tunnel test market if combined jet/intake test facilities were developed. If combined jet/intake testing is thought necessary by the manufacturers of STOVL aircraft then it could provide DERA Farnborough with a large customer research programme.

The majority of STOVL tests will continue to use blown jet 'force and moment' models with faired intakes as these are well within the capabilities of most test facilities. If jet/intake interference does prove important for modern STOVL configurations the additional interference effects may be found analytically using Navier-Stokes methods, or by further testing at a number of specialist facilities, such as the DERA Farnborough 5 m wind tunnel. It is still unlikely, however, that it will become general practice to simulate jet and intake flows simultaneously on 'force and moment' models because of the complexity of the models and high costs involved in establishing dedicated test facilities.

7.4 Procurement of a new low-speed wind tunnel

There are two features about aerodynamic research and development work which have a decisive bearing on the need for facilities and on their purpose. One is the fact that aerodynamics is largely an experimental science and that wind tunnels are, therefore, the main tools needed for the aerodynamic design of aircraft. The other is the widespread use of simulations, mathematical models and analogies. There is every reason to believe that these characteristics will continue to dominate work in aerodynamics for the future.

The need for experiments arises from the complexity of the flows to be investigated and to be applied in aircraft design. The flows are governed by highly non-linear equations and at present simplifications and approximations must be made before any mathematical modelling can proceed. Good modelling of practical usefulness tends to be particularly difficult at low flight speeds when high lift coefficients are to be generated or when aerodynamic lift is to be supplemented or replaced by lift forces associated with the propulsion system. Particular problems may include: large

pressure gradients on aerodynamic surfaces; the possibility of separated flow and the complexities introduced by deploying flaps, spoilers and undercarriage etc. Thus, reliable results which can be applied with confidence must still be provided partially if not wholly by experimental tools.

If, as a result of the experimental research carried out within this project, it is evident that there is a need for more rigorous wind tunnel testing of STOVL combined jet/intake models then it may be necessary to establish new experimental facilities which can accommodate models of the size and complexity which would be required.

7.4.1 Market impact from a new low-speed wind tunnel

There is an increasing requirement for a low-speed wind tunnel with a Reynolds number capability of approximately 20 million, which is much closer to full scale than current wind tunnels are capable of. Such a tunnel could provide the European aerospace industry with a competitive advantage over the USA by improving the ability to estimate aircraft low-speed performance in advance of the flight test stage.

Striving for ever increasing productivity and reduction in life-cycle costs, aerospace manufacturers focus heavily on improving aircraft performance and efficiency. This can only be achieved by obtaining accurate data on a particular configuration. The suppliers of wind tunnel test facilities such as DERA Farnborough need to be able to provide the aerospace companies with the required data and give them confidence in the accuracy of that data. The availability of an improved low-speed wind tunnel facility with high productivity and low operating costs, would enable European aircraft manufacturers to gain a competitive edge over their US counterparts.

The value of such a new wind tunnel lies in the capability to test models under simultaneous Reynolds number and Mach number conditions close to those experienced in flight. The flight Mach number is not difficult to match, but it is technologically difficult and expensive to build facilities capable of testing large aircraft at, or close to, the flight Reynolds number. Instead, most wind tunnel testing is performed at lower Reynolds numbers. The data are then extrapolated to the flight condition. The inherent uncertainty of this extrapolation leads to over-conservative aircraft design and performance estimates. High Reynolds number testing will reduce this uncertainty and thereby improve design and performance estimates.

One of the major areas to address is boundary layer transition. With future aircraft it may not be possible to simulate boundary layer transition artificially because of their design complexity. It must, therefore, be concluded that future low-speed wind tunnels should be able to provide Reynolds numbers which are high enough so that the dominating transition mechanism can be expected to be the same as that in flight. In addition, this project has shown (Chapter 4) that it is increasingly important to treat aircraft as integrated systems and not isolated components.

There are two options available to provide such a high Reynolds number. The first puts emphasis on the size of the tunnel and on the importance of being able to test the majority of actual aircraft. Such a tunnel would operate at atmospheric conditions and could deal with full-size STOVL aircraft. The working section would be sized so that the actual airflow which the aircraft sees in flight is reproduced accurately in the wind tunnel.

The second option puts the emphasis on being able to explore new and complex types of flow for lifting as well as propulsion purposes. To obtain reliable results with this kind of testing would require a large wind tunnel operated at moderate pressures above atmospheric, so that the kinds of flow encountered are accurately reproduced and so that the effects of Reynolds number and Mach number could be investigated separately. Extrapolation would then be applied to obtain full scale values for the recorded data. Such a tunnel could be smaller than the atmospheric one.

7.4.2 A review of low-speed wind tunnels in Europe

In Europe, two pressurised low-speed wind tunnels have been built in the last twenty years, the DERA 5 m tunnel [WILSON, 1973] and the ONERA F1 tunnel [ONERA, 1997], both completed in 1978. These tunnels can be pressurised up to 3 and 3.85 atmospheres respectively and their specifications are briefly summarised in Table 7.2. In both cases it was considered essential to be able to investigate Reynolds number and Mach number effects separately, particularly for aircraft in a high lift configuration, and it was this requirement which led to the tunnels being pressurised. The DNW tunnel [SEIDEL & JAARSMA, 1978], completed in 1979 provides a facility for larger models and has interchangeable test sections. It cannot be pressurised, however, and as such has a lower test Reynolds number than the two pressurised tunnels.

One of the main advantages of pressurising a low-speed wind tunnel is that it enables the effects of scale and compressibility to be investigated separately. In addition, a pressurised tunnel may have the advantage of a higher test Reynolds number than an atmospheric tunnel and this can be particularly important in tests of high lift wings and STOVL aircraft. Pressurised low-speed tunnels, however, do have disadvantages. Both tunnel and model design are more complicated, and capital, operating and model costs would be higher than for an atmospheric working section of the same size.

***Table 7.2** - Three large low-speed European Wind Tunnels.*

Establishment	***DERA 5 m, Farnborough, UK***	***ONERA F-1, Le Fauga, France***	***DNW, Noordoostpolder, The Netherlands***		
Working section (m)	5 × 4.2	4.5 × 3.5	9.5 × 9.5	8 × 6	6 × 6
M_{max} @ 310K	0.31[†]	0.35[‡]	0.18	0.31	0.41
Re_{max} [*] (×10^6)	7.9	7.3	3.5	4.6	5.2
Static pressure (atm.)	1 to 3	1 to 3.85	1		
Drive power (MW)	11	9.5	12.7		

7.4.3 The US National Wind Tunnel Complex

In the USA a proposal has been put forward by the National Facilities Study Team under the guidance of NASA for a 'National Wind Tunnel Complex'. The wind tunnel complex is designed to supplement the existing research-orientated NASA wind tunnels in meeting the needs of the US aerospace industry to develop and design advanced, efficient aircraft [YANG & GREY, 1995].

The US aerospace industry is feeling increasingly threatened by the high quality test facilities available in Europe. Currently, the DERA 5 m and ONERA F-1 wind tunnels are the subsonic wind tunnels of choice for industry. During the demolition and reconstruction of the NASA Ames 12 ft. wind tunnel in 1988-1995, US industry out of necessity utilised these European facilities (Boeing at DERA and McDonnell Douglas at ONERA) to do much of their low-speed testing. Whereas the Reynolds number capability of the 40 ft. × 80 ft. and 80 ft. × 120 ft. tunnels at NASA Ames may appear to make them likely candidates for development testing, their large size and low productivity make them unsuitable for use in commercial fixed-wing aircraft development. The now-operational NASA Ames 12 ft. wind tunnel will reduce this business for European tunnels, but a new high Reynolds number, low-speed wind tunnel may draw more testing away from the US. Their use can also be traded as part of the increasingly common offset deals tied to US equipment purchases.

The proposed site of the US wind tunnel complex would house a 7.3 m × 6.1 m pressurised low-speed tunnel with a maximum Reynolds number of 20.4 million and a 4.7 m × 3.4 m pressurised transonic tunnel with a maximum Reynolds num-

---

[†] *0.27 at 3 atm.*
[‡] *0.22 at 3.85 atm.*
[*] *Based on a length scale of* $0.1\sqrt{A_t}$ *and an air temperature of 310 K.*

ber of 28.1 million [MORRING, 1995]. The budget for the complex is $3.2 billion (1995) of which $400 million was spent on a feasibility study and initial design phase in 1995 and 1996. The estimated cost of the wind tunnel construction is $2.0 billion [YANG & GREY, 1995]. If construction costs are split 40 percent to the low-speed tunnel and 60 percent to the transonic tunnel then the low-speed tunnel will cost about $800 million (1995), approximately £500 million.

7.4.4 A proposed new low-speed wind tunnel

With the above considerations in mind, two proposals are put forward here for a new wind tunnel, a 29 m × 23.5 m atmospheric tunnel and an 11.5 m × 9.3 m pressurised tunnel. Both are of conventional layout (closed circuit, closed working section) and would have contraction ratios of approximately 10:1 to keep power consumption levels down and ensure low turbulence in the working section. The pressurised tunnel could operate at up to 4 bar(g) pressure. To avoid excessive wall interference and blockage effects, MATHESON, 1984, suggests that for STOVL testing, the wind tunnel working section should ideally be three times the width of the aircraft wing span. The atmospheric tunnel could, therefore, accommodate STOVL models of approximately 10 m span whereas in the pressurised tunnel models of only 4 m span could be tested. MATHESON, 1984, concluded that to obtain a sufficiently high test Reynolds number, and to allow the complex geometrical detail inherent in STOVL aircraft to be reproduced with sufficient accuracy, models with a wing span or rotor diameter of about 3 m are necessary for industrial development of aircraft. Both of the proposed tunnels could easily accommodate models of such a size.

The tunnels are designed to be development tunnels. In contrast to research tunnels, whose design is driven by the requirements associated with the collection of scientific data, development tunnels are designed and built to minimise cycle times and costs, so that industry can bring new aircraft to market more quickly and at a lower cost than the competition. Development tunnel design therefore emphasises not just aerodynamic capability but also high productivity and low operating cost.

Each tunnel would be powered to give a maximum speed of 130 ms^{-1} at atmospheric pressure. For the pressurised tunnel, the maximum speed is reduced at higher pressures (due to the increased air density), becoming 103 ms^{-1} at 2 atm., 90 ms^{-1} at 3 atm. and 82 ms^{-1} at 4 atm.

The construction and running cost estimates for the tunnels are derived from the work of SPENCE & SPEE, 1973 who based their estimates on the cost of constructing the DERA 5m wind tunnel. Their costs are given as 1971 prices and so a global multiplying factor has been applied to enable present day costs to be determined. The annual retail price index in the UK has increased on average at 8.5 percent per annum between 1971 and 1991 [REID & MYDDLETON, 1991]. Extrapolating this

increase also to the present day, the costs estimated by SPENCE & SPEE, 1973 have been multiplied by a factor of 8.34.

7.4.4.1 Construction costs

The tunnel shell

The working section for each tunnel has been sized to give a Reynolds number of approximately 20 million at maximum speed. The characteristic length used was one tenth of the square-root of the working section area. For the atmospheric tunnel, this gave a working section of 29 m by 23.5 m, whilst for the pressurised tunnel, the dimensions are 11.5 m by 9.3 m. The aspect ratio of the working section is approximately 5:4 for both tunnels, chosen to be similar to the DERA 5 m and ONERA F-1 tunnels.

For the pressurised tunnel, it was assumed that the pressure shell would be made of steel and that the cost was proportional to the weight and maximum tunnel gauge pressure [SPENCE & SPEE, 1973].

$$\text{Shell cost (£M)} = 160(p_t - 1)\left(\frac{A_t}{170}\right)^{1.5} \tag{7.1}$$

For the atmospheric tunnel, it was assumed that the shell would be made of reinforced concrete [SPENCE & SPEE, 1973]. Again the cost being proportional to the weight.

$$\text{Shell cost (£M)} = 20\left(\frac{A_t}{170}\right)^{1.5} \tag{7.2}$$

Main drive and tunnel cooling

The power for the main drive system was calculated as follows.

$$\text{Power} = \frac{1}{2\eta_t}\rho_a A_t V_t^3 \tag{7.3}$$

The tunnel power factor, η_t was assumed to be 3.6 for the atmospheric tunnel and 3.2 for the pressurised one. These figures were based on SPENCE & SPEE'S data.

The costs of the main drive were estimated to be £270,000 per megawatt. For the cooling and temperature control system of pressurised tunnels, a figure of £175,000 per megawatt was used. In the case of atmospheric tunnels, however, an air interchange system would suffice and a lower cost of £85,000 per megawatt has been taken for this. It was assumed that all the drive power was extracted by the tunnel cooling system and that the cooling system power consumption was 50 percent of the main drive power.

Compressed air supply

Provision of pressurised air supplies is of increasing importance as the tunnel size increases, both for pumping up the pressurised tunnel and for use in engine representation in both tunnels. For the tunnel pumping and model blowing installations, compressor and intercooler efficiency was assumed to be 80 percent. This figure is based on the compressor and intercooler efficiency of the compressed air facility at RMCS. For tunnel pressurisation, a two stage compressor was used (two 2:1 stages) whilst for model blowing, a three stage compressor was envisaged (4:1, 3:1 and 2:1 stages). The compressor stage power was calculated as follows.

$$\text{Power} = \frac{\dot{m} c_p \Delta T}{\eta} \tag{7.4}$$

For the pressurised tunnel, the cost for the air system assumed pumps sufficient to fill the tunnel to maximum pressure in 6 hours and storage of enough air for one fill. For model blowing, the air storage and mass flow rate required were based on the compressed air facilities at RMCS and scaled according to the linear dimensions of the wind tunnels.

The cost of pumping was estimated to be £300,000 per kgs^{-1} and the cost of storage was £18 per kg. SPENCE & SPEE, 1973, suggest that costs for additional equipment such as instrumentation, balances, model handling and preparation areas etc. would be of the order of 20 percent. Table 7.3 summarises the specifications of the two proposed tunnels and Table 7.4 provides a breakdown of the major construction costs. Table 7.5 gives details of the estimated operating costs of the two tunnel designs.

7.4.4.2 Operating costs

Operating costs have been estimated based on the following assumptions of SPENCE & SPEE, 1973 which are applicable for testing STOVL-type aircraft.

1. Tunnel usage is divided 40 percent to rotary wing aircraft (tested at 100 ms^{-1} on average) and 60 percent to fixed wing aircraft (tested at 75 ms^{-1} on average). It was assumed that the rotary wing aircraft will be tested at atmospheric pressure and the fixed wing aircraft will be tested at the maximum available pressure.
2. The maximum power has been taken as the sum of the main drive power, the cooling power and the tunnel pressurisation and model blowing power where appropriate.
3. Model blowing will only be required for fixed wing aircraft.
4. The electricity charges used are £20,000 per megawatt capacity and £47.50 per megawatthour.

5. The cost of labour, materials and equipment were assumed to be £3 million per year for a 1000 hour per year usage or £3.5 million per year at 2000 hours usage.

6. It has been assumed that the average rate of data recording is 5 test runs per hour for the atmospheric tunnel and 4 runs per hour for the pressurised tunnel.

***Table 7.3** - Proposed large low-speed wind tunnel designs.*

Item	*Atmospheric*	*Pressurised*
Working section (m)	29 × 23.5	11.5 × 9.3
M_{max} @ 310 K	0.37	0.37†
Re_{max}* (×10⁶)	20.4	20.4
Static pressure (atm.)	1	1 to 4
Power factor	3.6	3.2
Drive power (MW)	240	42
Cooling power (MW)	120	21
Pumping air (×10⁶ kg)	n/a	1.0
Pumping rate @ 4 bar (kgs^{-1})	n/a	46
Pumping power (MW)	n/a	8
Blowing air (×10⁶ kg)	0.02	0.01
Blowing rate @ 24 bar (kgs^{-1})	35	14
Blowing power (MW)	16	7

***Table 7.4** - Construction costs of the proposed wind tunnels.*

Item	*Atmospheric tunnel*	*Pressurised tunnel*
Shell (£M)	170	250
Drive (£M)	64	11
Cooling (£M)	10	4
Tunnel pressurisation pumps (£M)	n/a	14
Tunnel pressurisation storage (£M)	n/a	18
Model blowing pumps (£M)	10.5	4.2
Model blowing storage (£M)	0.5	0.2
Instrumentation etc. (20%)	51	60
Total (£M)	306	361

† *0.23 at 4 atmospheres.*

* *Based on a length scale of* $0.1\sqrt{A_t}$ *and a temperature of 310 K.*

***Table 7.5** - Operating costs of the proposed wind tunnels.*

Item	*Atmospheric*	*Pressurised*
Max. demand power (MW)	376	78
Mean demand power (MW)	116	49
Max. demand cost (£M)	7.5	1.6
For 1000 hours per year		
Power charge (£M)	5.5	2.3
Labour etc. (£M)	3	3
Total cost for 1 year (£M)	16	7
Cost per run @ 1000 hr/year (£)	3200	1750
For 2000 hours per year		
Power charge (£M)	11	4.6
Labour etc. (£M)	3.5	3.5
Total cost for 1 year (£M)	20	9.7
Cost per run @ 2000 hr/year (£)	2000	1200

The cost of the construction of the two tunnels is of the same order (£300 million to £350 million), with the cost of the atmospheric tunnel appearing slightly less than the pressurised one. This is mainly due to the much lower cost of the tunnel shell. Due to the much larger size of the atmospheric tunnel, its drive and cooling costs are much higher. This tends to offset against the lower shell cost. The provision for compressed air amounts to quite a small percentage, 3.6 percent for the atmospheric tunnel and 10 percent for the pressurised one. On the basis of construction costs, there is very little to choose between the two designs.

The big difference between the two tunnels is in their operating costs. As would be expected with such a large power consumption, the atmospheric tunnel costs nearly twice as much to run as the pressurised one. The combination of lower operating costs and the ability to investigate the effects of scale and compressibility separately would probably mean that the pressurised tunnel would be the better choice. Pressurisation of a particular tunnel greatly reduces the overall size for the same test Reynolds number which may be of importance when considering the cost of land on which to build the tunnel.

The costing of wind tunnels such as those being proposed is very difficult due to the unique nature of the project [WOODWARD, 1995]. Assuming that the proposed wind tunnel will be run as a business venture, a financial evaluation of the project must be made.

7.5 Capital investment decisions

Capital investment decisions are financial decisions which involve current outlays in return for benefits in future years. They are decisions which are generally consid-

ered to involve a significant period of time between the commitment of funds and the receipt of the benefits (usually greater than one year). Capital investment decisions normally represent the most important decisions which an organisation makes because they commit a substantial proportion of a company's resources to actions which are likely to be irreversible. Three main kinds of capital investment are: replacing equipment, to reduce costs or improve quality; expanding productive capacity, to meet growing demand; or providing new facilities. The construction of a new wind tunnel obviously falls into the final category.

7.6 The decision-making process

There are several key stages in the capital investment process (see Figure 7.4). The first stage indicates that the *objectives and goals of the company must be determined*, and the targets which the company wishes to achieve must be established. Not only should capital investments be profitable but they should also fulfil the objectives of the company. Modern capital investment theory suggests that the primary objective of a company is to maximise shareholders' wealth i.e. increase corporate value through net asset accumulation. In reality, companies may have other objectives which will influence the capital investment decision e.g. maximising sales, increasing market share and improving survival prospects.

Probably the most important stage is the second, *generating worthwhile ideas for capital investments*. These ideas may result from identifying business opportunities or from responding to recognised problems. Most will come from such company areas as sales, marketing, production, engineering and research and development. Good ideas are vital to the success of most companies.

The third stage in the decision process is to *gather information about the possible future business environment* which may affect the outcome of the project. Examples include changing technology, changing customer requirements, the state of the economy, inflation etc. Detailed engineering estimates, market forecasts etc. will be needed. Capital investment projects may often cover the whole range of a company, involving groups of people from many departments, and often covering quite long periods of time. If the future environment appears unfavourable to a particular project, then possible alternatives may be considered.

The fourth and fifth stages are to *list the possible outcomes* for each theoretical future business scenario and *measure the payoff* for each possible outcome in terms of the objectives of the company. Ways of measuring payoff will be discussed later in this chapter.

Stage six in the process is to *select the investment projects* which will give the maximum payoff and to include them in the company's long-term plan. Once authorisation has been obtained, the project can be implemented (stage 7). Finally, but im-

portantly, the capital investment decisions are reviewed at stage 8 to check their progress.

The 'feedback' loops signify that the process is continuous and dynamic and capital investment decisions should be continually reviewed to see if the actual results conform with expectations (list of possible outcomes). Environmental information should also be regularly monitored as this may indicate that a change is required in the idea-generating process and that the objectives and goals should be revised.

The application of these ideas to a wind tunnel construction project are difficult. Firstly, the standpoint from which the project is viewed must be identified. Wind tunnels of the scale which are being considered here are beyond the financial capabilities of any single European aerospace company. The wind tunnel would have to be run by a consortium of aerospace companies, or more likely, by a new company. The payment for the construction of the new wind tunnel may be along the lines of the European Transonic Wind Tunnel (ETW). ETW took nearly 10 years to design and build and became operational in 1994. The final cost was $350 million (1994) [COVAULT, 1994] and was paid for by the governments of Great Britain, France, Germany and The Netherlands. In 1995 the tunnel entered its business phase and the governments withdrew financial support and the facility became self financing [BOUIS, 1995]. For discussion purposes, the wind tunnel will be viewed from the standpoint of the company operating and running it.

The main reasons for building a new low-speed wind tunnel have already been discussed. The European aerospace industry has a requirement to obtain a better understanding of the aerodynamics of aircraft under high lift conditions. This will lead to the development of military and civil aircraft with a better performance and lower operating costs. These are the perceived benefits for the European aerospace industry and for them the wind tunnel is merely a tool in the design process. A market has therefore been established for a 20 million Reynolds number, low-speed wind tunnel. In the next sections the investment appraisal methods used to evaluate such a capital investment project will be discussed and critically evaluated.

7.7 Opportunity cost of investment

There are various options open to a company when investing money. It could be invested in low risk government securities which will yield a fixed return, or alternatively money could be invested in more risky securities but with the possibility of a higher return, such as ordinary shares of companies quoted on the stock exchange. Investors prefer to avoid risk if possible and will generally invest in risky securities only if they believe that they will obtain a significantly greater return for the increased risk. When making a capital investment decision, a company must evaluate the risk versus return for the project. It is pointless investing in a risky project which will return no more than putting the money in government securities.

The rates of return which are available from investments in securities in financial markets represent the opportunity cost of an investment in capital projects. If cash is invested in a capital project it cannot be invested elsewhere to yield a return. A company, therefore, should only invest in capital projects if they yield a return in excess of the opportunity cost of an investment.

7.8 Financial evaluation - appraisal methods

A wind tunnel construction project of the type described above will require extensive planning and a thorough financial evaluation of the project must be made. The financial risks are very high based on the estimated cost of the wind tunnel project. Capital investments may be for very large sums of money. Once implemented, they are often not reversible since, for many specialised pieces of equipment, there may be no second-hand market. Even if there were a potential buyer, it may only be possible to sell at a much reduced price. Large investments may also have important strategic implications, so companies are wary about capital spending necessitating thorough procedures for proposals to pass through before approval. The larger the amount of money involved, the higher up the company the capital project must go before approval. In this section, a summary of the techniques for financially evaluating a major project, such as is being considered here, are critically evaluated. Further details covering this area of the decision-making process may be found in, for example, ALLEN & MYDDLETON, 1992 or DRURY, 1996.

7.8.1 Traditional methods

7.8.1.1 Payback

Probably the most widely used financial evaluation method of all is the payback method, because it demonstrates the degree of risk associated with a particular project. It is defined as the length of time which is required for a stream of cash proceeds from an investment to recover the original cash outlay required by the investment. The shorter the payback period, the lower the risk.

For the payback period, it is usual to look at cash receipts from a project rather than accounting profits. Thus, in calculating a project's net cash inflows, only cash expenses should be deducted from sales revenues, not depreciation. Consider the example below of two projects A and B.

***Table 7.6** - Cash flows for projects A and B.*

		Project A (£)	***Project B (£)***
Investment	Year 0	-6,000	-12,000
Cash Inflows	Year 1	3,000	12,000
	Year 2	4,000	8,000
	Year 3	8,000	4,000

The payback period for project A is 21 months whereas for project B it is only 12 months. Therefore on the payback method, project B would be the better. The payback method has one clear advantage over the average accounting rate of return, it takes timing into account. The payback method, however, ignores cash receipts after payback. This is vital, there can be no profit unless cash inflows exceed the initial investment. From the two examples, project A's cash inflows are still rising after payback, whereas project B's are falling rapidly. Payback also has the disadvantage of only analysing the project up to the payback point. Quick payback of the original investment reduces the risk associated with a project by concentrating on the data in which there is the greatest confidence. As a result, the payback period is a particularly useful method when assessing projects whose cash flows are subject to uncertainty in the long term. It is popular with UK businesses but has a tendency to focus on the short-term and may lead to the rejection of many long-term, high risk but ultimately very profitable projects.

7.8.1.2 Average accounting rate of return

The accounting rate of return (ARR), also known as the return on capital employed or return on investment, is calculated by dividing the average annual profits from a project by the average investment costs.

$$\text{ARR} = \frac{\text{Average annual profit}}{\text{Average investment}} \times 100 \tag{7.5}$$

It differs from other methods in that 'profits' rather than cash flows are used. Profits differ from cash flows in that they include depreciation and other non-cash accounting transfers. The use of this method results from the wide use of the return on investment measure in financial statement analysis.

When the average annual net profits are calculated, only additional revenues and costs which follow from the investment are included in the calculation. The average annual net profit is therefore calculated by dividing the difference between incremental revenues and costs by the estimated life of the investment. The incremental costs include either the net investment cost or the total depreciation charges, these figures being identical. The average investment under this assumption is one-half of the amount of the initial investment plus one-half of the scrap value at the end of the projects life.

Consider again the projects A and B described above. Deducting the initial investment for each project from its total cash receipts gives the total net profit. The initial investment is then deducted from the total cash inflows. Project B produces a higher total net profit (£12,000 versus £9,000), but if we divide the average annual profit by the initial amount invested, project A produces a higher rate of return on investment than project B (50% versus 33%).

Table 7.7 - Average accounting rate of return for two projects

		Project A (£)		Project B (£)	
Investment Outflow	Year 0		-6,000		-12,000
Net Cash Inflows	Year 1	3,000	15,000	12,000	24,000
	Year 2	4,000		8,000	
	Year 3	8,000		4,000	
Net Profit (3 years)			9,000		12,000
Average annual profit			3,000		4,000
$\frac{\text{Average annual profit}}{\text{Initial investment}}$			$\frac{3}{6} = 50\%$		$\frac{4}{12} = 33\%$

The accounting rate of return is superior to the payback method in one respect; it allows for differences in the useful lives of the assets being compared. The accounting rate of return, however, suffers from the serious defect that it ignores the time value of money. When the method is used in relation to a project where the cash inflows do not occur until near the end of the project's life, it will show the same accounting rate of return as it would for a project where the cash inflows occur early in its life. Also, because the accounting rate of return is a ratio, the project's size, in terms of the absolute values of cash flows, is not considered.

7.8.2 Discounted cash flow methods

7.8.2.1 Net present value

Capital investment involves spending money now in the expectation of getting larger returns later. To tell whether the returns are large enough, a way is needed to compare returns in the future with investment now, to compare money amounts over time. A given amount of money now is worth more than the same amount of money in the future because it can be invested today to yield a return in the future. A way is therefore needed to determine the present value of money amounts in the future. This is done by using a discount rate. The discount rate normally reflects the company's cost of capital, the extent of essential projects which have no financial return and the 'riskiness' of the project concerned. While it is a difficult rate to measure, a

number of techniques may be adopted where appropriate. These include the capital asset pricing model, the weighted average cost of capital and the time preference.

The capital asset pricing model calculates the cost of capital as the return on equity required in a given period by the company's investors. It consists of two components: a risk-free element to represent the minimum level of return and a premium element which incorporates the risk attached to the investment.

The long term sources of finance are equity (retained profits or new issues of shares) and debt (borrowing). A company's weighted average cost of capital depends on the mix and the cost of equity and debt. If the proportion of equity to debt is 70/30, and the cost of equity is 18% and the cost of debt 7%, then the weighted average cost of capital is 14.7%.

In the public sector, the time-preference value of money is also assumed to estimate the cost of capital. It is the premium which the community is prepared to pay to enjoy benefits now rather than later.

Most companies invest in some necessary projects giving no direct financial return (e.g. for safety or to protect the environment). Attempts may be made to value such indirect benefits through cost-benefit analysis. Projects which do yield positive financial returns will need to make up for those that do not. Companies may use different discount rates for different types of project to allow for differences in risk. For example, cost saving projects may carry a lower discount rate than new product projects. How much to increase or reduce the average discount rate for high or low risk projects is hard to estimate.

Using an annual interest rate enables money amounts, receivable or payable, to be compared at different points in time. The net present value method of investment appraisal calculates a project's profit by comparing cash payments and cash receipts at the same point in time. Rather than look at the end of a project's life, however, it looks at the start. It does so by discounting expected future cash flows back to the present and then comparing the total present value of the future cash receipts with the initial capital investment in the project.

$$\text{NPV} = \sum_{y=1}^{n} \frac{C_y}{(1+k)^y} - C_0 \qquad (7.6)$$

Consider a company which wants to buy a new computer. The computer will cost £24,000 and be used for four years, after which time it would be obsolete with no second-hand value, giving a £6,000 p.a. straight-line depreciation charge. The company expects net cash inflows from the increased efficiency to be £6,000, £7,000, £9,000 and £11,000 in the four years of the computer's life. Using a discount rate of 15% (the assumed cost of capital), the net present value of the capital investment can be determined. Table 7.8 shows the details of the proposed computer purchase.

Clearly, the investment in the computer is not worthwhile. Its net terminal value is negative, indicating that the company would be better off investing the £24,000 at 15% interest. Thus the project amounts to a proposal to pay out £24,000 now in order to acquire the rights to future cash flows which have a present value of £21,429, representing a loss of £2,571.

***Table 7.8** - Net present value of proposed computer purchase*

End of year	Cash flow (£)	Discount Factor @ 15% p.a.	Amount at end of year 4 (£)	
0 (now)	-24,000	1.000	-------	-24,000
1	6,000	0.850	5,100	
2	7,000	0.723	5,061	
3	9,000	0.614	5,526	
4	11,000	0.522	5,742	21,429
Net present value				-2,571

The NPV method has a number of advantages. It focuses on the maximisation of the present value of future cash flows. It uses a discount rate reflecting the return required by the suppliers of funds. It is clear and unambiguous with a sound theoretical derivation to support the three fundamental financial decisions:

1. what proportion of the resources available should be consumed now ?
2. what proportion of the resources available should be invested to increase the future supply of resources ?
3. how much cash should be borrowed to finance the consumption and investment decisions ?

The NPV method relies on the accurate calculation of the cost of capital. Also, because it does not indicate financial efficiency, it cannot be used for ranking projects when resource constraints limit the level of investment. As well as the NPV of the initial investment, an investor will also be interested in the length of time before the return is achieved.

The profitability index addresses the problem of financial efficiency by showing the present value of benefits per £1 invested and is defined as the ratio of the present value of the benefits to the original investment.

$$\text{Profitability Index} = \frac{\text{Present value of benefits}}{\text{Original investment}} \tag{7.7}$$

In conjunction with the NPV, it can be a useful measure to rank competing projects when resources are limited.

7.8.2.2 Internal rate of return

Another method of discounting cash flows is often used instead of the net present value method. This is the internal rate of return (IRR) method. The net present value method lists the amount and timing of all the expected future cash flows from a project and the internal rate of return method does the same. The NPV method then applies a pre-determined discount rate based on the opportunity cost of capital, to see whether the net total of all the cash flows is positive or negative. If the NPV is positive, then the project is worthwhile (from a financial point of view), if the NPV is negative then it is not.

In contrast, the internal rate of return method determines what is the discount rate that when applied to the same cash flows will produce a net present value of exactly zero. This discount rate is the project's internal rate of return.

$$\sum_{y=1}^{n} \frac{C_y}{(1+\mathrm{IRR})^y} - C_0 = 0 \qquad (7.8)$$

It must then be compared with the criterion rate, to see whether or not the project is worthwhile. In Table 7.8, the net present value of the project was -£2,571 using a discount rate of 15%. Figure 7.5 shows the NPV of the same project for a variety of discount rates. The net present value is zero at a discount rate of 12.6%, the internal rate of return.

In most situations the internal rate of return method will result in the same decision as the net present value method. In the case of conventional projects, which are independent of each other, both NPV and IRR rules will lead to the same accept/reject decisions. There are, however, situations where the IRR method may lead to different decisions being made from those which would follow the adoption of the NPV procedure.

Where projects are mutually exclusive it is possible for the NPV and the IRR methods to suggest different rankings as to which project should be given priority. Mutually exclusive projects exist where the acceptance of one project excludes the acceptance of another project, for example the choice of one machine over another to perform a specific task. Consider a company investing in a new piece of equipment. Table 7.9 lists the estimated cash flows for the two options using a discount rate of 10%.

The IRR ranks project C first, but the NPV rate ranks project D first. If the projects were independent this would be irrelevant as both projects would be accepted. In the case of mutually exclusive projects, however, the ranking is crucial as only one project can be accepted. The NPV ranking depends on the discount rate used. Figure 7.6 shows that for a discount rate greater than 12% no contradictions arise as both the NPV and IRR rules rank project C first. The two methods give different rankings, however, for discount rates which are less than 12%, project D has a

higher NPV, but project C has a higher IRR. Logically one of them must be wrong and it is in fact the IRR method which is incorrect. Consider the incremental cash flows generated by moving from project D to project C. It would require an initial outlay of £5,000 and then an annual cash inflow of £2,090 for the 3 years the project runs. Figure 7.6 shows that the IRR of the incremental investment is 12%. As the cost of capital is 10%, the incremental project should be accepted. The IRR method has indicated that that the company should move from project C to project D, and the superiority of the NPV method is demonstrated.

***Table 7.9** - Mutually exclusive projects, NPV versus IRR*

		Project C (£)	Project D (£)
Investment	Year 0	-7,000	-12,000
Net Cash Inflows	Year 1	3,430	5,520
	Year 2	3,430	5,520
	Year 3	3,430	5,520
IRR (%)		22	18
NPV @10% (£)		1,530	1,728

Another problem with the IRR rule is that it expresses the result as a percentage rather than in monetary terms. Comparison of percentage returns can be misleading. Is an investment of £100 which returns 50% better than an investment of £1,000 which returns 25% ? Provided that all other factors are equal, the second investment is better, it yields £250 as opposed to £50, providing the company with more money for future investment.

7.8.2.3 Discounted payback

A modification to the payback method enables the time value of money to be taken into consideration. The payback period can only be a valid indicator of the time which an investment requires to pay for itself, if all cash flows are first discounted to their present values and the discounted values are then used to calculate the payback period. This adjustment gives rise to the discounted payback method. Even when such an adjustment is made the discounted payback method cannot be a complete measure of an investment's profitability. It can estimate whether an investment is likely to be profitable, but it cannot estimate how profitable that investment will be. The discounted payback method can be used as a supplementary indicator of the risk of an investment. This is only an approximation of risk, however, as it assumes that the risk of cash flows not being realised increases as they are deferred further into the future. This assumption may not always be true.

7.8.3 Problems associated with financial appraisal methods

The results from discounted cash flow calculations create an illusion of exactness which the underlying assumptions may not justify. Their accuracy is dependent on the selection of a realistic cost of capital. Small variations in the cost of capital can result in an investment decision being (sometimes incorrectly) reversed.

BREARLEY & MYERS, 1991, stress that a good capital budgeting system should contribute more than an accept/reject decision on individual projects. It should tie into both the organisation's long-term planning process and its procedure for measuring performance so that the organisation can learn from its experience. The financial analysis should only be a part of the decision-making process (item 5 in Figure 7.4). Qualitative judgement is also needed to assess the political, environmental, strategic and technological (PEST) issues affecting the profitability of the investment.

Although it is often an arbitrary process, the selection of the economic lifetime for a project is fundamental to the conduct of cost-benefit analysis, and this may be of the order of 50 years for a wind tunnel. Scenario and risk analysis can play an important role in identifying the long-term impact of decisions before making major policy choices [COYLE *et al.*, 1994]. Scenario analysis enables the effects of potential political, economic, social and technological changes to influence the choice of a project's life-time. Risk analysis determines the likely effect on the company if a particular scenario should become reality. As a consequence of risk analysis, additional premiums may be added to the discount rates used in determining net present values.

Cost-benefit analysis techniques ignore the full contribution of non-financial benefits which are uncertain and can be difficult to measure. Improvements in business performance due to the implementation of strategic systems are often qualitative and intangible. By focusing on return on investment figures and payback periods, companies tend to look short-term, and long-term innovation is discouraged. As long ago as the 1950s, it was stressed that post-project evaluations are needed for a company to assess progress and learn from its experience [DEAN, 1954]. In the early 1990s, however, more than 90 percent of companies failed to undertake a post-project evaluation to measure the actual performance of an investment against its original prediction [PETERS, 1990]. The lack of a post-project evaluation was attributed to a belief that it was unproductive and that it might reveal that the project was not cost effective.

In the following section, three broader frameworks are presented which, in addition to the financial appraisal, look at non-financial aspects of the decision-making process.

7.9 Broader frameworks for investment appraisal

7.9.1 Strategic methods

Corporate investment is normally undertaken in response to customer need. One way of gaining a deeper insight into customer need is through Porter's value chain analysis. A generic value chain is shown in Figure 7.7. The value chain breaks down the company into its strategically relevant activities. A company gains competitive advantage by performing these activities better or at lower cost than its rivals. Value is the amount customers are willing to pay for what a company provides them. The value chain displays total value and consists of value activities and margin. Value activities are the physically and technologically distinct activities that a company performs. Value activities are divided into two broad types, primary activities and support activities. Primary activities are those that are involved in the creation of the product or, in the case of wind tunnels, the service. These primary activities are divided into the following categories:

1. *Inbound logistics.* Activities associated with the receiving of goods. In the case of wind tunnels, this might include the delivery, handling and storage of the models to be tested.

2. *Operations.* Activities associated with the service itself. This would include the running of the wind tunnel, data collection for the customer and keeping the customer informed of the progress of the test programme.

3. *Outbound logistics.* Activities associated with delivering the end product or service. This would mainly involve the packaging and handling of the wind tunnel model ready for transportation but may also be extended to include the supply of test reports to the customer.

4. *Marketing and sales.* Activities associated with providing a means by which buyers can purchase the service and inducing them to do so (advertising, promotion, pricing structures).

5. *Service.* Activities the company may carry out for the customer upon supply of the product or completion of the service. This might include follow-up work for the customer to clarify any queries they may have with test data.

Each of these may be a source of competitive advantage and, depending on the industry, different activities will be emphasised. In the case of wind tunnel testing, the most important activity will be the operation of the wind tunnel and the associated data collection.

In addition, there are support activities; the company infrastructure, human resource management, technology development and procurement. These are factors which influence the running of the company supplying the product or service. In the

case of a company operating a wind tunnel, technological development will be especially important. The company needs to be able to provide the customer with the best instrumentation and data acquisition hardware available in order to retain their custom.

The value chain helps the company to identify its strengths and weaknesses in business areas which are important to it. Links between the company and the customer value chains can be important sources of competitive advantage. By tuning into the customer's business needs, the services provided can be tailored to their particular requirements. If the linkage is particularly good then the customer may perceive the supplier of the service as an essential part of their future business success. Thus, value chain analysis should be undertaken along side the formal capital budgeting evaluation.

7.9.2 The Information Economics Model

Another broader investment appraisal method which has been used in the field of information technology is the Information Economics Model. PARKER & BENSON, 1988 argued that, as the capability and strategic use of information technology increases, the costs and benefits of information systems projects become more difficult to assess. They asserted that the focus on finite costs and benefits was too restrictive to be successful in guiding corporate decisions. In an attempt to improve the effectiveness of investment appraisal, they developed the Information Economics Model to provide a broader approach to investment appraisal.

The purpose of information economics is to take economic tools, such as cost-benefit analysis, and expand them to consider competitive advantage in the decision-making process. Information economics replaces the concept of 'benefit' with the more generic idea of 'value', as used by Porter in his value chain discussed above. The company's processes and its interactions with its customers and markets are examined to identify how investment in a project can improve overall company performance. Similarly, 'cost' is expanded to cover the total cost to the organisation of implementing the project. Value and cost are considered throughout the company to ensure that the optimal solution is found rather than a solution which meets the financial appraisal criterion but which fails to meet the needs of the customer. Thus the true economic value of the project is defined in Figure 7.8. The Information Economics Model consists of three main components, the enhanced NPV, the business domain and the technology domain. The combination of these then gives the true economic value of the project.

The enhanced NPV is determined from five financial factors. Firstly, financial appraisal methods are used to determine if the project meets the company's accept/reject criteria. This will make use of one or more of the methods discussed in Section 7.8. It is most appropriate to use NPV or IRR to take account of the time

value of money. Secondly, 'value linking' assesses the improvement in business performance as a result of implementing the project. It represents the ripple effect of an improvement in one part of the company leading to improvements elsewhere. 'Value acceleration' considers the impact of time improvements generated by the project. In the case of a wind tunnel for example, the ability to obtain data at near full-scale Reynolds numbers could help to shorten the flight test programme of a new aircraft and reduce the number of modifications necessary before the production phase. 'Value restructuring' measures improvements in a company's performance resulting from organisational changes as a consequence of implementing the new project. Finally 'innovation valuation' estimates the value of new business opportunities afforded by the new project. This, undoubtedly, would be of major importance for a wind tunnel construction project. The construction of the new wind tunnel will in itself create a new company which will have to exploit the new business opportunities which this creates. In particular, a customer base will have to be developed if the wind tunnel operating company is to survive. The original NPV is reassessed to include the effect of the other four value factors.

In the business domain, five factors are used to determine this particular value. 'Strategic match' measures the degree to which the project supports the company's strategic goals. 'Competitive advantage' examines the extent to which the project improves the company's competitive position. In the case of the project being considered here, this is a major objective for the project. 'Management information' assesses the project's contribution in providing management information which directly contributes to the achievement of the company's mission. 'Competitive response' measures the degree to which failure to implement the project will cause competitive damage to the company. Competitive response is often a major driving force in investment decisions and the wind tunnel case is no exception. 'Organisational risk' considers whether the company has the necessary personnel, skills and experience to implement the project. This is an important consideration in risk analysis.

In the technology domain, the Information Economics Model considers how the project relates to the appropriate company activity or activities as contained in Porter's value chain e.g. technology development or sales and marketing. The 'strategic architecture' evaluates the degree to which the project is aligned with the overall company strategy for that activity. For example if a company has a mixture of computers with different operating systems and wishes to standardise on one, there is little logic in implementing a project which makes use of the operating system which is to be phased out. 'Definition uncertainty' assesses the degree to which the customer requirements are known. Similarly, 'technical uncertainty' assesses the project's dependence on new or untried technology, including operator skills and the reliability of new hardware and software. Finally 'infrastructure risk' assesses the

extra company infrastructure investment that may be required to implement the project.

The project's economic impact, as given by the enhanced NPV, is compared with a predefined company standard and scored in the range zero to five. Each of the business and technology domain factors is also scored in the range zero to five. The company then gives each factor a weight to reflect its relative importance. The selection of appropriate weights is important in the effective application of the Information Economics Model. Each company should set its own weights to suit its particular circumstances. Finally the weighted score for each proposal is calculated to produce a list of projects ranked according to their true economic value.

The Information Economics Model offers distinct advantages for the conduct of investment appraisal. It provides a holistic approach for analysing cost, benefit and risk. Although developed primarily for information systems projects, it is capable of being adapted to suit other corporate domains such as service industries, into which wind tunnel testing could be considered to be categorised. Non-financial aspects are quantified and considered alongside the direct economic costs and benefits. The Information Economics Model is particularly useful for appraising innovative projects whose benefits are often difficult to measure. It suits companies where resources are limited and competing projects have to be prioritised. The structured arrangement of the project enables easy auditing. Post project evaluation can be used to determine areas that are prone to optimistic or pessimistic bias.

The use of the Information Economics Model is not without its drawbacks, however. The application of the methodology may be inappropriate for small projects and the scoring can become subjective if the definitions contained within the model do not apply. Weights also have to be calculated carefully if the overall value obtained is to be realistic. The model applies quantitative measures to qualitative topics and there is the danger of placing too much emphasis on the single value which is generated as a result of applying the model.

7.9.3 Combined operational effectiveness and investment appraisal (COEIA)

The third of the investment appraisal frameworks in this selected review of broader capital budgeting techniques, is a new method for justifying procurement of military equipment for the tri-service UK Defence Staff, described at length by KIRKPATRICK, 1996. It combines operational effectiveness with financial appraisal methods to arrive at a procurement decision. Although primarily aimed at military procurement, it does provide ideas which are relevant to most large capital investment decisions.

COEIA has only been in use for a few years. It followed a review of UK equipment procurement procedures [BUCKLEY, 1991] which called for substantial changes in the decision-making process. The recommendation was that future proposals for

equipment procurement should be accompanied, among other things, by a cost-effectiveness report based on the results of operational analysis and on forecasts of the life cycle cost of the alternative equipment options. The result was the Combined Operational Effectiveness and Investment Appraisal (COEIA).

The COEIA procedure is intended to aid the selection of alternative options for defence equipment based on a military operational requirement. The first stage in any COEIA is the formulation of a concept of analysis. The concept of analysis sets out the alternative equipment options to be considered in the COEIA. The range of options available is extensive but falls into three main categories:

1. Do nothing.
2. Maintain present capability.
3. Improve capability.

The 'do nothing' option is important as it provides a datum from which increases in military capability and funding may be measured. It represents an inadequate and diminishing level of operational effectiveness in future years. The second alternative is to maintain the present capability. This can be achieved by refurbishing the existing equipment to extend its service life or by buying or leasing new or second-hand equipment with a broadly similar capability. The third alternative is to improve the current capability. This can be done by either upgrading existing equipment to enhance its capability; buying or leasing new or second-hand equipment with superior performance; or by developing the production of new equipment to meet the relevant requirement. The range of options chosen for the COEIA must include all practicable options which might offer best value for money. The concept of analysis must also define the scenario(s) within which the alternative equipment options will be assessed.

The second stage in the COEIA process is to determine the operational effectiveness of the procurement options. Within a COEIA, it is mandatory that the assessment should use military operational analysis. This method evaluates explicitly and quantitatively the overall effectiveness of the equipment being considered. Effectiveness is measured as the option's success relative to an enemy's current equipment. Databases of battle data enable trends to be identified linking the probability of victory to the number and effectiveness of the weapons involved. These trends enable operational analysis studies to conclude that one equipment option is likely to be better than another.

The third stage in the COEIA is to conduct a financial appraisal of the procurement options. There are four key factors in the financial appraisal of a COEIA.

The first is the production of a master data and assumptions list (MDAL) for each of the options considered. The list is extensive and includes such particulars as; a complete technical description of each of the options; the procurement strategy; the

delivery schedule; training and logistics support for the equipment; assumptions on the equipment's reliability and maintainability, and consequent estimates on the levels of support required.

Secondly, forecasts of all the components of the life cycle cost of each of the alternative options are required. This includes all the expenditure directly and indirectly associated with the project from its inception to its disposal. The forecasts are continually updated as more accurate information becomes available about the development, production, operation and support of the new equipment. A discounted cash flow method (NPV) is used for the financial appraisal with the discount rate set by the Treasury (currently 6 percent). Residual value must be included in the financial appraisal. It is therefore necessary to estimate the revenue from the sale of equipment or expenditure costs of disposal at the end of the project. Accurate estimates are not important as the discount factor ensures that these figures are relatively insignificant for a 25 year project.

Thirdly, consideration should be given to the risk and uncertainties in the forecast cost, performance and other characteristics of the alternative options, and to the effect of these uncertainties on the investment appraisal results. Uncertainties about any project arise from adverse events or delays which may affect the programme, and from variations in the equipment's performance, reliability, cost and other characteristics (e.g. Nimrod AEW). Uncertainties about equipment bought 'off-the-shelf' from a reliable contractor are much smaller than those associated with new equipment still undergoing development (e.g. Longbow Apache versus Eurocopter Tiger). Consequently, risk management plans should be drawn up to reduce the likelihood and/or the scale of potential variations in cost.

Finally, the assessments of operational effectiveness and forecasts of life-cycle costs of the alternative equipment options must be brought together in a comparison to determine which option offers best value for money. This may be done by plotting forecast values of force effectiveness against life-cycle cost (NPV) of each alternative option as shown in Figure 7.9. The procedure is not entirely satisfactory, however, because while option 3 is clearly better than 2 or 4, it is not obvious whether it is better than 1 or 5. Ideally the options should be formulated to reveal which force offers the lowest NPV of life-cycle cost at a given level of military effectiveness, or which offers the greatest level of military effectiveness at a chosen NPV. Treasury rules require the MoD to look for constant effectiveness options (Figure 7.10) i.e. provide a range of procurement options with the same operational effectiveness but differing NPVs. In practice, however, this can prove impossible. It is generally easier to tailor the alternative options to attain a specified NPV. A comparison of alternative options with NPV values which are similar, but not identical, is often adequate to identify the option offering best value for money.

There is no doubt that the COEIA system delivers a more thorough analysis of the options available than purely financial methods alone. There is a more formal assessment of the 'do nothing' option and a range of options is kept throughout the COEIA process which means that the decision makers can be better informed about the relative effects of different choices at the time they must make their decisions. The main penalties are the extra time and cost of carrying out the operational and financial analysis. The costs of COEIA studies can be high and may run into millions of pounds. This is, however, small (of the order of 0.5 percent) when compared with the life cycle cost of a major defence project.

7.10 Suitability of investment appraisal methods to wind tunnel construction projects

The application of solely financial appraisal methods to wind tunnel construction projects is inappropriate. As has already been stated, the reasons for building a wind tunnel of the type and size being considered here are essentially technology driven. Once a sufficient market has been established for a wind tunnel then construction will inevitably follow. The wind tunnel will probably be unique and will have to demonstrate the ability to provide technological and cost benefits for aircraft manufacturers over existing wind tunnels. WOODWARD, 1995, commented that investment appraisal was rarely, if at all, carried out on wind tunnel projects of the size considered here. Indeed, he said investment appraisal was not considered prior to the construction of the DERA 5 m wind tunnel at Farnborough. Technological factors were the driving force behind the decision to build that particular wind tunnel. The ability to carry out an accurate financial appraisal is complicated further by the long-term nature of the project. Construction would probably take at least 5 years and the life-span of the wind tunnel itself could conceivably be 50 years. Estimating the market demand and operating costs for a wind tunnel over this period of time is almost impossible.

Although the capital costs of wind tunnel construction projects have historically been funded by government, there is increasing pressure from governments for the aerospace industry to contribute to the capital cost. YANG & GREY, 1995, report that the US government is looking for a 10 percent contribution from industry towards the cost of the National Wind Tunnel Complex. Congress, however, prefers a greater contribution by industry to the shared cost, believing that a higher level of financial commitment would tangibly demonstrate the industry's need for the facilities. Industry, on the other hand, asserts that the majority of the long-term, low rate of return investment required to fund the capital cost should not be made by the private sector, arguing that in the competitive international aerospace market, US industry cannot justify a $2.0 billion short-term cost to gain such very long-term benefits. 'If you try to justify it on a return on investment basis for industry, it's not really possible to do that' [HARRINGTON, 1995]. Also, the need to finance the cost of the facility would

inflate the price of US aircraft, making them less competitive in the market place, partly defeating the purpose of constructing the wind tunnel complex.

Financial appraisal of the wind tunnel project should combine payback and NPV. Payback would be used to evaluate the financial 'riskiness' of the project and aim to determine the operational time required to recover the initial investment. NPV would evaluate the financial viability of the construction and operation of the wind tunnel based on a predetermined cost of capital. As already stated, however, due to the long life-span of the wind tunnel this could prove particularly difficult to determine accurately.

The broader frameworks discussed in Section 7.9 provide a more 'strategic' approach to investment appraisal which may be more appropriate to a project of the type considered here.

Porter's value chain is useful in determining which activities companies should focus on to enable them to develop a competitive advantage over their rivals. Once the wind tunnel is operational and has established a customer base, the aim will be to retain these customers and attract new ones. Value chain analysis would enable the company to analyse the strengths and weaknesses in its activities and then act on them in order to maintain a strong presence in the wind tunnel testing market.

The Information Economics Model looks at the impact of a new project on an existing company in terms of the financial, business and technological domains. The construction of the wind tunnel would necessitate the creation of a new company to run it and so the Information Economics Model would not be appropriate in this case. It would, however, be useful if, say, the wind tunnel required upgrading in the future to take account of new data acquisition hardware. The model would enable the company operating the wind tunnel to obtain a broader perspective on the impact of different upgrade options to the company.

COEIAs are useful in assessing procurement options where specifications and costs are expected to vary and hence could be used in a procurement decision such as is proposed. There are a number of permutations on tunnel design which COEIA-type frameworks could be used to analyse. These might include: the tunnel layout; geographic location; working section size; levels of pressurisation etc. The option which provides the best combination of technological capability, cost and productivity could then be determined.

Despite the availability of all the capital investment appraisal methods described above, in practice the decision often just comes down to 'rules-of-thumb' or 'intuition'. There have been many studies of investment criteria over the years. What emerges so strikingly from them is the major role rules-of-thumb still play in the appraisal tool kit [HIGSON, 1986]. In the case of the construction of a wind tunnel, decision-making may simply distil down to the fact that industry needs it, so build it. Such an approach, however, is not a recommendation of the author.

7.11 Summary

In this chapter the commercial justification for carrying out the research was first described. The overall management of the research project has been discussed with particular reference to the time schedule and costs, together with an analysis of the likely impact of the research findings for DERA Farnborough.

Based on these findings, a scenario was developed which called for the procurement of a new large-scale low-speed wind tunnel for the European aerospace industry. A brief review of existing low-speed European wind tunnels was presented, highlighting the need for a larger wind tunnel with a Reynolds number capability of 20 million. Design proposals were put forward for two low-speed wind tunnels, one atmospheric and the other pressurised, and estimates were made of their construction and operating costs. The two tunnels had similar construction costs but the pressurised tunnel was estimated to be less expensive to operate. The combination of this and the advantage of independent Mach number and Reynolds number testing, made the pressurised tunnel the preferred choice.

The decision-making process for capital investment decisions was then discussed followed by a review and critical analysis of appraisal methods which could be used in the financial evaluation of a wind tunnel construction project. This included traditional and modern 'discounted' methods. Following on from this, some of the broader non-financial considerations in the decision making process were discussed.

Finally the chapter looked at the application of these evaluation tools to a wind tunnel construction project and the company which would operate it. The review concluded that the application of solely financial investment appraisal methods to wind tunnel construction projects is inappropriate and that the use of broader-based appraisal methods should be considered.

	1993	1994				1995				1996				1997		
Project component	Oct.-Dec.	Jan.-Mar.	Apr.-Jun.	Jul.-Sep.	Oct.-Dec.	Jan.-Mar.	Apr.-Jun.	Jul.-Sep.	Oct.-Dec.	Jan.-Mar.	Apr.-Jun.	Jul.-Sep.	Oct.-Dec.	Jan.-Mar.	Apr.-Jun.	Jul.-Sep.
MBA course modules																
Additional modules																
Literature review																
Model design																
Model construction																
Set-up experimental facilities																
Model commissioning																
Data collection																
Data analysis																
CFD work																
Management theory																
Thesis write-up																

Figure 7.1 - Original schedule.

	1993	1994				1995				1996				1997		
Project component	Oct.-Dec.	Jan.-Mar.	Apr.-Jun.	Jul.-Sep.	Oct.-Dec.	Jan.-Mar.	Apr.-Jun.	Jul.-Sep.	Oct.-Dec.	Jan.-Mar.	Apr.-Jun.	Jul.-Sep.	Oct.-Dec.	Jan.-Mar.	Apr.-Jun.	Jul.-Sep.
MBA course modules																
Additional modules																
Literature review																
Model design																
Model construction																
Set-up experimental facilities																
Model commissioning																
Data collection																
Data analysis																
CFD work																
Management theory																
Thesis write-up																

Figure 7.2 - Actual Schedule

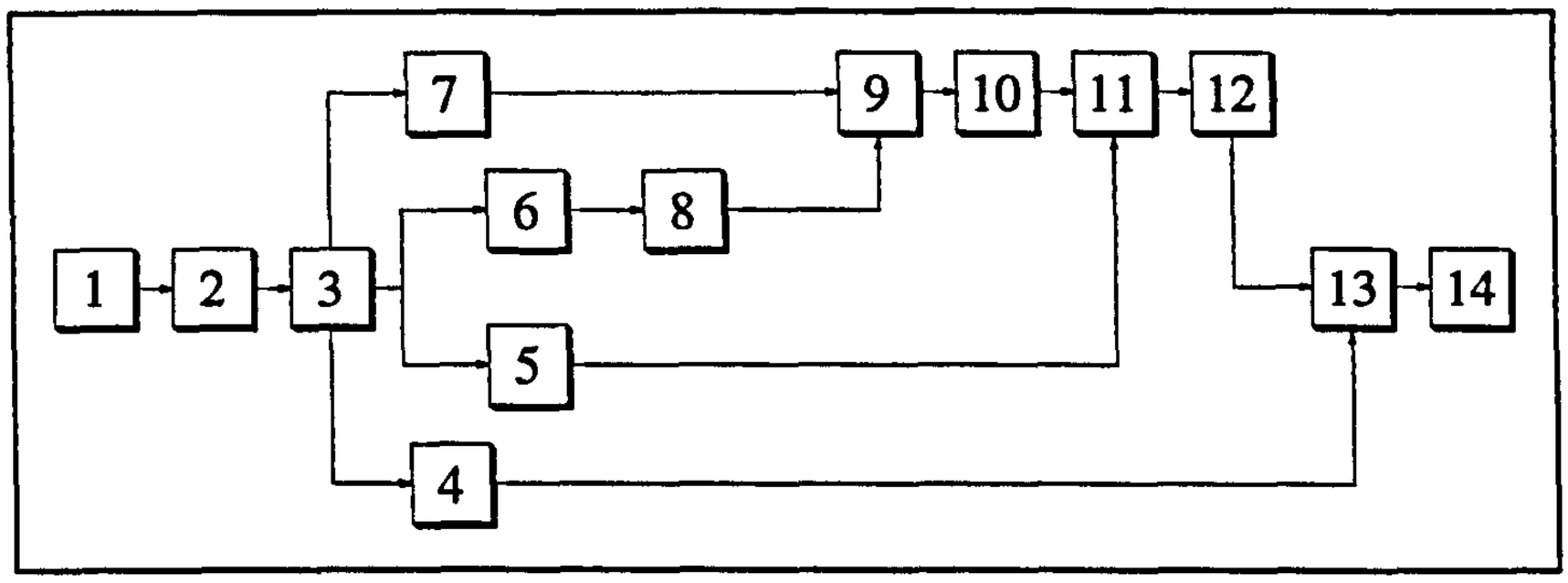

***Figure 7.3** - A Gantt chart for the project.*

1. Start
2. MBA course modules
3. Additional modules
4. Literature review
5. CFD
6. Model design
7. Set up experimental facilities
8. Model construction
9. Model commissioning
10. Experimental data collection
11. Data analysis
12. Management work
13. Thesis write-up
14. Finish

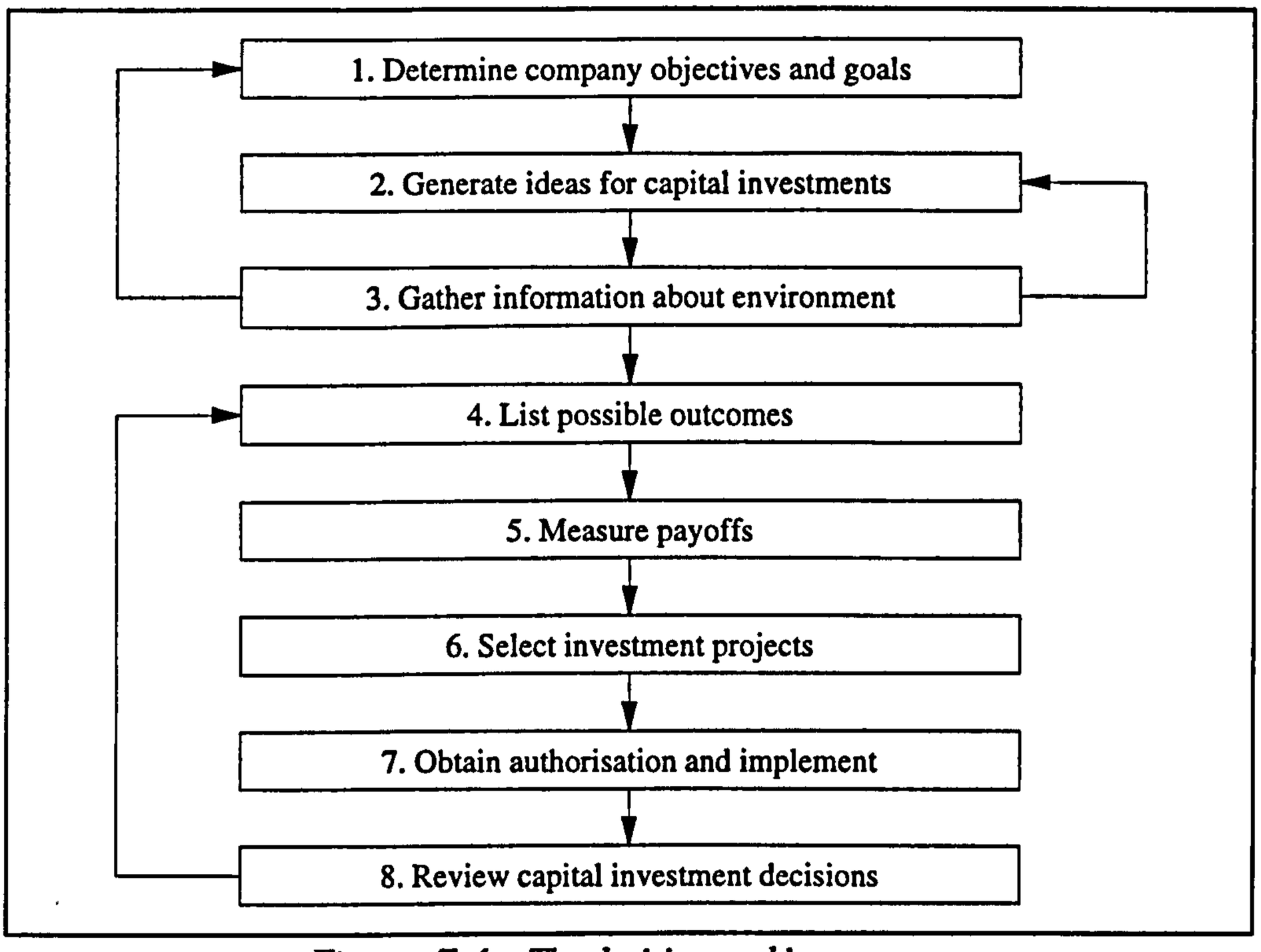

***Figure 7.4** - The decision-making process.*

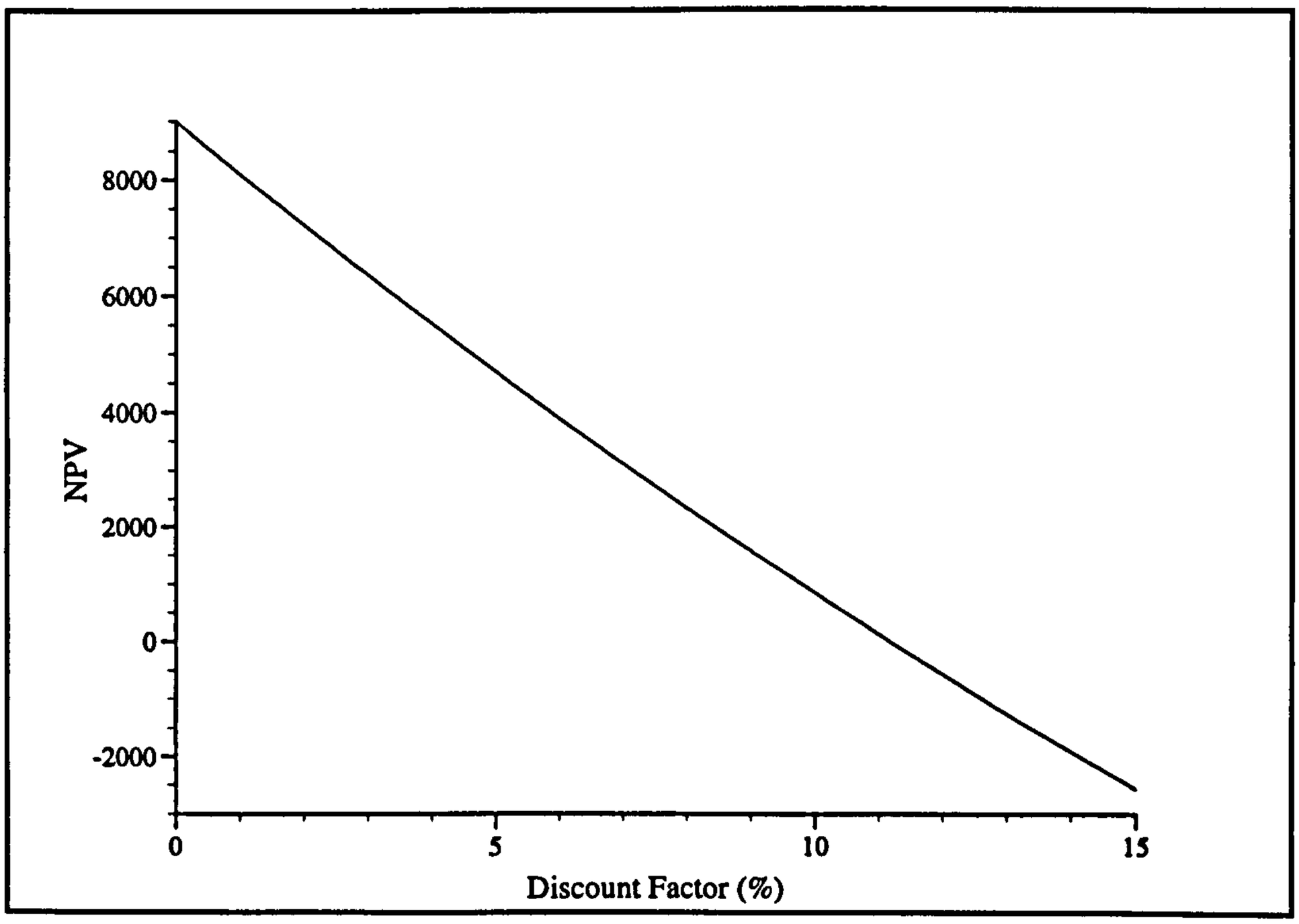

***Figure 7.5** - Net present value of computer purchase at various discount rates*

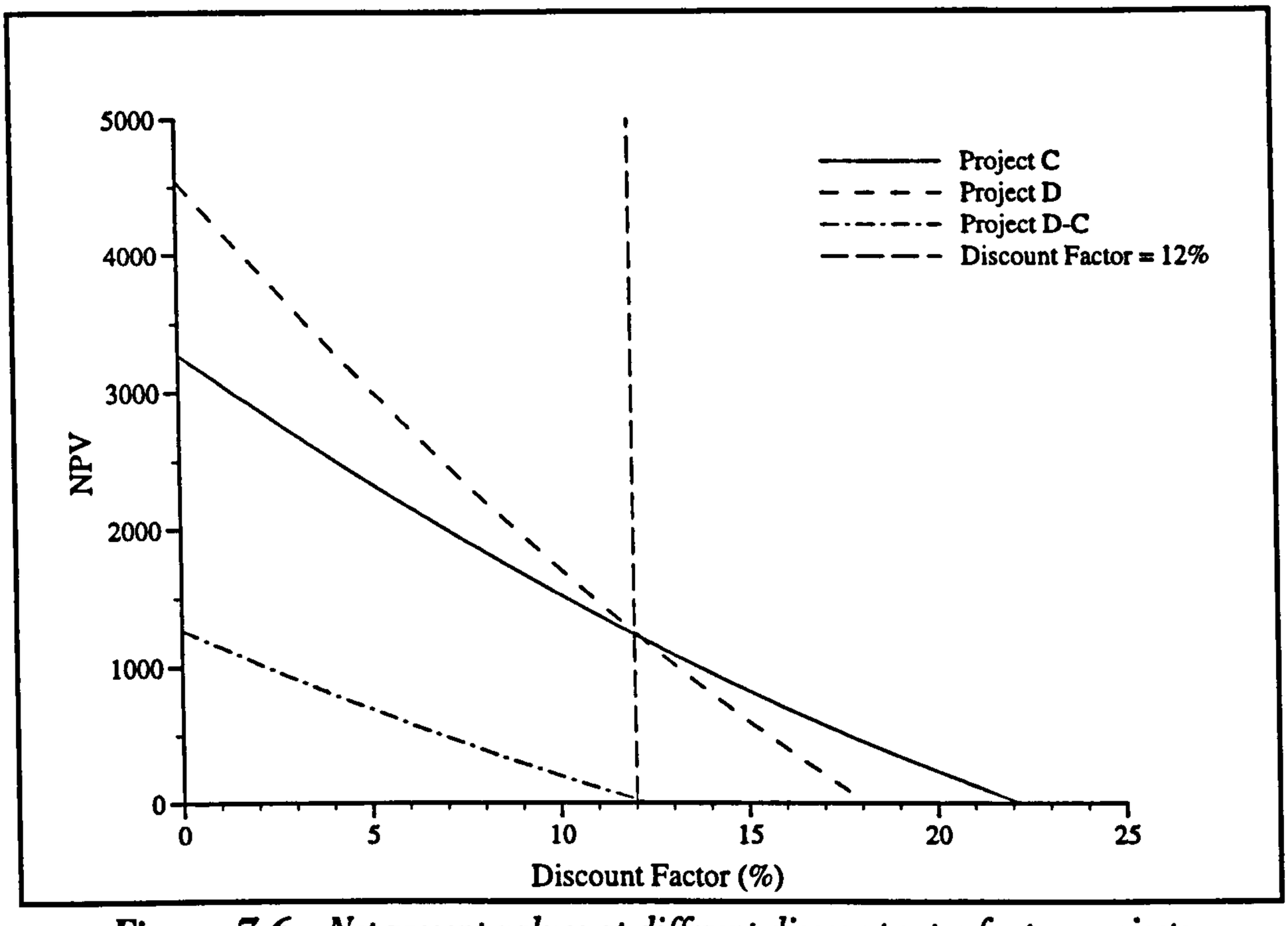

***Figure 7.6** - Net present values at different discount rates for two projects*

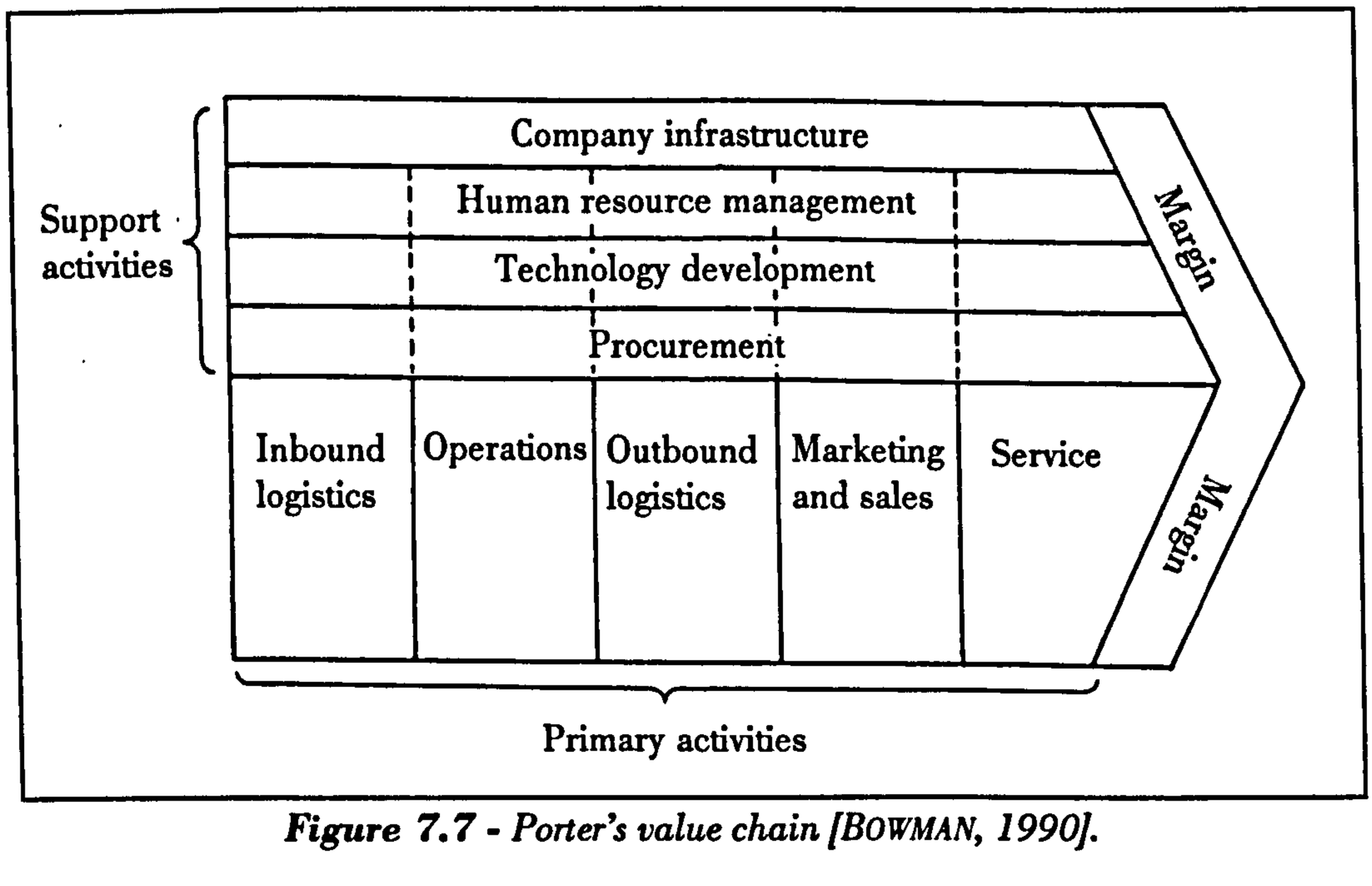

***Figure 7.7** - Porter's value chain [BOWMAN, 1990].*

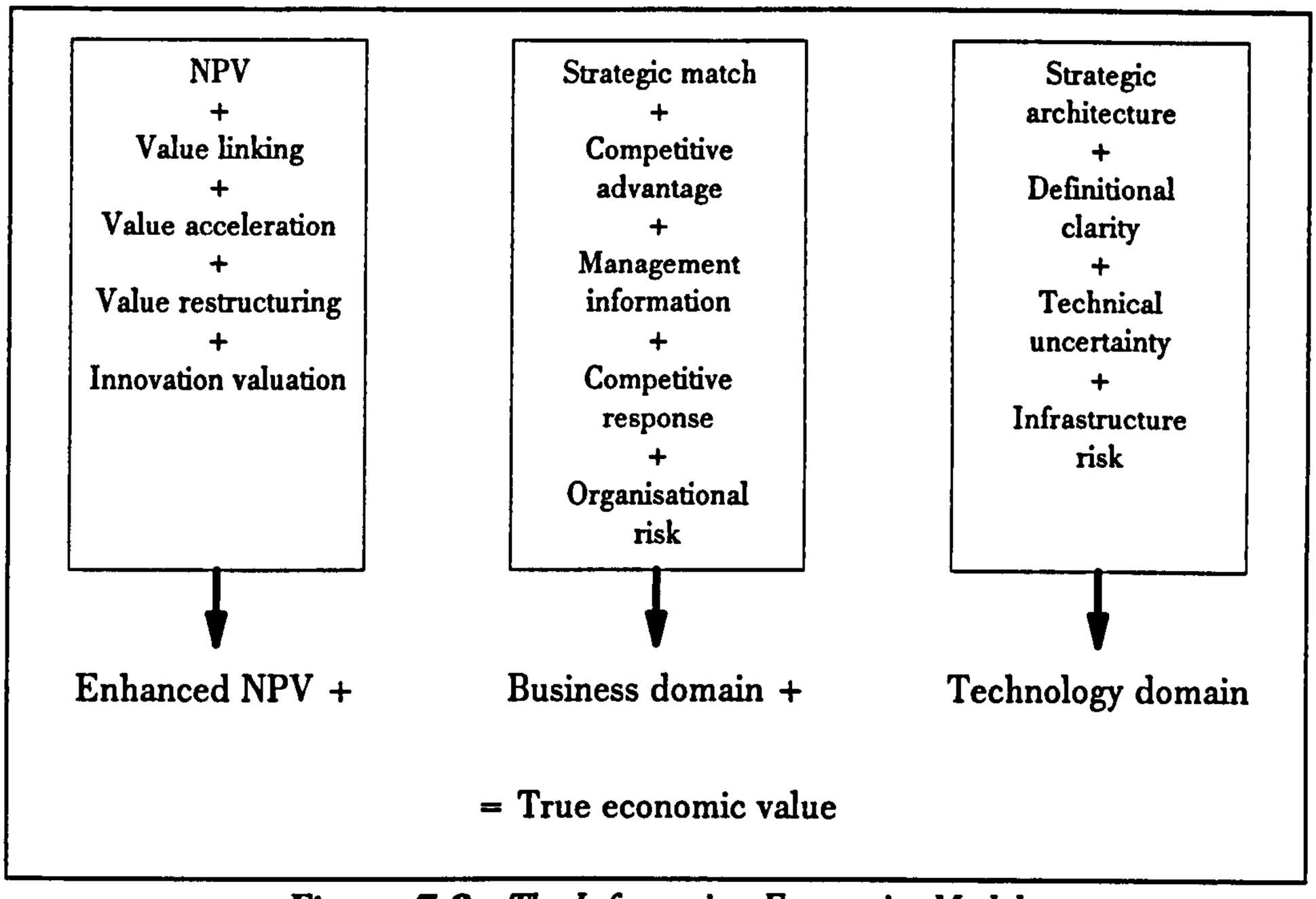

***Figure 7.8** - The Information Economics Model*

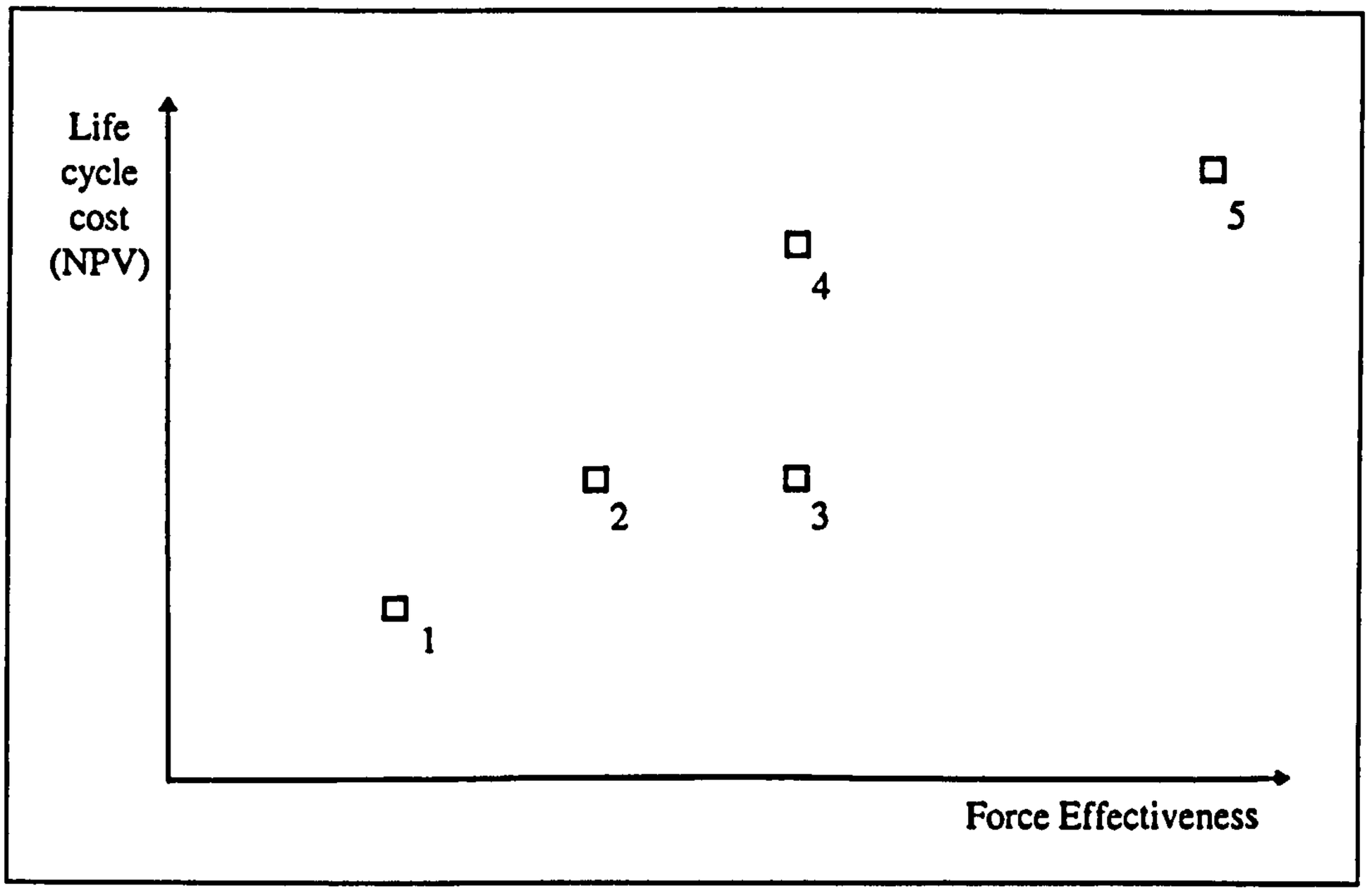

***Figure 7.9** - Comparison of cost and effectiveness of five alternative options.*

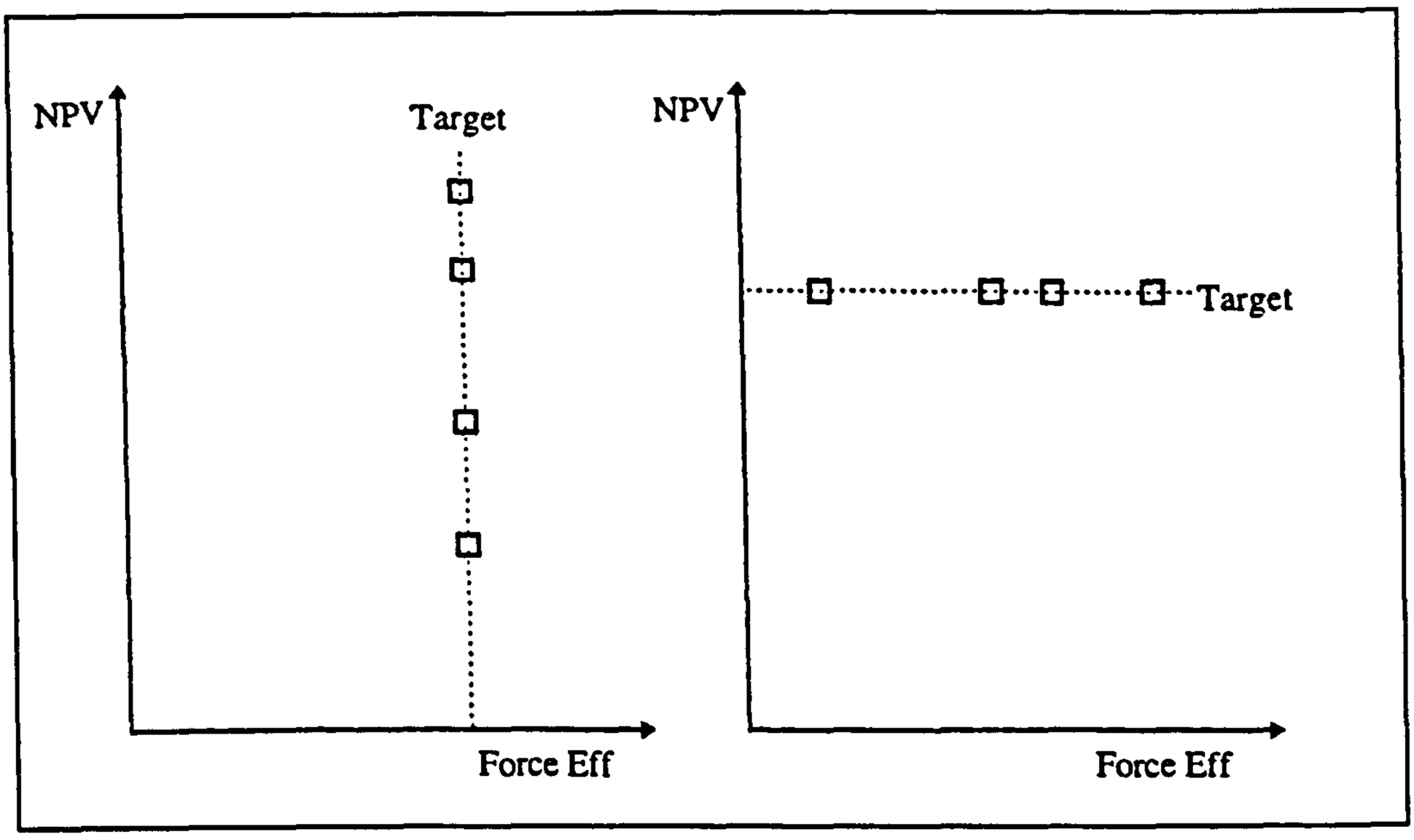

***Figure 7.10-** Comparison at constant effectiveness or constant cost.*

8 Conclusions and Recommendations

This final chapter summarises and draws conclusions from the experimental, numerical and management work undertaken in this project and discussed in the previous chapters.

Recommendations are also made for future research in the field of STOVL jet-lift aerodynamics.

8.1 Conclusions

This research has addressed some of the problems associated with wind tunnel testing of STOVL aircraft out of ground effect, in particular the question of whether jet and intake flows need to be represented simultaneously in such wind tunnel tests. There have been three aspects to this work: a wind tunnel test programme to investigate jet/intake interference effects, a CFD programme to investigate elements of these flow-fields and an analysis of management aspects of wind tunnel project work. Each of these aspects will be discussed in the following sections.

In Chapter 2 an extensive literature review was carried out on STOVL interference effects in order to gain a broad understanding of this research topic. The review included out of ground effect studies of free jets and jets in cross-flow as well as whole aircraft. Particular attention was paid to wind tunnel tests involving jets and intakes simulated together. The review concluded that although extensive research has been undertaken in the field of transition aerodynamics, attention has rarely focused on the area of jet/intake mutual interference and no conclusive evidence could be found to quantify the magnitude of such interference effects.

8.1.1 Experimental work

In order to investigate and measure jet/intake interference effects a suitable wind tunnel model was needed. Chapter 3 discussed the design and construction of a generic jet-lift STOVL wind tunnel model. A systematic experimental investigation was carried out to try to determine the magnitude of any jet and intake related interference effects on a generic jet-lift STOVL aircraft.

Chapter 4 described the results of the experimental work carried out to investigate STOVL jet- and intake-related interference effects. The following findings were made.

The jet-induced aerodynamic lift loss on the wing varied between -0.042 $C_{l\,(root)}$ and -0.234 $C_{l\,(root)}$. The latter was equivalent to a reduction in wing root incidence of over 2 degrees. Increasing effective velocity ratio reduced the jet-induced $\Delta C_{l\,(root)}$ increments for a constant NPR and nozzle position. The variation in $\Delta C_{l\,(root)}$ with V_e was found to be non-linear. Varying NPR with a constant nozzle mass flow rate showed no consistent effect on $\Delta C_{l\,(root)}$, however increasing NPR with a constant nozzle area increased the jet-induced $\Delta C_{l(root)}$ increment, particularly at low freestream dynamic pressures. Nozzle position showed a small influence on $\Delta C_{l\,(root)}$. Its effect was dependent on the particular combination of NPR and freestream dynamic pressure used during the test.

The effect of the powered intakes on the wing was to create a 'lift enhancement'. This was due to the intake flow altering the local magnitude and direction of the

freestream air ahead of the wing, in particular the combination of the high-mounted wing and the lack of intake plugs caused a reduction in velocity under the wing. At the lowest freestream dynamic pressure tested (61.3 Pa; $V_\infty \approx 10$ ms^{-1}) the lift enhancement was equivalent to a 0.5 degree increase in wing incidence. Increasing freestream dynamic pressure reduced the lift enhancing effect to 0.2 degrees at 245 Pa ($V_\infty \approx 20$ ms^{-1}) and 0.1 degrees at 551 Pa ($V_\infty \approx 30$ ms^{-1}).

The jet-induced interference introduced a velocity component into the freestream which affected the intake flow as well as the airflow over the wing. The interference created a download on the intakes which was determined from the intake static pressure distributions. The largest change in intake normal force coefficient, C_{ni} occurred at the lowest freestream dynamic pressure and reduced with increasing dynamic pressure. Increasing NPR at constant nozzle mass flow rate did not affect the value of C_{ni} for a particular nozzle position and freestream dynamic pressure. Increasing NPR with a constant nozzle area increased ΔC_{ni} particularly at the lowest freestream dynamic pressure. Jet-induced interference on the intake was greatest for the forward nozzle position, followed by the centre and rearward positions.

The numerical sum of the $\Delta C_{l\,(root)}$ values obtained from separate jet and intake configurations was not the same as the $\Delta C_{l\,(root)}$ values obtained with simultaneous jet and intake testing. The discrepancy between the two methods was thought to be due to the jet-induced interference on the intake flow. This brings into question the applicability of separate jet and intake testing for STOVL aircraft particularly at low transitional speeds.

The discrepancy between the two methods was found to be dependent on all the model configuration parameters and was determined to be as much as -0.08 $\Delta C_{l\,(root)}$ (0.75 degrees wing root incidence) depending on the model configuration and test parameters. The discrepancy was found to be greatest at the lowest effective velocity ratios but was still evident at the highest ones. Both methods of determining the combined interference effect of the jet and intakes on the wing followed the same trend with NPR (for both the constant mass flow rate and constant nozzle area tests). The discrepancy, therefore, was reasonably constant for variations in NPR. At the lowest freestream dynamic pressure (61.3 Pa; $V_\infty \approx 10$ ms^{-1}) the discrepancy was greatest at the forward nozzle position and reduced as the nozzle was moved further aft. At the two higher freestream dynamic pressures, the discrepancy was greatest at the centre nozzle position.

8.1.2 Numerical modelling

In addition to the experimental work, numerical modelling using the PHOENICS CFD code and the k-ε turbulence model was performed. Results were obtained for a NACA 1408 aerofoil, a round free jet at subcritical and underexpanded nozzle pressure ratios and a round jet in cross-flow with the same jet conditions. The re-

sults generated by the numerical modelling were compared with available experimental data and showed reasonable agreement. The following points were made regarding the numerical modelling work undertaken.

The suction pressures on an aerofoil modelled using the body-fitted co-ordinate system were underpredicted. The sectional lift coefficient, C_l, however, agreed with potential flow theory to within 5 percent.

The k-ε turbulence model was found to over-predict the spreading rate and hence the centre-line velocity decay of a round free jet. Contrary to experimental data, variations in NPR were found to have *no* effect on free jet spreading rate. In addition, PHOENICS tended to smear the shock structure of an underexpanded jet which led to near-field velocity profiles showing poor agreement with experimental data. The lack of a predicted NPR-effect is, perhaps, not surprising given this poor shock prediction and the lack of any effect of compressibility in the turbulence model. The centre-line trajectory of a round jet in cross-flow showed reasonably good agreement with established empirical correlations for the range of velocity ratios tested. The numerical model, however, predicted too much deflection at low velocity ratios and too little at higher ones.

Several unsuccessful attempts were made to simulate combined wing/jet and intake/jet configurations using the CFD software. Disappointingly, no satisfactory solutions were achieved for these particular flow-fields, mainly due to convergence and gridding problems.

8.1.3 Management work

This thesis finally addressed the management aspects of wind tunnel project work (Chapter 7). The management of time and cost elements of the research undertaken for this thesis was described. The research was completed on time and within budget.

The main focus of Chapter 7 was the hypothetical procurement of a new large-scale wind tunnel with a Reynolds number capability of 20 million for use by the European aerospace industry. A review of existing low-speed European wind tunnels established a need for such a tunnel especially in light of the proposed National Wind Tunnel Complex in the USA. Two tunnel designs, one atmospheric and the other pressurised, were proposed together with estimations of their construction and operating costs. The pressurised tunnel was chosen to be the more suitable due to its much lower operating costs and the ability to test independently the effects of Mach number and Reynolds number on aircraft designs.

The decision-making process for capital investment decisions (such as the construction of a new wind tunnel) was then discussed followed by a review and critical analysis of appraisal methods which could be used in the financial evaluation of a

wind tunnel construction project. This included traditional and modern 'discounted' methods. Following on from this, some of the broader non-financial considerations in the decision making process were discussed. The review concluded that the application of solely financial investment appraisal methods to wind tunnel construction projects is inappropriate. The broader investment appraisal frameworks discussed were thought to be more appropriate to the type of project being considered.

8.2 Recommendations for future work

The following recommendations are made for future work in the field of STOVL jet-lift aerodynamics. They have been grouped as: work needed to clarify the observed interference effects; developments needed to improve the productivity of the existing wind tunnel model; improvements to the CFD modelling and finally general recommendations relevant to STOVL wind tunnel testing.

Further work to clarify jet/intake interference effects

- Pressure measurements are needed at different span-wise locations to determine the span-wise extent of jet and intake interference effects on the wing.
- Tests should be conducted at even higher freestream dynamic pressures than were possible here, to determine if jet/intake mutual interference effects are confined solely to low speed transition. The current speed range could be increased by 50% by moving to the RMCS 2.75 m by 1.4 m open-jet wind tunnel.
- The effect of the ratio of jet to intake mass flow rate should be investigated. This would establish the sensitivity of the magnitude of the mutual interference effects to this parameter.
- The effect of wind tunnel interference on the results should be checked. This could be achieved by repositioning the model in the wind tunnel.
- Mapping of the flow-field around the wind tunnel model would help in understanding the interactions and would provide valuable CFD validation data.
- Pressure measurements on the fuselage underside in the vicinity of the jet would enable jet and intake interference effects on the fuselage to be determined.
- The effect of the intake mass flow rate (relative to the jet) should be investigated. The aim is to extrapolate back to zero intake mass flow rate in order to ascertain the effect of the intake plug.

- The effect of wind tunnel interference on the results should be checked. This could be achieved by repositioning the model in the wind tunnel. The aim is to determine the interference between the wind tunnel model and the wind tunnel jet in addition to the model jet/floor interaction.

Wind tunnel model developments

- Some of the additional work recommended above would require modifications to the model, specifically a new wing and modified fuselage underside. The following, however, would improve the utility of the model.
- The use of aluminium components and plastic mouldings for the wing and fuselage would improve the geometrical accuracy. This would be important when comparing the results with CFD, for which an accurately-specified geometry is required.
- The Scani-Valves and pressure transducers could be incorporated within the model. This would reduce the response time of the pressure measurement system. It would, however, necessitate modification to the fuselage design.

Future CFD modelling

- The use of alternatives to the k-ε turbulence model should be investigated. The k-ζ model, in particular, looks promising for jet flows.
- More jet and intake interaction effects should be modelled. For example, a jet/wing combination or a jet/intake/fuselage combination. The aim should be to develop a CFD model for a whole aircraft.
- The PHOENICS CFD code has proved unsuitable for modelling the complex geometries associated with STOVL aircraft. The use of an alternative code is advised. Cranfield University has recently changed to the 'Fluent' suite of CFD software. The ability to use unstructured meshes looks promising. In industry, the SAUNA CFD code is also used. It is also necessary, however, to have sufficient computing resources with which to run these codes.

Overall recommendations for STOVL wind tunnel testing

- Low-speed wind tunnel testing of future STOVL jet-lift aircraft which have close-coupled jet(s) and intake(s) should consider including simultaneous jet and intake flow simulation, ideally on a fully metric model. It is recognised, however, that this is a costly practice and further use of surface pressure measurements (from which forces may be inferred) may be necessary.

- The lack of direct force measurements may be compensated, to some extent, by CFD models of the particular configuration under investigation. At present, however, CFD validation data for complete STOVL aircraft is in short supply.

References

ABBOTT, I. H. & VON DOENHOFF, A. E., 1959, "Theory of Wing Sections", *Dover Publications Inc.*, New York, ISBN 486-60586-8.

ADLER, D. & BARON, A., 1978, "Prediction of a Three-dimensional Circular Turbulent Jet in Cross-flow", *AIAA Journal*, Vol. 17, No. 2, pp. 168-174.

AGARWAL, R. K., 1986, "Recent Advances in Prediction Methods for Jet-induced Effects on V/STOL Aircraft", *Recent Advances in Aerodynamics*, Ch. 21 pp. 471-521.

AHMED, S., 1996, "An Experimental Study of a Supersonic Jet in a Subsonic Cross-flow", *University of Surrey*, Department of Civil Engineering, unpublished work.

AIRSCREW COMPANY, 1961, "Airscrew Fans, General Data", *The Airscrew Company & Jicwood Ltd.*, Weybridge, Surrey, UK, p. 20.

ALLEN, M. W. & MYDDLETON D. R., 1992, "Essential Management Accounting", *Prentice Hall*, Hemel Hempstead, 2nd Edition, ISBN 0-13-284647-0.

ANDERSON, J. D. JR., 1990, "Modern Compressible Flow", *McGraw Hill*, London, ISBN 0-07-001673-9, pp. 161-162.

ARTS, T., CARBONARO, M. & VAN DEN BRAEMBUSSCHE, R. A., 1994, "Measurement Techniques in Fluid Dynamics", *Course Notes, Von Karman Institute for Fluid Dynamics*, 10-14 October, Ch. III, p. 42.

BAKER, A. J., SNYDER, P. K. & ORZECHOWSKI, J. A., 1993, "Three-dimensional Characterisation of the Near-field of a VSTOL Jet in a Turbulent Cross-flow", *Computer Methods in Applied Mechanics and Engineering*, No. 102, pp. 1-13.

BARCHE, J., 1974, "Jet-lift Problems of V/STOL Aircraft", *AGARD Conference Proceedings CP-143*, Fluid Dynamics Panel Symposium, Delft, Netherlands, April 24-26, pp. 16.1-16.18.

BARCHE, J., 1981, "Jet Interactions With Neighbouring Surfaces", *AGARD Conference Proceedings CP-308*, Fluid Dynamics Panel Symposium, Fundaçao Calouste Gulbenkian, Lisbon, Portugal, 2-5 November, pp. 2.1-2.18.

BOUIS, X.,1995, "Market Tests Europe's Wind Tunnels", *Aerospace America*, August 1995, pp. 28-31.

BOWMAN, C., 1990, "The Essence of Strategic Management", *Prentice Hall*, Hemel Hempstead, ISBN 0-13-284738-8.

BRADBURY, L. J. S., 1981, "Some Aspects of Jet Dynamics and Their Implications for VTOL Research", *AGARD Conference Proceedings CP-308*, Fluid Dynamics Panel Symposium, Fundaçao Calouste Gulbenkian, Lisbon, Portugal, 2-5 November, pp. 1.1-1.26.

BRAY, D., 1992, "Jets in Cross-flow and Ground Effect", *Cranfield Institute of Technology*, RMCS, PhD Thesis.

BREARLEY, R. & MYERS, S., 1991, "Principles of Corporate Finance", *McGraw-Hill*, New York, p. 261.

BRUCE, R. J., 1997, *private communication*, DERA (Farnborough), 8 January.

BRUUN, H. H., 1995, "Hot-wire Anemometry - Principles and Signal Analysis", *Oxford University Press*, Oxford, ISBN 0-19-856342-6.

BUCKLEY, 1991, "Report of the EPC Efficiency Scrutiny", *unpublished MoD report*, 17 May, (in KIRKPATRICK, 1996).

CEBECI, T. & SMITH, A. M. O., 1974, "Analysis of Turbulent Boundary Layers", *Academic Press Ltd.*, London, ISBN 0-12-164650-5.

CHAISSAING, P., GEORGE, J., CLARIA, A. & SANANES, F., 1974, "Physical Characteristics of Subsonic Jets in a Cross-stream", *Journal of Fluid Mechanics*, Vol. 62, No. 1, pp. 41-64.

CHAM, 1992, PHOENICS user manuals, TR99, TR100, TR140, TR141, TR200a, TR200b, TR217, TR218, TR219, *Concentration, Heat & Momentum Ltd.*, Wimbledon.

CORSIGLIA, V. R., WARDELL, D. A. & KUHN, R. E., 1990, "Small-scale Experiments in STOVL Ground Effects", *Proceedings of the International Powered Lift Conference*, London, UK, 29-31 August, pp. III.14.1-III.14.13.

COVAULT, C., 1994, "European Wind Tunnel Poses Challenge to US", *Aviation Week & Space Technology*, 7 November pp. 24-25.

COYLE, R. *et al.*, 1994, "Futures Assessment by Field Anomaly Relaxation: A Review and Appraisal", *Futures*, January, pp. 25-43.

CURTIS, P., 1992, "The Design and Testing of Short Duct Intakes for Supersonic STOVL Aircraft", *Proceedings of the RAeS/IMechE Conference on Engine Airframe Integration*, Nottingham, UK, 15-16 October 1992, pp. 10.1-10.12.

DEAN, J., 1954, "Measuring the Productivity of Capital", *Harvard Business Review*, January-February, pp. 120-130.

DONALDSON, C. DU P. & SNEDEKER, R. S., 1971, "A Study of Free Jet Impingement - Part 1: Mean Properties of Free and Impinging Jets", *Journal of Fluid Mechanics*, Vol. 45, pp. 281-319.

DRURY C., 1996, "Management and Cost Accounting", *Thompson International*, London, 4th Edition, ISBN 0-412-73360-9.

FAVRE, A., 1965, "Equations des Gaz Turbulents Compressibles", *Journal de Méchanique*, Vol. 4, No. 3, pp. 361-390.

FEARN, R. L., 1986, "Progress Towards a Model to Describe Jet/Aerodynamic-Surface Interference Effects", *Recent Advances in Aerodynamics*, pp. 407-434.

FEARN, R. L. & WESTON, R. P., 1978, "Induced Velocity Field of a Jet in a Cross-flow", *NASA Technical Proceedings TP-1087.*

FLUK, H., 1987, "Landing Surface Characteristics Unique to V/STOL Aircraft", *Proceedings of the International Powered Lift Conference*, Santa Clara, California, USA, December 7-10, pp. 87-99, SAE Paper No. 872310.

FÜTTERER, H. & HARMS, L., 1967, "Jet Interference Measurements on a VTOL Model With Jet Simulation by Fans", *Aerodynamische Versuchsanstalt*, Goettingen, pp. 17.1-17.26.

GENTRY, G. L. JR. & MARGASON, R. J., 1966, "Jet-induced Lift Losses on VTOL Configurations Hovering In and Out of Ground Effect", *NASA Technical Note TN D-3166.*

HAFTMANN, B., 1981, "Jet Effects on Forces and Moments of a VSTOL Fighter-type Aircraft", *AGARD Conference Proceedings CP-308*, Fluid Dynamics Panel Symposium, Fundaçao Calouste Gulbenkian, Lisbon, Portugal, 2-5 November, pp. 18.1-18.13.

HAMMOND, A. D., 1966, "Thrust Losses in Hovering for Jet VTOL Aircraft", *NASA Special Proceedings SP-116*, pp. 163-175.

HAMMOND, A. D. & MCLEMORE H. C., 1967, "Hot-gas Ingestion and Jet Interference Effects for Jet V/STOL Aircraft", *AGARD Conference Proceedings CP-27*, Fluid Dynamics Panel Symposium, Göttingen, Germany, 13-15 September, pp. 8.1-8.27.

HARRINGTON, L., 1995, quotation, in MORRING, 1995.

HARRIS, A. E. WILDE, G. L., SMITH, V. J., MUNDELL, A. R. G. & DAVIDSON, D. P., 1991, "ASTOVL Model Engine Simulators for Wind Tunnel Research", *AGARD Conference Proceedings CP-498*, Fluid Dynamics Panel Symposium, Fort Worth, Texas, USA, 7-10 October, pp. 15.1-15.10.

HEYSON, H. H., 1978, "Wind Tunnel Testing of VTOL and STOL Aircraft", *NASA Technical Memorandum TM-78750.*

HIGSON, C. J., 1986, "Business Finance", *Butterworth & Co. Ltd.*, ISBN 0-406-50141-6.

HIRSCHBERG, M. J., 1997, "V/STOL: The First Half-century", *The American Helicopter Society Web Site*, http://www.vtol.org/wheel/VSTOL.html.

INCE, N. Z. & LESCHZINER, M. A., 1993, "Calculation of Single and Multiple Jets in Cross-flow with and without Impingement using Reynolds-stress-transport Closure", *AGARD Conference Proceedings CP-534*, Fluid Dynamics Panel Symposium, Winchester, UK, 19-22 April.

ING, D. N. & ZHANG, X., 1994, "An Experimental and Computational Investigation of Ground Effect Lift Loss for Single Jet Impingement", *RAeS Aeronautical Journal*, Vol. 98, No. 974, pp. 127-136.

IVANOV, Y., 1963, "Shape of the Centreline of an Axisymmetric Fan-type Jet in a Cross-flow", *Izv. VUZ. Aviotsionnaya Teknika*, No. 4.

KAMOTANI, Y. & GREBER, I., 1972, "Experiments on a Turbulent Jet in a Cross-flow", *AIAA Journal*, Vol. 10, No. 11, pp. 1425-1429.

KEFFER, J. F. & BAINES, W. D., 1962, "The Round Turbulent Jet in a Cross-wind", *Journal of Fluid Mechanics*, Vol. 1, No. 31, pp. 481-496.

KIRKHAM, L., 1996, "Coaxial Jet Flows for ASTOVL Applications", *Cranfield University*, RMCS, MPhil Thesis.

KIRKPATRICK, D., 1996, "Choose Your Weapon: Combined Operational Effectiveness and Investment Appraisal (COEIA) and its Role in UK Defence Procurement", *RUSI Whitehall Paper No. 36*, ISBN 0-85516-135-3.

KNOTT, P. G., 1987, "The Ground Environment Created by High Specific Thrust Vertical Land Aircraft", *Proceedings of the International Powered Lift Conference*, Santa Clara, California, USA, December 7-10, pp. 75-85, SAE Paper No. 872309.

KNOTT, P. G. & HARGREAVES, J. J., 1974, "A Review of the Lifting Characteristics of Some Jet-lift V/STOL Configurations", *AGARD Conference Proceedings CP-143*, Fluid Dynamics Panel Symposium, Delft, Netherlands, April 24-26, pp. 24.1-24.12.

KNOWLES, K., 1996, "Scaling of Jet Flow-fields", *Proceedings of the 20th Congress of the International Council of Aeronautical Sciences*, Sorrento, Italy, 8-13 Sept., Vol. 2, pp. 1595-1605.

KNOWLES, K. & BRAY, D., 1991, "Recent Research into the Aerodynamics of ASTOVL Aircraft in Ground Environment", *Proceedings of the Institute of Mechanical Engineers, Part G, Journal of Aerospace Engineering*, Vol. 205, pp. 123-131.

KOTANSKY, D. R., 1984, "Jet Flow-fields", *AGARD Report R-710*, pp. 7.1-7.48.

KRENZ, G. & BARCHE, J., 1967, "Jet Influence on V/STOL Aircraft in the Transitional and High Speed Regime", *AGARD Conference Proceedings CP-27*, Fluid Dynamics Panel Symposium, Göttingen, Germany, 13-15 September, pp. 2.1-2.25.

KUENSTNER, R., DEUTENBACH, K. R. & VAGT J. D., 1992, "Measurement of Reference Dynamic Pressure in Open-jet Automotive Wind Tunnels", SAE Paper No. 920344, 24-28 February.

KUHN, R. E., 1986, "The Induced Aerodynamics of Jet and Fan Powered V/STOL Aircraft", *Recent Advances in Aerodynamics*, Ch. 21, pp. 337-373.

KUHN, R. E., 1987, "Hover Suckdown and Fountain Effects", *Proceedings of the International Powered Lift Conference*, Santa Clara, California, USA, December 7-10, pp. 1-17, SAE Paper No. 872305.

KUHN, R. E. & MCKINNEY, M. O. JR., 1965, "NASA Research on the Aerodynamics of Jet VTOL Engine Installations", *AGARDograph 103*, Specialists Meeting, Tennessee, USA, 25-27 October, pp. 689-713.

LAUNDER, B. E. & SHARMA, B. I., 1974, "Application of the Energy Dissipation Model of Turbulence to the Calculation of Flow Near a Spinning Disc", *Letters in Heat and Mass Transfer*, Vol. 1, No. 2, pp. 131-138.

LEYLAND, D. C., 1984, "Aerodynamics of V/STOL Aircraft - Performance Assessment", *AGARD Report R-710*, pp. 11.1-11.26.

MARGASON, R. J., 1966, "Jet-induced Effects in Transition Flight", *NASA Special Proceedings SP-116*, pp. 177-189.

MARGASON, R. J., 1968, "The Path of a Jet Directed at Large Angles to a Subsonic Freestream", *NASA Technical Note TN D-4919*.

MARGASON, R. J., 1987, "Propulsion-induced Effects Caused by Out-of-ground Effects", *Proceedings of the International Powered Lift Conference*, Santa Clara, California, USA, December 7-10, pp. 31-57, SAE Paper No. 872307.

MARGASON, R. J., 1993, "Fifty Years of Jet in Cross-flow Research", *AGARD Conference Proceedings CP-534*, Fluid Dynamics Panel Symposium, Winchester, UK, 19-22 April, pp. 1.1-1.41.

MARGASON, R. J. & GENTRY, G. L. JR., 1968, "Aerodynamic Characteristics of a Five-jet VTOL Configuration in the Transition Speed Range", *NASA Technical Note TN D-4812*.

MARGASON R. J., VOLGER, R. D. & WINSTON, M. M., 1972, "Wind Tunnel Investigation at Low Speeds of a Model of the Kestrel (XV-6A) Vectored Thrust V/STOL Airplane", *NASA Technical Note TN D-6826*.

MASKELL, E. C., 1966, "Bluff Bodies and High-lift Systems", *AGARDograph 109, Subsonic Wind Tunnel Wall Corrections*, pp. 437-465.

MASSEY, B. S., 1970, "Mechanics of Fluids", *Redwood Burn Ltd.*

MATHESON, N, 1984, "Atmospheric and Pressurised Low Speed Wind Tunnel Performance and Cost Comparisons", *Aeronautical Research Laboratories*, Melbourne, Report No. ARL-Aero-R-160.

MATSON, D. J., 1993, "Simulating V/STOL Aircraft Flow-fields using the PHOENICS CFD Package", *Cranfield University*, RMCS, MSc Thesis.

MCGUIRK, J. *et al.*, 1990, "Prediction and Measurement of Jet Flow-field Features for ASTOVL Aircraft", *Proceedings of the International Powered Lift Conference*, London, UK, 29-31 August, pp. III.6.1-III.6.9.

MCLEAN, R., SULLIVAN, J., & MURTHY S. N. B., 1990, "Hot Gas Environment Around STOVL Aircraft in Ground Proximity - Part 1: Experimental Study", *Proceedings of the AIAA/SAE/ASME/ASEE 26th Joint Propulsion Conference*, Orlando, Florida, Paper No. 90-2269, 16-18 July.

MCLEMORE, H. C., 1966, "Jet-induced Lift Loss of Jet VTOL Configurations in Hovering Condition", *NASA Technical Note TN D-3435.*

MILFORD, C. M., 1987, "Hot Gas Recirculation in V/STOL", *Proceedings of the International Powered Lift Conference*, Santa Clara, California, USA, December 7-10, pp. 19-29, SAE Paper No. 872306.

MINECK, R. E. & MARGASON, R. J., 1973, "Pressure Distribution on a Vectored Thrust V/STOL Fighter in the Transition-Speed Range", NASA Technical Memorandum TM X-2867.

MINECK, R. E. & SCHWENDEMANN, M. F., 1973, "Aerodynamic Characteristics of a Vectored Thrust V/STOL Fighter in the Transition Speed Range", *NASA Technical Note TN D-7191.*

MORRING, F., 1995, "Decision Nears on Wind Tunnels", *Aviation Week & Space Technology*, 20 February.

MYSZKO, M., 1997, "Experimental and Computational Studies of Factors Affecting Impinging Jet Flow-fields", *Cranfield University*, RMCS, PhD Thesis.

NANGIA, R. K., 1994, "Prediction & Evaluation of Vectored Jets-induced Interference on Aircraft Configurations in Low Speed Flight", *Proceedings of the 19th Congress of the International Council of Aeronautical Sciences*, Anaheim, California, 18-23 September, pp. 859-870.

ONERA, 1997, "ONERA Large Testing Facilities F1 Wind Tunnel", *ONERA Internet Web Site*, http://www.osiris.onera.fr/activities/en/grands-moyens-essais-f1.html.

OTIS, J. H. JR., 1962, "Induced Interference Effects on a Four-jet VTOL Configuration With Various Wing Planforms in the Transition Speed Range", *NASA Technical Note TN D-1400.*

PAPAMOSCHOU, D. & ROSHKO, A, 1988, "The Compressible Turbulent Shear Layer: An Experimental Study", *Journal of Fluid Mechanics*, Vol. 197, pp. 453-477.

PARKER, M. & BENSON, R., 1988, "Information Economics", *Prentice Hall.*

PATANKAR, S. V., 1980 "Numerical Heat Transfer and Fluid Flow", *Hemisphere Publishing Corporation*, London, ISBN 0-89116-522-3.

PATANKAR, S. V., 1981 "A Calculation Procedure for Two-dimensional Elliptic Problems", *Numerical Heat Transfer*, Vol. 4, pp. 409-426.

PATANKAR, S. V. & SPALDING, D. B., 1972, "A Calculation Procedure for Heat, Mass and Momentum Transfer in Three-dimensional Parabolic Flows", *International Journal of Heat and Mass Transfer*, Vol. 15, pp. 1787. (in PATANKER, 1980).

PENNEY, S., 1996, "Tomorrow's Fighter", *Aerospace*, December, pp. 8-12.

PETERS, G., 1990, "Beyond Strategy - Benefits Identification of Specific IT Investments", *Journal of Information Technology*, pp. 205-214.

POPE, S. B., 1978, "An Explanation of the Turbulent Round-jet/Plane-jet Anomaly", *AIAA Journal*, Vol. 16, No. 3, pp. 279-281.

POWER, LT. J., 1989, "V/STOL Aerodynamics - Development of Experimental Facilities", *41 Degree Course Project*, RMCS, Cranfield Institute of Technology.

RANSOM, E. C. P. & SMY, J. R., 1984, "Introduction and Review of Some Jet Interference Phenomena Relevant to V/STOL Aircraft", *AGARD Report R-710*, Part 2, pp. 1-23.

RANSOM, E. C. P. & WOOD, P. M., 1974, "A Literature Review on Jets in Cross-flow", *AGARD Conference Proceedings CP-143*, Fluid Dynamics Panel Symposium, Delft, Netherlands, April 24-26, Part 26, pp. 1-7.

REID, W. & MYDDLETON, D. R., 1992, "The Meaning of Company Accounts", *Gower Publishing Company Limited*, Aldershot, UK, ISBN 0-566-07350-1.

REYNOLDS, O., 1895, "On the Dynamical Theory of Incompressible Viscous Fluids and the Determination of the Criterion", *Philosophical Transactions of the Royal Society of London*, Series A, Vol. 186, pp. 123. (in WILCOX, 1994).

ROBINSON, D. F., HARRIS, J. E. & HASSAN, H. A., 1995, "Unified Turbulence Closure Model for Axisymmetric and Planar Free Shear Flows", *AIAA Journal*, Vol. 33, No. 12, pp. 2325-2331.

RODI, W., 1972, "The Prediction of Free Turbulent Boundary Layers by the Use of a Two-equation Model of Turbulence", *Imperial College London*, Mechanical Engineering Department, PhD Thesis.

RODI, W., 1984, "Turbulence Models and Their Application to Hydraulics", *International Association for Hydraulic Research*, Delft, The Netherlands.

ROTH, K. R. 1987, "Numerical Simulation of a Subsonic Jet in a Cross-flow", *Proceedings of the International Powered Lift Conference*, Santa Clara, California, USA, December 7-10, pp. 425-431, SAE Paper No. 872343.

SADDINGTON, A. J., 1996, "Mutual Interference Between Jets and Intakes in STOVL Aircraft - Phase 1: Experimental Test Report", *Cranfield University*, RMCS, Internal Report No. SEAS/DAGS/AJS/07/97.

SADDINGTON, A. J., 1997, "Mutual Interference Between Jets and Intakes in STOVL Aircraft - Phase 2: Experimental Test Report", *Cranfield University*, RMCS, Internal Report No. SEAS/DAGS/AJS/08/97.

SARKAR, S., 1995, "The Stabilising Effect of Compressibility in Turbulent Shear Flow", *Journal of Fluid Mechanics*, Vol. 282, pp. 163-186.

SARKAR, S. & LAKSHMANAN, B., 1991, "Application of a Reynolds Stress Turbulence Model to the Compressible Shear Layer", *AIAA Journal*, Vol. 29, No. 5, pp. 743-749.

SCHLICHTING, H., 1960, "Boundary Layer Theory", 7th Edition, *McGraw-Hill*, New York, ISBN 0-07-055334-3

SCHULTZ, G. & VIEHWEGER, G., 1974, "Detailed Experimental and Theoretical Analysis of the Aerodynamic Interference Between Lifting Jets and the Fuselage and Wing", *AGARD Conference Proceedings CP-150*, Fluid Dynamics Panel Symposium, Rome, Italy, 3-6 September, pp. 24.1-24.13.

SEIDEL, M., 1973, "The Influence of an Inclined Jet on the Flow Field in the Vicinity of a Lifting Surface and on its Aerodynamic Coefficients", *NASA Technical Translation TT F-14,956.*

SEIDEL, M. & JAARSMA, F., 1978, "The German-Dutch Low Speed Wind Tunnel DNW", *Aeronautical Journal*, April.

SENIOR, A. K., 1997, "A Numerical Study of Resistance in a Rough Walled Channel Flow where the Ratio of Roughness Length Scale to Depth of Flow Varies Over a Wide Range", *Cranfield University*, RMCS, PhD Thesis.

SHANDOROV, G., 1966, "Calculation of a Jet Axis in a Drifting Flow", *NASA Technical Translation TT F-10638.*

SHAW, C. S. & MARGASON, R. J., 1973, "An Experimental Investigation of a Highly Underexpanded Sonic Jet Ejecting From a Flat Plate into a Subsonic Crossflow", *NASA Technical Note TN D-7314.*

SHUMPERT, P. K. & TIBBETTS, J. G., 1969, "Model Tests of Jet-induced Lift Effects on a VTOL Aircraft in Hover", *NASA Contractor Report CR-1297.*

SICLARI, M. J., MIGDAL D. & PALCZA, J. L., 1975, "The Development of Theoretical Models for Jet-induced Effects on V/STOL Aircraft", *Proceedings of the AIAA/SAE 11th Propulsion Conference*, Anaheim, California, USA, September 29-October 1, AIAA Paper No. 75-1216.

SMITH, A. G., 1996, "Nozzle and Exhaust Plume Flow and Heat Transfer", *RAeS/IMechE Engine Airframe Integration Conference*, Bristol, 10-11 October, pp 5.1-5.10.

SNEL, H., 1974, "A Method for the Calculation of the Flow-field Induced by a Jet Exhausting Perpendicularly into a Cross-flow", *AGARD Conference Proceedings CP-143*, Fluid Dynamics Panel Symposium, Delft, Netherlands, April 24-26, pp. 18.1-18.16.

SPENCE, A. & SPEE, B. M., 1973, "Some Considerations of Future Low Speed Wind Tunnels For Europe", *AGARD Report R-600*, pp. 1.1-1.10.

SPREEMAN, K. P., 1960, "Induced Interference Effects on Jet and Buried-fan VTOL Configurations in Transition", *NASA Technical Note TN D-731*.

STEWART, V. R., 1987, "Effect of Ground Proximity on the Aerodynamic Characteristics of the STOL Aircraft", *Proceedings of the International Powered Lift Conference*, Santa Clara, California, USA, December 7-10, pp. 59-73, SAE Paper No. 872308.

STOY, R. L. & BEN-HAIM, Y., 1973, "Turbulent Jets in a Confined Cross-flow", *Transactions of the ASME, Journal of Fluids Engineering*, December, pp. 551-556.

SUCEC, J. & BOWLEY, W. W., 1976, "Prediction of the Trajectory of a Turbulent Jet Injecting into a Cross-flowing Stream", *Transactions of the ASME, Journal of Fluids Engineering*, December, pp. 667-673.

TAFTI, D. K. & VANKA, S. P., 1992, "Hot Gas Environment Around STOVL Aircraft in Ground Proximity - Part 2: Numerical Study", *Journal of Aircraft*, Vol. 29, No. 1, pp. 20-27.

TAPE, R. F., HARTILL, W. R., CURRY LT. S. & JONES T. J., 1983, "Vectoring Exhaust Systems for STOL Tactical Aircraft", *Transactions of the ASME, Journal of Engineering for Power*, Vol. 105, No. 3, pp. 654-662.

TAYLOR, P. & WATKINS, D. J., 1981, "An Investigation of Inclined Jets in a Cross-wind", *AGARD Conference Proceedings CP-308*, Fluid Dynamics Panel Symposium, Fundaçao Calouste Gulbenkian, Lisbon, Portugal, 2-5 November, pp. 6.1-6.14.

TOLHURST, W. H. JR. & KELLY, M. W., 1966, "Characteristics of Two Large Scale Jet-lift Propulsion Systems", *NASA Special Proceedings SP-116*, pp. 205-228.

VOLGER, R. D., 1964, "Interference Effects of Single and Multiple Round or Slotted Jets on a VTOL Model in Transition", *NASA Technical Note TN D-2380.*

VOLGER, R. D. & GOODSON, K. W., 1973, "Low Speed Aerodynamic Characteristics of a Fuselage Model With Various Arrangements of Elongated Lift-jets", *NASA Technical Note TN D-7299.*

WELTE, D., 1974, "Prediction of Aerodynamic Interference Effects With Jet-lift and Fan-lift VTOL Aircraft", *AGARD Conference Proceedings CP-143*, Fluid Dynamics Panel Symposium, Delft, Netherlands, April 24-26, pp. 23.1-23.9.

WILCOX, D. C., 1994, "Turbulence Modelling for CFD", *DCW Industries Inc.*, La Cañada, California, USA, ISBN 0-9636051-0-0.

WILES, W. F., 1965, "Jet-lift Intakes", *AGARDograph 103*, Specialists Meeting, Tennessee, USA, 25-27 October, pp. 559-586.

WILLIAMS, J. & WOOD, M. N., 1966, "Aerodynamic Interference Effects With Jet-lift V/STOL Aircraft Under Static and Forward Speed Conditions", *RAE Technical Report No. 66403.*

WILSON, M., 1973, "The RAE 5m Low Speed Wind Tunnel", *FLIGHT International*, 22 March, pp. 478-482.

WILSON, M. J., 1995, "Unsteady Aerodynamics of Impinging Jets", *Cranfield University*, RMCS, MPhil Thesis.

WINSTON, M. M., 1970, "Induced Interference Effects on the Aerodynamic Characteristics of a 0.16-Scale Six-Jet V/STOL Model in Transition", *NASA Technical Note TN D-5727.*

WINSTON, M. M., WESTON, R. P. & MINECK, R. E., 1975, "Propulsion-induced Interference Effects on Jet-lift VTOL Aircraft", *Proceedings of the AIAA/SAE 11th Propulsion Conference*, Anaheim, California, USA, September 29-October 1, AIAA Paper No. 75-1215.

WOOD, M. N., 1967, "Jet V/STOL Aircraft Aerodynamics", *Proceedings of the International Congress on Subsonic Aerodynamics*, New York, USA, 3-6 April, pp. 893-920.

WOODWARD, D. S., 1995, *private conversation*, DERA (Farnborough), 18 August.

WOOLER, P. T., 1969, "Flow of a Circular Jet into a Cross-flow", *Journal of Aircraft*, Vol. 6, No. 3, pp. 283-284.

WYATT, L. A., 1964, "Static Tests of Ground Effect on Planforms Fitted with a Centrally-located Round Lifting Jet", *Aeronautical Research Council*, C.P. No. 749.

YANG, A. & GREY, J., 1995, "The New National Wind Tunnel Complex", *AIAA Information Paper, AIAA Internet Web Site*, http://www.aiaa.org/policy/wind-tunnel.html, 20 January.

ZHANG, X. & HURST, D. W., 1990, "An Investigation of a Supersonic Jet in a Low Speed Cross-flow", *University of Southampton*, Department of Aeronautics and Astronautics, Report No. 301896.

A Determination of the Theoretical Effective Velocity Ratio

This appendix shows how the theoretical effective velocity ratios were determined for the experimental and numerical tests. Velocity ratio was defined as:

$$V_e = \frac{V_\infty}{V_j}\sqrt{\frac{\rho_\infty}{\rho_j}} = \frac{M_\infty}{M_j}\sqrt{\frac{p_\infty}{p_j}} \tag{A.1}$$

The local speed of sound may be determined from

$$a = \sqrt{\gamma RT} \tag{A.2}$$

Assuming that the static ambient temperature was 288.15 K, this gave a freestream speed of sound of 340.3 ms^{-1}. For freestream velocities of 10 ms^{-1}, 20 ms^{-1}, 30 ms^{-1} and 40 ms^{-1}, M_∞ values were 0.0294, 0.0588, 0.0882 and 0.1175 respectively.

A1.1 NPRs of 1.5 and 1.586

At NPRs of 1.5 and 1.586, the nozzle was not choked and so the exit static pressure, p_j was assumed to be equal to the ambient static pressure, p_∞. The exit Mach number was determined from the equation for the isentropic expansion of an ideal gas:

$$\frac{P}{p} = \left\{1 + \left(\frac{\gamma - 1}{2}\right)M^2\right\}^{\frac{\gamma}{\gamma-1}} \tag{A.3}$$

This gave a jet exit Mach number of 0.784 at an NPR of 1.5 and 0.839 at an NPR of 1.586. The effective velocity ratio can now be determined (see Table A1 below).

A1.2 NPRs of 2.0, 3.0 and 4.0

At NPRs of 2.0, 3.0 and 4.0 the nozzle will be choked since the critical pressure ratio of 1.893 has been exceeded and the exit Mach number will be fixed at unity. The nozzle, however, was operating in an underexpanded condition and the exit static pressure was higher than the freestream. The factor by which the jet exit static pressure exceeded the freestream static is the ratio of the operating NPR to the critical NPR. Hence for an NPR of 2.0, the ratio p_j/p_∞ was 2.0/1.893. The effective velocity ratio can therefore be determined (see Table A1 below).

***Table A1** - Effective velocity ratios for the test conditions*

V_∞	q_∞	M_∞	NPR	M_j	$\frac{p_\infty}{p_j}$	V_e
10.0	61.3	0.0294	1.5	0.784	1.0	0.038
20.0	245	0.0588	1.5	0.784	1.0	0.075
30.0	551	0.0882	1.5	0.784	1.0	0.113
40.0	981	0.1175	1.5	0.784	1.0	0.150
10.0	61.3	0.0294	1.586	0.839	1.0	0.035
20.0	245	0.0588	1.586	0.839	1.0	0.070
30.0	551	0.0882	1.586	0.839	1.0	0.105
40.0	981	0.1175	1.586	0.839	1.0	0.140
10.0	61.3	0.0294	2.0	1.0	0.946	0.029
20.0	245	0.0588	2.0	1.0	0.946	0.057
30.0	551	0.0882	2.0	1.0	0.946	0.086
40.0	981	0.1175	2.0	1.0	0.946	0.114
10.0	61.3	0.0294	3.0	1.0	0.631	0.023
20.0	245	0.0588	3.0	1.0	0.631	0.047
30.0	551	0.0882	3.0	1.0	0.631	0.070
40.0	981	0.1175	3.0	1.0	0.631	0.093
10.0	61.3	0.0294	4.0	1.0	0.473	0.020
20.0	245	0.0588	4.0	1.0	0.473	0.040
30.0	551	0.0882	4.0	1.0	0.473	0.061
40.0	981	0.1175	4.0	1.0	0.473	0.081

B Phase 1 Experimental Data

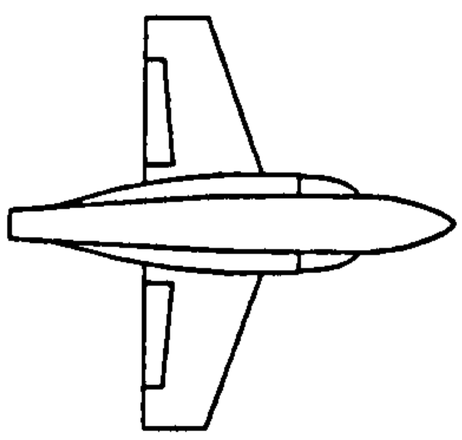

q_∞ = 61.3 Pa, NPR 1.0

	$C_{P\ (root)}$	
x/chord	upper	lower
0.0000	0.8431	0.8431
0.0459	-0.2680	-0.1966
0.0989	-0.3208	-0.1367
0.1519	-0.3819	-0.1215
0.2049	-0.4014	-0.1001
0.2580	-0.4077	-0.1132
0.3110	-0.3867	-0.0935
0.3640	-0.3640	-0.0531
0.4170	-0.3377	0.0020
0.4670	-0.3194	0.0432
0.5230	-0.2927	0.0705
0.5760	-0.2712	0.0889
0.6290	-0.2582	0.1068
0.6820	-0.2558	0.0997
0.7350	-0.2586	0.0001
0.7880	-0.3003	-0.1799
0.8410	-0.3120	-0.2815
1.0000	0.0000	0.0000

q_∞ = 245 Pa, NPR 1.0

$C_{P\ (root)}$	
upper	lower
0.8864	0.8864
-0.3114	-0.2209
-0.3566	-0.1543
-0.4202	-0.1499
-0.4444	-0.1376
-0.4498	-0.1268
-0.4262	-0.1545
-0.3986	-0.0860
-0.3748	-0.0208
-0.3514	0.0228
-0.3206	0.0555
-0.2926	0.0776
-0.2717	0.1016
-0.2678	0.1043
-0.2674	-0.0050
-0.3189	-0.2149
-0.3369	-0.3171
0.0000	0.0000

q_∞ = 551 Pa, NPR 1.0

$C_{P\ (root)}$	
upper	lower
0.8899	0.8899
-0.3301	-0.2399
-0.3676	-0.1687
-0.4275	-0.1721
-0.4461	-0.1674
-0.4497	-0.1464
-0.4216	-0.1657
-0.3933	-0.1206
-0.3654	-0.0508
-0.3477	-0.0087
-0.3231	0.0249
-0.2938	0.0468
-0.2776	0.0763
-0.2801	0.0847
-0.2867	-0.0150
-0.3452	-0.2092
-0.3398	-0.3055
0.0000	0.0000

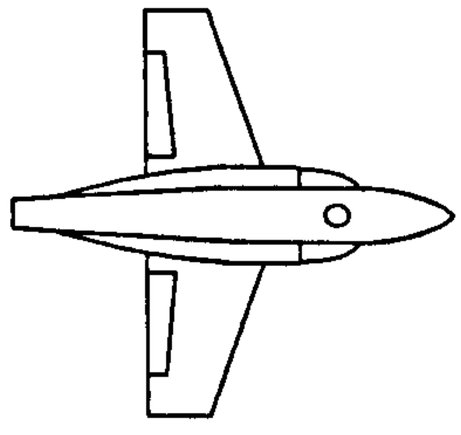

q_∞ = 61.3 Pa, NPR 2.0

	$C_{P\,(root)}$	
x/chord	upper	lower
0.0000	0.5537	0.5537
0.0459	-0.1812	-0.5107
0.0989	-0.2658	-0.3358
0.1519	-0.3344	-0.3128
0.2049	-0.3655	-0.2734
0.2580	-0.3836	-0.2548
0.3110	-0.3705	-0.2058
0.3640	-0.3588	-0.1467
0.4170	-0.3413	-0.0788
0.4670	-0.3255	-0.0240
0.5230	-0.3100	0.0132
0.5760	-0.2940	0.0402
0.6290	-0.2836	0.0636
0.6820	-0.2796	0.0654
0.7350	-0.2819	-0.0295
0.7880	-0.3223	-0.2333
0.8410	-0.3208	-0.2998
1.0000	0.0000	0.0000

q_∞ = 245 Pa, NPR 2.0

$C_{P\,(root)}$	
upper	lower
0.7491	0.7491
-0.2208	-0.4350
-0.2996	-0.2801
-0.3746	-0.2708
-0.4031	-0.2327
-0.4140	-0.2384
-0.3920	-0.1934
-0.3689	-0.1349
-0.3462	-0.0624
-0.3279	-0.0073
-0.3053	0.0293
-0.2781	0.0570
-0.2640	0.0832
-0.2631	0.0884
-0.2652	-0.0149
-0.3165	-0.2325
-0.3292	-0.3270
0.0000	0.0000

q_∞ = 551 Pa, NPR 2.0

$C_{P\,(root)}$	
upper	lower
0.8171	0.8171
-0.2656	-0.4058
-0.3269	-0.2733
-0.3919	-0.2651
-0.4139	-0.2447
-0.4216	-0.2509
-0.3957	-0.2166
-0.3706	-0.1640
-0.3437	-0.0888
-0.3258	-0.0383
-0.3032	0.0005
-0.2764	0.0261
-0.2622	0.0571
-0.2696	0.0693
-0.2798	-0.0292
-0.3360	-0.2311
-0.3306	-0.3208
0.0000	0.0000

q_∞ = 61.3 Pa, NPR 3.0

	$C_{P\,(root)}$	
x/chord	upper	lower
0.0000	0.5210	0.5210
0.0459	-0.1768	-0.5343
0.0989	-0.2551	-0.3489
0.1519	-0.3248	-0.3379
0.2049	-0.3553	-0.2580
0.2580	-0.3765	-0.2577
0.3110	-0.3620	-0.2010
0.3640	-0.3518	-0.1388
0.4170	-0.3377	-0.0721
0.4670	-0.3273	-0.0219
0.5230	-0.3062	0.0203
0.5760	-0.2873	0.0478
0.6290	-0.2760	0.0709
0.6820	-0.2737	0.0735
0.7350	-0.2773	-0.0142
0.7880	-0.3203	-0.2236
0.8410	-0.3211	-0.2849
1.0000	0.0000	0.0000

q_∞ = 245 Pa, NPR 3.0

$C_{P\,(root)}$	
upper	lower
0.7508	0.7508
-0.2254	-0.4265
-0.2978	-0.2724
-0.3649	-0.2682
-0.3900	-0.2170
-0.4017	-0.2511
-0.3775	-0.1913
-0.3570	-0.1313
-0.3361	-0.0608
-0.3237	-0.0081
-0.3068	0.0311
-0.2883	0.0572
-0.2805	0.0844
-0.2826	0.0902
-0.2831	-0.0128
-0.3311	-0.2248
-0.3415	-0.3175
0.0000	0.0000

q_∞ = 551 Pa, NPR 3.0

$C_{P\,(root)}$	
upper	lower
0.7980	0.7980
-0.2454	-0.4116
-0.3048	-0.2690
-0.3721	-0.2609
-0.3932	-0.2325
-0.4014	-0.2688
-0.3756	-0.2127
-0.3537	-0.1578
-0.3267	-0.0879
-0.3129	-0.0372
-0.2921	0.0017
-0.2687	0.0287
-0.2578	0.0579
-0.2655	0.0701
-0.2782	-0.0228
-0.3347	-0.2197
-0.3242	-0.3083
0.0000	0.0000

q_∞ = 61.3 Pa, NPR 4.0

	$C_{P\,(root)}$	
x/chord	upper	lower
0.0000	0.5303	0.5303
0.0459	-0.1753	-0.5522
0.0989	-0.2505	-0.3484
0.1519	-0.3169	-0.3879
0.2049	-0.3542	-0.2598
0.2580	-0.3683	-0.2603
0.3110	-0.3562	-0.2084
0.3640	-0.3422	-0.1441
0.4170	-0.3327	-0.0726
0.4670	-0.3207	-0.0165
0.5230	-0.3016	0.0228
0.5760	-0.2868	0.0500
0.6290	-0.2736	0.0738
0.6820	-0.2699	0.0783
0.7350	-0.2710	-0.0083
0.7880	-0.3169	-0.2219
0.8410	-0.3149	-0.2888
1.0000	0.0000	0.0000

q_∞ = 245 Pa, NPR 4.0

$C_{P\,(root)}$	
upper	lower
0.7826	0.7826
-0.2522	-0.3997
-0.3159	-0.2553
-0.3794	-0.2610
-0.4025	-0.1990
-0.4175	-0.2541
-0.3917	-0.1848
-0.3694	-0.1254
-0.3478	-0.0551
-0.3371	-0.0018
-0.3210	0.0351
-0.2989	0.0608
-0.2917	0.0871
-0.2936	0.0904
-0.2907	-0.0120
-0.3394	-0.2266
-0.3436	-0.3219
0.0000	0.0000

q_∞ = 551 Pa, NPR 4.0

$C_{P\,(root)}$	
upper	lower
0.7957	0.7957
-0.2422	-0.4025
-0.3051	-0.2603
-0.3664	-0.2551
-0.3869	-0.2198
-0.3980	-0.2734
-0.3718	-0.2128
-0.3494	-0.1549
-0.3241	-0.0858
-0.3133	-0.0351
-0.2960	0.0040
-0.2748	0.0313
-0.2654	0.0609
-0.2737	0.0716
-0.2855	-0.0218
-0.3419	-0.2192
-0.3266	-0.3087
0.0000	0.0000

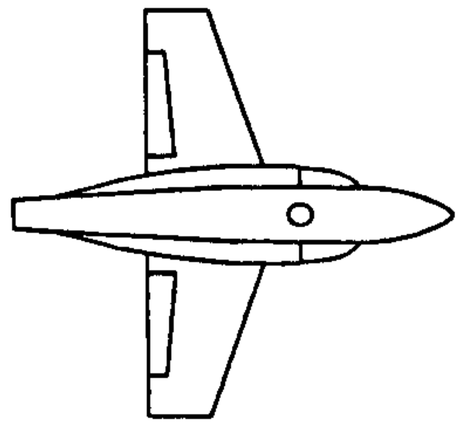

q_∞ = 61.3 Pa, NPR 2.0

	$C_{P\ (root)}$	
x/chord	upper	lower
0.0000	0.6239	0.6239
0.0459	-0.1855	-0.5134
0.0989	-0.2678	-0.3496
0.1519	-0.3396	-0.3206
0.2049	-0.3721	-0.2818
0.2580	-0.3810	-0.2612
0.3110	-0.3658	-0.2154
0.3640	-0.3498	-0.1565
0.4170	-0.3325	-0.0847
0.4670	-0.3206	-0.0254
0.5230	-0.3001	0.0136
0.5760	-0.2837	0.0410
0.6290	-0.2742	0.0660
0.6820	-0.2710	0.0716
0.7350	-0.2705	-0.0245
0.7880	-0.3103	-0.2212
0.8410	-0.3173	-0.2916
1.0000	0.0000	0.0000

q_∞ = 245 Pa, NPR 2.0

$C_{P\ (root)}$	
upper	lower
0.7670	0.7670
-0.2385	-0.4534
-0.3133	-0.3050
-0.3855	-0.2969
-0.4120	-0.2565
-0.4199	-0.2682
-0.3978	-0.2198
-0.3736	-0.1581
-0.3529	-0.0818
-0.3359	-0.0251
-0.3127	0.0152
-0.2900	0.0432
-0.2775	0.0747
-0.2764	0.0819
-0.2751	-0.0207
-0.3234	-0.2374
-0.3368	-0.3292
0.0000	0.0000

q_∞ = 551 Pa, NPR 2.0

$C_{P\ (root)}$	
upper	lower
0.8370	0.8370
-0.2821	-0.3894
-0.3380	-0.2717
-0.4004	-0.2664
-0.4198	-0.2518
-0.4252	-0.2570
-0.3985	-0.2263
-0.3719	-0.1766
-0.3445	-0.1002
-0.3294	-0.0491
-0.3047	-0.0088
-0.2793	0.0178
-0.2656	0.0504
-0.2705	0.0644
-0.2815	-0.0338
-0.3397	-0.2345
-0.3339	-0.3229
0.0000	0.0000

q_∞ = 61.3 Pa, NPR 3.0

	$C_{P\ (root)}$	
x/chord	upper	lower
0.0000	0.5652	0.5652
0.0459	-0.1743	-0.5621
0.0989	-0.2676	-0.3642
0.1519	-0.3378	-0.3504
0.2049	-0.3674	-0.2759
0.2580	-0.3839	-0.2792
0.3110	-0.3726	-0.2192
0.3640	-0.3570	-0.1537
0.4170	-0.3375	-0.0824
0.4670	-0.3273	-0.0257
0.5230	-0.3055	0.0156
0.5760	-0.2881	0.0439
0.6290	-0.2759	0.0673
0.6820	-0.2732	0.0699
0.7350	-0.2718	-0.0171
0.7880	-0.3113	-0.2177
0.8410	-0.3124	-0.2784
1.0000	0.0000	0.0000

q_∞ = 245 Pa, NPR 3.0

$C_{P\ (root)}$	
upper	lower
0.7617	0.7617
-0.2374	-0.4498
-0.3111	-0.2949
-0.3778	-0.2884
-0.4020	-0.2387
-0.4079	-0.2767
-0.3868	-0.2139
-0.3645	-0.1502
-0.3440	-0.0771
-0.3323	-0.0221
-0.3133	0.0182
-0.2956	0.0475
-0.2860	0.0763
-0.2909	0.0834
-0.2908	-0.0177
-0.3393	-0.2309
-0.3466	-0.3195
0.0000	0.0000

q_∞ = 551 Pa, NPR 3.0

$C_{P\ (root)}$	
upper	lower
0.8233	0.8233
-0.2695	-0.3871
-0.3239	-0.2611
-0.3847	-0.2549
-0.4043	-0.2335
-0.4082	-0.2685
-0.3831	-0.2260
-0.3569	-0.1669
-0.3327	-0.0961
-0.3174	-0.0454
-0.2984	-0.0049
-0.2743	0.0233
-0.2624	0.0541
-0.2685	0.0679
-0.2792	-0.0252
-0.3368	-0.2219
-0.3259	-0.3104
0.0000	0.0000

q_∞ = 61.3 Pa, NPR 4.0

	$C_{P\,(root)}$	
x/chord	upper	lower
0.0000	0.5245	0.5245
0.0459	-0.2119	-0.5864
0.0989	-0.2992	-0.3943
0.1519	-0.3588	-0.4329
0.2049	-0.3894	-0.3046
0.2580	-0.4058	-0.2977
0.3110	-0.3940	-0.2471
0.3640	-0.3804	-0.1799
0.4170	-0.3662	-0.1064
0.4670	-0.3567	-0.0487
0.5230	-0.3386	-0.0051
0.5760	-0.3228	0.0225
0.6290	-0.3111	0.0488
0.6820	-0.3125	0.0543
0.7350	-0.3141	-0.0382
0.7880	-0.3541	-0.2551
0.8410	-0.3594	-0.3179
1.0000	0.0000	0.0000

q_∞ = 245 Pa, NPR 4.0

$C_{P\,(root)}$	
upper	lower
0.7891	0.7891
-0.2632	-0.4150
-0.3251	-0.2772
-0.3871	-0.2758
-0.4093	-0.2173
-0.4211	-0.2846
-0.3993	-0.2082
-0.3781	-0.1438
-0.3587	-0.0743
-0.3466	-0.0189
-0.3295	0.0202
-0.3046	0.0483
-0.2932	0.0761
-0.2922	0.0822
-0.2943	-0.0226
-0.3389	-0.2366
-0.3381	-0.3296
0.0000	0.0000

q_∞ = 551 Pa, NPR 4.0

$C_{P\,(root)}$	
upper	lower
0.8111	0.8111
-0.2607	-0.3936
-0.3165	-0.2594
-0.3755	-0.2575
-0.3964	-0.2289
-0.4034	-0.2747
-0.3757	-0.2327
-0.3526	-0.1674
-0.3279	-0.0980
-0.3188	-0.0460
-0.3035	-0.0054
-0.2816	0.0233
-0.2732	0.0537
-0.2805	0.0671
-0.2903	-0.0246
-0.3437	-0.2228
-0.3312	-0.3117
0.0000	0.0000

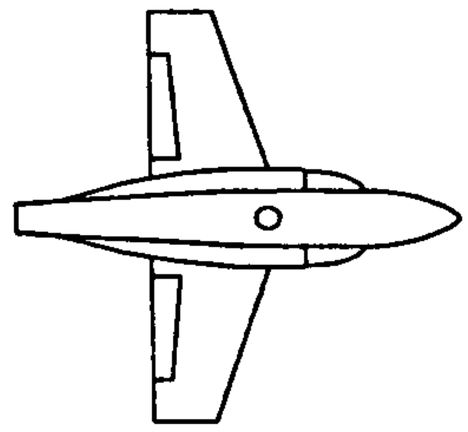

q_∞ = 61.3 Pa, NPR 2.0

	$C_{P\ (root)}$	
x/chord	upper	lower
0.0000	0.6770	0.6770
0.0459	-0.2326	-0.5080
0.0989	-0.3053	-0.3623
0.1519	-0.3725	-0.3472
0.2049	-0.3992	-0.3088
0.2580	-0.4068	-0.3015
0.3110	-0.3899	-0.2550
0.3640	-0.3728	-0.1980
0.4170	-0.3563	-0.1262
0.4670	-0.3421	-0.0635
0.5230	-0.3195	-0.0185
0.5760	-0.3026	0.0109
0.6290	-0.2909	0.0374
0.6820	-0.2857	0.0425
0.7350	-0.2917	-0.0493
0.7880	-0.3305	-0.2417
0.8410	-0.3337	-0.3137
1.0000	0.0000	0.0000

q_∞ = 245 Pa, NPR 2.0

$C_{P\ (root)}$	
upper	lower
0.8194	0.8194
-0.2784	-0.3839
-0.3419	-0.2715
-0.4044	-0.2704
-0.4280	-0.2438
-0.4333	-0.2575
-0.4111	-0.2180
-0.3874	-0.1621
-0.3643	-0.0881
-0.3489	-0.0336
-0.3261	0.0065
-0.3058	0.0370
-0.2911	0.0662
-0.2915	0.0756
-0.2892	-0.0273
-0.3324	-0.2420
-0.3437	-0.3299
0.0000	0.0000

q_∞ = 551 Pa, NPR 2.0

$C_{P\ (root)}$	
upper	lower
0.8657	0.8657
-0.3192	-0.3344
-0.3622	-0.2413
-0.4228	-0.2448
-0.4402	-0.2395
-0.4437	-0.2554
-0.4148	-0.2281
-0.3888	-0.1826
-0.3603	-0.1075
-0.3444	-0.0590
-0.3203	-0.0183
-0.2919	0.0093
-0.2765	0.0437
-0.2781	0.0582
-0.2884	-0.0382
-0.3353	-0.2369
-0.3323	-0.3260
0.0000	0.0000

q_∞ = 61.3 Pa, NPR 3.0

	$C_{P\ (root)}$	
x/chord	upper	lower
0.0000	0.6199	0.6199
0.0459	-0.2248	-0.5645
0.0989	-0.3080	-0.3897
0.1519	-0.3741	-0.3919
0.2049	-0.3985	-0.3147
0.2580	-0.4083	-0.3310
0.3110	-0.3946	-0.2751
0.3640	-0.3774	-0.2077
0.4170	-0.3645	-0.1351
0.4670	-0.3549	-0.0758
0.5230	-0.3305	-0.0287
0.5760	-0.3131	0.0032
0.6290	-0.3029	0.0303
0.6820	-0.2984	0.0350
0.7350	-0.2955	-0.0562
0.7880	-0.3391	-0.2508
0.8410	-0.3413	-0.3143
1.0000	0.0000	0.0000

q_∞ = 245 Pa, NPR 3.0

$C_{P\ (root)}$	
upper	lower
0.7966	0.7966
-0.2729	-0.4122
-0.3347	-0.2811
-0.3899	-0.2846
-0.4130	-0.2389
-0.4216	-0.2895
-0.3945	-0.2264
-0.3734	-0.1667
-0.3544	-0.0931
-0.3440	-0.0378
-0.3258	0.0031
-0.3105	0.0323
-0.3010	0.0625
-0.3041	0.0703
-0.3045	-0.0286
-0.3540	-0.2411
-0.3583	-0.3305
0.0000	0.0000

q_∞ = 551 Pa, NPR 3.0

$C_{P\ (root)}$	
upper	lower
0.8545	0.8545
-0.3013	-0.3526
-0.3470	-0.2483
-0.4066	-0.2520
-0.4222	-0.2338
-0.4284	-0.2722
-0.3999	-0.2307
-0.3752	-0.1776
-0.3472	-0.1056
-0.3321	-0.0557
-0.3115	-0.0154
-0.2862	0.0131
-0.2733	0.0458
-0.2779	0.0603
-0.2860	-0.0375
-0.3416	-0.2411
-0.3330	-0.3287
0.0000	0.0000

q_∞ = 61.3 Pa, NPR 4.0

	$C_{P\,(root)}$	
x/chord	upper	lower
0.0000	0.5783	0.5783
0.0459	-0.2364	-0.5679
0.0989	-0.3112	-0.3941
0.1519	-0.3703	-0.4445
0.2049	-0.3928	-0.3136
0.2580	-0.4053	-0.3247
0.3110	-0.3932	-0.2748
0.3640	-0.3795	-0.2060
0.4170	-0.3627	-0.1310
0.4670	-0.3502	-0.0693
0.5230	-0.3322	-0.0245
0.5760	-0.3132	0.0063
0.6290	-0.3020	0.0328
0.6820	-0.3001	0.0392
0.7350	-0.3016	-0.0489
0.7880	-0.3447	-0.2514
0.8410	-0.3490	-0.3186
1.0000	0.0000	0.0000

q_∞ = 245 Pa, NPR 4.0

$C_{P\,(root)}$	
upper	lower
0.8082	0.8082
-0.2769	-0.4009
-0.3328	-0.2738
-0.3913	-0.2850
-0.4133	-0.2290
-0.4193	-0.2983
-0.3967	-0.2234
-0.3747	-0.1626
-0.3562	-0.0908
-0.3459	-0.0350
-0.3291	0.0057
-0.3082	0.0352
-0.2944	0.0635
-0.2953	0.0706
-0.2939	-0.0307
-0.3410	-0.2420
-0.3475	-0.3338
0.0000	0.0000

q_∞ = 551 Pa, NPR 4.0

$C_{P\,(root)}$	
upper	lower
0.8448	0.8448
-0.2896	-0.3545
-0.3378	-0.2461
-0.3932	-0.2502
-0.4091	-0.2277
-0.4136	-0.2748
-0.3855	-0.2428
-0.3612	-0.1768
-0.3364	-0.1078
-0.3255	-0.0569
-0.3092	-0.0156
-0.2881	0.0129
-0.2769	0.0441
-0.2811	0.0596
-0.2904	-0.0324
-0.3446	-0.2273
-0.3340	-0.3169
0.0000	0.0000

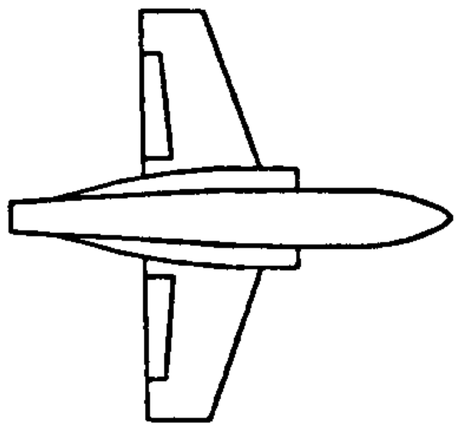

q_∞ = 61.3 Pa, NPR 1.0

	$C_{P\,(root)}$	
x/chord	upper	lower
0.0000	0.9839	0.9839
0.0459	-0.1929	0.1032
0.0989	-0.2512	0.0775
0.1519	-0.3173	0.0604
0.2049	-0.3518	0.0595
0.2580	-0.3830	0.0190
0.3110	-0.3792	0.0328
0.3640	-0.3682	0.0521
0.4170	-0.3469	0.0893
0.4670	-0.3339	0.1248
0.5230	-0.3058	0.1501
0.5760	-0.2833	0.1608
0.6290	-0.2741	0.1706
0.6820	-0.2715	0.1814
0.7350	-0.3086	0.0608
0.7880	-0.3231	-0.1476
0.8410	-0.3421	-0.2583
1.0000	0.0000	0.0000

q_∞ = 245 Pa, NPR 1.0

$C_{P\,(root)}$	
upper	lower
0.9484	0.9484
-0.3411	-0.0446
-0.3539	-0.0365
-0.4059	-0.0638
-0.4277	-0.0618
-0.4359	-0.0692
-0.4167	-0.1029
-0.3982	-0.0421
-0.3802	0.0192
-0.3608	0.0588
-0.3335	0.0875
-0.3096	0.1091
-0.2947	0.1368
-0.2938	0.1409
-0.2930	0.0152
-0.3516	-0.2108
-0.3614	-0.3250
0.0000	0.0000

q_∞ = 551 Pa, NPR 1.0

$C_{P\,(root)}$	
upper	lower
0.9304	0.9304
-0.3763	-0.1169
-0.3881	-0.0932
-0.4299	-0.1186
-0.4453	-0.1196
-0.4495	-0.1155
-0.4261	-0.1508
-0.4016	-0.0899
-0.3809	-0.0237
-0.3593	0.0168
-0.3328	0.0481
-0.3053	0.0702
-0.2875	0.1012
-0.2910	0.1084
-0.2959	-0.0067
-0.3606	-0.2093
-0.3417	-0.3169
0.0000	0.0000

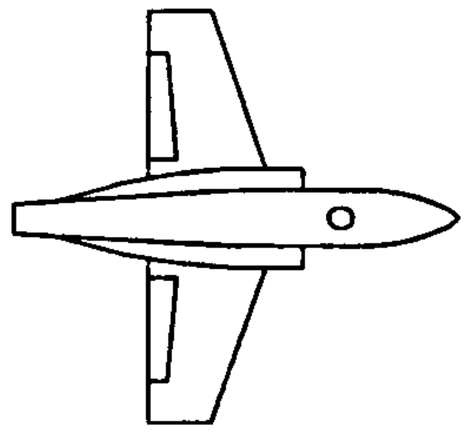

q_∞ = 61.3 Pa, NPR 2.0

	$C_{P\ (root)}$	
x/chord	upper	lower
0.0000	0.7764	0.7764
0.0459	0.0432	-0.2125
0.0989	-0.0768	-0.1110
0.1519	-0.1792	-0.0913
0.2049	-0.2431	-0.0800
0.2580	-0.2786	-0.0690
0.3110	-0.2818	-0.0443
0.3640	-0.2845	-0.0107
0.4170	-0.2801	0.0435
0.4670	-0.2714	0.0933
0.5230	-0.2569	0.1305
0.5760	-0.2373	0.1508
0.6290	-0.2266	0.1792
0.6820	-0.2227	0.1836
0.7350	-0.2309	0.0729
0.7880	-0.2934	-0.1409
0.8410	-0.3077	-0.2355
1.0000	0.0000	0.0000

q_∞ = 245 Pa, NPR 2.0

$C_{P\ (root)}$	
upper	lower
0.8711	0.8711
-0.2010	-0.2688
-0.2705	-0.1923
-0.3401	-0.1963
-0.3770	-0.1821
-0.3937	-0.1671
-0.3824	-0.1643
-0.3688	-0.1087
-0.3533	-0.0380
-0.3391	0.0151
-0.3167	0.0509
-0.2939	0.0759
-0.2805	0.1071
-0.2801	0.1158
-0.2797	-0.0032
-0.3441	-0.2265
-0.3519	-0.3351
0.0000	0.0000

q_∞ = 551 Pa, NPR 2.0

$C_{P\ (root)}$	
upper	lower
0.8826	0.8826
-0.2998	-0.3116
-0.3369	-0.2267
-0.3938	-0.2371
-0.4179	-0.2304
-0.4302	-0.2242
-0.4059	-0.2119
-0.3869	-0.1592
-0.3655	-0.0851
-0.3492	-0.0370
-0.3246	0.0003
-0.2996	0.0247
-0.2852	0.0590
-0.2903	0.0704
-0.2932	-0.0371
-0.3562	-0.2429
-0.3490	-0.3386
0.0000	0.0000

q_∞ = 61.3 Pa, NPR 3.0

	$C_{P\ (root)}$	
x/chord	upper	lower
0.0000	0.7241	0.7241
0.0459	0.0774	-0.2494
0.0989	-0.0520	-0.1397
0.1519	-0.1573	-0.1250
0.2049	-0.2235	-0.1181
0.2580	-0.2649	-0.0854
0.3110	-0.2748	-0.0643
0.3640	-0.2734	-0.0297
0.4170	-0.2704	0.0303
0.4670	-0.2647	0.0792
0.5230	-0.2469	0.1133
0.5760	-0.2302	0.1369
0.6290	-0.2206	0.1627
0.6820	-0.2181	0.1669
0.7350	-0.2235	0.0558
0.7880	-0.2900	-0.1528
0.8410	-0.3023	-0.2433
1.0000	0.0000	0.0000

q_∞ = 245 Pa, NPR 3.0

$C_{P\ (root)}$	
upper	lower
0.8587	0.8587
-0.1936	-0.2619
-0.2553	-0.1808
-0.3278	-0.1893
-0.3603	-0.1757
-0.3777	-0.1710
-0.3662	-0.1493
-0.3544	-0.1005
-0.3414	-0.0306
-0.3284	0.0183
-0.3063	0.0529
-0.2869	0.0798
-0.2762	0.1075
-0.2758	0.1167
-0.2746	0.0015
-0.3416	-0.2195
-0.3483	-0.3243
0.0000	0.0000

q_∞ = 551 Pa, NPR 3.0

$C_{P\ (root)}$	
upper	lower
0.8850	0.8850
-0.3248	-0.2583
-0.3475	-0.1917
-0.3945	-0.2110
-0.4092	-0.2032
-0.4145	-0.2281
-0.3903	-0.1883
-0.3696	-0.1468
-0.3485	-0.0773
-0.3347	-0.0317
-0.3112	0.0044
-0.2883	0.0292
-0.2769	0.0618
-0.2820	0.0750
-0.2880	-0.0294
-0.3469	-0.2265
-0.3406	-0.3219
0.0000	0.0000

q_∞ = 61.3 Pa, NPR 4.0

	$C_{P\,(root)}$	
x/chord	upper	lower
0.0000	0.7121	0.7121
0.0459	0.0995	-0.2406
0.0989	-0.0325	-0.1188
0.1519	-0.1470	-0.1116
0.2049	-0.2129	-0.0733
0.2580	-0.2460	-0.0951
0.3110	-0.2553	-0.0540
0.3640	-0.2581	-0.0106
0.4170	-0.2510	0.0496
0.4670	-0.2481	0.0948
0.5230	-0.2284	0.1256
0.5760	-0.2153	0.1511
0.6290	-0.1998	0.1746
0.6820	-0.2031	0.1811
0.7350	-0.2069	0.0701
0.7880	-0.2618	-0.1416
0.8410	-0.2817	-0.2282
1.0000	0.0000	0.0000

q_∞ = 245 Pa, NPR 4.0

$C_{P\,(root)}$	
upper	lower
0.8625	0.8625
-0.2149	-0.2629
-0.2762	-0.1787
-0.3460	-0.2000
-0.3807	-0.1725
-0.4077	-0.2108
-0.3928	-0.1652
-0.3771	-0.1139
-0.3638	-0.0439
-0.3560	0.0057
-0.3346	0.0408
-0.3126	0.0662
-0.3000	0.0933
-0.3007	0.1020
-0.2988	-0.0155
-0.3575	-0.2375
-0.3721	-0.3492
0.0000	0.0000

q_∞ = 551 Pa, NPR 4.0

$C_{P\,(root)}$	
upper	lower
0.8946	0.8946
-0.3202	-0.2449
-0.3412	-0.1741
-0.3872	-0.1990
-0.4013	-0.1860
-0.4081	-0.2235
-0.3828	-0.1767
-0.3624	-0.1361
-0.3416	-0.0663
-0.3292	-0.0217
-0.3075	0.0142
-0.2851	0.0392
-0.2737	0.0718
-0.2808	0.0836
-0.2854	-0.0197
-0.3465	-0.2187
-0.3360	-0.3149
0.0000	0.0000

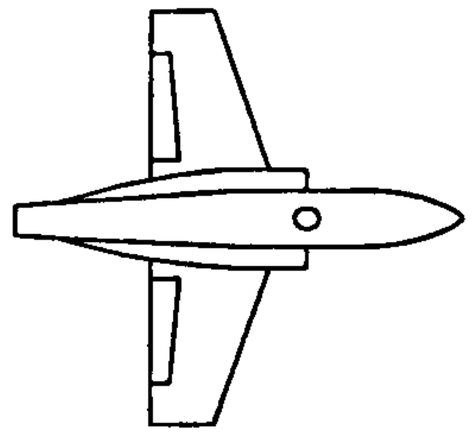

q_∞ = 61.3 Pa, NPR 2.0

	$C_{P\ (root)}$	
x/chord	upper	lower
0.0000	0.7605	0.7605
0.0459	0.0410	-0.2355
0.0989	-0.0747	-0.1412
0.1519	-0.1734	-0.1304
0.2049	-0.2316	-0.1118
0.2580	-0.2645	-0.0979
0.3110	-0.2637	-0.0748
0.3640	-0.2712	-0.0392
0.4170	-0.2578	0.0174
0.4670	-0.2454	0.0675
0.5230	-0.2324	0.1083
0.5760	-0.2153	0.1293
0.6290	-0.2053	0.1574
0.6820	-0.1981	0.1692
0.7350	-0.2024	0.0614
0.7880	-0.2565	-0.1434
0.8410	-0.2702	-0.2309
1.0000	0.0000	0.0000

q_∞ = 245 Pa, NPR 2.0

$C_{P\ (root)}$	
upper	lower
0.8442	0.8442
-0.2211	-0.3071
-0.2836	-0.2215
-0.3509	-0.2310
-0.3870	-0.2234
-0.4018	-0.2097
-0.3872	-0.1978
-0.3743	-0.1448
-0.3595	-0.0738
-0.3454	-0.0205
-0.3228	0.0180
-0.3019	0.0441
-0.2881	0.0769
-0.2883	0.0897
-0.2885	-0.0225
-0.3473	-0.2419
-0.3577	-0.3459
0.0000	0.0000

q_∞ = 551 Pa, NPR 2.0

$C_{P\ (root)}$	
upper	lower
0.8688	0.8688
-0.3014	-0.3131
-0.3395	-0.2342
-0.3938	-0.2461
-0.4149	-0.2425
-0.4234	-0.2409
-0.4016	-0.2241
-0.3837	-0.1765
-0.3625	-0.1033
-0.3486	-0.0549
-0.3248	-0.0176
-0.3018	0.0095
-0.2895	0.0436
-0.2956	0.0590
-0.3021	-0.0428
-0.3668	-0.2396
-0.3563	-0.3314
0.0000	0.0000

q_∞ = 61.3 Pa, NPR 3.0

	$C_{P\ (root)}$	
x/chord	upper	lower
0.0000	0.6519	0.6519
0.0459	0.0259	-0.3307
0.0989	-0.1007	-0.2085
0.1519	-0.2005	-0.1893
0.2049	-0.2650	-0.1808
0.2580	-0.3057	-0.1603
0.3110	-0.3126	-0.1327
0.3640	-0.3169	-0.0856
0.4170	-0.3127	-0.0175
0.4670	-0.3009	0.0247
0.5230	-0.2841	0.0644
0.5760	-0.2667	0.0929
0.6290	-0.2552	0.1152
0.6820	-0.2523	0.1300
0.7350	-0.2600	0.0192
0.7880	-0.3134	-0.1905
0.8410	-0.3364	-0.2800
1.0000	0.0000	0.0000

q_∞ = 245 Pa, NPR 3.0

$C_{P\ (root)}$	
upper	lower
0.8450	0.8450
-0.2116	-0.2911
-0.2769	-0.2078
-0.3444	-0.2193
-0.3795	-0.2065
-0.3917	-0.2128
-0.3799	-0.1807
-0.3687	-0.1332
-0.3556	-0.0612
-0.3393	-0.0096
-0.3182	0.0281
-0.2947	0.0559
-0.2822	0.0883
-0.2853	0.0975
-0.2863	-0.0153
-0.3415	-0.2386
-0.3561	-0.3400
0.0000	0.0000

q_∞ = 551 Pa, NPR 3.0

$C_{P\ (root)}$	
upper	lower
0.8865	0.8865
-0.3510	-0.2556
-0.3639	-0.1946
-0.4087	-0.2174
-0.4198	-0.2113
-0.4237	-0.2375
-0.3946	-0.2023
-0.3753	-0.1593
-0.3536	-0.0891
-0.3397	-0.0434
-0.3185	-0.0058
-0.2959	0.0193
-0.2850	0.0542
-0.2904	0.0677
-0.2973	-0.0348
-0.3575	-0.2321
-0.3455	-0.3278
0.0000	0.0000

q_∞ = 61.3 Pa, NPR 4.0

	$C_{P\,(root)}$	
x/chord	upper	lower
0.0000	0.6871	0.6871
0.0459	0.1187	-0.2887
0.0989	-0.0181	-0.1603
0.1519	-0.1276	-0.1439
0.2049	-0.1933	-0.1031
0.2580	-0.2362	-0.1195
0.3110	-0.2475	-0.0727
0.3640	-0.2454	-0.0230
0.4170	-0.2444	0.0432
0.4670	-0.2357	0.0988
0.5230	-0.2154	0.1296
0.5760	-0.2019	0.1559
0.6290	-0.1854	0.1798
0.6820	-0.1834	0.1914
0.7350	-0.1954	0.0813
0.7880	-0.2406	-0.1256
0.8410	-0.2667	-0.2128
1.0000	0.0000	0.0000

q_∞ = 245 Pa, NPR 4.0

$C_{P\,(root)}$	
upper	lower
0.8238	0.8238
-0.2145	-0.2939
-0.2762	-0.2063
-0.3439	-0.2308
-0.3803	-0.1974
-0.4014	-0.2434
-0.3896	-0.1909
-0.3791	-0.1399
-0.3643	-0.0708
-0.3540	-0.0202
-0.3314	0.0163
-0.3106	0.0432
-0.2982	0.0749
-0.3015	0.0844
-0.3014	-0.0271
-0.3585	-0.2433
-0.3684	-0.3434
0.0000	0.0000

q_∞ = 551 Pa, NPR 4.0

$C_{P\,(root)}$	
upper	lower
0.8852	0.8852
-0.3260	-0.2425
-0.3417	-0.1807
-0.3880	-0.1997
-0.3982	-0.1944
-0.4033	-0.2309
-0.3776	-0.1912
-0.3583	-0.1469
-0.3385	-0.0793
-0.3272	-0.0337
-0.3071	0.0030
-0.2858	0.0285
-0.2748	0.0618
-0.2818	0.0766
-0.2874	-0.0221
-0.3493	-0.2161
-0.3312	-0.3087
0.0000	0.0000

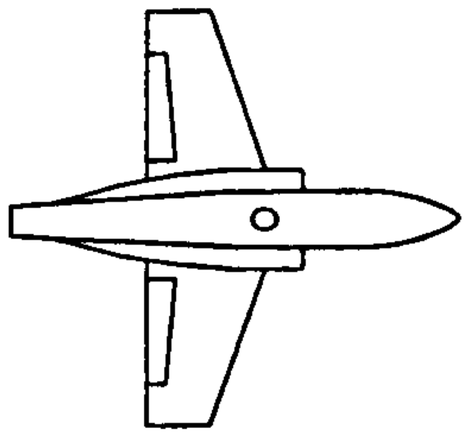

q_∞ = 61.3 Pa, NPR 2.0

	$C_{P\ (root)}$	
x/chord	upper	lower
0.0000	0.8279	0.8279
0.0459	-0.0003	-0.1865
0.0989	-0.1031	-0.1166
0.1519	-0.1975	-0.1174
0.2049	-0.2527	-0.1171
0.2580	-0.2824	-0.0994
0.3110	-0.2871	-0.0824
0.3640	-0.2855	-0.0480
0.4170	-0.2768	0.0089
0.4670	-0.2651	0.0461
0.5230	-0.2453	0.0853
0.5760	-0.2325	0.1143
0.6290	-0.2189	0.1487
0.6820	-0.2127	0.1659
0.7350	-0.2148	0.0595
0.7880	-0.2739	-0.1389
0.8410	-0.2920	-0.2322
1.0000	0.0000	0.0000

q_∞ = 245 Pa, NPR 2.0

$C_{P\ (root)}$	
upper	lower
0.8776	0.8776
-0.2691	-0.2455
-0.3150	-0.1928
-0.3724	-0.2053
-0.4034	-0.2096
-0.4194	-0.2008
-0.4053	-0.1977
-0.3877	-0.1464
-0.3708	-0.0761
-0.3564	-0.0285
-0.3307	0.0075
-0.3094	0.0348
-0.2961	0.0702
-0.2928	0.0835
-0.2966	-0.0311
-0.3550	-0.2498
-0.3638	-0.3511
0.0000	0.0000

q_∞ = 551 Pa, NPR 2.0

$C_{P\ (root)}$	
upper	lower
0.8905	0.8905
-0.3363	-0.2501
-0.3579	-0.1910
-0.4066	-0.2151
-0.4258	-0.2209
-0.4330	-0.2307
-0.4092	-0.2157
-0.3905	-0.1739
-0.3676	-0.1034
-0.3531	-0.0587
-0.3317	-0.0203
-0.3064	0.0045
-0.2945	0.0418
-0.2999	0.0577
-0.3084	-0.0470
-0.3686	-0.2440
-0.3569	-0.3345
0.0000	0.0000

q_∞ = 61.3 Pa, NPR 3.0

	$C_{P\ (root)}$	
x/chord	upper	lower
0.0000	0.7990	0.7990
0.0459	0.0270	-0.2358
0.0989	-0.0843	-0.1431
0.1519	-0.1852	-0.1529
0.2049	-0.2400	-0.1413
0.2580	-0.2743	-0.1343
0.3110	-0.2759	-0.1065
0.3640	-0.2731	-0.0646
0.4170	-0.2693	-0.0051
0.4670	-0.2570	0.0395
0.5230	-0.2420	0.0801
0.5760	-0.2294	0.1110
0.6290	-0.2162	0.1445
0.6820	-0.2139	0.1587
0.7350	-0.2257	0.0499
0.7880	-0.2648	-0.1456
0.8410	-0.2927	-0.2388
1.0000	0.0000	0.0000

q_∞ = 245 Pa, NPR 3.0

$C_{P\ (root)}$	
upper	lower
0.8577	0.8577
-0.2302	-0.2667
-0.2857	-0.1990
-0.3510	-0.2151
-0.3813	-0.2100
-0.4012	-0.2207
-0.3865	-0.1907
-0.3732	-0.1453
-0.3585	-0.0735
-0.3442	-0.0263
-0.3221	0.0103
-0.3063	0.0381
-0.2933	0.0731
-0.2929	0.0860
-0.2937	-0.0268
-0.3552	-0.2412
-0.3623	-0.3396
0.0000	0.0000

q_∞ = 551 Pa, NPR 3.0

$C_{P\ (root)}$	
upper	lower
0.8911	0.8911
-0.3807	-0.2050
-0.3830	-0.1639
-0.4203	-0.1956
-0.4299	-0.2024
-0.4306	-0.2282
-0.4053	-0.2058
-0.3819	-0.1674
-0.3607	-0.0979
-0.3462	-0.0536
-0.3233	-0.0167
-0.3012	0.0086
-0.2898	0.0439
-0.2957	0.0601
-0.2998	-0.0396
-0.3593	-0.2325
-0.3472	-0.3242
0.0000	0.0000

q_∞ = 61.3 Pa, NPR 4.0

	$C_{P\,(root)}$	
x/chord	upper	lower
0.0000	0.6533	0.6533
0.0459	-0.0593	-0.3675
0.0989	-0.1819	-0.2647
0.1519	-0.2792	-0.2593
0.2049	-0.3379	-0.2455
0.2580	-0.3785	-0.2603
0.3110	-0.3822	-0.2255
0.3640	-0.3777	-0.1827
0.4170	-0.3717	-0.1182
0.4670	-0.3629	-0.0668
0.5230	-0.3417	-0.0299
0.5760	-0.3206	-0.0047
0.6290	-0.3088	0.0247
0.6820	-0.3097	0.0365
0.7350	-0.3084	-0.0708
0.7880	-0.3697	-0.2710
0.8410	-0.3870	-0.3585
1.0000	0.0000	0.0000

q_∞ = 245 Pa, NPR 4.0

$C_{P\,(root)}$	
upper	lower
0.8459	0.8459
-0.2405	-0.2492
-0.2886	-0.1843
-0.3542	-0.2163
-0.3877	-0.1929
-0.4076	-0.2318
-0.3922	-0.1857
-0.3806	-0.1412
-0.3642	-0.0710
-0.3514	-0.0226
-0.3282	0.0143
-0.3102	0.0417
-0.2978	0.0737
-0.2927	0.0857
-0.2914	-0.0250
-0.3467	-0.2417
-0.3586	-0.3428
0.0000	0.0000

q_∞ = 551 Pa, NPR 4.0

$C_{P\,(root)}$	
upper	lower
0.9037	0.9037
-0.3669	-0.2012
-0.3700	-0.1557
-0.4081	-0.1901
-0.4142	-0.1897
-0.4191	-0.2278
-0.3915	-0.1948
-0.3723	-0.1524
-0.3493	-0.0856
-0.3374	-0.0416
-0.3157	-0.0054
-0.2934	0.0199
-0.2806	0.0551
-0.2873	0.0711
-0.2944	-0.0299
-0.3486	-0.2278
-0.3387	-0.3167
0.0000	0.0000

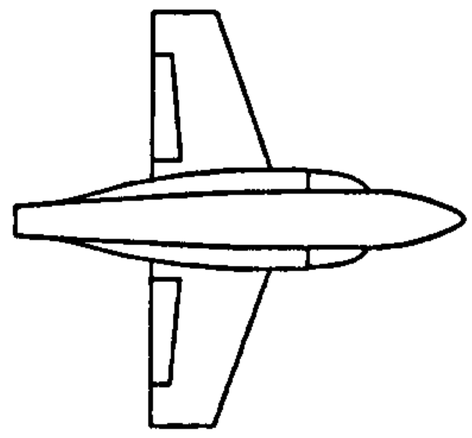

q_∞ = 61.3 Pa, NPR 1.0

	C_{Pi}	
x/d_e	lower outer	upper outer
0.0000	0.4113	-0.1076
0.1189	-0.2660	-0.1767
0.2081	-0.3378	-0.2365
0.2973	-0.2471	-0.1466
0.3963	-0.1561	-0.0587
0.4954	-0.1051	0.0081
0.5945	-0.0784	0.0751
0.6963	-0.0596	0.1465
0.7927	-0.0444	0.2273
0.8918	-0.0260	0.3127
0.9908	-0.0420	0.3844
1.0899	-0.0275	0.4453

q_∞ = 245 Pa, NPR 1.0

C_{Pi}	
lower outer	upper outer
0.4882	-0.1512
-0.3379	-0.2568
-0.4070	-0.3119
-0.2878	-0.2066
-0.1787	-0.0973
-0.1232	-0.0058
-0.0932	0.0716
-0.0832	0.1497
-0.0635	0.2347
-0.0493	0.3307
-0.0658	0.4142
-0.0486	0.4679

q_∞ = 551 Pa, NPR 1.0

C_{Pi}	
lower outer	upper outer
0.5045	-0.1549
-0.3689	-0.2936
-0.4395	-0.3488
-0.3053	-0.2319
-0.1840	-0.1041
-0.1311	-0.0135
-0.1013	0.0625
-0.0962	0.1425
-0.0733	0.2310
-0.0581	0.3329
-0.0812	0.4197
-0.0593	0.4687

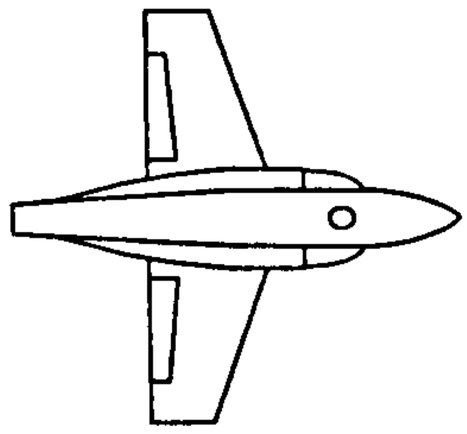

q_∞ = 61.3 Pa, NPR 2.0

	C_{Pi}	
x/d_{ie}	lower outer	upper outer
0.0000	-0.0992	-0.0315
0.1189	-0.6822	-0.2521
0.2081	-0.6564	-0.3171
0.2973	-0.5611	-0.2310
0.3963	-0.4683	-0.1423
0.4954	-0.4086	-0.0704
0.5945	-0.3628	-0.0085
0.6963	-0.3452	0.0675
0.7927	-0.3065	0.1405
0.8918	-0.2743	0.2249
0.9908	-0.2634	0.3069
1.0899	-0.2413	0.3730

q_∞ = 245 Pa, NPR 2.0

C_{Pi}	
lower outer	upper outer
0.3312	-0.0267
-0.5789	-0.2778
-0.6049	-0.3352
-0.4715	-0.2304
-0.3396	-0.1177
-0.2873	-0.0292
-0.2492	0.0471
-0.2348	0.1246
-0.2015	0.2091
-0.1802	0.3072
-0.1928	0.3946
-0.1686	0.4504

q_∞ = 551 Pa, NPR 2.0

C_{Pi}	
lower outer	upper outer
0.4167	-0.0297
-0.6115	-0.3210
-0.6654	-0.3759
-0.4973	-0.2556
-0.3497	-0.1280
-0.2944	-0.0381
-0.2560	0.0379
-0.2455	0.1190
-0.2124	0.2089
-0.1891	0.3131
-0.2134	0.4042
-0.1810	0.4539

q_∞ = 61.3 Pa, NPR 3.0

	C_{Pi}	
x/d_{ie}	lower outer	upper outer
0.0000	-0.1122	-0.0137
0.1189	-0.6614	-0.2494
0.2081	-0.6314	-0.3218
0.2973	-0.5493	-0.2354
0.3963	-0.4472	-0.1434
0.4954	-0.3923	-0.0786
0.5945	-0.3483	-0.0112
0.6963	-0.3213	0.0529
0.7927	-0.2945	0.1268
0.8918	-0.2665	0.2168
0.9908	-0.2463	0.3057
1.0899	-0.2403	0.3762

q_∞ = 245 Pa, NPR 3.0

C_{Pi}	
lower outer	upper outer
0.3344	-0.0231
-0.5787	-0.2823
-0.6010	-0.3406
-0.4645	-0.2335
-0.3337	-0.1228
-0.2802	-0.0370
-0.2456	0.0392
-0.2295	0.1134
-0.1988	0.1976
-0.1747	0.2976
-0.1876	0.3873
-0.1632	0.4488

q_∞ = 551 Pa, NPR 3.0

C_{Pi}	
lower outer	upper outer
0.4349	-0.0274
-0.5885	-0.3090
-0.6404	-0.3647
-0.4725	-0.2450
-0.3289	-0.1197
-0.2735	-0.0327
-0.2340	0.0417
-0.2263	0.1207
-0.1911	0.2099
-0.1681	0.3142
-0.1943	0.4055
-0.1623	0.4572

q_∞ = 61.3 Pa, NPR 4.0

	C_{Pi}	
x/d_e	lower outer	upper outer
0.0000	-0.0929	-0.0086
0.1189	-0.6779	-0.2290
0.2081	-0.6463	-0.2977
0.2973	-0.5512	-0.2163
0.3963	-0.4567	-0.1297
0.4954	-0.3976	-0.0647
0.5945	-0.3562	-0.0060
0.6963	-0.3283	0.0598
0.7927	-0.2985	0.1340
0.8918	-0.2678	0.2229
0.9908	-0.2563	0.3132
1.0899	-0.2381	0.3885

q_∞ = 245 Pa, NPR 4.0

C_{Pi}	
lower outer	upper outer
0.3580	-0.0293
-0.5542	-0.3105
-0.5804	-0.3707
-0.4452	-0.2612
-0.3151	-0.1482
-0.2614	-0.0604
-0.2244	0.0144
-0.2090	0.0886
-0.1782	0.1751
-0.1559	0.2771
-0.1696	0.3750
-0.1459	0.4390

q_∞ = 551 Pa, NPR 4.0

C_{Pi}	
lower outer	upper outer
0.4442	-0.0306
-0.5586	-0.3034
-0.6160	-0.3603
-0.4486	-0.2436
-0.3074	-0.1179
-0.2522	-0.0329
-0.2145	0.0385
-0.2035	0.1159
-0.1728	0.2034
-0.1493	0.3086
-0.1739	0.4036
-0.1453	0.4589

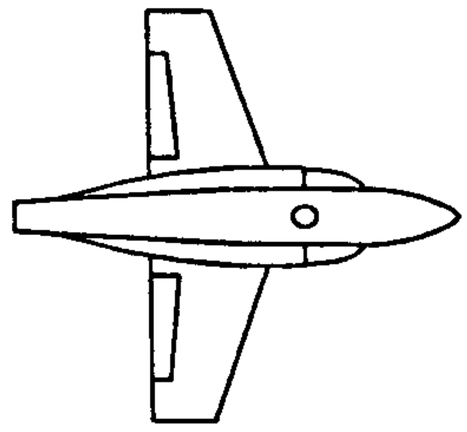

q_∞ = 61.3 Pa, NPR 2.0

	C_{Pi}	
x/d_e	lower outer	upper outer
0.0000	0.1416	-0.0151
0.1189	-0.8109	-0.2600
0.2081	-0.8475	-0.3266
0.2973	-0.7112	-0.2345
0.3963	-0.5869	-0.1424
0.4954	-0.5252	-0.0718
0.5945	-0.4856	-0.0007
0.6963	-0.4606	0.0739
0.7927	-0.4254	0.1542
0.8918	-0.3998	0.2397
0.9908	-0.3990	0.3224
1.0899	-0.3711	0.3856

q_∞ = 245 Pa, NPR 2.0

C_{Pi}	
lower outer	upper outer
0.4180	-0.0236
-0.6308	-0.2887
-0.7120	-0.3463
-0.5610	-0.2376
-0.4245	-0.1231
-0.3638	-0.0330
-0.3298	0.0441
-0.3193	0.1224
-0.2919	0.2083
-0.2732	0.3061
-0.2929	0.3932
-0.2695	0.4472

q_∞ = 551 Pa, NPR 2.0

C_{Pi}	
lower outer	upper outer
0.4549	-0.0296
-0.5924	-0.3240
-0.6815	-0.3778
-0.5209	-0.2566
-0.3807	-0.1236
-0.3280	-0.0344
-0.2949	0.0417
-0.2939	0.1228
-0.2680	0.2127
-0.2500	0.3157
-0.2822	0.4031
-0.2503	0.4529

q_∞ = 61.3 Pa, NPR 3.0

	C_{Pi}	
x/d_e	lower outer	upper outer
0.0000	0.1068	-0.0069
0.1189	-0.8481	-0.2412
0.2081	-0.8646	-0.3079
0.2973	-0.7377	-0.2207
0.3963	-0.6181	-0.1264
0.4954	-0.5412	-0.0628
0.5945	-0.4928	0.0016
0.6963	-0.4724	0.0766
0.7927	-0.4418	0.1511
0.8918	-0.4100	0.2410
0.9908	-0.3924	0.3270
1.0899	-0.3667	0.3924

q_∞ = 245 Pa, NPR 3.0

C_{Pi}	
lower outer	upper outer
0.4365	-0.0221
-0.6167	-0.2903
-0.6986	-0.3511
-0.5459	-0.2420
-0.4079	-0.1302
-0.3487	-0.0408
-0.3118	0.0330
-0.3014	0.1119
-0.2757	0.1962
-0.2540	0.2974
-0.2566	0.3885
-0.2421	0.4457

q_∞ = 551 Pa, NPR 3.0

C_{Pi}	
lower outer	upper outer
0.4690	-0.0291
-0.5792	-0.3105
-0.6681	-0.3657
-0.5042	-0.2461
-0.3616	-0.1162
-0.3081	-0.0291
-0.2757	0.0457
-0.2732	0.1258
-0.2460	0.2143
-0.2263	0.3173
-0.2568	0.4058
-0.2259	0.4560

q_∞ = 61.3 Pa, NPR 4.0

	C_{Pi}	
x/d_{ie}	lower outer	upper outer
0.0000	0.0986	-0.0410
0.1189	-0.8508	-0.2593
0.2081	-0.8798	-0.3350
0.2973	-0.7489	-0.2463
0.3963	-0.6197	-0.1596
0.4954	-0.5484	-0.0916
0.5945	-0.5094	-0.0294
0.6963	-0.4745	0.0359
0.7927	-0.4513	0.1144
0.8918	-0.4053	0.2004
0.9908	-0.4087	0.2920
1.0899	-0.3797	0.3619

q_∞ = 245 Pa, NPR 4.0

C_{Pi}	
lower outer	upper outer
0.4439	-0.0316
-0.5962	-0.3176
-0.6792	-0.3784
-0.5287	-0.2645
-0.3890	-0.1513
-0.3266	-0.0588
-0.2927	0.0175
-0.2784	0.0960
-0.2526	0.1800
-0.2255	0.2829
-0.2471	0.3758
-0.2214	0.4331

q_∞ = 551 Pa, NPR 4.0

C_{Pi}	
lower outer	upper outer
0.4706	-0.0330
-0.5677	-0.3052
-0.6584	-0.3613
-0.4966	-0.2459
-0.3528	-0.1189
-0.2985	-0.0325
-0.2641	0.0401
-0.2618	0.1187
-0.2337	0.2048
-0.2116	0.3115
-0.2409	0.4036
-0.2113	0.4568

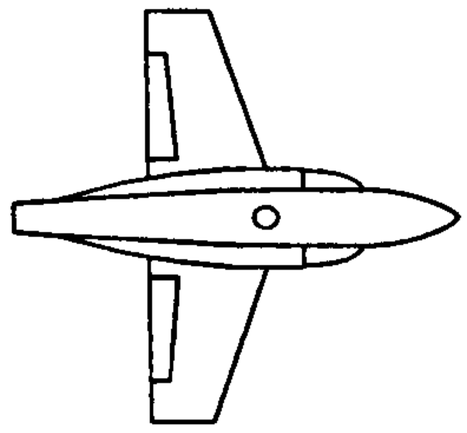

q_∞ = 61.3 Pa, NPR 2.0

	C_{Pi}	
x/d_e	lower outer	upper outer
0.0000	0.2829	-0.0236
0.1189	-0.5644	-0.2757
0.2081	-0.6297	-0.3453
0.2973	-0.5166	-0.2398
0.3963	-0.4101	-0.1584
0.4954	-0.3548	-0.0875
0.5945	-0.3344	-0.0165
0.6963	-0.3246	0.0623
0.7927	-0.3026	0.1409
0.8918	-0.2993	0.2329
0.9908	-0.3213	0.3149
1.0899	-0.3161	0.3755

q_∞ = 245 Pa, NPR 2.0

C_{Pi}	
lower outer	upper outer
0.4515	-0.0280
-0.4561	-0.2877
-0.5313	-0.3470
-0.3998	-0.2366
-0.2877	-0.1252
-0.2291	-0.0346
-0.2004	0.0426
-0.1979	0.1213
-0.1774	0.2040
-0.1671	0.3046
-0.1945	0.3909
-0.1800	0.4458

q_∞ = 551 Pa, NPR 2.0

C_{Pi}	
lower outer	upper outer
0.4786	-0.0327
-0.4406	-0.3238
-0.5183	-0.3779
-0.3768	-0.2574
-0.2498	-0.1249
-0.1982	-0.0344
-0.1721	0.0402
-0.1697	0.1216
-0.1487	0.2101
-0.1386	0.3131
-0.1707	0.4009
-0.1519	0.4506

q_∞ = 61.3 Pa, NPR 3.0

	C_{Pi}	
x/d_e	lower outer	upper outer
0.0000	0.2619	-0.0250
0.1189	-0.6053	-0.2595
0.2081	-0.6715	-0.3276
0.2973	-0.5572	-0.2424
0.3963	-0.4428	-0.1558
0.4954	-0.3885	-0.0862
0.5945	-0.3656	-0.0224
0.6963	-0.3583	0.0485
0.7927	-0.3371	0.1228
0.8918	-0.3273	0.2110
0.9908	-0.3501	0.3017
1.0899	-0.3437	0.3731

q_∞ = 245 Pa, NPR 3.0

C_{Pi}	
lower outer	upper outer
0.4565	-0.0291
-0.4761	-0.2962
-0.5525	-0.3558
-0.4220	-0.2462
-0.2988	-0.1338
-0.2447	-0.0466
-0.2157	0.0263
-0.2102	0.1053
-0.1936	0.1890
-0.1801	0.2886
-0.2054	0.3795
-0.1933	0.4390

q_∞ = 551 Pa, NPR 3.0

C_{Pi}	
lower outer	upper outer
0.4877	-0.0356
-0.4582	-0.3151
-0.5351	-0.3700
-0.3894	-0.2499
-0.2599	-0.1221
-0.2091	-0.0347
-0.1806	0.0411
-0.1805	0.1205
-0.1590	0.2094
-0.1467	0.3127
-0.1783	0.4030
-0.1591	0.4543

q_∞ = 61.3 Pa, NPR 4.0

	C_{Pi}	
x/d_e	lower outer	upper outer
0.0000	0.2630	-0.0310
0.1189	-0.6076	-0.2599
0.2081	-0.6752	-0.3318
0.2973	-0.5578	-0.2413
0.3963	-0.4431	-0.1609
0.4954	-0.3922	-0.0925
0.5945	-0.3622	-0.0307
0.6963	-0.3511	0.0356
0.7927	-0.3382	0.1113
0.8918	-0.3247	0.2011
0.9908	-0.3428	0.2940
1.0899	-0.3368	0.3626

q_∞ = 245 Pa, NPR 4.0

C_{Pi}	
lower outer	upper outer
0.4654	-0.0295
-0.4762	-0.3127
-0.5563	-0.3742
-0.4213	-0.2608
-0.2985	-0.1477
-0.2446	-0.0590
-0.2171	0.0160
-0.2093	0.0949
-0.1940	0.1807
-0.1783	0.2823
-0.2039	0.3746
-0.1897	0.4358

q_∞ = 551 Pa, NPR 4.0

C_{Pi}	
lower outer	upper outer
0.4880	-0.0317
-0.4555	-0.3103
-0.5350	-0.3666
-0.3892	-0.2483
-0.2583	-0.1202
-0.2066	-0.0358
-0.1788	0.0380
-0.1783	0.1167
-0.1572	0.2044
-0.1434	0.3079
-0.1761	0.4017
-0.1570	0.4545

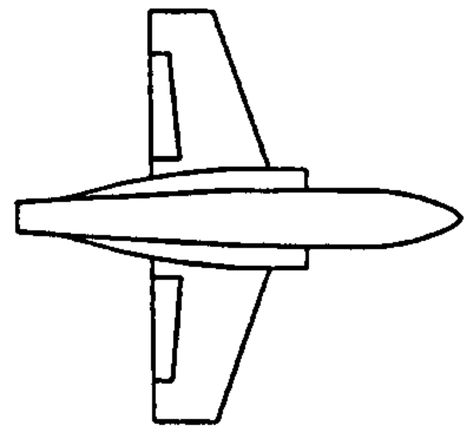

q_∞ = 61.3 Pa, NPR 1.0

	C_{Pi}			
x/d_{ie}	lower outer	lower inner	upper inner	upper outer
0.0000	-83.0956	-83.0956	-108.6351	-108.6351
0.1189	0.3915	-101.5079	-116.6924	-34.9485
0.2081	1.0120	-101.2498	-102.7953	0.8522
0.2973	0.9308	-94.9384	-95.3395	0.8908
0.3963	0.7715	-90.8454	-90.7768	0.7802
0.4954	0.6241	-87.8538	-88.1568	0.7189
0.5945	0.5212	-88.1621	-87.4115	0.6687
0.6963	0.4333	-86.3982	-87.1973	0.6552
0.7927	0.3810	-85.9575	-86.8649	0.6608
0.8918	0.3311	-85.7596	-88.9785	0.6781
0.9908	0.2799	-86.4501	-88.4358	0.7102
1.0899	0.2607	-86.6876	-86.2218	0.7149

q_∞ = 245 Pa, NPR 1.0

	C_{Pi}			
x/d_{ie}	lower outer	lower inner	upper inner	upper outer
0.0000	-13.2756	-13.2756	-20.3044	-20.3044
0.1189	0.8552	-23.2505	-27.9307	-4.8205
0.2081	0.4702	-24.7594	-24.9386	0.4729
0.2973	0.3389	-23.2479	-23.2435	0.3085
0.3963	0.2687	-21.8595	-22.3404	0.2289
0.4954	0.2093	-21.3930	-21.6812	0.2047
0.5945	0.1777	-21.5977	-21.4999	0.2019
0.6963	0.1400	-21.1981	-21.3682	0.2290
0.7927	0.1265	-20.9772	-21.3748	0.2857
0.8918	0.1121	-20.8893	-21.9840	0.3488
0.9908	0.0884	-21.0625	-21.7690	0.4238
1.0899	0.0881	-21.1160	-21.0098	0.5948

q_∞ = 551 Pa, NPR 1.0

	C_{Pi}			
x/d_{i_e}	lower outer	lower inner	upper inner	upper outer
0.0000	-3.0995	-3.0995	-6.4069	-6.4069
0.1189	0.3124	-8.6982	-11.3422	-0.7483
0.2081	-0.0039	-10.4159	-10.6845	0.1356
0.2973	0.0079	-9.8057	-9.9763	0.0683
0.3963	0.0336	-9.2400	-9.4391	0.0779
0.4954	0.0278	-8.9366	-9.1045	0.0935
0.5945	0.0263	-9.0666	-9.0135	0.1297
0.6963	0.0225	-8.8828	-9.0073	0.1837
0.7927	0.0206	-8.7881	-8.9823	0.2344
0.8918	0.0223	-8.7392	-9.2892	0.2999
0.9908	0.0100	-8.8211	-9.1771	0.5095
1.0899	0.0147	-8.8275	-8.8325	0.6509

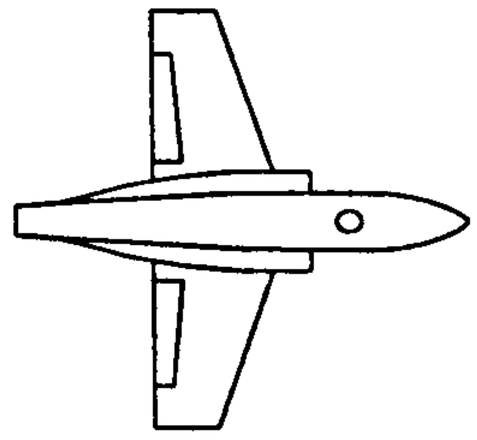

q_∞ = 61.3 Pa, NPR 2.0

	C_{Pi}			
x/d_{ie}	lower outer	lower inner	upper inner	upper outer
0.0000	-103.6473	-103.6473	-117.2256	-117.2256
0.1189	0.6260	-98.0287	-119.5431	-1.0293
0.2081	0.9271	-100.4921	-104.7707	0.8828
0.2973	0.7546	-93.3552	-97.1473	0.8863
0.3963	0.5790	-89.2269	-92.3312	0.7645
0.4954	0.4408	-86.9904	-89.5193	0.6659
0.5945	0.3747	-87.9202	-88.7855	0.6394
0.6963	0.2918	-86.7786	-88.3438	0.6132
0.7927	0.2591	-85.7096	-87.6736	0.6353
0.8918	0.2275	-85.4485	-89.6568	0.6728
0.9908	0.1859	-86.1420	-89.1957	0.6870
1.0899	0.1643	-86.3800	-86.8644	0.7011

q_∞ = 245 Pa, NPR 2.0

	C_{Pi}			
x/d_{ie}	lower outer	lower inner	upper inner	upper outer
0.0000	-14.3551	-14.3551	-20.3943	-20.3943
0.1189	0.6374	-23.1757	-29.4858	0.7062
0.2081	0.1990	-24.4144	-25.9521	0.4511
0.2973	0.1108	-22.8082	-24.0079	0.3228
0.3963	0.0805	-21.6927	-22.7719	0.2609
0.4954	0.0495	-21.1076	-21.9391	0.2440
0.5945	0.0327	-21.4278	-21.6951	0.2461
0.6963	0.0100	-20.9561	-21.6935	0.2781
0.7927	0.0129	-20.8994	-21.5525	0.3248
0.8918	0.0070	-20.8571	-22.2109	0.3981
0.9908	-0.0106	-21.0837	-21.9878	0.4934
1.0899	-0.0067	-21.1499	-21.2282	0.6291

q_∞ = 551 Pa, NPR 2.0

	C_{Pi}			
x/d_{in}	lower outer	lower inner	upper inner	upper outer
0.0000	-2.1111	-2.1111	-5.4649	-5.4649
0.1189	-0.0319	-9.2593	-11.9136	0.4421
0.2081	-0.3439	-10.0332	-10.9792	0.1092
0.2973	-0.2644	-9.4829	-10.1795	0.0553
0.3963	-0.1914	-9.0273	-9.5735	0.0520
0.4954	-0.1642	-8.7730	-9.1982	0.0596
0.5945	-0.1436	-8.9578	-9.0896	0.0867
0.6963	-0.1382	-8.7657	-9.0584	0.1287
0.7927	-0.1221	-8.6838	-9.0041	0.1857
0.8918	-0.1109	-8.6611	-9.3027	0.2612
0.9908	-0.1115	-8.7650	-9.2148	0.4281
1.0899	-0.1012	-8.7937	-8.8764	0.6115

q_∞ = 61.3 Pa, NPR 3.0

	C_{Pi}			
x/d_{in}	lower outer	lower inner	upper inner	upper outer
0.0000	-104.7108	-104.7108	-120.8188	-120.8188
0.1189	0.6280	-98.2959	-123.3734	-0.7518
0.2081	0.9456	-100.3002	-106.8330	0.7745
0.2973	0.7766	-93.1088	-98.0819	0.7714
0.3963	0.6129	-89.0312	-92.7032	0.6742
0.4954	0.4886	-86.7257	-89.4208	0.6182
0.5945	0.4011	-87.8629	-88.4463	0.5999
0.6963	0.3294	-86.2565	-87.8745	0.6115
0.7927	0.2978	-85.7617	-87.7562	0.6502
0.8918	0.2604	-85.7533	-89.3301	0.6830
0.9908	0.2185	-86.5428	-89.0629	0.6983
1.0899	0.1971	-86.5974	-86.7523	0.7079

q_∞ = 245 Pa, NPR 3.0

	C_{Pi}			
x/d_{in}	lower outer	lower inner	upper inner	upper outer
0.0000	-14.1136	-14.1136	-20.7468	-20.7468
0.1189	0.6341	-22.9888	-29.3929	0.5846
0.2081	0.2045	-23.9974	-25.8604	0.4401
0.2973	0.1162	-22.4620	-23.8483	0.3182
0.3963	0.0891	-21.4742	-22.5167	0.2623
0.4954	0.0580	-20.8980	-21.8264	0.2449
0.5945	0.0431	-21.2894	-21.5600	0.2499
0.6963	0.0273	-20.7761	-21.5218	0.2695
0.7927	0.0225	-20.6731	-21.3157	0.3234
0.8918	0.0185	-20.7044	-21.9957	0.3900
0.9908	0.0047	-20.8918	-21.8492	0.4921
1.0899	0.0084	-20.9583	-21.0636	0.6210

q_∞ = 551 Pa, NPR 3.0

	C_{Pi}			
x/d_e	lower outer	lower inner	upper inner	upper outer
0.0000	-2.2561	-2.2561	-5.2265	-5.2265
0.1189	0.0136	-9.3081	-11.7960	0.3848
0.2081	-0.3014	-10.0225	-10.9364	0.0749
0.2973	-0.2296	-9.4739	-10.0986	0.0286
0.3963	-0.1612	-8.9970	-9.4898	0.0282
0.4954	-0.1377	-8.7385	-9.1391	0.0387
0.5945	-0.1212	-8.9171	-9.0618	0.0630
0.6963	-0.1120	-8.7357	-9.0439	0.1041
0.7927	-0.1006	-8.6557	-8.9779	0.1612
0.8918	-0.0877	-8.6112	-9.2718	0.2409
0.9908	-0.0888	-8.7108	-9.1708	0.3926
1.0899	-0.0788	-8.7560	-8.8429	0.5689

q_∞ = 61.3 Pa, NPR 4.0

	C_{Pi}			
x/d_e	lower outer	lower inner	upper inner	upper outer
0.0000	-102.9416	-102.9416	-119.4906	-119.4906
0.1189	0.6288	-96.9663	-122.1921	-0.4958
0.2081	0.9471	-99.3563	-106.1586	0.6560
0.2973	0.7818	-92.8652	-97.6481	0.7572
0.3963	0.6368	-88.8434	-92.5086	0.7153
0.4954	0.5005	-86.5727	-88.9201	0.6735
0.5945	0.4194	-87.4827	-88.3519	0.6568
0.6963	0.3576	-85.7811	-88.1220	0.6546
0.7927	0.3022	-85.1066	-87.3125	0.6848
0.8918	0.2754	-84.9046	-89.5515	0.7092
0.9908	0.2352	-85.3263	-89.1211	0.7394
1.0899	0.2120	-85.7707	-86.3714	0.7384

q_∞ = 245 Pa, NPR 4.0

	C_{Pi}			
x/d_e	lower outer	lower inner	upper inner	upper outer
0.0000	-13.5985	-13.5985	-20.7055	-20.7055
0.1189	0.6400	-22.8124	-29.1832	0.5741
0.2081	0.2136	-24.0167	-25.7485	0.3881
0.2973	0.1246	-22.5078	-23.8174	0.2674
0.3963	0.0982	-21.3717	-22.6311	0.2144
0.4954	0.0624	-20.9175	-21.8663	0.1935
0.5945	0.0474	-21.2891	-21.6793	0.2042
0.6963	0.0321	-20.9493	-21.6180	0.2428
0.7927	0.0239	-20.7304	-21.4549	0.2912
0.8918	0.0235	-20.6853	-22.1258	0.3688
0.9908	0.0086	-20.8833	-21.8895	0.4682
1.0899	0.0098	-20.9606	-21.1071	0.5895

q_∞ = 551 Pa, NPR 4.0

	C_{Pi}			
x/d_e	lower outer	lower inner	upper inner	upper outer
0.0000	-2.0994	-2.0994	-5.1108	-5.1108
0.1189	0.0405	-9.1749	-11.6534	0.3926
0.2081	-0.2726	-9.9485	-10.8312	0.0833
0.2973	-0.2038	-9.4457	-10.0467	0.0409
0.3963	-0.1380	-8.9629	-9.4557	0.0383
0.4954	-0.1151	-8.7453	-9.1157	0.0487
0.5945	-0.1025	-8.9096	-9.0402	0.0732
0.6963	-0.0956	-8.7316	-9.0207	0.1148
0.7927	-0.0821	-8.6479	-8.9576	0.1713
0.8918	-0.0719	-8.6314	-9.2540	0.2510
0.9908	-0.0731	-8.7214	-9.1809	0.4015
1.0899	-0.0655	-8.7560	-8.8388	0.5787

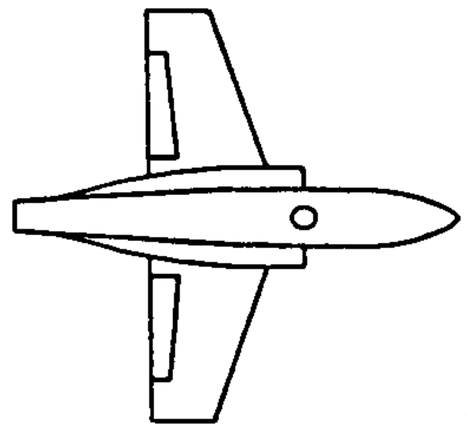

q_∞ = 61.3 Pa, NPR 2.0

	C_{Pi}			
x/d_{ie}	lower outer	lower inner	upper inner	upper outer
0.0000	-103.7072	-103.7072	-113.2872	-113.2872
0.1189	0.7193	-96.7495	-120.1035	-0.4852
0.2081	0.9282	-99.6758	-104.9284	0.8436
0.2973	0.7073	-93.4634	-96.6024	0.8600
0.3963	0.5013	-89.2475	-91.9789	0.7616
0.4954	0.3497	-86.5809	-89.0031	0.6924
0.5945	0.2427	-87.2018	-88.1148	0.6505
0.6963	0.1586	-85.7032	-87.8870	0.6319
0.7927	0.1096	-85.1380	-87.2632	0.6444
0.8918	0.0852	-84.9641	-89.0693	0.6812
0.9908	0.0170	-85.6452	-88.5009	0.7029
1.0899	0.0004	-85.9579	-86.1256	0.7179

q_∞ = 245 Pa, NPR 2.0

	C_{Pi}			
x/d_{ie}	lower outer	lower inner	upper inner	upper outer
0.0000	-14.6953	-14.6953	-18.7356	-18.7356
0.1189	0.6428	-22.8993	-28.3300	0.6683
0.2081	0.1701	-23.9536	-25.2372	0.4149
0.2973	0.0583	-22.4714	-23.3825	0.2859
0.3963	0.0109	-21.2908	-22.1599	0.2393
0.4954	-0.0413	-20.7863	-21.4693	0.2155
0.5945	-0.0697	-21.0663	-21.2891	0.2241
0.6963	-0.1035	-20.7035	-21.2417	0.2562
0.7927	-0.1091	-20.5662	-21.0784	0.3071
0.8918	-0.1182	-20.4330	-21.7590	0.3766
0.9908	-0.1372	-20.6516	-21.5446	0.4677
1.0899	-0.1353	-20.7481	-20.8253	0.6084

q_∞ = 551 Pa, NPR 2.0

	C_{Pi}			
x/d_{ie}	lower outer	lower inner	upper inner	upper outer
0.0000	-2.6780	-2.6780	-4.9790	-4.9790
0.1189	0.0685	-9.3816	-11.3907	0.4127
0.2081	-0.2841	-10.0675	-10.6704	0.0906
0.2973	-0.2372	-9.5371	-9.9626	0.0450
0.3963	-0.1939	-8.9955	-9.4019	0.0440
0.4954	-0.1892	-8.7727	-9.0632	0.0544
0.5945	-0.1889	-8.9163	-8.9575	0.0819
0.6963	-0.1960	-8.7190	-8.9601	0.1239
0.7927	-0.1910	-8.6477	-8.8671	0.1825
0.8918	-0.1877	-8.5888	-9.1806	0.2561
0.9908	-0.2015	-8.6636	-9.1123	0.4239
1.0899	-0.1942	-8.7010	-8.7836	0.5983

q_∞ = 61.3 Pa, NPR 3.0

	C_{Pi}			
x/d_{ie}	lower outer	lower inner	upper inner	upper outer
0.0000	-103.4151	-103.4151	-116.3918	-116.3918
0.1189	0.6860	-97.9729	-121.9891	-0.3694
0.2081	0.8992	-100.3810	-105.9983	0.7429
0.2973	0.6737	-94.2077	-97.7591	0.7919
0.3963	0.4768	-89.4833	-92.5516	0.7095
0.4954	0.3287	-87.3540	-89.8861	0.6456
0.5945	0.2255	-87.8922	-89.0246	0.6047
0.6963	0.1568	-86.6127	-88.2992	0.6021
0.7927	0.0995	-85.9434	-87.8047	0.6269
0.8918	0.0612	-85.5947	-89.8887	0.6555
0.9908	0.0189	-86.1317	-89.3495	0.6639
1.0899	0.0063	-86.5425	-87.0393	0.6780

q_∞ = 245 Pa, NPR 3.0

	C_{Pi}			
x/d_{ie}	lower outer	lower inner	upper inner	upper outer
0.0000	-14.6976	-14.6976	-19.3830	-19.3830
0.1189	0.6376	-23.0218	-28.4590	0.5993
0.2081	0.1711	-24.0921	-25.3736	0.3946
0.2973	0.0612	-22.5643	-23.5315	0.2778
0.3963	0.0128	-21.4151	-22.3246	0.2163
0.4954	-0.0300	-20.9053	-21.6105	0.2033
0.5945	-0.0640	-21.2068	-21.4020	0.2095
0.6963	-0.0910	-20.8330	-21.3796	0.2416
0.7927	-0.1015	-20.6480	-21.2729	0.2887
0.8918	-0.1063	-20.5641	-21.9102	0.3659
0.9908	-0.1218	-20.7427	-21.6961	0.4530
1.0899	-0.1199	-20.8175	-20.9525	0.5879

q_∞ = 551 Pa, NPR 3.0

	C_{Pi}			
x/d_e	lower outer	lower inner	upper inner	upper outer
0.0000	-2.8045	-2.8045	-4.7880	-4.7880
0.1189	0.0980	-9.5001	-11.3734	0.3731
0.2081	-0.2557	-10.1678	-10.7018	0.0583
0.2973	-0.2142	-9.6088	-9.9851	0.0206
0.3963	-0.1709	-9.0689	-9.4308	0.0239
0.4954	-0.1675	-8.8247	-9.0881	0.0380
0.5945	-0.1672	-8.9745	-9.0125	0.0665
0.6963	-0.1714	-8.7954	-9.0006	0.1095
0.7927	-0.1662	-8.7000	-8.9344	0.1685
0.8918	-0.1614	-8.6712	-9.2276	0.2459
0.9908	-0.1738	-8.7585	-9.1650	0.4085
1.0899	-0.1662	-8.7760	-8.8349	0.5787

q_∞ = 61.3 Pa, NPR 4.0

	C_{Pi}			
x/d_e	lower outer	lower inner	upper inner	upper outer
0.0000	-103.7301	-103.7301	-118.2732	-118.2732
0.1189	0.7176	-97.6172	-122.6136	-0.4858
0.2081	0.9316	-100.2357	-106.1858	0.6735
0.2973	0.7123	-93.9264	-97.9344	0.7578
0.3963	0.5219	-89.5743	-93.0359	0.7127
0.4954	0.3696	-87.1538	-89.9221	0.6617
0.5945	0.2685	-87.5641	-88.9547	0.6498
0.6963	0.1873	-86.2953	-88.5517	0.6654
0.7927	0.1427	-85.5171	-88.0418	0.6924
0.8918	0.1108	-85.3865	-90.1315	0.7239
0.9908	0.0657	-86.0413	-89.5441	0.7436
1.0899	0.0359	-86.3691	-86.9137	0.7725

q_∞ = 245 Pa, NPR 4.0

	C_{Pi}			
x/d_e	lower outer	lower inner	upper inner	upper outer
0.0000	-14.5336	-14.5336	-20.2363	-20.2363
0.1189	0.6431	-23.0176	-28.6940	0.5148
0.2081	0.1800	-24.0976	-25.5808	0.3434
0.2973	0.0685	-22.6003	-23.6741	0.2386
0.3963	0.0184	-21.4233	-22.4603	0.1962
0.4954	-0.0241	-20.9318	-21.7448	0.1717
0.5945	-0.0493	-21.1951	-21.5171	0.1783
0.6963	-0.0808	-20.8585	-21.4765	0.2032
0.7927	-0.0826	-20.7051	-21.3518	0.2510
0.8918	-0.0858	-20.6112	-21.9300	0.3336
0.9908	-0.1047	-20.8371	-21.7213	0.4259
1.0899	-0.1030	-20.8843	-21.0355	0.5511

q_∞ = 551 Pa, NPR 4.0

	C_{Pi}			
x/d_{ie}	lower outer	lower inner	upper inner	upper outer
0.0000	-2.7606	-2.7606	-4.7970	-4.7970
0.1189	0.1064	-9.4424	-11.3347	0.3725
0.2081	-0.2465	-10.1106	-10.6492	0.0654
0.2973	-0.2077	-9.5505	-9.9243	0.0278
0.3963	-0.1638	-9.0207	-9.3719	0.0302
0.4954	-0.1590	-8.7782	-9.0316	0.0442
0.5945	-0.1572	-8.9204	-8.9543	0.0692
0.6963	-0.1613	-8.7431	-8.9471	0.1137
0.7927	-0.1558	-8.6409	-8.8700	0.1672
0.8918	-0.1500	-8.6046	-9.1749	0.2494
0.9908	-0.1615	-8.7010	-9.1141	0.4006
1.0899	-0.1537	-8.7195	-8.7957	0.5723

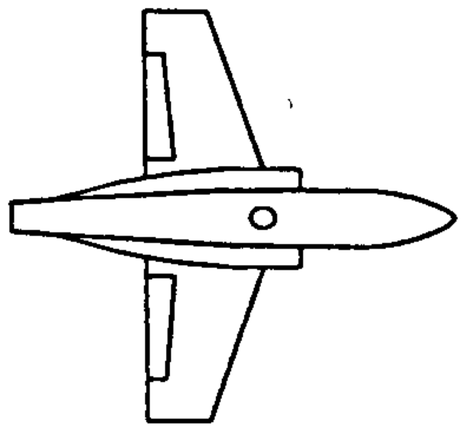

q_∞ = 61.3 Pa, NPR 2.0

	C_{Pi}			
x/d_e	lower outer	lower inner	upper inner	upper outer
0.0000	-110.3122	-110.3122	-110.6632	-110.6632
0.1189	0.5596	-97.2088	-119.1249	-0.0371
0.2081	0.9735	-100.1379	-104.7327	0.8273
0.2973	0.7983	-93.7780	-96.8113	0.8250
0.3963	0.6085	-89.3482	-91.7949	0.7323
0.4954	0.4549	-86.9919	-88.9299	0.6670
0.5945	0.3357	-87.8298	-88.0730	0.6190
0.6963	0.2446	-85.8012	-87.6774	0.6195
0.7927	0.1832	-85.3194	-87.2643	0.6422
0.8918	0.1315	-85.2477	-89.0307	0.6749
0.9908	0.0668	-85.7634	-88.7351	0.6887
1.0899	0.0407	-86.1020	-86.1850	0.6942

q_∞ = 245 Pa, NPR 2.0

	C_{Pi}			
x/d_e	lower outer	lower inner	upper inner	upper outer
0.0000	-16.2723	-16.2723	-18.3061	-18.3061
0.1189	0.7670	-23.1559	-28.0174	0.6574
0.2081	0.3442	-24.0887	-24.9771	0.4022
0.2973	0.2134	-22.5857	-23.1774	0.2827
0.3963	0.1518	-21.3994	-22.0506	0.2233
0.4954	0.0935	-20.8577	-21.3796	0.2038
0.5945	0.0567	-21.0980	-21.1617	0.2154
0.6963	0.0209	-20.7075	-21.1593	0.2422
0.7927	0.0017	-20.4931	-21.0370	0.2948
0.8918	-0.0115	-20.4433	-21.6286	0.3671
0.9908	-0.0446	-20.6252	-21.4799	0.4574
1.0899	-0.0510	-20.6979	-20.7634	0.5986

q_∞ = 551 Pa, NPR 2.0

	C_{Pi}			
x/d_e	lower outer	lower inner	upper inner	upper outer
0.0000	-3.3627	-3.3627	-4.8011	-4.8011
0.1189	0.2500	-9.6284	-11.3261	0.4049
0.2081	-0.0904	-10.2135	-10.6893	0.0872
0.2973	-0.0689	-9.6438	-9.9624	0.0454
0.3963	-0.0417	-9.0905	-9.4198	0.0484
0.4954	-0.0455	-8.8142	-9.0673	0.0602
0.5945	-0.0479	-8.9903	-9.0037	0.0866
0.6963	-0.0587	-8.7815	-8.9833	0.1352
0.7927	-0.0602	-8.7147	-8.9194	0.1932
0.8918	-0.0643	-8.6662	-9.2076	0.2622
0.9908	-0.0845	-8.7611	-9.1604	0.4390
1.0899	-0.0859	-8.7811	-8.8418	0.6060

q_∞ = 61.3 Pa, NPR 3.0

	C_{Pi}			
x/d_e	lower outer	lower inner	upper inner	upper outer
0.0000	-108.8832	-108.8832	-111.9973	-111.9973
0.1189	0.6149	-97.9718	-120.9294	-0.2759
0.2081	0.9810	-99.8544	-105.3093	0.7116
0.2973	0.7905	-93.8738	-97.0922	0.7654
0.3963	0.5902	-89.3232	-92.4484	0.6949
0.4954	0.4422	-86.3446	-89.1806	0.6497
0.5945	0.3304	-87.2233	-88.3441	0.6396
0.6963	0.2455	-86.1031	-87.6472	0.6440
0.7927	0.1778	-85.4333	-87.4148	0.6703
0.8918	0.1348	-85.3027	-89.0651	0.7016
0.9908	0.0594	-86.0779	-88.8884	0.7152
1.0899	0.0264	-86.0334	-86.6781	0.7402

q_∞ = 245 Pa, NPR 3.0

	C_{Pi}			
x/d_e	lower outer	lower inner	upper inner	upper outer
0.0000	-16.0818	-16.0818	-18.9855	-18.9855
0.1189	0.7506	-23.1461	-28.2047	0.6064
0.2081	0.3225	-24.1123	-25.1962	0.3796
0.2973	0.1981	-22.5687	-23.3289	0.2677
0.3963	0.1389	-21.4178	-22.1663	0.2136
0.4954	0.0790	-20.8661	-21.4729	0.1956
0.5945	0.0450	-21.1286	-21.3062	0.1973
0.6963	0.0083	-20.7532	-21.2636	0.2293
0.7927	-0.0044	-20.5577	-21.1308	0.2820
0.8918	-0.0202	-20.4797	-21.7415	0.3504
0.9908	-0.0522	-20.6893	-21.5876	0.4427
1.0899	-0.0611	-20.7286	-20.8829	0.5808

q_∞ = 551 Pa, NPR 3.0

	C_{Pi}			
x/d_e	lower outer	lower inner	upper inner	upper outer
0.0000	-3.3749	-3.3749	-4.5726	-4.5726
0.1189	0.2513	-9.6459	-11.1614	0.3561
0.2081	-0.0921	-10.2054	-10.5547	0.0441
0.2973	-0.0737	-9.6442	-9.8822	0.0096
0.3963	-0.0454	-9.0807	-9.3463	0.0198
0.4954	-0.0515	-8.8041	-8.9955	0.0345
0.5945	-0.0545	-8.9424	-8.9636	0.0650
0.6963	-0.0665	-8.7549	-8.9444	0.1125
0.7927	-0.0645	-8.6550	-8.8735	0.1702
0.8918	-0.0675	-8.5899	-9.1582	0.2473
0.9908	-0.0874	-8.7218	-9.0968	0.4181
1.0899	-0.0881	-8.7297	-8.7893	0.5817

q_∞ = 61.3 Pa, NPR 4.0

	C_{Pi}			
x/d_e	lower outer	lower inner	upper inner	upper outer
0.0000	-107.1363	-107.1363	-113.8353	-113.8353
0.1189	0.6154	-97.1676	-119.3757	-0.5419
0.2081	0.9525	-99.6793	-104.0415	0.5420
0.2973	0.7521	-93.4700	-96.1938	0.5726
0.3963	0.5617	-88.8679	-91.6669	0.5184
0.4954	0.4095	-86.6344	-88.4442	0.4852
0.5945	0.2990	-87.2172	-87.5614	0.4853
0.6963	0.2062	-85.8412	-87.3867	0.5064
0.7927	0.1519	-84.8135	-86.7320	0.5333
0.8918	0.1051	-84.6651	-88.6917	0.5770
0.9908	0.0414	-85.3752	-88.3605	0.6036
1.0899	0.0075	-85.7452	-86.1391	0.6366

q_∞ = 245 Pa, NPR 4.0

	C_{Pi}			
x/d_e	lower outer	lower inner	upper inner	upper outer
0.0000	-15.6667	-15.6667	-19.3087	-19.3087
0.1189	0.7397	-22.8581	-27.8086	0.4977
0.2081	0.3157	-23.7788	-24.8776	0.3392
0.2973	0.1883	-22.2424	-23.0432	0.2281
0.3963	0.1327	-21.1399	-21.8820	0.1801
0.4954	0.0776	-20.5675	-21.1767	0.1675
0.5945	0.0401	-20.8431	-21.0143	0.1769
0.6963	0.0053	-20.4801	-20.9612	0.2048
0.7927	-0.0100	-20.2960	-20.8559	0.2485
0.8918	-0.0202	-20.2114	-21.4348	0.3203
0.9908	-0.0521	-20.4040	-21.2851	0.4178
1.0899	-0.0579	-20.4408	-20.5671	0.5431

q_∞ = 551 Pa, NPR 4.0

	C_{Pi}			
x/d_e	lower outer	lower inner	upper inner	upper outer
0.0000	-3.3031	-3.3031	-4.5817	-4.5817
0.1189	0.2454	-9.5907	-11.1678	0.3573
0.2081	-0.0940	-10.2094	-10.5451	0.0473
0.2973	-0.0780	-9.6218	-9.8488	0.0157
0.3963	-0.0476	-9.0671	-9.3143	0.0235
0.4954	-0.0525	-8.8153	-8.9918	0.0389
0.5945	-0.0542	-8.9341	-8.9280	0.0674
0.6963	-0.0673	-8.7523	-8.9218	0.1125
0.7927	-0.0665	-8.6595	-8.8472	0.1708
0.8918	-0.0666	-8.6132	-9.1242	0.2521
0.9908	-0.0894	-8.7050	-9.0749	0.4120
1.0899	-0.0882	-8.7135	-8.7659	0.5788

C Phase 2a Experimental Data (Constant Nozzle Mass Flow Rate)

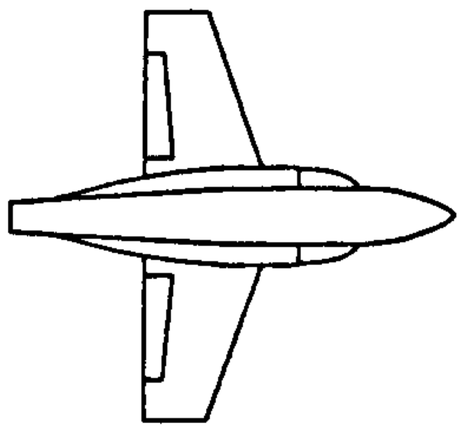

q_∞ = 61.3 Pa, NPR 1.0

	$C_{P\ (root)}$	
x/chord	upper	lower
0.0000	0.9100	0.9100
0.0459	-0.3519	-0.1655
0.0989	-0.3764	-0.1250
0.1519	-0.4193	-0.1180
0.2049	-0.4376	-0.0969
0.2580	-0.4427	-0.1038
0.3110	-0.4202	-0.0934
0.3640	-0.3945	-0.0534
0.4170	-0.3734	0.0094
0.4670	-0.3504	0.0517
0.5230	-0.3243	0.0758
0.5760	-0.2974	0.1006
0.6290	-0.2821	0.1193
0.6820	-0.2720	0.1136
0.7350	-0.2808	0.0193
0.7880	-0.2756	-0.1846
0.8410	-0.3251	-0.2774
1.0000	0.0000	0.0000

q_∞ = 245 Pa, NPR 1.0

$C_{P\ (root)}$	
upper	lower
0.9304	0.9304
-0.3620	-0.2191
-0.3852	-0.1538
-0.4349	-0.1502
-0.4490	-0.1345
-0.4557	-0.1167
-0.4321	-0.1548
-0.4087	-0.0793
-0.3873	-0.0103
-0.3651	0.0352
-0.3360	0.0692
-0.3068	0.0941
-0.2901	0.1199
-0.2822	0.1235
-0.2829	0.0130
-0.3341	-0.2082
-0.3408	-0.3065
0.0000	0.0000

q_∞ = 551 Pa, NPR 1.0

$C_{P\ (root)}$	
upper	lower
0.9169	0.9169
-0.3810	-0.2413
-0.4007	-0.1655
-0.4453	-0.1729
-0.4574	-0.1531
-0.4601	-0.1437
-0.4336	-0.1405
-0.4091	-0.1439
-0.3803	-0.0405
-0.3612	0.0043
-0.3374	0.0419
-0.3027	0.0647
-0.2868	0.0948
-0.2825	0.1088
-0.2887	0.0051
-0.3417	-0.2045
-0.3338	-0.2980
0.0000	0.0000

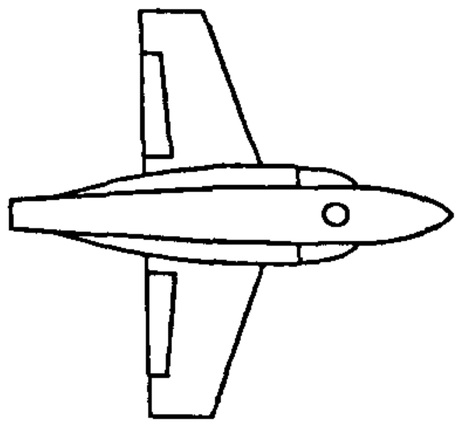

q_∞ = 61.3 Pa, NPR 1.586

	$C_{P\,(root)}$	
x/chord	upper	lower
0.0000	0.6739	0.6739
0.0459	-0.2086	-0.5781
0.0989	-0.3007	-0.3833
0.1519	-0.3737	-0.3496
0.2049	-0.4134	-0.3062
0.2580	-0.4296	-0.2695
0.3110	-0.4190	-0.2222
0.3640	-0.3957	-0.1521
0.4170	-0.3815	-0.0760
0.4670	-0.3599	-0.0124
0.5230	-0.3362	0.0295
0.5760	-0.3136	0.0571
0.6290	-0.3009	0.0841
0.6820	-0.2924	0.0881
0.7350	-0.2986	-0.0139
0.7880	-0.3256	-0.2465
0.8410	-0.3554	-0.3167
1.0000	0.0000	0.0000

q_∞=245 Pa, NPR 1.586

$C_{P\,(root)}$	
upper	lower
0.7932	0.7932
-0.2721	-0.4725
-0.3410	-0.3124
-0.4034	-0.2944
-0.4265	-0.2650
-0.4385	-0.2380
-0.4183	-0.2164
-0.3982	-0.1481
-0.3777	-0.0716
-0.3597	-0.0133
-0.3329	0.0264
-0.3036	0.0567
-0.2886	0.0860
-0.2825	0.0939
-0.2877	-0.0153
-0.3397	-0.2445
-0.3492	-0.3322
0.0000	0.0000

q_∞=551 Pa, NPR 1.586

$C_{P\,(root)}$	
upper	lower
0.8401	0.8401
-0.3230	-0.4141
-0.3710	-0.2942
-0.4288	-0.2800
-0.4421	-0.2675
-0.4499	-0.2522
-0.4277	-0.2204
-0.4037	-0.1831
-0.3801	-0.0983
-0.3615	-0.0448
-0.3376	-0.0002
-0.3054	0.0257
-0.2896	0.0595
-0.2914	0.0760
-0.2994	-0.0233
-0.3502	-0.2379
-0.3448	-0.3196
0.0000	0.0000

q_∞ = 61.3 Pa, NPR 2.0

	$C_{P\,(root)}$	
x/chord	upper	lower
0.0000	0.6463	0.6463
0.0459	-0.2041	-0.5275
0.0989	-0.2846	-0.3446
0.1519	-0.3573	-0.3159
0.2049	-0.3842	-0.2761
0.2580	-0.3983	-0.2490
0.3110	-0.3888	-0.2060
0.3640	-0.3746	-0.1400
0.4170	-0.3598	-0.0706
0.4670	-0.3442	-0.0094
0.5230	-0.3193	0.0286
0.5760	-0.2964	0.0546
0.6290	-0.2831	0.0771
0.6820	-0.2768	0.0833
0.7350	-0.2829	-0.0152
0.7880	-0.3294	-0.2253
0.8410	-0.3373	-0.2936
1.0000	0.0000	0.0000

q_∞ = 245 Pa, NPR 2.0

$C_{P\,(root)}$	
upper	lower
0.7889	0.7889
-0.2565	-0.4491
-0.3174	-0.3013
-0.3821	-0.2754
-0.4061	-0.2462
-0.4145	-0.2392
-0.3973	-0.1966
-0.3785	-0.1318
-0.3577	-0.0559
-0.3376	-0.0008
-0.3106	0.0389
-0.2901	0.0685
-0.2729	0.0982
-0.2657	0.1059
-0.2733	0.0003
-0.3269	-0.2277
-0.3327	-0.3098
0.0000	0.0000

q_∞ = 551 Pa, NPR 2.0

$C_{P\,(root)}$	
upper	lower
0.8630	0.8630
-0.3287	-0.3885
-0.3688	-0.2805
-0.4216	-0.2616
-0.4338	-0.2488
-0.4355	-0.2406
-0.4098	-0.2077
-0.3849	-0.1717
-0.3614	-0.0856
-0.3423	-0.0319
-0.3206	0.0115
-0.2864	0.0382
-0.2715	0.0723
-0.2721	0.0895
-0.2827	-0.0106
-0.3280	-0.2232
-0.3287	-0.3095
0.0000	0.0000

q_∞ = 61.3 Pa, NPR 3.0

	$C_{P\,(root)}$	
x/chord	upper	lower
0.0000	0.5755	0.5755
0.0459	-0.1545	-0.5559
0.0989	-0.2366	-0.3522
0.1519	-0.3087	-0.3183
0.2049	-0.3355	-0.2677
0.2580	-0.3590	-0.2522
0.3110	-0.3481	-0.1962
0.3640	-0.3409	-0.1266
0.4170	-0.3332	-0.0564
0.4670	-0.3166	0.0061
0.5230	-0.2983	0.0423
0.5760	-0.2736	0.0682
0.6290	-0.2680	0.0947
0.6820	-0.2578	0.0992
0.7350	-0.2661	0.0124
0.7880	-0.3892	-0.2092
0.8410	-0.3115	-0.2708
1.0000	0.0000	0.0000

q_∞ = 245 Pa, NPR 3.0

$C_{P\,(root)}$	
upper	lower
0.8086	0.8086
-0.2707	-0.4203
-0.3344	-0.2735
-0.3901	-0.2617
-0.4098	-0.2245
-0.4162	-0.2376
-0.3991	-0.1846
-0.3785	-0.1238
-0.3626	-0.0510
-0.3461	0.0028
-0.3200	0.0429
-0.2930	0.0684
-0.2781	0.0985
-0.2726	0.1061
-0.2770	0.0013
-0.3219	-0.2235
-0.3310	-0.3105
0.0000	0.0000

q_∞ = 551 Pa, NPR 3.0

$C_{P\,(root)}$	
upper	lower
0.8776	0.8776
-0.3340	-0.3747
-0.3713	-0.2655
-0.4193	-0.2470
-0.4299	-0.2362
-0.4310	-0.2470
-0.4055	-0.2033
-0.3802	-0.1572
-0.3537	-0.0811
-0.3341	-0.0263
-0.3103	0.0152
-0.2780	0.0433
-0.2639	0.0757
-0.2643	0.0914
-0.2742	-0.0071
-0.3297	-0.2221
-0.3202	-0.3082
0.0000	0.0000

q_∞ = 61.3 Pa, NPR 4.0

	$C_{P\,(root)}$	
x/chord	upper	lower
0.0000	0.5917	0.5917
0.0459	-0.1746	-0.5510
0.0989	-0.2529	-0.3537
0.1519	-0.3081	-0.3547
0.2049	-0.3458	-0.2639
0.2580	-0.3642	-0.2668
0.3110	-0.3570	-0.2090
0.3640	-0.3464	-0.1411
0.4170	-0.3402	-0.0705
0.4670	-0.3358	-0.0104
0.5230	-0.3148	0.0291
0.5760	-0.2955	0.0563
0.6290	-0.2877	0.0783
0.6820	-0.2759	0.0848
0.7350	-0.2876	-0.0058
0.7880	-0.2950	-0.2275
0.8410	-0.3167	-0.2891
1.0000	0.0000	0.0000

q_∞ = 245 Pa, NPR 4.0

$C_{P\,(root)}$	
upper	lower
0.8259	0.8259
-0.2867	-0.3963
-0.3375	-0.2606
-0.3923	-0.2478
-0.4106	-0.2070
-0.4197	-0.2452
-0.3993	-0.1774
-0.3804	-0.1187
-0.3609	-0.0477
-0.3454	0.0067
-0.3215	0.0449
-0.2958	0.0730
-0.2811	0.1017
-0.2770	0.1070
-0.2778	0.0031
-0.3193	-0.2210
-0.3261	-0.3073
0.0000	0.0000

q_∞ = 551 Pa, NPR 4.0

$C_{P\,(root)}$	
upper	lower
0.8739	0.8739
-0.3382	-0.3448
-0.3719	-0.2481
-0.4172	-0.2314
-0.4251	-0.2164
-0.4267	-0.2422
-0.4008	-0.2114
-0.3755	-0.1466
-0.3518	-0.0761
-0.3335	-0.0235
-0.3105	0.0176
-0.2778	0.0463
-0.2644	0.0767
-0.2636	0.0918
-0.2723	-0.0042
-0.3189	-0.2145
-0.3146	-0.3013
0.0000	0.0000

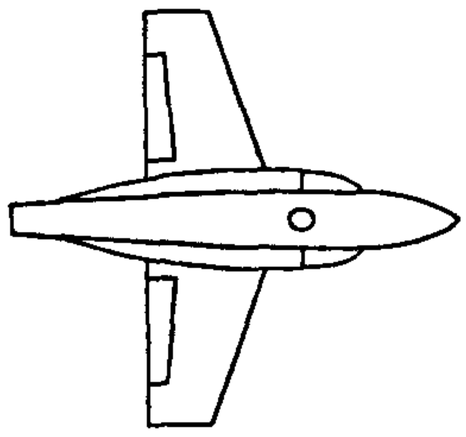

q_∞ = 61.3 Pa, NPR 1.586

	$C_{P\,(root)}$	
x/chord	upper	lower
0.0000	0.6988	0.6988
0.0459	-0.2083	-0.5786
0.0989	-0.2947	-0.3893
0.1519	-0.3659	-0.3471
0.2049	-0.3937	-0.3103
0.2580	-0.4089	-0.2703
0.3110	-0.3974	-0.2208
0.3640	-0.3812	-0.1530
0.4170	-0.3668	-0.0748
0.4670	-0.3482	-0.0071
0.5230	-0.3214	0.0358
0.5760	-0.3000	0.0646
0.6290	-0.2825	0.0914
0.6820	-0.2804	0.0958
0.7350	-0.2819	-0.0036
0.7880	-0.3718	-0.2210
0.8410	-0.3450	-0.2989
1.0000	0.0000	0.0000

q_∞=245 Pa, NPR 1.586

$C_{P\,(root)}$	
upper	lower
0.8311	0.8311
-0.2831	-0.4318
-0.3481	-0.2967
-0.4054	-0.2836
-0.4240	-0.2600
-0.4339	-0.2357
-0.4147	-0.2110
-0.3943	-0.1462
-0.3722	-0.0663
-0.3522	-0.0075
-0.3252	0.0323
-0.2960	0.0643
-0.2799	0.0952
-0.2742	0.1054
-0.2803	-0.0035
-0.3308	-0.2299
-0.3392	-0.3228
0.0000	0.0000

q_∞=551 Pa, NPR 1.586

$C_{P\,(root)}$	
upper	lower
0.8642	0.8642
-0.3431	-0.4154
-0.3882	-0.2911
-0.4386	-0.2850
-0.4531	-0.2732
-0.4561	-0.2587
-0.4316	-0.2310
-0.4074	-0.2009
-0.3803	-0.1076
-0.3615	-0.0548
-0.3375	-0.0098
-0.3031	0.0171
-0.2888	0.0545
-0.2880	0.0706
-0.2956	-0.0300
-0.3420	-0.2409
-0.3401	-0.3232
0.0000	0.0000

q_∞ = 61.3 Pa, NPR 2.0

	$C_{P\,(root)}$	
x/chord	upper	lower
0.0000	0.6978	0.6978
0.0459	-0.1838	-0.5029
0.0989	-0.2650	-0.3331
0.1519	-0.3289	-0.3045
0.2049	-0.3555	-0.2687
0.2580	-0.3664	-0.2253
0.3110	-0.3567	-0.1868
0.3640	-0.3477	-0.1207
0.4170	-0.3321	-0.0474
0.4670	-0.3148	0.0166
0.5230	-0.2888	0.0568
0.5760	-0.2691	0.0844
0.6290	-0.2555	0.1114
0.6820	-0.2444	0.1168
0.7350	-0.2500	0.0210
0.7880	-0.2982	-0.1921
0.8410	-0.3066	-0.2591
1.0000	0.0000	0.0000

q_∞ = 245 Pa, NPR 2.0

$C_{P\,(root)}$	
upper	lower
0.8212	0.8212
-0.2748	-0.4326
-0.3330	-0.2974
-0.3921	-0.2811
-0.4076	-0.2491
-0.4209	-0.2431
-0.4035	-0.2053
-0.3820	-0.1397
-0.3599	-0.0618
-0.3411	-0.0039
-0.3118	0.0370
-0.2856	0.0672
-0.2703	0.0977
-0.2625	0.1065
-0.2735	0.0004
-0.3541	-0.2240
-0.3337	-0.3088
0.0000	0.0000

q_∞ = 551 Pa, NPR 2.0

$C_{P\,(root)}$	
upper	lower
0.8808	0.8808
-0.3561	-0.3647
-0.3859	-0.2717
-0.4326	-0.2617
-0.4440	-0.2533
-0.4451	-0.2427
-0.4194	-0.2157
-0.3932	-0.1847
-0.3692	-0.0958
-0.3504	-0.0416
-0.3249	0.0025
-0.2915	0.0302
-0.2767	0.0655
-0.2769	0.0822
-0.2857	-0.0177
-0.3502	-0.2285
-0.3319	-0.3153
0.0000	0.0000

q_∞ = 61.3 Pa, NPR 3.0

	$C_{P\,(root)}$	
x/chord	upper	lower
0.0000	0.6156	0.6156
0.0459	-0.1819	-0.5712
0.0989	-0.2601	-0.3776
0.1519	-0.3190	-0.3351
0.2049	-0.3510	-0.2935
0.2580	-0.3697	-0.2825
0.3110	-0.3601	-0.2183
0.3640	-0.3506	-0.1485
0.4170	-0.3409	-0.0797
0.4670	-0.3244	-0.0181
0.5230	-0.3037	0.0231
0.5760	-0.2809	0.0507
0.6290	-0.2725	0.0759
0.6820	-0.2646	0.0823
0.7350	-0.2599	-0.0063
0.7880	-0.2561	-0.2204
0.8410	-0.3121	-0.2795
1.0000	0.0000	0.0000

q_∞ = 245 Pa, NPR 3.0

$C_{P\,(root)}$	
upper	lower
0.8230	0.8230
-0.2863	-0.4197
-0.3467	-0.2820
-0.3994	-0.2719
-0.4171	-0.2384
-0.4208	-0.2535
-0.4021	-0.1988
-0.3864	-0.1388
-0.3666	-0.0624
-0.3489	-0.0068
-0.3235	0.0348
-0.2947	0.0633
-0.2794	0.0947
-0.2742	0.1024
-0.2763	-0.0036
-0.3207	-0.2245
-0.3282	-0.3102
0.0000	0.0000

q_∞ = 551 Pa, NPR 3.0

$C_{P\,(root)}$	
upper	lower
0.8836	0.8836
-0.3619	-0.3430
-0.3882	-0.2588
-0.4317	-0.2413
-0.4384	-0.2368
-0.4354	-0.2512
-0.4097	-0.2154
-0.3839	-0.1678
-0.3568	-0.0904
-0.3376	-0.0372
-0.3118	0.0067
-0.2789	0.0336
-0.2664	0.0672
-0.2667	0.0841
-0.2750	-0.0144
-0.3181	-0.2241
-0.3259	-0.3097
0.0000	0.0000

q_∞ = 61.3 Pa, NPR 4.0

	$C_{P\,(root)}$	
x/chord	upper	lower
0.0000	0.7060	0.7060
0.0459	-0.3004	-0.7032
0.0989	-0.3749	-0.4807
0.1519	-0.4469	-0.4749
0.2049	-0.4729	-0.3801
0.2580	-0.4912	-0.3793
0.3110	-0.4787	-0.3135
0.3640	-0.4691	-0.2323
0.4170	-0.4565	-0.1483
0.4670	-0.4409	-0.0780
0.5230	-0.4167	-0.0263
0.5760	-0.3937	0.0125
0.6290	-0.3765	0.0385
0.6820	-0.3656	0.0408
0.7350	-0.3632	-0.0744
0.7880	-0.4139	-0.3353
0.8410	-0.4192	-0.4102
1.0000	0.0000	0.0000

q_∞ = 245 Pa, NPR 4.0

$C_{P\,(root)}$	
upper	lower
0.8631	0.8631
-0.3202	-0.4364
-0.3717	-0.2909
-0.4293	-0.2908
-0.4465	-0.2354
-0.4552	-0.2749
-0.4327	-0.2102
-0.4114	-0.1486
-0.3900	-0.0704
-0.3751	-0.0103
-0.3524	0.0311
-0.3218	0.0621
-0.3071	0.0931
-0.3005	0.0997
-0.3016	-0.0103
-0.3525	-0.2460
-0.3533	-0.3403
0.0000	0.0000

q_∞ = 551 Pa, NPR 4.0

$C_{P\,(root)}$	
upper	lower
0.9076	0.9076
-0.3651	-0.3468
-0.3948	-0.2511
-0.4391	-0.2460
-0.4455	-0.2290
-0.4451	-0.2580
-0.4174	-0.2205
-0.3914	-0.1600
-0.3650	-0.0855
-0.3453	-0.0321
-0.3224	0.0105
-0.2893	0.0397
-0.2746	0.0739
-0.2746	0.0910
-0.2858	-0.0140
-0.3327	-0.2336
-0.3301	-0.3175
0.0000	0.0000

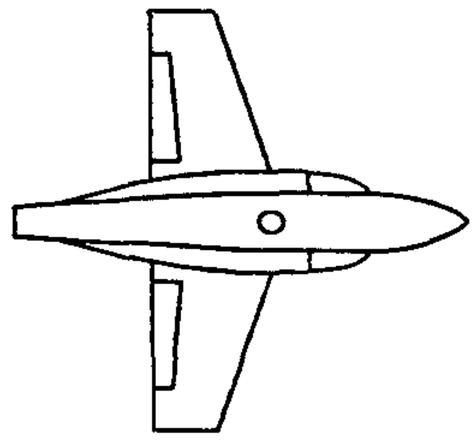

q_∞ = 61.3 Pa, NPR 1.586

	$C_{P\,(root)}$	
x/chord	upper	lower
0.0000	0.7464	0.7464
0.0459	-0.2701	-0.6156
0.0989	-0.3492	-0.4635
0.1519	-0.4246	-0.4246
0.2049	-0.4540	-0.3871
0.2580	-0.4675	-0.3520
0.3110	-0.4517	-0.3123
0.3640	-0.4344	-0.2398
0.4170	-0.4115	-0.1508
0.4670	-0.3899	-0.0791
0.5230	-0.3630	-0.0240
0.5760	-0.3390	0.0173
0.6290	-0.3254	0.0471
0.6820	-0.3172	0.0561
0.7350	-0.3208	-0.0513
0.7880	-0.3759	-0.2840
0.8410	-0.3825	-0.3557
1.0000	0.0000	0.0000

q_∞=245 Pa, NPR 1.586

$C_{P\,(root)}$	
upper	lower
0.8743	0.8743
-0.3247	-0.4244
-0.3761	-0.3059
-0.4370	-0.2965
-0.4540	-0.2767
-0.4609	-0.2563
-0.4416	-0.2444
-0.4181	-0.1760
-0.3944	-0.0935
-0.3732	-0.0339
-0.3441	0.0068
-0.3156	0.0413
-0.2992	0.0737
-0.2955	0.0861
-0.2997	-0.0236
-0.3503	-0.2554
-0.3607	-0.3440
0.0000	0.0000

q_∞=551 Pa, NPR 1.586

$C_{P\,(root)}$	
upper	lower
0.9074	0.9074
-0.3886	-0.3467
-0.4113	-0.2584
-0.4573	-0.2742
-0.4660	-0.2662
-0.4693	-0.2526
-0.4407	-0.2389
-0.4136	-0.2062
-0.3887	-0.1151
-0.3671	-0.0639
-0.3441	-0.0162
-0.3071	0.0119
-0.2916	0.0516
-0.2891	0.0717
-0.2979	-0.0349
-0.3452	-0.2501
-0.3441	-0.3367
0.0000	0.0000

q_∞ = 61.3 Pa, NPR 2.0

	$C_{P\,(root)}$	
x/chord	upper	lower
0.0000	0.7155	0.7155
0.0459	-0.2394	-0.5853
0.0989	-0.3289	-0.4237
0.1519	-0.3870	-0.3942
0.2049	-0.4218	-0.3514
0.2580	-0.4332	-0.3314
0.3110	-0.4235	-0.2810
0.3640	-0.4033	-0.2090
0.4170	-0.3864	-0.1241
0.4670	-0.3659	-0.0548
0.5230	-0.3432	-0.0037
0.5760	-0.3172	0.0268
0.6290	-0.3099	0.0587
0.6820	-0.2985	0.0648
0.7350	-0.2996	-0.0354
0.7880	-0.3901	-0.2511
0.8410	-0.3595	-0.3227
1.0000	0.0000	0.0000

q_∞ = 245 Pa, NPR 2.0

$C_{P\,(root)}$	
upper	lower
0.8721	0.8721
-0.3120	-0.4054
-0.3599	-0.2850
-0.4167	-0.2808
-0.4348	-0.2559
-0.4447	-0.2471
-0.4243	-0.2216
-0.4037	-0.1587
-0.3841	-0.0801
-0.3618	-0.0214
-0.3326	0.0227
-0.3038	0.0542
-0.2876	0.0872
-0.2814	0.0977
-0.2856	-0.0110
-0.3481	-0.2405
-0.3504	-0.3280
0.0000	0.0000

q_∞ = 551 Pa, NPR 2.0

$C_{P\,(root)}$	
upper	lower
0.9130	0.9130
-0.3853	-0.3256
-0.4065	-0.2424
-0.4490	-0.2516
-0.4559	-0.2430
-0.4579	-0.2335
-0.4309	-0.2191
-0.4051	-0.1951
-0.3773	-0.1007
-0.3574	-0.0486
-0.3345	-0.0048
-0.3001	0.0229
-0.2857	0.0612
-0.2845	0.0796
-0.2931	-0.0244
-0.3389	-0.2396
-0.3393	-0.3279
0.0000	0.0000

q_∞ = 61.3 Pa, NPR 3.0

	$C_{P\,(root)}$	
x/chord	upper	lower
0.0000	0.6648	0.6648
0.0459	-0.2379	-0.6479
0.0989	-0.3172	-0.4537
0.1519	-0.3826	-0.4251
0.2049	-0.4073	-0.3695
0.2580	-0.4272	-0.3706
0.3110	-0.4140	-0.3072
0.3640	-0.3990	-0.2276
0.4170	-0.3854	-0.1471
0.4670	-0.3726	-0.0779
0.5230	-0.3480	-0.0299
0.5760	-0.3257	0.0064
0.6290	-0.3135	0.0381
0.6820	-0.3053	0.0482
0.7350	-0.3203	-0.0524
0.7880	-0.3933	-0.2749
0.8410	-0.3582	-0.3327
1.0000	0.0000	0.0000

q_∞ = 245 Pa, NPR 3.0

$C_{P\,(root)}$	
upper	lower
0.8559	0.8559
-0.3180	-0.4070
-0.3637	-0.2911
-0.4184	-0.2866
-0.4337	-0.2511
-0.4407	-0.2711
-0.4205	-0.2192
-0.3984	-0.1597
-0.3796	-0.0795
-0.3619	-0.0241
-0.3356	0.0203
-0.3066	0.0519
-0.2926	0.0814
-0.2872	0.0964
-0.2900	-0.0138
-0.3485	-0.2403
-0.3430	-0.3275
0.0000	0.0000

q_∞ = 551 Pa, NPR 3.0

$C_{P\,(root)}$	
upper	lower
0.9071	0.9071
-0.3819	-0.3138
-0.4034	-0.2414
-0.4436	-0.2436
-0.4491	-0.2383
-0.4512	-0.2538
-0.4221	-0.2241
-0.3951	-0.1794
-0.3672	-0.0991
-0.3480	-0.0479
-0.3246	-0.0038
-0.2886	0.0246
-0.2752	0.0613
-0.2767	0.0791
-0.2861	-0.0210
-0.3411	-0.2373
-0.3335	-0.3207
0.0000	0.0000

q_∞ = 61.3 Pa, NPR 4.0

	$C_{P\,(root)}$	
x/chord	upper	lower
0.0000	0.6761	0.6761
0.0459	-0.2902	-0.6821
0.0989	-0.3564	-0.4770
0.1519	-0.4182	-0.4793
0.2049	-0.4479	-0.3849
0.2580	-0.4590	-0.4009
0.3110	-0.4534	-0.3371
0.3640	-0.4391	-0.2541
0.4170	-0.4269	-0.1684
0.4670	-0.4113	-0.0968
0.5230	-0.3861	-0.0501
0.5760	-0.3637	-0.0149
0.6290	-0.3478	0.0215
0.6820	-0.3437	0.0301
0.7350	-0.3390	-0.0794
0.7880	-0.3890	-0.3155
0.8410	-0.3847	-0.3815
1.0000	0.0000	0.0000

q_∞ = 245 Pa, NPR 4.0

$C_{P\,(root)}$	
upper	lower
0.8657	0.8657
-0.3221	-0.4131
-0.3707	-0.2893
-0.4201	-0.2866
-0.4334	-0.2431
-0.4444	-0.2916
-0.4254	-0.2234
-0.4054	-0.1587
-0.3839	-0.0841
-0.3635	-0.0239
-0.3404	0.0193
-0.3121	0.0500
-0.3007	0.0813
-0.2967	0.0928
-0.3005	-0.0158
-0.3500	-0.2459
-0.3482	-0.3368
0.0000	0.0000

q_∞ = 551 Pa, NPR 4.0

$C_{P\,(root)}$	
upper	lower
0.9098	0.9098
-0.3841	-0.3220
-0.4040	-0.2416
-0.4467	-0.2409
-0.4516	-0.2323
-0.4500	-0.2587
-0.4222	-0.2350
-0.3960	-0.1719
-0.3698	-0.0978
-0.3491	-0.0449
-0.3275	-0.0012
-0.2925	0.0280
-0.2791	0.0622
-0.2778	0.0813
-0.2911	-0.0193
-0.3330	-0.2358
-0.3310	-0.3212
0.0000	0.0000

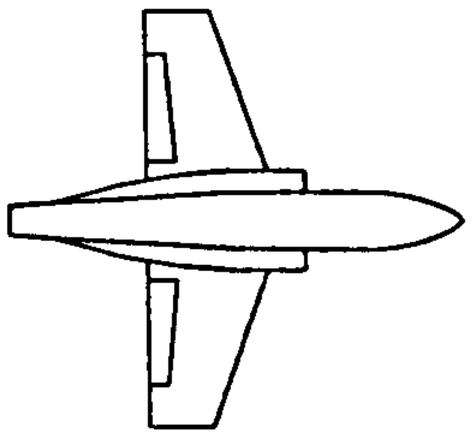

q_∞ = 61.3 Pa, NPR 1.0

	$C_{P\,(root)}$	
x/chord	upper	lower
0.0000	1.0086	1.0086
0.0459	-0.2147	0.0391
0.0989	-0.2458	0.0453
0.1519	-0.3510	0.0397
0.2049	-0.3976	0.0354
0.2580	-0.4132	0.0293
0.3110	-0.4081	0.0296
0.3640	-0.3966	0.0417
0.4170	-0.3921	0.0721
0.4670	-0.3636	0.0796
0.5230	-0.2944	0.1039
0.5760	-0.2777	0.1224
0.6290	-0.2600	0.1606
0.6820	-0.2516	0.1831
0.7350	-0.2598	0.0611
0.7880	-0.3786	-0.1909
0.8410	-0.3951	-0.2696
1.0000	0.0000	0.0000

q_∞ = 245 Pa, NPR 1.0

$C_{P\,(root)}$	
upper	lower
0.9470	0.9470
-0.2993	-0.1074
-0.3331	-0.0639
-0.3917	-0.0870
-0.4265	-0.0733
-0.4329	-0.0704
-0.4241	-0.1158
-0.3981	-0.0439
-0.3689	0.0154
-0.3561	0.0627
-0.3294	0.1056
-0.3097	0.1170
-0.2896	0.1470
-0.2802	0.1516
-0.2922	0.0279
-0.3505	-0.1998
-0.3575	-0.3139
0.0000	0.0000

q_∞ = 551 Pa, NPR 1.0

$C_{P\,(root)}$	
upper	lower
0.9303	0.9303
-0.3602	-0.1625
-0.3792	-0.1177
-0.4277	-0.1332
-0.4398	-0.1302
-0.4453	-0.1193
-0.4279	-0.1465
-0.4017	-0.0952
-0.3789	-0.0237
-0.3582	0.0156
-0.3310	0.0502
-0.3008	0.0705
-0.2809	0.1088
-0.2782	0.1172
-0.2891	0.0071
-0.3523	-0.2159
-0.3488	-0.3117
0.0000	0.0000

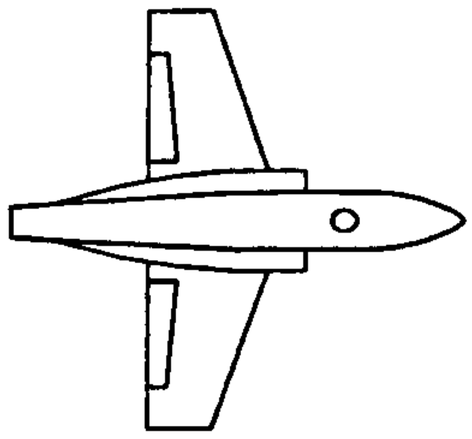

q_∞ = 61.3 Pa, NPR 1.586

	$C_{P\,(root)}$	
x/chord	upper	lower
0.0000	0.8464	0.8464
0.0459	-0.0085	-0.4046
0.0989	-0.1116	-0.2678
0.1519	-0.3001	-0.2337
0.2049	-0.3244	-0.1861
0.2580	-0.3603	-0.1636
0.3110	-0.3587	-0.1079
0.3640	-0.3537	-0.0509
0.4170	-0.3447	-0.0231
0.4670	-0.3315	0.0020
0.5230	-0.3149	0.0157
0.5760	-0.3122	0.0412
0.6290	-0.3088	0.1047
0.6820	-0.3072	0.1208
0.7350	-0.3127	-0.0012
0.7880	-0.3277	-0.2884
0.8410	-0.3965	-0.3232
1.0000	0.0000	0.0000

q_∞=245 Pa, NPR 1.586

$C_{P\,(root)}$	
upper	lower
0.8444	0.8444
-0.1712	-0.3397
-0.2709	-0.2217
-0.3529	-0.2151
-0.3800	-0.1948
-0.4123	-0.1668
-0.3960	-0.1627
-0.3759	-0.1249
-0.3644	-0.0469
-0.3543	0.0198
-0.3187	0.0364
-0.2856	0.0918
-0.2813	0.1103
-0.2811	0.1146
-0.2812	0.0064
-0.3544	-0.2257
-0.3630	-0.3344
0.0000	0.0000

q_∞=551 Pa, NPR 1.586

$C_{P\,(root)}$	
upper	lower
0.8719	0.8719
-0.2844	-0.3205
-0.3319	-0.2292
-0.4003	-0.2504
-0.4163	-0.2294
-0.4297	-0.2035
-0.4025	-0.2105
-0.3827	-0.1549
-0.3572	-0.0818
-0.3376	-0.0222
-0.3156	0.0130
-0.2899	0.0430
-0.2684	0.0733
-0.2727	0.0879
-0.2909	-0.0180
-0.3470	-0.2350
-0.3443	-0.3270
0.0000	0.0000

q_∞ = 61.3 Pa, NPR 2.0

	$C_{P\,(root)}$	
x/chord	upper	lower
0.0000	0.8271	0.8271
0.0459	-0.0284	-0.3529
0.0989	-0.0871	-0.2105
0.1519	-0.3218	-0.1344
0.2049	-0.3431	-0.1160
0.2580	-0.3487	-0.0882
0.3110	-0.3486	-0.0817
0.3640	-0.3482	-0.0639
0.4170	-0.3476	-0.0317
0.4670	-0.3460	-0.0178
0.5230	-0.3395	0.0085
0.5760	-0.3359	0.0684
0.6290	-0.3317	0.1148
0.6820	-0.3336	0.1158
0.7350	-0.3245	-0.0222
0.7880	-0.3438	-0.2178
0.8410	-0.3791	-0.3389
1.0000	0.0000	0.0000

q_∞ = 245 Pa, NPR 2.0

$C_{P\,(root)}$	
upper	lower
0.8149	0.8149
-0.1630	-0.3594
-0.2509	-0.2295
-0.3412	-0.2071
-0.3838	-0.1843
-0.3949	-0.1710
-0.3883	-0.1628
-0.3815	-0.1215
-0.3559	-0.0475
-0.3397	0.0088
-0.3089	0.0658
-0.2960	0.0800
-0.2743	0.1034
-0.2666	0.1146
-0.2849	0.0067
-0.3379	-0.2196
-0.3558	-0.3192
0.0000	0.0000

q_∞ = 551 Pa, NPR 2.0

$C_{P\,(root)}$	
upper	lower
0.8838	0.8838
-0.2804	-0.3429
-0.3259	-0.2372
-0.3862	-0.2419
-0.4084	-0.2346
-0.4170	-0.2163
-0.3930	-0.2035
-0.3719	-0.1550
-0.3481	-0.0785
-0.3310	-0.0182
-0.3029	0.0087
-0.2795	0.0367
-0.2724	0.0729
-0.2745	0.0943
-0.2828	-0.0100
-0.3356	-0.2320
-0.3424	-0.3173
0.0000	0.0000

q_∞ = 61.3 Pa, NPR 3.0

	$C_{P\,(root)}$	
x/chord	upper	lower
0.0000	0.5767	0.5767
0.0459	0.0292	-0.3637
0.0989	-0.0635	-0.2671
0.1519	-0.2712	-0.2441
0.2049	-0.2826	-0.2260
0.2580	-0.2990	-0.1808
0.3110	-0.3058	-0.0979
0.3640	-0.3018	-0.0245
0.4170	-0.2990	0.0022
0.4670	-0.2905	0.0307
0.5230	-0.2841	0.0432
0.5760	-0.2798	0.0436
0.6290	-0.2784	0.0476
0.6820	-0.2788	0.0755
0.7350	-0.2777	0.0252
0.7880	-0.3406	-0.2626
0.8410	-0.3359	-0.2866
1.0000	0.0000	0.0000

q_∞ = 245 Pa, NPR 3.0

$C_{P\,(root)}$	
upper	lower
0.8299	0.8299
-0.1604	-0.3017
-0.2433	-0.1900
-0.3168	-0.1952
-0.3561	-0.1702
-0.3753	-0.1712
-0.3619	-0.1352
-0.3504	-0.0996
-0.3372	-0.0273
-0.3185	0.0364
-0.2856	0.0597
-0.2713	0.1052
-0.2685	0.1216
-0.2666	0.1278
-0.2653	0.0311
-0.3297	-0.2001
-0.3462	-0.2936
0.0000	0.0000

q_∞ = 551 Pa, NPR 3.0

$C_{P\,(root)}$	
upper	lower
0.8763	0.8763
-0.2707	-0.3071
-0.3170	-0.2100
-0.3715	-0.2197
-0.3893	-0.2077
-0.4005	-0.2251
-0.3739	-0.1842
-0.3526	-0.1412
-0.3303	-0.0635
-0.3135	-0.0157
-0.2926	0.0175
-0.2646	0.0487
-0.2593	0.0840
-0.2616	0.0949
-0.2732	-0.0019
-0.3305	-0.2195
-0.3270	-0.3051
0.0000	0.0000

q_∞ = 61.3 Pa, NPR 4.0

	$C_{P\,(root)}$	
x/chord	upper	lower
0.0000	0.6468	0.6468
0.0459	-0.0026	-0.3794
0.0989	-0.1201	-0.2388
0.1519	-0.2977	-0.1960
0.2049	-0.3167	-0.1647
0.2580	-0.3505	-0.1866
0.3110	-0.3571	-0.0991
0.3640	-0.3499	-0.0486
0.4170	-0.3451	-0.0244
0.4670	-0.3396	0.0046
0.5230	-0.3200	0.0210
0.5760	-0.3098	0.0422
0.6290	-0.3059	0.1094
0.6820	-0.3075	0.1179
0.7350	-0.3053	-0.0035
0.7880	-0.3385	-0.2737
0.8410	-0.4245	-0.3254
1.0000	0.0000	0.0000

q_∞ = 245 Pa, NPR 4.0

$C_{P\,(root)}$	
upper	lower
0.8331	0.8331
-0.2091	-0.3213
-0.2906	-0.1956
-0.3716	-0.2112
-0.3878	-0.1702
-0.4224	-0.2201
-0.3954	-0.1557
-0.3865	-0.1341
-0.3792	-0.0595
-0.3694	0.0052
-0.3376	0.0276
-0.3091	0.0801
-0.3013	0.0938
-0.2996	0.0970
-0.2989	-0.0105
-0.3653	-0.2327
-0.3716	-0.3437
0.0000	0.0000

q_∞ = 551 Pa, NPR 4.0

$C_{P\,(root)}$	
upper	lower
0.8888	0.8888
-0.2801	-0.2820
-0.3208	-0.2015
-0.3752	-0.2095
-0.3912	-0.1951
-0.4018	-0.2284
-0.3745	-0.1836
-0.3546	-0.1331
-0.3306	-0.0674
-0.3162	-0.0092
-0.2974	0.0191
-0.2659	0.0509
-0.2613	0.0850
-0.2626	0.0982
-0.2692	0.0028
-0.3362	-0.2192
-0.3263	-0.3070
0.0000	0.0000

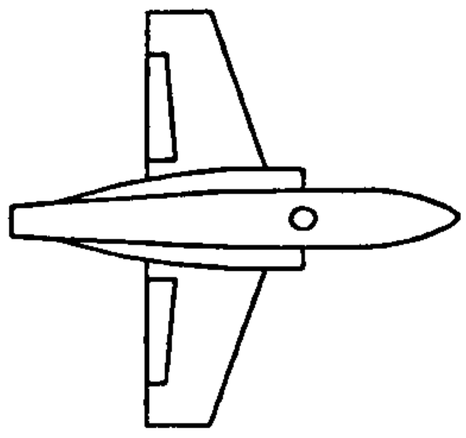

q_∞ = 61.3 Pa, NPR 1.586

	$C_{P\ (root)}$	
x/chord	upper	lower
0.0000	0.6069	0.6069
0.0459	0.0065	-0.4455
0.0989	-0.1834	-0.2499
0.1519	-0.2442	-0.2175
0.2049	-0.3455	-0.2092
0.2580	-0.3811	-0.1946
0.3110	-0.3861	-0.1868
0.3640	-0.3784	-0.1784
0.4170	-0.3610	-0.0647
0.4670	-0.3509	0.0522
0.5230	-0.3339	0.0768
0.5760	-0.2973	0.0833
0.6290	-0.2687	0.1033
0.6820	-0.2598	0.1152
0.7350	-0.2827	0.0493
0.7880	-0.3618	-0.2101
0.8410	-0.4644	-0.3284
1.0000	0.0000	0.0000

q_∞=245 Pa, NPR 1.586

$C_{P\ (root)}$	
upper	lower
0.8728	0.8728
-0.2103	-0.3460
-0.2841	-0.2371
-0.3703	-0.2319
-0.3985	-0.2123
-0.4278	-0.1791
-0.4109	-0.1882
-0.3912	-0.1435
-0.3799	-0.0650
-0.3559	-0.0065
-0.3368	0.0373
-0.3034	0.0763
-0.2873	0.0940
-0.2800	0.1128
-0.2857	-0.0141
-0.3471	-0.2361
-0.3680	-0.3464
0.0000	0.0000

q_∞=551 Pa, NPR 1.586

$C_{P\ (root)}$	
upper	lower
0.8813	0.8813
-0.2936	-0.3538
-0.3417	-0.2551
-0.4075	-0.2623
-0.4253	-0.2596
-0.4410	-0.2400
-0.4171	-0.2305
-0.3978	-0.1815
-0.3766	-0.1014
-0.3599	-0.0478
-0.3322	-0.0003
-0.3014	0.0179
-0.2854	0.0536
-0.2873	0.0743
-0.3052	-0.0302
-0.3603	-0.2495
-0.3579	-0.3375
0.0000	0.0000

q_∞ = 61.3 Pa, NPR 2.0

	$C_{P\ (root)}$	
x/chord	upper	lower
0.0000	0.6461	0.6461
0.0459	-0.0486	-0.4213
0.0989	-0.1545	-0.2064
0.1519	-0.2793	-0.1879
0.2049	-0.3346	-0.1792
0.2580	-0.4134	-0.1578
0.3110	-0.4180	-0.1528
0.3640	-0.3971	-0.1446
0.4170	-0.3807	-0.0710
0.4670	-0.3486	0.0584
0.5230	-0.3177	0.1111
0.5760	-0.3068	0.1163
0.6290	-0.3026	0.1214
0.6820	-0.2974	0.1289
0.7350	-0.3017	0.0347
0.7880	-0.4430	-0.1982
0.8410	-0.4550	-0.3132
1.0000	0.0000	0.0000

q_∞ = 245 Pa, NPR 2.0

$C_{P\ (root)}$	
upper	lower
0.8515	0.8515
-0.2028	-0.3330
-0.2868	-0.2271
-0.3536	-0.2278
-0.4007	-0.2077
-0.4169	-0.1847
-0.4100	-0.1831
-0.3816	-0.1159
-0.3539	-0.0432
-0.3432	-0.0087
-0.3235	0.0432
-0.2970	0.0565
-0.2795	0.1164
-0.2720	0.1213
-0.2844	-0.0109
-0.3375	-0.2311
-0.3481	-0.3341
0.0000	0.0000

q_∞ = 551 Pa, NPR 2.0

$C_{P\ (root)}$	
upper	lower
0.8875	0.8875
-0.2901	-0.3186
-0.3344	-0.2352
-0.3986	-0.2476
-0.4190	-0.2390
-0.4269	-0.2273
-0.4033	-0.2103
-0.3850	-0.1680
-0.3626	-0.0889
-0.3410	-0.0378
-0.3198	0.0098
-0.2925	0.0255
-0.2737	0.0622
-0.2765	0.0873
-0.2904	-0.0188
-0.3517	-0.2364
-0.3460	-0.3253
0.0000	0.0000

q_∞ = 61.3 Pa, NPR 3.0

	$C_{P\,(root)}$	
x/chord	upper	lower
0.0000	0.7215	0.7215
0.0459	-0.0264	-0.4648
0.0989	-0.1801	-0.3060
0.1519	-0.3072	-0.2987
0.2049	-0.3505	-0.2657
0.2580	-0.4253	-0.2422
0.3110	-0.4375	-0.1940
0.3640	-0.4167	-0.0857
0.4170	-0.3905	-0.0382
0.4670	-0.3668	0.0003
0.5230	-0.3438	0.0129
0.5760	-0.3187	0.0339
0.6290	-0.3115	0.0872
0.6820	-0.3122	0.1010
0.7350	-0.3168	-0.0168
0.7880	-0.3903	-0.2981
0.8410	-0.4582	-0.3567
1.0000	0.0000	0.0000

q_∞ = 245 Pa, NPR 3.0

$C_{P\,(root)}$	
upper	lower
0.8641	0.8641
-0.2048	-0.3229
-0.2949	-0.2070
-0.3746	-0.2280
-0.3980	-0.1936
-0.4218	-0.2022
-0.4002	-0.1688
-0.3910	-0.1384
-0.3809	-0.0626
-0.3656	0.0042
-0.3403	0.0521
-0.3047	0.0772
-0.2996	0.0963
-0.2935	0.1165
-0.2979	0.0027
-0.3499	-0.2354
-0.3811	-0.3430
0.0000	0.0000

q_∞ = 551 Pa, NPR 3.0

$C_{P\,(root)}$	
upper	lower
0.9166	0.9166
-0.3269	-0.2777
-0.3584	-0.2038
-0.4089	-0.2239
-0.4192	-0.2168
-0.4251	-0.2337
-0.3969	-0.1977
-0.3751	-0.1531
-0.3498	-0.0792
-0.3290	-0.0211
-0.3066	0.0073
-0.2774	0.0377
-0.2716	0.0738
-0.2736	0.0978
-0.2796	-0.0087
-0.3475	-0.2383
-0.3396	-0.3285
0.0000	0.0000

q_∞ = 61.3 Pa, NPR 4.0

	$C_{P\,(root)}$	
x/chord	upper	lower
0.0000	0.6797	0.6797
0.0459	-0.0284	-0.4163
0.0989	-0.0998	-0.3019
0.1519	-0.3197	-0.2683
0.2049	-0.3421	-0.2091
0.2580	-0.3609	-0.2295
0.3110	-0.3620	-0.1288
0.3640	-0.3612	-0.0763
0.4170	-0.3542	-0.0397
0.4670	-0.3474	-0.0179
0.5230	-0.3400	0.0085
0.5760	-0.3370	0.0383
0.6290	-0.3297	0.1028
0.6820	-0.3368	0.1137
0.7350	-0.3402	-0.0281
0.7880	-0.4765	-0.2939
0.8410	-0.3887	-0.3423
1.0000	0.0000	0.0000

q_∞ = 245 Pa, NPR 4.0

$C_{P\,(root)}$	
upper	lower
0.8839	0.8839
-0.2159	-0.2914
-0.2935	-0.1831
-0.3686	-0.2151
-0.3885	-0.1712
-0.4182	-0.2179
-0.3975	-0.1590
-0.3841	-0.1286
-0.3715	-0.0588
-0.3574	0.0096
-0.3349	0.0440
-0.2994	0.0816
-0.2889	0.1004
-0.2935	0.1122
-0.2973	0.0029
-0.3729	-0.2301
-0.3721	-0.3331
0.0000	0.0000

q_∞ = 551 Pa, NPR 4.0

$C_{P\,(root)}$	
upper	lower
0.9075	0.9075
-0.3233	-0.2721
-0.3499	-0.1989
-0.4011	-0.2145
-0.4143	-0.2057
-0.4198	-0.2392
-0.3932	-0.1958
-0.3708	-0.1477
-0.3462	-0.0766
-0.3290	-0.0185
-0.3077	0.0082
-0.2775	0.0387
-0.2714	0.0742
-0.2742	0.0972
-0.2794	-0.0080
-0.3322	-0.2320
-0.3364	-0.3206
0.0000	0.0000

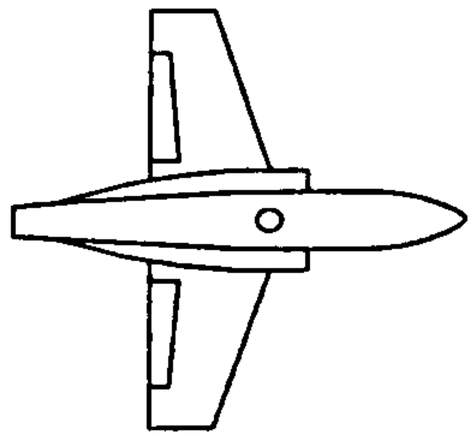

q_∞ = 61.3 Pa, NPR 1.586

	$C_{P\ (root)}$	
x/chord	upper	lower
0.0000	0.7626	0.7626
0.0459	-0.0639	-0.4412
0.0989	-0.2605	-0.3092
0.1519	-0.3391	-0.2966
0.2049	-0.4506	-0.2937
0.2580	-0.4657	-0.2854
0.3110	-0.4657	-0.2528
0.3640	-0.4629	-0.1800
0.4170	-0.4544	-0.0655
0.4670	-0.4336	-0.0375
0.5230	-0.3624	-0.0092
0.5760	-0.3411	0.0088
0.6290	-0.3289	0.0261
0.6820	-0.3210	0.0545
0.7350	-0.3339	-0.0333
0.7880	-0.3036	-0.3064
0.8410	-0.4685	-0.3963
1.0000	0.0000	0.0000

q_∞=245 Pa, NPR 1.586

$C_{P\ (root)}$	
upper	lower
0.9027	0.9027
-0.2505	-0.2911
-0.3135	-0.1997
-0.3726	-0.2130
-0.4163	-0.2051
-0.4339	-0.1792
-0.4199	-0.2068
-0.3937	-0.1319
-0.3691	-0.0547
-0.3563	-0.0146
-0.3265	0.0322
-0.3113	0.0521
-0.2883	0.1010
-0.2815	0.1089
-0.2820	-0.0164
-0.3452	-0.2418
-0.3620	-0.3429
0.0000	0.0000

q_∞=551 Pa, NPR 1.586

$C_{P\ (root)}$	
upper	lower
0.8991	0.8991
-0.3260	-0.3074
-0.3642	-0.2273
-0.4195	-0.2462
-0.4374	-0.2451
-0.4466	-0.2250
-0.4305	-0.2308
-0.4013	-0.1876
-0.3785	-0.1082
-0.3616	-0.0570
-0.3336	-0.0088
-0.3024	0.0142
-0.2863	0.0507
-0.2893	0.0682
-0.3013	-0.0391
-0.3552	-0.2535
-0.3554	-0.3380
0.0000	0.0000

q_∞ = 61.3 Pa, NPR 2.0

	$C_{P\ (root)}$	
x/chord	upper	lower
0.0000	0.7310	0.7310
0.0459	-0.0375	-0.3500
0.0989	-0.0929	-0.2184
0.1519	-0.3271	-0.1995
0.2049	-0.3405	-0.1626
0.2580	-0.3496	-0.1136
0.3110	-0.3495	-0.0950
0.3640	-0.3470	-0.0772
0.4170	-0.3464	-0.0392
0.4670	-0.3425	-0.0260
0.5230	-0.3385	-0.0181
0.5760	-0.3363	0.0375
0.6290	-0.3211	0.1139
0.6820	-0.3330	0.0705
0.7350	-0.3357	-0.0230
0.7880	-0.3379	-0.1689
0.8410	-0.3658	-0.3359
1.0000	0.0000	0.0000

q_∞ = 245 Pa, NPR 2.0

$C_{P\ (root)}$	
upper	lower
0.8957	0.8957
-0.2198	-0.2832
-0.3016	-0.1807
-0.3722	-0.1902
-0.3947	-0.1849
-0.4090	-0.1743
-0.3938	-0.1708
-0.3835	-0.1402
-0.3585	-0.0626
-0.3414	0.0026
-0.3116	0.0487
-0.2977	0.0751
-0.2748	0.0956
-0.2624	0.1155
-0.2686	0.0036
-0.3278	-0.2225
-0.3513	-0.3228
0.0000	0.0000

q_∞ = 551 Pa, NPR 2.0

$C_{P\ (root)}$	
upper	lower
0.9037	0.9037
-0.3080	-0.2838
-0.3465	-0.2066
-0.4091	-0.2283
-0.4321	-0.2312
-0.4365	-0.2187
-0.4147	-0.2106
-0.3878	-0.1720
-0.3657	-0.0952
-0.3470	-0.0393
-0.3203	-0.0018
-0.2881	0.0297
-0.2812	0.0653
-0.2814	0.0780
-0.2889	-0.0200
-0.3536	-0.2417
-0.3461	-0.3274
0.0000	0.0000

q_∞ = 61.3 Pa, NPR 3.0

	$C_{P\,(root)}$	
x/chord	upper	lower
0.0000	0.6910	0.6910
0.0459	-0.0604	-0.4452
0.0989	-0.1921	-0.3156
0.1519	-0.3424	-0.3293
0.2049	-0.3706	-0.3030
0.2580	-0.4116	-0.2885
0.3110	-0.4181	-0.2417
0.3640	-0.3941	-0.1372
0.4170	-0.3879	-0.0763
0.4670	-0.3754	-0.0392
0.5230	-0.3504	-0.0273
0.5760	-0.3428	-0.0026
0.6290	-0.3406	0.0735
0.6820	-0.3390	0.0857
0.7350	-0.3406	-0.0374
0.7880	-0.3666	-0.3211
0.8410	-0.4452	-0.3660
1.0000	0.0000	0.0000

q_∞ = 245 Pa, NPR 3.0

$C_{P\,(root)}$	
upper	lower
0.8905	0.8905
-0.2497	-0.3028
-0.3191	-0.1992
-0.3823	-0.2278
-0.4110	-0.2143
-0.4445	-0.2209
-0.4185	-0.1734
-0.3897	-0.1452
-0.3791	-0.0673
-0.3678	-0.0227
-0.3393	0.0176
-0.3089	0.0691
-0.2984	0.0905
-0.2970	0.0959
-0.2988	-0.0205
-0.3672	-0.2397
-0.3780	-0.3439
0.0000	0.0000

q_∞ = 551 Pa, NPR 3.0

$C_{P\,(root)}$	
upper	lower
0.9228	0.9228
-0.3537	-0.2448
-0.3707	-0.1835
-0.4147	-0.2083
-0.4261	-0.2116
-0.4326	-0.2274
-0.4022	-0.1979
-0.3748	-0.1596
-0.3521	-0.0850
-0.3318	-0.0296
-0.3052	0.0097
-0.2728	0.0397
-0.2661	0.0712
-0.2680	0.0858
-0.2772	-0.0158
-0.3397	-0.2338
-0.3366	-0.3264
0.0000	0.0000

q_∞ = 61.3 Pa, NPR 4.0

	$C_{P\,(root)}$	
x/chord	upper	lower
0.0000	0.7418	0.7418
0.0459	-0.0215	-0.4095
0.0989	-0.1775	-0.2934
0.1519	-0.3028	-0.2920
0.2049	-0.3250	-0.2776
0.2580	-0.3483	-0.2991
0.3110	-0.3490	-0.2708
0.3640	-0.3467	-0.1298
0.4170	-0.3433	-0.0415
0.4670	-0.3312	-0.0081
0.5230	-0.3130	0.0053
0.5760	-0.3075	0.0183
0.6290	-0.3077	0.0292
0.6820	-0.3061	0.0373
0.7350	-0.3216	-0.0077
0.7880	-0.4185	-0.2868
0.8410	-0.3895	-0.3233
1.0000	0.0000	0.0000

q_∞ = 245 Pa, NPR 4.0

$C_{P\,(root)}$	
upper	lower
0.8856	0.8856
-0.2262	-0.2686
-0.2939	-0.1802
-0.3678	-0.2086
-0.3863	-0.1697
-0.4101	-0.2211
-0.3837	-0.1586
-0.3716	-0.1313
-0.3615	-0.0539
-0.3407	0.0049
-0.3212	0.0289
-0.2885	0.0853
-0.2837	0.1033
-0.2807	0.1058
-0.2855	0.0098
-0.3487	-0.2190
-0.3620	-0.3235
0.0000	0.0000

q_∞ = 551 Pa, NPR 4.0

$C_{P\,(root)}$	
upper	lower
0.9096	0.9096
-0.3393	-0.2492
-0.3650	-0.1897
-0.4088	-0.2075
-0.4201	-0.2070
-0.4228	-0.2371
-0.3963	-0.2050
-0.3733	-0.1627
-0.3464	-0.0880
-0.3297	-0.0323
-0.3074	0.0045
-0.2769	0.0362
-0.2714	0.0715
-0.2724	0.0825
-0.2771	-0.0103
-0.3505	-0.2325
-0.3381	-0.3198
0.0000	0.0000

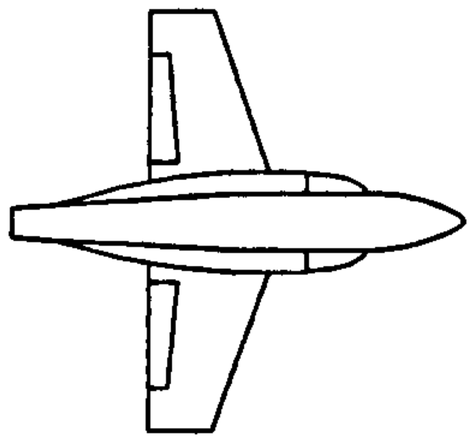

q_∞ = 61.3 Pa, NPR 1.0

	C_{Pi}	
x/d_{ie}	lower outer	upper outer
0.0000	0.4328	0.0024
0.1189	-0.3013	-0.2636
0.2081	-0.3652	-0.3104
0.2973	-0.2699	-0.2091
0.3963	-0.1843	-0.1126
0.4954	-0.1178	-0.0520
0.5945	-0.0953	0.0311
0.6963	-0.0837	0.1193
0.7927	-0.0592	0.2035
0.8918	-0.0531	0.2856
0.9908	-0.0545	0.3665
1.0899	-0.0467	0.4369

q_∞ = 245 Pa, NPR 1.0

C_{Pi}	
lower outer	upper outer
0.5087	-0.0033
-0.3432	-0.2993
-0.4181	-0.3630
-0.2952	-0.2492
-0.1859	-0.1298
-0.1261	-0.0351
-0.0947	0.0458
-0.0846	0.1253
-0.0660	0.2127
-0.0523	0.3190
-0.0698	0.4081
-0.0490	0.4670

q_∞ = 551 Pa, NPR 1.0

C_{Pi}	
lower outer	upper outer
0.5255	-0.0080
-0.3682	-0.3304
-0.4433	-0.3899
-0.3079	-0.2672
-0.1836	-0.1367
-0.1276	-0.0459
-0.0980	0.0319
-0.0930	0.1160
-0.0702	0.2076
-0.0550	0.3174
-0.0782	0.4134
-0.0564	0.4672

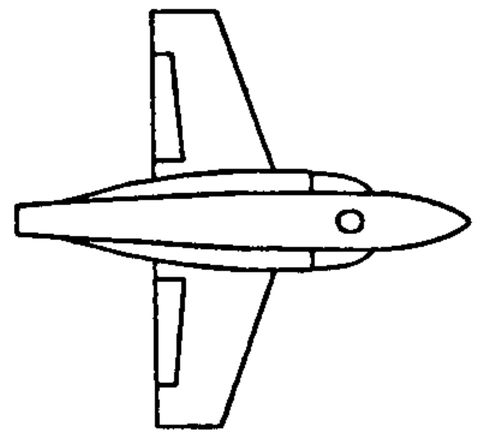

q_∞ = 61.3 Pa, NPR 1.586

	C_{Pi}	
x/d_{ie}	lower outer	upper outer
0.0000	-0.0469	-0.0211
0.1189	-0.7808	-0.2931
0.2081	-0.7853	-0.3687
0.2973	-0.6639	-0.2733
0.3963	-0.5555	-0.1690
0.4954	-0.4663	-0.0796
0.5945	-0.4183	-0.0035
0.6963	-0.3830	0.0796
0.7927	-0.3281	0.1656
0.8918	-0.3130	0.2717
0.9908	-0.2872	0.3718
1.0899	-0.2670	0.4444

q_∞=245 Pa, NPR 1.586

C_{Pi}	
lower outer	upper outer
0.3756	-0.0116
-0.6354	-0.3212
-0.6723	-0.3885
-0.5274	-0.2740
-0.3843	-0.1583
-0.3265	-0.0633
-0.2785	0.0183
-0.2621	0.1027
-0.2341	0.1931
-0.2044	0.3027
-0.2182	0.4000
-0.1885	0.4628

q_∞=551 Pa, NPR 1.586

C_{Pi}	
lower outer	upper outer
0.4524	-0.0165
-0.6373	-0.3635
-0.7007	-0.4252
-0.5328	-0.3019
-0.3782	-0.1695
-0.3176	-0.0739
-0.2774	0.0032
-0.2642	0.0900
-0.2310	0.1833
-0.2092	0.2956
-0.2301	0.3951
-0.1991	0.4526

q_∞ = 61.3 Pa, NPR 2.0

	C_{Pi}	
x/d_{ie}	lower outer	upper outer
0.0000	-0.0302	-0.0180
0.1189	-0.6735	-0.2765
0.2081	-0.6460	-0.3528
0.2973	-0.5635	-0.2473
0.3963	-0.4423	-0.1588
0.4954	-0.3782	-0.0884
0.5945	-0.3494	-0.0108
0.6963	-0.3160	0.0649
0.7927	-0.2774	0.1423
0.8918	-0.2400	0.2522
0.9908	-0.2407	0.3399
1.0899	-0.2221	0.4138

q_∞ = 245 Pa, NPR 2.0

C_{Pi}	
lower outer	upper outer
0.3786	-0.0043
-0.6005	-0.3209
-0.6342	-0.3818
-0.4888	-0.2662
-0.3522	-0.1521
-0.2960	-0.0639
-0.2575	0.0165
-0.2396	0.0993
-0.2082	0.1878
-0.1897	0.2949
-0.2005	0.3979
-0.1701	0.4587

q_∞ = 551 Pa, NPR 2.0

C_{Pi}	
lower outer	upper outer
0.4566	-0.0102
-0.6182	-0.3667
-0.6786	-0.4279
-0.5073	-0.3022
-0.3545	-0.1677
-0.2946	-0.0738
-0.2558	0.0046
-0.2433	0.0906
-0.2099	0.1856
-0.1850	0.2972
-0.2085	0.3959
-0.1761	0.4522

q_∞ = 61.3 Pa, NPR 3.0

	C_{Pi}	
x/d_e	lower outer	upper outer
0.0000	-0.0518	0.0028
0.1189	-0.7017	-0.2855
0.2081	-0.6961	-0.3539
0.2973	-0.5726	-0.2640
0.3963	-0.4652	-0.1567
0.4954	-0.3911	-0.0899
0.5945	-0.3704	-0.0124
0.6963	-0.3281	0.0544
0.7927	-0.3225	0.1335
0.8918	-0.2804	0.2277
0.9908	-0.2559	0.3348
1.0899	-0.2388	0.4160

q_∞ = 245 Pa, NPR 3.0

C_{Pi}	
lower outer	upper outer
0.4050	-0.0054
-0.5590	-0.3167
-0.5898	-0.3862
-0.4497	-0.2716
-0.3214	-0.1565
-0.2591	-0.0653
-0.2247	0.0108
-0.2071	0.0942
-0.1792	0.1812
-0.1600	0.2900
-0.1733	0.3906
-0.1443	0.4534

q_∞ = 551 Pa, NPR 3.0

C_{Pi}	
lower outer	upper outer
0.4907	-0.0132
-0.5801	-0.3750
-0.6412	-0.4358
-0.4712	-0.3092
-0.3202	-0.1727
-0.2616	-0.0775
-0.2215	0.0002
-0.2103	0.0856
-0.1755	0.1803
-0.1522	0.2936
-0.1770	0.3949
-0.1455	0.4514

q_∞ = 61.3 Pa, NPR 4.0

	C_{Pi}	
x/d_e	lower outer	upper outer
0.0000	-0.0113	-0.0168
0.1189	-0.6926	-0.2928
0.2081	-0.6596	-0.3578
0.2973	-0.5614	-0.2584
0.3963	-0.4626	-0.1653
0.4954	-0.4023	-0.1009
0.5945	-0.3679	-0.0277
0.6963	-0.3352	0.0391
0.7927	-0.3044	0.1276
0.8918	-0.2650	0.2848
0.9908	-0.2616	0.3142
1.0899	-0.2431	0.3902

q_∞ = 245 Pa, NPR 4.0

C_{Pi}	
lower outer	upper outer
0.4310	-0.0088
-0.5176	-0.3267
-0.5549	-0.3942
-0.4221	-0.2801
-0.2888	-0.1658
-0.2336	-0.0792
-0.1997	-0.0017
-0.1820	0.0814
-0.1559	0.1712
-0.1293	0.2812
-0.1510	0.3829
-0.1265	0.4514

q_∞ = 551 Pa, NPR 4.0

C_{Pi}	
lower outer	upper outer
0.4912	-0.0141
-0.5361	-0.3654
-0.6074	-0.4258
-0.4403	-0.3007
-0.2930	-0.1667
-0.2347	-0.0757
-0.1949	0.0013
-0.1846	0.0854
-0.1530	0.1776
-0.1288	0.2895
-0.1529	0.3905
-0.1249	0.4478

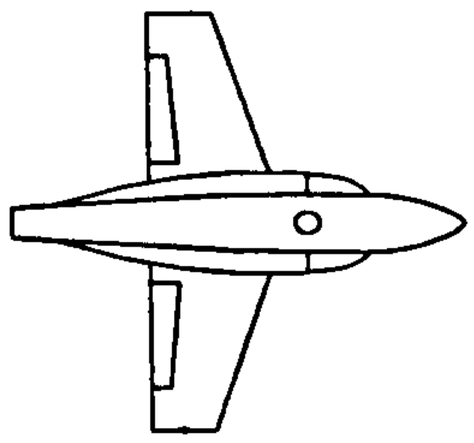

q_∞ = 61.3 Pa, NPR 1.586

x/d_e	C_{Pi} lower outer	C_{Pi} upper outer
0.0000	0.2355	-0.0062
0.1189	-0.8823	-0.3001
0.2081	-0.9637	-0.3640
0.2973	-0.8117	-0.2742
0.3963	-0.6681	-0.1704
0.4954	-0.6158	-0.0774
0.5945	-0.5638	-0.0016
0.6963	-0.5364	0.0720
0.7927	-0.5102	0.1669
0.8918	-0.4787	0.2738
0.9908	-0.4891	0.3674
1.0899	-0.4583	0.4319

q_∞=245 Pa, NPR 1.586

C_{Pi} lower outer	C_{Pi} upper outer
0.4668	-0.0043
-0.6348	-0.3201
-0.7337	-0.3910
-0.5822	-0.2708
-0.4397	-0.1552
-0.3763	-0.0583
-0.3384	0.0260
-0.3242	0.1084
-0.2996	0.1983
-0.2789	0.3053
-0.2984	0.4035
-0.2712	0.4639

q_∞=551 Pa, NPR 1.586

C_{Pi} lower outer	C_{Pi} upper outer
0.4778	-0.0170
-0.6330	-0.3664
-0.7279	-0.4277
-0.5660	-0.3056
-0.4199	-0.1674
-0.3618	-0.0745
-0.3281	0.0033
-0.3274	0.0902
-0.2998	0.1836
-0.2817	0.2951
-0.3127	0.3941
-0.2783	0.4494

q_∞ = 61.3 Pa, NPR 2.0

x/d_e	C_{Pi} lower outer	C_{Pi} upper outer
0.0000	0.2420	0.0088
0.1189	-0.7812	-0.2683
0.2081	-0.8452	-0.3241
0.2973	-0.6968	-0.2304
0.3963	-0.5672	-0.1385
0.4954	-0.5076	-0.0488
0.5945	-0.4539	0.0101
0.6963	-0.4559	0.0940
0.7927	-0.4108	0.1680
0.8918	-0.3959	0.2660
0.9908	-0.3979	0.3667
1.0899	-0.3528	0.4308

q_∞ = 245 Pa, NPR 2.0

C_{Pi} lower outer	C_{Pi} upper outer
0.4618	-0.0021
-0.6122	-0.3219
-0.7064	-0.3879
-0.5559	-0.2752
-0.4184	-0.1551
-0.3499	-0.0600
-0.3139	0.0212
-0.3040	0.1020
-0.2770	0.1924
-0.2542	0.2989
-0.2776	0.3958
-0.2500	0.4621

q_∞ = 551 Pa, NPR 2.0

C_{Pi} lower outer	C_{Pi} upper outer
0.4837	-0.0133
-0.5910	-0.3707
-0.6848	-0.4310
-0.5270	-0.3032
-0.3817	-0.1694
-0.3242	-0.0740
-0.2927	0.0040
-0.2902	0.0912
-0.2633	0.1842
-0.2468	0.2957
-0.2760	0.3919
-0.2443	0.4478

q_∞ = 61.3 Pa, NPR 3.0

	C_{Pi}	
x/d_e	lower outer	upper outer
0.0000	0.1691	-0.0007
0.1189	-0.8366	-0.2714
0.2081	-0.8659	-0.3503
0.2973	-0.7297	-0.2541
0.3963	-0.5898	-0.1618
0.4954	-0.5258	-0.0825
0.5945	-0.4893	-0.0137
0.6963	-0.4643	0.0586
0.7927	-0.4390	0.1348
0.8918	-0.4166	0.2390
0.9908	-0.3963	0.3336
1.0899	-0.3651	0.4001

q_∞ = 245 Pa, NPR 3.0

C_{Pi}	
lower outer	upper outer
0.4708	-0.0058
-0.6070	-0.3240
-0.6919	-0.3906
-0.5401	-0.2768
-0.3978	-0.1633
-0.3341	-0.0670
-0.2971	0.0127
-0.2855	0.0946
-0.2617	0.1814
-0.2368	0.2868
-0.2540	0.3853
-0.2277	0.4493

q_∞ = 551 Pa, NPR 3.0

C_{Pi}	
lower outer	upper outer
0.4903	-0.0147
-0.5805	-0.3740
-0.6740	-0.4323
-0.5120	-0.3078
-0.3659	-0.1723
-0.3062	-0.0794
-0.2734	-0.0022
-0.2679	0.0840
-0.2440	0.1766
-0.2231	0.2894
-0.2528	0.3863
-0.2221	0.4414

q_∞ = 61.3 Pa, NPR 4.0

	C_{Pi}	
x/d_e	lower outer	upper outer
0.0000	0.2765	-0.0564
0.1189	-0.9691	-0.3871
0.2081	-1.0241	-0.4715
0.2973	-0.8539	-0.3588
0.3963	-0.6826	-0.2446
0.4954	-0.6094	-0.1465
0.5945	-0.5615	-0.0682
0.6963	-0.5292	0.0271
0.7927	-0.4814	0.1202
0.8918	-0.4510	0.2327
0.9908	-0.4480	0.3387
1.0899	-0.4261	0.4187

q_∞ = 245 Pa, NPR 4.0

C_{Pi}	
lower outer	upper outer
0.5036	-0.0187
-0.6251	-0.3694
-0.7165	-0.4360
-0.5567	-0.3166
-0.4076	-0.1917
-0.3381	-0.0953
-0.3009	-0.0143
-0.2863	0.0712
-0.2618	0.1631
-0.2298	0.2797
-0.2487	0.3865
-0.2228	0.4560

q_∞ = 551 Pa, NPR 4.0

C_{Pi}	
lower outer	upper outer
0.5021	-0.0179
-0.5823	-0.3735
-0.6812	-0.4371
-0.5147	-0.3099
-0.3630	-0.1705
-0.3059	-0.0765
-0.2699	0.0018
-0.2655	0.0885
-0.2377	0.1835
-0.2145	0.2972
-0.2438	0.3965
-0.2122	0.4530

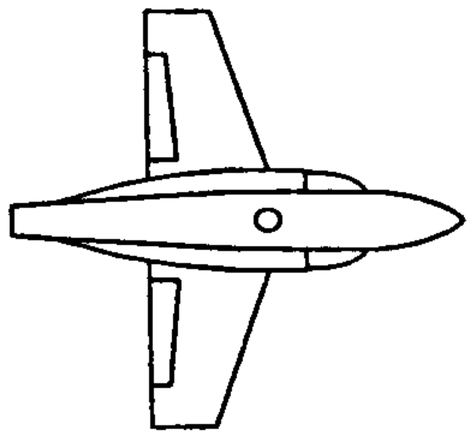

q_∞ = 61.3 Pa, NPR 1.586

	C_{Pi}	
x/d_e	lower outer	upper outer
0.0000	0.3679	-0.0250
0.1189	-0.6504	-0.3316
0.2081	-0.7453	-0.4038
0.2973	-0.6043	-0.3104
0.3963	-0.4767	-0.2042
0.4954	-0.4145	-0.1141
0.5945	-0.3869	-0.0125
0.6963	-0.3793	0.0599
0.7927	-0.3834	0.1559
0.8918	-0.3623	0.2676
0.9908	-0.3870	0.3545
1.0899	-0.3764	0.4359

q_∞=245 Pa, NPR 1.586

C_{Pi}	
lower outer	upper outer
0.4957	-0.0136
-0.4795	-0.3351
-0.5545	-0.3983
-0.4294	-0.2828
-0.3076	-0.1616
-0.2462	-0.0651
-0.2162	0.0137
-0.2076	0.1013
-0.1958	0.1918
-0.1847	0.3018
-0.2163	0.4004
-0.2020	0.4659

q_∞=551 Pa, NPR 1.586

C_{Pi}	
lower outer	upper outer
0.5107	-0.0150
-0.4512	-0.3700
-0.5347	-0.4369
-0.3915	-0.3062
-0.2614	-0.1680
-0.2074	-0.0729
-0.1792	0.0041
-0.1797	0.0925
-0.1614	0.1872
-0.1525	0.2997
-0.1874	0.3999
-0.1678	0.4535

q_∞ = 61.3 Pa, NPR 2.0

	C_{Pi}	
x/d_e	lower outer	upper outer
0.0000	0.3398	-0.0148
0.1189	-0.6085	-0.3070
0.2081	-0.6974	-0.3858
0.2973	-0.5725	-0.2787
0.3963	-0.4612	-0.1740
0.4954	-0.3874	-0.0901
0.5945	-0.3611	-0.0150
0.6963	-0.3488	0.0657
0.7927	-0.3508	0.1481
0.8918	-0.3271	0.2681
0.9908	-0.3341	0.3574
1.0899	-0.3433	0.4366

q_∞ = 245 Pa, NPR 2.0

C_{Pi}	
lower outer	upper outer
0.4922	-0.0053
-0.4705	-0.3278
-0.5579	-0.3918
-0.4230	-0.2734
-0.3013	-0.1570
-0.2420	-0.0627
-0.2133	0.0167
-0.2022	0.1039
-0.1870	0.1942
-0.1793	0.3037
-0.2074	0.3999
-0.1884	0.4634

q_∞ = 551 Pa, NPR 2.0

C_{Pi}	
lower outer	upper outer
0.5085	-0.0129
-0.4529	-0.3712
-0.5368	-0.4315
-0.3910	-0.3053
-0.2599	-0.1670
-0.2062	-0.0717
-0.1763	0.0067
-0.1768	0.0948
-0.1563	0.1882
-0.1450	0.3007
-0.1770	0.3975
-0.1572	0.4531

q_∞ = 61.3 Pa, NPR 3.0

	C_{Pi}	
x/d_{ie}	lower outer	upper outer
0.0000	0.3358	-0.0261
0.1189	-0.6563	-0.3245
0.2081	-0.7322	-0.3997
0.2973	-0.6148	-0.2965
0.3963	-0.4718	-0.1973
0.4954	-0.4314	-0.1196
0.5945	-0.3870	-0.0326
0.6963	-0.3833	0.0393
0.7927	-0.3692	0.1221
0.8918	-0.3677	0.2939
0.9908	-0.3684	0.3318
1.0899	-0.3799	0.4077

q_∞ = 245 Pa, NPR 3.0

C_{Pi}	
lower outer	upper outer
0.4975	-0.0068
-0.4854	-0.3301
-0.5665	-0.3959
-0.4341	-0.2820
-0.3095	-0.1592
-0.2490	-0.0672
-0.2179	0.0112
-0.2120	0.0939
-0.1970	0.1798
-0.1829	0.2917
-0.2095	0.3924
-0.1955	0.4577

q_∞ = 551 Pa, NPR 3.0

C_{Pi}	
lower outer	upper outer
0.5113	-0.0139
-0.4635	-0.3749
-0.5465	-0.4351
-0.3994	-0.3077
-0.2638	-0.1710
-0.2112	-0.0771
-0.1817	0.0005
-0.1801	0.0880
-0.1603	0.1810
-0.1487	0.2933
-0.1785	0.3912
-0.1601	0.4480

q_∞ = 61.3 Pa, NPR 4.0

	C_{Pi}	
x/d_{ie}	lower outer	upper outer
0.0000	0.3585	-0.0431
0.1189	-0.6754	-0.3595
0.2081	-0.7689	-0.4442
0.2973	-0.6254	-0.3273
0.3963	-0.4932	-0.2206
0.4954	-0.4393	-0.1364
0.5945	-0.4099	-0.0758
0.6963	-0.3936	0.0238
0.7927	-0.3769	0.1075
0.8918	-0.3587	0.2341
0.9908	-0.3718	0.3188
1.0899	-0.3747	0.4014

q_∞ = 245 Pa, NPR 4.0

C_{Pi}	
lower outer	upper outer
0.5060	-0.0126
-0.4926	-0.3584
-0.5817	-0.4262
-0.4396	-0.3028
-0.3119	-0.1874
-0.2522	-0.0939
-0.2204	-0.0128
-0.2156	0.0705
-0.1993	0.1639
-0.1832	0.2766
-0.2110	0.3823
-0.1953	0.4541

q_∞ = 551 Pa, NPR 4.0

C_{Pi}	
lower outer	upper outer
0.5144	-0.0144
-0.4654	-0.3685
-0.5518	-0.4295
-0.4018	-0.3029
-0.2662	-0.1677
-0.2111	-0.0756
-0.1830	0.0026
-0.1806	0.0873
-0.1609	0.1808
-0.1474	0.2939
-0.1799	0.3944
-0.1599	0.4509

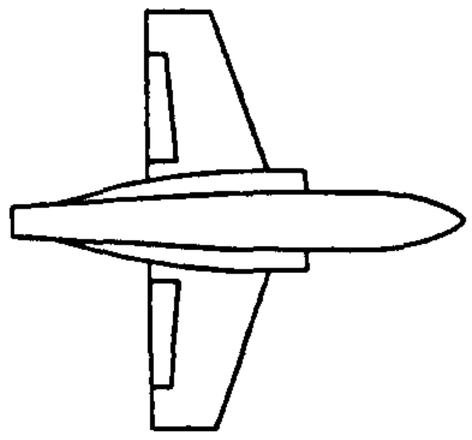

q_∞ = 61.3 Pa, NPR 1.0

	C_{Pi}			
x/d_{ie}	lower outer	lower inner	upper inner	upper outer
0.0000	-121.2229	-121.2229	-108.4668	-108.4668
0.1189	0.4323	-101.0957	-119.7248	0.0834
0.2081	1.0563	-103.5131	-106.0033	0.9729
0.2973	0.9635	-97.0780	-98.3093	0.9412
0.3963	0.8114	-92.6135	-93.8389	0.8278
0.4954	0.6729	-90.0089	-91.1665	0.7545
0.5945	0.5471	-90.0792	-90.3236	0.7034
0.6963	0.4761	-88.6688	-90.2819	0.6907
0.7927	0.4192	-87.7601	-89.5958	0.6982
0.8918	0.3659	-87.8304	-91.4754	0.7235
0.9908	0.3138	-88.4402	-91.0283	0.7496
1.0899	0.2862	-88.5410	-88.9407	0.7515

q_∞ = 245 Pa, NPR 1.0

	C_{Pi}			
x/d_{ie}	lower outer	lower inner	upper inner	upper outer
0.0000	-17.3081	-17.3081	-17.6893	-17.6893
0.1189	0.8683	-23.2979	-27.7720	0.8514
0.2081	0.4645	-24.1744	-24.6692	0.4769
0.2973	0.3323	-22.4939	-22.9371	0.3199
0.3963	0.2696	-21.3797	-21.8581	0.2500
0.4954	0.1971	-20.8185	-21.1927	0.2285
0.5945	0.0630	-21.0563	-21.0167	0.2304
0.6963	0.1341	-20.6484	-20.9983	0.2647
0.7927	0.1203	-20.4648	-20.8492	0.3199
0.8918	0.1184	-20.3814	-21.4276	0.3810
0.9908	0.1036	-20.5810	-21.3082	0.4616
1.0899	0.1026	-20.6062	-20.6439	0.6397

q_∞ = 551 Pa, NPR 1.0

	C_{Pi}			
x/d_e	lower outer	lower inner	upper inner	upper outer
0.0000	-3.5058	-3.5058	-4.6644	-4.6644
0.1189	0.3154	-9.5942	-11.1180	0.4482
0.2081	-0.0122	-10.2488	-10.5628	0.1198
0.2973	0.0083	-9.5738	-9.8818	0.0736
0.3963	0.0299	-9.0649	-9.3219	0.0798
0.4954	0.0215	-8.8024	-8.9967	0.0992
0.5945	0.0195	-8.9367	-8.9173	0.1306
0.6963	0.0156	-8.7467	-8.9096	0.1785
0.7927	0.0173	-8.6520	-8.8368	0.2401
0.8918	0.0177	-8.6133	-9.1323	0.3097
0.9908	0.0123	-8.7131	-9.0843	0.5246
1.0899	0.0135	-8.7246	-8.7552	0.6618

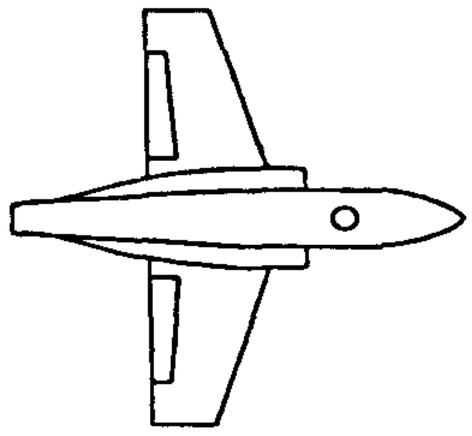

q_∞ = 61.3 Pa, NPR 1.586

	C_{Pi}			
x/d_{ie}	lower outer	lower inner	upper inner	upper outer
0.0000	-98.0403	-98.0403	-114.7043	-114.7043
0.1189	0.8458	-96.4073	-120.5531	0.1021
0.2081	0.9500	-99.4255	-105.5511	0.9854
0.2973	0.7602	-93.1117	-97.5966	0.9611
0.3963	0.5376	-88.8833	-92.7191	0.8264
0.4954	0.4183	-86.8588	-89.7141	0.7477
0.5945	0.3062	-87.5229	-88.5123	0.6846
0.6963	0.1598	-85.8143	-88.2169	0.6621
0.7927	0.1091	-85.5057	-87.5382	0.6778
0.8918	0.0934	-85.2090	-89.0837	0.7275
0.9908	0.1368	-86.0144	-89.0026	0.7500
1.0899	0.1216	-86.1943	-86.4359	0.7467

q_∞ = 245 Pa, NPR 1.586

	C_{Pi}			
x/d_{ie}	lower outer	lower inner	upper inner	upper outer
0.0000	-13.0148	-13.0148	-19.6097	-19.6097
0.1189	0.5715	-22.5373	-29.1540	0.7813
0.2081	0.1249	-23.8268	-25.6870	0.4727
0.2973	0.0544	-22.3755	-23.7196	0.3247
0.3963	0.0329	-21.3090	-22.5561	0.2722
0.4954	0.0115	-20.7933	-21.7700	0.2514
0.5945	-0.0135	-21.1836	-21.5180	0.2585
0.6963	-0.0329	-20.7733	-21.4590	0.2944
0.7927	-0.0294	-20.6487	-21.3198	0.3389
0.8918	-0.0322	-20.6085	-21.8754	0.4161
0.9908	-0.0469	-20.7994	-21.7238	0.5090
1.0899	-0.0458	-20.8461	-21.0279	0.6669

q_∞ = 551 Pa, NPR 1.586

	C_{Pi}			
x/d_e	lower outer	lower inner	upper inner	upper outer
0.0000	-1.9015	-1.9015	-5.2077	-5.2077
0.1189	-0.0545	-9.0360	-11.5967	0.4610
0.2081	-0.3623	-9.8229	-10.8012	0.1211
0.2973	-0.2804	-9.3162	-10.0497	0.0771
0.3963	-0.2041	-8.8900	-9.4330	0.0651
0.4954	-0.1826	-8.6756	-9.0786	0.0838
0.5945	-0.1584	-8.8501	-8.9855	0.1118
0.6963	-0.1535	-8.6613	-8.9721	0.1424
0.7927	-0.1362	-8.5957	-8.8982	0.2159
0.8918	-0.1266	-8.5645	-9.1584	0.2859
0.9908	-0.1253	-8.6712	-9.1075	0.4779
1.0899	-0.1209	-8.6866	-8.7826	0.6423

q_∞ = 61.3 Pa, NPR 2.0

	C_{Pi}			
x/d_e	lower outer	lower inner	upper inner	upper outer
0.0000	-101.3796	-101.3796	-116.8056	-116.8056
0.1189	0.7289	-96.9208	-120.8671	-0.1066
0.2081	0.9448	-99.7479	-105.7442	0.8159
0.2973	0.7659	-93.1796	-97.7138	0.9089
0.3963	0.5929	-89.0976	-92.8902	0.7906
0.4954	0.4627	-86.8233	-89.8811	0.7229
0.5945	0.3712	-87.4387	-88.7543	0.6694
0.6963	0.3005	-86.1060	-88.4372	0.6321
0.7927	0.2368	-85.4610	-87.7112	0.6550
0.8918	0.1229	-85.1766	-89.3059	0.7036
0.9908	0.0540	-86.0655	-88.9516	0.7190
1.0899	0.0739	-86.0198	-86.7787	0.7290

q_∞ = 245 Pa, NPR 2.0

	C_{Pi}			
x/d_e	lower outer	lower inner	upper inner	upper outer
0.0000	-13.3587	-13.3587	-20.0952	-20.0952
0.1189	0.6070	-22.4874	-29.0205	0.7272
0.2081	0.1474	-23.7520	-25.6347	0.4804
0.2973	0.0839	-22.3401	-23.6872	0.3536
0.3963	0.0722	-21.2819	-22.4614	0.3015
0.4954	0.0215	-20.7895	-21.7520	0.2837
0.5945	0.0088	-21.1076	-21.4826	0.2905
0.6963	0.0020	-20.7856	-21.4436	0.3193
0.7927	-0.0026	-20.6158	-21.3154	0.3667
0.8918	-0.0021	-20.5405	-21.8914	0.4360
0.9908	-0.0281	-20.7940	-21.7237	0.5298
1.0899	-0.0237	-20.7934	-21.0071	0.6758

q_∞ = 551 Pa, NPR 2.0

	C_{Pi}			
x/d_e	lower outer	lower inner	upper inner	upper outer
0.0000	-1.8479	-1.8479	-5.2653	-5.2653
0.1189	-0.0442	-8.9843	-11.6491	0.4466
0.2081	-0.3551	-9.7792	-10.8349	0.1143
0.2973	-0.2721	-9.2928	-10.0394	0.0653
0.3963	-0.1911	-8.8469	-9.4544	0.0599
0.4954	-0.1702	-8.6530	-9.0776	0.0682
0.5945	-0.1431	-8.8191	-8.9763	0.0981
0.6963	-0.1393	-8.6412	-8.9661	0.1254
0.7927	-0.1286	-8.5731	-8.8876	0.1961
0.8918	-0.1097	-8.5397	-9.1668	0.2734
0.9908	-0.1111	-8.6361	-9.1127	0.4434
1.0899	-0.1055	-8.6574	-8.7761	0.6273

q_∞ = 61.3 Pa, NPR 3.0

	C_{Pi}			
x/d_e	lower outer	lower inner	upper inner	upper outer
0.0000	-100.2539	-100.2539	-118.9236	-118.9236
0.1189	0.7535	-96.6359	-121.8567	-0.3087
0.2081	0.9500	-99.2850	-106.2430	0.7171
0.2973	0.7922	-92.7402	-97.7408	0.8195
0.3963	0.6123	-88.7323	-92.8152	0.7300
0.4954	0.4839	-86.5102	-89.4873	0.6732
0.5945	0.4052	-87.3699	-88.8084	0.6497
0.6963	0.3037	-85.8865	-88.4155	0.6457
0.7927	0.1681	-85.3021	-87.3815	0.6628
0.8918	0.1542	-85.1282	-89.5265	0.7027
0.9908	0.1780	-85.9161	-89.1697	0.7189
1.0899	0.1735	-86.0853	-86.7078	0.7628

q_∞ = 245 Pa, NPR 3.0

	C_{Pi}			
x/d_e	lower outer	lower inner	upper inner	upper outer
0.0000	-13.3780	-13.3780	-20.6857	-20.6857
0.1189	0.6421	-22.5181	-28.9606	0.6955
0.2081	0.1974	-23.7257	-25.5569	0.4916
0.2973	0.1210	-22.2676	-23.6637	0.3773
0.3963	0.1092	-21.1820	-22.4842	0.3198
0.4954	0.0802	-20.7267	-21.7303	0.3031
0.5945	0.0440	-21.0764	-21.4936	0.3082
0.6963	0.0388	-20.7162	-21.4513	0.3264
0.7927	0.0355	-20.5757	-21.2923	0.3737
0.8918	0.0373	-20.5300	-21.8945	0.4411
0.9908	0.0272	-20.7738	-21.7356	0.5210
1.0899	0.0264	-20.8076	-21.0310	0.6568

q_∞ = 551 Pa, NPR 3.0

	C_{Pi}			
x/d_e	lower outer	lower inner	upper inner	upper outer
0.0000	-1.9396	-1.9396	-5.2652	-5.2652
0.1189	-0.0014	-9.0107	-11.7199	0.3938
0.2081	-0.3047	-9.7870	-10.8264	0.0926
0.2973	-0.2278	-9.2935	-10.0102	0.0526
0.3963	-0.1586	-8.8595	-9.4318	0.0520
0.4954	-0.1273	-8.6479	-9.0821	0.0543
0.5945	-0.1172	-8.8273	-8.9985	0.0814
0.6963	-0.1059	-8.6444	-8.9821	0.1165
0.7927	-0.0929	-8.5661	-8.9106	0.1669
0.8918	-0.0861	-8.5515	-9.1791	0.2610
0.9908	-0.0867	-8.6576	-9.1144	0.3960
1.0899	-0.0819	-8.6666	-8.7884	0.5722

q_∞ = 61.3 Pa, NPR 4.0

	C_{Pi}			
x/d_e	lower outer	lower inner	upper inner	upper outer
0.0000	-104.1223	-104.1223	-123.0706	-123.0706
0.1189	0.7338	-99.1140	-123.8775	-0.4136
0.2081	0.9633	-101.3106	-107.8189	0.6999
0.2973	0.8004	-94.7700	-99.2232	0.7870
0.3963	0.6221	-90.5664	-94.1032	0.7042
0.4954	0.4859	-88.2725	-91.1583	0.6357
0.5945	0.4120	-89.1609	-90.1620	0.5883
0.6963	0.3213	-87.0889	-89.9332	0.6012
0.7927	0.2673	-86.9737	-89.2209	0.6377
0.8918	0.1397	-86.6118	-91.3072	0.7025
0.9908	0.1499	-87.5912	-90.6191	0.7202
1.0899	0.1614	-87.7317	-88.2748	0.7429

q_∞ = 245 Pa, NPR 4.0

	C_{Pi}			
x/d_e	lower outer	lower inner	upper inner	upper outer
0.0000	-13.8686	-13.8686	-21.7149	-21.7149
0.1189	0.6442	-23.0650	-29.6414	0.6189
0.2081	0.2082	-24.2800	-26.1105	0.4239
0.2973	0.1261	-22.6728	-24.1467	0.3038
0.3963	0.0942	-21.6448	-22.9520	0.2605
0.4954	0.0756	-21.1797	-22.1931	0.2263
0.5945	0.0442	-21.5363	-21.9572	0.2270
0.6963	0.0186	-21.1685	-21.9128	0.2569
0.7927	0.0164	-21.0284	-21.7783	0.3012
0.8918	0.0167	-20.9922	-22.3944	0.3718
0.9908	0.0068	-21.1843	-22.1924	0.4764
1.0899	0.0081	-21.2411	-21.4759	0.6062

q_∞ = 551 Pa, NPR 4.0

	C_{Pi}			
x/d_e	lower outer	lower inner	upper inner	upper outer
0.0000	-2.1214	-2.1214	-5.3857	-5.3857
0.1189	0.0419	-9.2142	-11.9163	0.3845
0.2081	-0.2673	-10.0010	-10.9857	0.0929
0.2973	-0.2063	-9.4775	-10.1624	0.0516
0.3963	-0.1358	-9.0242	-9.5579	0.0503
0.4954	-0.1189	-8.8045	-9.2255	0.0531
0.5945	-0.0970	-8.9804	-9.1496	0.0723
0.6963	-0.0917	-8.7963	-9.1470	0.1153
0.7927	-0.0827	-8.7439	-9.0642	0.1587
0.8918	-0.0709	-8.7169	-9.3270	0.2474
0.9908	-0.0763	-8.8267	-9.2652	0.3828
1.0899	-0.0699	-8.8411	-8.9497	0.5592

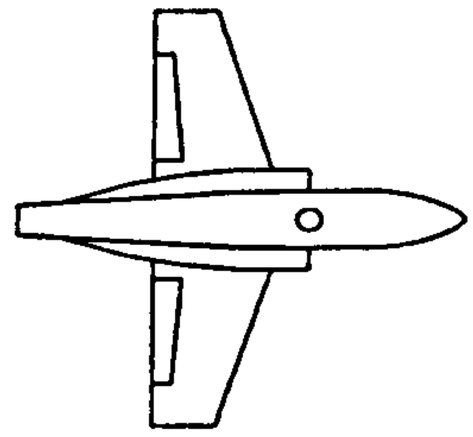

q_∞ = 61.3 Pa, NPR 1.586

	C_{Pi}			
x/d_e	lower outer	lower inner	upper inner	upper outer
0.0000	-105.2581	-105.2581	-115.7461	-115.7461
0.1189	0.7565	-98.3559	-121.1562	-0.1519
0.2081	0.9220	-101.2650	-106.3848	0.8637
0.2973	0.6503	-94.5843	-98.3482	0.9021
0.3963	0.3271	-90.6345	-93.8224	0.7679
0.4954	0.2543	-88.3009	-90.9192	0.6520
0.5945	0.1244	-88.8645	-89.9105	0.6077
0.6963	0.0776	-87.2978	-89.5717	0.5961
0.7927	0.0617	-86.6971	-88.7934	0.6018
0.8918	0.0084	-86.4977	-90.4226	0.6305
0.9908	-0.0886	-87.2361	-90.1574	0.6480
1.0899	-0.1435	-87.3052	-87.1968	0.6398

q_∞ = 245 Pa, NPR 1.586

	C_{Pi}			
x/d_e	lower outer	lower inner	upper inner	upper outer
0.0000	-14.9981	-14.9981	-18.6042	-18.6042
0.1189	0.6747	-23.0403	-28.5732	0.7943
0.2081	0.1631	-24.1574	-25.2372	0.4511
0.2973	0.0763	-22.5050	-23.4481	0.3060
0.3963	0.0107	-21.4266	-22.3184	0.2484
0.4954	-0.0510	-20.9192	-21.6026	0.2200
0.5945	-0.0734	-21.1839	-21.3680	0.2287
0.6963	-0.1106	-20.7841	-21.3388	0.2640
0.7927	-0.1226	-20.5934	-21.1576	0.3119
0.8918	-0.1385	-20.5452	-21.7347	0.3856
0.9908	-0.1478	-20.7642	-21.5988	0.4861
1.0899	-0.1461	-20.7960	-20.9216	0.6610

q_∞ = 551 Pa, NPR 1.586

	C_{Pi}			
x/d_e	lower outer	lower inner	upper inner	upper outer
0.0000	-2.7620	-2.7620	-4.8816	-4.8816
0.1189	0.0669	-9.4409	-11.4009	0.4330
0.2081	-0.2908	-10.1301	-10.6999	0.1048
0.2973	-0.2562	-9.5148	-9.9608	0.0485
0.3963	-0.2119	-9.0187	-9.3939	0.0523
0.4954	-0.2097	-8.7754	-9.0484	0.0654
0.5945	-0.2076	-8.9194	-8.9759	0.0994
0.6963	-0.2193	-8.7360	-8.9780	0.1349
0.7927	-0.2159	-8.6638	-8.8989	0.2023
0.8918	-0.2145	-8.6249	-9.1693	0.2768
0.9908	-0.2243	-8.7248	-9.1036	0.4676
1.0899	-0.2208	-8.7355	-8.8018	0.6379

q_∞ = 61.3 Pa, NPR 2.0

	C_{Pi}			
x/d_e	lower outer	lower inner	upper inner	upper outer
0.0000	-103.8432	-103.8432	-112.9750	-112.9750
0.1189	0.7529	-96.1838	-119.6337	-0.0957
0.2081	0.9496	-99.4017	-104.7267	0.8103
0.2973	0.6844	-93.2473	-96.8503	0.9099
0.3963	0.3991	-89.0379	-92.1381	0.7749
0.4954	0.3120	-86.6807	-89.2641	0.6587
0.5945	0.1698	-87.0088	-88.2604	0.6280
0.6963	0.1494	-85.6941	-87.9303	0.6158
0.7927	0.1171	-85.0552	-87.1564	0.6293
0.8918	0.1088	-84.4746	-88.8612	0.6572
0.9908	0.0460	-85.6998	-88.1349	0.6711
1.0899	-0.0340	-85.6872	-86.3519	0.6722

q_∞ = 245 Pa, NPR 2.0

	C_{Pi}			
x/d_e	lower outer	lower inner	upper inner	upper outer
0.0000	-14.7083	-14.7083	-18.8573	-18.8573
0.1189	0.6478	-22.8149	-28.2514	0.7003
0.2081	0.1625	-23.8247	-25.0345	0.4355
0.2973	0.0570	-22.2525	-23.2643	0.3090
0.3963	0.0170	-21.2092	-22.0806	0.2513
0.4954	-0.0285	-20.7035	-21.4032	0.2439
0.5945	-0.0527	-21.0183	-21.2069	0.2440
0.6963	-0.1002	-20.5254	-21.1764	0.2845
0.7927	-0.1035	-20.4264	-21.0245	0.3344
0.8918	-0.1040	-20.3814	-21.6120	0.4057
0.9908	-0.1146	-20.6010	-21.4413	0.4965
1.0899	-0.1145	-20.5929	-20.7760	0.6445

q_∞ = 551 Pa, NPR 2.0

	C_{Pi}			
x/d_e	lower outer	lower inner	upper inner	upper outer
0.0000	-2.7552	-2.7552	-4.8801	-4.8801
0.1189	0.0915	-9.3908	-11.4005	0.4134
0.2081	-0.2596	-10.0877	-10.6865	0.0886
0.2973	-0.2226	-9.5119	-9.9602	0.0454
0.3963	-0.1758	-9.0038	-9.3687	0.0537
0.4954	-0.1784	-8.7620	-9.0436	0.0584
0.5945	-0.1768	-8.9047	-8.9630	0.0888
0.6963	-0.1794	-8.7146	-8.9650	0.1316
0.7927	-0.1762	-8.6345	-8.8830	0.1859
0.8918	-0.1724	-8.5826	-9.1531	0.2759
0.9908	-0.1891	-8.6953	-9.0991	0.4395
1.0899	-0.1816	-8.7039	-8.7788	0.6203

q_∞ = 61.3 Pa, NPR 3.0

	C_{Pi}			
x/d_e	lower outer	lower inner	upper inner	upper outer
0.0000	-103.8209	-103.8209	-117.2247	-117.2247
0.1189	0.8948	-99.6294	-123.7540	0.0095
0.2081	0.9861	-102.2009	-107.5743	0.7606
0.2973	0.7368	-95.5875	-99.2706	0.8927
0.3963	0.4955	-91.1613	-94.3453	0.7847
0.4954	0.2714	-88.8142	-91.4508	0.7091
0.5945	-0.0463	-89.4751	-90.3907	0.6399
0.6963	0.1388	-87.8685	-90.1533	0.6217
0.7927	0.1064	-87.3388	-89.5260	0.6516
0.8918	0.0790	-87.1690	-91.3909	0.7173
0.9908	0.0077	-87.9638	-90.8967	0.7413
1.0899	0.0035	-88.1003	-88.4774	0.7857

q_∞ = 245 Pa, NPR 3.0

	C_{Pi}			
x/d_e	lower outer	lower inner	upper inner	upper outer
0.0000	-14.9183	-14.9183	-19.7708	-19.7708
0.1189	0.6723	-23.2734	-28.9389	0.6836
0.2081	0.1655	-24.3900	-25.7265	0.4295
0.2973	0.0794	-22.7504	-23.7087	0.3070
0.3963	0.0140	-21.6315	-22.5883	0.2508
0.4954	-0.0299	-21.1190	-21.9094	0.2306
0.5945	-0.0656	-21.4524	-21.6937	0.2432
0.6963	-0.0764	-21.0233	-21.6720	0.2796
0.7927	-0.0814	-20.9110	-21.5154	0.3085
0.8918	-0.0830	-20.8084	-22.1287	0.3895
0.9908	-0.1219	-21.0421	-21.8305	0.4895
1.0899	-0.0934	-21.0982	-21.1588	0.6340

q_∞ = 551 Pa, NPR 3.0

	C_{Pi}			
x/d_e	lower outer	lower inner	upper inner	upper outer
0.0000	-2.8632	-2.8632	-4.8673	-4.8673
0.1189	0.1100	-9.6494	-11.5948	0.3789
0.2081	-0.2451	-10.3347	-10.8644	0.0661
0.2973	-0.2071	-9.6959	-10.1288	0.0292
0.3963	-0.1648	-9.1869	-9.5557	0.0357
0.4954	-0.1634	-8.9421	-9.2128	0.0404
0.5945	-0.1600	-9.0902	-9.1531	0.0726
0.6963	-0.1663	-8.9025	-9.1379	0.1136
0.7927	-0.1624	-8.8163	-9.0688	0.1675
0.8918	-0.1612	-8.7892	-9.3623	0.2622
0.9908	-0.1697	-8.8703	-9.2988	0.4211
1.0899	-0.1641	-8.9098	-8.9703	0.6022

q_∞ = 61.3 Pa, NPR 4.0

	C_{Pi}			
x/d_e	lower outer	lower inner	upper inner	upper outer
0.0000	-103.4512	-103.4512	-119.2954	-119.2954
0.1189	0.8820	-98.9454	-123.4490	-0.3673
0.2081	0.9930	-101.4364	-107.1805	0.6968
0.2973	0.7472	-94.8458	-98.8088	0.7626
0.3963	0.5102	-90.5223	-93.9041	0.6826
0.4954	0.3718	-88.3231	-90.9339	0.6142
0.5945	0.1551	-88.9372	-89.9657	0.5858
0.6963	0.0636	-87.4809	-89.8492	0.5958
0.7927	0.1043	-86.8836	-89.2249	0.6360
0.8918	0.0964	-86.7448	-91.2376	0.6966
0.9908	0.0480	-87.4992	-90.7291	0.7441
1.0899	0.0109	-87.6481	-88.1932	0.7756

q_∞ = 245 Pa, NPR 4.0

	C_{Pi}			
x/d_e	lower outer	lower inner	upper inner	upper outer
0.0000	-14.7346	-14.7346	-20.1339	-20.1339
0.1189	0.6767	-23.1259	-28.7919	0.6014
0.2081	0.1850	-24.2036	-25.6259	0.4005
0.2973	0.0874	-22.6245	-23.5674	0.2851
0.3963	0.0249	-21.5581	-22.4710	0.2210
0.4954	-0.0131	-21.0578	-21.8365	0.2159
0.5945	-0.0504	-21.3399	-21.5704	0.2068
0.6963	-0.0662	-20.8971	-21.5816	0.2325
0.7927	-0.0744	-20.7905	-21.3733	0.2824
0.8918	-0.0678	-20.7083	-22.0983	0.3686
0.9908	-0.0895	-20.9714	-21.7946	0.4721
1.0899	-0.0786	-21.0163	-21.1865	0.6102

q_∞ = 551 Pa, NPR 4.0

	C_{Pi}			
x/d_e	lower outer	lower inner	upper inner	upper outer
0.0000	-2.8136	-2.8136	-4.9225	-4.9225
0.1189	0.1159	-9.5674	-11.4981	0.3761
0.2081	-0.2417	-10.2641	-10.8484	0.0715
0.2973	-0.2059	-9.6599	-10.1086	0.0344
0.3963	-0.1618	-9.0740	-9.5120	0.0365
0.4954	-0.1551	-8.8923	-9.1371	0.0423
0.5945	-0.1568	-9.0599	-9.0651	0.0680
0.6963	-0.1593	-8.8692	-9.1052	0.1082
0.7927	-0.1534	-8.7719	-8.9564	0.1611
0.8918	-0.1426	-8.7427	-9.3234	0.2573
0.9908	-0.1581	-8.8513	-9.2604	0.4064
1.0899	-0.1480	-8.8303	-8.9505	0.5822

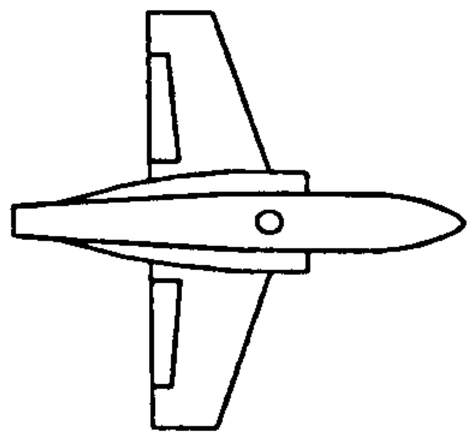

q_∞ = 61.3 Pa, NPR 1.586

	C_{Pi}			
x/d_e	lower outer	lower inner	upper inner	upper outer
0.0000	-106.5418	-106.5418	-108.2959	-108.2959
0.1189	0.8313	-96.6047	-117.6386	0.2519
0.2081	1.0495	-99.6058	-103.5552	1.0282
0.2973	0.8172	-93.1883	-95.9295	0.9325
0.3963	0.5978	-89.0690	-91.3613	0.7970
0.4954	0.4293	-86.7317	-88.5734	0.7059
0.5945	0.2214	-87.1670	-87.0591	0.6389
0.6963	-0.0473	-85.6890	-87.4829	0.6049
0.7927	0.1351	-85.0713	-86.7900	0.6292
0.8918	0.0805	-84.9086	-88.5844	0.6693
0.9908	0.0043	-85.4076	-88.1774	0.7035
1.0899	-0.0058	-85.7806	-86.0622	0.7092

q_∞ = 245 Pa, NPR 1.586

	C_{Pi}			
x/d_e	lower outer	lower inner	upper inner	upper outer
0.0000	-15.8614	-15.8614	-17.8296	-17.8296
0.1189	0.7837	-22.8863	-27.7048	0.7414
0.2081	0.3383	-23.7886	-24.6622	0.4405
0.2973	0.1958	-22.1618	-22.9183	0.3030
0.3963	0.1492	-21.1050	-21.7636	0.2418
0.4954	0.1021	-20.5365	-21.0906	0.2156
0.5945	0.0513	-20.8259	-20.9100	0.2173
0.6963	0.0221	-20.4398	-20.8544	0.2481
0.7927	-0.0050	-20.2355	-20.7383	0.3105
0.8918	-0.0203	-20.1551	-21.2848	0.3788
0.9908	-0.0518	-20.3655	-21.1939	0.4768
1.0899	-0.0533	-20.4000	-20.5271	0.6481

q_∞ = 551 Pa, NPR 1.586

	C_{Pi}			
x/d_e	lower outer	lower inner	upper inner	upper outer
0.0000	-3.2449	-3.2449	-4.6787	-4.6787
0.1189	0.2414	-9.4581	-11.1289	0.4176
0.2081	-0.0934	-10.0918	-10.5105	0.0872
0.2973	-0.0724	-9.4624	-9.8003	0.0493
0.3963	-0.0415	-8.9425	-9.2529	0.0519
0.4954	-0.0464	-8.6845	-8.9122	0.0678
0.5945	-0.0516	-8.8368	-8.8467	0.1002
0.6963	-0.0683	-8.6441	-8.8430	0.1220
0.7927	-0.0696	-8.5618	-8.7699	0.2071
0.8918	-0.0729	-8.5277	-9.0304	0.2787
0.9908	-0.0938	-8.5956	-8.9876	0.4737
1.0899	-0.0959	-8.6167	-8.6790	0.6390

q_∞ = 61.3 Pa, NPR 2.0

	C_{Pi}			
x/d_e	lower outer	lower inner	upper inner	upper outer
0.0000	-106.6190	-106.6190	-108.8480	-108.8480
0.1189	0.7451	-95.7078	-117.2283	0.0458
0.2081	1.0370	-98.5682	-102.9807	0.9748
0.2973	0.8152	-92.3329	-95.2884	0.8977
0.3963	0.6109	-88.2477	-90.7586	0.7711
0.4954	0.4734	-85.9658	-87.8921	0.7014
0.5945	0.3285	-86.3464	-87.0099	0.6090
0.6963	0.1561	-84.9103	-86.7723	0.6080
0.7927	-0.1335	-84.3228	-85.2613	0.6397
0.8918	0.0702	-84.1298	-87.8243	0.7013
0.9908	-0.0172	-84.8040	-87.4065	0.7450
1.0899	-0.0253	-84.9492	-85.2572	0.7426

q_∞ = 245 Pa, NPR 2.0

	C_{Pi}			
x/d_e	lower outer	lower inner	upper inner	upper outer
0.0000	-15.6299	-15.6299	-18.1368	-18.1368
0.1189	0.7733	-22.7089	-27.5866	0.6974
0.2081	0.3393	-23.6303	-24.6176	0.4386
0.2973	0.2053	-22.0669	-22.7928	0.3062
0.3963	0.1083	-20.9668	-21.6492	0.2544
0.4954	0.0843	-20.4886	-20.9958	0.2394
0.5945	0.0676	-20.7520	-20.8179	0.2447
0.6963	0.0055	-20.3167	-20.7725	0.2742
0.7927	-0.0019	-20.1577	-20.7022	0.3142
0.8918	-0.0063	-20.0922	-21.2604	0.4042
0.9908	-0.0618	-20.2313	-21.0608	0.4925
1.0899	-0.0706	-20.2604	-20.4472	0.6461

q_∞ = 551 Pa, NPR 2.0

	C_{Pi}			
x/d_{ie}	lower outer	lower inner	upper inner	upper outer
0.0000	-3.1124	-3.1124	-4.6909	-4.6909
0.1189	0.2272	-9.4134	-11.1202	0.3988
0.2081	-0.1052	-10.0660	-10.5183	0.0814
0.2973	-0.0811	-9.4406	-9.7906	0.0402
0.3963	-0.0446	-8.9260	-9.2528	0.0516
0.4954	-0.0486	-8.6809	-8.9176	0.0662
0.5945	-0.0476	-8.8265	-8.8534	0.0982
0.6963	-0.0682	-8.6230	-8.8489	0.1238
0.7927	-0.0672	-8.5055	-8.7731	0.2028
0.8918	-0.0692	-8.4845	-9.0432	0.2761
0.9908	-0.0897	-8.5983	-8.9806	0.4421
1.0899	-0.0921	-8.6062	-8.6730	0.6236

q_∞ = 61.3 Pa, NPR 3.0

	C_{Pi}			
x/d_{ie}	lower outer	lower inner	upper inner	upper outer
0.0000	-106.6023	-106.6023	-112.3570	-112.3570
0.1189	0.8589	-98.4073	-120.9490	0.0784
0.2081	1.0548	-100.8560	-105.3695	0.7203
0.2973	0.8030	-94.2412	-97.3709	0.8078
0.3963	0.5924	-89.8833	-92.5819	0.6952
0.4954	0.4308	-87.5614	-89.7252	0.6337
0.5945	0.2605	-88.0958	-88.7417	0.5928
0.6963	-0.0958	-86.5894	-88.5824	0.6090
0.7927	0.1214	-86.0218	-88.0365	0.6343
0.8918	0.0863	-85.8028	-90.0376	0.6932
0.9908	-0.0080	-86.6038	-89.5320	0.7177
1.0899	-0.0296	-86.7392	-87.1638	0.7705

q_∞ = 245 Pa, NPR 3.0

	C_{Pi}			
x/d_{ie}	lower outer	lower inner	upper inner	upper outer
0.0000	-15.8085	-15.8085	-18.9495	-18.9495
0.1189	0.7592	-22.9864	-27.9827	0.6642
0.2081	0.3041	-23.9993	-24.9649	0.4280
0.2973	0.1600	-22.3489	-23.1831	0.2985
0.3963	0.1208	-21.2562	-22.0565	0.2345
0.4954	0.0775	-20.6780	-21.3111	0.2148
0.5945	0.0233	-20.9835	-21.1303	0.2137
0.6963	-0.0040	-20.5524	-21.1149	0.2374
0.7927	-0.0258	-20.3997	-21.0306	0.3006
0.8918	-0.0404	-20.3092	-21.5969	0.3696
0.9908	-0.0671	-20.5083	-21.4231	0.4745
1.0899	-0.0717	-20.5894	-20.7543	0.6141

q_∞ = 551 Pa, NPR 3.0

	C_{Pi}			
x/d_e	lower outer	lower inner	upper inner	upper outer
0.0000	-3.2545	-3.2545	-4.5515	-4.5515
0.1189	0.2353	-9.5878	-11.2753	0.3556
0.2081	-0.1036	-10.2381	-10.6257	0.0513
0.2973	-0.0808	-9.5987	-9.9059	0.0166
0.3963	-0.0479	-9.0536	-9.3379	0.0294
0.4954	-0.0535	-8.8033	-9.0055	0.0473
0.5945	-0.0586	-8.9614	-8.9733	0.0720
0.6963	-0.0705	-8.7632	-8.9682	0.1187
0.7927	-0.0709	-8.6775	-8.8960	0.1721
0.8918	-0.0732	-8.6428	-9.1553	0.2643
0.9908	-0.0920	-8.7326	-9.1103	0.4305
1.0899	-0.0924	-8.7420	-8.7458	0.6098

q_∞ = 61.3 Pa, NPR 4.0

	C_{Pi}			
x/d_e	lower outer	lower inner	upper inner	upper outer
0.0000	-106.9808	-106.9808	-114.6974	-114.6974
0.1189	0.7894	-97.6108	-120.1333	-0.3689
0.2081	1.0042	-99.9288	-104.7223	0.6562
0.2973	0.7932	-93.3520	-96.7105	0.7404
0.3963	0.5911	-89.0617	-91.8842	0.6352
0.4954	0.4204	-86.7679	-89.0564	0.5550
0.5945	0.2369	-87.3266	-88.1947	0.5347
0.6963	0.0302	-85.8277	-88.0180	0.5509
0.7927	0.1438	-85.3030	-87.2115	0.5973
0.8918	0.0375	-85.0495	-87.7959	0.6571
0.9908	0.0066	-85.8415	-88.9098	0.6846
1.0899	-0.0080	-85.9816	-86.0354	0.7395

q_∞ = 245 Pa, NPR 4.0

	C_{Pi}			
x/d_e	lower outer	lower inner	upper inner	upper outer
0.0000	-15.7024	-15.7024	-19.2986	-19.2986
0.1189	0.7669	-22.8788	-27.8715	0.5928
0.2081	0.3184	-23.7974	-25.0140	0.3945
0.2973	0.1790	-22.0914	-23.1818	0.2786
0.3963	0.1324	-21.0707	-21.9868	0.2201
0.4954	0.0927	-20.5543	-21.2406	0.1984
0.5945	0.0341	-20.8755	-21.1210	0.1998
0.6963	0.0070	-20.4511	-21.0396	0.2195
0.7927	-0.0108	-20.2620	-20.8651	0.2809
0.8918	-0.0169	-20.2506	-21.5490	0.3541
0.9908	-0.0553	-20.4304	-21.3181	0.4555
1.0899	-0.0617	-20.4596	-20.6310	0.5935

q_∞ = 551 Pa, NPR 4.0

	C_{Pi}			
x/d_e	lower outer	lower inner	upper inner	upper outer
0.0000	-3.1962	-3.1962	-4.6085	-4.6085
0.1189	0.2356	-9.5438	-11.2670	0.3619
0.2081	-0.1036	-10.1417	-10.5861	0.0510
0.2973	-0.0845	-9.5572	-9.8454	0.0136
0.3963	-0.0549	-9.0310	-9.3388	0.0354
0.4954	-0.0602	-8.7778	-9.0003	0.0401
0.5945	-0.0616	-8.9189	-8.9347	0.0664
0.6963	-0.0726	-8.7271	-8.9340	0.1108
0.7927	-0.0704	-8.6393	-8.8669	0.1626
0.8918	-0.0688	-8.6013	-9.0707	0.2539
0.9908	-0.0994	-8.6958	-9.0763	0.4109
1.0899	-0.0967	-8.7038	-8.7820	0.5893

D Phase 2b Experimental Data (Constant Nozzle Area)

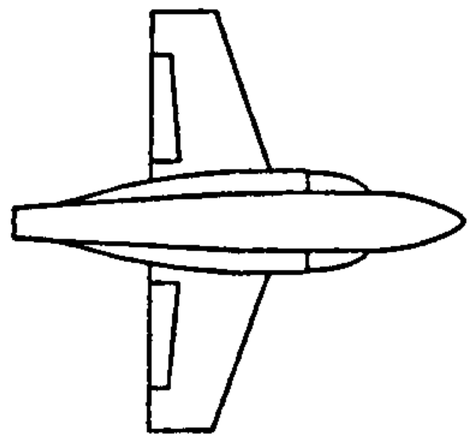

q_∞ = 61.3 Pa, NPR 1.0

	$C_{P\,(root)}$	
x/chord	upper	lower
0.0000	0.9100	0.9100
0.0459	-0.3519	-0.1655
0.0989	-0.3764	-0.1250
0.1519	-0.4193	-0.1180
0.2049	-0.4376	-0.0969
0.2580	-0.4427	-0.1038
0.3110	-0.4202	-0.0934
0.3640	-0.3945	-0.0534
0.4170	-0.3734	0.0094
0.4670	-0.3504	0.0517
0.5230	-0.3243	0.0758
0.5760	-0.2974	0.1006
0.6290	-0.2821	0.1193
0.6820	-0.2720	0.1136
0.7350	-0.2808	0.0193
0.7880	-0.2756	-0.1846
0.8410	-0.3251	-0.2774
1.0000	0.0000	0.0000

q_∞ = 245 Pa, NPR 1.0

$C_{P\,(root)}$	
upper	lower
0.9304	0.9304
-0.3620	-0.2191
-0.3852	-0.1538
-0.4349	-0.1502
-0.4490	-0.1345
-0.4557	-0.1167
-0.4321	-0.1548
-0.4087	-0.0793
-0.3873	-0.0103
-0.3651	0.0352
-0.3360	0.0692
-0.3068	0.0941
-0.2901	0.1199
-0.2822	0.1235
-0.2829	0.0130
-0.3341	-0.2082
-0.3408	-0.3065
0.0000	0.0000

q_∞ = 551 Pa, NPR 1.0

$C_{P\,(root)}$	
upper	lower
0.9169	0.9169
-0.3810	-0.2413
-0.4007	-0.1655
-0.4453	-0.1729
-0.4574	-0.1531
-0.4601	-0.1437
-0.4336	-0.1405
-0.4091	-0.1439
-0.3803	-0.0405
-0.3612	0.0043
-0.3374	0.0419
-0.3027	0.0647
-0.2868	0.0948
-0.2825	0.1088
-0.2887	0.0051
-0.3417	-0.2045
-0.3338	-0.2980
0.0000	0.0000

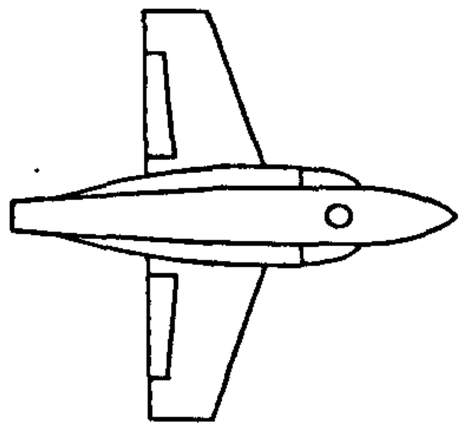

q_∞ = 61.3 Pa, NPR 1.586

	$C_{P\,(root)}$	
x/chord	upper	lower
0.0000	0.7843	0.7843
0.0459	-0.2450	-0.4611
0.0989	-0.3227	-0.3161
0.1519	-0.3898	-0.2830
0.2049	-0.4203	-0.2505
0.2580	-0.4280	-0.2169
0.3110	-0.4169	-0.1900
0.3640	-0.4008	-0.1284
0.4170	-0.3801	-0.0563
0.4670	-0.3597	0.0021
0.5230	-0.3371	0.0495
0.5760	-0.3111	0.0716
0.6290	-0.2984	0.0964
0.6820	-0.2900	0.0965
0.7350	-0.2884	-0.0098
0.7880	-0.2803	-0.2205
0.8410	-0.3471	-0.2968
1.0000	0.0000	0.0000

q_∞=245 Pa, NPR 1.586

$C_{P\,(root)}$	
upper	lower
0.8263	0.8263
-0.2774	-0.4416
-0.3427	-0.2926
-0.4060	-0.2743
-0.4286	-0.2476
-0.4386	-0.2226
-0.4227	-0.2052
-0.4019	-0.1383
-0.3837	-0.0600
-0.3626	-0.0037
-0.3341	0.0370
-0.3062	0.0662
-0.2886	0.0959
-0.2845	0.1037
-0.2899	-0.0056
-0.3595	-0.2353
-0.3456	-0.3235
0.0000	0.0000

q_∞=551 Pa, NPR 1.586

$C_{P\,(root)}$	
upper	lower
0.8706	0.8706
-0.3283	-0.3845
-0.3757	-0.2703
-0.4285	-0.2616
-0.4437	-0.2472
-0.4508	-0.2197
-0.4280	-0.2038
-0.4051	-0.1709
-0.3800	-0.0802
-0.3609	-0.0271
-0.3368	0.0132
-0.3041	0.0417
-0.2892	0.0750
-0.2869	0.0900
-0.2983	-0.0119
-0.3428	-0.2299
-0.3403	-0.3162
0.0000	0.0000

q_∞ = 61.3 Pa, NPR 2.0

	$C_{P\,(root)}$	
x/chord	upper	lower
0.0000	0.6463	0.6463
0.0459	-0.2041	-0.5275
0.0989	-0.2846	-0.3446
0.1519	-0.3573	-0.3159
0.2049	-0.3842	-0.2761
0.2580	-0.3983	-0.2490
0.3110	-0.3888	-0.2060
0.3640	-0.3746	-0.1400
0.4170	-0.3598	-0.0706
0.4670	-0.3442	-0.0094
0.5230	-0.3193	0.0286
0.5760	-0.2964	0.0546
0.6290	-0.2831	0.0771
0.6820	-0.2768	0.0833
0.7350	-0.2829	-0.0152
0.7880	-0.3294	-0.2253
0.8410	-0.3373	-0.2936
1.0000	0.0000	0.0000

q_∞ = 245 Pa, NPR 2.0

$C_{P\,(root)}$	
upper	lower
0.7889	0.7889
-0.2565	-0.4491
-0.3174	-0.3013
-0.3821	-0.2754
-0.4061	-0.2462
-0.4145	-0.2392
-0.3973	-0.1966
-0.3785	-0.1318
-0.3577	-0.0559
-0.3376	-0.0008
-0.3106	0.0389
-0.2901	0.0685
-0.2729	0.0982
-0.2657	0.1059
-0.2733	0.0003
-0.3269	-0.2277
-0.3327	-0.3098
0.0000	0.0000

q_∞ = 551 Pa, NPR 2.0

$C_{P\,(root)}$	
upper	lower
0.8630	0.8630
-0.3287	-0.3885
-0.3688	-0.2805
-0.4216	-0.2616
-0.4338	-0.2488
-0.4355	-0.2406
-0.4098	-0.2077
-0.3849	-0.1717
-0.3614	-0.0856
-0.3423	-0.0319
-0.3206	0.0115
-0.2864	0.0382
-0.2715	0.0723
-0.2721	0.0895
-0.2827	-0.0106
-0.3280	-0.2232
-0.3287	-0.3095
0.0000	0.0000

q_∞ = 61.3 Pa, NPR 3.0

	$C_{P\,(root)}$	
x/chord	upper	lower
0.0000	0.4418	0.4418
0.0459	-0.1329	-0.6557
0.0989	-0.2246	-0.4194
0.1519	-0.3003	-0.3720
0.2049	-0.3448	-0.3108
0.2580	-0.3617	-0.2914
0.3110	-0.3578	-0.2209
0.3640	-0.3485	-0.1470
0.4170	-0.3345	-0.0764
0.4670	-0.3313	-0.0094
0.5230	-0.3110	0.0255
0.5760	-0.2855	0.0574
0.6290	-0.2775	0.0824
0.6820	-0.2724	0.0897
0.7350	-0.2744	-0.0025
0.7880	-0.3329	-0.2309
0.8410	-0.3293	-0.2730
1.0000	0.0000	0.0000

q_∞ = 245 Pa, NPR 3.0

$C_{P\,(root)}$	
upper	lower
0.8052	0.8052
-0.2721	-0.4470
-0.3317	-0.2904
-0.3901	-0.2744
-0.4146	-0.2318
-0.4228	-0.2444
-0.4052	-0.1901
-0.3868	-0.1274
-0.3651	-0.0514
-0.3488	0.0031
-0.3251	0.0421
-0.2968	0.0712
-0.2838	0.1001
-0.2795	0.1081
-0.2822	0.0006
-0.3353	-0.2285
-0.3388	-0.3144
0.0000	0.0000

q_∞ = 551 Pa, NPR 3.0

$C_{P\,(root)}$	
upper	lower
0.8604	0.8604
-0.3169	-0.4079
-0.3576	-0.2848
-0.4088	-0.2693
-0.4211	-0.2501
-0.4248	-0.2633
-0.4020	-0.2155
-0.3779	-0.1652
-0.3525	-0.0869
-0.3336	-0.0342
-0.3109	0.0085
-0.2797	0.0359
-0.2660	0.0693
-0.2674	0.0858
-0.2804	-0.0134
-0.3241	-0.2267
-0.3245	-0.3113
0.0000	0.0000

q_∞ = 61.3 Pa, NPR 4.0

	$C_{P\,(root)}$	
x/chord	upper	lower
0.0000	0.1572	0.1572
0.0459	-0.0337	-0.7362
0.0989	-0.1327	-0.4810
0.1519	-0.2087	-0.4505
0.2049	-0.2516	-0.3453
0.2580	-0.2906	-0.3012
0.3110	-0.2955	-0.2270
0.3640	-0.2947	-0.1593
0.4170	-0.2919	-0.0888
0.4670	-0.2805	-0.0255
0.5230	-0.2707	0.0222
0.5760	-0.2484	0.0518
0.6290	-0.2435	0.0727
0.6820	-0.2422	0.0857
0.7350	-0.2473	0.0011
0.7880	-0.2349	-0.2066
0.8410	-0.2902	-0.2237
1.0000	0.0000	0.0000

q_∞ = 245 Pa, NPR 4.0

$C_{P\,(root)}$	
upper	lower
0.7728	0.7728
-0.2626	-0.4718
-0.3272	-0.3088
-0.3870	-0.2849
-0.4084	-0.2409
-0.4231	-0.2725
-0.4050	-0.2019
-0.3852	-0.1379
-0.3651	-0.0641
-0.3496	-0.0103
-0.3253	0.0302
-0.2988	0.0582
-0.2857	0.0883
-0.2839	0.0962
-0.2892	-0.0089
-0.3281	-0.2349
-0.3410	-0.3239
0.0000	0.0000

q_∞ = 551 Pa, NPR 4.0

$C_{P\,(root)}$	
upper	lower
0.8424	0.8424
-0.2924	-0.4363
-0.3399	-0.2915
-0.3931	-0.2716
-0.4070	-0.2438
-0.4135	-0.2749
-0.3884	-0.2186
-0.3659	-0.1599
-0.3444	-0.0863
-0.3237	-0.0295
-0.3037	0.0130
-0.2722	0.0440
-0.2617	0.0738
-0.2641	0.0900
-0.2790	-0.0098
-0.3272	-0.2287
-0.3204	-0.3136
0.0000	0.0000

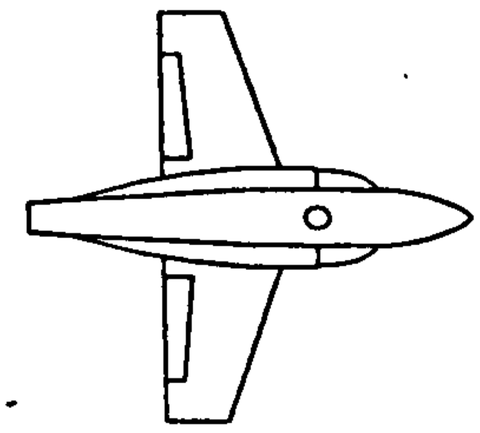

q_∞ = 61.3 Pa, NPR 1.586

	$C_{P\,(root)}$	
x/chord	upper	lower
0.0000	0.7864	0.7864
0.0459	-0.2707	-0.4804
0.0989	-0.3412	-0.3379
0.1519	-0.4041	-0.3086
0.2049	-0.4350	-0.2766
0.2580	-0.4467	-0.2439
0.3110	-0.4326	-0.2157
0.3640	-0.4104	-0.1502
0.4170	-0.3945	-0.0753
0.4670	-0.3743	-0.0097
0.5230	-0.3474	0.0316
0.5760	-0.3217	0.0599
0.6290	-0.3087	0.0868
0.6820	-0.3021	0.0895
0.7350	-0.3108	-0.0179
0.7880	-0.3806	-0.2308
0.8410	-0.3558	-0.3224
1.0000	0.0000	0.0000

q_∞=245 Pa, NPR 1.586

$C_{P\,(root)}$	
upper	lower
0.8618	0.8618
-0.3044	-0.4046
-0.3604	-0.2885
-0.4235	-0.2716
-0.4403	-0.2521
-0.4515	-0.2241
-0.4321	-0.2184
-0.4100	-0.1499
-0.3905	-0.0692
-0.3689	-0.0128
-0.3433	0.0292
-0.3127	0.0598
-0.2963	0.0903
-0.2896	0.1005
-0.2922	-0.0104
-0.3493	-0.2410
-0.3520	-0.3296
0.0000	0.0000

q_∞=551 Pa, NPR 1.586

$C_{P\,(root)}$	
upper	lower
0.8998	0.8998
-0.3616	-0.3486
-0.3946	-0.2491
-0.4417	-0.2531
-0.4523	-0.2407
-0.4593	-0.2204
-0.4346	-0.2075
-0.4108	-0.1830
-0.3854	-0.0860
-0.3642	-0.0359
-0.3395	0.0074
-0.3066	0.0350
-0.2885	0.0717
-0.2885	0.0877
-0.2963	-0.0155
-0.3402	-0.2336
-0.3397	-0.3201
0.0000	0.0000

q_∞ = 61.3 Pa, NPR 2.0

	$C_{P\,(root)}$	
x/chord	upper	lower
0.0000	0.6978	0.6978
0.0459	-0.1838	-0.5029
0.0989	-0.2650	-0.3331
0.1519	-0.3289	-0.3045
0.2049	-0.3555	-0.2687
0.2580	-0.3664	-0.2253
0.3110	-0.3567	-0.1868
0.3640	-0.3477	-0.1207
0.4170	-0.3321	-0.0474
0.4670	-0.3148	0.0166
0.5230	-0.2888	0.0568
0.5760	-0.2691	0.0844
0.6290	-0.2555	0.1114
0.6820	-0.2444	0.1168
0.7350	-0.2500	0.0210
0.7880	-0.2982	-0.1921
0.8410	-0.3066	-0.2591
1.0000	0.0000	0.0000

q_∞ = 245 Pa, NPR 2.0

$C_{P\,(root)}$	
upper	lower
0.8212	0.8212
-0.2748	-0.4326
-0.3330	-0.2974
-0.3921	-0.2811
-0.4076	-0.2491
-0.4209	-0.2431
-0.4035	-0.2053
-0.3820	-0.1397
-0.3599	-0.0618
-0.3411	-0.0039
-0.3118	0.0370
-0.2856	0.0672
-0.2703	0.0977
-0.2625	0.1065
-0.2735	0.0004
-0.3541	-0.2240
-0.3337	-0.3088
0.0000	0.0000

q_∞ = 551 Pa, NPR 2.0

$C_{P\,(root)}$	
upper	lower
0.8808	0.8808
-0.3561	-0.3647
-0.3859	-0.2717
-0.4326	-0.2617
-0.4440	-0.2533
-0.4451	-0.2427
-0.4194	-0.2157
-0.3932	-0.1847
-0.3692	-0.0958
-0.3504	-0.0416
-0.3249	0.0025
-0.2915	0.0302
-0.2767	0.0655
-0.2769	0.0822
-0.2857	-0.0177
-0.3502	-0.2285
-0.3319	-0.3153
0.0000	0.0000

q_∞ = 61.3 Pa, NPR 3.0

	$C_{P\,(root)}$	
x/chord	upper	lower
0.0000	0.5192	0.5192
0.0459	-0.1505	-0.7130
0.0989	-0.2433	-0.4667
0.1519	-0.3179	-0.4190
0.2049	-0.3536	-0.3601
0.2580	-0.3736	-0.3354
0.3110	-0.3687	-0.2561
0.3640	-0.3548	-0.1793
0.4170	-0.3433	-0.0992
0.4670	-0.3307	-0.0337
0.5230	-0.3111	0.0159
0.5760	-0.2898	0.0464
0.6290	-0.2748	0.0727
0.6820	-0.2707	0.0828
0.7350	-0.2789	-0.0085
0.7880	-0.3229	-0.2426
0.8410	-0.3288	-0.2850
1.0000	0.0000	0.0000

q_∞ = 245 Pa, NPR 3.0

$C_{P\,(root)}$	
upper	lower
0.8183	0.8183
-0.2836	-0.4612
-0.3467	-0.3160
-0.4062	-0.2989
-0.4253	-0.2592
-0.4335	-0.2662
-0.4150	-0.2149
-0.3960	-0.1504
-0.3753	-0.0727
-0.3573	-0.0128
-0.3336	0.0278
-0.3091	0.0590
-0.2934	0.0907
-0.2856	0.0983
-0.2867	-0.0066
-0.3457	-0.2387
-0.3435	-0.3237
0.0000	0.0000

q_∞ = 551 Pa, NPR 3.0

$C_{P\,(root)}$	
upper	lower
0.8805	0.8805
-0.3401	-0.3786
-0.3756	-0.2766
-0.4222	-0.2671
-0.4330	-0.2530
-0.4353	-0.2670
-0.4084	-0.2232
-0.3827	-0.1743
-0.3566	-0.0946
-0.3369	-0.0404
-0.3141	0.0038
-0.2817	0.0327
-0.2686	0.0672
-0.2700	0.0852
-0.2785	-0.0158
-0.3244	-0.2305
-0.3252	-0.3140
0.0000	0.0000

q_∞ = 61.3 Pa, NPR 4.0

	$C_{P\,(root)}$	
x/chord	upper	lower
0.0000	0.1872	0.1872
0.0459	-0.0779	-0.8342
0.0989	-0.1753	-0.5311
0.1519	-0.2524	-0.4928
0.2049	-0.2858	-0.3975
0.2580	-0.3163	-0.3482
0.3110	-0.3166	-0.2700
0.3640	-0.3088	-0.1912
0.4170	-0.3020	-0.1073
0.4670	-0.2978	-0.0422
0.5230	-0.2833	0.0051
0.5760	-0.2644	0.0400
0.6290	-0.2521	0.0659
0.6820	-0.2540	0.0742
0.7350	-0.2623	-0.0126
0.7880	-0.2829	-0.2311
0.8410	-0.3079	-0.2365
1.0000	0.0000	0.0000

q_∞ = 245 Pa, NPR 4.0

$C_{P\,(root)}$	
upper	lower
0.8175	0.8175
-0.2808	-0.4834
-0.3434	-0.3216
-0.4023	-0.3097
-0.4259	-0.2553
-0.4354	-0.2847
-0.4165	-0.2197
-0.3985	-0.1487
-0.3787	-0.0738
-0.3631	-0.0146
-0.3387	0.0272
-0.3111	0.0586
-0.2973	0.0879
-0.2926	0.0972
-0.2915	-0.0056
-0.3488	-0.2457
-0.3509	-0.3310
0.0000	0.0000

q_∞ = 551 Pa, NPR 4.0

$C_{P\,(root)}$	
upper	lower
0.8640	0.8640
-0.3217	-0.4064
-0.3618	-0.2891
-0.4131	-0.2744
-0.4217	-0.2544
-0.4236	-0.2855
-0.4003	-0.2406
-0.3760	-0.1769
-0.3536	-0.1033
-0.3346	-0.0451
-0.3132	-0.0003
-0.2819	0.0302
-0.2695	0.0622
-0.2709	0.0804
-0.2802	-0.0173
-0.3210	-0.2342
-0.3234	-0.3192
0.0000	0.0000

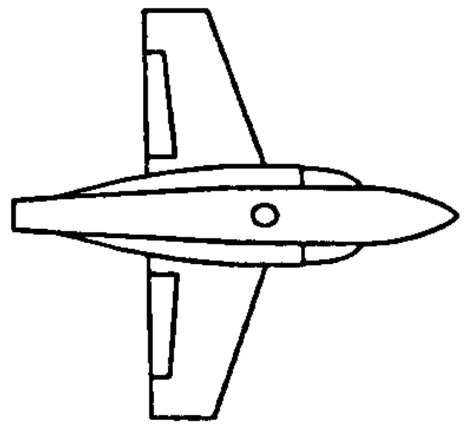

q_∞ = 61.3 Pa, NPR 1.586

	$C_{P\,(root)}$	
x/chord	upper	lower
0.0000	0.7968	0.7968
0.0459	-0.2629	-0.4733
0.0989	-0.3432	-0.3429
0.1519	-0.3945	-0.3203
0.2049	-0.4285	-0.2904
0.2580	-0.4350	-0.2575
0.3110	-0.4169	-0.2317
0.3640	-0.4030	-0.1714
0.4170	-0.3823	-0.0973
0.4670	-0.3615	-0.0325
0.5230	-0.3351	0.0142
0.5760	-0.3122	0.0455
0.6290	-0.2898	0.0749
0.6820	-0.2867	0.0812
0.7350	-0.3098	-0.0173
0.7880	-0.2149	-0.2361
0.8410	-0.3509	-0.3160
1.0000	0.0000	0.0000

q_∞=245 Pa, NPR 1.586

$C_{P\,(root)}$	
upper	lower
0.8900	0.8900
-0.3277	-0.3607
-0.3735	-0.2581
-0.4287	-0.2521
-0.4456	-0.2433
-0.4526	-0.2158
-0.4317	-0.2199
-0.4102	-0.1517
-0.3908	-0.0725
-0.3679	-0.0176
-0.3387	0.0246
-0.3110	0.0558
-0.2963	0.0891
-0.2897	0.0977
-0.2946	-0.0145
-0.3183	-0.2404
-0.3459	-0.3315
0.0000	0.0000

q_∞=551 Pa, NPR 1.586

$C_{P\,(root)}$	
upper	lower
0.9065	0.9065
-0.3677	-0.3191
-0.3969	-0.2359
-0.4436	-0.2456
-0.4547	-0.2327
-0.4589	-0.2198
-0.4346	-0.2070
-0.4093	-0.1857
-0.3826	-0.0934
-0.3626	-0.0419
-0.3395	0.0013
-0.3037	0.0292
-0.2871	0.0649
-0.2863	0.0827
-0.2936	-0.0203
-0.3513	-0.2326
-0.3374	-0.3194
0.0000	0.0000

q_∞ = 61.3 Pa, NPR 2.0

	$C_{P\,(root)}$	
x/chord	upper	lower
0.0000	0.7155	0.7155
0.0459	-0.2394	-0.5853
0.0989	-0.3289	-0.4237
0.1519	-0.3870	-0.3942
0.2049	-0.4218	-0.3514
0.2580	-0.4332	-0.3314
0.3110	-0.4235	-0.2810
0.3640	-0.4033	-0.2090
0.4170	-0.3864	-0.1241
0.4670	-0.3659	-0.0548
0.5230	-0.3432	-0.0037
0.5760	-0.3172	0.0268
0.6290	-0.3099	0.0587
0.6820	-0.2985	0.0648
0.7350	-0.2996	-0.0354
0.7880	-0.3901	-0.2511
0.8410	-0.3595	-0.3227
1.0000	0.0000	0.0000

q_∞ = 245 Pa, NPR 2.0

$C_{P\,(root)}$	
upper	lower
0.8721	0.8721
-0.3120	-0.4054
-0.3599	-0.2850
-0.4167	-0.2808
-0.4348	-0.2559
-0.4447	-0.2471
-0.4243	-0.2216
-0.4037	-0.1587
-0.3841	-0.0801
-0.3618	-0.0214
-0.3326	0.0227
-0.3038	0.0542
-0.2876	0.0872
-0.2814	0.0977
-0.2856	-0.0110
-0.3481	-0.2405
-0.3504	-0.3280
0.0000	0.0000

q_∞ = 551 Pa, NPR 2.0

$C_{P\,(root)}$	
upper	lower
0.9130	0.9130
-0.3853	-0.3256
-0.4065	-0.2424
-0.4490	-0.2516
-0.4559	-0.2430
-0.4579	-0.2335
-0.4309	-0.2191
-0.4051	-0.1951
-0.3773	-0.1007
-0.3574	-0.0486
-0.3345	-0.0048
-0.3001	0.0229
-0.2857	0.0612
-0.2845	0.0796
-0.2931	-0.0244
-0.3389	-0.2396
-0.3393	-0.3279
0.0000	0.0000

q_∞ = 61.3 Pa, NPR 3.0

	$C_{P\,(root)}$	
x/chord	upper	lower
0.0000	0.5380	0.5380
0.0459	-0.1452	-0.7117
0.0989	-0.2304	-0.4851
0.1519	-0.3011	-0.4238
0.2049	-0.3295	-0.3723
0.2580	-0.3522	-0.3662
0.3110	-0.3484	-0.2925
0.3640	-0.3377	-0.2061
0.4170	-0.3207	-0.1194
0.4670	-0.3123	-0.0529
0.5230	-0.2873	-0.0048
0.5760	-0.2644	0.0353
0.6290	-0.2585	0.0657
0.6820	-0.2503	0.0790
0.7350	-0.2553	-0.0145
0.7880	-0.3326	-0.2277
0.8410	-0.3101	-0.2700
1.0000	0.0000	0.0000

q_∞ = 245 Pa, NPR 3.0

$C_{P\,(root)}$	
upper	lower
0.8463	0.8463
-0.3039	-0.4236
-0.3530	-0.3025
-0.4083	-0.2953
-0.4300	-0.2614
-0.4333	-0.2742
-0.4135	-0.2263
-0.3942	-0.1647
-0.3720	-0.0851
-0.3549	-0.0274
-0.3292	0.0163
-0.2998	0.0502
-0.2846	0.0827
-0.2810	0.0927
-0.2837	-0.0108
-0.3489	-0.2381
-0.3407	-0.3287
0.0000	0.0000

q_∞ = 551 Pa, NPR 3.0

$C_{P\,(root)}$	
upper	lower
0.9212	0.9212
-0.3726	-0.3377
-0.3935	-0.2486
-0.4372	-0.2526
-0.4446	-0.2442
-0.4454	-0.2571
-0.4191	-0.2212
-0.3916	-0.1744
-0.3642	-0.0915
-0.3442	-0.0362
-0.3216	0.0090
-0.2868	0.0388
-0.2746	0.0775
-0.2746	0.0970
-0.2853	-0.0095
-0.3382	-0.2371
-0.3334	-0.3227
0.0000	0.0000

q_∞ = 61.3 Pa, NPR 4.0

	$C_{P\,(root)}$	
x/chord	upper	lower
0.0000	0.3361	0.3361
0.0459	-0.1667	-0.9010
0.0989	-0.2633	-0.6550
0.1519	-0.3396	-0.6231
0.2049	-0.3761	-0.4779
0.2580	-0.4024	-0.4864
0.3110	-0.3998	-0.4062
0.3640	-0.3904	-0.2949
0.4170	-0.3734	-0.2012
0.4670	-0.3698	-0.1264
0.5230	-0.3446	-0.0833
0.5760	-0.3256	-0.0418
0.6290	-0.3192	-0.0050
0.6820	-0.3110	0.0082
0.7350	-0.3259	-0.0878
0.7880	-0.3906	-0.3337
0.8410	-0.3728	-0.3279
1.0000	0.0000	0.0000

q_∞ = 245 Pa, NPR 4.0

$C_{P\,(root)}$	
upper	lower
0.8398	0.8398
-0.3098	-0.4576
-0.3665	-0.3177
-0.4237	-0.3155
-0.4416	-0.2708
-0.4482	-0.3121
-0.4268	-0.2431
-0.4034	-0.1774
-0.3838	-0.0971
-0.3673	-0.0331
-0.3424	0.0122
-0.3148	0.0462
-0.3004	0.0780
-0.2965	0.0950
-0.2983	-0.0134
-0.3490	-0.2489
-0.3488	-0.3366
0.0000	0.0000

q_∞ = 551 Pa, NPR 4.0

$C_{P\,(root)}$	
upper	lower
0.8943	0.8943
-0.3557	-0.3584
-0.3855	-0.2638
-0.4290	-0.2614
-0.4373	-0.2461
-0.4389	-0.2697
-0.4134	-0.2350
-0.3885	-0.1769
-0.3631	-0.1004
-0.3434	-0.0427
-0.3203	0.0015
-0.2848	0.0312
-0.2720	0.0672
-0.2695	0.0880
-0.2817	-0.0114
-0.3264	-0.2320
-0.3237	-0.3194
0.0000	0.0000

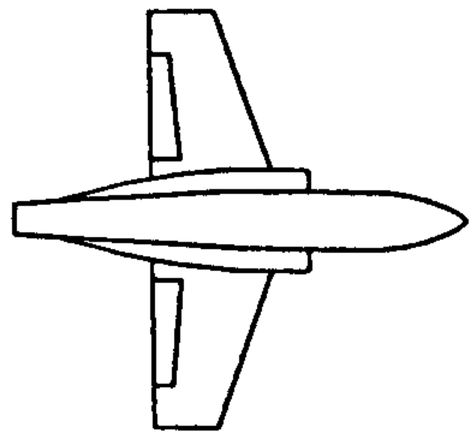

q_∞ = 61.3 Pa, NPR 1.0

	$C_{P\,(root)}$	
x/chord	upper	lower
0.0000	1.0086	1.0086
0.0459	-0.2147	0.0391
0.0989	-0.2458	0.0453
0.1519	-0.3510	0.0397
0.2049	-0.3976	0.0354
0.2580	-0.4132	0.0293
0.3110	-0.4081	0.0296
0.3640	-0.3966	0.0417
0.4170	-0.3921	0.0721
0.4670	-0.3636	0.0796
0.5230	-0.2944	0.1039
0.5760	-0.2777	0.1224
0.6290	-0.2600	0.1606
0.6820	-0.2516	0.1831
0.7350	-0.2598	0.0611
0.7880	-0.3786	-0.1909
0.8410	-0.3951	-0.2696
1.0000	0.0000	0.0000

q_∞ = 245 Pa, NPR 1.0

$C_{P\,(root)}$	
upper	lower
0.9470	0.9470
-0.2993	-0.1074
-0.3331	-0.0639
-0.3917	-0.0870
-0.4265	-0.0733
-0.4329	-0.0704
-0.4241	-0.1158
-0.3981	-0.0439
-0.3689	0.0154
-0.3561	0.0627
-0.3294	0.1056
-0.3097	0.1170
-0.2896	0.1470
-0.2802	0.1516
-0.2922	0.0279
-0.3505	-0.1998
-0.3575	-0.3139
0.0000	0.0000

q_∞ = 551 Pa, NPR 1.0

$C_{P\,(root)}$	
upper	lower
0.9303	0.9303
-0.3602	-0.1625
-0.3792	-0.1177
-0.4277	-0.1332
-0.4398	-0.1302
-0.4453	-0.1193
-0.4279	-0.1465
-0.4017	-0.0952
-0.3789	-0.0237
-0.3582	0.0156
-0.3310	0.0502
-0.3008	0.0705
-0.2809	0.1088
-0.2782	0.1172
-0.2891	0.0071
-0.3523	-0.2159
-0.3488	-0.3117
0.0000	0.0000

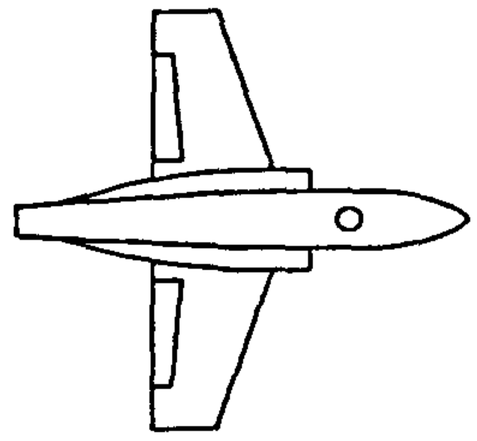

q_∞ = 61.3 Pa, NPR 1.586

	$C_{P\,(root)}$	
x/chord	upper	lower
0.0000	0.9826	0.9826
0.0459	-0.0346	-0.3038
0.0989	-0.1316	-0.0997
0.1519	-0.3054	-0.0671
0.2049	-0.3150	-0.0488
0.2580	-0.3442	-0.0523
0.3110	-0.3427	-0.0454
0.3640	-0.3305	-0.0389
0.4170	-0.3217	-0.0007
0.4670	-0.3142	0.0079
0.5230	-0.3122	0.0135
0.5760	-0.3082	0.0487
0.6290	-0.3023	0.1225
0.6820	-0.3011	0.1454
0.7350	-0.3060	0.0043
0.7880	-0.3161	-0.2182
0.8410	-0.3548	-0.3103
1.0000	0.0000	0.0000

q_∞=245 Pa, NPR 1.586

$C_{P\,(root)}$	
upper	lower
0.8690	0.8690
-0.1662	-0.2948
-0.2571	-0.1891
-0.3399	-0.1811
-0.3695	-0.1614
-0.3910	-0.1463
-0.3730	-0.1544
-0.3624	-0.1194
-0.3528	-0.0429
-0.3249	0.0249
-0.2939	0.0460
-0.2779	0.0973
-0.2693	0.1113
-0.2580	0.1178
-0.2697	0.0205
-0.3194	-0.2108
-0.3441	-0.3098
0.0000	0.0000

q_∞=551 Pa, NPR 1.586

$C_{P\,(root)}$	
upper	lower
0.8789	0.8789
-0.2673	-0.3216
-0.3157	-0.2226
-0.3838	-0.2263
-0.4086	-0.2184
-0.4196	-0.1990
-0.4016	-0.1818
-0.3789	-0.1509
-0.3580	-0.0703
-0.3413	-0.0072
-0.3134	0.0203
-0.2827	0.0444
-0.2730	0.0800
-0.2738	0.1044
-0.2823	-0.0009
-0.3432	-0.2241
-0.3386	-0.3095
0.0000	0.0000

q_∞ = 61.3 Pa, NPR 2.0

	$C_{P\,(root)}$	
x/chord	upper	lower
0.0000	0.8271	0.8271
0.0459	-0.0284	-0.3529
0.0989	-0.0871	-0.2105
0.1519	-0.3218	-0.1344
0.2049	-0.3431	-0.1160
0.2580	-0.3487	-0.0882
0.3110	-0.3486	-0.0817
0.3640	-0.3482	-0.0639
0.4170	-0.3476	-0.0317
0.4670	-0.3460	-0.0178
0.5230	-0.3395	0.0085
0.5760	-0.3359	0.0684
0.6290	-0.3317	0.1148
0.6820	-0.3336	0.1158
0.7350	-0.3245	-0.0222
0.7880	-0.3438	-0.2178
0.8410	-0.3791	-0.3389
1.0000	0.0000	0.0000

q_∞ = 245 Pa, NPR 2.0

$C_{P\,(root)}$	
upper	lower
0.8149	0.8149
-0.1630	-0.3594
-0.2509	-0.2295
-0.3412	-0.2071
-0.3838	-0.1843
-0.3949	-0.1710
-0.3883	-0.1628
-0.3815	-0.1215
-0.3559	-0.0475
-0.3397	0.0088
-0.3089	0.0658
-0.2960	0.0800
-0.2743	0.1034
-0.2666	0.1146
-0.2849	0.0067
-0.3379	-0.2196
-0.3558	-0.3192
0.0000	0.0000

q_∞ = 551 Pa, NPR 2.0

$C_{P\,(root)}$	
upper	lower
0.8838	0.8838
-0.2804	-0.3429
-0.3259	-0.2372
-0.3862	-0.2419
-0.4084	-0.2346
-0.4170	-0.2163
-0.3930	-0.2035
-0.3719	-0.1550
-0.3481	-0.0785
-0.3310	-0.0182
-0.3029	0.0087
-0.2795	0.0367
-0.2724	0.0729
-0.2745	0.0943
-0.2828	-0.0100
-0.3356	-0.2320
-0.3424	-0.3173
0.0000	0.0000

q_∞ = 61.3 Pa, NPR 3.0

	$C_{P\,(root)}$	
x/chord	upper	lower
0.0000	0.4168	0.4168
0.0459	0.0446	-0.5551
0.0989	-0.0519	-0.3170
0.1519	-0.1950	-0.2913
0.2049	-0.3107	-0.2375
0.2580	-0.3234	-0.2246
0.3110	-0.3265	-0.1155
0.3640	-0.3274	-0.0608
0.4170	-0.3262	-0.0293
0.4670	-0.3261	-0.0064
0.5230	-0.3199	0.0131
0.5760	-0.3174	0.0348
0.6290	-0.3108	0.0939
0.6820	-0.3086	0.1104
0.7350	-0.3112	-0.0113
0.7880	-0.3216	-0.2894
0.8410	-0.3620	-0.3243
1.0000	0.0000	0.0000

q_∞ = 245 Pa, NPR 3.0

$C_{P\,(root)}$	
upper	lower
0.8236	0.8236
-0.1602	-0.3500
-0.2543	-0.2114
-0.3438	-0.2114
-0.3799	-0.1800
-0.3889	-0.1786
-0.3813	-0.1546
-0.3738	-0.1167
-0.3560	-0.0427
-0.3379	0.0146
-0.3078	0.0610
-0.2953	0.0849
-0.2869	0.1013
-0.2810	0.1133
-0.2928	0.0119
-0.3464	-0.2212
-0.3631	-0.3144
0.0000	0.0000

q_∞ = 551 Pa, NPR 3.0

$C_{P\,(root)}$	
upper	lower
0.8872	0.8872
-0.2726	-0.3374
-0.3145	-0.2359
-0.3774	-0.2386
-0.3913	-0.2238
-0.4041	-0.2430
-0.3794	-0.1947
-0.3581	-0.1520
-0.3326	-0.0796
-0.3168	-0.0152
-0.2890	0.0195
-0.2685	0.0427
-0.2549	0.0798
-0.2603	0.1010
-0.2773	-0.0041
-0.3260	-0.2293
-0.3253	-0.3166
0.0000	0.0000

q_∞ = 61.3 Pa, NPR 4.0

	$C_{P\,(root)}$	
x/chord	upper	lower
0.0000	0.1145	0.1145
0.0459	0.0954	-0.7414
0.0989	-0.0197	-0.4032
0.1519	-0.0972	-0.3450
0.2049	-0.2211	-0.2700
0.2580	-0.2730	-0.2704
0.3110	-0.3008	-0.1643
0.3640	-0.3192	-0.0966
0.4170	-0.3162	-0.0476
0.4670	-0.3092	-0.0175
0.5230	-0.2894	0.0303
0.5760	-0.2573	0.0551
0.6290	-0.2586	0.0953
0.6820	-0.2454	0.0982
0.7350	-0.2883	-0.0204
0.7880	-0.3447	-0.2567
0.8410	-0.3421	-0.2931
1.0000	0.0000	0.0000

q_∞ = 245 Pa, NPR 4.0

$C_{P\,(root)}$	
upper	lower
0.8047	0.8047
-0.1615	-0.3525
-0.2486	-0.2119
-0.3398	-0.2197
-0.3745	-0.1767
-0.3875	-0.2168
-0.3822	-0.1560
-0.3724	-0.1249
-0.3515	-0.0498
-0.3392	0.0118
-0.3122	0.0507
-0.2914	0.0813
-0.2827	0.0973
-0.2791	0.1102
-0.2952	0.0044
-0.3431	-0.2246
-0.3609	-0.3288
0.0000	0.0000

q_∞ = 551 Pa, NPR 4.0

$C_{P\,(root)}$	
upper	lower
0.8644	0.8644
-0.2483	-0.3408
-0.2917	-0.2400
-0.3584	-0.2358
-0.3783	-0.2174
-0.3909	-0.2472
-0.3675	-0.1966
-0.3449	-0.1487
-0.3213	-0.0745
-0.3083	-0.0140
-0.2865	0.0241
-0.2629	0.0455
-0.2519	0.0800
-0.2572	0.0994
-0.2787	-0.0050
-0.3268	-0.2252
-0.3231	-0.3115
0.0000	0.0000

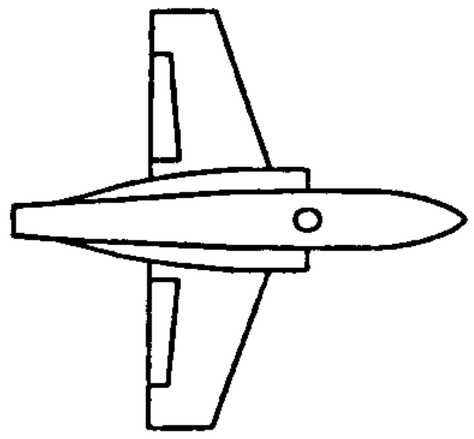

q_∞ = 61.3 Pa, NPR 1.586

	$C_{P\ (root)}$	
x/chord	upper	lower
0.0000	0.7971	0.7971
0.0459	0.0278	-0.2347
0.0989	-0.1341	-0.1124
0.1519	-0.2355	-0.0862
0.2049	-0.2719	-0.0508
0.2580	-0.3140	-0.0461
0.3110	-0.3209	0.0001
0.3640	-0.2989	0.0242
0.4170	-0.2778	0.0398
0.4670	-0.2658	0.0758
0.5230	-0.2421	0.0826
0.5760	-0.2352	0.0881
0.6290	-0.2348	0.1336
0.6820	-0.2336	0.1785
0.7350	-0.2352	0.0725
0.7880	-0.2241	-0.1779
0.8410	-0.3234	-0.2390
1.0000	0.0000	0.0000

q_∞=245 Pa, NPR 1.586

$C_{P\ (root)}$	
upper	lower
0.8694	0.8694
-0.2168	-0.2785
-0.2906	-0.1808
-0.3671	-0.1898
-0.3911	-0.1756
-0.4105	-0.1548
-0.3923	-0.1683
-0.3804	-0.1332
-0.3714	-0.0585
-0.3429	0.0077
-0.3138	0.0330
-0.2956	0.0810
-0.2801	0.0951
-0.2723	0.1129
-0.2842	0.0068
-0.3389	-0.2228
-0.3574	-0.3204
0.0000	0.0000

q_∞=551 Pa, NPR 1.586

$C_{P\ (root)}$	
upper	lower
0.8925	0.8925
-0.2946	-0.2936
-0.3397	-0.2149
-0.4010	-0.2255
-0.4195	-0.2159
-0.4288	-0.1995
-0.4086	-0.1865
-0.3843	-0.1684
-0.3646	-0.0789
-0.3467	-0.0212
-0.3209	0.0112
-0.2881	0.0389
-0.2778	0.0777
-0.2790	0.0975
-0.2873	-0.0071
-0.3537	-0.2295
-0.3464	-0.3170
0.0000	0.0000

q_∞ = 61.3 Pa, NPR 2.0

	$C_{P\ (root)}$	
x/chord	upper	lower
0.0000	0.6461	0.6461
0.0459	-0.0486	-0.4213
0.0989	-0.1545	-0.2064
0.1519	-0.2793	-0.1879
0.2049	-0.3346	-0.1792
0.2580	-0.4134	-0.1578
0.3110	-0.4180	-0.1528
0.3640	-0.3971	-0.1446
0.4170	-0.3807	-0.0710
0.4670	-0.3486	0.0584
0.5230	-0.3177	0.1111
0.5760	-0.3068	0.1163
0.6290	-0.3026	0.1214
0.6820	-0.2974	0.1289
0.7350	-0.3017	0.0347
0.7880	-0.4430	-0.1982
0.8410	-0.4550	-0.3132
1.0000	0.0000	0.0000

q_∞ = 245 Pa, NPR 2.0

$C_{P\ (root)}$	
upper	lower
0.8515	0.8515
-0.2028	-0.3330
-0.2868	-0.2271
-0.3536	-0.2278
-0.4007	-0.2077
-0.4169	-0.1847
-0.4100	-0.1831
-0.3816	-0.1159
-0.3539	-0.0432
-0.3432	-0.0087
-0.3235	0.0432
-0.2970	0.0565
-0.2795	0.1164
-0.2720	0.1213
-0.2844	-0.0109
-0.3375	-0.2311
-0.3481	-0.3341
0.0000	0.0000

q_∞ = 551 Pa, NPR 2.0

$C_{P\ (root)}$	
upper	lower
0.8875	0.8875
-0.2901	-0.3186
-0.3344	-0.2352
-0.3986	-0.2476
-0.4190	-0.2390
-0.4269	-0.2273
-0.4033	-0.2103
-0.3850	-0.1680
-0.3626	-0.0889
-0.3410	-0.0378
-0.3198	0.0098
-0.2925	0.0255
-0.2737	0.0622
-0.2765	0.0873
-0.2904	-0.0188
-0.3517	-0.2364
-0.3460	-0.3253
0.0000	0.0000

q_∞ = 61.3 Pa, NPR 3.0

	$C_{P\,(root)}$	
x/chord	upper	lower
0.0000	0.3545	0.3545
0.0459	0.0602	-0.5710
0.0989	-0.0022	-0.3098
0.1519	-0.2026	-0.2736
0.2049	-0.2596	-0.2632
0.2580	-0.2666	-0.2485
0.3110	-0.2705	-0.1926
0.3640	-0.2690	-0.0843
0.4170	-0.2721	0.0007
0.4670	-0.2664	0.0285
0.5230	-0.2641	0.0491
0.5760	-0.2599	0.0549
0.6290	-0.2601	0.0644
0.6820	-0.2601	0.0788
0.7350	-0.2626	0.0300
0.7880	-0.2640	-0.2531
0.8410	-0.3124	-0.2653
1.0000	0.0000	0.0000

q_∞ = 245 Pa, NPR 3.0

$C_{P\,(root)}$	
upper	lower
0.8626	0.8626
-0.1613	-0.3341
-0.2537	-0.2079
-0.3340	-0.2115
-0.3608	-0.1788
-0.3765	-0.1867
-0.3648	-0.1454
-0.3551	-0.1172
-0.3406	-0.0392
-0.3229	0.0248
-0.2942	0.0493
-0.2720	0.1018
-0.2681	0.1175
-0.2604	0.1225
-0.2710	0.0282
-0.3101	-0.2035
-0.3417	-0.3017
0.0000	0.0000

q_∞ = 551 Pa, NPR 3.0

$C_{P\,(root)}$	
upper	lower
0.8936	0.8936
-0.2918	-0.3008
-0.3270	-0.2250
-0.3822	-0.2295
-0.4005	-0.2229
-0.4058	-0.2386
-0.3809	-0.2018
-0.3574	-0.1612
-0.3326	-0.0848
-0.3140	-0.0221
-0.2867	0.0074
-0.2681	0.0391
-0.2505	0.0757
-0.2564	0.1001
-0.2736	-0.0028
-0.3262	-0.2217
-0.3191	-0.3077
0.0000	0.0000

q_∞ = 61.3 Pa, NPR 4.0

	$C_{P\,(root)}$	
x/chord	upper	lower
0.0000	-0.0323	-0.0323
0.0459	0.0415	-0.8148
0.0989	-0.0146	-0.4591
0.1519	-0.0859	-0.4163
0.2049	-0.2260	-0.3390
0.2580	-0.2924	-0.3250
0.3110	-0.2917	-0.2848
0.3640	-0.3035	-0.1822
0.4170	-0.2987	-0.0754
0.4670	-0.3108	-0.0375
0.5230	-0.2891	-0.0180
0.5760	-0.2768	-0.0005
0.6290	-0.2612	0.0197
0.6820	-0.2643	0.0262
0.7350	-0.3018	-0.0327
0.7880	-0.2976	-0.2951
0.8410	-0.3331	-0.3032
1.0000	0.0000	0.0000

q_∞ = 245 Pa, NPR 4.0

$C_{P\,(root)}$	
upper	lower
0.8926	0.8926
-0.1831	-0.3248
-0.2696	-0.2049
-0.3565	-0.2208
-0.3886	-0.1786
-0.4022	-0.2277
-0.3901	-0.1629
-0.3766	-0.1157
-0.3548	-0.0441
-0.3472	0.0105
-0.3148	0.0673
-0.2885	0.0818
-0.2754	0.1135
-0.2743	0.1184
-0.2796	0.0087
-0.3462	-0.2235
-0.3570	-0.3401
0.0000	0.0000

q_∞ = 551 Pa, NPR 4.0

$C_{P\,(root)}$	
upper	lower
0.8692	0.8692
-0.2874	-0.3460
-0.3275	-0.2528
-0.3860	-0.2552
-0.4033	-0.2433
-0.4151	-0.2682
-0.3866	-0.2243
-0.3661	-0.1741
-0.3442	-0.1026
-0.3268	-0.0414
-0.3044	-0.0021
-0.2790	0.0287
-0.2721	0.0620
-0.2761	0.0745
-0.2844	-0.0193
-0.3421	-0.2428
-0.3378	-0.3269
0.0000	0.0000

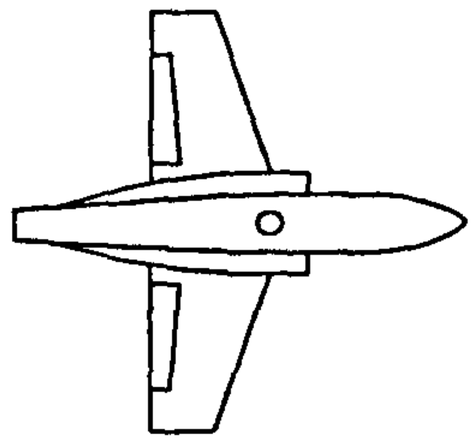

q_∞ = 61.3 Pa, NPR 1.586

	$C_{P\,(root)}$	
x/chord	upper	lower
0.0000	0.8321	0.8321
0.0459	-0.0650	-0.2909
0.0989	-0.1501	-0.1111
0.1519	-0.3284	-0.1039
0.2049	-0.3451	-0.0891
0.2580	-0.3599	-0.0915
0.3110	-0.3575	-0.0832
0.3640	-0.3511	-0.0743
0.4170	-0.3475	-0.0360
0.4670	-0.3463	-0.0248
0.5230	-0.3350	-0.0086
0.5760	-0.3220	0.0496
0.6290	-0.3295	0.1038
0.6820	-0.3241	0.1199
0.7350	-0.3315	-0.0193
0.7880	-0.3437	-0.1653
0.8410	-0.3663	-0.3365
1.0000	0.0000	0.0000

q_∞=245 Pa, NPR 1.586

$C_{P\,(root)}$	
upper	lower
0.9024	0.9024
-0.2322	-0.2480
-0.3067	-0.1704
-0.3801	-0.1773
-0.4019	-0.1707
-0.4255	-0.1590
-0.4026	-0.1742
-0.3888	-0.1394
-0.3780	-0.0630
-0.3496	0.0018
-0.3191	0.0341
-0.3011	0.0741
-0.2840	0.0936
-0.2749	0.1148
-0.2807	0.0031
-0.3569	-0.2256
-0.3525	-0.3236
0.0000	0.0000

q_∞=551 Pa, NPR 1.586

$C_{P\,(root)}$	
upper	lower
0.9226	0.9226
-0.3320	-0.2319
-0.3638	-0.1716
-0.4156	-0.2032
-0.4305	-0.2002
-0.4373	-0.1865
-0.4144	-0.1835
-0.3876	-0.1751
-0.3660	-0.0826
-0.3406	-0.0274
-0.3189	0.0077
-0.2819	0.0356
-0.2755	0.0761
-0.2752	0.0991
-0.2818	-0.0073
-0.3349	-0.2322
-0.3368	-0.3199
0.0000	0.0000

q_∞ = 61.3 Pa, NPR 2.0

	$C_{P\,(root)}$	
x/chord	upper	lower
0.0000	0.7310	0.7310
0.0459	-0.0375	-0.3500
0.0989	-0.0929	-0.2184
0.1519	-0.3271	-0.1995
0.2049	-0.3405	-0.1626
0.2580	-0.3496	-0.1136
0.3110	-0.3495	-0.0950
0.3640	-0.3470	-0.0772
0.4170	-0.3464	-0.0392
0.4670	-0.3425	-0.0260
0.5230	-0.3385	-0.0181
0.5760	-0.3363	0.0375
0.6290	-0.3211	0.1139
0.6820	-0.3330	0.0705
0.7350	-0.3357	-0.0230
0.7880	-0.3379	-0.1689
0.8410	-0.3658	-0.3359
1.0000	0.0000	0.0000

q_∞ = 245 Pa, NPR 2.0

$C_{P\,(root)}$	
upper	lower
0.8957	0.8957
-0.2198	-0.2832
-0.3016	-0.1807
-0.3722	-0.1902
-0.3947	-0.1849
-0.4090	-0.1743
-0.3938	-0.1708
-0.3835	-0.1402
-0.3585	-0.0626
-0.3414	0.0026
-0.3116	0.0487
-0.2977	0.0751
-0.2748	0.0956
-0.2624	0.1155
-0.2686	0.0036
-0.3278	-0.2225
-0.3513	-0.3228
0.0000	0.0000

q_∞ = 551 Pa, NPR 2.0

$C_{P\,(root)}$	
upper	lower
0.9037	0.9037
-0.3080	-0.2838
-0.3465	-0.2066
-0.4091	-0.2283
-0.4321	-0.2312
-0.4365	-0.2187
-0.4147	-0.2106
-0.3878	-0.1720
-0.3657	-0.0952
-0.3470	-0.0393
-0.3203	-0.0018
-0.2881	0.0297
-0.2812	0.0653
-0.2814	0.0780
-0.2889	-0.0200
-0.3536	-0.2417
-0.3461	-0.3274
0.0000	0.0000

q_∞ = 61.3 Pa, NPR 3.0

	$C_{P\,(root)}$	
x/chord	upper	lower
0.0000	0.5265	0.5265
0.0459	-0.0074	-0.5659
0.0989	-0.0641	-0.3635
0.1519	-0.2782	-0.3390
0.2049	-0.3207	-0.3256
0.2580	-0.3299	-0.3189
0.3110	-0.3319	-0.2796
0.3640	-0.3307	-0.1583
0.4170	-0.3286	-0.0650
0.4670	-0.3279	-0.0318
0.5230	-0.3245	-0.0039
0.5760	-0.3171	-0.0006
0.6290	-0.3169	0.0270
0.6820	-0.3123	0.0716
0.7350	-0.3091	-0.0177
0.7880	-0.3371	-0.2941
0.8410	-0.3671	-0.3279
1.0000	0.0000	0.0000

q_∞ = 245 Pa, NPR 3.0

$C_{P\,(root)}$	
upper	lower
0.8541	0.8541
-0.2092	-0.3364
-0.2858	-0.2219
-0.3682	-0.2310
-0.3895	-0.2225
-0.4075	-0.2200
-0.3942	-0.1790
-0.3806	-0.1483
-0.3655	-0.0706
-0.3450	-0.0186
-0.3134	0.0195
-0.2944	0.0596
-0.2887	0.0916
-0.2881	0.1006
-0.2933	-0.0028
-0.3565	-0.2320
-0.3673	-0.3358
0.0000	0.0000

q_∞ = 551 Pa, NPR 3.0

$C_{P\,(root)}$	
upper	lower
0.9038	0.9038
-0.3283	-0.2725
-0.3534	-0.2131
-0.4056	-0.2291
-0.4161	-0.2288
-0.4186	-0.2403
-0.3946	-0.2115
-0.3701	-0.1737
-0.3441	-0.0961
-0.3250	-0.0381
-0.2993	0.0019
-0.2749	0.0318
-0.2660	0.0677
-0.2688	0.0852
-0.2774	-0.0093
-0.3308	-0.2333
-0.3322	-0.3173
0.0000	0.0000

q_∞ = 61.3 Pa, NPR 4.0

	$C_{P\,(root)}$	
x/chord	upper	lower
0.0000	0.2193	0.2193
0.0459	0.0399	-0.8416
0.0989	-0.0723	-0.5600
0.1519	-0.2357	-0.5042
0.2049	-0.3183	-0.4543
0.2580	-0.3515	-0.4414
0.3110	-0.3679	-0.3661
0.3640	-0.3601	-0.2890
0.4170	-0.3562	-0.1804
0.4670	-0.3463	-0.1029
0.5230	-0.3290	-0.0549
0.5760	-0.3116	-0.0343
0.6290	-0.3168	-0.0097
0.6820	-0.3200	0.0119
0.7350	-0.3250	-0.0658
0.7880	-0.3642	-0.3493
0.8410	-0.4667	-0.3654
1.0000	0.0000	0.0000

q_∞ = 245 Pa, NPR 4.0

$C_{P\,(root)}$	
upper	lower
0.8616	0.8616
-0.2236	-0.3252
-0.2909	-0.2264
-0.3632	-0.2347
-0.3903	-0.2111
-0.4040	-0.2464
-0.3896	-0.1838
-0.3790	-0.1499
-0.3596	-0.0722
-0.3442	-0.0221
-0.3227	0.0259
-0.2876	0.0679
-0.2748	0.0901
-0.2757	0.1097
-0.2808	-0.0034
-0.3479	-0.2314
-0.3621	-0.3394
0.0000	0.0000

q_∞ = 551 Pa, NPR 4.0

$C_{P\,(root)}$	
upper	lower
0.9073	0.9073
-0.2961	-0.2685
-0.3304	-0.2067
-0.3786	-0.2130
-0.3944	-0.2126
-0.4019	-0.2346
-0.3751	-0.2053
-0.3492	-0.1582
-0.3257	-0.0831
-0.3078	-0.0253
-0.2820	0.0113
-0.2634	0.0430
-0.2497	0.0799
-0.2551	0.1032
-0.2683	0.0031
-0.3320	-0.2189
-0.3181	-0.3052
0.0000	0.0000

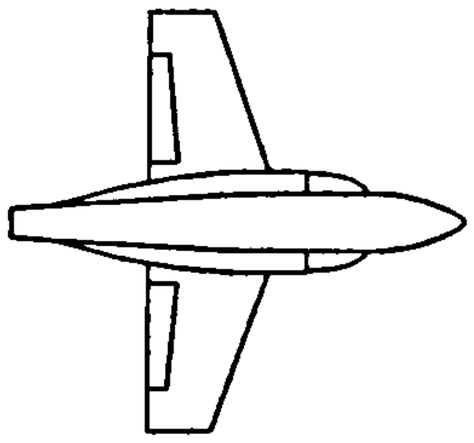

q_∞ = 61.3 Pa, NPR 1.0

	C_{Pi}	
x/d_e	lower outer	upper outer
0.0000	0.4328	0.0024
0.1189	-0.3013	-0.2636
0.2081	-0.3652	-0.3104
0.2973	-0.2699	-0.2091
0.3963	-0.1843	-0.1126
0.4954	-0.1178	-0.0520
0.5945	-0.0953	0.0311
0.6963	-0.0837	0.1193
0.7927	-0.0592	0.2035
0.8918	-0.0531	0.2856
0.9908	-0.0545	0.3665
1.0899	-0.0467	0.4369

q_∞ = 245 Pa, NPR 1.0

C_{Pi}	
lower outer	upper outer
0.5087	-0.0033
-0.3432	-0.2993
-0.4181	-0.3630
-0.2952	-0.2492
-0.1859	-0.1298
-0.1261	-0.0351
-0.0947	0.0458
-0.0846	0.1253
-0.0660	0.2127
-0.0523	0.3190
-0.0698	0.4081
-0.0490	0.4670

q_∞ = 551 Pa, NPR 1.0

C_{Pi}	
lower outer	upper outer
0.5255	-0.0080
-0.3682	-0.3304
-0.4433	-0.3899
-0.3079	-0.2672
-0.1836	-0.1367
-0.1276	-0.0459
-0.0980	0.0319
-0.0930	0.1160
-0.0702	0.2076
-0.0550	0.3174
-0.0782	0.4134
-0.0564	0.4672

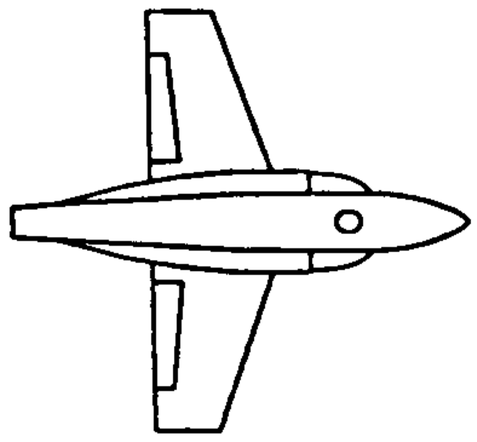

q_∞ = 61.3 Pa, NPR 1.586

	C_{Pi}	
x/d_{ie}	lower outer	upper outer
0.0000	0.1205	-0.0261
0.1189	-0.6224	-0.2843
0.2081	-0.5981	-0.3654
0.2973	-0.5088	-0.2267
0.3963	-0.4079	-0.1444
0.4954	-0.3362	-0.0733
0.5945	-0.2890	-0.0168
0.6963	-0.2631	0.0640
0.7927	-0.2337	0.1806
0.8918	-0.2030	0.2842
0.9908	-0.1931	0.3635
1.0899	-0.1821	0.4406

q_∞=245 Pa, NPR 1.586

C_{Pi}	
lower outer	upper outer
0.4238	-0.0065
-0.6003	-0.3198
-0.6447	-0.3862
-0.4956	-0.2719
-0.3584	-0.1548
-0.2957	-0.0575
-0.2554	0.0209
-0.2416	0.1075
-0.2096	0.1925
-0.1885	0.3058
-0.2027	0.4060
-0.1743	0.4669

q_∞=551 Pa, NPR 1.586

C_{Pi}	
lower outer	upper outer
0.4742	-0.0102
-0.6078	-0.3559
-0.6687	-0.4182
-0.4992	-0.2910
-0.3461	-0.1609
-0.2878	-0.0644
-0.2463	0.0139
-0.2356	0.1000
-0.2019	0.1927
-0.1780	0.3060
-0.2012	0.4060
-0.1683	0.4623

q_∞ = 61.3 Pa, NPR 2.0

	C_{Pi}	
x/d_{ie}	lower outer	upper outer
0.0000	-0.0302	-0.0180
0.1189	-0.6735	-0.2765
0.2081	-0.6460	-0.3528
0.2973	-0.5635	-0.2473
0.3963	-0.4423	-0.1588
0.4954	-0.3782	-0.0884
0.5945	-0.3494	-0.0108
0.6963	-0.3160	0.0649
0.7927	-0.2774	0.1423
0.8918	-0.2400	0.2522
0.9908	-0.2407	0.3399
1.0899	-0.2221	0.4138

q_∞ = 245 Pa, NPR 2.0

C_{Pi}	
lower outer	upper outer
0.3786	-0.0043
-0.6005	-0.3209
-0.6342	-0.3818
-0.4888	-0.2662
-0.3522	-0.1521
-0.2960	-0.0639
-0.2575	0.0165
-0.2396	0.0993
-0.2082	0.1878
-0.1897	0.2949
-0.2005	0.3979
-0.1701	0.4587

q_∞ = 551 Pa, NPR 2.0

C_{Pi}	
lower outer	upper outer
0.4566	-0.0102
-0.6182	-0.3667
-0.6786	-0.4279
-0.5073	-0.3022
-0.3545	-0.1677
-0.2946	-0.0738
-0.2558	0.0046
-0.2433	0.0906
-0.2099	0.1856
-0.1850	0.2972
-0.2085	0.3959
-0.1761	0.4522

q_∞ = 61.3 Pa, NPR 3.0

	C_{Pi}	
x/d_e	lower outer	upper outer
0.0000	-0.1527	0.0009
0.1189	-0.8045	-0.3053
0.2081	-0.7713	-0.3914
0.2973	-0.6580	-0.2699
0.3963	-0.5387	-0.1840
0.4954	-0.4725	-0.0984
0.5945	-0.4383	-0.0261
0.6963	-0.3871	0.0460
0.7927	-0.3562	0.1164
0.8918	-0.3432	0.2497
0.9908	-0.3338	0.3374
1.0899	-0.3144	0.4204

q_∞ = 245 Pa, NPR 3.0

C_{Pi}	
lower outer	upper outer
0.3739	-0.0085
-0.5935	-0.3279
-0.6213	-0.3974
-0.4769	-0.2769
-0.3465	-0.1612
-0.2861	-0.0697
-0.2476	0.0112
-0.2269	0.0925
-0.1984	0.1827
-0.1680	0.2915
-0.1836	0.3942
-0.1571	0.4581

q_∞ = 551 Pa, NPR 3.0

C_{Pi}	
lower outer	upper outer
0.4689	-0.0149
-0.6158	-0.3740
-0.6675	-0.4363
-0.4986	-0.3105
-0.3479	-0.1751
-0.2863	-0.0803
-0.2499	-0.0033
-0.2361	0.0845
-0.2010	0.1764
-0.1758	0.2912
-0.2030	0.3898
-0.1685	0.4480

q_∞ = 61.3 Pa, NPR 4.0

	C_{Pi}	
x/d_e	lower outer	upper outer
0.0000	-0.2947	0.0068
0.1189	-0.8834	-0.2856
0.2081	-0.8608	-0.3466
0.2973	-0.7267	-0.2484
0.3963	-0.6061	-0.1429
0.4954	-0.5237	-0.0833
0.5945	-0.4778	-0.0159
0.6963	-0.4538	0.0512
0.7927	-0.4210	0.1213
0.8918	-0.3815	0.2218
0.9908	-0.3620	0.3184
1.0899	-0.3663	0.4007

q_∞ = 245 Pa, NPR 4.0

C_{Pi}	
lower outer	upper outer
0.3397	-0.0136
-0.6319	-0.3384
-0.6519	-0.4047
-0.5154	-0.2908
-0.3688	-0.1717
-0.3120	-0.0822
-0.2696	-0.0036
-0.2440	0.0752
-0.2180	0.1649
-0.1880	0.2773
-0.2007	0.3807
-0.1738	0.4521

q_∞ = 551 Pa, NPR 4.0

C_{Pi}	
lower outer	upper outer
0.4670	-0.0152
-0.6149	-0.3619
-0.6715	-0.4242
-0.5002	-0.2973
-0.3509	-0.1609
-0.2874	-0.0694
-0.2496	0.0073
-0.2364	0.0931
-0.2022	0.1871
-0.1719	0.3029
-0.2014	0.4033
-0.1685	0.4596

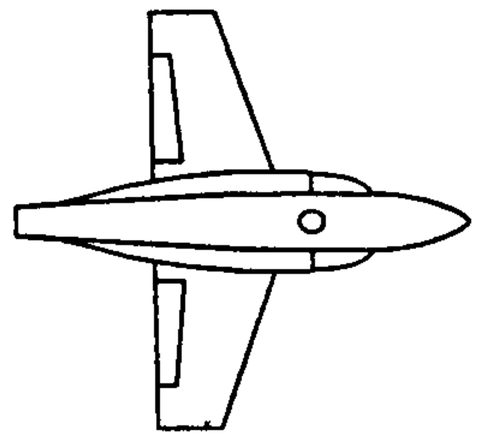

q_∞ = 61.3 Pa, NPR 1.586

	C_{Pi}	
x/d_{ie}	lower outer	upper outer
0.0000	0.3122	-0.0269
0.1189	-0.7164	-0.3075
0.2081	-0.7805	-0.3776
0.2973	-0.6629	-0.2920
0.3963	-0.5104	-0.1612
0.4954	-0.4342	-0.0870
0.5945	-0.3888	-0.0114
0.6963	-0.3881	0.0804
0.7927	-0.3337	0.1682
0.8918	-0.3260	0.2633
0.9908	-0.3265	0.3641
1.0899	-0.3045	0.4259

q_∞=245 Pa, NPR 1.586

C_{Pi}	
lower outer	upper outer
0.4740	-0.0087
-0.5931	-0.3278
-0.6839	-0.3932
-0.5338	-0.2793
-0.3978	-0.1574
-0.3348	-0.0641
-0.3005	0.0191
-0.2876	0.1000
-0.2633	0.1959
-0.2462	0.3043
-0.2649	0.4014
-0.2368	0.4626

q_∞=551 Pa, NPR 1.586

C_{Pi}	
lower outer	upper outer
0.4948	-0.0140
-0.5644	-0.3618
-0.6552	-0.4236
-0.4991	-0.2987
-0.3597	-0.1613
-0.3037	-0.0677
-0.2712	0.0120
-0.2694	0.0987
-0.2428	0.1912
-0.2267	0.3064
-0.2575	0.4032
-0.2301	0.4582

q_∞ = 61.3 Pa, NPR 2.0

	C_{Pi}	
x/d_{ie}	lower outer	upper outer
0.0000	0.2420	0.0088
0.1189	-0.7812	-0.2683
0.2081	-0.8452	-0.3241
0.2973	-0.6968	-0.2304
0.3963	-0.5672	-0.1385
0.4954	-0.5076	-0.0488
0.5945	-0.4539	0.0101
0.6963	-0.4559	0.0940
0.7927	-0.4108	0.1680
0.8918	-0.3959	0.2660
0.9908	-0.3979	0.3667
1.0899	-0.3528	0.4308

q_∞ = 245 Pa, NPR 2.0

C_{Pi}	
lower outer	upper outer
0.4618	-0.0021
-0.6122	-0.3219
-0.7064	-0.3879
-0.5559	-0.2752
-0.4184	-0.1551
-0.3499	-0.0600
-0.3139	0.0212
-0.3040	0.1020
-0.2770	0.1924
-0.2542	0.2989
-0.2776	0.3958
-0.2500	0.4621

q_∞ = 551 Pa, NPR 2.0

C_{Pi}	
lower outer	upper outer
0.4837	-0.0133
-0.5910	-0.3707
-0.6848	-0.4310
-0.5270	-0.3032
-0.3817	-0.1694
-0.3242	-0.0740
-0.2927	0.0040
-0.2902	0.0912
-0.2633	0.1842
-0.2468	0.2957
-0.2760	0.3919
-0.2443	0.4478

q_∞ = 61.3 Pa, NPR 3.0

	C_{Pi}	
x/d_e	lower outer	upper outer
0.0000	0.1224	-0.0022
0.1189	-1.0787	-0.3198
0.2081	-1.0888	-0.3948
0.2973	-0.9180	-0.2799
0.3963	-0.7859	-0.1879
0.4954	-0.6997	-0.0990
0.5945	-0.6594	-0.0177
0.6963	-0.6309	0.0581
0.7927	-0.5973	0.1489
0.8918	-0.5397	0.2558
0.9908	-0.5281	0.3526
1.0899	-0.4929	0.4235

q_∞ = 245 Pa, NPR 3.0

C_{Pi}	
lower outer	upper outer
0.4773	-0.0118
-0.6561	-0.3411
-0.7480	-0.4074
-0.5875	-0.2901
-0.4428	-0.1674
-0.3742	-0.0745
-0.3323	0.0032
-0.3260	0.0909
-0.2982	0.1805
-0.2651	0.2927
-0.2874	0.3911
-0.2563	0.4549

q_∞ = 551 Pa, NPR 3.0

C_{Pi}	
lower outer	upper outer
0.4935	-0.0152
-0.6180	-0.3774
-0.7152	-0.4389
-0.5458	-0.3130
-0.3929	-0.1741
-0.3354	-0.0795
-0.2996	-0.0012
-0.2955	0.0860
-0.2670	0.1807
-0.2433	0.2919
-0.2730	0.3912
-0.2411	0.4460

q_∞ = 61.3 Pa, NPR 4.0

	C_{Pi}	
x/d_e	lower outer	upper outer
0.0000	0.0276	0.0068
0.1189	-1.2348	-0.2936
0.2081	-1.2557	-0.3781
0.2973	-1.0811	-0.2662
0.3963	-0.9126	-0.1710
0.4954	-0.8126	-0.1034
0.5945	-0.7836	-0.0250
0.6963	-0.7240	0.0510
0.7927	-0.6883	0.1284
0.8918	-0.6436	0.2423
0.9908	-0.5985	0.3302
1.0899	-0.5489	0.4091

q_∞ = 245 Pa, NPR 4.0

C_{Pi}	
lower outer	upper outer
0.4820	-0.0124
-0.6699	-0.3505
-0.7842	-0.4164
-0.6186	-0.3026
-0.4589	-0.1808
-0.3888	-0.0849
-0.3531	-0.0030
-0.3365	0.0834
-0.3097	0.1740
-0.2815	0.2892
-0.3036	0.3917
-0.2742	0.4578

q_∞ = 551 Pa, NPR 4.0

C_{Pi}	
lower outer	upper outer
0.4825	-0.0176
-0.6269	-0.3656
-0.7338	-0.4300
-0.5593	-0.3039
-0.4037	-0.1679
-0.3459	-0.0739
-0.3115	0.0037
-0.3046	0.0905
-0.2771	0.1850
-0.2482	0.2971
-0.2828	0.3964
-0.2506	0.4535

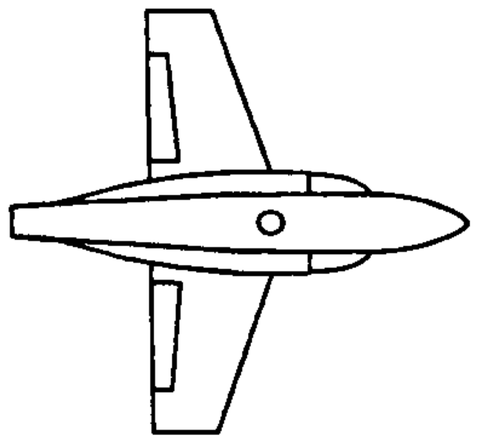

q_∞ = 61.3 Pa, NPR 1.586

	C_{Pi}	
x/d_e	lower outer	upper outer
0.0000	0.3933	-0.0051
0.1189	-0.4974	-0.3250
0.2081	-0.6045	-0.3694
0.2973	-0.4955	-0.2623
0.3963	-0.3783	-0.1687
0.4954	-0.3041	-0.0724
0.5945	-0.2751	0.0086
0.6963	-0.2564	0.0795
0.7927	-0.2725	0.1556
0.8918	-0.2668	0.2604
0.9908	-0.2604	0.3565
1.0899	-0.2614	0.4298

q_∞=245 Pa, NPR 1.586

C_{Pi}	
lower outer	upper outer
0.4884	-0.0075
-0.4418	-0.3249
-0.5232	-0.3807
-0.3911	-0.2668
-0.2747	-0.1502
-0.2142	-0.0590
-0.1861	0.0223
-0.1775	0.1074
-0.1630	0.1951
-0.1501	0.3071
-0.1827	0.4013
-0.1635	0.4623

q_∞=551 Pa, NPR 1.586

C_{Pi}	
lower outer	upper outer
0.5059	-0.0092
-0.4260	-0.3490
-0.5039	-0.4140
-0.3663	-0.2889
-0.2405	-0.1564
-0.1860	-0.0600
-0.1580	0.0180
-0.1545	0.0999
-0.1374	0.1974
-0.1271	0.3074
-0.1590	0.4040
-0.1426	0.4612

q_∞ = 61.3 Pa, NPR 2.0

	C_{Pi}	
x/d_e	lower outer	upper outer
0.0000	0.3398	-0.0148
0.1189	-0.6085	-0.3070
0.2081	-0.6974	-0.3858
0.2973	-0.5725	-0.2787
0.3963	-0.4612	-0.1740
0.4954	-0.3874	-0.0901
0.5945	-0.3611	-0.0150
0.6963	-0.3488	0.0657
0.7927	-0.3508	0.1481
0.8918	-0.3271	0.2681
0.9908	-0.3341	0.3574
1.0899	-0.3433	0.4366

q_∞ = 245 Pa, NPR 2.0

C_{Pi}	
lower outer	upper outer
0.4922	-0.0053
-0.4705	-0.3278
-0.5579	-0.3918
-0.4230	-0.2734
-0.3013	-0.1570
-0.2420	-0.0627
-0.2133	0.0167
-0.2022	0.1039
-0.1870	0.1942
-0.1793	0.3037
-0.2074	0.3999
-0.1884	0.4634

q_∞ = 551 Pa, NPR 2.0

C_{Pi}	
lower outer	upper outer
0.5085	-0.0129
-0.4529	-0.3712
-0.5368	-0.4315
-0.3910	-0.3053
-0.2599	-0.1670
-0.2062	-0.0717
-0.1763	0.0067
-0.1768	0.0948
-0.1563	0.1882
-0.1450	0.3007
-0.1770	0.3975
-0.1572	0.4531

q_∞ = 61.3 Pa, NPR 3.0

	C_{Pi}	
x/d_{i_e}	lower outer	upper outer
0.0000	0.2960	0.0045
0.1189	-0.7211	-0.2954
0.2081	-0.8047	-0.3648
0.2973	-0.6671	-0.2687
0.3963	-0.5334	-0.1604
0.4954	-0.4760	-0.0800
0.5945	-0.4609	-0.0208
0.6963	-0.4464	0.0559
0.7927	-0.4338	0.1415
0.8918	-0.4193	0.2545
0.9908	-0.4450	0.3511
1.0899	-0.4433	0.4246

q_∞ = 245 Pa, NPR 3.0

C_{Pi}	
lower outer	upper outer
0.4867	-0.0092
-0.5056	-0.3330
-0.5923	-0.3930
-0.4541	-0.2820
-0.3222	-0.1632
-0.2637	-0.0697
-0.2344	0.0099
-0.2297	0.0924
-0.2147	0.1821
-0.1982	0.2927
-0.2286	0.3895
-0.2131	0.4544

q_∞ = 551 Pa, NPR 3.0

C_{Pi}	
lower outer	upper outer
0.5261	-0.0085
-0.4835	-0.3750
-0.5725	-0.4379
-0.4231	-0.3088
-0.2836	-0.1688
-0.2264	-0.0728
-0.1956	0.0070
-0.1958	0.0941
-0.1737	0.1900
-0.1600	0.3050
-0.1939	0.4042
-0.1758	0.4622

q_∞ = 61.3 Pa, NPR 4.0

	C_{Pi}	
x/d_{i_e}	lower outer	upper outer
0.0000	0.3135	-0.0239
0.1189	-0.8806	-0.3860
0.2081	-0.9578	-0.4482
0.2973	-0.8126	-0.3391
0.3963	-0.6582	-0.2236
0.4954	-0.5828	-0.1644
0.5945	-0.5664	-0.0802
0.6963	-0.5536	-0.0100
0.7927	-0.5663	0.1055
0.8918	-0.5337	0.2842
0.9908	-0.5419	0.3088
1.0899	-0.5585	0.4055

q_∞ = 245 Pa, NPR 4.0

C_{Pi}	
lower outer	upper outer
0.5052	-0.0111
-0.5282	-0.3650
-0.6257	-0.4363
-0.4887	-0.3165
-0.3556	-0.1873
-0.2914	-0.0978
-0.2655	-0.0175
-0.2596	0.0696
-0.2467	0.1622
-0.2256	0.2767
-0.2544	0.3862
-0.2464	0.4551

q_∞ = 551 Pa, NPR 4.0

C_{Pi}	
lower outer	upper outer
0.5131	-0.0132
-0.4820	-0.3645
-0.5752	-0.4262
-0.4255	-0.3031
-0.2843	-0.1661
-0.2297	-0.0744
-0.2030	0.0024
-0.2010	0.0883
-0.1835	0.1809
-0.1685	0.2941
-0.2035	0.3961
-0.1875	0.4524

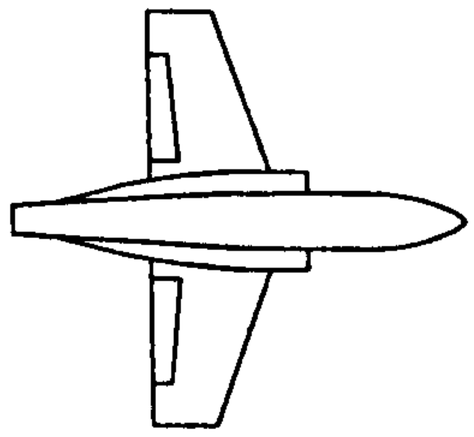

q_∞ = 61.3 Pa, NPR 1.0

	C_{Pi}			
x/d_e	lower outer	lower inner	upper inner	upper outer
0.0000	-121.2229	-121.2229	-108.4668	-108.4668
0.1189	0.4323	-101.0957	-119.7248	0.0834
0.2081	1.0563	-103.5131	-106.0033	0.9729
0.2973	0.9635	-97.0780	-98.3093	0.9412
0.3963	0.8114	-92.6135	-93.8389	0.8278
0.4954	0.6729	-90.0089	-91.1665	0.7545
0.5945	0.5471	-90.0792	-90.3236	0.7034
0.6963	0.4761	-88.6688	-90.2819	0.6907
0.7927	0.4192	-87.7601	-89.5958	0.6982
0.8918	0.3659	-87.8304	-91.4754	0.7235
0.9908	0.3138	-88.4402	-91.0283	0.7496
1.0899	0.2862	-88.5410	-88.9407	0.7515

q_∞ = 245 Pa, NPR 1.0

	C_{Pi}			
x/d_e	lower outer	lower inner	upper inner	upper outer
0.0000	-17.3081	-17.3081	-17.6893	-17.6893
0.1189	0.8683	-23.2979	-27.7720	0.8514
0.2081	0.4645	-24.1744	-24.6692	0.4769
0.2973	0.3323	-22.4939	-22.9371	0.3199
0.3963	0.2696	-21.3797	-21.8581	0.2500
0.4954	0.1971	-20.8185	-21.1927	0.2285
0.5945	0.0630	-21.0563	-21.0167	0.2304
0.6963	0.1341	-20.6484	-20.9983	0.2647
0.7927	0.1203	-20.4648	-20.8492	0.3199
0.8918	0.1184	-20.3814	-21.4276	0.3810
0.9908	0.1036	-20.5810	-21.3082	0.4616
1.0899	0.1026	-20.6062	-20.6439	0.6397

q_∞ = 551 Pa, NPR 1.0

	C_{Pi}			
x/d_e	lower outer	lower inner	upper inner	upper outer
0.0000	-3.5058	-3.5058	-4.6644	-4.6644
0.1189	0.3154	-9.5942	-11.1180	0.4482
0.2081	-0.0122	-10.2488	-10.5628	0.1198
0.2973	0.0083	-9.5738	-9.8818	0.0736
0.3963	0.0299	-9.0649	-9.3219	0.0798
0.4954	0.0215	-8.8024	-8.9967	0.0992
0.5945	0.0195	-8.9367	-8.9173	0.1306
0.6963	0.0156	-8.7467	-8.9096	0.1785
0.7927	0.0173	-8.6520	-8.8368	0.2401
0.8918	0.0177	-8.6133	-9.1323	0.3097
0.9908	0.0123	-8.7131	-9.0843	0.5246
1.0899	0.0135	-8.7246	-8.7552	0.6618

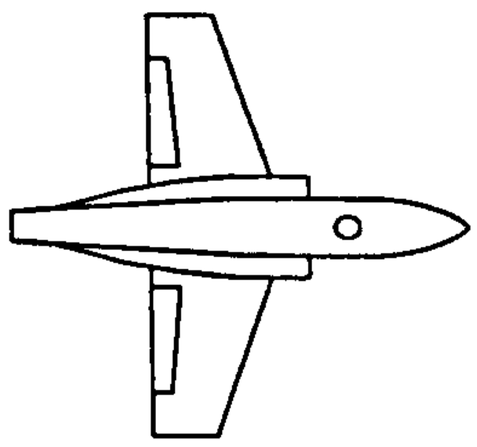

q_∞ = 61.3 Pa, NPR 1.586

	C_{Pi}			
x/d_e	lower outer	lower inner	upper inner	upper outer
0.0000	-104.1346	-104.1346	-113.0540	-113.0540
0.1189	0.7163	-96.6199	-119.2147	-0.0413
0.2081	0.9775	-99.4061	-103.3009	0.8344
0.2973	0.8094	-93.0090	-96.7680	0.9246
0.3963	0.6357	-88.8313	-92.0361	0.8101
0.4954	0.5048	-86.6469	-89.0955	0.7253
0.5945	0.4313	-87.1641	-88.1062	0.6522
0.6963	0.3420	-85.6918	-87.6103	0.6320
0.7927	0.2707	-85.0364	-87.0266	0.6329
0.8918	0.1358	-84.9150	-87.5867	0.7021
0.9908	-0.0073	-85.4963	-88.3370	0.7213
1.0899	0.0730	-85.6240	-85.9117	0.7339

q_∞ = 245 Pa, NPR 1.586

	C_{Pi}			
x/d_e	lower outer	lower inner	upper inner	upper outer
0.0000	-13.4717	-13.4717	-19.0369	-19.0369
0.1189	0.6352	-22.3988	-28.6344	0.7848
0.2081	0.1843	-23.5952	-25.3342	0.4719
0.2973	0.1095	-21.9638	-23.3535	0.3269
0.3963	0.0933	-21.0411	-22.2441	0.2731
0.4954	0.0350	-20.4760	-21.5102	0.2500
0.5945	0.0294	-20.8542	-21.2552	0.2617
0.6963	0.0175	-20.4117	-21.2641	0.2961
0.7927	0.0032	-20.4183	-20.9725	0.3478
0.8918	0.0028	-20.3794	-21.4902	0.4202
0.9908	-0.0160	-20.5927	-21.4659	0.5075
1.0899	-0.0127	-20.5453	-20.8188	0.6770

q_∞ = 551 Pa, NPR 1.586

	C_{Pi}			
$x/d_{i\infty}$	lower outer	lower inner	upper inner	upper outer
0.0000	-2.0318	-2.0318	-5.2440	-5.2440
0.1189	-0.0037	-9.0697	-11.5755	0.4725
0.2081	-0.3209	-9.8485	-10.7968	0.1401
0.2973	-0.2402	-9.3365	-10.0265	0.0777
0.3963	-0.1719	-8.8797	-9.4212	0.0788
0.4954	-0.1470	-8.6629	-9.0597	0.0869
0.5945	-0.1315	-8.8405	-8.9753	0.1128
0.6963	-0.1281	-8.6586	-8.9607	0.1540
0.7927	-0.1100	-8.5843	-8.8844	0.2207
0.8918	-0.0988	-8.5570	-9.1211	0.2936
0.9908	-0.1018	-8.6451	-9.0870	0.4705
1.0899	-0.0966	-8.6599	-8.7807	0.6452

q_∞ = 61.3 Pa, NPR 2.0

	C_{Pi}			
$x/d_{i\infty}$	lower outer	lower inner	upper inner	upper outer
0.0000	-101.3796	-101.3796	-116.8056	-116.8056
0.1189	0.7289	-96.9208	-120.8671	-0.1066
0.2081	0.9448	-99.7479	-105.7442	0.8159
0.2973	0.7659	-93.1796	-97.7138	0.9089
0.3963	0.5929	-89.0976	-92.8902	0.7906
0.4954	0.4627	-86.8233	-89.8811	0.7229
0.5945	0.3712	-87.4387	-88.7543	0.6694
0.6963	0.3005	-86.1060	-88.4372	0.6321
0.7927	0.2368	-85.4610	-87.7112	0.6550
0.8918	0.1229	-85.1766	-89.3059	0.7036
0.9908	0.0540	-86.0655	-88.9516	0.7190
1.0899	0.0739	-86.0198	-86.7787	0.7290

q_∞ = 245 Pa, NPR 2.0

	C_{Pi}			
$x/d_{i\infty}$	lower outer	lower inner	upper inner	upper outer
0.0000	-13.3587	-13.3587	-20.0952	-20.0952
0.1189	0.6070	-22.4874	-29.0205	0.7272
0.2081	0.1474	-23.7520	-25.6347	0.4804
0.2973	0.0839	-22.3401	-23.6872	0.3536
0.3963	0.0722	-21.2819	-22.4614	0.3015
0.4954	0.0215	-20.7895	-21.7520	0.2837
0.5945	0.0088	-21.1076	-21.4826	0.2905
0.6963	0.0020	-20.7856	-21.4436	0.3193
0.7927	-0.0026	-20.6158	-21.3154	0.3667
0.8918	-0.0021	-20.5405	-21.8914	0.4360
0.9908	-0.0281	-20.7940	-21.7237	0.5298
1.0899	-0.0237	-20.7934	-21.0071	0.6758

q_∞ = 551 Pa, NPR 2.0

	C_{Pi}			
x/d_e	lower outer	lower inner	upper inner	upper outer
0.0000	-1.8479	-1.8479	-5.2653	-5.2653
0.1189	-0.0442	-8.9843	-11.6491	0.4466
0.2081	-0.3551	-9.7792	-10.8349	0.1143
0.2973	-0.2721	-9.2928	-10.0394	0.0653
0.3963	-0.1911	-8.8469	-9.4544	0.0599
0.4954	-0.1702	-8.6530	-9.0776	0.0682
0.5945	-0.1431	-8.8191	-8.9763	0.0981
0.6963	-0.1393	-8.6412	-8.9661	0.1254
0.7927	-0.1286	-8.5731	-8.8876	0.1961
0.8918	-0.1097	-8.5397	-9.1668	0.2734
0.9908	-0.1111	-8.6361	-9.1127	0.4434
1.0899	-0.1055	-8.6574	-8.7761	0.6273

q_∞ = 61.3 Pa, NPR 3.0

	C_{Pi}			
x/d_e	lower outer	lower inner	upper inner	upper outer
0.0000	-96.0608	-96.0608	-121.4527	-121.4527
0.1189	0.7604	-95.0464	-122.0914	-0.3183
0.2081	0.8412	-98.5702	-106.3988	0.7615
0.2973	0.6823	-92.3370	-97.7927	0.8238
0.3963	0.4884	-88.2868	-92.0468	0.7530
0.4954	0.3708	-86.1430	-89.6572	0.6848
0.5945	0.2939	-87.0341	-88.7906	0.6222
0.6963	0.1330	-85.5317	-88.5199	0.6370
0.7927	-0.0397	-85.1820	-87.4484	0.6802
0.8918	0.0505	-85.0141	-88.4532	0.7131
0.9908	0.1059	-85.7975	-88.8737	0.7440
1.0899	0.1107	-85.5694	-86.6388	0.7660

q_∞ = 245 Pa, NPR 3.0

	C_{Pi}			
x/d_e	lower outer	lower inner	upper inner	upper outer
0.0000	-12.7888	-12.7888	-20.7518	-20.7518
0.1189	0.5975	-22.2309	-28.9933	0.6922
0.2081	0.1364	-23.6167	-25.4033	0.4849
0.2973	0.0880	-22.2140	-23.6199	0.3579
0.3963	0.0791	-21.0014	-22.3930	0.2966
0.4954	0.0301	-20.6423	-21.7168	0.2863
0.5945	0.0196	-21.0228	-21.4776	0.2844
0.6963	0.0134	-20.6416	-21.4468	0.3071
0.7927	0.0125	-20.5511	-21.2765	0.3621
0.8918	0.0120	-20.5094	-21.7653	0.4278
0.9908	-0.0090	-20.6001	-21.6343	0.5223
1.0899	0.0037	-20.6885	-20.9910	0.6432

q_∞ = 551 Pa, NPR 3.0

	C_{Pi}			
x/d_e	lower outer	lower inner	upper inner	upper outer
0.0000	-1.7766	-1.7766	-5.3857	-5.3857
0.1189	-0.0508	-9.0971	-11.9778	0.4119
0.2081	-0.3582	-9.9374	-11.0290	0.1074
0.2973	-0.2710	-9.4477	-10.2031	0.0548
0.3963	-0.1910	-8.9953	-9.6051	0.0517
0.4954	-0.1640	-8.7963	-9.2348	0.0579
0.5945	-0.1406	-8.9738	-9.1815	0.0772
0.6963	-0.1331	-8.7924	-9.1627	0.1179
0.7927	-0.1136	-8.7416	-9.0567	0.1693
0.8918	-0.1044	-8.7007	-9.3279	0.2585
0.9908	-0.1048	-8.8262	-9.2690	0.4082
1.0899	-0.0983	-8.8356	-8.9398	0.5879

q_∞ = 61.3 Pa, NPR 4.0

	C_{Pi}			
x/d_e	lower outer	lower inner	upper inner	upper outer
0.0000	-91.8065	-91.8065	-126.6017	-126.6017
0.1189	0.7672	-95.8038	-124.3921	-0.4551
0.2081	0.7779	-98.6813	-107.8194	0.7368
0.2973	0.5727	-92.4938	-99.2395	0.8044
0.3963	0.3969	-88.3870	-93.1580	0.7151
0.4954	0.2029	-86.2366	-90.8375	0.6589
0.5945	0.0816	-87.9441	-89.9507	0.6136
0.6963	0.0738	-86.5439	-89.6060	0.6150
0.7927	0.0644	-85.6164	-88.2947	0.6335
0.8918	0.0951	-85.9424	-89.6283	0.7011
0.9908	0.0539	-86.2978	-89.5957	0.7225
1.0899	0.0353	-86.2428	-87.1651	0.7491

q_∞ = 245 Pa, NPR 4.0

	C_{Pi}			
x/d_e	lower outer	lower inner	upper inner	upper outer
0.0000	-12.4469	-12.4469	-21.5470	-21.5470
0.1189	0.5760	-22.2797	-29.4835	0.6438
0.2081	0.0974	-23.5093	-25.8590	0.4405
0.2973	0.0753	-22.1294	-24.0482	0.3143
0.3963	0.0640	-21.2906	-22.6266	0.2663
0.4954	0.0371	-20.9061	-21.9545	0.2459
0.5945	0.0249	-21.2900	-21.7678	0.2672
0.6963	0.0067	-20.9422	-21.7672	0.2770
0.7927	0.0033	-20.6986	-21.5125	0.3197
0.8918	0.0087	-20.7100	-22.1510	0.3935
0.9908	-0.0037	-20.9006	-21.9050	0.4970
1.0899	-0.0181	-20.9980	-21.1705	0.6234

q_∞ = 551 Pa, NPR 4.0

	C_{Pi}			
x/d_{ie}	lower outer	lower inner	upper inner	upper outer
0.0000	-1.7204	-1.7204	-5.6580	-5.6580
0.1189	-0.0433	-9.1051	-12.2039	0.4063
0.2081	-0.3467	-9.8780	-11.1182	0.1191
0.2973	-0.2677	-9.4704	-10.2393	0.0700
0.3963	-0.1840	-9.0261	-9.6726	0.0665
0.4954	-0.1525	-8.8242	-9.3058	0.0675
0.5945	-0.1360	-9.0094	-9.2414	0.0898
0.6963	-0.1185	-8.8482	-9.2205	0.1101
0.7927	-0.1063	-8.7760	-9.1634	0.1693
0.8918	-0.0912	-8.7719	-9.4036	0.2569
0.9908	-0.0933	-8.8394	-9.3445	0.3935
1.0899	-0.0838	-8.9076	-9.0050	0.5643

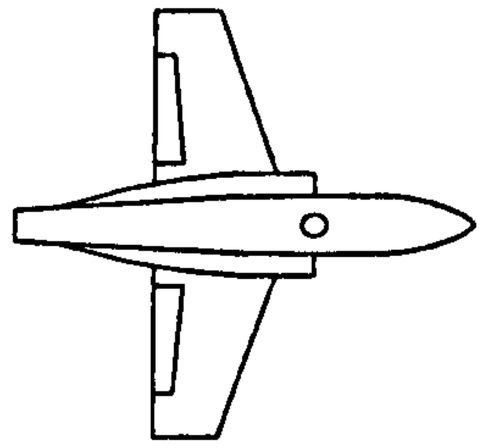

q_∞ = 61.3 Pa, NPR 1.586

	C_{Pi}			
x/d_e	lower outer	lower inner	upper inner	upper outer
0.0000	-110.0983	-110.0983	-114.4619	-114.4619
0.1189	0.7189	-99.2518	-121.3107	-0.0038
0.2081	1.0198	-101.9238	-106.2486	0.8346
0.2973	0.8115	-95.5017	-98.4579	0.9368
0.3963	0.5996	-91.1319	-93.8402	0.8521
0.4954	0.4729	-88.7793	-90.9080	0.7620
0.5945	0.2252	-89.2183	-90.0311	0.6991
0.6963	0.2302	-87.7252	-89.7843	0.6612
0.7927	0.2025	-87.1349	-88.9985	0.6827
0.8918	0.1496	-86.8642	-90.7353	0.7144
0.9908	0.0897	-87.5455	-90.4518	0.7462
1.0899	0.0798	-87.6513	-88.2994	0.7364

q_∞ = 245 Pa, NPR 1.586

	C_{Pi}			
x/d_e	lower outer	lower inner	upper inner	upper outer
0.0000	-15.8746	-15.8746	-18.8482	-18.8482
0.1189	0.7171	-23.3148	-28.6322	0.7578
0.2081	0.2268	-24.3806	-25.3868	0.4485
0.2973	0.1152	-22.6947	-23.6138	0.3037
0.3963	0.2338	-21.6935	-22.4493	0.2533
0.4954	0.0098	-21.0349	-21.7271	0.2237
0.5945	-0.0294	-21.3341	-21.5177	0.2358
0.6963	-0.0641	-20.9296	-21.5375	0.2736
0.7927	-0.0714	-20.7846	-21.3321	0.3259
0.8918	-0.0752	-20.6703	-21.8965	0.3954
0.9908	-0.1000	-20.9389	-21.8134	0.4839
1.0899	-0.1104	-20.9644	-21.1314	0.6518

q_∞ = 551 Pa, NPR 1.586

	C_{Pi}			
x/d_e	lower outer	lower inner	upper inner	upper outer
0.0000	-3.1927	-3.1927	-5.0758	-5.0758
0.1189	0.1589	-9.7026	-11.4381	0.4480
0.2081	-0.2022	-10.3547	-10.9039	0.1120
0.2973	-0.1726	-9.7444	-10.1485	0.0618
0.3963	-0.1369	-9.2248	-9.5495	0.0671
0.4954	-0.1386	-8.9764	-9.2163	0.0780
0.5945	-0.1432	-9.1264	-9.1381	0.1090
0.6963	-0.1553	-8.9202	-9.1510	0.1466
0.7927	-0.1544	-8.8330	-9.0704	0.2121
0.8918	-0.1519	-8.7992	-9.3121	0.2874
0.9908	-0.1691	-8.9010	-9.2965	0.4739
1.0899	-0.1667	-8.8975	-8.9877	0.6446

q_∞ = 61.3 Pa, NPR 2.0

	C_{Pi}			
x/d_e	lower outer	lower inner	upper inner	upper outer
0.0000	-103.8432	-103.8432	-112.9750	-112.9750
0.1189	0.7529	-96.1838	-119.6337	-0.0957
0.2081	0.9496	-99.4017	-104.7267	0.8103
0.2973	0.6844	-93.2473	-96.8503	0.9099
0.3963	0.3991	-89.0379	-92.1381	0.7749
0.4954	0.3120	-86.6807	-89.2641	0.6587
0.5945	0.1698	-87.0088	-88.2604	0.6280
0.6963	0.1494	-85.6941	-87.9303	0.6158
0.7927	0.1171	-85.0552	-87.1564	0.6293
0.8918	0.1088	-84.4746	-88.8612	0.6572
0.9908	0.0460	-85.6998	-88.1349	0.6711
1.0899	-0.0340	-85.6872	-86.3519	0.6722

q_∞ = 245 Pa, NPR 2.0

	C_{Pi}			
x/d_e	lower outer	lower inner	upper inner	upper outer
0.0000	-14.7083	-14.7083	-18.8573	-18.8573
0.1189	0.6478	-22.8149	-28.2514	0.7003
0.2081	0.1625	-23.8247	-25.0345	0.4355
0.2973	0.0570	-22.2525	-23.2643	0.3090
0.3963	0.0170	-21.2092	-22.0806	0.2513
0.4954	-0.0285	-20.7035	-21.4032	0.2439
0.5945	-0.0527	-21.0183	-21.2069	0.2440
0.6963	-0.1002	-20.5254	-21.1764	0.2845
0.7927	-0.1035	-20.4264	-21.0245	0.3344
0.8918	-0.1040	-20.3814	-21.6120	0.4057
0.9908	-0.1146	-20.6010	-21.4413	0.4965
1.0899	-0.1145	-20.5929	-20.7760	0.6445

q_∞ = 551 Pa, NPR 2.0

	C_{Pi}			
x/d_{ie}	lower outer	lower inner	upper inner	upper outer
0.0000	-2.7552	-2.7552	-4.8801	-4.8801
0.1189	0.0915	-9.3908	-11.4005	0.4134
0.2081	-0.2596	-10.0877	-10.6865	0.0886
0.2973	-0.2226	-9.5119	-9.9602	0.0454
0.3963	-0.1758	-9.0038	-9.3687	0.0537
0.4954	-0.1784	-8.7620	-9.0436	0.0584
0.5945	-0.1768	-8.9047	-8.9630	0.0888
0.6963	-0.1794	-8.7146	-8.9650	0.1316
0.7927	-0.1762	-8.6345	-8.8830	0.1859
0.8918	-0.1724	-8.5826	-9.1531	0.2759
0.9908	-0.1891	-8.6953	-9.0991	0.4395
1.0899	-0.1816	-8.7039	-8.7788	0.6203

q_∞ = 61.3 Pa, NPR 3.0

	C_{Pi}			
x/d_{ie}	lower outer	lower inner	upper inner	upper outer
0.0000	-101.2855	-101.2855	-121.0629	-121.0629
0.1189	0.8325	-98.3384	-124.3099	-0.2663
0.2081	0.8795	-100.5128	-107.9777	0.7566
0.2973	0.6408	-94.7849	-99.4736	0.8605
0.3963	0.3459	-90.3910	-94.5376	0.7527
0.4954	0.0391	-88.1652	-91.6227	0.6629
0.5945	0.0930	-88.7802	-90.5953	0.6618
0.6963	0.0410	-87.3864	-89.3177	0.6401
0.7927	0.0109	-86.7740	-89.4745	0.6652
0.8918	-0.0105	-86.6491	-90.6294	0.6972
0.9908	-0.0093	-86.9546	-90.6284	0.7411
1.0899	-0.0164	-87.5725	-88.4087	0.7713

q_∞ = 245 Pa, NPR 3.0

	C_{Pi}			
x/d_{ie}	lower outer	lower inner	upper inner	upper outer
0.0000	-14.4474	-14.4474	-19.7676	-19.7676
0.1189	0.6430	-22.9271	-28.5030	0.6848
0.2081	0.1394	-24.0031	-25.5444	0.4633
0.2973	0.0443	-22.5549	-23.5956	0.3277
0.3963	0.0091	-21.3918	-22.3759	0.2927
0.4954	-0.0407	-20.8967	-21.6514	0.2596
0.5945	-0.0551	-21.2164	-21.4407	0.2721
0.6963	-0.1049	-20.8228	-21.4873	0.3048
0.7927	-0.1031	-20.5439	-21.2795	0.3598
0.8918	-0.1151	-20.5746	-21.8063	0.4239
0.9908	-0.1189	-20.7318	-21.6632	0.5129
1.0899	-0.1176	-20.7809	-21.0049	0.6525

q_∞ = 551 Pa, NPR 3.0

	C_{Pi}			
x/d_e	lower outer	lower inner	upper inner	upper outer
0.0000	-2.7893	-2.7893	-4.9982	-4.9982
0.1189	0.0759	-9.5753	-11.6594	0.3923
0.2081	-0.2810	-10.2727	-10.9006	0.0744
0.2973	-0.2418	-9.7033	-10.1447	0.0346
0.3963	-0.1973	-9.1750	-9.5253	0.0384
0.4954	-0.1935	-8.9069	-9.2210	0.0440
0.5945	-0.1873	-9.0996	-9.1537	0.0748
0.6963	-0.1883	-8.8984	-9.1524	0.1148
0.7927	-0.1861	-8.8039	-9.0658	0.1910
0.8918	-0.1774	-8.7874	-9.3283	0.2630
0.9908	-0.1886	-8.8857	-9.2850	0.4214
1.0899	-0.1792	-8.8893	-8.9458	0.6009

q_∞ = 61.3 Pa, NPR 4.0

	C_{Pi}			
x/d_e	lower outer	lower inner	upper inner	upper outer
0.0000	-96.8120	-96.8120	-126.3039	-126.3039
0.1189	0.8269	-97.4879	-124.4968	-0.4063
0.2081	0.8033	-100.6447	-108.2828	0.6989
0.2973	0.5062	-94.4254	-99.8288	0.7933
0.3963	0.1744	-90.2191	-94.7411	0.6851
0.4954	0.0992	-87.4241	-91.7189	0.5581
0.5945	-0.0127	-88.7508	-90.5980	0.5066
0.6963	-0.0538	-87.3399	-90.2539	0.5008
0.7927	-0.1323	-86.6917	-89.4607	0.5412
0.8918	-0.1665	-86.5291	-90.8934	0.6201
0.9908	-0.2212	-87.4614	-90.5824	0.6494
1.0899	-0.2580	-87.6114	-88.5146	0.6863

q_∞ = 245 Pa, NPR 4.0

	C_{Pi}			
x/d_e	lower outer	lower inner	upper inner	upper outer
0.0000	-14.2540	-14.2540	-20.3006	-20.3006
0.1189	0.6169	-23.3070	-29.1480	0.6337
0.2081	0.1179	-24.4118	-25.8391	0.4123
0.2973	0.0139	-22.8960	-24.0476	0.2902
0.3963	-0.0297	-21.7392	-22.8342	0.2384
0.4954	-0.0737	-21.2163	-22.1000	0.2233
0.5945	-0.0869	-21.5648	-21.8330	0.2191
0.6963	-0.1241	-21.2018	-21.8204	0.2565
0.7927	-0.1376	-21.0430	-21.7053	0.2985
0.8918	-0.1202	-20.9058	-22.2157	0.3775
0.9908	-0.1477	-21.1624	-22.0969	0.4857
1.0899	-0.1432	-21.1890	-21.4262	0.6251

q_∞ = 551 Pa, NPR 4.0

	C_{Pi}			
x/d_{is}	lower outer	lower inner	upper inner	upper outer
0.0000	-2.5917	-2.5917	-5.1527	-5.1527
0.1189	0.0432	-9.5489	-11.8264	0.3802
0.2081	-0.3158	-10.2824	-10.8683	0.0713
0.2973	-0.2767	-9.7196	-10.2308	0.0322
0.3963	-0.2301	-9.2125	-9.6533	0.0335
0.4954	-0.2234	-8.9666	-9.1646	0.0397
0.5945	-0.2205	-9.0784	-9.2291	0.0569
0.6963	-0.2244	-8.8764	-9.2321	0.1028
0.7927	-0.2107	-8.8652	-9.0878	0.1557
0.8918	-0.2038	-8.8425	-9.4197	0.2446
0.9908	-0.2135	-8.9352	-9.3174	0.3936
1.0899	-0.2054	-8.9160	-9.0507	0.5709

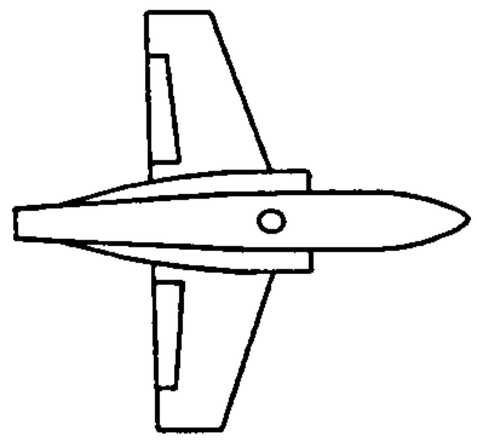

q_∞ = 61.3 Pa, NPR 1.586

	C_{Pi}			
x/d_{ie}	lower outer	lower inner	upper inner	upper outer
0.0000	-114.2149	-114.2149	-112.4718	-112.4718
0.1189	0.5931	-98.5673	-120.7820	-0.0226
0.2081	1.0374	-102.3513	-106.1168	1.0443
0.2973	0.8325	-95.9953	-98.3619	0.9125
0.3963	0.6620	-91.6379	-93.7662	0.7868
0.4954	0.4929	-89.1889	-91.0192	0.7124
0.5945	0.4055	-89.3731	-90.1386	0.6554
0.6963	0.2980	-87.9495	-89.9513	0.6338
0.7927	0.1501	-87.1601	-89.2402	0.6436
0.8918	0.0366	-87.1572	-90.8960	0.6879
0.9908	0.0995	-87.8067	-90.6966	0.7137
1.0899	0.0672	-87.9405	-88.5412	0.7012

q_∞ = 245 Pa, NPR 1.586

	C_{Pi}			
x/d_{ie}	lower outer	lower inner	upper inner	upper outer
0.0000	-17.0076	-17.0076	-18.6019	-18.6019
0.1189	0.8158	-23.5945	-28.5751	0.7671
0.2081	0.3780	-24.4777	-25.4390	0.4486
0.2973	0.2536	-22.8767	-23.5444	0.3019
0.3963	0.1637	-21.7606	-22.3460	0.2534
0.4954	0.1191	-21.1788	-21.7338	0.2273
0.5945	0.0830	-21.4668	-21.5424	0.2306
0.6963	0.0405	-21.0284	-21.5727	0.2689
0.7927	0.0118	-20.8041	-21.3584	0.3165
0.8918	0.0066	-20.8075	-21.9736	0.3898
0.9908	-0.0322	-20.9370	-21.8202	0.4802
1.0899	-0.0391	-20.9702	-21.1357	0.6578

q_∞ = 551 Pa, NPR 1.586

	C_{Pi}			
x/d_e	lower outer	lower inner	upper inner	upper outer
0.0000	-3.6399	-3.6399	-4.8339	-4.8339
0.1189	0.2980	-9.9000	-11.4670	0.4327
0.2081	-0.0428	-10.5205	-10.8555	0.1023
0.2973	-0.0337	-9.8634	-10.1422	0.0591
0.3963	-0.0072	-9.3008	-9.5642	0.0577
0.4954	-0.0124	-9.0349	-9.2369	0.0819
0.5945	-0.0197	-9.1747	-9.1669	0.1068
0.6963	-0.0380	-8.9787	-9.1783	0.1514
0.7927	-0.0392	-8.8874	-9.0985	0.2168
0.8918	-0.0457	-8.8437	-9.3639	0.2920
0.9908	-0.0682	-8.9484	-9.3319	0.4976
1.0899	-0.0712	-8.9415	-9.0250	0.6544

q_∞ = 61.3 Pa, NPR 2.0

	C_{Pi}			
x/d_e	lower outer	lower inner	upper inner	upper outer
0.0000	-106.6190	-106.6190	-108.8480	-108.8480
0.1189	0.7451	-95.7078	-117.2283	0.0458
0.2081	1.0370	-98.5682	-102.9807	0.9748
0.2973	0.8152	-92.3329	-95.2884	0.8977
0.3963	0.6109	-88.2477	-90.7586	0.7711
0.4954	0.4734	-85.9658	-87.8921	0.7014
0.5945	0.3285	-86.3464	-87.0099	0.6090
0.6963	0.1561	-84.9103	-86.7723	0.6080
0.7927	-0.1335	-84.3228	-85.2613	0.6397
0.8918	0.0702	-84.1298	-87.8243	0.7013
0.9908	-0.0172	-84.8040	-87.4065	0.7450
1.0899	-0.0253	-84.9492	-85.2572	0.7426

q_∞ = 245 Pa, NPR 2.0

	C_{Pi}			
x/d_e	lower outer	lower inner	upper inner	upper outer
0.0000	-15.6299	-15.6299	-18.1368	-18.1368
0.1189	0.7733	-22.7089	-27.5866	0.6974
0.2081	0.3393	-23.6303	-24.6176	0.4386
0.2973	0.2053	-22.0669	-22.7928	0.3062
0.3963	0.1083	-20.9668	-21.6492	0.2544
0.4954	0.0843	-20.4886	-20.9958	0.2394
0.5945	0.0676	-20.7520	-20.8179	0.2447
0.6963	0.0055	-20.3167	-20.7725	0.2742
0.7927	-0.0019	-20.1577	-20.7022	0.3142
0.8918	-0.0063	-20.0922	-21.2604	0.4042
0.9908	-0.0618	-20.2313	-21.0608	0.4925
1.0899	-0.0706	-20.2604	-20.4472	0.6461

q_∞ = 551 Pa, NPR 2.0

	C_{Pi}			
x/d_e	lower outer	lower inner	upper inner	upper outer
0.0000	-3.1124	-3.1124	-4.6909	-4.6909
0.1189	0.2272	-9.4134	-11.1202	0.3988
0.2081	-0.1052	-10.0660	-10.5183	0.0814
0.2973	-0.0811	-9.4406	-9.7906	0.0402
0.3963	-0.0446	-8.9260	-9.2528	0.0516
0.4954	-0.0486	-8.6809	-8.9176	0.0662
0.5945	-0.0476	-8.8265	-8.8534	0.0982
0.6963	-0.0682	-8.6230	-8.8489	0.1238
0.7927	-0.0672	-8.5055	-8.7731	0.2028
0.8918	-0.0692	-8.4845	-9.0432	0.2761
0.9908	-0.0897	-8.5983	-8.9806	0.4421
1.0899	-0.0921	-8.6062	-8.6730	0.6236

q_∞ = 61.3 Pa, NPR 3.0

	C_{Pi}			
x/d_e	lower outer	lower inner	upper inner	upper outer
0.0000	-107.3730	-107.3730	-117.1868	-117.1868
0.1189	0.7635	-99.1999	-123.1985	-0.0462
0.2081	0.9978	-101.7910	-107.2774	0.8112
0.2973	0.7654	-95.2884	-99.0401	0.7814
0.3963	0.5206	-90.9382	-94.2087	0.6751
0.4954	0.3722	-88.6332	-91.1888	0.6308
0.5945	0.1585	-89.0927	-90.2723	0.5567
0.6963	0.1297	-87.5346	-89.9885	0.6129
0.7927	0.0477	-86.9441	-89.1780	0.6239
0.8918	0.0114	-86.7943	-90.8362	0.6831
0.9908	-0.0448	-87.5684	-90.5549	0.6913
1.0899	-0.0546	-87.6262	-88.3463	0.7230

q_∞ = 245 Pa, NPR 3.0

	C_{Pi}			
x/d_e	lower outer	lower inner	upper inner	upper outer
0.0000	-15.9604	-15.9604	-19.4099	-19.4099
0.1189	0.7532	-23.3138	-28.4541	0.6788
0.2081	0.3039	-24.2368	-25.4332	0.4302
0.2973	0.1656	-22.7013	-23.5100	0.3002
0.3963	0.1110	-21.5913	-22.2833	0.2550
0.4954	0.0723	-21.0293	-21.7224	0.2373
0.5945	0.0172	-21.2976	-21.5117	0.2328
0.6963	-0.0218	-20.8912	-21.5143	0.2872
0.7927	-0.0417	-20.8068	-21.3307	0.3209
0.8918	-0.0626	-20.6962	-21.8080	0.3895
0.9908	-0.0749	-20.8100	-21.8228	0.4894
1.0899	-0.0889	-20.8982	-21.1370	0.6339

q_∞ = 551 Pa, NPR 3.0

	C_{Pi}			
x/d_e	lower outer	lower inner	upper inner	upper outer
0.0000	-3.3234	-3.3234	-4.8349	-4.8349
0.1189	0.2270	-9.7708	-11.4980	0.3753
0.2081	-0.1163	-10.3618	-10.8279	0.0654
0.2973	-0.0975	-9.7940	-10.1357	0.0329
0.3963	-0.0652	-9.2544	-9.5651	0.0340
0.4954	-0.0733	-9.0062	-9.1941	0.0405
0.5945	-0.0779	-9.0785	-9.1129	0.0722
0.6963	-0.0897	-8.8898	-9.1610	0.1168
0.7927	-0.0933	-8.8543	-9.0360	0.1694
0.8918	-0.0947	-8.8084	-9.3469	0.2615
0.9908	-0.1163	-8.9091	-9.3107	0.4268
1.0899	-0.1200	-8.8209	-9.0037	0.6059

q_∞ = 61.3 Pa, NPR 4.0

	C_{Pi}			
x/d_e	lower outer	lower inner	upper inner	upper outer
0.0000	-103.8062	-103.8062	-121.2771	-121.2771
0.1189	0.8428	-99.1042	-122.9296	-0.1458
0.2081	0.9484	-100.7492	-108.0207	0.7944
0.2973	0.6906	-95.4768	-99.6593	0.7843
0.3963	0.4512	-90.8883	-94.8213	0.6227
0.4954	0.2041	-88.9089	-91.8962	0.4949
0.5945	0.1406	-89.4255	-90.8394	0.4686
0.6963	0.0226	-87.6837	-90.5967	0.4720
0.7927	-0.0081	-87.3474	-89.8077	0.4900
0.8918	-0.0365	-87.2059	-91.2436	0.5523
0.9908	-0.0951	-87.6346	-90.9573	0.5864
1.0899	-0.1994	-88.0615	-88.9067	0.5930

q_∞ = 245 Pa, NPR 4.0

	C_{Pi}			
x/d_e	lower outer	lower inner	upper inner	upper outer
0.0000	-15.7015	-15.7015	-19.8243	-19.8243
0.1189	0.7396	-23.1931	-28.4582	0.6006
0.2081	0.3179	-24.2375	-25.4716	0.3886
0.2973	0.1301	-22.7078	-23.6011	0.2731
0.3963	0.0947	-21.5542	-22.3629	0.2071
0.4954	0.0433	-21.0421	-21.7391	0.1939
0.5945	0.0036	-21.2399	-21.4774	0.2029
0.6963	-0.0355	-20.9815	-21.5297	0.2260
0.7927	-0.0648	-20.7329	-21.3737	0.2755
0.8918	-0.0670	-20.6834	-21.9849	0.3504
0.9908	-0.0886	-20.9461	-21.7665	0.4545
1.0899	-0.1078	-20.8785	-21.0495	0.6053

q_∞ = 551 Pa, NPR 4.0

	C_{Pi}			
x/d_{is}	lower outer	lower inner	upper inner	upper outer
0.0000	-3.2846	-3.2846	-4.8868	-4.8868
0.1189	0.2348	-9.7411	-11.5561	0.3904
0.2081	-0.1151	-10.3363	-10.8278	0.0811
0.2973	-0.0961	-9.7680	-10.0603	0.0440
0.3963	-0.0678	-9.2294	-9.5531	0.0450
0.4954	-0.0729	-8.9745	-9.1436	0.0535
0.5945	-0.0735	-9.1272	-9.1503	0.0816
0.6963	-0.0909	-8.8702	-9.0810	0.1208
0.7927	-0.0850	-8.8414	-9.0376	0.1741
0.8918	-0.0831	-8.8092	-9.3514	0.2675
0.9908	-0.1264	-8.9184	-9.2986	0.4211
1.0899	-0.1208	-8.8476	-9.0021	0.5934

E PHOENICS q1 Input Files

E.1 NACA 1408 aerofoil

```
TALK=F;RUN(1,1);VDU=X11-TERM
    *
    ** NACA 1408 Aerofoil at 0' AOA
    ** Flight speed = 10 m/s to 40 m/s
    ** Incompressible flow (M<0.2)
    ** K-e turbulence model
    ** PA=101325Pa, Temp=15'C
    *
    ****************************************************************************
    *
    ** Run identifiers and other preliminaries
    *
TEXT(NACA 1408,AOA=0',10m/s)
    *
    ** Declare variables
    *
REAL(PAMB,TAMB,DAMB,CFLOW,TINT,TKEIN,EPIN,MINL,MAXV)
REAL(RGAS,RELXV,RELXW,RELXKE,RELXEP)
    *
    ** Define constants
    *
RGAS=287.05
PAMB=101325.0
TAMB=288.15
DAMB=PAMB/(RGAS*TAMB)
CFLOW=10.0
TINT=0.03
    *
    ** Elliptic simulation
    *
PARAB=F
    *
    ****************************************************************************
    *
    ** Group 2 Time-dependence and related parameters
    *
    ** Steady state simulation
    *
STEADY=T
    *
    ****************************************************************************
    *
    ** Group 3 X-direction grid
    *
    ** Total number of grid cells in X direction = 1
    *
    ****************************************************************************
    *
    ** Group 4 Y-direction grid
    *
    ** Total number of grid cells in Y direction = 101
    *
    ****************************************************************************
    *
    ** Group 5 Z-direction grid
    *
    ** Total number of grid cells in Z direction = 90
    *
    ****************************************************************************
    *
    ** Group 6 Body fitting and other grid distortions
    *
BFC=T
```

```
NONORT=T
    *
    ** Define flow domain
    *
GSET(D,1,101,90,0.01,3.0,2.0)
    *
    ** Set points
    *
GSET(P,PT1,0.0,0.0,0.0)
GSET(P,PT2,0.0,0.0,0.85)
GSET(P,PT3,0.0,0.0,1.15)
GSET(P,PT4,0.0,0.0,2.0)
GSET(P,PT5,0.0,1.499900,2.0)
GSET(P,PT6,0.0,1.500100,2.0)
GSET(P,PT7,0.0,3.0,2.0)
GSET(P,PT8,0.0,3.0,1.15)
GSET(P,PT9,0.0,3.0,0.85)
GSET(P,PT10,0.0,3.0,0.0)
GSET(P,PT11,0.0,1.500100,0.0)
GSET(P,PT12,0.0,1.499900,0.0)
GSET(P,PT13,0.0,1.500100,0.85)
GSET(P,PT14,0.0,1.513339,1.001945)
GSET(P,PT15,0.0,1.500100,1.15)
GSET(P,PT16,0.0,1.499900,1.15)
GSET(P,PT17,0.0,1.492472,1.001822)
GSET(P,PT18,0.0,1.499900,0.85)
    *
    ** Set lines
    *
GSET(L,LN1,PT1,PT2,30,-1.5)
GSET(L,LN2,PT2,PT3,30,1.0)
GSET(L,LN3,PT3,PT4,30,1.5)
GSET(L,LN4,PT4,PT5,50,-1.85)
GSET(L,LN5,PT5,PT6,1,1.0)
GSET(L,LN6,PT6,PT7,50,1.85)
GSET(L,LN7,PT7,PT8,30,-1.5)
GSET(L,LN8,PT8,PT9,30,1.0)
GSET(L,LN9,PT9,PT10,30,1.5)
GSET(L,LN10,PT10,PT11,50,-1.85)
GSET(L,LN11,PT11,PT12,1,1.0)
GSET(L,LN12,PT12,PT1,50,1.85)
GSET(L,LN13,PT11,PT13,30,-1.5)
GSET(L,LN14,PT12,PT18,30,-1.5)
GSET(L,LN15,PT13,PT18,1,1.0)
GSET(L,LN16,PT15,PT16,1,1.0)
GSET(L,LN17,PT15,PT6,30,1.5)
GSET(L,LN18,PT16,PT5,30,1.5)
    *
    ** Set curves
    *
    ** Curve 1 lower surface trailing edge
    *
GSET(V,CV1,S,PT16,SPLINE)
GSET(V,0.0,1.499713,1.145273)
GSET(V,0.0,1.499459,1.141036)
GSET(V,0.0,1.499143,1.135684)
GSET(V,0.0,1.498893,1.131395)
GSET(V,0.0,1.498616,1.126588)
GSET(V,0.0,1.498315,1.121281)
GSET(V,0.0,1.497990,1.115495)
GSET(V,0.0,1.497759,1.111334)
GSET(V,0.0,1.497523,1.107030)
GSET(V,0.0,1.497280,1.102582)
GSET(V,0.0,1.496994,1.097275)
GSET(V,0.0,1.496702,1.091780)
GSET(V,0.0,1.496403,1.086104)
GSET(V,0.0,1.496098,1.080256)
```

```
GSET(V,0.0,1.495785,1.074171)
GSET(V,0.0,1.495576,1.070044)
GSET(V,0.0,1.495364,1.065846)
GSET(V,0.0,1.495152,1.061585)
GSET(V,0.0,1.494938,1.057262)
GSET(V,0.0,1.494725,1.052885)
GSET(V,0.0,1.494511,1.048454)
GSET(V,0.0,1.494298,1.043978)
GSET(V,0.0,1.494086,1.039457)
GSET(V,0.0,1.493896,1.035359)
GSET(V,0.0,1.493729,1.031684)
GSET(V,0.0,1.493564,1.028009)
GSET(V,0.0,1.493399,1.024291)
GSET(V,0.0,1.493238,1.020572)
GSET(V,0.0,1.493079,1.016839)
GSET(V,0.0,1.492922,1.013092)
GSET(V,0.0,1.492769,1.009345)
GSET(V,0.0,1.492619,1.005584)
GSET(V,CV1,E,PT17)
GSET(L,LN19,PT16,PT17,15,1.3,CRV,CV1)
   *
   ** Curve 2 lower surface leading edge
   *
GSET(V,CV2,S,PT17,SPLINE)
GSET(V,0.0,1.492330,0.998061)
GSET(V,0.0,1.492192,0.994301)
GSET(V,0.0,1.492059,0.990540)
GSET(V,0.0,1.491932,0.986795)
GSET(V,0.0,1.491810,0.983049)
GSET(V,0.0,1.491694,0.979319)
GSET(V,0.0,1.491584,0.975604)
GSET(V,0.0,1.491480,0.971889)
GSET(V,0.0,1.491383,0.968226)
GSET(V,0.0,1.491292,0.964564)
GSET(V,0.0,1.491194,0.960481)
GSET(V,0.0,1.491093,0.955980)
GSET(V,0.0,1.491002,0.951523)
GSET(V,0.0,1.490919,0.947113)
GSET(V,0.0,1.490849,0.942756)
GSET(V,0.0,1.490790,0.938454)
GSET(V,0.0,1.490746,0.934214)
GSET(V,0.0,1.490716,0.930036)
GSET(V,0.0,1.490699,0.925928)
GSET(V,0.0,1.490696,0.921891)
GSET(V,0.0,1.490708,0.917933)
GSET(V,0.0,1.490735,0.914052)
GSET(V,0.0,1.490779,0.910257)
GSET(V,0.0,1.490838,0.906548)
GSET(V,0.0,1.490929,0.902344)
GSET(V,0.0,1.491063,0.897646)
GSET(V,0.0,1.491225,0.893213)
GSET(V,0.0,1.491421,0.888922)
GSET(V,0.0,1.491653,0.884773)
GSET(V,0.0,1.491911,0.880922)
GSET(V,0.0,1.492205,0.877229)
GSET(V,0.0,1.492538,0.873694)
GSET(V,0.0,1.493091,0.868882)
GSET(V,0.0,1.493717,0.864582)
GSET(V,0.0,1.494415,0.860811)
GSET(V,0.0,1.495183,0.857584)
GSET(V,0.0,1.496919,0.852814)
GSET(V,0.0,1.498912,0.850351)
GSET(V,CV2,E,PT18)
GSET(L,LN20,PT17,PT18,15,-1.3,CRV,CV2)
   *
```

```
   ** Curve 3 upper surface leading edge
   *
GSET(V,CV3,S,PT13,SPLINE)
GSET(V,0.0,1.501117,0.850241)
GSET(V,0.0,1.503343,0.852500)
GSET(V,0.0,1.505529,0.857099)
GSET(V,0.0,1.506592,0.860256)
GSET(V,0.0,1.507625,0.863970)
GSET(V,0.0,1.508621,0.868226)
GSET(V,0.0,1.509570,0.873008)
GSET(V,0.0,1.510181,0.876531)
GSET(V,0.0,1.510757,0.880220)
GSET(V,0.0,1.511295,0.884073)
GSET(V,0.0,1.511816,0.888231)
GSET(V,0.0,1.512296,0.892536)
GSET(V,0.0,1.512736,0.896990)
GSET(V,0.0,1.513049,0.900533)
GSET(V,0.0,1.513331,0.904079)
GSET(V,0.0,1.513597,0.907815)
GSET(V,0.0,1.513834,0.911553)
GSET(V,0.0,1.514053,0.915465)
GSET(V,0.0,1.514242,0.919379)
GSET(V,0.0,1.514410,0.923452)
GSET(V,0.0,1.514550,0.927527)
GSET(V,0.0,1.514667,0.931745)
GSET(V,0.0,1.514756,0.935964)
GSET(V,0.0,1.514818,0.940309)
GSET(V,0.0,1.514853,0.944655)
GSET(V,0.0,1.514861,0.949111)
GSET(V,0.0,1.514842,0.953566)
GSET(V,0.0,1.514809,0.957204)
GSET(V,0.0,1.514760,0.960842)
GSET(V,0.0,1.514695,0.964508)
GSET(V,0.0,1.514614,0.968203)
GSET(V,0.0,1.514519,0.971897)
GSET(V,0.0,1.514411,0.975628)
GSET(V,0.0,1.514290,0.979358)
GSET(V,0.0,1.514158,0.983103)
GSET(V,0.0,1.514015,0.986863)
GSET(V,0.0,1.513862,0.990623)
GSET(V,0.0,1.513698,0.994397)
GSET(V,0.0,1.513523,0.998172)
GSET(V,CV3,E,PT14)
GSET(L,LN21,PT13,PT14,15,1.3,CRV,CV3)
   *
   ** Curve 4 upper surface trailing edge
   *
GSET(V,CV4,S,PT14,SPLINE)
GSET(V,0.0,1.513146,1.005719)
GSET(V,0.0,1.512943,1.009492)
GSET(V,0.0,1.512733,1.013250)
GSET(V,0.0,1.512513,1.017008)
GSET(V,0.0,1.512287,1.020751)
GSET(V,0.0,1.512053,1.024478)
GSET(V,0.0,1.511811,1.028205)
GSET(V,0.0,1.511564,1.031888)
GSET(V,0.0,1.511310,1.035570)
GSET(V,0.0,1.511018,1.039675)
GSET(V,0.0,1.510685,1.044203)
GSET(V,0.0,1.510346,1.048684)
GSET(V,0.0,1.509999,1.053120)
GSET(V,0.0,1.509648,1.057500)
GSET(V,0.0,1.509291,1.061825)
GSET(V,0.0,1.508930,1.066087)
GSET(V,0.0,1.508566,1.070285)
GSET(V,0.0,1.508200,1.074411)
GSET(V,0.0,1.507832,1.078465)
```

```
GSET(V,0.0,1.507464,1.082440)
GSET(V,0.0,1.507096,1.086334)
GSET(V,0.0,1.506729,1.090142)
GSET(V,0.0,1.506363,1.093862)
GSET(V,0.0,1.506001,1.097487)
GSET(V,0.0,1.505641,1.101017)
GSET(V,0.0,1.505228,1.105001)
GSET(V,0.0,1.504759,1.109437)
GSET(V,0.0,1.504312,1.113585)
GSET(V,0.0,1.503873,1.117581)
GSET(V,0.0,1.503443,1.121424)
GSET(V,0.0,1.503042,1.124949)
GSET(V,0.0,1.502561,1.129104)
GSET(V,0.0,1.502026,1.133631)
GSET(V,0.0,1.501545,1.137631)
GSET(V,0.0,1.501122,1.141089)
GSET(V,0.0,1.500597,1.145302)
GSET(V,0.0,1.500151,1.148821)
GSET(V,0.0,1.500038,1.149705)
GSET(V,CV4,E,PT15)
GSET(L,LN22,PT14,PT15,15,-1.3,CRV,CV4)
   *
   ** Set frames
   *
GSET(F,FR1,PT1,PT2.PT3,PT4,-,PT5,PT16.PT17.PT18,PT12,-)
GSET(F,FR2,PT11,PT13.PT14.PT15,PT6,-,PT7,PT8.PT9,PT10,-)
GSET(F,FR3,PT12,PT18.PT17.PT16,PT5,-,PT6,PT15.PT14.PT13,PT11,-)
   *
   ** Match frames
   *
GSET(M,FR1,+K+J,1,1,1,LAP5)
GSET(M,FR2,+K+J,1,52,1,LAP5)
GSET(M,FR3,+K+J,1,51,1,TRANS)
   *
GSET(C,I2,F,I1,1,101,1,90,+,0.01,0.0,0.0,INC,1.0)
   *
   ************************************************************
   *
   ** Group 7 variables stored and solved for
   *
SOLVE(P1,V1,W1)
STORE(RHO1,TMP1)
SOLUTN(P1,Y,Y,Y,N,N,N)
   *
   ************************************************************
   *
   ** Group 8 terms and devices
   *
   ************************************************************
   *
   ** Group 9 properties of the medium
   *
PRESS0=PAMB
TMP1=TAMB
RHO1=DAMB
   *
   ** KE and EP values for wind-tunnel modelling
   *
TURMOD(KEMODL)
ENUL=1.461E-5
TKEIN=(CFLOW*TINT)**2
EPIN=0.009*(TKEIN**2)/(50*ENUL)
   *
   ************************************************************
   *
   ** Group 10 interphase transfer processes and properties
   *
```

```
   ************************************************************
   *
   ** Group 11 initialisation of fields, variables and porosities
   *
   ** Set initial field values
   *
FIINIT(P1)=0.0
FIINIT(V1)=0.0
FIINIT(W1)=CFLOW
FIINIT(TMP1)=TAMB
FIINIT(RHO1)=DAMB
FIINIT(KE)=TKEIN
FIINIT(EP)=EPIN
   *
CONPOR(WING,-1,CELL,-1,-1,-51,-51,-31,-60)
COVAL(WING,PRPS,0.0,198)
   *
   ************************************************************
   *
   ** Group 12 convection and diffusion adjustments
   *
   ************************************************************
   *
   ** Group 13 boundary conditions and special sources
   *
PATCH(UPSTRM,LOW,1,1,1,101,1,1,1,1)
COVAL(UPSTRM,P1,FIXFLU,CFLOW*DAMB)
COVAL(UPSTRM,W1,ONLYMS,CFLOW)
COVAL(UPSTRM,KE,ONLYMS,TKEIN)
COVAL(UPSTRM,EP,ONLYMS,EPIN)
   *
PATCH(DNSTRM,HIGH,1,1,1,101,90,90,1,1)
COVAL(DNSTRM,P1,FIXP,0.0)
   *
   ************************************************************
   *
   ** Group 14 downstream pressure (for parabolic flow)
   *
   ************************************************************
   *
   ** Group 15 termination criteria for sweeps
   *
FSWEEP=1
LSWEEP=5000
SELREF=T
RESFAC=1.0E-3
   *
   ************************************************************
   *
   ** Group 16 termination criteria for inner iterations
   *
   ************************************************************
   *
   ** Group 17 under relaxation and related devices
   *
MAXV=CFLOW
MINL=1.0E-4
   *
RELXV=30
RELXW=30
RELXKE=10
RELXEP=10
   *
RELAX(P1,LINRLX,0.8)
RELAX(V1,FALSDT,(MINL/MAXV)*RELXV)
RELAX(W1,FALSDT,(MINL/MAXV)*RELXW)
RELAX(KE,FALSDT,(MINL/MAXV)*RELXKE)
```

```
RELAX(EP,FALSDT,(MINL/MAXV)*RELXEP)
   *
   ************************************************************
   *
   ** Group 18 limits on variables, values or increments to them
   *
   ************************************************************
   *
   ** Group 19 data communicated by SATELLITE to GROUND
   *
USEGRD=T
   *
   ************************************************************
   *
   ** Group 20 control of preliminary printout
   *
   ************************************************************
   *
   ** Group 21 frequency and extent of field printout
   *
   ************************************************************
   *
   ** Group 22 location of spot values
   *
IXMON=1
IYMON=20
IZMON=45
TSTSWP=10
UWATCH=F
USTEER=F
   *
   ************************************************************
   *
   ** Group 23 variable by variable field printout
   *
YZPR=T
NYPRIN=1
NZPRIN=1
   *
   ************************************************************
   *
   ** Group 24 preparation of continuation of runs
   *
   ************************************************************
   *
NOWIPE=T
STOP
```

E.2 Round free-jet

```
TALK=F;RUN(1,1);VDU=X11-TERM
    *
    ** Open jet tunnel representation
    ** Only half of domain modelled (assume symmetry)
    ** 3d Single jet (cartesian grid)
    ** Compressible flow
    ** K-e turbulence model
    ** NPR=1.5, Temp=15'C, PAMB=101325 Pa
    *
    ************************************************************
    *
    ** Group 1 run identifiers and other preliminaries
    *
TEXT(Dn=0.03673, NPR=1.5)
    *
    ** Declare variables
    *
REAL(NPR,TAMB,PAMB,DAMB,MACH,DIAM)
REAL(TJETT,TJETS,DJETT,DJETS,WJET)
REAL(CGAS,RGAS,GAMMA)
REAL(TINT,TKEJET,EPINJET)
REAL(MAXV,MINL,RELXU,RELXV,RELXW,RELXKE,RELXEP)
REAL(XPWR,YPWR,ZPWR)
    *
    ** Define constants
    *
NPR=1.5
DIAM=0.03673
XPWR=1.476
YPWR=1.454
ZPWR=1.414
    *
PAMB=101325.0
TAMB=288.15
TJETT=TAMB
CGAS=1005.0
RGAS=287.05
GAMMA=1.4
TINT=0.03
    *
    ** Calculate ambient density
    *
DAMB=PAMB/(RGAS*TAMB)
    *
    ** Calculate Mach number
    *
MACH=(2*(NPR**((GAMMA-1)/GAMMA)-1)/(GAMMA-1))**0.5
    *
    ** Calculation of jet exit static temperature
    *
TJETS=TJETT*(1.0/NPR)**((GAMMA-1.0)/GAMMA)
    *
    ** Calculation of jet exit velocity (only for NPR<1.893)
    *
WJET=MACH*((GAMMA*RGAS*TJETS)**0.5)
    *
    ** Calculation of jet exit total density
    *
DJETT=(PAMB*NPR)/(RGAS*TJETT)
    *
    ** Calculation of jet exit static density
    *
DJETS=DJETT*(1/NPR)**(1/GAMMA)
```

```
    *
    ** Elliptic simulation
    *
PARAB=F
    *
    ************************************************************
    *
    ** Group 2 time dependence and other related parameters
    *
    ** Steady state simulation
    *
STEADY=T
    *
    ************************************************************
    *
    ** Group 3 X-direction grid
    *
    ** Total number of cells in grid X direction = 24
    *
NX=24
NREGX=2
XULAST=0.5
IREGX=1;GRDPWR(X,20,(0.5-(DIAM/2)),-XPWR)
IREGX=2;GRDPWR(X,4,(DIAM/2),1.0)
    *
    ************************************************************
    *
    ** Group 4 Y-direction grid
    *
    ** Total number of cells in grid Y direction = 88
    *
NY=88
NREGY=3
YVLAST=2.0
IREGY=1;GRDPWR(Y,40,(1.0-(DIAM/2)),-YPWR)
IREGY=2;GRDPWR(Y,8,DIAM,1.0)
IREGY=3;GRDPWR(Y,40,(1.0-(DIAM/2)),YPWR)
    *
    ************************************************************
    *
    ** Group 5 Z-direction grid
    *
    ** Total number of cells in Z direction = 60
    *
NZ=60
NREGZ=1
ZWLAST=1.5
IREGZ=1;GRDPWR(Z,60,1.5,ZPWR)
    *
    ************************************************************
    *
    ** Group 6 body fitting and other grid distortions
    *
    ************************************************************
    *
    ** Group 7 variables stored and solved for
    *
SOLVE(P1,U1,V1,W1)
STORE(RHO1,TMP1)
SOLUTN(P1,Y,Y,Y,N,N,N)
    *
    ************************************************************
    *
    ** Group 8 terms and devices
    *
    ************************************************************
    *
```

```
   ** Group 9 properties of the medium
   *
   ** Pressure, temperature and density
   *
PRESS0=PAMB
TMP1=GRND5;TMP1A=CGAS*TAMB;TMP1B=CGAS
RHO1=GRND5;RHO1B=1/RGAS;DRH1DP=GRND5
ENUL=GRND6;ENULA=1.458E-6;ENULB=110.4
   *
   ** Turbulence
   *
TURMOD(KEMODL)
TKEJET=(WJET*TINT)**2
EPINJET=3/7*(TKEJET**1.5)/DIAM
   *
   ***************************************************************
   *
   ** Group 10 interphase transfer processes and properties
   *
   ***************************************************************
   *
   ** Group 11 initialisation of fields, variables and porosities
   *
   ** Set initial field values
   *
FIINIT(P1)=0.0
FIINIT(U1)=0.0
FIINIT(V1)=0.0
FIINIT(W1)=0.0
FIINIT(TMP1)=TAMB
FIINIT(RHO1)=DAMB
FIINIT(KE)=TKEJET
FIINIT(EP)=EPINJET
   *
   ***************************************************************
   *
   ** Group 12 convection and diffusion adjustments
   *
   ***************************************************************
   *
   ** Group 13 boundary conditions and special sources
   *
   ** Nozzle inlet
   *
PATCH(JET1,LOW,21,21,44,45,1,1,1,1)
COVAL(JET1,P1,FIXFLU,WJET*DJETS)
COVAL(JET1,W1,ONLYMS,WJET)
COVAL(JET1,KE,ONLYMS,TKEJET)
COVAL(JET1,EP,ONLYMS,EPINJET)
   *
PATCH(JET2,LOW,22,23,42,47,1,1,1,1)
COVAL(JET2,P1,FIXFLU,WJET*DJETS)
COVAL(JET2,W1,ONLYMS,WJET)
COVAL(JET2,KE,ONLYMS,TKEJET)
COVAL(JET2,EP,ONLYMS,EPINJET)
   *
PATCH(JET3,LOW,24,24,41,48,1,1,1,1)
COVAL(JET3,P1,FIXFLU,WJET*DJETS)
COVAL(JET3,W1,ONLYMS,WJET)
COVAL(JET3,KE,ONLYMS,TKEJET)
COVAL(JET3,EP,ONLYMS,EPINJET)
   *
   ** Upstream boundary
   *
PATCH(UPSTRM,SOUTH,1,24,1,1,1,60,1,1)
COVAL(UPSTRM,P1,FIXP,0.0)
   *
```

```
   ** Collector
   *
PATCH(DNSTRM,NORTH,1,24,88,88,1,60,1,1)
COVAL(DNSTRM,P1,FIXP,0.0)
   *
   ** Tunnel side (only west side defined,
   **              east is plane of symmetry)
   *
PATCH(SIDE,WEST,1,1,1,88,1,60,1,1)
COVAL(SIDE,P1,FIXP,0.0)
   *
   ** Upper surface
   *
PATCH(FSE1,LWALL,1,20,1,88,1,1,1,1)
COVAL(FSE1,U1,GRND2,0.0)
COVAL(FSE1,V1,GRND2,0.0)
COVAL(FSE1,W1,GRND2,0.0)
COVAL(FSE1,KE,GRND2,GRND2)
COVAL(FSE1,EP,GRND2,GRND2)
   *
PATCH(FSE2,LWALL,21,21,1,43,1,1,1,1)
COVAL(FSE2,U1,GRND2,0.0)
COVAL(FSE2,V1,GRND2,0.0)
COVAL(FSE2,W1,GRND2,0.0)
COVAL(FSE2,KE,GRND2,GRND2)
COVAL(FSE2,EP,GRND2,GRND2)
   *
PATCH(FSE3,LWALL,21,21,46,88,1,1,1,1)
COVAL(FSE3,U1,GRND2,0.0)
COVAL(FSE3,V1,GRND2,0.0)
COVAL(FSE3,W1,GRND2,0.0)
COVAL(FSE3,KE,GRND2,GRND2)
COVAL(FSE3,EP,GRND2,GRND2)
   *
PATCH(FSE4,LWALL,22,23,1,41,1,1,1,1)
COVAL(FSE4,U1,GRND2,0.0)
COVAL(FSE4,V1,GRND2,0.0)
COVAL(FSE4,W1,GRND2,0.0)
COVAL(FSE4,KE,GRND2,GRND2)
COVAL(FSE4,EP,GRND2,GRND2)
   *
PATCH(FSE5,LWALL,22,23,48,88,1,1,1,1)
COVAL(FSE5,U1,GRND2,0.0)
COVAL(FSE5,V1,GRND2,0.0)
COVAL(FSE5,W1,GRND2,0.0)
COVAL(FSE5,KE,GRND2,GRND2)
COVAL(FSE5,EP,GRND2,GRND2)
   *
PATCH(FSE6,LWALL,24,24,1,40,1,1,1,1)
COVAL(FSE6,U1,GRND2,0.0)
COVAL(FSE6,V1,GRND2,0.0)
COVAL(FSE6,W1,GRND2,0.0)
COVAL(FSE6,KE,GRND2,GRND2)
COVAL(FSE6,EP,GRND2,GRND2)
   *
PATCH(FSE7,LWALL,24,24,49,88,1,1,1,1)
COVAL(FSE7,U1,GRND2,0.0)
COVAL(FSE7,V1,GRND2,0.0)
COVAL(FSE7,W1,GRND2,0.0)
COVAL(FSE7,KE,GRND2,GRND2)
COVAL(FSE7,EP,GRND2,GRND2)
   *
   ** Tunnel floor
   *
PATCH(BOTTOM,HWALL,1,24,1,88,60,60,1,1)
COVAL(BOTTOM,U1,GRND2,0.0)
COVAL(BOTTOM,V1,GRND2,0.0)
```

```
COVAL(BOTTOM,W1,GRND2,0.0)
COVAL(BOTTOM,KE,GRND2,GRND2)
COVAL(BOTTOM,EP,GRND2,GRND2)
    *
    ************************************************************
    *
    ** Group 14 downstream pressure (for parabolic flow)
    *
    ************************************************************
    *
    ** Group 15 termination criteria for sweeps
    *
 FSWEEP=1
 LSWEEP=5000
 SELREF=T
 RESFAC=1.0E-3
    *
    ************************************************************
    *
    ** Group 16 termination criteria for inner iterations
    *
    ************************************************************
    *
    ** Group 17 under relaxation and related devices
    *
 MAXV=WJET
 MINL=DIAM/8
 RELXU=30.0
 RELXV=30.0
 RELXW=30.0
 RELXKE=10.0
 RELXEP=10.0

 RELAX(P1,LINRLX,0.8)
 RELAX(U1,FALSDT,(MINL/MAXV)*RELXU)
 RELAX(V1,FALSDT,(MINL/MAXV)*RELXV)
 RELAX(W1,FALSDT,(MINL/MAXV)*RELXW)
 RELAX(KE,FALSDT,(MINL/MAXV)*RELXKE)
 RELAX(EP,FALSDT,(MINL/MAXV)*RELXEP)
    *
    ************************************************************
    *
    ** Group 18 limits on variables, values or increments to them
    *
    ************************************************************
    *
    ** Group 19 data communicated by SATELLITE to GROUND
    *
 USEGRD=T
    *
    ************************************************************
    *
    ** Group 20 control of preliminary printout
    *
    ************************************************************
    *
    ** Group 21 frequency and extent of field printout
    *
    ************************************************************
    *
    ** Group 22 location of spot values
    *
 IXMON=10
 IYMON=44
 IZMON=20
 TSTSWP=10
 UWATCH=F
```

```
USTEER=F
    *
    ************************************************************************
    *
    ** Group 23 variable by variable fields printout
    *
YZPR=T
NXPRIN=1
NYPRIN=1
NZPRIN=1
    *
    ************************************************************************
    *
    ** Group 24 preparation for continuation of runs
    *
    ************************************************************************
    *
NOWIPE=T
STOP
```

E.3 Round jet in crossflow

```
TALK=F;RUN(1,1);VDU=X11-TERM
    *
    ** Open jet tunnel representation
    ** Only half of domain modelled (assume symmetry)
    ** 3d Single jet with crossflow (cartesian grid)
    ** Compressible flow
    ** K-e turbulence model
    ** NPR=4.0, Temp=15'C, PAMB=101325 Pa
    ** Crossflow=10,20,30,40 m/s
    *
    ************************************************************
    *
    ** Group 1 run identifiers and other preliminaries
    *
TEXT(Dn=0.01796, NPR=4.0, CFLOW=10 m/s)
    *
    ** Declare variables
    *
REAL(NPR,TAMB,PAMB,DAMB,DIAM)
REAL(TJETT,TJETS,DJETT,DJETS,WJET,CFLOW)
REAL(CGAS,RGAS,GAMMA)
REAL(TINT,TKEIN,EPINJET,EPINCF)
REAL(MAXV,MINL,RELXU,RELXV,RELXW,RELXKE,RELXEP)
REAL(XPWR,YPWR,ZPWR)
    *
    ** Define constants
    *
NPR=4.0
CFLOW=10.0
DIAM=0.01796
XPWR=1.798
YPWR=1.651
ZPWR=1.589
    *
PAMB=101325.0
TAMB=288.15
TJETT=TAMB
CGAS=1005.0
RGAS=287.05
GAMMA=1.4
TINT=0.03
    *
    ** Calculate ambient density
    *
DAMB=PAMB/(RGAS*TAMB)
    *
    ** Calculation of jet exit static temperature
    *
TJETS=TJETT/(1.0+((GAMMA-1.0)/2.0))
    *
    ** Calculation of jet exit velocity (only for NPR>1.893)
    *
WJET=(GAMMA*RGAS*TJETS)**0.5
    *
    ** Calculation of jet exit total density
    *
DJETT=(PAMB*NPR)/(RGAS*TJETT)
    *
    ** Calculation of jet exit static density
    *
DJETS=DJETT/(1+(GAMMA-1)/2)**(1/(GAMMA-1))
    *
    ** Elliptic simulation
```

```
    *
PARAB=F
    *
    ************************************************************
    *
    ** Group 2 time dependence and other related parameters
    *
    ** Steady state simulation
    *
STEADY=T
    *
    ************************************************************
    *
    ** Group 3 X-direction grid
    *
    ** Total number of cells in grid X direction = 24
    *
NX=24
NREGX=2
XULAST=0.5
IREGX=1;GRDPWR(X,20,(0.5-(DIAM/2)),-XPWR)
IREGX=2;GRDPWR(X,4,(DIAM/2),1.0)
    *
    ************************************************************
    *
    ** Group 4 Y-direction grid
    *
    ** Total number of cells in grid Y direction = 88
    *
NY=88
NREGY=3
YVLAST=2.0
IREGY=1;GRDPWR(Y,40,(1.0-(DIAM/2)),-YPWR)
IREGY=2;GRDPWR(Y,8,DIAM,1.0)
IREGY=3;GRDPWR(Y,40,(1.0-(DIAM/2)),YPWR)
    *
    ************************************************************
    *
    ** Group 5 Z-direction grid
    *
    ** Total number of cells in Z direction = 60
    *
NZ=60
NREGZ=1
ZWLAST=1.5
IREGZ=1;GRDPWR(Z,60,1.5,ZPWR)
    *
    ************************************************************
    *
    ** Group 6 body fitting and other grid distortions
    *
    ************************************************************
    *
    ** Group 7 variables stored and solved for
    *
SOLVE(P1,U1,V1,W1)
STORE(RHO1,TMP1)
SOLUTN(P1,Y,Y,Y,N,N,N)
    *
    ************************************************************
    *
    ** Group 8 terms and devices
    *
    ************************************************************
    *
    ** Group 9 properties of the medium
    *
```

```
   ** Pressure, temperature and density
   *
PRESS0=PAMB
TMP1=GRND5;TMP1A=CGAS*TAMB;TMP1B=CGAS
RHO1=GRND5;RHO1B=1/RGAS;DRH1DP=GRND5
ENUL=GRND6;ENULA=1.458E-6;ENULB=110.4
   *
   ** Turbulence
   *
TURMOD(KEMODL)
TKEIN=(WJET*TINT)**2
EPINJET=3/7*(TKEIN**1.5))/DIAM
EPINCF=0.009*(TKEIN**2)/(50*1.461E-5)
   *
   ***********************************************************
   *
   ** Group 10 interphase transfer processes and properties
   *
   ***********************************************************
   *
   ** Group 11 initialisation of fields, variables and porosities
   *
   ** Set initial field values
   *
FIINIT(P1)=0.0
FIINIT(U1)=0.0
FIINIT(V1)=CFLOW
FIINIT(W1)=0.0
FIINIT(TMP1)=TAMB
FIINIT(RHO1)=DAMB
FIINIT(KE)=TKEIN
FIINIT(EP)=EPINCF
   *
   ***********************************************************
   *
   ** Group 12 convection and diffusion adjustments
   *
   ***********************************************************
   *
   ** Group 13 boundary conditions and special sources
   *
   ** Nozzle inlet
   *
PATCH(JET1,LOW,21,21,44,45,1,1,1,1)
COVAL(JET1,P1,FIXFLU,WJET*DJETS)
COVAL(JET1,W1,ONLYMS,WJET)
COVAL(JET1,KE,ONLYMS,TKEIN)
COVAL(JET1,EP,ONLYMS,EPINJET)
   *
PATCH(JET2,LOW,22,23,42,47,1,1,1,1)
COVAL(JET2,P1,FIXFLU,WJET*DJETS)
COVAL(JET2,W1,ONLYMS,WJET)
COVAL(JET2,KE,ONLYMS,TKEIN)
COVAL(JET2,EP,ONLYMS,EPINJET)
   *
PATCH(JET3,LOW,24,24,41,48,1,1,1,1)
COVAL(JET3,P1,FIXFLU,WJET*DJETS)
COVAL(JET3,W1,ONLYMS,WJET)
COVAL(JET3,KE,ONLYMS,TKEIN)
COVAL(JET3,EP,ONLYMS,EPINJET)
   *
   ** Crossflow
   *
PATCH(UPSTRM,SOUTH,1,24,1,1,1,60,1,1)
COVAL(UPSTRM,P1,FIXFLU,CFLOW*DAMB)
COVAL(UPSTRM,V1,ONLYMS,CFLOW)
COVAL(UPSTRM,KE,ONLYMS,TKEIN)
```

```
COVAL(UPSTRM,EP,ONLYMS,EPINCF)
   *
   ** Collector
   *
PATCH(DNSTRM,NORTH,1,24,88,88,1,60,1,1)
COVAL(DNSTRM,P1,FIXP,0.0)
   *
   ** Tunnel side (only west side defined,
   **              east is plane of symmetry)
   *
PATCH(PORT,WEST,1,1,1,88,1,60,1,1)
COVAL(PORT,P1,FIXP,0.0)
   *
   ** Upper surface
   *
PATCH(FSE1,LWALL,1,20,1,88,1,1,1,1)
COVAL(FSE1,U1,GRND2,0.0)
COVAL(FSE1,V1,GRND2,0.0)
COVAL(FSE1,W1,GRND2,0.0)
COVAL(FSE1,KE,GRND2,GRND2)
COVAL(FSE1,EP,GRND2,GRND2)
   *
PATCH(FSE2,LWALL,21,21,1,43,1,1,1,1)
COVAL(FSE2,U1,GRND2,0.0)
COVAL(FSE2,V1,GRND2,0.0)
COVAL(FSE2,W1,GRND2,0.0)
COVAL(FSE2,KE,GRND2,GRND2)
COVAL(FSE2,EP,GRND2,GRND2)
   *
PATCH(FSE3,LWALL,21,21,46,88,1,1,1,1)
COVAL(FSE3,U1,GRND2,0.0)
COVAL(FSE3,V1,GRND2,0.0)
COVAL(FSE3,W1,GRND2,0.0)
COVAL(FSE3,KE,GRND2,GRND2)
COVAL(FSE3,EP,GRND2,GRND2)
   *
PATCH(FSE4,LWALL,22,23,1,41,1,1,1,1)
COVAL(FSE4,U1,GRND2,0.0)
COVAL(FSE4,V1,GRND2,0.0)
COVAL(FSE4,W1,GRND2,0.0)
COVAL(FSE4,KE,GRND2,GRND2)
COVAL(FSE4,EP,GRND2,GRND2)
   *
PATCH(FSE5,LWALL,22,23,48,88,1,1,1,1)
COVAL(FSE5,U1,GRND2,0.0)
COVAL(FSE5,V1,GRND2,0.0)
COVAL(FSE5,W1,GRND2,0.0)
COVAL(FSE5,KE,GRND2,GRND2)
COVAL(FSE5,EP,GRND2,GRND2)
   *
PATCH(FSE6,LWALL,24,24,1,40,1,1,1,1)
COVAL(FSE6,U1,GRND2,0.0)
COVAL(FSE6,V1,GRND2,0.0)
COVAL(FSE6,W1,GRND2,0.0)
COVAL(FSE6,KE,GRND2,GRND2)
COVAL(FSE6,EP,GRND2,GRND2)
   *
PATCH(FSE7,LWALL,24,24,49,88,1,1,1,1)
COVAL(FSE7,U1,GRND2,0.0)
COVAL(FSE7,V1,GRND2,0.0)
COVAL(FSE7,W1,GRND2,0.0)
COVAL(FSE7,KE,GRND2,GRND2)
COVAL(FSE7,EP,GRND2,GRND2)
   *
   ** Tunnel floor
   *
PATCH(BOTTOM,HWALL,1,24,1,88,60,60,1,1)
```

```
COVAL(BOTTOM,U1,GRND2,0.0)
COVAL(BOTTOM,V1,GRND2,0.0)
COVAL(BOTTOM,W1,GRND2,0.0)
COVAL(BOTTOM,KE,GRND2,GRND2)
COVAL(BOTTOM,EP,GRND2,GRND2)
    *
    ************************************************************
    *
    ** Group 14 downstream pressure (for parabolic flow)
    *
    ************************************************************
    *
    ** Group 15 termination criteria for sweeps
    *
FSWEEP=1
LSWEEP=5000
SELREF=T
RESFAC=1.0E-3
    *
    ************************************************************
    *
    ** Group 16 termination criteria for inner iterations
    *
    ************************************************************
    *
    ** Group 17 under relaxation and related devices
    *
MAXV=WJET
MINL=DIAM/8
RELXU=30.0
RELXV=30.0
RELXW=30.0
RELXKE=10.0
RELXEP=10.0

RELAX(P1,LINRLX,0.8)
RELAX(U1,FALSDT,(MINL/MAXV)*RELXU)
RELAX(V1,FALSDT,(MINL/MAXV)*RELXV)
RELAX(W1,FALSDT,(MINL/MAXV)*RELXW)
RELAX(KE,FALSDT,(MINL/MAXV)*RELXKE)
RELAX(EP,FALSDT,(MINL/MAXV)*RELXEP)
    *
    ************************************************************
    *
    ** Group 18 limits on variables, values or increments to them
    *
    ************************************************************
    *
    ** Group 19 data communicated by SATELLITE to GROUND
    *
USEGRD=T
    *
    ************************************************************
    *
    ** Group 20 control of preliminary printout
    *
    ************************************************************
    *
    ** Group 21 frequency and extent of field printout
    *
    ************************************************************
    *
    ** Group 22 location of spot values
    *
IXMON=10
IYMON=44
IZMON=20
```

```
TSTSWP=10
UWATCH=F
USTEER=F
   *
   ************************************************************
   *
   ** Group 23 variable by variable fields printout
   *
YZPR=T
NXPRIN=1
NYPRIN=1
NZPRIN=1
   *
   ************************************************************
   *
   ** Group 24 preparation for continuation of runs
   *
   ************************************************************
   *
NOWIPE=T
STOP
```